7. DOSE-ASSESSMENT MODULE

R.B. Neel/NMSS

7.1 BACKGROUND

A major difference between the Iterative Performance Assessment (IPA) Phase 1 and IPA Phase 2 studies was the incorporation of a dose-assessment capability into the total-system performance assessment (TPA) computer code in IPA Phase 2. A dose assessment for the proposed repository at Yucca Mountain was not included in IPA Phase 1 for the following reasons. First, the U.S. Environmental Protection Agency (EPA) adopted, as its primary criterion for compliance with the containment regulations in 40 CFR 191.13[1] (*Code of Federal Regulations*, Title 40, "Protection of Environment") a restriction on the quantity of any radionuclide that could be released to the accessible environment for 10,000 years after permanent closure, not on the exposures of individuals or populations that might result from these releases. Second, it appeared there was little likelihood of any non-compliance with the individual dose provisions in 40 CFR 191.15, "Individual Protection Requirements" (and therefore little need for a dose assessment capability) because EPA calculations showed that radionuclides released from a geologic repository located in volcanic tuff would not reasonably be expected to expose any human being for at least 1000 years after disposal. Section 191.15 restricts the annual dose to any individual only during the first 1000 years after permanent closure of the geologic repository operations area (GROA). Third, the staff believed that, if needed, existing computer codes for dose assessment could readily be assimilated into the TPA computer code.

In its original form, the criteria to be used for licensing a geologic repository were published in 1985 by EPA as: "Environmental Standards for the Management and Disposal of Spent Nuclear Fuel, High-Level and Transuranic Radioactive Wastes; Final Rule," 40 CFR Part 191 (EPA, 1985; 50 *FR* 38066). On July 17, 1987, the U.S. Court of Appeals for the First Circuit in Boston vacated Subpart B of this 1985 version of 40 CFR Part 191 and remanded the rule to the EPA for further consideration (see EPA, 1993; 58 *FR* 7924).

In response to this action by the court, the EPA published a final revision to 40 CFR Part 191 on December 20, 1993 (EPA, 1993; 58 *FR* 66398). The revised dose provisions in the draft included an extension of the period that applied to individual dose, from 1000 to 10,000 years after disposal. This proposal would significantly increase the probability for a subsequent exposure of a member of the public to releases of radionuclides from the geologic repository. Under the Waste Isolation Pilot Project (WIPP) Land Withdrawal Act and the Energy Policy Act of 1992, this revision is not applicable to a potential Yucca Mountain Repository. However, since the Energy Policy Act of 1992 directed the EPA to evaluate a health-based standard based on doses to individuals, the staff believed that addition of a dose-assessment capability in the total-system code for a potential Yucca Mountain site would be prudent.

---

[1] The Energy Policy Act of 1992 (Public Law 102-486), dated October 24, 1992, directs the Nuclear Regulatory Commission to promulgate a rule, modifying 10 CFR Part 60 of its regulations, so that these regulations are consistent with EPA's public health and safety standards for protection of the public, from releases to the accessible environment, from radioactive materials stored or disposed of at Yucca Mountain, Nevada, consistent with the findings and recommendations made by the National Academy of Sciences, to EPA, on issues relating to the environmental standards governing the Yucca Mountain repository.

7.2 BASIS FOR THE CALCULATION OF HUMAN EXPOSURES IN IPA PHASE 2

7.2.1 Concept of the "Reference Biosphere"

The NRC staff adopted a concept of a stable, or reference biosphere for its studies in IPA Phase 2 (see Federline, 1993). This "reference biosphere" implies that the locations, lifestyles, and physiology of persons who live and work in the vicinity of Yucca Mountain over the future periods of interest (up to 10,000 years and beyond) are difficult to predict. A reference biosphere will provide a basis for quantification of dose. The reference biosphere used in the environmental pathways that could result in human exposure to ionizing radiation will remain unchanged from those that exist in today's biosphere. In IPA Phase 2, scenarios that impacted the geosphere at Yucca Mountain were assumed not to disrupt this reference biosphere.

7.2.2 Similarity to Assumptions in 40 CFR Part 191

The use of a "reference biosphere" in NRC's approach to dose assessment is similar to that taken by EPA during the development of the background information for 40 CFR Part 191 (see EPA, 1985, p. 7-1). EPA's approach to dose assessment for the final rule contained the following caveat: "... it is pointless to try to make precise projections of the actual risks due to radionuclide releases from repositories. Population distributions, food chains, living habits, and technological capabilities will undoubtedly change in major ways over 10,000 years. Unlike geological processes, they can be realistically predicted only for relatively short times ...." (*op. cit.*). The conceptual model for the human physiology adopted by EPA included the concept of a present-day "reference man" (see ICRP, 1975).

EPA also proposed a definition for a "reference population" as another revision to 40 CFR Part 191 (see EPA, 1992). The "reference population" was defined as the entity of persons that, for 10,000 years after disposal, has the following features: (a) major population relocations or emergencies have not occurred; (b) the size of the (world) population is 10 billion; and (c) characteristics and behavior affecting estimates of radiation exposure and its effects are assumed to be as today; this includes level of knowledge, technical capability, human physiology, nutritional needs, societal structure, and access to pathways of exposure."

7.2.3 Similarity to the Approach Taken by BIOMOVS

The use of a "reference biosphere" in NRC's approach to dose assessment is also similar to that taken by a working group in BIOMOVS, the Biospheric Model Validation Study. BIOMOVS is a cooperative effort by the selected members of the international nuclear community to develop and test models that were designed to quantify the transfer and bio-accumulation of radionuclides in the environment (see INTERA, 1992). BIOMOVS recommends that long-term assessments of dose be based on the conceptual model of a "reference biosphere," that is analogous to the "reference-man" concept developed by the International Commission on Radiological Protection (ICRP). The participants in BIOMOVS believe that it is impossible to predict all the possible future evolutions (future states) of the biosphere. However, they believe it may be possible to identify a comprehensive list of important features, events, and processes that are essential for safe disposal of high-level radioactive waste (HLW) for a geologic repository sited in the present-day environments. The range of present-day environments is expected to bound the biospheres expected in the various future states. (Because of the diversity of nature, BIOMOVS recognizes that it may be necessary to define a number of different "reference biospheres".) NRC staff is currently considering this concept.

7.3 COMPUTER CODE SELECTED FOR DOSE ASSESSMENT

Human exposures in the IPA Phase 2 study were evaluated by *DITTY* (Dose Integrated for Ten Thousand Years) (see Napier *et al.*, 1988a, pp. 3-16 - 3-18), a new module added to the version of the total-system code. *DITTY* was selected for IPA Phase 2 because: (a) it could be used to calculate the relative variation in doses for the various scenarios used in Phase 2, rather than to predict the absolute doses for comparison with other performance-assessment studies; (b) it was easily interfaced to the outputs of other consequence modules used in the total-system performance code; (c) it could calculate population doses over durations of 10,000 years or more; and (d) it was available and could be executed with little further development.

7.3.1 Overview of DITTY

DITTY estimates the time integral of collective dose over a 10,000-year duration for releases (or concentrations) of radionuclides to the accessible environment. *DITTY* can treat both chronic and acute releases of radionuclides. Only a few input parameters to *DITTY* can be entered as input variables at various times during the 10,000-year period. These include:

- Annual releases of radioactivity to air and water;
- The number of persons in the exposed regional population; and
- The dispersion factors in the terrestrial and aquatic environments.

DITTY breaks the 10,000-year duration into 143 periods of 70 years (each period is considered to be the length of a human lifetime), and the total population dose is determined for each of the 143 periods. The radioactivity present during any 70-year period is the sum of the activity in the nuclides released during that period and the residual radioactivity in the environment caused by releases in previous periods. For radionuclides whose effective half-life in the environment is very long compared to a human life span, and whose release rate to the accessible environment is relatively constant, division of the 70-year lifetime dose calculated by *DITTY* by a factor of 70 gives a crude estimate of annual individual dose.
In IPA Phase 2, the exposure pathways to the accessible environment that were of interest are illustrated in Figure 7-1. These include: the atmosphere, land surfaces, the top 15 centimeters of surface soil, vegetation, animal products (milk, beef), and drinking water. Aquatic pathways were not considered in this study because they are not credible pathways near Yucca Mountain. The quantities of radionuclides released from the repository that move into the environmental media along these pathways are used to calculate concentrations and dose in the reference biosphere. *DITTY* cannot calculate concentrations of radionuclides in the lithosphere or the ground water contained therein.

For IPA Phase 2, the annual releases to the air or water pathways at selected times, during the 10,000-year period of interest (the source terms), were provided as input to *DITTY* by other TPA computer code modules in the form of average annual concentrations. Up to 450 of these paired values can be entered as an input file (e.g., as curies per year/time or curies per volume/time). The values for these concentration-time pairs were obtained as outputs directly from the *NEFTRAN* module, or indirectly, from the *C14*, *DRILL02*, and *VOLCANO* modules (see Figure 2-1).

DITTY calculates the downwind regional air concentrations as the product of the release rate of radionuclide (from the ground surfaces above the geologic repository into the atmosphere) and a

dispersion factor, commonly designated as *X/Q*. For waterborne releases, in addition to the calculation of collective doses, *DITTY* will identify that 70-year period when the individual lifetime (70-year) dose is highest.

7.3.2 General Approach to Dose Calculations in DITTY

A calculation of internal dose to a human-body organ in *DITTY* can be visualized as the product of four parameters, so that for any single radionuclide:

$$D = C \times FTC \times U \times DCF,$$

where *D* is the dose to a body organ from the radionuclide per year of intake; *C* is the concentration of radionuclide in a specific media (e.g., curies per kilogram of pasture grass eaten by beef cattle); *FTC*, is identified in *DITTY* as the food-transfer coefficient, is a dimensionless factor that expresses the distribution ratio of a radionuclide between two media at steady-state (e.g., the ratio of the steady-state concentration in the edible tissues of the beef cattle to the steady-state concentration in pasture grass); *U* is the human-use factor (e.g., kilograms of beef eaten per year) for the media; and *DCF* (dose-conversion factor) is the quantity that will convert radioactivity ingested or inhaled into dose (e.g., rem per curie). The *DCF* values and the *FTC* values used in this study, which are described in Section 7.7, are different from values in the original *DITTY* databases.

7.3.3 Calculation of Total Dose in DITTY

The total population dose is expressed in terms of an effective dose equivalent (EDE). This dose is the sum (over all organs) of internal and external doses that result from direct radiation or uptakes of radionuclides into the human body along the pathways illustrated in Figure 7-1.

Internal doses to body organs can result from the inhalation of airborne radioactivity or from the ingestion of radionuclides in contaminated food and water. In *DITTY*, these organ doses are multiplied by a risk-based weighting factor to give "effective" organ doses (i.e, committed EDE). The values used for these organ-weighting factors in *DITTY* are the same as those given in ICRP-26 (ICRP, 1977). All internal doses are integrated over the 50-year period that follows an intake of radionuclides (i.e., for a dose-commitment period of 50 years in the human body). The integrated dose is formed from the sum of the doses to six designated body organs and to the five remaining organs with the highest doses.

External exposures can result either from submersion of the human body in airborne radioactivity or from exposure to direct radiation (ground shine) that emanates from the surface of contaminated soil. In *DITTY*, organ doses caused by external exposures are expressed in terms of the EDE, instead of the more common dose equivalent quantities. A special energy-dependent dose factor (rem/rad) is used in *DITTY* to convert external doses to the body surfaces to deep organ-doses (Kocher, 1981). The use of these conversion factors in *DITTY* has preceded any guidance by the Commission on acceptable methods for calculation of EDE from external photon and particulate radiation.

7.3.4 Selection of *DITTY* Model Parameters

For IPA Phase 2, default values for the model parameters from *DITTY* were used in the dose-assessment models unless indicated otherwise. Probability density functions (PDFs) were not defined, and Latin Hypercube Sampling (LHS -- discussed in Chapter 8) was not attempted, for any parameter used in the

Figure 7-1. Human exposure pathways in the accessible environment, as calculated by the *DITTY* computer code.

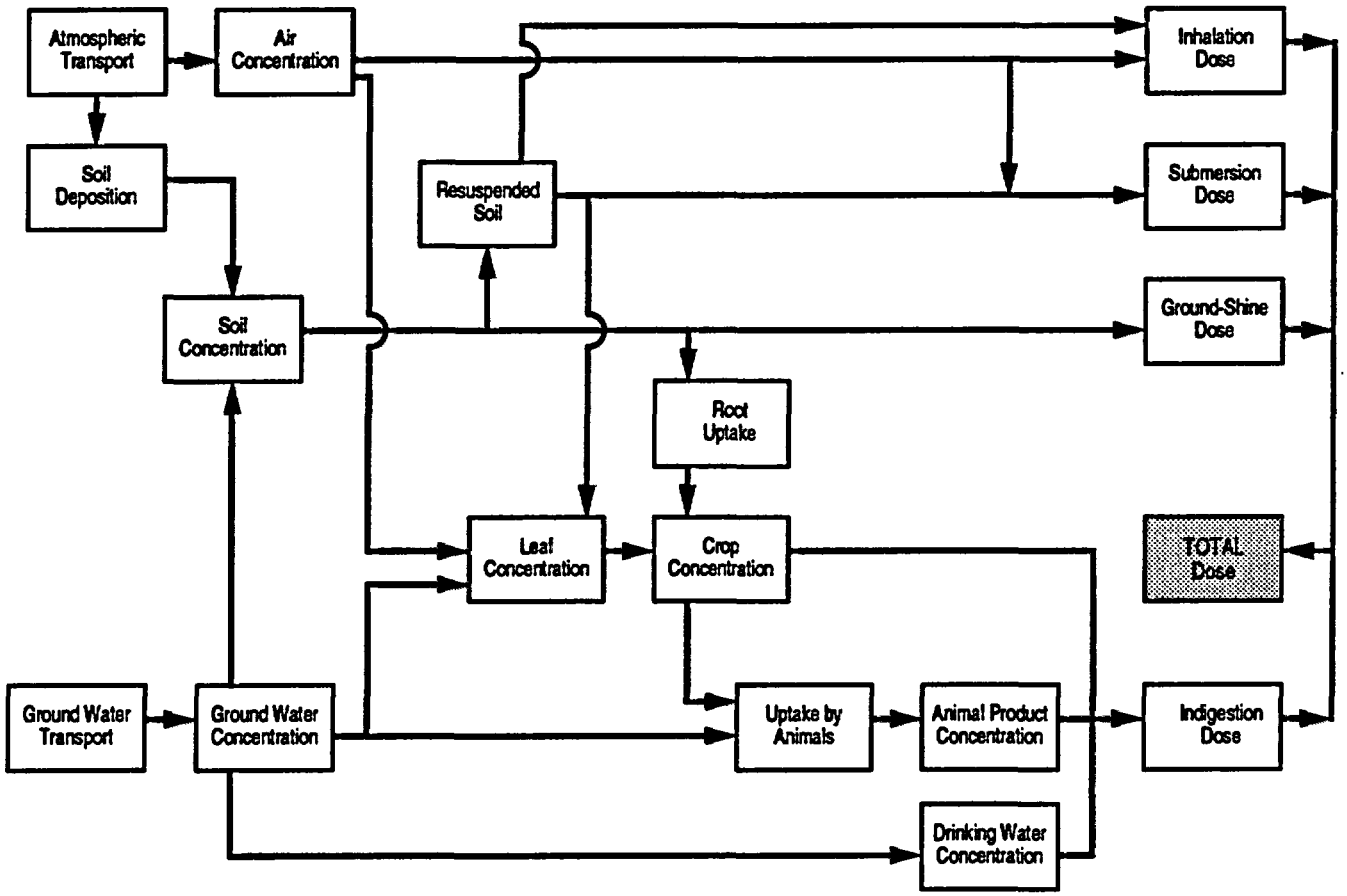
Atmospheric Transport
Air Concentration
Inhalation Dose
Soil Deposition
Resuspended Soil
Submersion Dose
Soil Concentration
Ground-Shine Dose
Root Uptake
Leaf Concentration
Crop Concentration
TOTAL Dose
Ground Water Transport
Ground Water Concentration
Uptake by Animals
Animal Product Concentration
Indigestion Dose
Drinking Water Concentration

dose-assessment models. This was done intentionally to focus attention on the magnitude of the uncertainties introduced into the resulting doses by the collective uncertainties associated with the source term and geosphere models used in IPA Phase 2. In the future, it will be necessary to estimate site-specific values for the *DITTY* model parameters to make the most meaningful calculations of dose. In many cases, a literature study will be sufficient to select these values. However, for those radionuclides that are major contributors to the dose, laboratory and field studies may also be desirable. Sensitivity studies, similar to those conducted in other IPA Phase 2 modules (see Chapter 9, "Sensitivity and Uncertainty Analysis"), should also be carried out for parameters in the biosphere models. In this way, the parameters that significantly influence the magnitude of the doses and that may require further study in the field may be identified.

7.4 DIFFERENCES FROM INTERNAL DOSIMETRY MODELS IN ICRP-30

The major differences of the biokinetic models in *DITTY* from those in ICRP-30 -- "Limits for Intakes of Radionuclides by Workers" (ICRP, 1979) -- are found in the computer program *GENMOD*. *GENMOD* (Johnson and Carver, 1981), which was adapted directly from ICRP-30, incorporates additional models other than those developed by the International Commission for Radiation Protection (such as the alkaline earth model, the *MIRD* iron model, and the ^{14}C model). *GENMOD* was used to generate databases that include values for the following metabolic parameters for each radionuclide used in *DITTY*: organ uptake, transfer coefficients from compartment to compartment, and elimination rates from compartments. The metabolic models for carbon assume it is inhaled as carbon dioxide gas, and that ingested carbon is in the form of carbohydrates that are readily absorbed through the gut and rapidly distributed throughout the body.

Although metabolic parameters for various ages, sexes, and ethnic groups were not available when this study was undertaken, they may require further consideration when guidance for members of the public becomes available. A rough estimate of the variation of dose with the age of exposure may be inferred from the Statement of Considerations for the final rule for 10 CFR Part 20 (*Code of Federal Regulations*, Title 10, "Energy") "... those organs for which age dependency is important, such as the thyroid gland, are of lesser importance because of the lower w_T values [risk-weighting factors] ... used to calculate the effective dose. A factor of 2 is included ... which, in part, accounts for age dependency ...." (NRC, 1991; 56 *FR* 23390). This appears to be a reasonable assumption, given the observation recently made by Charles and Smith (1991, p. 10) that "... the generally higher committed doses per unit intakes for non-adult age groups are in the main cancelled by the lower consumption of foodstuffs ...."

7.5 SELECTION OF DCFs FOR THIS STUDY

7.5.1 DCFs for Ingestion and Inhalation

In IPA Phase 2, the *DCFs'* values were assumed to be without bias and of the highest precision. Since it was assumed that a "reference man" in a "reference biosphere" was exposed over the 10,000-year period when radionuclides were released from the geologic repository, the same *DCFs* were used for calculations of dose during each of the 70-year human lifetimes considered in *DITTY*. The *DCFs* for the radioactive daughters that are produced *in vivo* were generally also described with the same metabolic parameters as those for the parent radionuclide.

The *DCFs* for inhalation and ingestion, used in IPA Phase 2, which were prepared by Dr. Paul Rittman

of Westinghouse Hanford Company, from the revised computer code *INTDF* (Version 1.483) (see Napier *et al.*, 1988a, pp. 3-13 - 3-16), are the "worst-case" values. These parameters, which pertain to each radionuclide used in *DITTY*, maximize either the inhalation dose by an intentional selection of the chemical form with the worst-case solubility in the lung, or the ingestion dose, by selection of the chemical form that results in the largest uptake in the small intestine (*f1* value) for each radionuclide, or both. When normalized to an annual basis, the *DCFs* generated by *INTDF*, a *DITTY* sub-routine, are essentially the same as those reported in EPA's Federal Guidance Report No. 11 (i.e., to within two significant figures, but with a few differences for very short-lived nuclides) (EPA, 1988).

The dose-commitment period for all *DCFs* used in this study is 50 years. This is consistent with 10 CFR Part 20 and also with the recommendations of both national and international committees on radiation protection. A 50-year dose-commitment period was also suggested by EPA for Appendix B of 40 CFR Part 191 (see EPA, 1993; 58 *FR* 7936). Since *DITTY* assumes that an individual will experience an annual intake of radionuclides during each year of his 70-year lifetime, the use of this 50-year dose commitment period will overestimate his lifetime dose for those radionuclides with a long biological half-life (but in no case by more than a factor of 2).

7.5.2 DCFs for External Exposure

The *DCFs* for air submersion and for direct radiation exposure to radionuclides deposited on land surfaces (ground shine) were used in this study unchanged from those as found in the databases of the *DITTY* code. These values will be reviewed when EPA publishes Federal Guidance No. 12 (in preparation), a tabulation of dose coefficients for external exposure to photons and electrons emitted by radionuclides distributed in environmental media.

7.6 SELECTION OF PARAMETERS FOR THE INGESTION PATHWAYS

The bases for selection of data used in the terrestrial-ingestion pathway models of *DITTY* are discussed below.

7.6.1 Drinking-Water Parameters

The original version of the database *BIOACI.DAT* contained factors to simulate the treatment of drinking water by a municipal water-treatment plant. For IPA Phase 2, drinking water was assumed to be taken from a surface well without any treatments to remove radionuclides (all treatment factors were set to a value of 1). This is equivalent to the assumption that the concentration of a radionuclide in drinking water has the same concentration as it had in the ground water that feeds the well. The IPA Phase 2 analysis did not consider mitigating measures available in present-day technology. These measures may include devices to monitor waterborne radiation or procedures, such as water treatment or condemnation of the well.

7.6.2 Food-Transfer Parameters

The documentation in *DITTY* does not identify the sources of the soil-to-food transfer parameters stored in the *DITTY* file *FTRANS.DAT*. (The user's manual for *DITTY* indicates that the "... sources of these parameters are to be published in a separate document" (see Napier *et al.*, 1988b, pp. 2.28 - 2.29). Since literature citations were not available during IPA Phase 2, *FTRANS.DAT* parameters were replaced by "generic" parameters taken from the well-known study by Baes *et al.* (1984).

The Baes parameters used in this study (*Bv, Br, Ff,* and *Fm*) are based on clearly- defined protocols that were used to select them from the multiplicity of experimental values reported in the literature. For example, for the soil-to-crop values, the Baes study attempted to select concentration ratios that were based on detailed literature studies in which the soil and plant concentrations were both measured at "edible maturity" of the plant. These literature citations show that large variations (orders of magnitude) of these parameters in various environmental settings are not uncommon, and therefore most studies use site-specific values to increase the reliability of dose estimates.

The *DITTY* parameters for each chemical element that was stored in the file *FTRANS.DAT* were replaced by the following types of Baes parameters (dry-weight to dry-weight basis):

- A *Bv* value (Baes *et al.*, 1984; Figure 2.1) replaced each soil-to-leafy-vegetable concentration ratio;
- The same *Br* value (Baes *et al.*, 1984; Figure 2.2) replaced each of the four soil-to-edible-crop concentration ratios (these crops are vegetable, root, grain, and fruit);
- A *Ff* value (Baes *et al.*, 1984; Figure 2.25) replaced the feed-to-meat transfer coefficient; and
- A *Fm* value (Baes *et al.*, 1984; Figure 2.24) replaced the feed-to-milk transfer coefficient. The poultry and egg pathways were not used in the IPA Phase 2 studies, and therefore these food-transfer coefficients were not modified. These new values, which are stored in a new file *FTRANS.CFB*, were used for all calculations of dose in IPA Phase 2.

The leaching factors for soil in *FTRANS.CFB* are unchanged from the values in *FTRANS.DAT*. The magnitudes of the leaching factors in *DITTY* are directly proportional to the percolation rate of water through the rooting zone and into deeper soil layers (an over-watering term of 15 cm/year was assumed in *DITTY*). In IPA Phase 2, small variations in the leaching factors for very mobile radionuclides (e.g. technecium and iodine), were shown to have a significant impact on the magnitude of dose. For models like *DITTY*, that involve long-term deposition of radionuclides in soil, the leaching factors should be obtained from site-specific investigations, to properly characterize the retention of radionuclides in soil and their biological availability to crops (IAEA, 1982).

7.6.3 Growing-Season Parameters

The site-specific agricultural parameters for Yucca Mountain that were entered as input data to *DITTY* included: the length of the growing season, the irrigation rate for crops during the growing season, and the yields of the various types of crops. There are two periods in Nevada when vegetables can be grown – one that begins in February, and the other that begins as early as mid-August. The lengths of the growing season depend on the crop type. One of the most important crops in Nevada is alfalfa, which can grow up to 250 days each year and produce up to eight harvests each year. For most vegetables, the first growing season begins in February and ends in early March; the second season begins in mid-August and ends in mid October. Very little appears to grow during the hot, dry summer months between late May and late August (Mills, 1993).

The lengths of the growing period selected for this study were: For leafy vegetables, 45 days; for "other" vegetables, 90 days. For alfalfa, and for those pasture grasses that are consumed as by animals as forage, the growing season was taken as 30 days (Kennedy and Strenge, 1992, Table 6.12).

7.6.4 Irrigation Rate for Crops

The State of Nevada issues water-use permits that limit the maximum pumping rate from wells in the vicinity of Yucca Mountain to 127 liters per month per square meter (~152 cm per year) of irrigated land (Personal comm., Nevada State Engineer's Office). For areas within 100 kilometers of the geologic repository, the irrigation period was assumed to coincide with the average length of the growing season (i.e. 60 days). Irrigation was assumed to proceed at the maximum pumping rate allowed by the water permit (see "Rate of Irrigation," in Section 7.8.2).

7.6.5 Crop Yields (Human Consumption)

The yields of the irrigated crops (in kilograms per square meter), and the quantities consumed by humans (in kilograms per year in parenthesis) are taken from Tables 6.14 and 6.15, respectively, in Kennedy and Strenge (1992, Vol. 1). The values used in *DITTY* are: leafy vegetables, 2.0 (11); "other" vegetables, including grains, fruits and root vegetables, 4.0 (172); the pasture grasses and alfalfa that fatten beef cattle and leads to milk production, 1.5 (milk, 100 kg/year and beef, 59 kg/year). These values are not inconsistent with those found to grow in Nevada lowlands (Nevada Agricultural Statistics Service, 1988).

Milk cows are assumed to consume vegetation at the rate of 55 kilograms per day and beef cattle at 68 kilograms per day. Milk cows are assumed to drink water at the rate of 60 liters per day and beef cattle at 50 liters per day. These parameters are default values in *DITTY* (found in data statements).

7.7 SELECTION OF PARAMETERS FOR THE INHALATION PATHWAYS

7.7.1 Meteorological Data

The meteorological data selected for *DITTY* was a composite of the annual averaged STAR (Stability Array) data measured by the National Oceanographic and Atmospheric Administration between 1986 and 1990, at Station Number 03160, Desert Rock, Nevada, which is 935 meters above sea level (U.S. Department of Commerce, 1992). Data were available for seven stability classes, six wind speeds and for 16 compass directions. Data from this particular location were selected because of their availability. These data was used to calculate the concentrations of airborne radionuclides in the region surrounding the geologic repository.

All releases of radioactivity from the geologic repository were assumed to occur at ground level and to disperse radially out to a distance of 100 kilometers. (The distance between radial segments illustrated in Figure 7-2 is 20 kilometers.) A Gaussian plume model was used to convert releases of radioactivity to long-term, sector-averaged X/Q values (expressed in units of seconds per cubic meter released). In this study, X/Q values were estimated by *DITTY* at the following distances: 2.5, 7.5, 15, 30, 50, 70, and 90 kilometers. These distances are measured radially from the release point in the GROA to the midpoints of the wedge-shaped sectors shown in Figure 7-2 (e.g., a mid-point distance of 30 kilometer (North) is midway between the 20 kilometer (North) and 40 kilometer (North) distance intervals).

7.7.2 Regional Population Distribution at Yucca Mountain

The size of the regional population exposed to airborne releases of radioactivity was assumed to be stable

throughout the entire 10,000-year period. Members of this population were located at the mid-points of the wedge-shaped sectors shown in Figure 7-2 (i.e., those distances identified in Item (1), above).

The dispersion studies were extended to 100 kilometers, to include the 5500 persons who were residents of the city of Pahrump in 1988. This regional population distribution in Figure 7-2 was taken from SAND 81-2375 (Logan *et al.*, 1982) and was updated with information obtained from DOE's 1988 Site Characterization Plan (see DOE, 1988, Table 3-21).

7.8 APPLICATION OF THE DOSE ASSESSMENT METHODOLOGY TO YUCCA MOUNTAIN: BIOSPHERE SCENARIOS

7.8.1 Application of the Critical-Group Concept

Whenever a radiological assessment is undertaken before the operation of a new nuclear facility, the specific individuals who may receive the highest exposures and greatest risks in future time cannot be identified. In these circumstances, it is appropriate to define a hypothetical critical group (those persons who receive the highest exposures) because this approach avoids the need to forecast future lifestyles, attitudes to risk, and developments in the diagnosis and treatment of disease. In principle, the critical group should be defined by age, sex, and ethnic origins since intakes, metabolism, and dosimetry of radionuclides are all strongly conditioned by these factors (IAEA, 1982). As noted in Section 7.4, a rough estimate of the variation of dose with the age of exposure may be inferred from the Statement of Considerations for the final 10 CFR Part 20 rule.

7.8.2 Hypothetical Biosphere Scenario: Waterborne Release

Section 191.15 of 40 CFR Part 191 requires that "... all potential pathways...from the disposal system to people shall be considered ... including the assumption that individuals consume 2 liters per day of drinking water from a significant source of ground water outside of the controlled area." A contemporary farm family of three persons was selected as the hypothetical critical group, to illustrate the capability for dose assessment that was incorporated into the total-system computer code in IPA Phase 2.

Location: The hypothetical family is assumed to maintain a year-round residence on an average-sized farm (approximately 1093 hectares) located at the boundary of the controlled area (10 CFR 60.2) that surrounds the geologic repository at Yucca Mountain. Contaminated water pumped from a local well irrigates two areas on this farm: a 88-hectare tract, an area which is set aside as irrigated pasture land for calves (yearlings) and other cattle (Agricultural Statistics for Nevada for the 1987-88 period estimates that approximately 100 farms, with a irrigated land area of 12,146 hectares, are irrigated in Nye County); and a fenced-in tract of 1.2 hectares, which is used to grow a large portion of the family vegetables (leafy and other), fruits and grains for home consumption (the growing periods and yields of crops, and the human consumption of meats and crops were adopted from Kennedy and Strenge, 1992, Tables 6.12 - 6.15). The remaining 1004 hectares of un-irrigated and un-contaminated land are used to graze mature beef cattle.

Drinking Water: Each member of this contemporary family is assumed to obtain all of his/her drinking water (2 liters per day of drinking water for 365 days per year) from a contaminated well at the boundary of the controlled area. The composition of this well water is assumed to be similar to that found in U.S. Geological Survey Well J-13. Well J-13 is located approximately 13 kilometers southeast from the controlled area boundary of the repository. The current capacity of the pump at Well J-13 is 2385 liters

(The population distribution shown is as of December 1988. It was adopted from Logan, *et al.* (1982) and DOE (1988)).

Figure 7-2. Estimated population distribution in the vicinity of Yucca Mountain, Nevada.

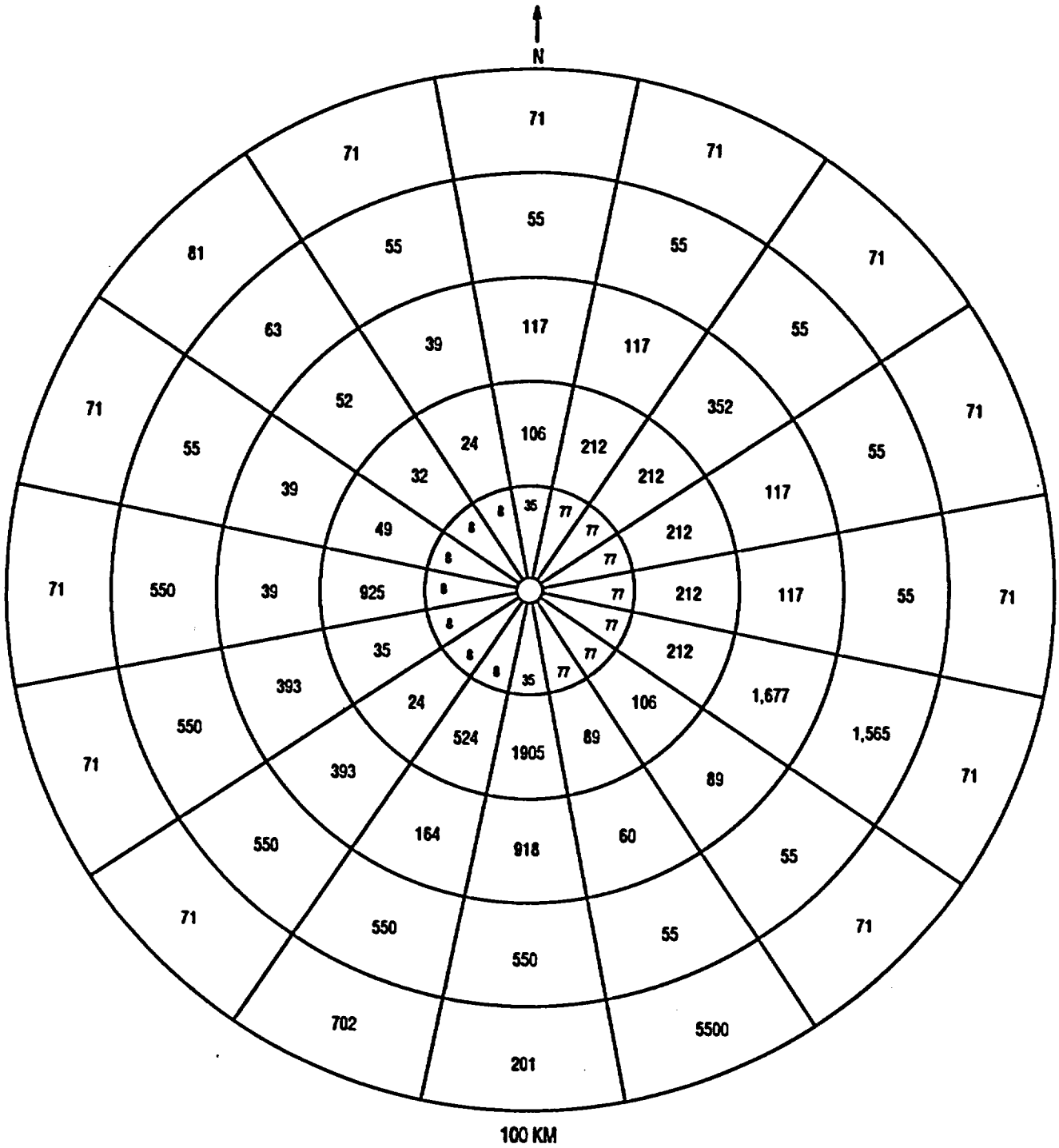
N
71
71
71
55
55
55
81
71
63
39
117
117
55
71
52
352
71
55
24
106
212
55
39
32
212
117
49
212
71
550
39
925
212
117
55
71
35
212
393
24
106
1,677
550
524
1905
89
1,565
71
393
89
550
164
918
60
55
71
550
550
55
71
702
5500
201
100 KM

per minute (maximum) which is approximately 4 million liters per day (see Czarnecki, 1992, Table 1).

Rate of Irrigation: Fluxes of radionuclides to the well used by the farm family emanate from the seven subareas in the model of the repository for the Yucca Mountain site, as depicted in Figure 4.6, and are calculated by the TPA computer code that invokes the models for source term releases, flow, and transport. The seven geologic repository sub-areas have different physical and chemical properties that govern the times of release of the radionuclides from the waste form and the travel time through the geosphere. Thus, the concentration of the radionuclides in the well at the point of use by the farm family is a complicated function of time.

To obtain the concentrations of radionuclides in the contaminated well water after a waterborne release, the fluxes of radionuclides in the aquifer (calculated at the location of the well) were diluted to a volume of 4 million liters per day. Approximately 4 millon liters per day would be required to irrigate the garden plot and the pasture area (89 hectares irrigated at a rate of 127 liters/square meter-month). This dilution flow was considered consistent with the water usage by the farm family and for stock watering. These concentrations were calculated at selected times during the 10,000-year period of study and were used as input to *DITTY*.

Consumption of Foods: Reports by the U.S. Department of Commerce indicate that no farms in Nye County sell dairy products for profit (USDC, 1989, p. 138). The farm family is therefore assumed to own cows only to provide dairy products for their own consumption. Of the 136 farms identified in Nye County in 1987, only eight farms raised poultry, and only nine farms raised hogs and pigs (*op. cit.*). The family is assumed to purchase pork, poultry, eggs, and small quantities of fruits, vegetables, and grains at a local supermarket supplied with un-contaminated foodstuffs by a distributor from another geographical area. The family is assumed to consume 100 percent of their beef and milk from farm animals that feed on vegetation irrigated by contaminated well water.

Inside/Outside Activities: Annually, the hypothetical person is assumed to spend 6424 hours (73 percent) inside his home (TV, sleep, etc.), and to spend 2336 hours outside the home (farming, herding cattle, and recreation). If the hours spent inside the home are weighted by a shielding factor of 0.5 (NRC, Regulatory Guide 1.109, p. 43) and added to the hours spent outside, the effective time that this person would be exposed to external ionizing radiation (ground shine and submersion in airborne radioactivity) would be 5548 hours per year.

Exported Beef Cattle: Beef cattle (60 percent mature and 40 percent calves) sold for profit are assumed to obtain 100 percent of their feed from the contaminated vegetation raised on the 88 hectares of irrigated pasture land on the family farm. Half of the these animals (43 calves and 32 cattle), that are exported off the farm and sold for profit each year, are estimated to produce 10,377 pounds per year of edible beef. This quantity of beef will feed 177 persons per year, if it is assumed that one person consumes 129 pounds (59 kilograms) of beef each year (approximately 1½ hamburgers per day every day of the year).

7.8.3 More Realistic Biosphere Scenario: Waterborne Release

A more realistic biosphere scenario would involve exploitation of ground waters near Yucca Mountain, to supplement the municipal water supply for regional populations. Water consumers in the region would then form the critical group whose doses would be limited by an individual protection standard (Federline, 1993). This scenario may be explored further in future IPA analyses.

7.8.4 Hypothetical Biosphere Scenarios: Airborne Releases

Mechanisms of Release to the Atmosphere: In IPA Phase 2, contaminated soil (or gaseous ^{14}C) was assumed to be transported to the ground surface above the repository as a result of disruptions of the geologic repository either by human intrusion (e.g., by exploratory drilling) or by an extrusive volcano (only for cone magma events). As many as 20 radionuclides might contribute to the radioactivity in this contaminated soil. During the 10,000-year period in this study, the times that the releases to the atmosphere from the contaminated ground surface could occur are governed by model parameters. The time of release is therefore a variable, because it depends on the particular vector set used to generate the dose for any given scenario (these times and the vector sets are determined by LHS sampling of appropriate model parameters).

Only a fraction of this released radioactivity was assumed to become available for transport by the air pathway to members of the public beyond the controlled area of the repository. The fractions of the radioactivity that were assumed to become airborne were: 0.04 for the human intrusion scenarios; 0.30 for the magmatic eruption scenarios; and 1.0 for the ^{14}C scenarios. (These values were stored in the *AIRCOM* module of the TPA computer code.) All the airborne radioactivity was assumed to be respirable (whether in the solid, liquid, or gaseous states). Any radioactivity that did not become airborne was considered to remain undisturbed at the point of release to the above-ground surface.

The NRC staff made preliminary estimates of the fractions of radioactivity, released from the human intrusion and volcano scenarios, that became airborne, as described below. For the human intrusion scenario, a company that manufactures drill bits advised the staff that for a large hole, which was drilled into a hard formation such as granite, approximately 25 percent of the drilling would pass through a 200-mesh screen. (This means that 25 percent of the cuttings would be smaller than 62 microns). The staff assumed that the grain sizes of cuttings below 62 microns followed a uniform distribution. From a typical plot of grain size versus cumulative percentage of cuttings retained in the various-sized sieves (e.g., see Freeze and Cherry, 1979, p. 351), the staff estimated that one-sixth of this material would be smaller than 10 microns. It follows that roughly 4 percent of the total mass of the drill cuttings would be smaller than 10 microns (25/6 = 4 percent). For the volcano scenario, the NRC staff obtained the respirable airborne fractions from Fisher and Schmincke (1984). For "explosive" volcanic eruptions, they claim that between 10 to 30 percent of the material that becomes airborne is smaller than 10 microns.

Calculation of Dose for Airborne Releases: The sequence of calculations by the TPA computer code that results in an estimate of the doses to the regional population (or the farm family) after exposure to an airborne release of radioactivity from the geologic repository is as follows. First, the consequence modules *DRILLO2*, *VOLCANO*, and *C14* calculate the quantities of radionuclides in contaminated soil (or gaseous ^{14}C) that are released to the ground surface in any given year. These quantities of surface radioactivity are then multiplied by the corresponding fractions stored in the *AIRCOM* module to generate the quantities of radioactivity that becomes airborne and respirable during that year. These latter values are in a format that is compatible with the *DITTY* module (curies per year released to air at various times).

DITTY calculates the concentrations of radionuclide in the various media (refer to Figure 7-1) that result from an airborne release and converts these to dose with the appropriate *DCFs*. The semi-infinite plume model was used to calculate doses caused by submersion in contaminated air. For this exercise, wind speeds measured at the Desert Rock Station were not corrected to ground-level.

Airborne Releases of ^{14}Carbon: The models for ^{14}C (gaseous release), human intrusion, and magmatic eruption were used to estimate the releases of gaseous ^{14}C to the atmosphere. All of the ^{14}C that escapes from degraded waste package canisters emplaced in the repository is assumed to travel through the geosphere and to be gradually released to the atmosphere as carbon dioxide gas. In *DITTY*, this ^{14}C is further assumed to be incorporated into vegetation by the photosynthesis process, with a resulting specific activity in the plant that is identical to that in the contaminated atmosphere. *DITTY* also assumes that 10 percent of the specific activity in soil is transferred to the edible plant, to augment the photosynthesis process.

In Section 4.3, the releases of ^{14}C were estimated to occur over an area of several square kilometers. But, in this study, all ^{14}C releases to the atmosphere were assumed to emanate from a point source located at the approximate center of the GROA. The exposure values reported in IPA Phase 2 for ^{14}C are therefore expected to over-estimate collective dose, since the concentrations of gaseous ^{14}C from the area source would be more diffused, and therefore smaller, than those from a point source.

7.9 CONCLUSIONS AND POSSIBLE CONSIDERATIONS FOR FUTURE DOSE ASSESSMENTS

7.9.1 Conclusions

Although dose-related parameters were not sampled in this total-system performance assessment, the uncertainty inherent in the dose assessment calculation can be significant, and adds to the uncertainty being propagated in the release model. Much of the uncertainty in dose is associated with inherent uncertainties in the parameters used for the human physiology and environmental pathway models in the *DITTY* computer code. The *DCF* may not always reflect the individual differences (e.g., age, metabolism, sex, etc.) in human response to ionizing radiation. The parameters used in this study for the environmental pathway analyses are not always site-specific, and furthermore, are considered to be invariant in space and time. Nevertheless, the results of the dose assessment provide valuable insights regarding the performance of the geologic repository, and are summarized below:

- A gaseous release of ^{14}C makes a significant contribution to the EPA sum, but its corresponding impact on the cumulative population dose is insignificant.

- The radionuclides that made the largest contributions to the population doses (accumulated over 10,000 years) were: ^{94}Nb, ^{210}Pb, ^{243}Am, and ^{237}Np. (Refer to Section 8.3.2. for additional discussion.)

- The scenario classes most likely to impact dose were those composed of some combination of the following independent events: drilling into a waste package canister, plus a change in climate, plus a seismic event. (Refer to Figure 9-7b in Section 9.3 and the discussion of climate in Section 9.2.3 for additional discussion.)

- The average annual inhalation dose to an individual in the Yucca Mountain region was negligible compared to the average annual dose caused by the ingestion of contaminated drinking water, and locally-grown contaminated food (both averaged over a 10,000-year period as discussed in Section 9.6).

- Further data development and site characterization are desirable, if not necessary, to help reduce the uncertainty in many important parameters in the biosphere model (such as the leaching rates in soil).

7.9.2 Considerations for Future Dose Assessments

The following recommendations should be considered for adoption in future dose assessments that might be conducted by the staff as part of its IPA work.

Recommendation 1. Improve the DITTY Dose-Assessment Model

- Display the results of dose assessments with multi-dimensional plots (cumulative and organ doses should be functions of both the type of radionuclide and the exposure pathway).

- Re-calculate the *DCFs* used in IPA Phase 2, to obtain a more accurate estimate of population doses for long-lived radionuclides (as discussed in Section 7.6).

- Verify that the model parameters currently used in *DITTY* are applicable to the Yucca Mountain site; identify the ranges of these parameters.

Recommendation 2. Evaluate Other Dose Assessment Computer Codes

- Evaluate other computer codes that could be used to estimate long-term individual and collective exposures and should be explored if dose becomes a performance requirement. One code that has these capabilities to be explored is *GENII-S* (see Leigh *et al.*, 1993). Many of the databases in this code are common to the *DITTY* code used in this study.

- Evaluate atmospheric dispersion models that can calculate atmospheric concentrations caused by releases of radionuclides from area sources. These models could be used to obtain better dose estimates for releases of gaseous ^{14}C.

- Evaluate atmospheric dispersion models that consider aerosols of a variety of particle sizes, shapes, and densities.

- Evaluate demographic models that can project the growth of a population. This feature would be useful for calculation of collective dose.

- Evaluate methods employed by international organizations for calculation of dose into the far future (e.g., BIOMOVS and NEA).

- Incorporate the "1990 Recommendations of the International Commission on Radiological Protection" (ICRP, 1990), into the codes used for dose calculations, when adopted by the Agency.

Recommendation 3. Conduct Sensitivity/Uncertainty Analyses

- Apply the statistical sensitivity and uncertainty methodology developed in IPA Phase 2 for the geosphere models to the dose-assessment models.

8. SENSITIVITY AND UNCERTAINTY ANALYSIS[1]

V.A. Colten-Bradley/NMSS, R.B. Codell/NMSS, and M.R. Byrne/NMSS

8.1 INTRODUCTION

The purpose of sensitivity and uncertainty analyses is to gain an understanding of the relationships between the repository performance measures and the input parameters used to formulate the models. The overall performance measures for the geologic repository used in the Iterative Performance Assessment (IPA) Phase 2 analysis are cumulative total releases of radionuclides at the accessible environment (*Normalized Release*) and doses to the exposed population (*Effective Dose Equivalent (EDE)*). Because of the complexity of the systems comprising a geologic repository, it is not usually possible to develop exact analytical expressions for the functional relationship between repository performance and the input parameters used to formulate the models. Empirical relationships may be inferred by inspecting the model performance measures and input parameters in a variety of ways. This section will illustrate a number of techniques used for determining the relationships among parameters and their importance to the model performance.

Performance assessments for the geologic repository are based on conceptual models, embodied as computer programs, and measured field and laboratory data. Because of the inherent variabilities and sparsity of the measured data and the underlying uncertainty concerning the processes included in the models, the results of any performance assessment have significant uncertainty. An important aspect of conducting a performance assessment for a geologic repository is quantifying the sensitivity of the results to, and the uncertainty associated with, the values of the input parameters. An analysis of model sensitivity will provide information concerning which input parameters are most important to the results. A better understanding of those parameters that have the most influence on the results can hopefully lead to improvement in the models. Likewise, from a review standpoint, identification of the most sensitive parameters provides a means of comparing and evaluating different performance assessment models and indicates where reviews of data should be concentrated. This section discusses how variation in model output reflects variation in the input parameters.

8.2 OVERVIEW OF TECHNIQUES AND METHODS

8.2.1 Background

A variety of techniques have been used to quantify the uncertainty and sensitivity in complex models for assessing radiological impact on man and the environment. These include: the Monte Carlo method (Helton 1961); fractional factorial design (Cochran, 1963); differential analysis (Baybutt *et al.*, 1981); response surface methodology; Fourier amplitude sensitivity (Helton *et al.*, 1991); and the limit-state approach (Wu *et al.*, 1992). No one technique is definitive and several can be used together to evaluate total-system performance assessments. Because comparisons of the methods employed in each approach may be found in several works (Zimmerman *et al.*, 1991; Helton *et al.*, 1991; Wu *et al.*, 1992), only a limited evaluation is provided here. The Monte Carlo approach was used in the present performance assessment. Regression analysis and differential analysis as means of

[1] The figures shown in this chapter present the results from a demonstration of staff capability to review a performance assessment. These figures, like the demonstration, are limited by the use of many simplifying assumptions and sparse data.

determining sensitivity to individual parameters are compared in Section 8.4.4.

8.2.2 IPA Phase 1 Sensitivity and Uncertainty Analysis

IPA Phase 1 examined sensitivity and uncertainty for radionuclide releases at the accessible environment for a geologic repository in unsaturated tuff (see Section 9.5, "Sensitivities and Uncertainties for Liquid-Pathway Analysis," in Codell *et al.*, 1992). The consequence models were significantly simpler than those in the present study, and there was a narrower range of scenarios considered.

8.2.2.1 Sensitivity Analyses

Four sensitivity analyses were performed for IPA Phase 1: (a) sensitivity analyses demonstrating the effect of individual parameters on the resultant Complementary Cumulative Distribution Function (CCDF) for cumulative release to the accessible environment (10 CFR 60.112); (b) regression analyses using stepwise linear regression to estimate the sensitivity to key parameters in the consequence models; (c) determination of relative importance of radionuclides in the waste; and (d) sensitivity of CCDFs to performance of the natural and engineered barriers. The sensitivity analyses considered only liquid releases, not those from drilling. Gas release was not part of the IPA Phase 1 total-system performance assessment results, but was included as an auxiliary analysis (see Appendix D, "Gaseous Release of C14," in Codell *et al.*, 1992).

8.2.2.2 Uncertainty Analyses

The Phase 1 IPA included only two events and processes different from the base-case conditions: pluvial conditions and drilling. These were combined into four scenarios (i.e., base case, base case plus drilling, pluvial conditions without drilling, and pluvial conditions with drilling). Uncertainty analyses were restricted to presentation of CCDF plots of cumulative release at the accessible environment (*Normalized Release*) for each of the scenarios, separately, and a combined CCDF for all scenarios factored by the scenario probability. The CCDFs were the result of the uncertainty in the sampled parameters propagated through the analysis. *EDE* was not calculated as a performance measure for the IPA Phase 1 study. Construction of CCDFs is described in Section 9.2 of this report.

8.2.3 Techniques

The techniques used in the evaluation of the performance assessment model include studying the distributions of the input and output variables, evaluating correlations between individual input parameters and the performance measures, and overall model sensitivity to independent variables. The techniques used in this analysis have been described by a number of authors (Draper and Smith, 1966; Mendenhall and Schaeffer, 1973; Bowen and Bennett, 1988; Sen and Srivastava, 1990) and several have been applied previously to total-system performance assessments (Iman and Conover, 1979; Helton *et al.*, 1991; McKay, 1992).

The use of regression analysis in this work was an extension of the regression analyses done in IPA Phase 1. Previously, the regression analysis was used to determine the most important variables and estimate sensitivities of the total-system performance assessment model output to individual independent variables. In IPA Phase 2, the following techniques for development of a regression equation to emulate the total-system performance assessment model were investigated: transformation of data (Iman and Conover, 1979; Seitz *et al.*, 1991); test for heteroscedasticity (residual variation;

Draper and Smith, 1966; Bowen and Bennett, 1988; Sen and Srivastava, 1990); and Mallows' C_p statistic (Sen and Srivastava, 1990). In addition to several techniques used in previous performance assessment work (e.g., the stepwise linear regression), the following techniques were evaluated for determining parameter importance and sensitivity (Kolmogorov-Smirnov and Sign tests (Bowen and Bennett, 1988)); and differential analysis (Helton *et al.*, 1991).

The sensitivity and uncertainty analyses were done with the commercially-available statistical package, *S-plus* (Version 3.1) (Statistical Sciences, Inc., 1992). Programs written in *S-plus* were used in this work to do the compartmental-component analysis, stepwise linear regression analysis, multilinear regression analysis, and statistical tests such as the Kolmogorov-Smirnov test and Mallows' C_p statistic.

8.3 SELECTION OF MOST INFLUENTIAL INDEPENDENT VARIABLES

8.3.1 Subset Selection by Stepwise Regression Analysis

Stepwise regression analysis has been used in previous total-system performance assessment work (Codell *et al.*, 1992; Helton *et al.*, 1991) to determine the independent variables that have the most influence on the model output. Stepwise regression analysis (Draper and Smith, 1966) selects variables to be in a linear equation based on the correlation coefficient between a single independent variable and the dependent variable (Iman *et al.*, 1980).

Selection of variables for the linear model by stepwise regression analysis may be based on a variety of criteria, such as the *F*-statistic, the Mean Square Error, the correlation coefficient, or the C_p statistic. As variables are added to the regression equation, the coefficient of determination, R^2, is calculated (Seitz *et al.*, 1991). The coefficient of determination is the square of the multiple correlation coefficient (Walpole and Myers, 1978) and is proportional to the total variance of the dependent variable that is explained by the regression model; it increases as more variables are added to the model (Intriligator, 1978). In this analysis, the *F*-statistic was used for variable selection; the subset giving the largest R^2 was chosen.

In stepwise regression, variables are ranked in order of importance to the total-system performance assessment model by their effect on the coefficient of determination, R^2 (Seitz *et al.*, 1991). The variable associated with the largest change in R^2 is ranked as the most important.

Subset selection by the stepwise regression technique may be performed at varying levels of significance, α. The level of significance α is the probability that a variable will be rejected from the regression equation when it should be included. Helton *et al.* (1991) performed stepwise regression analyses at the 0.01 level of significance. In this analysis, the stepwise regression analyses were done for 0.01 and 0.05 level of significance. For the base case (*oooo*) scenario, fifteen variables were selected by the stepwise regression from a suite of 195 variables at the 0.01 level of significance, whereas 24 variables were selected at the 0.05 level of significance. Six variables were selected at the 0.01 level of significance, from a suite of 29 independent variables by Helton *et al.*, for the Waste Isolation Pilot Project performance assessment. Helton *et al.* noted that as the number of independent variables increases, there is more chance for selection of a spurious variable. An analysis of the relationship between the number of independent variables used as input to the total-system

performance assessment model, the level of significance, and the number of the stepwise-selected variables was not done in IPA Phase 2. However, such an analysis is needed in order to establish the most appropriate number of variables for the selected subset. A discussion of Mallow's C_p statistic for determining the number of variables for the "best" fit of a model by a regression equation is given in Section 8.6.2.2.

A small set of variables that were important in all IPA Phase 2 scenarios were the corrosion potential parameters, *ecorr6, ecorr7,* and *ecorr8* that were used in the *SOTEC* module (see Chapter 5 and Appendix A). Infiltration was the most important parameter for the scenarios (see Table 8-1) in which climatic (pluvial) consequences were not considered (*oooo, oodo, osoo, ooov*). The gas retardation coefficient (*betaf*) and fracture permeability (*permf*) for the Topapah Springs member (*C14* gas module) were also included in the list of the most important variables. The UO_2 alteration rate for sub-area 2 of the repository, *forwar2 (SOTEC),* was among the important parameters for the scenarios with climatic consequences, *cooo* and *csdv*. Tables 8-2 to 8-5 list the variables selected by stepwise regression for the base case (*oooo*) and fully disturbed case (*csdv*) for the 0.01 level of significance.

Table 8-1
Scenario Classes Modeled in the IPA Phase 2 Analysis

Scenario Class	*Scenario Class Identifier*
Base Case	oooo
Climate Change Only (Pluvial)	cooo
Seismicity Only	osoo
Drilling Only	oodo
Magmatic Activity Only	ooov
Drilling + Seismicity	osdo
Drilling + Seismicity + Magmatic Activity	osdv
Drilling + Seismicity + Climate Change	csdo
Drilling + Seismicity + Magmatic Activity + Climate Change *	csdv

* Fully disturbed

It should be noted that the same subsets were selected for all scenarios without climatic disturbances, *oooo, oodo, osoo, ooov.* Similarly, the scenarios with climatic effects, *cooo* and *csdv*, had the same subsets of important variables.

A means of confirming the selection of the most important variables for the model is through the use of scatter plots (Helton *et al.*, 1991). By plotting the performance measure (*Normalized Release* or *EDE*) against the input variable (e.g., undisturbed infiltration) linear or discontinuous relationships

among the variables may be seen. However, because the performance measures are a function of many independent parameters, distinct relationships may be difficult to detect from scatter plots alone.

Table 8-2
Results of Stepwise and Multilinear Regression: Normalized Release for Base Case (*oooo*) Scenario [a]

Variable Name	*Regression Coefficient*	*Confidence Interval*	*Standardized Regression Coefficient*	*Rank Regression Coefficient*	*Partial Correlation Coefficient*
INFIL(UN)	4.86E+02	±1.12E+02	0.400	0.417	0.390
ECORR6	-3.35E-03	±1.06E-06	-0.312	-0.348	-0.269
ECORR7	-2.68E-03	±1.06E-03	-0.248	-0.282	-0.219
RETARD3	-1.44E-03	5.57E-03	-0.242	-0.216	-0.510
ECORR8	1.28E+03	±5.72E+02	0.205	0.243	0.178
AKR3	9.34E+14	±4.03E+04	0.213	0.274	0.256
Kd39Th	-7.18E-01	±4.78E-01	-0.148	-0.092	-0.119
ECORR5	-2.79E+01	±2.25E+01	-0.114	-0.082	-0.219
RETARD1	-6.20E-03	±5.56E-03	-0.104	-0.110	-0.219
KdCm1	1.43E-01	±1.27E-01	0.104	0.066	0.089
AKR2	9.79E+13	±8.24E+13	0.110	0.106	0.132
AKR4	1.60E+14	±1.34E+14	0.120	0.126	0.131
Kd26Am	4.12E-02	±4.21E-02	0.090	0.074	0.078
SOL4Am	2.03E+03	±2.00E+03	0.094	--[b]	0.059
FORWAR2	5.69E+02	±5.71E+02	0.092	--[b]	0.068

[a] See Appendix A for a description of the variable names. Coefficients are described in Section 8.4.

[b] Variable not selected.

Table 8-3
Results of Stepwise and Multilinear Regression: EDE for Base Case (*oooo*) Scenario[a]

Variable Name	*Regression Coefficient*	*Confidence Interval*	*Standardized Regression Coefficient*	*Rank Regression Coefficient*	*Elasticity Coefficient*	*Uncertainty Coefficient*
INFIL(UN)	2.91E+07	±4.20E+06	0.657	0.870	1.03	0.432
FUNNEL2	8.27E+04	±4.63E+04	0.169	0.091	0.469	0.0286
ECORR6	-6.45E+01	±3.708E+01	-0.165	-0.138	-2.29	0.0272
FORWAR2	3.57E+07	±2.15E+07	0.158	0.101	0.217	0.0249
SOL4AM	1.04E+08	±7.46E+07	0.132	0.042	0.154	0.0175
RDIFF13	4.38E+07	±3.77E+07	0.110	0.072	0.151	0.0121
KD39Th	-1.87E+04	±1.78E+04	-0.099	-0.038	-0.136	0.0098
ECORR5	-8.18E+05	±8.43E+05	-0.092	-0.053	-0.278	0.0085
RPOR21	1.51E+05	±1.54E+05	0.093	0.043	0.061	0.0087
ECORR7	-3.62E+01	±3.71E+01	-0.093	-0.140	-1.28	0.0086

[a] See Appendix A for a definition of the variable names. Coefficients are described in Section 8.4.

Table 8-4
Results of Stepwise and Multilinear Regression: Normalized Release for Fully Disturbed (*csdv*) Scenario[a]

Variable Name	*Regression Coefficient*	*Confidence Interval*	*Standardized Regression Coefficient*	*Rank Regression Coefficient*	*Elasticity Coefficient*	*Uncertainty Coefficient*
ECORR6	-6.71E-03	±1.4E-03	-0.36	-0.385	-2.22	0.133
ECORR7	-4.55E-03	±1.4E-03	-0.25	-0.333	-1.50	0.061
FORWAR2	2.09E+03	±8.4E+02	0.20	0.158	0.12	0.038
ECORR8	1.93E+03	±8.4E+02	0.18	0.179	0.11	0.033
FORWAR3	1.46E+03	±8.4E+02	0.137	0.121	0.083	0.019
KD39TH	-1.25E+00	±7.0E-01	-0.141	-0.124	-0.085	0.020
RETARD3	-1.33E-02	±8.0E-03	-0.131	-0.148	-0.194	0.017
FUNNEL2	2.87E+00	±1.82E+00	0.125	0.120	0.152	0.016
VOLMAX2	-8.64E+01	±6.1E-01	0.113	0.032	0.137	0.013
HIT19	1.017E+00	±7.3E-01	0.111	0.118	0.134	0.012

[a] See Appendix A for a definition of the variable names. Coefficients are described in Section 8.4.

Table 8-5
Results of Stepwise and Multilinear Regression: EDE for Fully Disturbed (*csdv*) Scenario[a]

Variable Name	*Regression Coefficient*	*Confidence Interval*	*Standardized Regression Coefficient*	*Rank Regression Coefficient*	*Elasticity Coefficient*	*Uncertainty Coefficient*
FORWAR2	2.13E+08	±8.5E+07	0.219	0.378	0.407	0.048
FORWAR3	1.63E+08	±8.5E=08	0.167	0.126	0.310	0.028
ECORR6	-2.60E+02	±1.5E+02	-0.154	0.346	-2.88	0.024
ECORR8	1.39E+08	±8.5E+07	0.143	0.087	0.215	0.020
Kd114Se	3.75E+06	±2.8E+06	0.115	–[b]	0.215	0.013
DRILL21	9.85E+00	±7.5E+00	0.114	0.099	0.437	0.013
VOLMAX4	-8.07E+04	±6.1E+04	-0.115	-0.046	-0.430	0.013
Kd104Ni	1.14E+06	±8.5E+05	0.116	–[b]	0.217	0.014
ZONE7	-8.65E+04	±7.4E+04	-0.102	–[b]	-0.383	0.010
Kd44Ra	6.65E+03	±5.7E+04	0.102	–[b]	0.191	0.010
WAREA4	8.97E+04	±7.4E+04	0.106	–[b]	0.398	0.011
FUNNEL2	2.13E+05	±1.9E+05	0.101	0.237	0.380	0.010
PERMF1	1.82E+21	±1.7E+21	0.096	0.119	2.34	0.009
HIT19	8.37E+04	±7.4E+04	0.099	0.086	0.037	0.010
Kd50Pb	1.36E+04	±1.3E+04	0.095	–[b]	0.177	0.009
BETAF3	-3.94E+04	±3.5E+04	-0.098	–[b]	-1.49	0.010
PORM1	5.08E+05	7.3E+05	0.060	–[b]	0.050	0.004
BETAM	3.5E+04	±3.5E+04	-0.088	-0.058	-0.709	0.008
VOLMAX6	-6.0E+04	±6.1E+04	-0.086	–[b]	-0.321	0.007

[a] See Appendix A for a definition of the variable names. Coefficients are described in Section 8.4.

[b] Variable not selected.

8.3.2 Compartmental Component Analysis

Compartmental component analysis was used to illustrate the relative importance of individual radionuclides or release pathways to the *Normalized Release* or *EDE*. The compartmental component analysis was done primarily with the use of boxplots. The boxplot (Tukey, 1977; Helton *et al.*, 1991) is a means of assessing the effect of the full range and distribution of a given component (radionuclide or geosphere pathway) on the output. The boxplot (Figure 8-1) consists of a "box," the ends of which represent the lower and upper quartiles of the distribution (25th percentile ($x_{.25}$) and 75th percentile ($x_{.75}$), respectively). The "]" symbol (whisker) represents the values in the distribution that are $x_{.25} - 1.5(x_{.75} - x_{.25})$ and $x_{.75} + 1.5(x_{.75} - x_{.25})$; Helton *et al.*, 1991). Values outside the whiskers ("outliers") are represented with lines.

8.3.2.1 Contribution of Individual Nuclides to the *Normalized Release* and *EDE*

The contribution of individual nuclides to the *Normalized Release* was evaluated in terms of the absolute contribution, the fraction of the total contribution, and the contribution of different transport pathways to the collective release to the accessible environment. The contributions by seven representative radionuclides to the *Normalized Release* and to the *EDE* for the base case (*oooo*) are shown in Figures 8-2 and 8-3, respectively. Corresponding results for the fully disturbed case (*csdv*) are illustrated in Figures 8-4 and 8-5.

The dominant radionuclide contributor to the *Normalized Release* is ^{14}C, primarily in the gaseous pathway (Figures 8-2 and 8-4). Fifty percent of the vectors in the base case (*oooo*) have ^{14}C releases greater than 0.8 × (EPA limit). Although gaseous ^{14}C is important to the *Normalized Release*, it is a very small contributor to the *EDE* (Figures 8-3 and 8-5). ^{243}Am is an important contributor to the *Normalized Release* and *EDE*, whereas ^{240}Pu and ^{99}Tc are important contributors to the fully disturbed scenario (*csdv*) *Normalized Release*. In some cases, these nuclides exhibit releases greater than the EPA limit.

Federal Regulation 40 CFR Part 191 provides that 10 percent of the total releases to the accessible environment may have a *Normalized Release* between 1 and 10. In the IPA Phase 2 total-system performance assessment, more than fifty percent of the vectors gave a *Normalized Release* greater than 1, in large part because of the gaseous ^{14}C release. More than 25 percent of the liquid pathway releases have *Normalized Releases* greater than 1.

The nuclides making the largest contribution to the *EDE* are ^{94}Nb, ^{210}Pb, ^{237}Np, and ^{243}Am. ^{94}Nb, ^{237}Np, and ^{243}Am are important because of their long half-lives, whereas ^{210}Pb continues to build up over time with decay of nuclides in the ^{238}U series, particularly ^{234}U.

8.3.2.2 Releases by Pathway

The relative release by pathway differs between the base (*oooo*) and the fully disturbed (*csdv*) cases. In the base case (*oooo*) scenario, the contribution to the *Normalized Release* is roughly divided between the liquid and the gaseous pathways. The mean contribution to the *Normalized Release* is higher in the liquid pathway for *Normalized Releases* less than 1, whereas the mean contribution to the total release is higher in the gaseous pathways for *Normalized Release* between 1 and 10. This is anticipated because much of the exceedence of the EPA limit of 1 is because of gaseous ^{14}C release. The releases for the fully disturbed scenario (*csdv*) are divided much differently among liquid,

Figure 8-1. Example Boxplot Showing Interquartile Region, the Whiskers at 1.5 X (interquartile) and Outliers in the Distribution

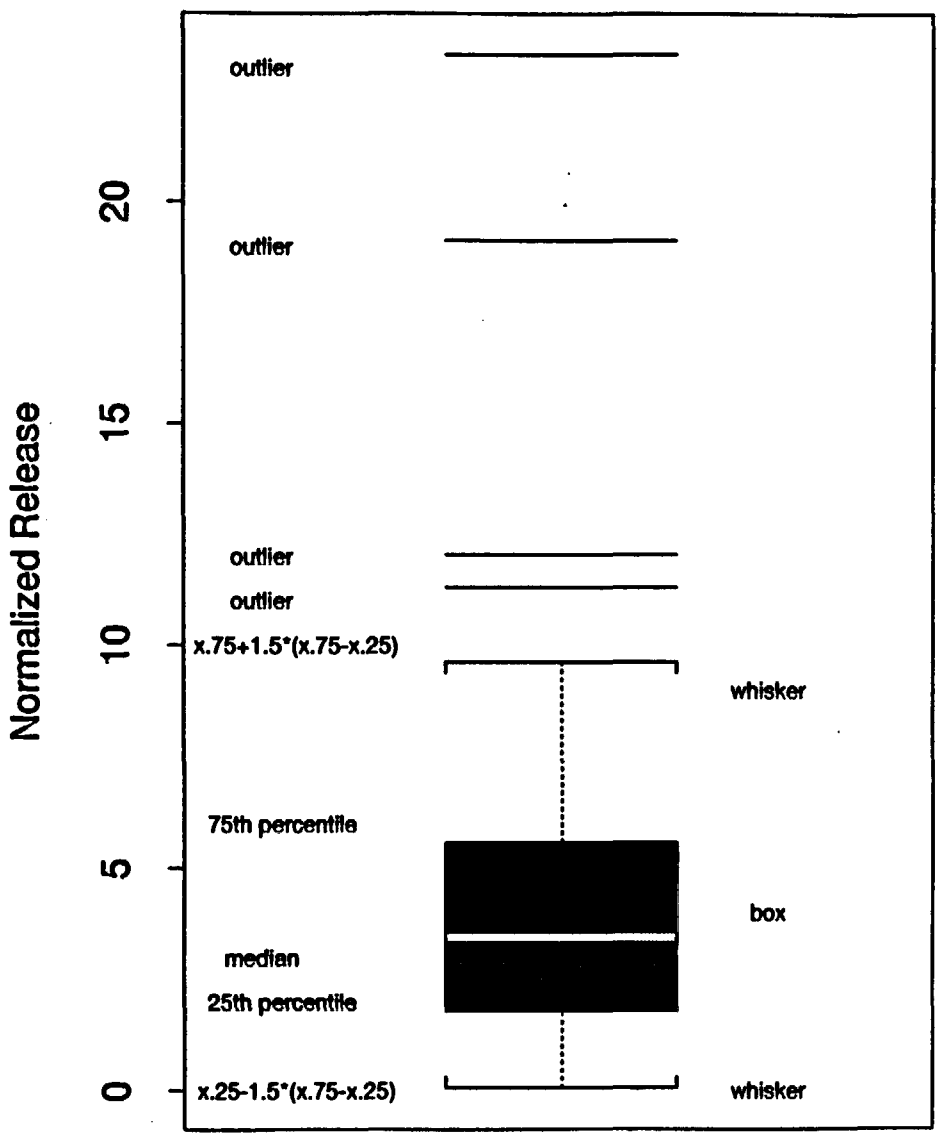
Normalized Release
0
5
10
15
20
outlier
outlier
outlier
outlier
x.75+1.5*(x.75-x.25)
whisker
75th percentile
box
median
25th percentile
x.25-1.5*(x.75-x.25)
whisker

FIG 9-1

Figure 8-2. Absolute contributions to Normalized Releases by Selected Radionuclides, Base Case (oooo) Scenario.

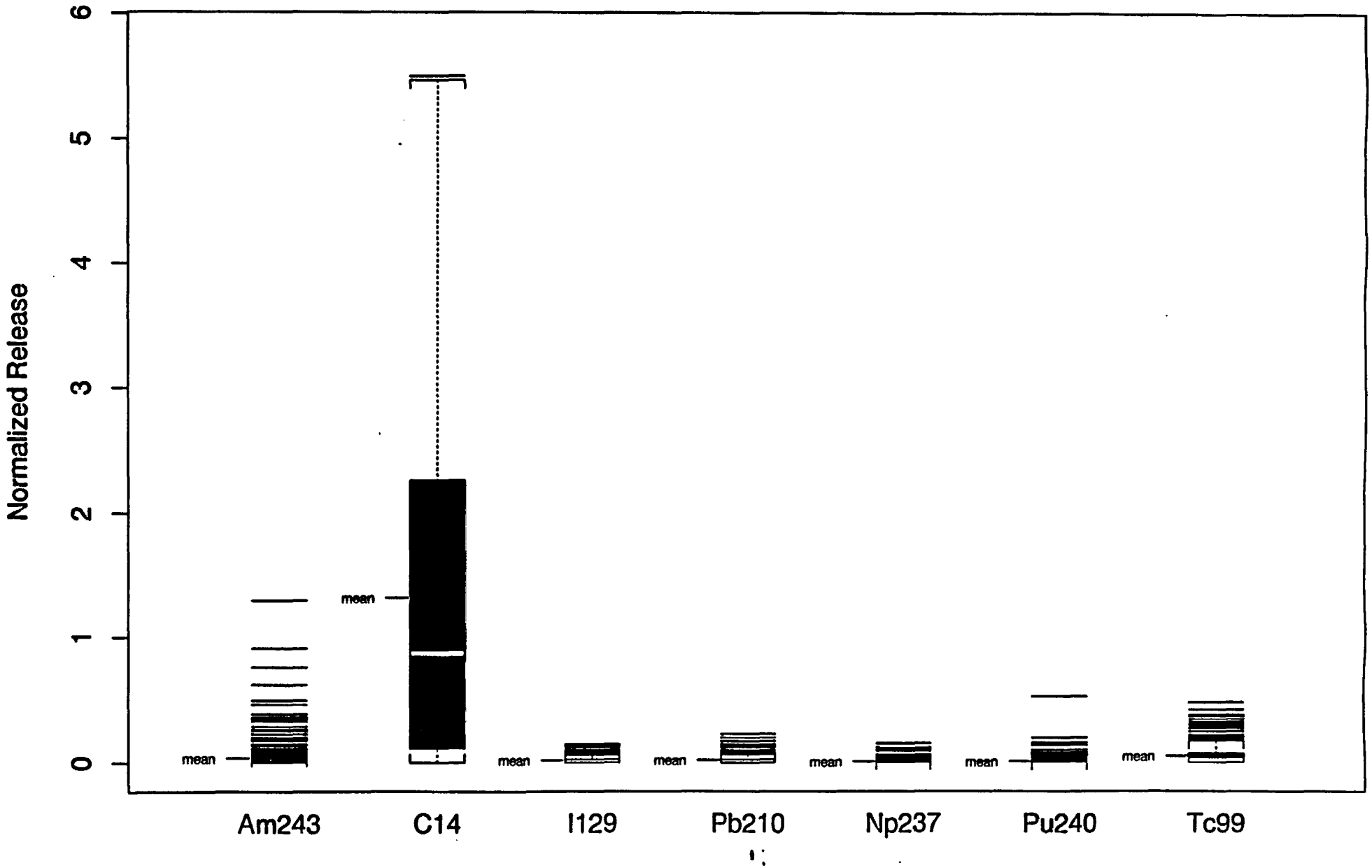
Normalized Release
0
1
2
3
4
5
6
mean
mean
mean
mean
mean
mean
mean
Am243
C14
I129
Pb210
Np237
Pu240
Tc99

FIG. 5-2

Figure 8-3. Absolute Contribution to Effective Dose Equivalent by Selected Radionuclides.

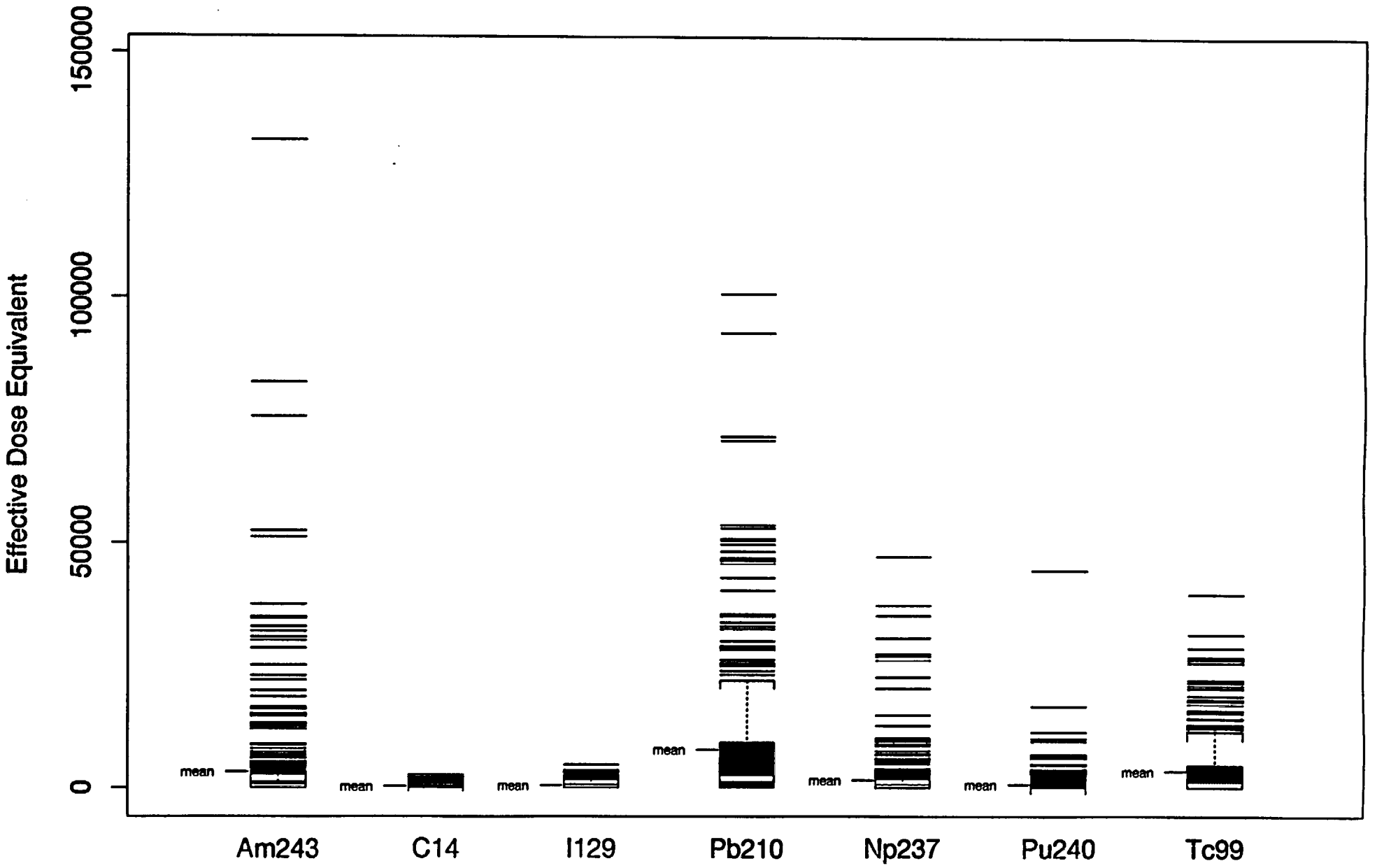
Effective Dose Equivalent
150000
100000
50000
0
mean
mean
mean
mean
mean
mean
mean
Am243
C14
I129
Pb210
Np237
Pu240
Tc99

Fig 8-3

Figure 8-4. Absolute Contributions to Normalized Releases by Selected Radionuclides - Fully Disturbed (csdv) Scenario.

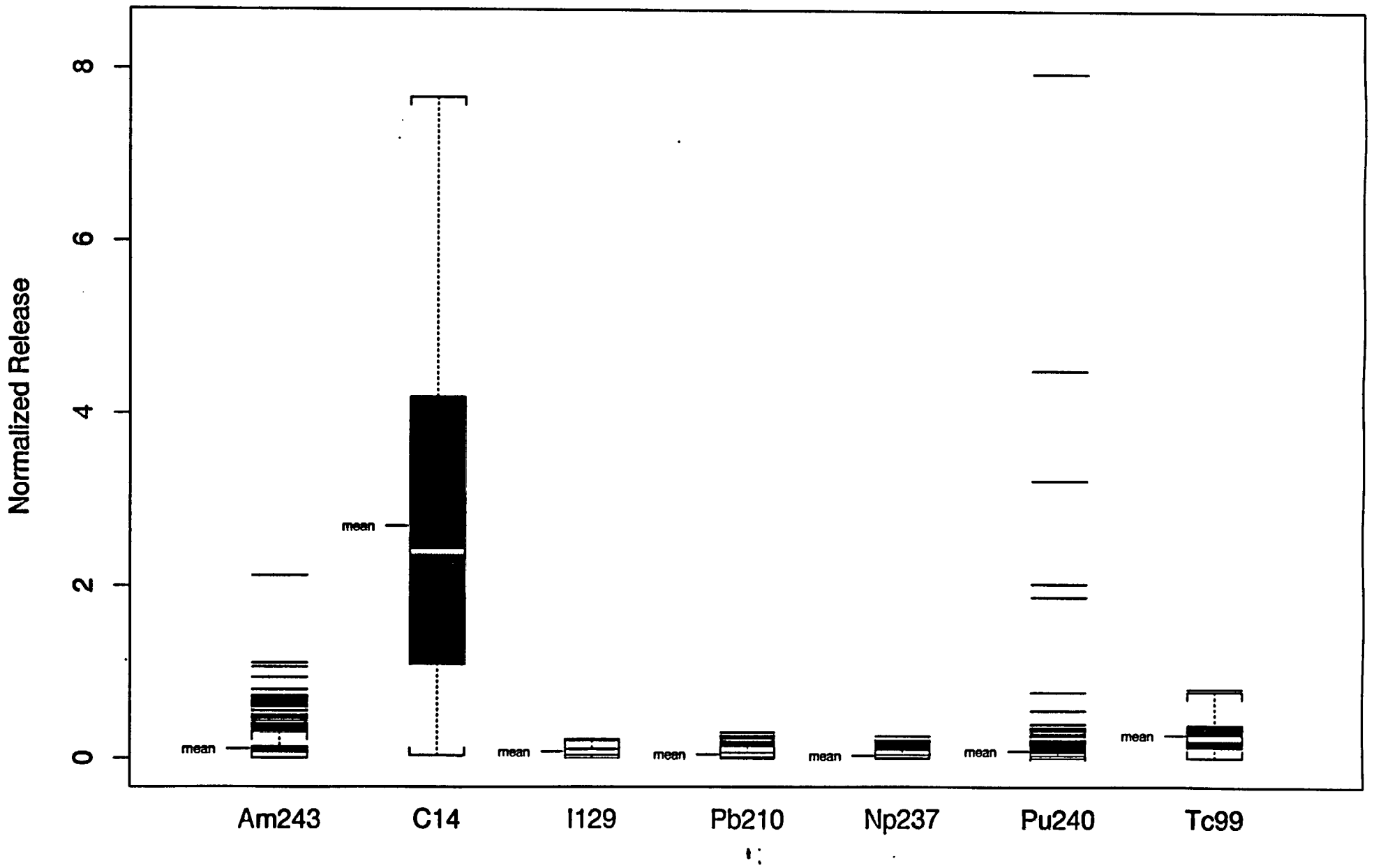
Normalized Release
0
2
4
6
8
mean
mean
mean
mean
mean
mean
mean
Am243
C14
I129
Pb210
Np237
Pu240
Tc99

FIG 8-4

Figure 8-5. Absolute Contribution to Effective Dose Equivalent by Selected Radionuclides, Fully Disturbed (csdv) Scenario.

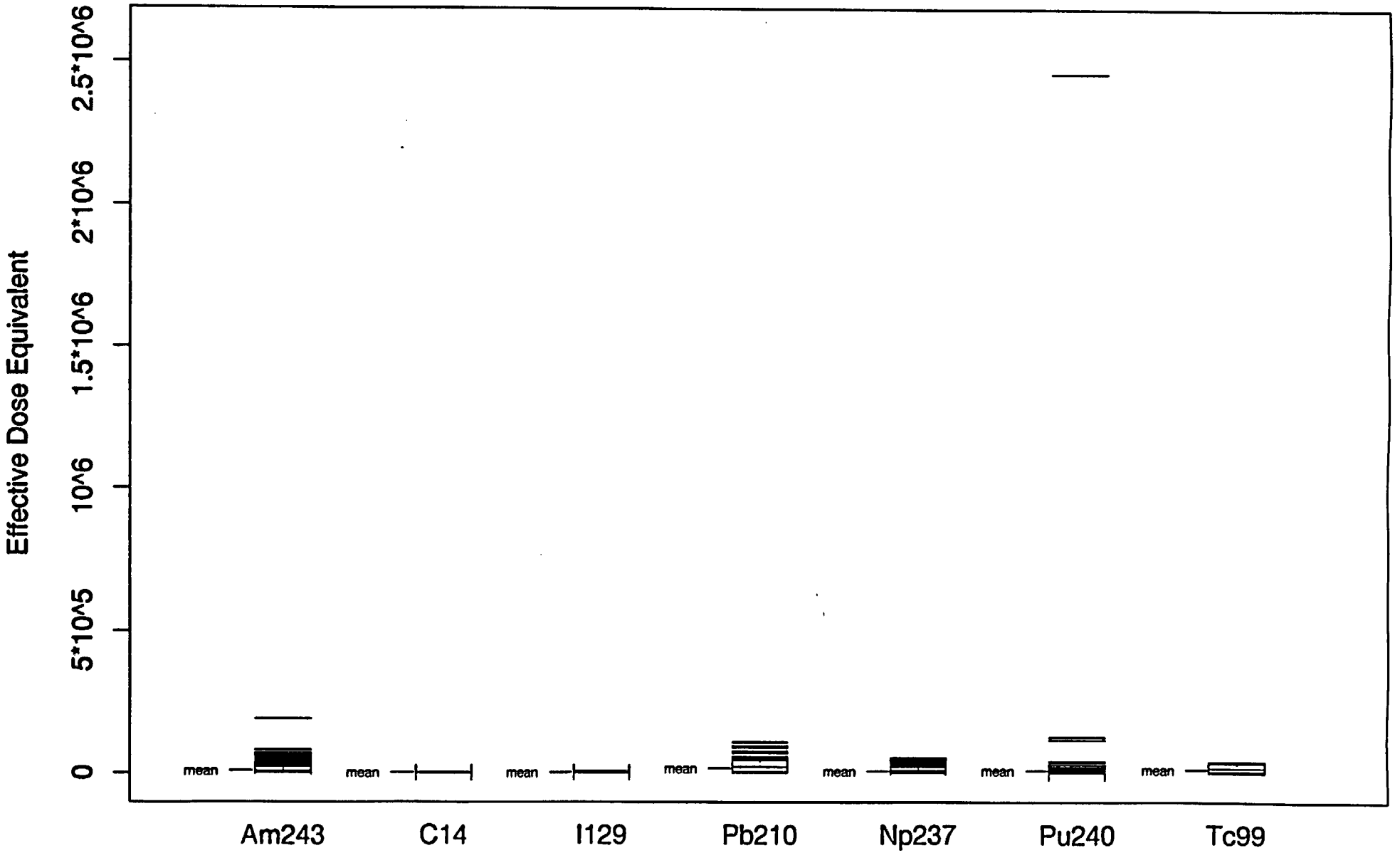
Effective Dose Equivalent
0
5*10^5
10^6
1.5*10^6
2*10^6
2.5*10^6
mean
mean
mean
mean
mean
mean
mean
Am243
C14
I129
Pb210
Np237
Pu240
Tc99

FIG 9-5

gaseous, and direct pathways (Figure 8-6). The mean fractional contribution to the *Normalized Release* for the liquid pathway is 0.8, whereas the mean fractional contribution to the *Normalized Release* is 0.2 for the gaseous pathway. The direct pathway (via drilling or volcanism), while a much smaller contributor to the total release, exhibits *Normalized Releases* as high as 15.

8.3.3 Significance of Independent Variables – Kolmogorov-Smirnov Test and Sign Test

The stepwise regression analysis used the change in the coefficient of determination, R^2, to determine which variables were the most important in the total-system performance assessment model. The Kolmogorov-Smirnov (*K-S*) test and the Sign test were also used to determine the importance of the input parameters (Bowen and Bennett, 1988). These tests, unlike stepwise regression analysis, test the relationship between the parameters and results, without assuming a specific functional form.

8.3.3.1 The Kolmogorov-Smirnov Test

The *K-S* test (Bowen and Bennett, 1988) is generally used to test whether two distributions are the same. It was used in the present context as a test of whether a subset of the LHS-determined values for a given input variable conforms to the distribution defined for the variable. The subsets of input values used in the *K-S* analysis correspond to the vectors in which the 40 largest values for *Normalized Release* or *EDE* were generated in a given scenario. For each input variable, the defined or theoretical distribution was compared to the distribution of the values in the subsets (Figure 8-7). If the theoretical and subset distributions are similar, the interpretation is that the input variable will have little or no effect on the results. Conversely, a significant difference between the theoretical distribution and subset distribution would indicate that the parameter is important to the performance measure. Figure 8-7a is a plot of the theoretical distribution (solid line) and the distribution of the sampled values (dots) for the fracture beta parameter. The two distributions are very similar, whereas the distributions for undisturbed infiltration (Figure 8-7b) are very different. Fifty percent of the values (cumulative density = 0.5 to 1.0) from the theoretical distribution (solid line) for infiltration rate are greater than 0.00075, whereas 80 percent (cumulative density = 0.2 to 1) of the sampled values (dots) are greater than 0.00075. These large values for the *infiltration rate* are thus significant in affecting the total-system performance assessment (TPA) computer model output as *Normalized Release*.

8.3.3.2 The Sign Test

The Sign test (Bowen and Bennett, 1988) is another test for comparing whether two distributions are the same. Each observation in the subset sample is represented by a plus (+) sign or a minus (-) sign, depending whether it is smaller or larger than the median of the known distribution. The test statistic is the total number of plus (+) signs, and is compared to the number of plus signs expected for a given theoretical distribution and number of samples. If the distributions are significantly different, the independent variable is considered to have an important effect on the total-system performance assessment model output.

Table 8-6 presents the results of applying the *K-S* and Sign tests to the base case (*oooo*) scenario results for the 0.05 level of significance. The variables are listed in order of their values for the *K-S* test. In general, when the *K-S* test and Sign test were performed on a set of independent variables one-at-a-time, the resulting subset of important independent variables agreed with the set of independent variables selected by the stepwise regression. However, this agreement is conditional on

Figure 8-6. Fractional Contributions to Normalized Releases by Geosphere Path.

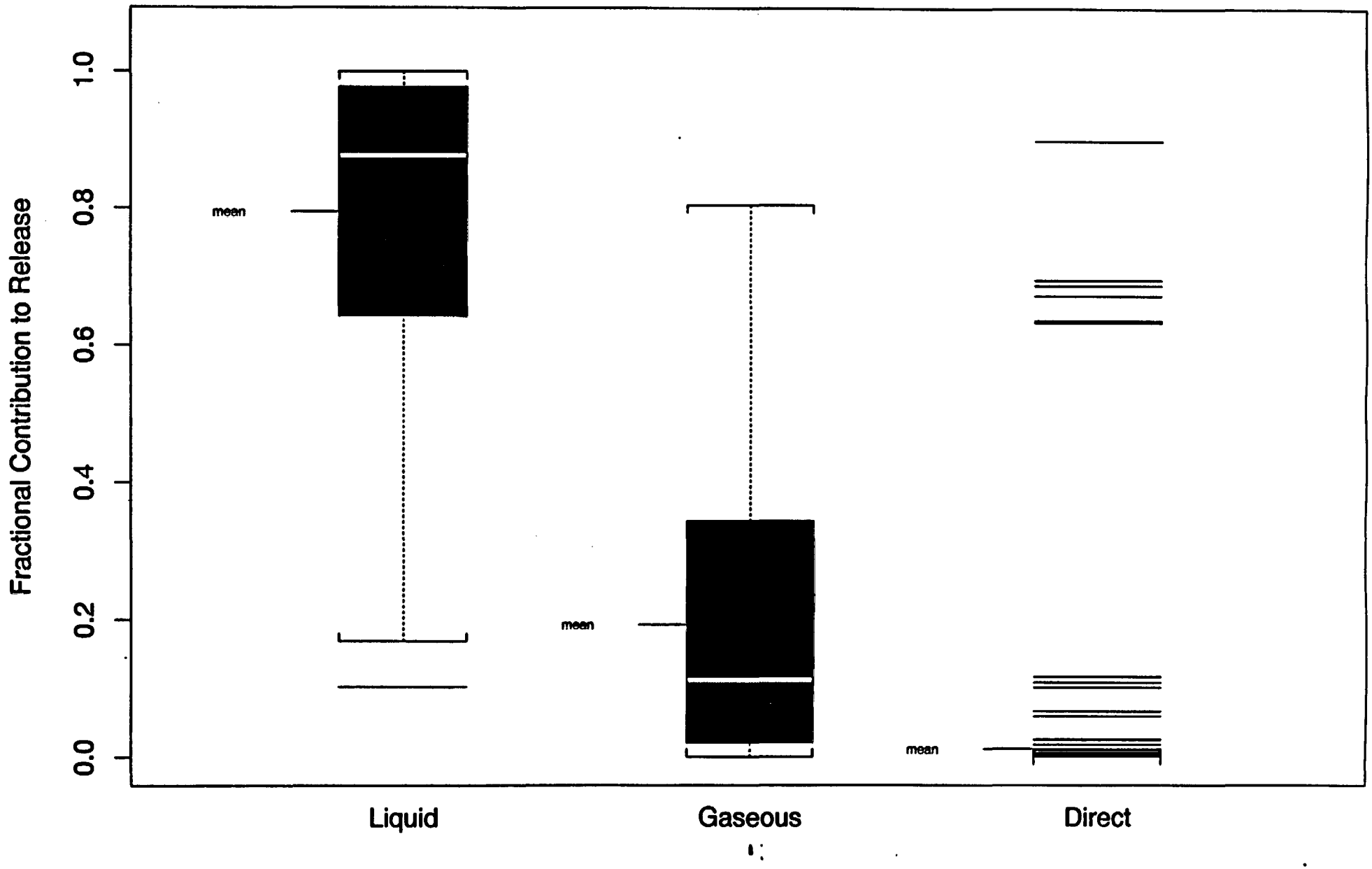
Fractional Contribution to Release
0.0
0.2
0.4
0.6
0.8
1.0
mean
mean
mean
Liquid
Gaseous
Direct

FIG 3-6

Figure 8-7. Distributions Used in the Kolmogorov-Smirnov Test; a)Beta coefficient for Fractures; b)Undisturbed Infiltration Rate.

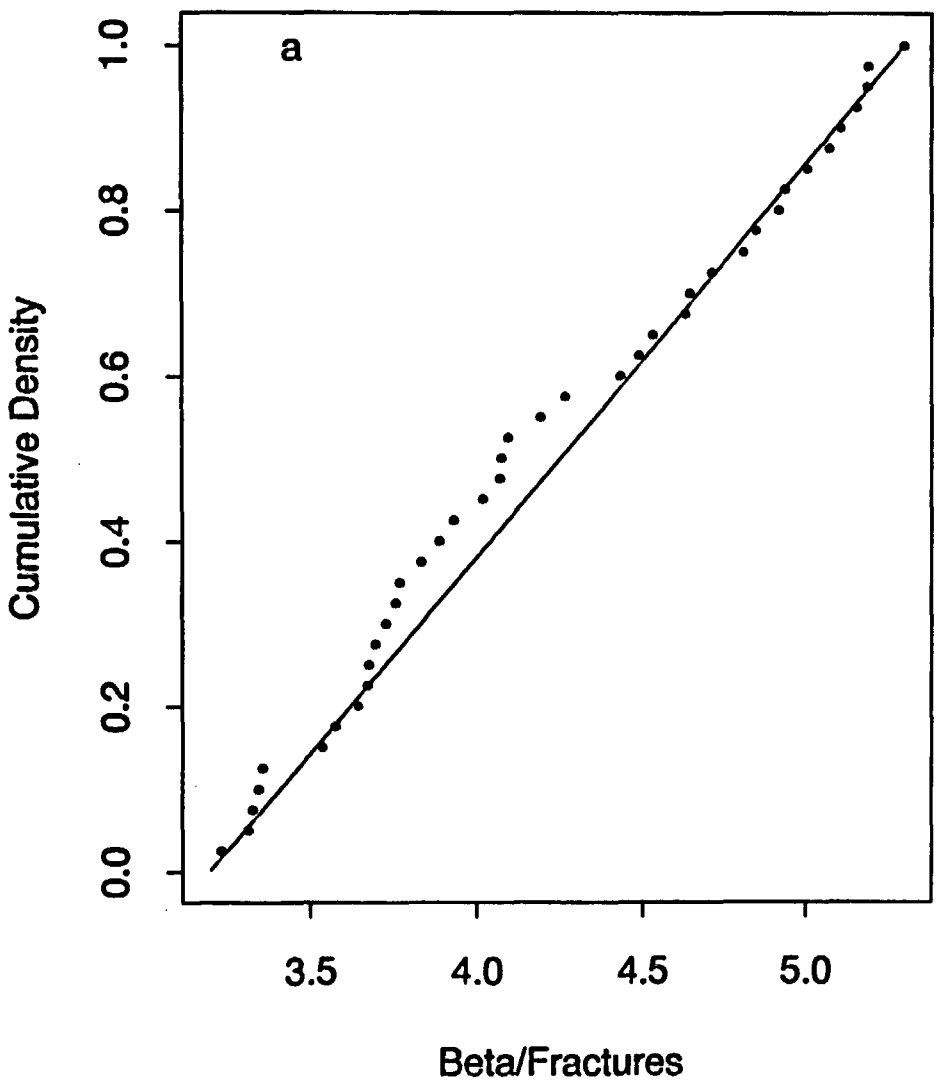
a
Cumulative Density
0.0
0.2
0.4
0.6
0.8
1.0
3.5
4.0
4.5
5.0
Beta/Fractures

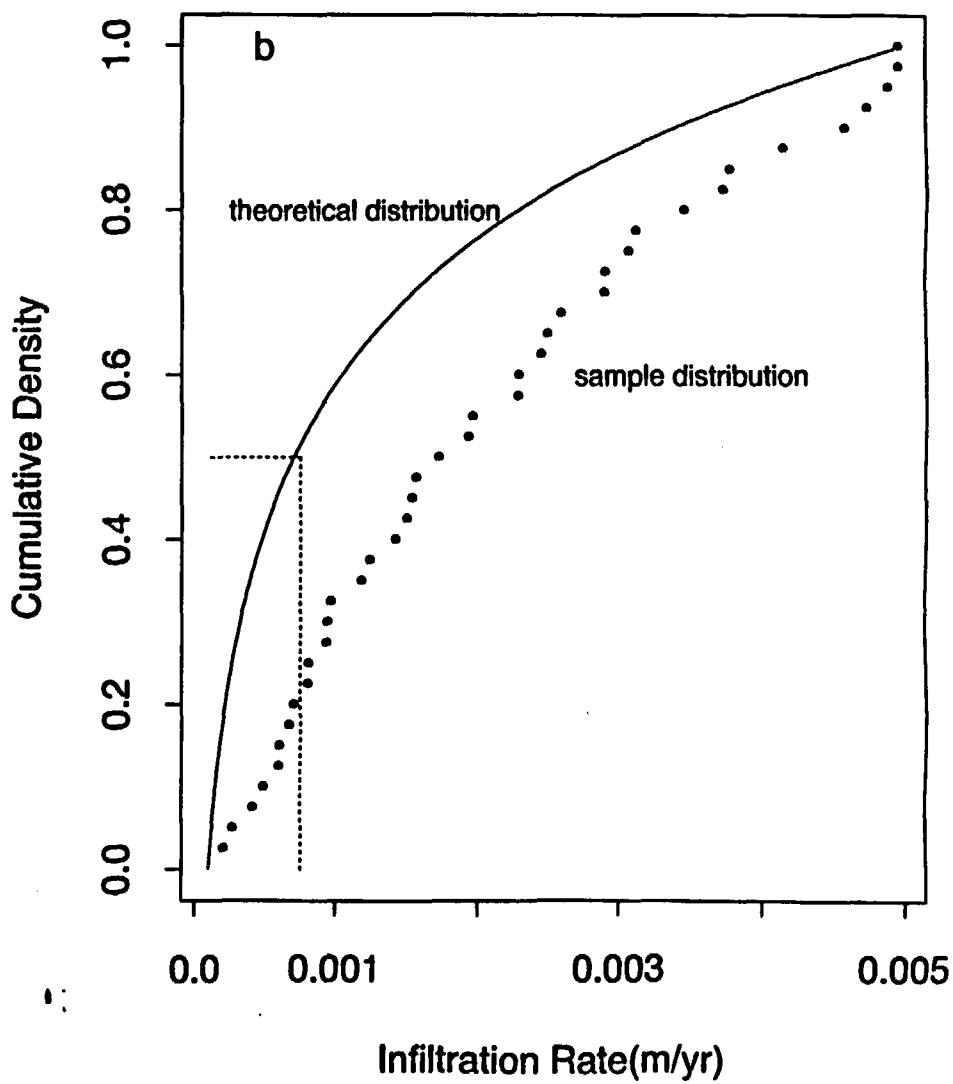
b
theoretical distribution
sample distribution
Cumulative Density
0.0
0.2
0.4
0.6
0.8
1.0
0.0
0.001
0.003
0.005
Infiltration Rate(m/yr)

Fig. 9-7

the fact that the samples tested were made up of only the largest values of the *Normalized Release* or *EDE*.

The advantage of the *K-S* and Sign tests over the stepwise regression analysis is that the correlation with the performance measure is strictly related to the distribution of the independent variable. Different ranges of the performance measure can also be explored to determine the most significant parameters in other parts of the parameter space.

Table 8-6
Important Variables Selected by the Kolmogorov-Smirnov and Sign Tests for the Base Case (*oooo*) Scenario at the 0.05 Level of Significance[a]

Normalized Release	*TPA Module*	*Collective Effective Dose Equivalent*	*TPA Module*
INFIL(UN)	*FLOWMOD*	INFIL(UN)	*FLOWMOD*
ECORR8	*SOTEC*	FUNNEL2	*SOTEC*
AKR3	*C14*	RPOR(1,2)	*SOTEC*
RETARD2	*C14*	ECORR6	*SOTEC*
SOL4Am	*SOTEC*	FORWAR2	*SOTEC*

[a] See Appendix A for a definition of the variable names.

8.4 SENSITIVITY ANALYSIS

8.4.1 Introduction

The objective of sensitivity analysis is to establish the relative importance of parameters to the conceptual model. One measure of model sensitivity is the amount of variation in model output affected by variation in the model input. The model output, *Y*, cumulative release of radionuclides at the accessible environment (*Normalized Release* or *EDE*) can be expressed in terms of the independent variables:

$$Y = f(x_1, x_2, \ldots\ldots x_n) \quad . \tag{8-1}$$

Model sensitivity can be defined as the first partial derivative of the model output response *Y* with respect to the input variables x_i:

$$s_i = \frac{\partial Y}{\partial x_i} \quad . \tag{8-2}$$

The sensitivity, as defined in the above relationship, has dimensions. To compare sensitivity among variables in the model, the sensitivities can be normalized and made dimensionless. This may be

done in a variety of ways. One method of making the sensitivities dimensionless is to multiply the sensitivity by a ratio of Y and x_i:

$$s' = \frac{\partial Y}{\partial x_i} \frac{x_i}{Y} \quad . \tag{8-3}$$

If the values for x_i and Y used in the ratio x_i/Y are the estimated means of x_i and Y, the sensitivity is known as the "elasticity" (Intriligator, 1978).

Another way to remove the dimensions and the differences in scale is to standardize each value for the input and response variables by subtracting the estimated mean $\bar{x}$ and dividing by the standard deviation σ_x (Seitz *et al.*, 1991):

$$x_i^* = \frac{x_i - \bar{x}}{\sigma_x} \quad . \tag{8-4}$$

The sensitivities $\partial Y^*/\partial x^*_i$ will have values between 0 and ± 1, which facilitates comparison between disparate variables.

A number of methods may be used to estimate the sensitivity of the model output to a given independent parameter. Differential analysis (Helton *et al.*, 1991), involves determining the local sensitivity of the response to an individual parameter. Regression analysis may be used to estimate the sensitivity of the model in relation to an individual parameter, or to a group of parameters. Estimations of model performance and overall model sensitivity may be generated with a regression equation.

Generally, a linear regression equation is represented as a linear combination of the independent variables:

$$Y = \alpha_o + \sum_{i=1}^{N} \beta_i x_i + \epsilon_i \quad , \tag{8-5}$$

where α_o is the intercept, β_i are the regression coefficients and $\in_i$ is the error (Sen and Srivastava, 1990).

Many submodels in a typical performance assessment behave non-linearly with respect to the values of the input variables. Regression can include polynomials and cross products of the N independent variables, for example:

$$Y = \alpha_o + \sum_{i=1}^{N} \beta_i x_i + \sum_{i=1}^{N}\sum_{j=1}^{N} \beta_{ij} x_j x_i + \epsilon_i \quad . \tag{8-6}$$

the regression analyses for IPA Phase 2 considered only linear forms and combinations of the variables, such as that expressed in Equation (8-5).

8.4.2 Estimation of Sensitivities by Regression Analysis

Multilinear regression was used to estimate the sensitivities of the model with respect to the most important variables selected by stepwise regression analysis. The estimated regression coefficients for the untransformed data have dimensions. To compare sensitivities for the individual variables, two different transformations of the data were executed before doing the regression analysis: standardization (Seitz *et al.*, 1991) and rank transformation (Iman and Conover, 1979).

8.4.2.1 Standardization

Data can be standardized to eliminate the dimensions and any scale effects, as illustrated in Equation (8-4) above. The result of this transformation is that all transformed variables have a mean of zero and a standard deviation of one. The regression coefficients estimated, using standardized data, are also a measure of the fraction of the standard deviation change in the dependent variable Y, as affected by a fraction of the standard deviation σ_x change in the independent variable (Helton *et al.*, 1991). Thus, the coefficients estimated from regression of the standardized data will be indicative of the importance to the model.

8.4.2.2 Rank Transformation

Rank transformation of the data also eliminates the dimensions and scale associated with the variables (Iman and Conover, 1979). The rank transformation involves replacing the data used in the model with their corresponding ranks, as determined by ordering the 400 observations from the minimum (1) to maximum (400). The same transformation is done to values of the model output.

The estimated regression coefficients for regressions done with untransformed data, the standardized, and rank-transformed data for the base (*oooo*), and the fully-disturbed (*csdv*) cases are given in Tables 8-2 to 8-5. Because the regression coefficients are estimates, the 95 percent confidence interval was determined for each of the raw regression coefficients. It should be noted that while the regression coefficients are a measure of sensitivity of the model output to the input variables, they are particular to specific models and are not generically applicable.

8.4.3 Estimation of Sensitivities by Differential Analysis

Another method, used primarily for sensitivity analyses, is differential analysis. This approach consists of approximating the response surface by its Taylor series expansion about a reference point (x^o) such as the mean:

$$Y = Y(x^o) + \sum_{i=1}^{N} \frac{\partial Y(x^o)}{\partial x_i}(x_i - x_i^o) + (\textit{higher order terms}) + \epsilon_i \quad . \tag{8-7}$$

By truncating the Taylor series at the first term, the partial derivative of the response with respect to variable x_i for a small perturbation from the reference point is defined:

$$\frac{\partial Y(x^*)}{\partial x_i} = \frac{Y - Y(x^*)}{x_i - x_i^*} \quad . \tag{8-8}$$

The partial derivatives can be evaluated analytically in some cases, but it is often too difficult to do this directly. A number of techniques, such as the adjoint method and Green's function method, have also been developed (Zimmerman *et al.*, 1990) to increase the efficiency of the evaluation of derivatives analytically within complex computer codes. The partial derivatives can also be evaluated numerically by calculating the performance at the reference point and at points nearby, by perturbing one independent variable at a time.

There are important drawbacks to differential analysis. The Taylor series approximation of the partial derivatives is inherently local, and may not reflect accurately the sensitivity at points far from the evaluation point. Another drawback to differential analysis is that the evaluation of the derivatives is often difficult and expensive. Numerical evaluation of the derivatives, as in Equation (8-8), requires one or more evaluations of the performance assessment model for each derivative, and is often too costly to consider for a large number of input variables.

Differential analysis provides no information on the possible existence of thresholds or discontinuities in either the independent variables or the response of the model to the distribution (Helton *et al.*, 1991) (e.g., the change from matrix to fracture flow in unsaturated media). It is possible, however, to evaluate the partial derivatives at any point in the parameter space. Efficient techniques for finding points in the parameter space that are highly significant (e.g., sensitive or high-consequence) have been developed, and demonstrated on a simple representations of a geologic repository (Wu *et al.*, 1992).

8.4.4 Comparison of Sensitivity Coefficients Estimated from Regression and Differential Analyses

Multilinear regression was used to estimate the first derivatives of *Normalized Release (Y)* with respect to the input variables x_i (i.e., $\partial Y/\partial x_i$). These first derivatives are estimates of the coefficients of the multilinear regression equation. In differential analysis, the first derivatives are estimated at a "reference" point; in this analysis, the mean of each input variable. Each input variable is perturbed a small amount from the mean value, one variable at a time, and the first derivatives calculated as described in Equation (8-8).

Differential analysis should not give the same results as regression analysis for the first derivatives (Wu *et al.*, 1992) because multilinear regression analysis uses information from all regions of the parameter space, whereas differential analysis estimates the derivatives at only one point in parameter space.

The analysis for the present comparison was performed for the base case (*oooo*) scenario and the 14 most significant input variables in the following manner:

(1) Calculate the mean value of each variable in the 400-vector Latin Hypercube Sampler (LHS) input file;

(2) Generate a new input file containing 15 vectors. The first vector will be the average values for each variable. The next 14 vectors will contain the average values for each variable except for one of the most significant variables, which will differ from its average by a small amount (e.g., 10 percent);

(3) Run the TPA computer code using the new input file for the base case, to generate 15 output vectors of *Normalized Release*; and

(4) Estimate the partial derivatives for Normalized Release with respect to the 14 independent variables, using Equation (8-8); the difference between the *Normalized Release* from vector 1 and vectors 2 through 15, divided by the difference in the independent variable.

The sensitivity coefficients from the differential analysis and multilinear regression for the 14 most significant variables are compared in Table 8-7. The results agree reasonably well in some cases (e.g., *INFIL(UN), undisturbed infiltration*) and generally have the same sense. The most striking difference is the large number of cases in which differential analysis gave a zero sensitivity. This could be a reflection of the insensitivity of those parameters in the region of the reference point. Additionally, many of the TPA modules switch from one behavior to another rather abruptly, depending on the input parameters. For example, the transition from matrix flow to fracture flow in the module *FLOWMOD* is non-linear over the range of infiltration rates. The insensitivity of the model to several variables at the reference point indicates the need to apply differential analysis at several points on the response surface.

8.4.5 Model Sensitivity Analysis

8.4.5.1 CCDF Sensitivity

In this work, the CCDF, that is (1 - CDF (Cumulative Distribution Function)), which, in a single figure, plots the magnitude and uncertainty of the *Normalized Release* at the accessible environment, is the main vehicle for conveying uncertainty results. However, the CCDF gives no explicit information on the contribution to total uncertainty by each of the input parameters.

Plots illustrating the sensitivity of the CCDF to a single parameter or condition were generated by screening the output vectors according to a criterion, and using only the remaining vectors to produce the CCDFs. The CCDFs of screened data illustrating the sensitivity to performance measures of individual natural and engineered barriers are presented in Section 9.5.

8.4.5.2 Sensitivity of Results to Number of Vectors

The sensitivity of the results to the number of LHS vectors in each scenario is illustrated by comparing spurious correlations among the input variables and by the sensitivity of the CCDF to the number of vectors.

8.4.5.2.1 Spurious Correlations

Although it is possible to specify correlations among variables when generating input vectors with the

LHS method, this feature was not evoked in IPA Phase 2 (i.e., there was no deliberate attempt to produce correlations among input variables). Spurious correlations are apparent correlations of the input variables among themselves, when no correlations were intended. Although computer programs for generating LHS (Iman *et al.*, 1980) generally contain algorithms for minimizing these effects, correlation of the dependent variables to the independent variables is confounded by spurious correlations, if too few vectors are available for the statistical tests.

Table 8-7
Comparison of First Derivatives of Normalized Release by Regression and Differential Analysis[a]

Variable Name	$\partial Y/\partial x_i$ *Regression*	$\partial Y/\partial x_i$ *Differential*	*Elasticity Regression*	*Elasticity Differential*
INFIL(UN)	502	377.4	0.403	0.495
ECORR6	-0.0033	0	-2.66	0
ECORR7	-0.0027	0	-2.14	0
RETARD3	-0.015	-0.00194	-0.518	-0.112
ECORR8	1317	0	0.182	0
AKR3	9.6E+14	3.65E+13	0.264	0.016
KD39Th	-0.713	0	-0.118	0
ECORR5	-27.3	0	-0.213	0
RETARD1	-0.0062	-0.0021	-0.219	-0.036
KD1Cm	0.014	0	0.049	0
AKR2	9.79E+13	5.66E+13	0.132	0.012
AKR4	1.6E+14	-1.7E+13	0.131	-0.0022
Kd26Am	0.041	0	0.077	0
SOL4Am	2030	597	0.068	0.0033

[a] See Appendix A for a definition of the variable names.

To demonstrate the problem with spurious correlations, three computations of *Normalized Release* were done with inputs of 100, 200, and 400 vectors generated by the LHS technique. Each vector had 445 parameters, 195 of which were sampled for the base case (*oooo*). The correlation coefficient between each input variable x_i and the *Normalized Release*, Y, calculated from the performance assessment model was calculated and plotted against the largest correlation between x_i and any other independent variable. These plots illustrate a limitation of the sensitivity analyses; if the spurious correlations among independent variables are as large or larger than the correlation between the dependent independent variables, then one cannot determine the validity of the latter correlations. Figure 8-8 for 100 vectors clearly shows that the correlations among independent variables are as large or larger than the correlations between the independent and dependent variables for a significant

Figure 8-8. Maximum Spurious Correlations Among Independent Variables vs. Correlations Between Dependent and Independent Variables for 100 Vectors.

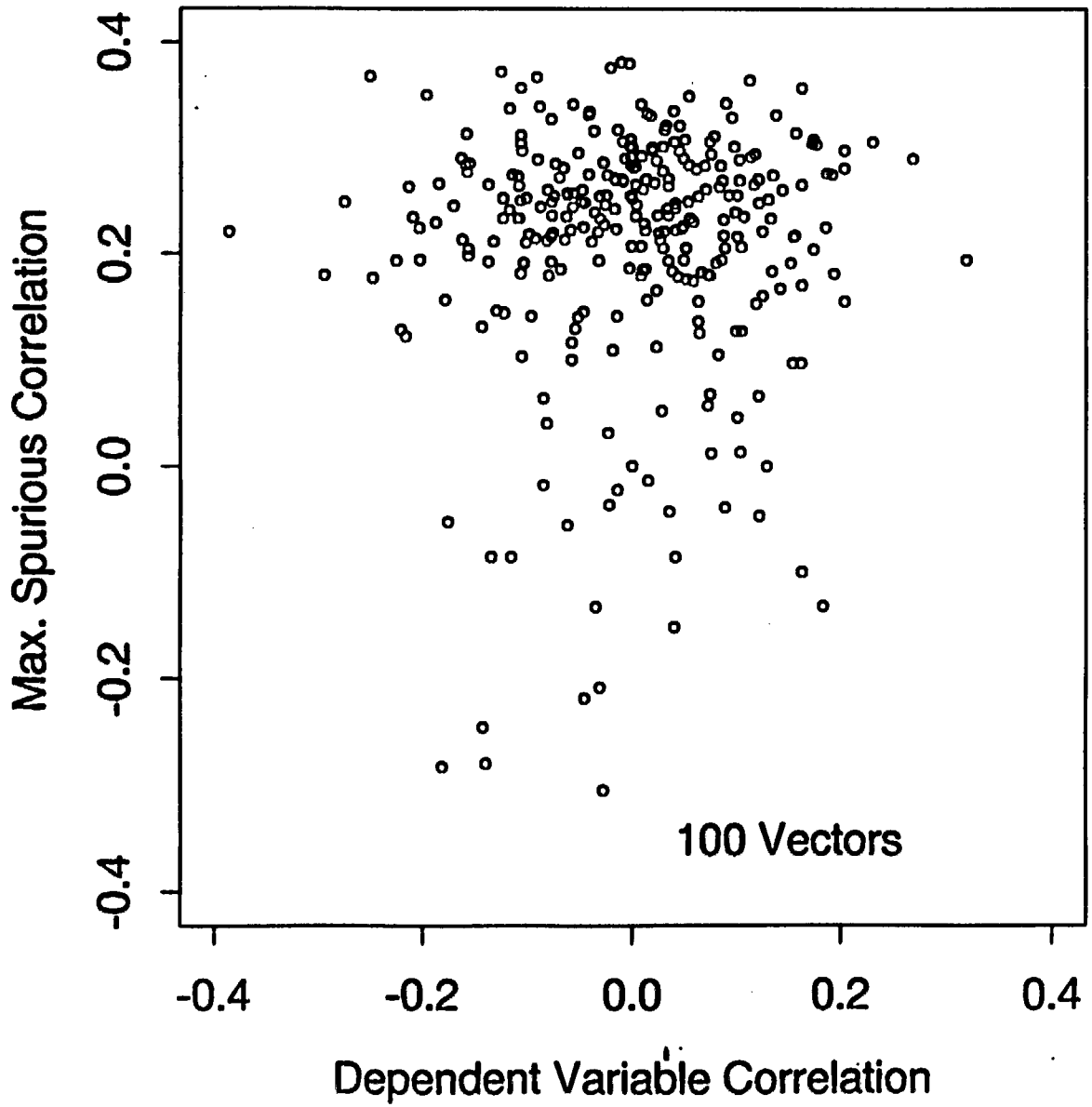
Max. Spurious Correlation
0.4
0.2
0.0
-0.2
-0.4
100 Vectors
-0.4
-0.2
0.0
0.2
0.4
Dependent Variable Correlation

FIG 3-8

fraction of the vectors, thereby confounding interpretation of the results for sensitivity. The results are similar for 200 vectors, but are not shown here. Figure 8-9 illustrates that for 400 vectors, the largest correlations between the independent and dependent variables are distinctly larger than the correlations among the independent variables.

8.4.5.2.2 Sensitivity of the CCDF to Number of Vectors

CCDFs of total release were generated from runs of 50, 100, 150, 200, and 400 vectors, and presented in Figure 8-10. Visually, the CCDFs were quite similar, suggesting a relative lack of sensitivity to the number of vectors.

The conclusions that can be drawn from this analysis are that the usefulness of the sensitivity analysis was limited for fewer than 400 vectors per scenario, as shown by comparing the magnitude of the largest spurious correlations to the dependent-independent variable correlations. However CCDFs were much less sensitive to the number of vectors per scenario.

8.5 UNCERTAINTY ANALYSIS

Different types of uncertainty associated with the modeling of physicochemical processes can be distinguished -- in particular:

- The statistical uncertainty because of the inherent random nature of the processes, and
- The state-of-knowledge uncertainty.

The latter uncertainty may be subdivided further into parameter and model uncertainty. Parameter uncertainty is caused by insufficient knowledge about the input information, and can manifest itself in several forms. For example, if a single parameter characterizes a facet of the model (e.g., hydraulic conductivity of a rock unit), then uncertainty about its value would lead to selecting a distribution for the probabilistic sampling of that parameter with wider limits than if the parameter were well characterized. Because it usually is not possible to characterize a spatially varying property of the rock, such as permeability by a single parameter, using a single parameter value over the entire field of calculation to represent a spatially varying parameter also introduces uncertainty.

For IPA Phase 2, the repository was represented by a highly simplified conceptual model, which in many cases, ignored the large spatial variability of the geosphere (e.g, the hydraulic properties of each layer were considered spatially homogeneous for each vector, ignoring the considerable heterogeneity). These variables could be made to vary in time and space; however, this would make the modeling much more complicated. Models within the system representing the performance assessment do in fact include spatial and temporal variability, but these are only indirectly a result of the values of the input parameters. For example, gas flow is represented in two dimensions and is transient in time. Additionally, some of the parameters such as hydraulic conductivity implicitly take into consideration the spatial scales of correlation, to account for the length of flow paths.

Modeling uncertainty is caused by simplifying assumptions and the fact that the models used may not accurately simulate the true physical process. This study, as was the case in the IPA Phase 1 study (Codell *et al.*, 1992), deals primarily with the effects of parameter uncertainty.

Figure 8-9. Maximum Spurious Correlations Among Independent Variables vs. Correlations Between Dependent and Independent Variables for 400 Vectors.

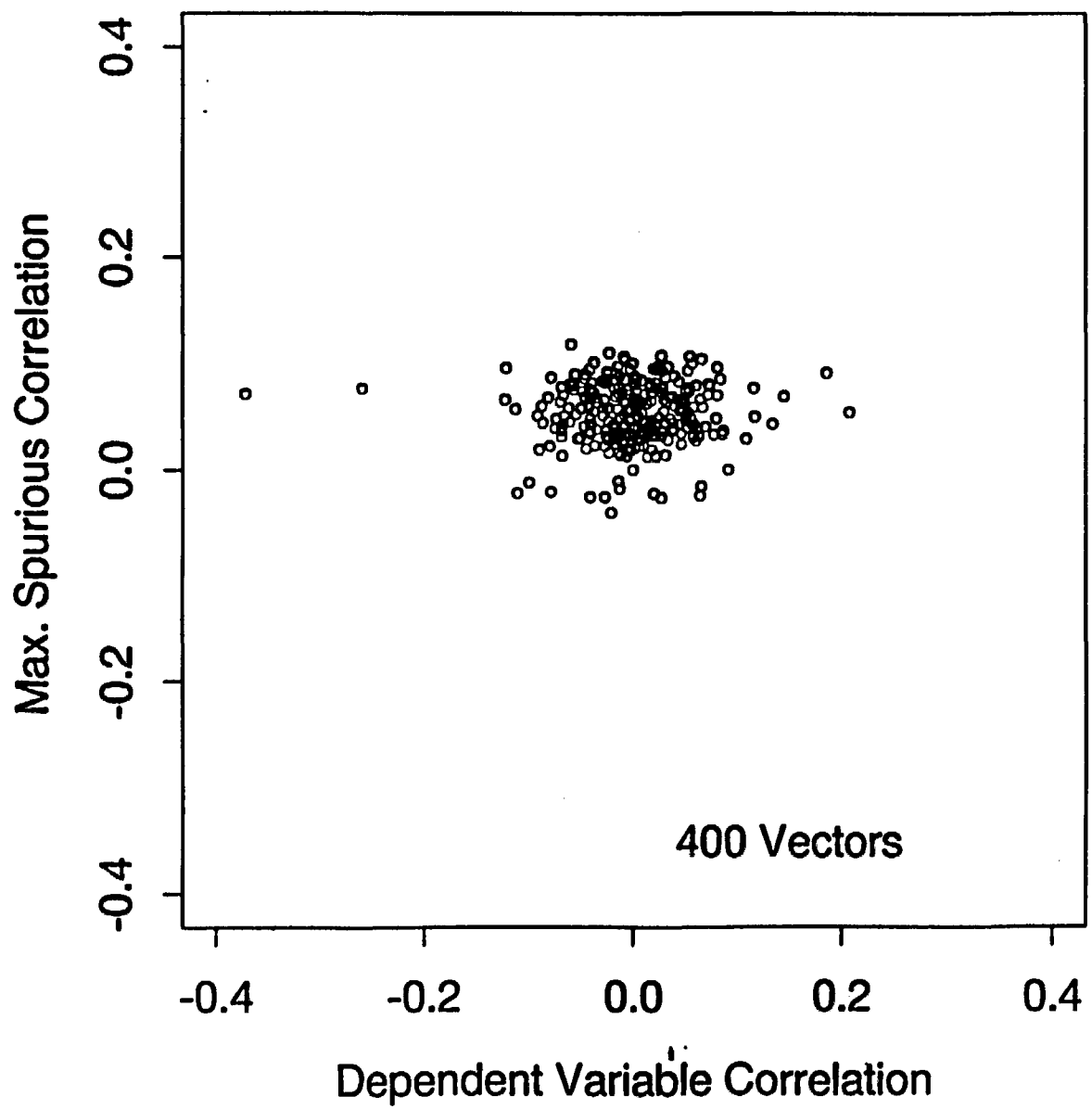
Max. Spurious Correlation
0.4
0.2
0.0
-0.2
-0.4
400 Vectors
-0.4
-0.2
0.0
0.2
0.4
Dependent Variable Correlation

FIG 3-9

Figure 8-10. Sensitivity of Base Case Scenario CCDF to the Number of Vectors.

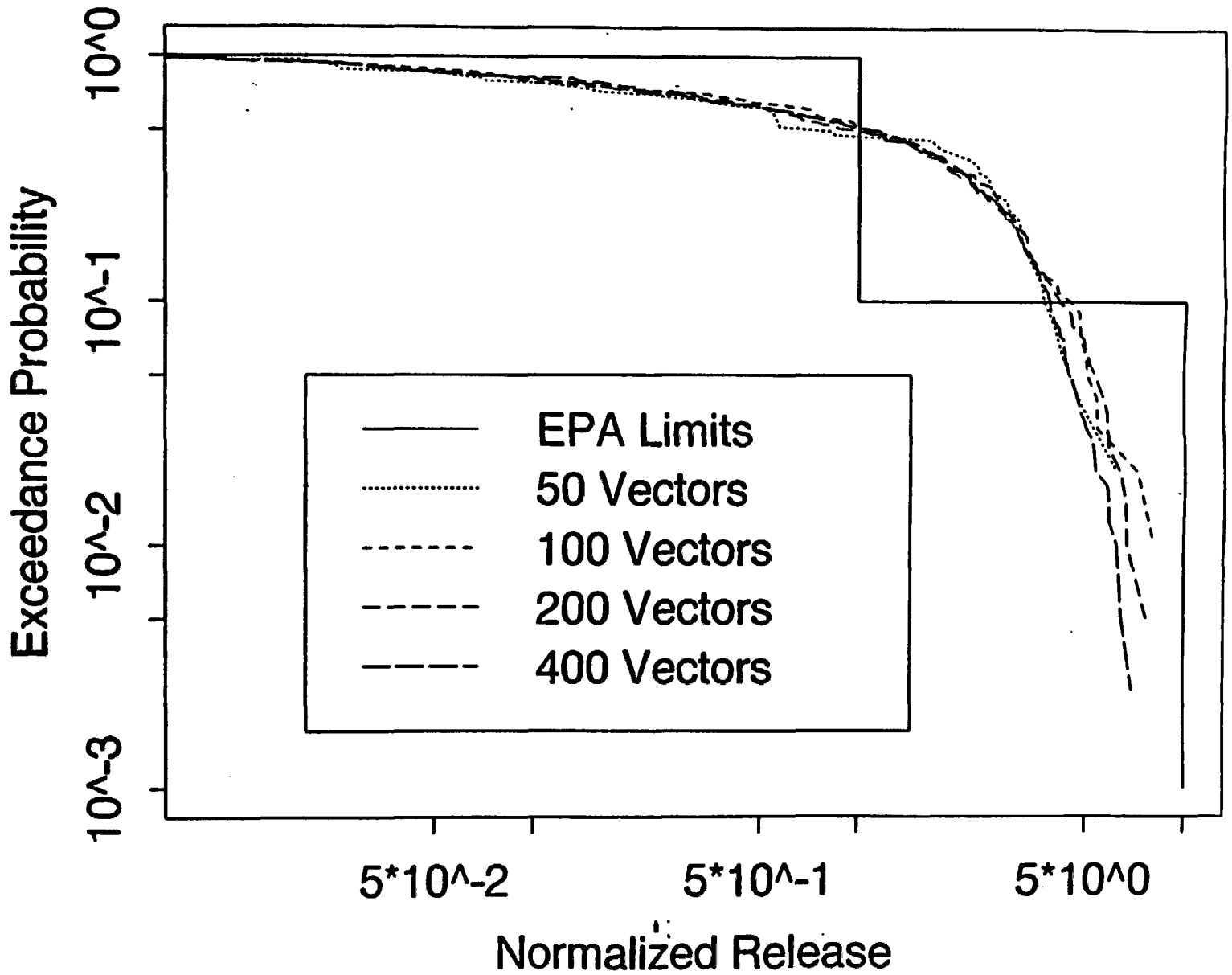
Exceedance Probability
10^0
10^-1
10^-2
10^-3
5*10^-2
5*10^-1
5*10^0
Normalized Release
EPA Limits
50 Vectors
100 Vectors
200 Vectors
400 Vectors

FIG 3-10

Iman and Helton (1985, p. 1-1) give an apt definition of uncertainty, which has been adopted for the present study:

> "Uncertainty analysis is defined here to be the determination of the variation or model imprecision in Y that results from the collective variation in the model variables $x_1 \ldots x_k \ldots$. A convenient tool for providing such information is the estimated cumulative distribution function (CDF) for Y since it summarizes the variability in computer model output which results from the input assumptions."

Although the main presentation of uncertainty in IPA Phase 2 will rest on the CCDF, an additional means of describing uncertainty, the "Uncertainty Coefficient," has also been developed.

Uncertainty Coefficient

It would be useful to define an "uncertainty coefficient" to represent the contribution of uncertainty from each of the input parameters, but there does not appear to be any standard definition of such a term. Leading toward a definition that can be used in the present work, Zimmerman *et al.* (1990) present an expression for the uncertainty, using the response surface in which the actual model is represented by the multilinear regression of the model results:

$$Var(Y) = E\left[(Y - \bar{Y})^2\right] = \sum_i \beta_i^2 \, Var\,(x_i) + \sum_i \sum_j \beta_i \beta_j Cov(x_i, x_j) \quad . \tag{8-9}$$

where "Y" is the value of the dependent variable for the fitted surface, "β_i" is the regression coefficient $\partial Y/\partial x_i$, "$E[\ ]$" is the expected value, "$\bar{Y}$" is the estimated mean of Y, "Var" is the variance, and "Cov" is the covariance. For the IPA Phase 2 calculations, the independent variables are not deliberately correlated, so we assume that the covariance term is zero. In this analysis, we estimate the quantity $Var(Y)$ by estimating β_i and $Var(x_i)$.

Assuming that there is no covariance among the independent variables, Equation (8-9) presents a way in which the variance of the dependent variable can be tied to variance and sensitivity of each of the independent variables. Based on this assumption, it is possible to define an "uncertainty" coefficient U_i:

$$U_i = \frac{\beta_i^2 \, Var(x_i)}{Var\,(Y)} \quad . \tag{8-10}$$

This term is numerically equivalent to the square of the "standardized regression coefficient" described in Section 8.4.2. Ideally, if all the independent variables were included in the model, the sum of U_i for all independent variables would be unity. Non-zero covariance of the independent variables will cause ΣU_i to deviate from unity. The sums of the uncertainty coefficients presented in Tables 8-2 to 8-5 are equal to the coefficient of determination, R^2, for each regression analysis.

8.6 EMULATION OF THE TOTAL-SYSTEM PERFORMANCE ASSESSMENT MODEL USING MULTILINEAR REGRESSION

One aspect of doing multilinear regression that has not been explored previously by the NRC staff is the application to emulating the total-system performance assessment model. The regression equation can be used with the suite of values for the input variables to estimate the response variable. The estimated response variable, $\hat{Y}$, may then be compared with the full model output *(Normalized Release* or *EDE)* to determine how good the regression equation approximation of the model is. The following discussion outlines some of the procedures used to better fit the regression equation to the model and illustrates how the regression equation can be used to estimate model performance.

8.6.1 Estimation of the Response Variable

Values of the response variable for the simplest form of the multilinear regression equation were calculated using the raw data for the input variables (x_i) and the estimated regression coefficients, b_i (Tables 8-2 to 8-5).

$$\hat{Y} = a_0 + b_1x_1 + \ldots + b_nx_n \quad . \tag{8-11}$$

It should be noted that although the form of the regression described here is linear, several parameters used in IPA Phase 2 do not exhibit a linear relationship with the performance measure.

A non-linear relationship between independent and dependent variables can often be determined by plotting the residuals for the regression against the values for a given independent variable (Figure 8-11). If the residuals $e_i = (Y_i - \hat{Y}_i)$ are a function of an independent variable, there will be a grouping or trend in the residuals as a function of the independent variable (Figure 8-11a). In Figure 8-11a, there is a skewed distribution of the points toward low infiltration values. Transformation of the independent variable to a non-linear form (e.g., $1/x$, $log(x)$, x^2) may be appropriate (Sen and Srivastava, 1990). By transforming the independent variable (e.g., *infiltration* to *log(infiltration)*), the residuals plot (Figure 8-11b) is changed to indicate no functional relationship between the residuals and the independent variable. This indicates that the new form of the variable may help provide a better fit of the model.

The process of transforming variables, doing subset selection and regression analysis, is an iterative process. Several iterations may be required to get the best fit of the model by the regression equation. Nonlinear regression techniques are also available, but beyond the scope of the present project.

A regression equation was constructed for the purpose of emulating the total-system performance assessment model. Twenty variables selected by stepwise regression analysis were used; some variables were transformed as discussed above. Figure 8-12 is a plot of the estimated values for *Normalized Release*, $\hat{Y}$, from the regression equation versus the *Normalized Release* for the base case (*oooo*) computed by the TPA computer code. It should be noted that the estimated response variable $\hat{Y}$ is a function of specific b_i and specific values of x_i. Other regression equations will give different results. The purpose of the plot is to illustrate the degree of fit between the response variable determined by the regression equation and the performance measure computed by the TPA computer

Figure 8-11. Plot of Residuals From Multilinear Regression as a Test for Heteroscedasticity.

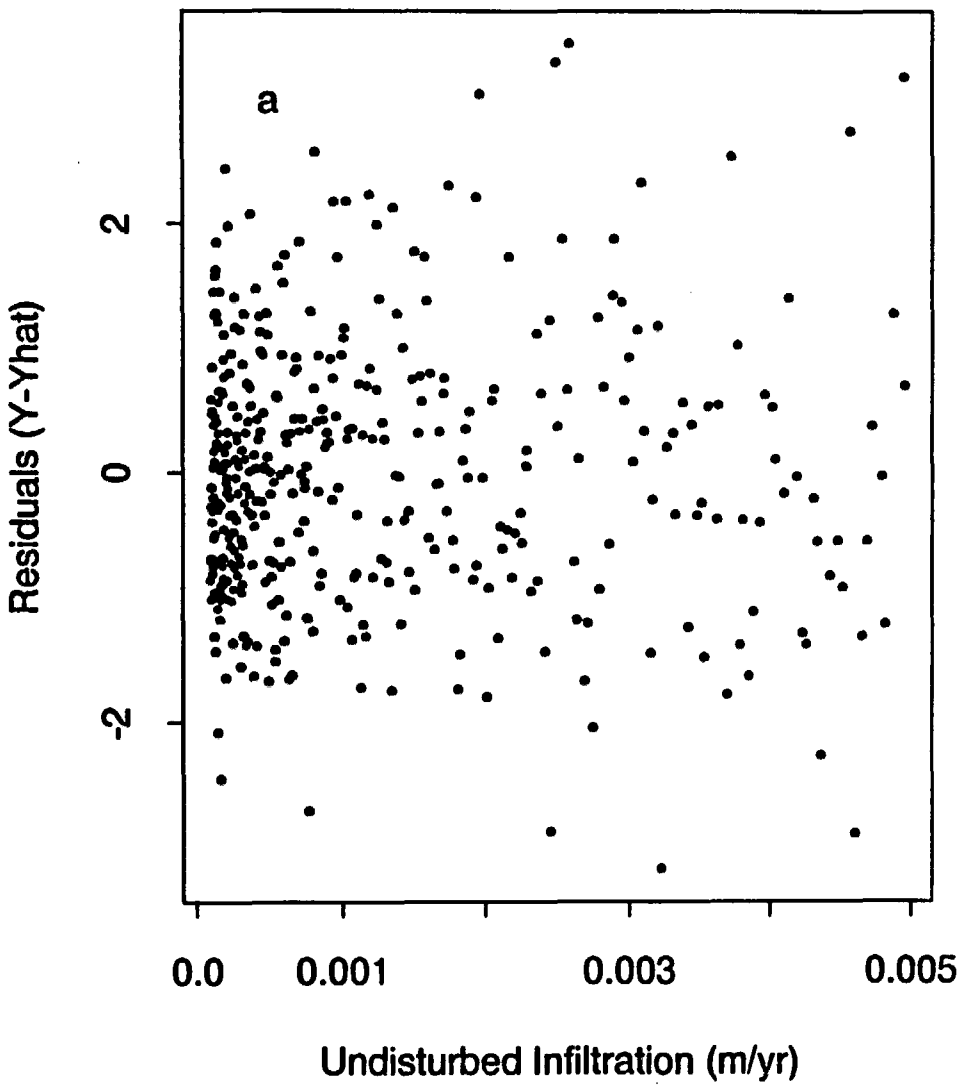
a
Residuals (Y-Yhat)
2
0
-2
0.0
0.001
0.003
0.005
Undisturbed Infiltration (m/yr)

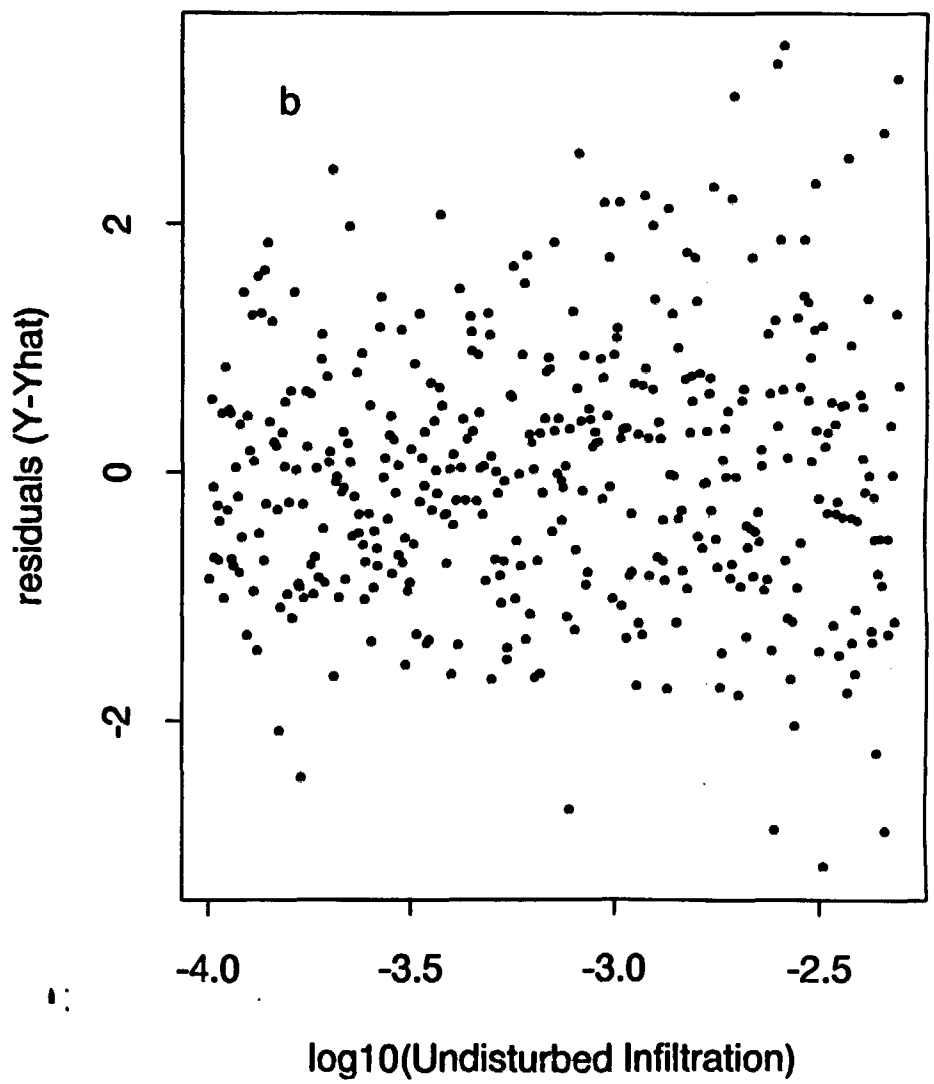
b
residuals (Y-Yhat)
2
0
-2
-4.0
-3.5
-3.0
-2.5
log10(Undisturbed Infiltration)

FIG 3-11

Figure 8-12. Plot of Predicted Normalized Releases (YHAT.RAW) From Multilinear Regression Analysis vs Normalized Releases Calculated bythe TPA Computer Code, Bas case (oooo) Scenario.

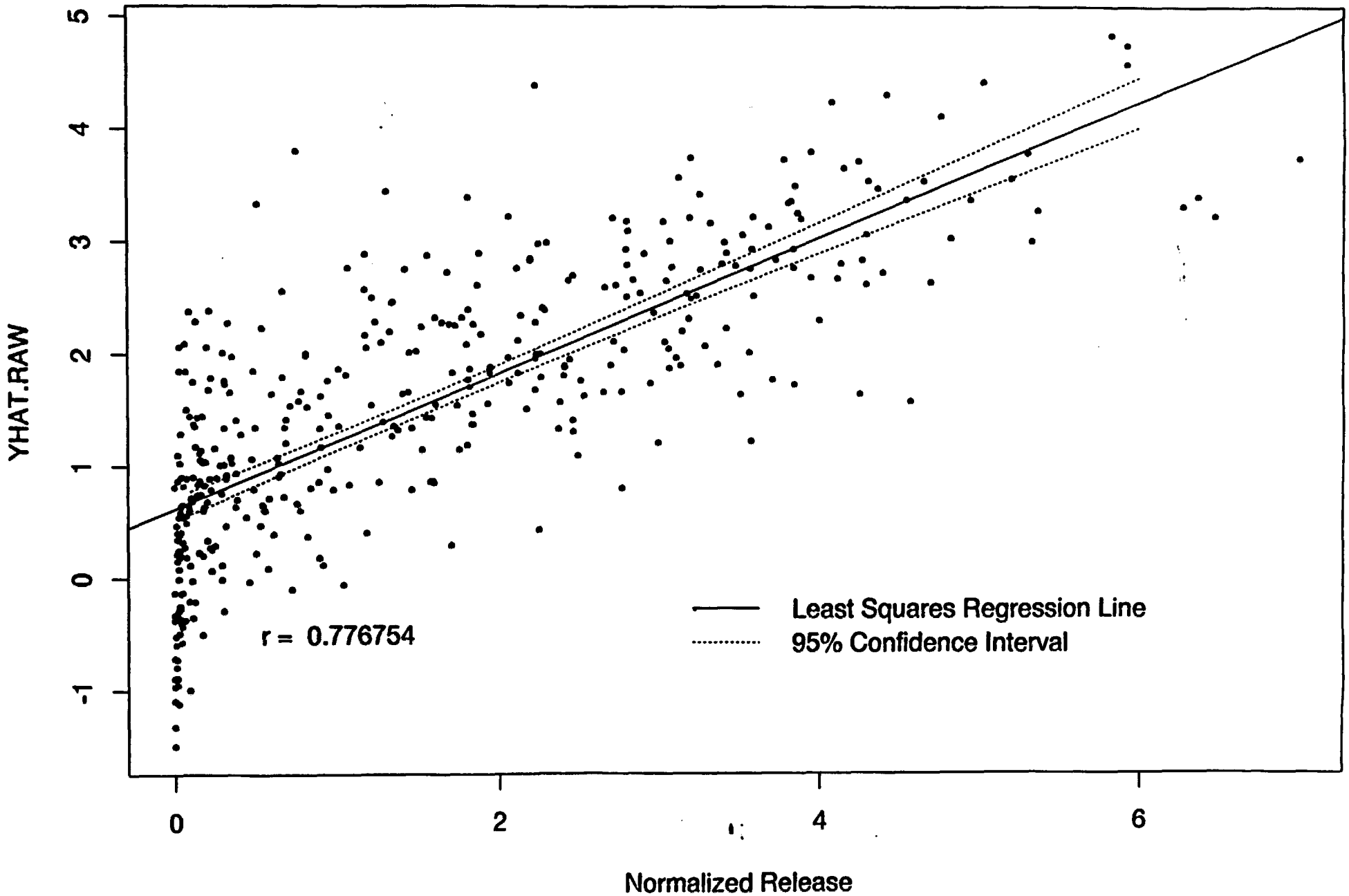
YHAT.RAW
5
4
3
2
1
0
-1
0
2
4
6
Normalized Release
r = 0.776754
Least Squares Regression Line
95% Confidence Interval

FIG B-12

code. The correlation coefficient between the estimated releases $\hat{Y}$ and the *Normalized Release* is 0.78, which corresponds to a coefficient of determination of 0.61. The 95 percent confidence interval is noted on the plot and indicates the region in which there is high confidence of finding the least-squares fit line. Figure 8-13 illustrates the CCDFs for the estimated releases $\hat{Y}$ and the *Normalized Release* from the TPA model.

8.6.2 Evaluation of the Goodness of Fit

8.6.2.1 Correlation Coefficient

The correlation coefficient is often used to estimate the linear relationship between two variables (Walpole and Myers, 1978). The more linear the relationship, the closer the correlation coefficient is to unity. Ideally, the better the regression equation estimates the full total-system performance assessment model, the closer the correlation coefficient is to 1 (or -1). The square of the correlation coefficient, the coefficient of determination (R^2) indicates the percent of the full model that is explained by the regression model. The coefficient of determination for the regression equation with twenty variables is 0.61. Because the coefficient of determination and the absolute value of the correlation coefficient increase as more variables are added to the model, they are not necessarily good indicators of the optimal number of variables to be included in the regression model. Proper selection of the form of the independent variables is essential to constructing a regression equation that will emulate the total-system performance assessment model well.

8.6.2.2 Mallow's C_p Statistic

Helton *et al.* (1991) stated that as the number of independent variables increases, there is a greater chance for spurious correlations that result in the inclusion of a variable in the regression model. Mallow's C_p statistic (Mallow, 1973; Sen and Srivastava, 1990) was used in this analysis, in an attempt to evaluate the optimal number of variables that should be included in the regression model.

Mallows' C_p statistic compares the error of the restricted model (the regression equation for the subset of variables) to the error of the full (total-system performance assessment) model (all of the independent variables):

$$C_p = \frac{\sum_{i=1}^{p} (Y-\hat{Y})^2}{s^2} - (n-2p) \quad , \quad (8\text{-}12)$$

where Y is the response for the full model with all parameters, $\hat{Y}$ is the response for the restricted model, s^2 is the unbiased estimate of the variance (mean square error) for the full model, n is the number of observations, and p is the number of independent variables in restricted model, plus one (Walpole and Meyers, 1978).

When $C_p = p$, the optimal number of variables for the regression equation has been chosen. In this analysis, the use of the C_p statistic for selecting the optimal number of variables did not give results that were easily interpretable. The C_p statistic is very sensitive to small changes in the fit if $(n - 2p)$ is large (Gunst and Mason, 1980). Attempts were made to reduce the number of independent variables to consider, by first performing stepwise linear regression, with the F-test criterion using $\alpha = 0.1$, and then doing a subsequent subset selection, with $\alpha = 0.05$. The comparison of the $\alpha_{.05}$

Figure 8-13. Comparison of CCDFs for Predicted Normalized Releases From the TPA Computer Code. Base Case (oooo) Scenario.

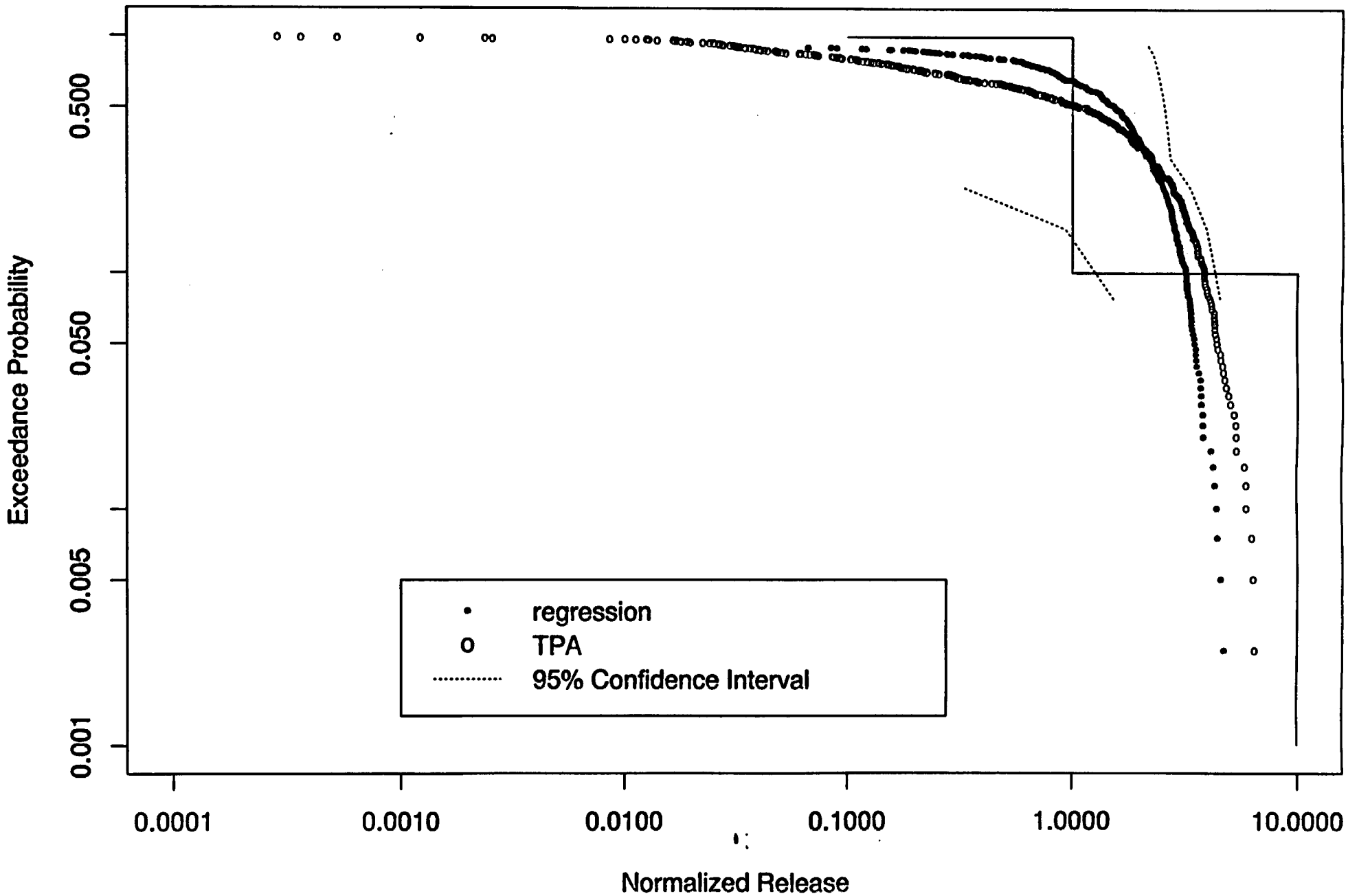
Exceedance Probability
0.500
0.050
0.005
0.001
0.0001
0.0010
0.0100
0.1000
1.0000
10.0000
Normalized Release
regression
TPA
95% Confidence Interval

FIG 8-13

model with the $\alpha_{0.1}$ model still did not provide easily interpretable results. More work is needed to establish the optimal number of variables for subset selection and multilinear regression. One aspect that should be considered is the predictive capability of the individual independent variables. Another aspect to consider is how effectively this statistic might be applied to highly non-linear models.

8.7 SENSITIVITY AND UNCERTAINTY AUXILIARY ANALYSIS

Y.T. Wu/CNWRA, A.B. Gureghian/CNWRA, and R.B. Codell/NMSS

The IPA Phase 2 staff took part in a computational exercise to evaluate several methods of sensitivity and uncertainty analyses. The purpose of these analyses was to demonstrate, on relatively simple flow and transport problems, several methods for sensitivity and uncertainty analysis useful for evaluation of total-system performance assessments.

The work was presented in two reports. The first report (Gureghian *et al*, 1992) covers the derivation and verification of the closed-form analytical solutions for one-dimensional saturated transport of a radionuclide in a fractured, layered system with diffusion into the rock matrix. The material properties of individual fractures and rock matrix layers were assumed to be homogeneous and isotropic. The sorption phenomenon in fractures and matrix was described by a retardation coefficients. The solutions of the model are based on analytical inversions of the Laplace transforms, verified with inversions performed numerically. The first module of the computer program calculates the space-time dependent concentration of a decaying species migrating in the fractures and the surrounding matrix. The second module predicts the local sensitivities of releases to the independent variables.

The second report (Wu *et al*, 1992) evaluates and demonstrates the use of several sensitivity and uncertainty analysis methods using the analytical model developed by Gureghian *et al*. The Limit State Approach, which was developed initially for structural reliability analyses, was investigated for its usefulness in IPA. This approach is based on partitioning the performance results into two parts, one in which the performance measure is smaller than a chosen value called the Limit State, and the other in which the performance measure is larger. The optimal expansion point in parameter space, known as the Most Probable Point (MPP), has the property that its location on the Limit State surface is closest to the origin. Additionally, the projections onto the parameter axes of the vector from the origin to the MPP are the sensitivity coefficients. Once the MPP is determined and the Limit State surface approximated, the probability of the performance measure being less than the Limit State can be evaluated. By choosing a succession of Limit States, the entire cumulative distribution of the performance measure can be determined. Determining the location of the MPP is the crux of the methodology. Methods for determining the MPP and improving the estimate of probability are discussed in the report.

The Limit State Approach is significantly more complex than the more commonly used Monte Carlo or Latin Hypercube sampling methods. To aid understanding of the Limit State Approach, all steps of the method were explained by applying it to two simple examples. The first involved calculation of the cumulative probability distribution of the Darcy velocity V, given by $V = -KI$, where K and I are the hydraulic conductivity and hydraulic gradient, respectively. Although simple, this example turned out to be difficult for the application of the Limit State Approach, because of the possibility of change of sign of I and hence V.

The second example applied the Limit State Approach to a one-dimensional transport problem developed in Gureghian *et al.*, and compared the results among the more conventional methods such as Monte Carlo, LHS, and differential analysis for computing both the CCDF and the sensitivity coefficients. This problem included 25 independent variables. The uncertainty analysis used the CCDF for cumulative release as the basis for comparison between the methods. Results indicated that the Limit State Approach had the potential of being much more efficient in terms of computational resources than Latin Hypercube or Monte Carlo Sampling. In one case, the Limit State Approach was able to duplicate the CCDF produced by a 5000-vector Monte Carlo run with only about 600 vectors, and in other cases far fewer.

In general, computational efficiency is proportional to the desired accuracy and the choice of an approach will depend on the nature of the problem. However, the reports demonstrate that the Limit State Approach permits the analyst to concentrate on the critical performance region, with the potential for optimizing the use of the consequence model where it can contribute the most information. By contrast, sampling methods such as Monte Carlo or LHS must cover the entire parameter space, regardless of its importance. In addition, the Limit State Approach leads to probabilistic sensitivity analyses, with essentially no additional work. In particular, the efficiency of the Limit State Approach is independent of the probability level. Therefore, it is more suitable for evaluating the tails of the distribution than LHS or Monte Carlo sampling. However, the Limit State Approach is relatively difficult to implement.

The computational efficiency of the Limit State Approach in general depends on the number of independent variables and the efficiency of evaluating local sensitivities. When the number of independent variables is large, the Limit State Approach may no longer be efficient unless the sensitivities can be determined efficiently, but at the expense of simplicity. The efficiency of the standard Monte Carlo method depends only on the probability level and desired accuracy. It is not clear that the Limit State Approach will be the best approach for problems involving large numbers of independent variables.

8.8 CONCLUSIONS AND SUGGESTIONS FOR FURTHER WORK

The sensitivity and uncertainty analyses in IPA Phase 2 involved evaluation of a number of techniques that have potential use in the evaluation of license application performance assessment models. Many of the techniques used have been used in previous performance assessment work: stepwise regression analysis, CCDFs, differential analysis, and boxplots. In addition, the Kolmogorov-Smirnov and Sign tests were used to determine parameters important to the total-system performance assessment model. Techniques for developing regression equation to emulate the total-system performance assessment model were examined for potential use in determining CCDF sensitivity to changes in parameter distribution type, for example.

Selection of the significant parameters by stepwise regression analysis, the *K-S* test, and the Sign test gave similar results. Regression analysis can only be applied over the entire parameter space. The *K-S* test can also be applied to different parts of the parameter space, in order to test for locally important parameters.

The use of standardized data for stepwise regression gave the same results as the untransformed/raw

data and had the advantage of giving dimensionless coefficients that could then be compared. The estimated multilinear regression coefficients for the standardized data were used to determine the "uncertainty coefficient" that defined the percentage of the variance of the dependent variable, attributable to variance in the independent variable.

The results of differential analysis for 14 variables about the mean for all parameters agreed fairly well with the multilinear regression coefficients. Several variables exhibited zero sensitivity about the mean, which points to the importance of determining local sensitivities at several points in the parameter space.

The question of how many vectors (observations) will give valid results needs to be explored. The Latin Hypercube sampling strategy reduces the number of vectors needed to do a Monte Carlo simulation. The covariance of the independent variables for 400 vectors was small but non-zero. Difficulties associated with application of the C_p statistic indicates that perhaps more vectors are needed. The sampling of more vectors will have the disadvantage of requiring longer run times. Yet, it should significantly reduce the number of spurious correlations that can result in picking the wrong variables by stepwise regression.

The assumption that covariance was zero was made in the sensitivity and uncertainty analyses. Future work to consider grouping of parameters or covariance among the input variables is important to developing a better understanding of model sensitivities.

The development of a regression equation for the purpose of verifying important parameter selection b y emulating the total-system performance assessment model has potential use in the license application review process. It should be emphasized that regression equations can never replace the total-system performance assessment model, but are a tool by which to study the sensitivities associated with performance assessment models. The linear estimation used in this analysis is the simplest technique; a number of others can be explored in future phases of this work.

In general, the techniques used in the IPA Phase 2 sensitivity and uncertainty analysis were easy to implement. No single technique is valid for the sensitivity and uncertainty analyses. The use of a combination of techniques is essential to bringing out various aspects of the total-system performance assessment model. Future evaluation of other techniques such as the hat function or the Limit State Approach will help to establish which techniques will be most useful to the license application review process.

9. ANALYTICAL RESULTS[1]

R.G. Wescott/NMSS, R.B. Codell/NMSS, and V. Colten-Bradley/NMSS

9.1 INTRODUCTION AND CAVEATS CONCERNING THE RESULTS OF IPA PHASE 2

This chapter presents the results of the simulation runs of the total-system performance assessment (TSPA) computer code using the parameter distributions presented in Appendix A of this report. The results of the simulations are presented as Complimentary Cumulative Distribution Functions (CCDFs) of release and effective dose equivalent, distribution bar graphs, and scatter plots.

The results are presented for demonstration purposes and are not intended to indicate the potential for repository compliance or non-compliance with any of the 10 CFR Part 60 performance requirements.

The following caveats should be taken into consideration when reviewing the results of IPA Phase 2:

1. The models used here are based on limited site data and have had limited review.

Preliminary results from some models such as the gas transport and ^{14}C retardation model have been presented at U.S. Nuclear Regulatory Commission / U.S. Department of Energy Technical Exchanges and before the U.S. Environmental Protection Agency's (EPA's) Scientific Advisory Board. Although the overall modeling was more sophisticated than that of IPA Phase 1, it was recognized that input data were still very limited. In addition, scientists do not yet agree on how adequately the various models represent repository processes.

2. The results presented here can not be confirmed as accurately representing the behavior of the repository.

The staff has examined the results of runs for individual vectors to ensure that for these limited cases, the TSPA model appears to be performing as designed. However, other than software quality assurance and the above mentioned checks, there is no comprehensive validation procedure for the TSPA model available at present, to ensure that the computed CCDFs are accurate representations of the behavior of the repository system.

3. There are numerous unverified simplifying assumptions in many of the models.

The models for flow and transport considered only a steady rate of infiltration and a constant environment, and did not take into account the significant variations in the driving forces likely to occur over the performance assessment period. Also, the models considered that the geosphere was

---

[1] The figures shown in this chapter present the results from a demonstration of staff capability to review a performance assessment. These figures, like the demonstration, are limited by the use of many simplifying assumptions and sparse data.

spatially uniform in the lateral direction, and did not take into account the large variations in material properties that exist at the site. In addition, the behavior of many thousands of waste packages was represented by ensemble averages, using seven representative waste packages.

4. There are large uncertainties in the input data.

Although the TSPA model is intended to deal with some data uncertainty through the Latin Hypercube Sampling (LHS) process, many of the most important parameters have variations over several orders of magnitude. For many parameter distributions, the means and distribution shapes are based on only a few measurements. Also, the analysis did not recognize correlations among the independent variables in the Monte Carlo analyses, and treated all variables as independent. These situations are likely to lead to extremes in consequences. However, spatial correlations were considered , somewhat, in choosing hydrogeologic variables.

5. Coupled effects between processes and events in the scenarios have not been fully modeled nor evaluated.

In IPA Phase 2, an attempt was made to couple some events and processes such as corrosion and repository cooling. However, complex coupled interactions such as moisture movement (including infiltration) and gas transport have not been modeled in IPA Phase 2.

6. The dose calculation is for illustrative purposes.

The dose calculation is based on assumptions regarding a postulated biosphere consisting of a farm irrigated by well water, a family living on the farm, and a distant population consuming cattle raised on the farm. There has been relatively little research, as a part of IPA Phase 2, on the likelihood of these or other assumptions regarding future biospheres. In addition, many of the coefficients in the dose model are generic and not specific to the repository region.

9.2 CONDITIONAL CCDFS AND EXCEEDANCE PROBABILITY CURVES

9.2.1 Construction of the CCDFs

The CCDFs, which express the uncertainty in the model results for population doses and EPA limits for cumulative release over 10,000 years, are presented in different forms including:

- Conditional CCDFs for each scenario;
- Conditional CCDFs showing performance of individual and engineered barriers; and
- Total CCDFs combining all scenarios for both release and dose.

Normalized release, which is the primary measure of consequences displayed by the CCDF is computed by dividing each radionuclide which enters the accessible environment by its limit specified in 40 CFR Part 191, Appendix A, Table 1 and summing the resulting ratios. Effective dose

equivalent, the other measure of consequences displayed by the CCDF is described in Section 7.3.3.

Both conventional mean CCDFs and "hair" diagrams have been constructed. The following discussion presents salient points of CCDF construction for IPA Phase 2.

9.2.1.1 Conditional CCDFs

A conditional CCDF is a CCDF constructed for a single scenario class with the assumption that the scenario class has a probability of occurrence of 1.0. For each scenario class evaluated under IPA Phase 2, a conditional CCDF was constructed in the following manner:

- A vector represents a single sampling for all of the sampled variables. The total number of vectors to be selected has to be known before sampling so that each selection for each variable is made from equally probable distributions;

- Each vector is assigned an equal probability within the scenario (i.e., for 400 vectors, each vector has a probability $p_i = 1/400$);

- The set of vectors is sorted from lowest to highest consequences "R" (cumulative release or dose)

- The exceedance probability "E" of the sorted consequences is calculated by the following formula:

$$E_i = 1 - \sum_{i=1}^{N'} p'_i \quad , \tag{9-1}$$

  where "p'_i" is the probability of the ith vector of the sorted set, and "N'" = the number of vectors in the set; and

- The CCDF is the graph of "E_i" versus its sorted consequences, "R".

9.2.1.2 Screened Conditional CCDFs

This CCDF uses a set of vectors derived from the 400-vector base case scenario by screening for compliance with regulations or ranges of model input parameters. It is constructed identically to the conditional CCDF described above, but for N'' = the number of remaining vectors, and still assuming equal probability for each remaining vector, $p_{i''} = 1/N''$. Examples of possible screening criteria are waste package lifetimes greater than 300 years (or 1000 years) and infiltration rates less than .3 mm/year.

9.2.1.3 Total CCDF

The total CCDF is constructed by combining vectors from all scenarios. The probability of each

vector "p_k.", however, is taken to be the scenario probability "p_j" divided by the number of vectors, "N_j", in the scenario:

$$p_k' = \frac{p_j}{N_j} \quad . \tag{9-2}$$

The consequences are then sorted, as before, from lowest to highest. The exceedance probability is then defined:

$$E_k = \sum_{k=1}^{N'} p'_k \quad , \tag{9-3}$$

where N' the total number of vectors, and p'_k = the probabilities for the sorted consequences.

9.2.1.4 "Hair" Diagrams

Helton, *et al.* (1991, Section VI) develops an alternative method of displaying uncertainty about scenarios and parameters for probabilistic models. In this technique, "hair diagrams," there is one CCDF or "hair" per vector, which displays the cumulative probability for each vector (for which there is a new set of sampled parameters) displayed over the range of scenarios. Among the advantage of hair diagrams, Helton states the following:

> "... they maintain the distinction between scenarios, probabilities for scenarios, consequences and fixed but imprecisely known quantities....Further, these representations lead naturally to CCDFs and distributions of CCDFs. The distributions of CCDFs are important because they display the variability that is averaged over to obtain the mean CCDFs that are typically used for comparison with the EPA release limits."

Because one line is plotted for each vector, hair diagrams are complicated and difficult to interpret. To simplify them visually, yet preserve the statistical information they contain, the boundaries of the hair diagram are summarized by finding the density function of the exceedance probability at a range of values of cumulative release, and plotting only the 5th, 50th, and 95th percentiles of this density function; (i.e., for a given value of cumulative release R_i, the exceedance probabilities are interpreted from all hairs, their values sorted, and the 20th, 200th, and 380th values saved to be plotted as the 5th, 50th, and 95th percentile of the hairs.

9.2.2 Conditional CCDFs for Various Scenario Classes

Four-hundred (400) vector runs were made for nine scenario classes. These classes are identified in the following table along with their estimated probabilities of occurrence over the next 10,000 years.

Estimated Probabilities for the Scenario Classes Modeled in the IPA Phase 2 Analysis

Scenario Class	*Scenario Class Identifier*	*Estimated Probability*
Base Case	oooo	≈ 0.0
Climate Change Only (Pluvial)	cooo	≈ 0.0
Seismicity Only	osoo	7.9×10^{-5}
Drilling Only	oodo	≈ 0.0
Magmatic Activity Only	ooov	≈ 0.0
Drilling + Seismicity	osdo	0.35
Drilling + Seismicity + Magmatic Activity	osdv	1.0×10^{-2}
Drilling + Seismicity + Climate Change	csdo	0.62
Drilling + Seismicity + Magmatic Activity + Climate Change*	csdv	2.0×10^{-2}

* Fully disturbed.

Scenario classes *csdv, csdo, osdv,* and *osdo* were chosen from the 16 possible scenarios (see Section 3) to calculate the exceedance probabilities of the releases and doses from their conditional exceedance probability curves (CCDFs). These are the only scenario classes with occurrence probabilities large enough to make a significant contribution to total performance. The other cases were chosen to evaluate the effect on exceedance probabilities by disruptive events acting alone. It is assumed that any significant interaction between disruptive events (within the capabilities of the models to predict) will be picked up in the fully disturbed case *(csdv).*

9.2.3 Basic Scenarios

The basic scenarios computed for the purpose of comparison are: the base (or undisturbed) scenario *(oooo)*; the fully disturbed scenario *(csdv)*; the base case disturbed by climate-only, *(cooo)* scenario; the base case disturbed by drilling-only, *(oodo)* scenario; the base case disturbed by seismic-only, *(osoo)*; and the base case disturbed by volcanism-only, *(ooov).* The conditional exceedance probabilities (or CCDFs) for the normalized release for each scenario are presented in Figure 9-1. The dotted lines represent compliance with the EPA release standard.[2] The conditional exceedance probabilities for dose estimates[3] are

[2] Pursuant to the Nuclear Waste Policy Act of 1982, as amended, § 60.112 is to be modified to conform to EPA's containment requirements for radioactive materials.

[3] Those persons who were assumed to be exposed in the CCDFs for dose include: the members of the farm family (3 persons); and members of the regional population (177 of them are assumed to consume contaminated beef).

Figure 9-1. Conditional CCDFs for normalized releases for basic scenarios.

DEMONSTRATION PLOT ONLY, DOES NOT REPRESENT
EXPECTED REPOSITORY PERFORMANCE

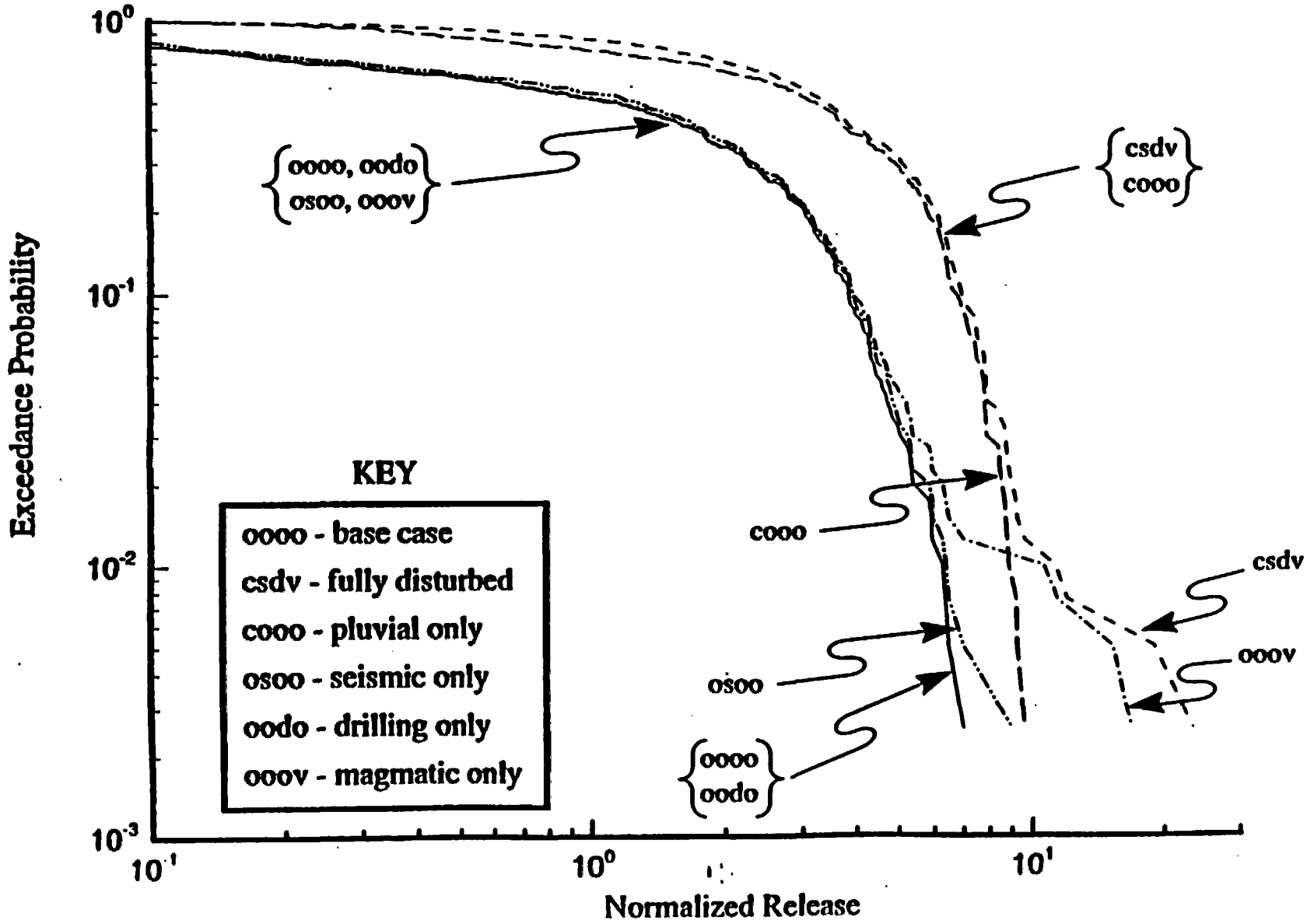

presented in Figure 9-2.

Figure 9-2. Conditional CCDFs for effective dose equivalents.

DEMONSTRATION PLOT ONLY, DOES NOT REPRESENT
EXPECTED REPOSITORY PERFORMANCE

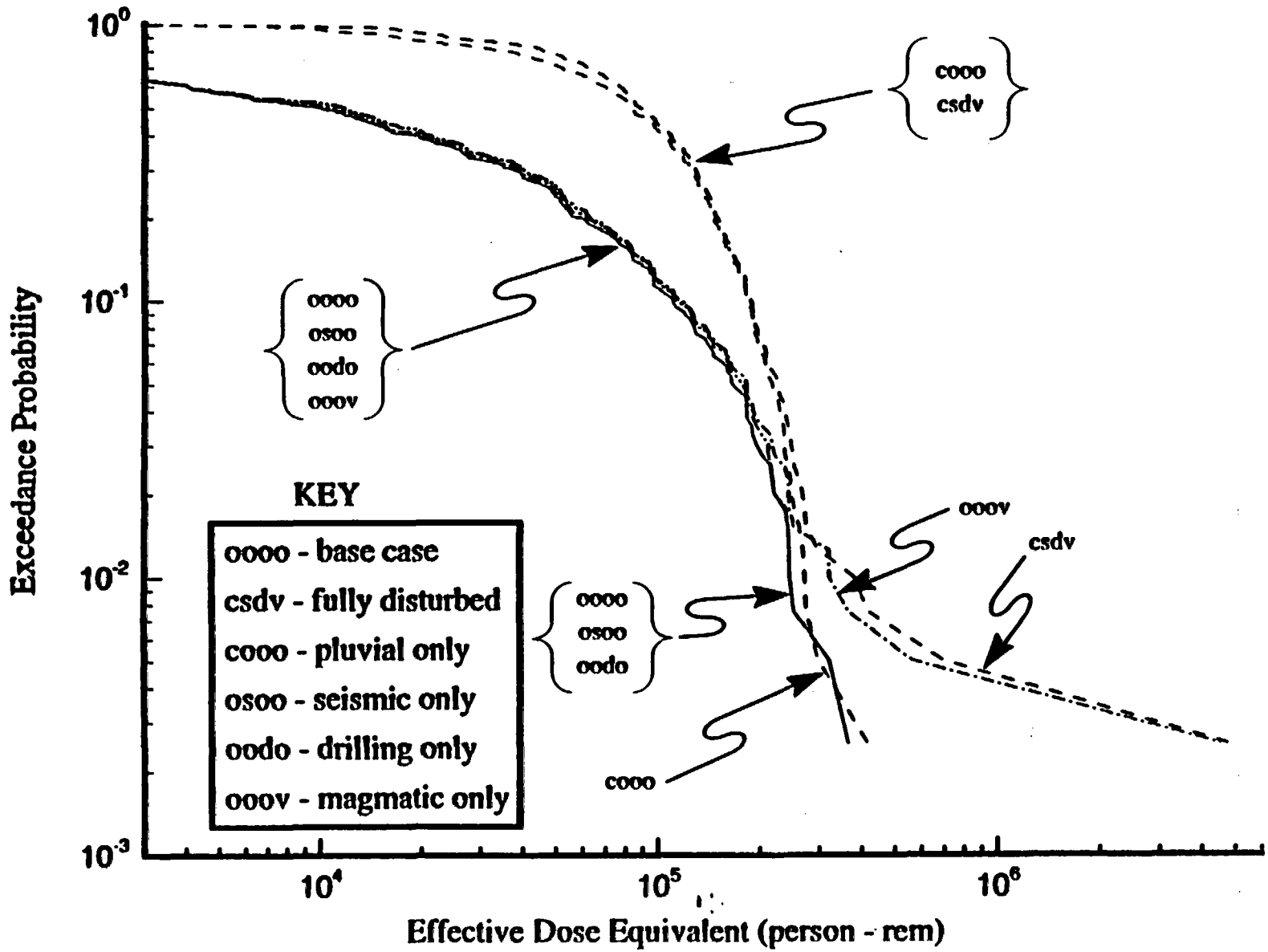

Scenario plots as defined in this report are scatter plots of the results for one scenario plotted against the results of another scenario. For the IPA Phase 2 analysis, the LHS sets contained 400 vectors for all production runs. Since all scenario runs used the same LHS set and most of the same independent variables, these plots allow the visual inspection of the effects of the scenario on the model outputs. Scenario plots were used to compare the single-event scenarios against the base case; that is, scenario *cooo* (pluvial infiltration and higher water table); *osoo* (seismicity); *oodo* (human intrusion by drilling); and *ooov* (volcanism); against *oooo* (undisturbed or base case).

The base case scenario represents the calculated releases and doses from the repository over a 10,000-year performance period, under conditions as they are presently perceived to exist (allowing for parameter uncertainty) and without disturbing events such as drilling, earthquakes, volcanism, or change to a pluvial climate. The thresholds defined for two of these disturbing events, earthquakes and drilling, give them probabilities of occurrence of almost 1.0 during the period of performance. Hence, the probability of occurrence of scenarios not containing these events is almost 0.0. The probability of having a pluvial climate within the performance assessment period is estimated to be 0.64. Therefore, the probability of the base case is very low, and is computed primarily for comparison rather than as a major contributor to the total exceedance probability curve. The fully disturbed scenario *(csdv)* represents the opposite extreme from the base case. In the fully disturbed case, all disruptive events being considered (seismicity, drilling, volcanism, and pluvial) are allowed to act on the repository. This scenario is expected to show the effects of interactions among events, as well as the effects of the events, themselves. An example of an expected interaction is pluvial climate (high water level and increased infiltration) and seismically induced waste package failures.

As can be seen by comparing the climate-only, scenario *(cooo)* with the fully disturbed case *(csdv)* in Figure 9-1, almost all the increase in normalized release in the high probability part of the fully disturbed CCDF over the base case CCDF is due to the influence of the pluvial-climate. Figure 9-3 is a scenario plot comparing the releases from the pluvial scenario with the releases from the base case for the same vectors. The influence of climate on the total releases is very significant for most vectors, even though the gas pathway is insensitive to infiltration (the IPA Phase 2 models did not explicitly consider the effects of infiltrating water on either the release of gaseous radionuclides, nor their transport in the geosphere). Although the effect of the pluvial conditions is large, there are some vectors that are nearly the same or even smaller for the pluvial case. This observation is probably caused by the following conditions:

- Contributions to cumulative release from the gas pathway are relatively large, compared with the liquid pathway.

- The higher water table during the pluvial scenario causes radionuclides to be released from the vadose zone into a less permeable and slower moving saturated zone than would be the case for the non-pluvial conditions. This results in a smaller release to the accessible environment for the same release to the saturated zone.

Human intrusion, as presented in the base case disturbed by drilling only *(oodo)*, in Figure 9-1, does not appear to have a discernable effect on the exceedance probabilities. There appears to be a low likelihood of a direct hit and relatively minor consequences when a hit is actually made. The scenario plot, Figure

Figure 9-3. Scenario plot of pluvial vs. base case.

DEMONSTRATION PLOT ONLY, DOES NOT REPRESENT
EXPECTED REPOSITORY PERFORMANCE

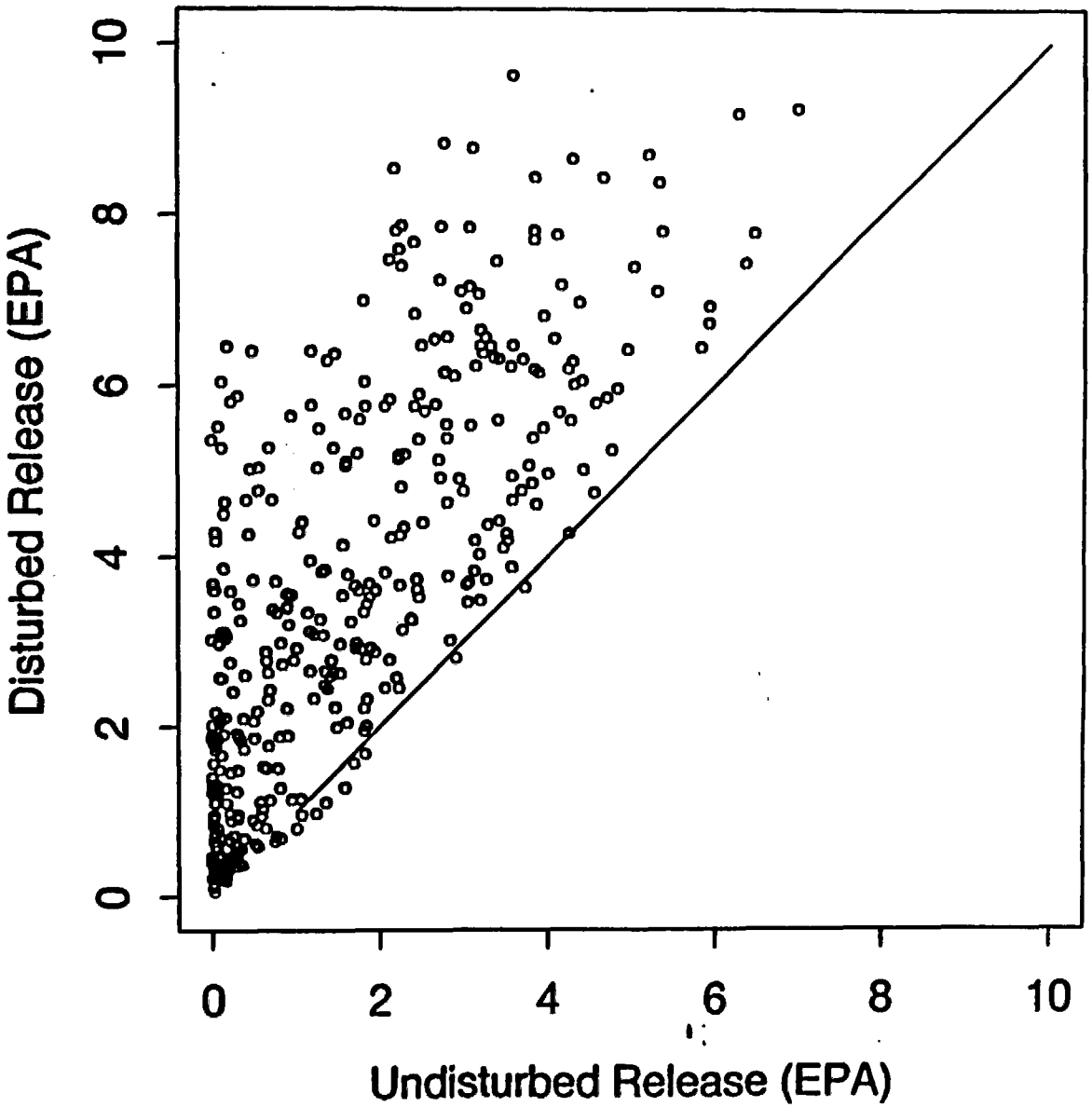

9-4, shows the releases from the liquid, gas, and direct pathways for the drilling-only scenario compared with the base case. There are only minor differences in the releases from drilling, virtually all caused by the direct releases of contaminated rock. Without the releases of contaminated rock, the comparison would plot almost perfectly as a straight line. There are only minor differences in liquid and gas releases caused by a few prematurely failed waste packages, but the results are too small to be visible on a plot. It should be noted that a more in-depth analysis, for example, one accounting for the effects of drilling fluid, could show an increase in consequences and the significance of the scenario.

The seismic-failure mechanism is considered to be very conservative. However seismic failure appears to have only a small effect on the CCDF, as shown by the comparison in Figure 9-1. Seismic loading usually shortens waste package lifetime by a small amount, resulting in little increase in the normalized releases.

The effect of seismicity is more apparent on the scenario plot, Figure 9-5a. This figure shows the total releases for the seismic-only scenario compared with the base case scenario. There are a significant number of vectors with higher releases. The way in which the seismic model is employed must permit all containers in any zone to fail simultaneously when the seismic criteria are exceeded. The vectors having the largest relative release for the seismic scenario had seismic parameters allowing relatively early seismic failure, which contributed mostly to large gaseous releases from the temperature-dependent ^{14}C source term and transport models. Liquid-only releases, presented in scenario plot, Figure 9-5b, showed a more modest effect of early seismic failures.

Like pluvial-climate, volcanism *(ooov)* appears to be the only other event to have a significant, discernable effect on the shape of the exceedance probability plot, as shown in Figure 9-1. Unlike climate, however, volcanism appears to affect only the low probability part of the curve. The likely explanation is that as with drilling into a waste package, the probability of a dike intersection with the repository is very low even under the conditional assumption that the scenario exists. With the volcanism model the probability of an intersection when coupled with the scenario probability and its consequences is high enough and the consequences high enough, that the event of volcanism was able to make a discernable modification to the base case exceedance probabilities at the tail of the distribution function.

The scenario plot in Figure 9-6 shows the total releases from liquid, gas, and direct pathways for the volcanic scenarios. There are a relatively few vectors with large releases. Most of the releases are identical with the base case because there were no volcanic events that happened within the repository area and affected releases. The largest releases were caused by volcanic cones that were assumed to bring radioactive contaminants directly to the surface. In a few cases, volcanic dikes caused premature container failure, but did not bring any contaminant directly to the surface. Subtracting out the direct releases, premature failure caused only minor excess releases of liquid and gas, too small to be visible on a plot.

9.3 TOTAL SYSTEM CCDF

The total CCDF for cumulative release for the significant scenarios, csdo, osdo, csdv and osdv, was constructed by the procedure described in Section 9.2.1 and is shown in Figure 9-7a. The corresponding

Figure 9-4. Scenario plot of drilling scenario vs. base case.

Figure 8-9

DEMONSTRATION PLOT ONLY, DOES NOT REPRESENT
EXPECTED REPOSITORY PERFORMANCE

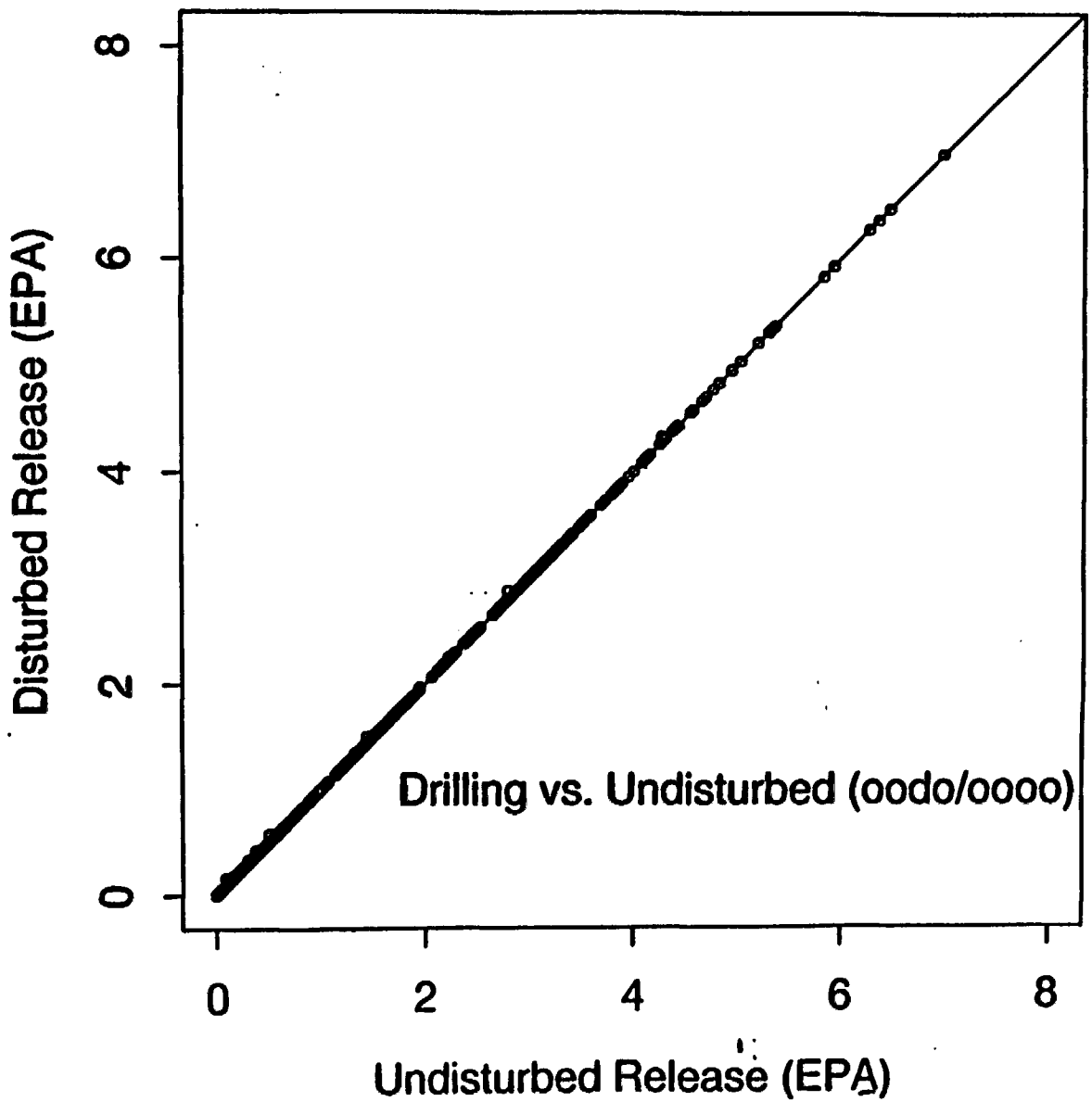

Figure 9-5a. Scenario plot of seismic scenario vs. base case.

Figure E.5a

DEMONSTRATION PLOT ONLY, DOES NOT REPRESENT
EXPECTED REPOSITORY PERFORMANCE

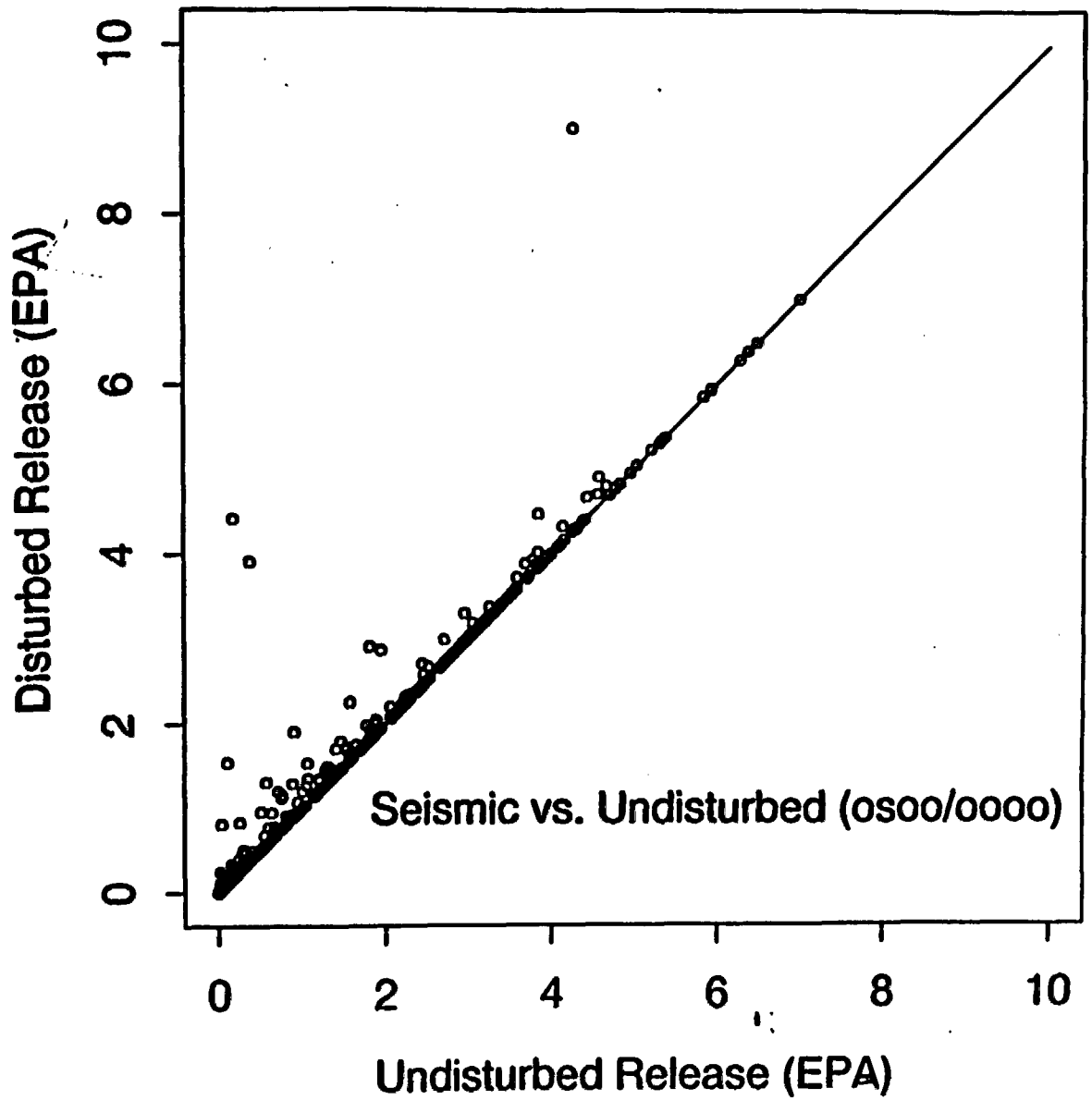

Figure 9-5b. Scenario plot of seismic scenario vs. base case (liquid only).

0500 vs 0000

Liquid only

Fig 8.5b

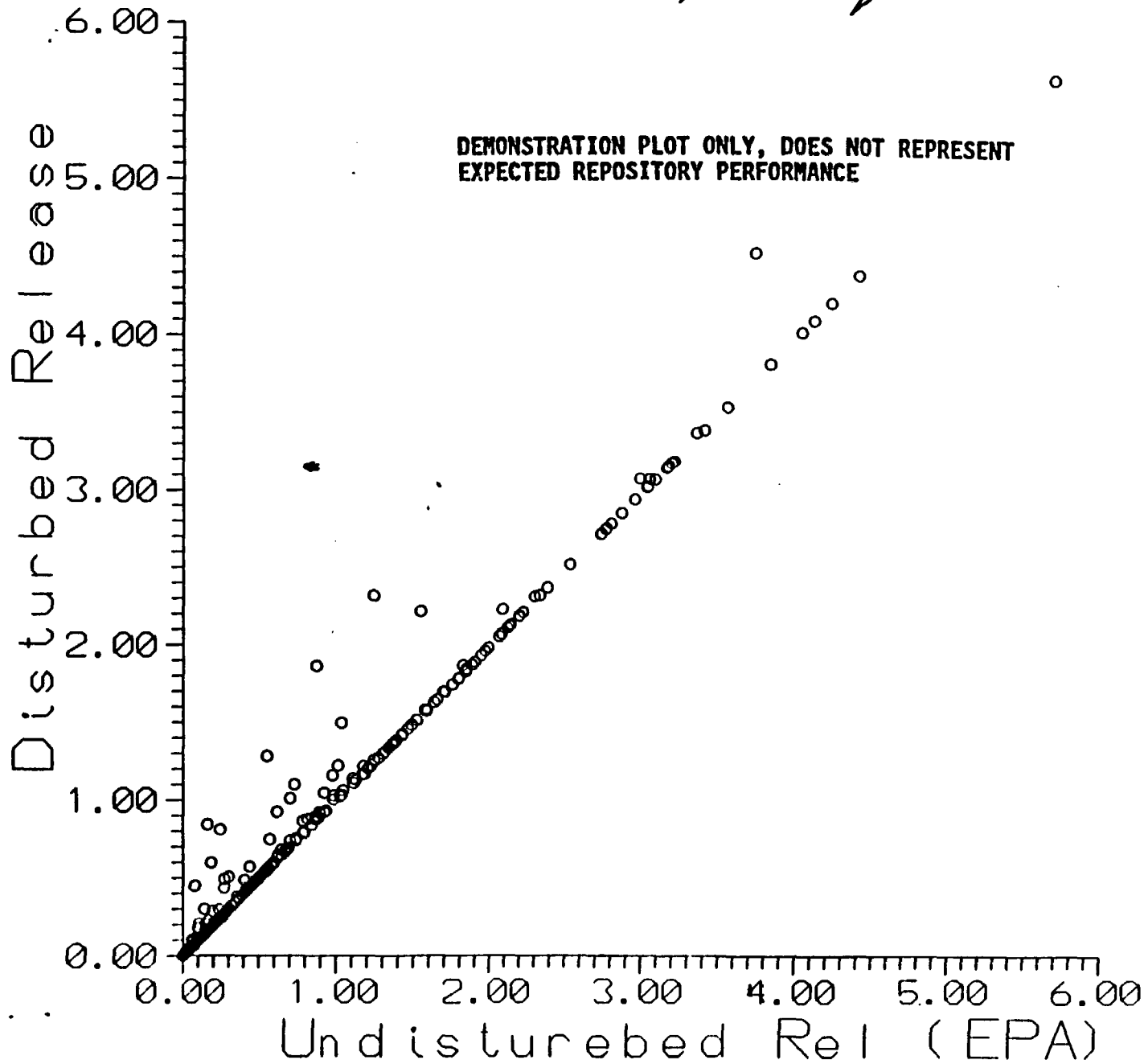

Figure 9-6. Scenario plot of magmatic scenario.

Fig 8.2-6

DEMONSTRATION PLOT ONLY, DOES NOT REPRESENT
EXPECTED REPOSITORY PERFORMANCE

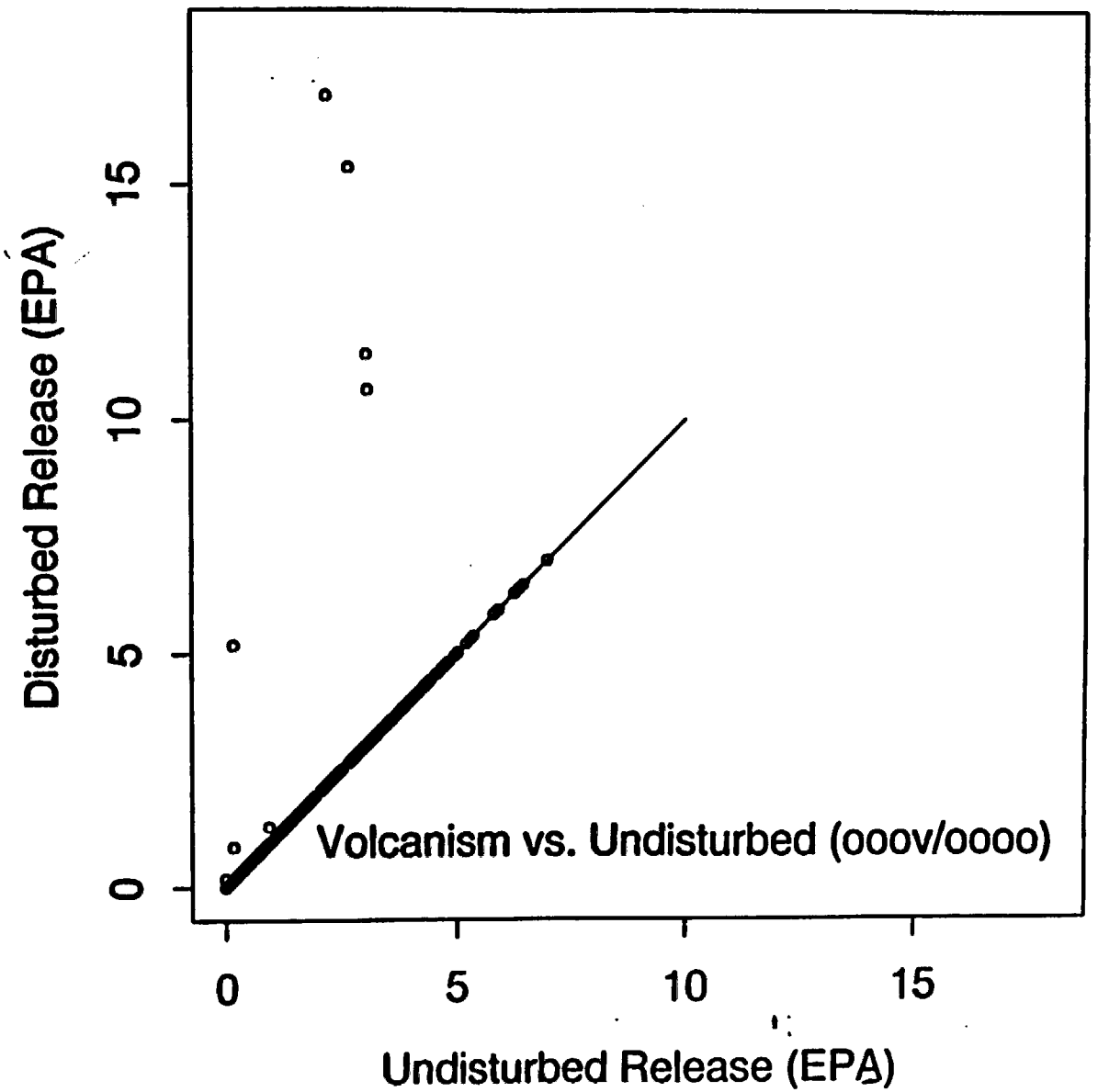

Figure 9-7a Total CCDF For normalized releases from significant scenarios

DEMONSTRATION PLOT ONLY, DOES NOT REPRESENT
EXPECTED REPOSITORY PERFORMANCE

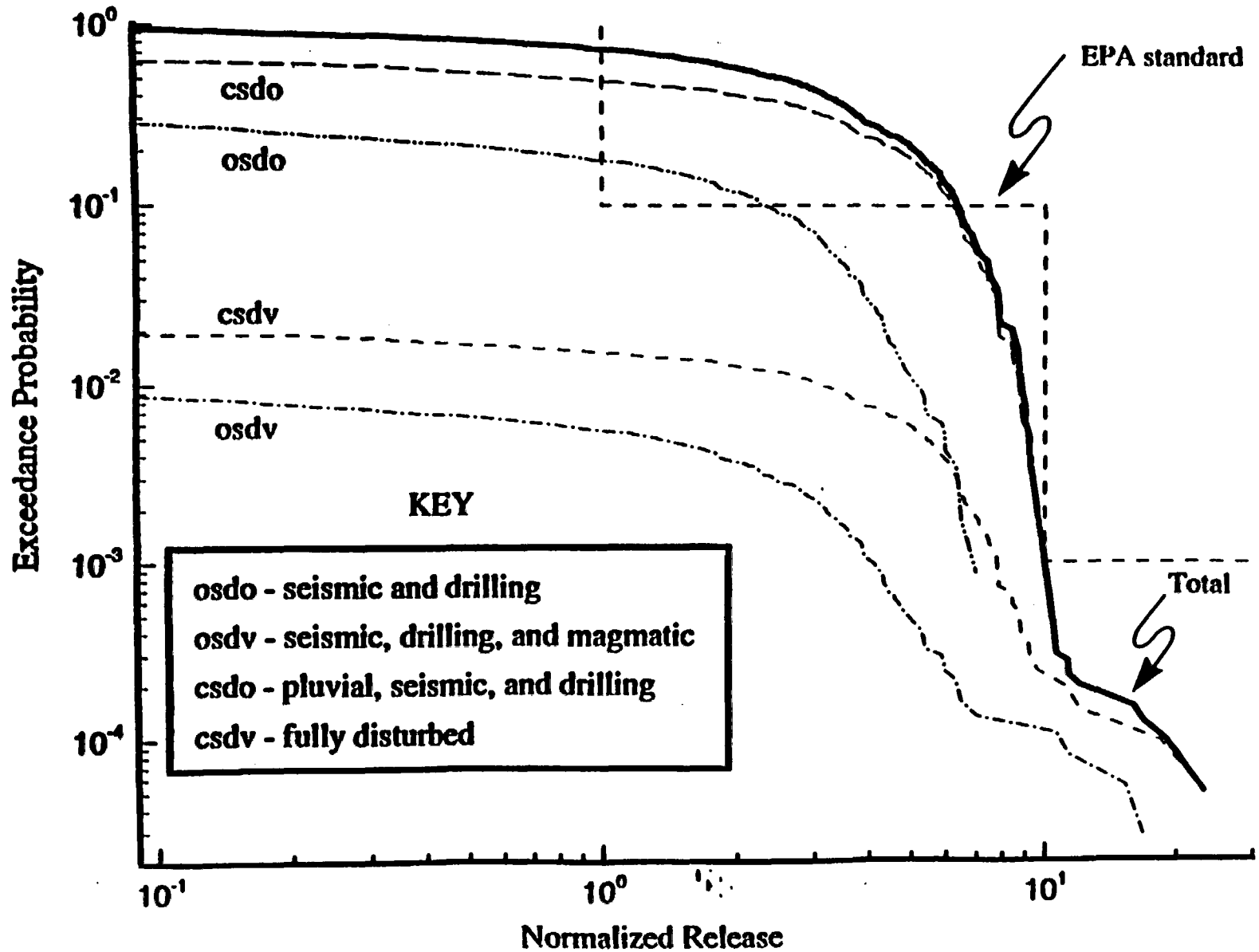

CCDF for dose is shown in Figure 9-7b. It should be noted that although the effects of a high-probability

Figure 9-7b Total CCDF for effective dose equivalent from Significant Scenarios

DEMONSTRATION PLOT ONLY, DOES NOT REPRESENT
EXPECTED REPOSITORY PERFORMANCE

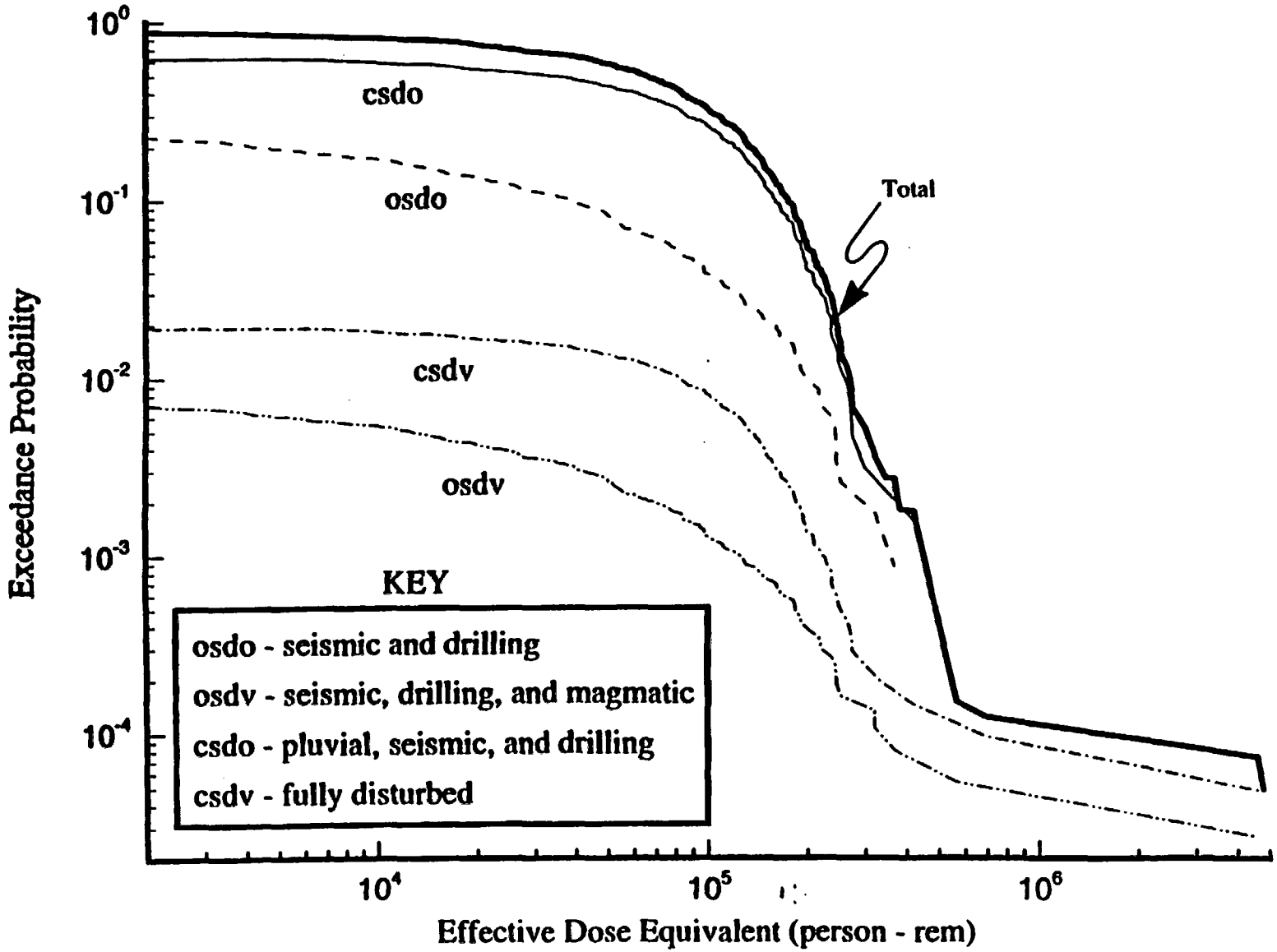

event such as pluvial-climate can still be recognized in the total CCDF, the effects of low-probability events such as volcanism are obscured. To better preserve the effects of both low- and high-probability events, Figure 9-8a shows the same information used to construct the total CCDF, but plotted as a "hair" diagram, as described in Section 9.2.1. Figure 9-8b shows the 5th, 50th and 95th percentiles of the hairs, as boundaries from the hair diagram. The significance of the "hair diagram" is to present the entire range of credible releases from the repository as a function of scenario probability and parameter uncertainty. The curve shown in Figure 9-7a incorporates scenario probability and parameter uncertainty into a single curve, without providing a means of separately evaluating the effects of either.

9.4 DIFFERENCES BETWEEN IPA PHASES 1 AND 2, AND COMPARISON OF RESULTS

A complete discussion of results from this TSPA and future TSPAs must include an evaluation of why the results differ among various analyses. If a baseline CCDF is established, the effects of changing assumptions and parameter values can be quantitatively examined. At the present time, the only baseline developed by the staff for comparison is the CCDF from the IPA Phase 1 study. IPA Phases 1 and 2 were significantly different in terms of scope and approach, in many areas. A description of the major improvements in Phase 2 over Phase 1 provides an indication of the amount and relative significance of factors that may be influencing the difference.

9.4.1 Improvements in IPA Phase 2 Likely to Affect Results

9.4.1.1 Scenarios

Only a limited set of scenario classes was considered in IPA Phase 1, drilling and pluvial conditions, resulting in four scenarios. However, for the IPA Phase 2 analysis, the staff applied the Sandia National Laboratories (SNL) scenario-selection methodology for use in the consequence analysis of a potential high-level waste (HLW) disposal site (see Cranwell, *et al.*, 1990). Based on the staff evaluation and modification of the SNL methodology, four scenario classes were considered (climate change, seismicity, magamatism, and human intrusion) from which 16 scenarios resulted. In phase 1, the occurrence probability of pluvial-climate was assumed to be 0.10. In phase 2, the occurrence probability of pluvial climate was determined to be 0.64 (Chapter 3). The probability of the drilling scenario class at the site was determined to be approximately equal to 1.0 in both Phase 1 and Phase 2.

9.4.1.2 Pathways

The IPA Phase 1 effort identified and accounted for a number of important attributes of the Yucca Mountain site (e.g., stratigraphic changes below the repository in the unsaturated zone and differences between matrix and fracture flow). As discussed in Chapter 4, the IPA Phase 2 effort not only has maintained the important attributes identified in the Phase 1, study but has added further modeling complexity such as:

- saturated zone pathways to the accessible environment;
- calculation of radionuclide concentration for dose assessment; and

Figure 9-8a. "hair diagram" showing all normalized release vectors.

Figure 8a

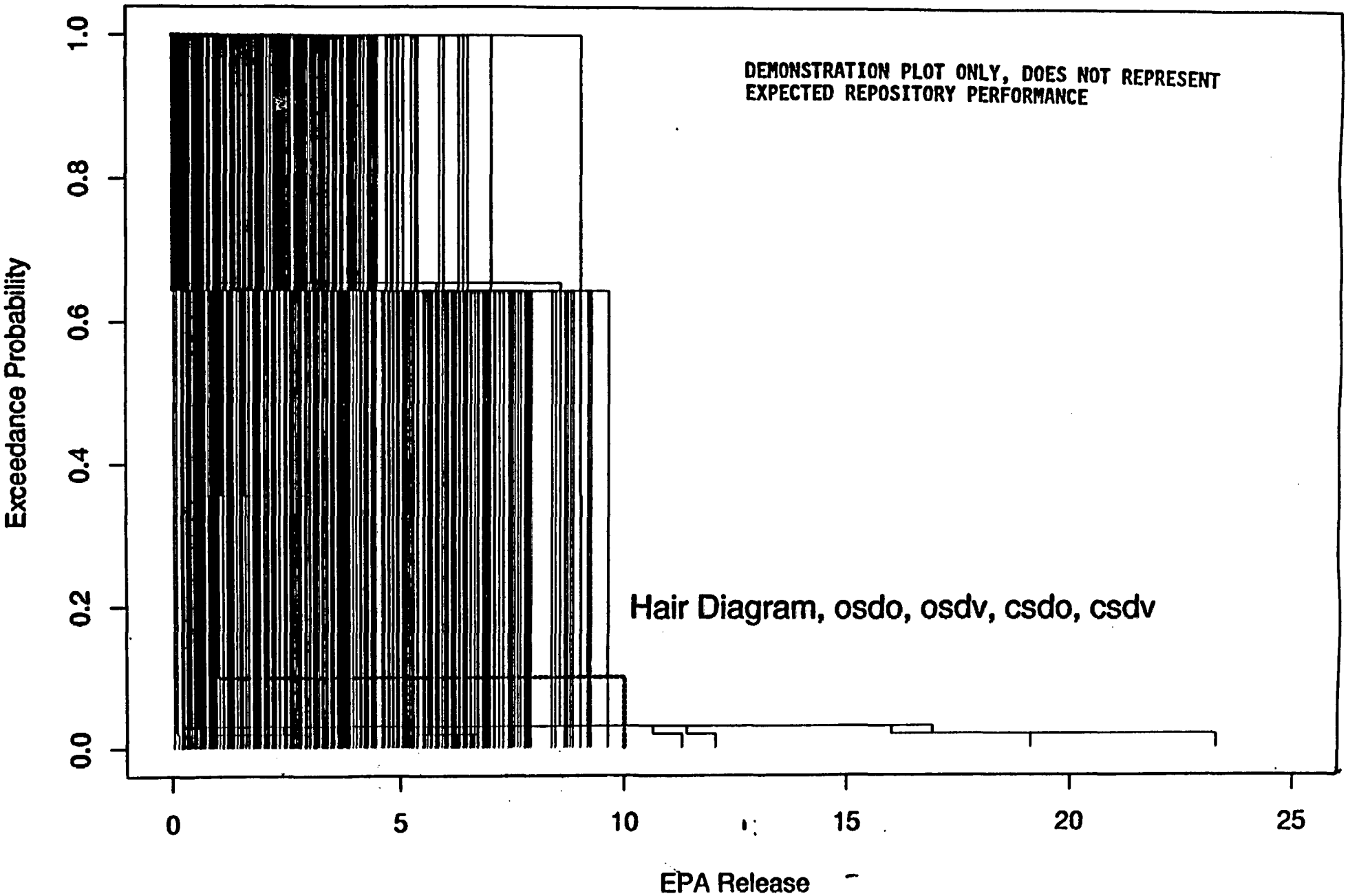
DEMONSTRATION PLOT ONLY, DOES NOT REPRESENT
EXPECTED REPOSITORY PERFORMANCE
Hair Diagram, osdo, osdv, csdo, csdv
Exceedance Probability
0.0
0.2
0.4
0.6
0.8
1.0
0
5
10
15
20
25
EPA Release

Figure 9-8b. Percentile values of release vectors from "hair diagrams."

Figure 8-86

DEMONSTRATION PLOT ONLY, DOES NOT REPRESENT
EXPECTED REPOSITORY PERFORMANCE

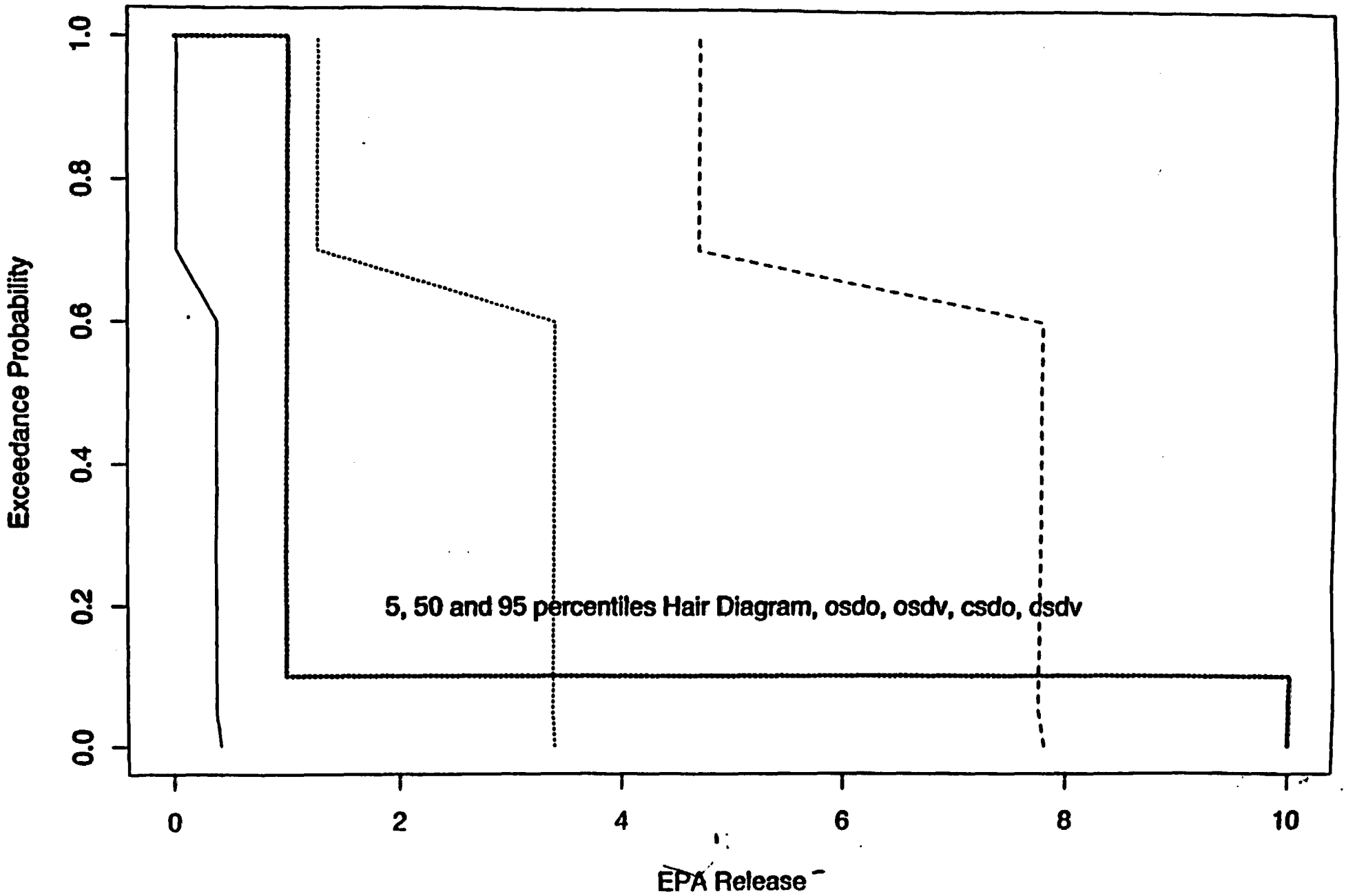

- both fracture and matrix pathways allowed within a vector.

The additional complexity provided additional insights into: the performance of fractured rock as geologic barrier; data requirements; and the capabilities of the utilized computational methods.

Also, three transport pathways were considered in IPA Phase 2 (i.e., gaseous, aqueous, and direct) compared with one transport pathway (i.e., aqueous) in IPA Phase 1. In the gas-phase transport calculations, advection, radioactive decay, and temperature effects were considered. The retardation coefficients used for the gas-phase calculation also accounted for equilibrium speciation.

9.4.1.3 Source Term

The modeling of waste-package failure was nonmechanistic in IPA Phase 1. The model used by the staff to calculate the source term in IPA Phase 1 was that incorporated in the *NEFTRAN* computer code obtained from SNL (see Longsine *et al.*, 1987). In this model, radionuclide releases would occur only after failure of the waste package, characterized as a single failure time for the entire repository.

As discussed in Chapter 5, the staff developed its own computer code to calculate the source term in IPA Phase 2. The *SOTEC* module (see Sagar, *et al.* (1992)) deals with the calculation of aqueous and gaseous radionuclide time- and space-dependent source terms for the geologic repository. It does so by considering the variations in those physical processes expected to be important for the release of radionuclides from the engineered barrier system (EBS).

Three primary calculations are done in *SOTEC:* (a) failure of waste packages because of a combination of corrosion processes and mechanical stresses; (b) the leaching of spent fuel; and (c) the release of $^{14}CO_2$ gas from the oxidation of UO_2 and other components in spent nuclear fuel and hardware. Other principal features of the IPA Phase 2 source-term model include representation of the repository by seven separate regions and the consideration of 20 radionuclides, based on a screening analysis. The IPA Phase 1 analysis considered 28 radionuclides. The screening analysis for radionuclides is described in Section 5.2.4 of this report.

9.4.2 Possible Reasons for Differences in Results

Figure 9-9 shows the total system CCDFs for the IPA Phase 1 and Phase 2 analyses. The Phase 1 CCDF has relatively higher releases in the high-risk portion of the curve (i.e., the left side), but lower releases in the low-risk portion. As discussed in Section 9.4.1, the Phase 1 and Phase 2 models were quite different in a number of important aspects, so it is difficult to pinpoint the exact causes of the differences in results. Some of the differences in the Total system CCDFs may have been caused by the following specific factors:

1. *Waste package failure model* – The IPA Phase 1 study had a non-mechanistic model of canister failure, which assumed a probability distribution of failure times. Furthermore, all canisters in the four modeled repository zones were assumed to fail at the same time. The IPA Phase 2 model employs a mechanistic model of canister failure that calculates the failure time based on

Figure 9-9. Comparision of CCDFs for IPA Phases 1 and 2.

(2D) || Print || 22 Nov 1993 || tot1and2.plt || Total ccdf for Phase 1 & xsdx scenarios in Phase 2.

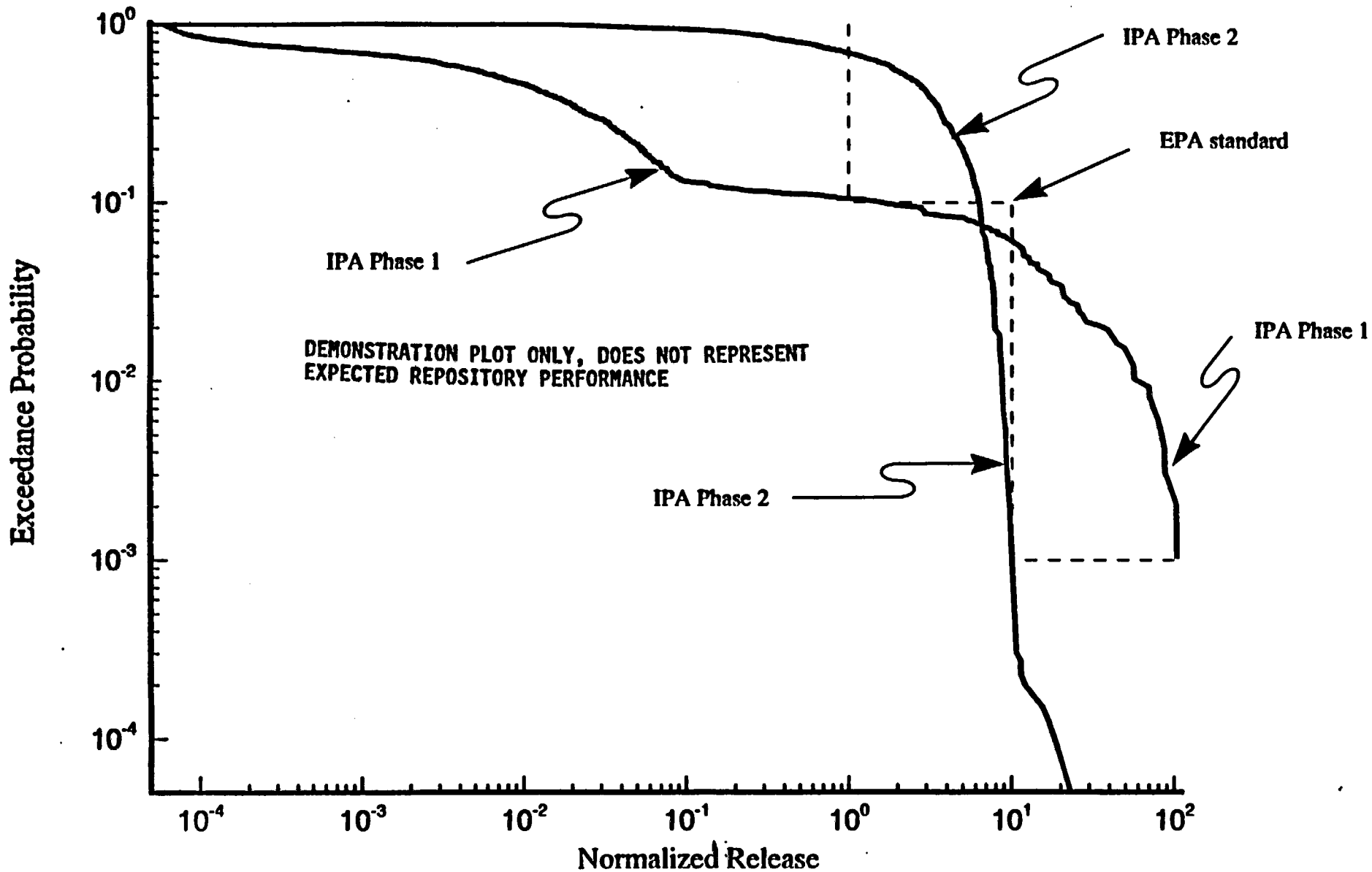

assumptions about canister wetting, corrosion, and seismic forces. Furthermore, the failure times of the canisters in the seven modeled zones were independent of each other.

2. *Release rate from failed canisters* -- The IPA Phase 1 model for source term based release rate of dissolved radionuclides from the waste form on the solubility of either the uranium matrix or the individual radionuclides for a given flow rate through the canister, and carried away only in the advective flow. Carbon-14 gaseous releases were not included explicitly in the IPA Phase 1 model. The IPA Phase 2 model includes several important improvements:

   - solubility limited by collection of isotopes of each element
   - a temperature-dependent model for ^{14}C release from several compartments of the fuel
   - diffusive as well as advective transport from the canister

3. *Several of the parameters common to both IPA Phases 1 and 2 had different values.*
   Rate of water influx -- this value was an assumed fraction of the infiltration rate in IPA Phase 1, but was calculated explicitly from the fracture-flow modeling in Phase 2. Only fracture flow at the repository horizon contributed to advective transport through the canister.

   Contact fraction with waste -- The fraction of infiltrating water contacting the waste was chosen from a uniform distribution in both the Phase 1 and 2 models from a range related to the cross sectional area of the boreholes. The contact fraction was chosen to be 0.002 to 0.01 in Phase 1. The equivalent range for Phase 2 was about 0 to 0.002, which is considerably lower. Furthermore, only the fracture flow portion of the total infiltration could reach the waste package in Phase 2, whereas both the fracture and matrix flow parts of the flow could be involved in Phase 1.

   Infiltration Rate -- The range of infiltration rates for the base case and the pluvial-climate case was the same in both IPA Phase 1 and Phase 2. The type of distribution chosen was different, however. A uniform distribution was chosen in Phase 1 for both the base case and the pluvial case. For IPA Phase 2, a log-uniform distribution was assumed for both cases.

4. *Radionuclide contributions* -- The largest contributors to cumulative release at the accessible environment for the IPA Phase 1 study were the isotopes of plutonium, but they were relatively unimportant in Phase 2. The solubility range of plutonium for IPA Phase 1 was 5.0E-5 to 3.0E-3 Kg/m^3 sampled from a log-uniform distribution. In IPA Phase 2, thermodynamic calculations and the consideration of both oxidizing and reducing environments resulted in a range of 2.0E-7 to 5.0E-4, which is considerably smaller. Furthermore, solubility in Phase 1 was based on single radionuclides, wherever the IPA Phase 2 model considered all isotopes of an element in this determination.

5. *Carbon-14 gaseous releases* -- The IPA Phase 1 model did not include the releases of ^{14}C gas to

the accessible environment. The release of ^{14}C gas was a major contributor to the cumulative release to the accessible environment in the IPA Phase 2 model. Furthermore, the IPA Phase 2 model predicted this release to occur at high conditional probabilities and independent of the release of the dissolved radionuclides.

6. *Scenario probabilities* -- Except as noted under item 3 above; the application of the pluvial-climate scenario has been reasonably similar in both IPA Phases 1 and 2. However, the probability of the pluvial-climate was arbitrarily assumed to be 0.10 in IPA Phase 1 and determined by analysis of paleo-hydrologic data to be 0.64 in IPA Phase 2. In both IPA phases, pluvial-climate conditions result in a significant increase in releases at high conditional probabilities.

9.4.3 Conclusions

The modeling improvements from phase 1 to phase 2 were numerous and in some cases cannot be easily separated, such as in the case of canister-failure mechanisms resulting in the release of ^{14}C and other radionuclides and the incorporation of a gas-transport pathway. Hence, the calculation of a quantitative measure of the effect of each individual change or improvement is not considered feasible. A visual inspection of the curves indicates that the difference in occurrence probabilities assigned to the pluvial-climate scenario, and the incorporation of the gas pathway in Phase 2 may be the primary factors. In future IPA phases it will be feasible to analyze the effect on the CCDF for every significant change in the analysis, including modifications to models, parameter distributions, and scenario classes.

9.5 EFFECTS OF MODELED PERFORMANCE OF NATURAL AND ENGINEERED BARRIERS ON TOTAL SYSTEM PERFORMANCE

This section presents repository performance in terms of factors related to the behavior of the engineered and natural barriers. In IPA Phase 2, the factors investigated were the integrity of the waste packages, the rate of release of radionuclides from the engineered barriers and the travel time of water through the geosphere. One of the primary goals of IPA is to give insight to the effectiveness and ability to implement the regulations applicable to the repository. The regulations in 10 CFR 60.113[19] address three "subsystem performance factors," namely ground-water travel time (GWTT), substantially complete containment (SCC) and release rate from the engineered barrier system (EBS). The results presented in this section portray the total system performance in terms of our understanding of the primary factors of waste containment. The calculations are not for the purpose of directly drawing a comparison between total system performance in terms of release or dose and the subsystem performance measure. There are primarily two reasons for this distinction: (1) the subsystem performance measures are supposed to be independent requirements ensuring a minimal performance of each of the multiple barriers in a repository, unrelated to the total system performance; and (2) the characterizations of GWTT, SCC, and EBS release rate used in IPA Phase 2 are crude and incomplete, and do not exactly conform to the definitions of those quantities in 10 CFR 60. For example, travel time, as used here, does not include the concept of the disturbed zone and is for post-emplacement rather than pre-emplacement conditions. Furthermore, travel time calculated in the system program is an abstraction based on the fastest combination of possible fracture and matrix pathways, and does not correspond to a realistic flow path. Nevertheless, the

following comparisons shed light on the importance of the engineered and natural barriers to the total system performance.

Screened Conditional CCDFs are used for these comparisons. As explained in Section 9.2.1, these plots are generated by "screening out" vectors according to a criterion, and using only the remaining vectors to produce the CCDFs. The criteria used in the present study were:

- Infiltration less than 1 or 2 mm/year (discussed in Section 10.3).
- Travel time of water in geosphere less than 1200, 1100, and 1000 years (discussed in Section 9.5.1).
- Release rates of radionuclides from the EBS less than 10^{-5}/year of the 1000 year inventory (discussed in Section 9.5.2).
- Waste package lifetimes of 300 or 1000 years (discussed in Section 9.5.3).

9.5.1 Effect of Travel Time of Water through the Geosphere

The NRC regulations in 10 CFR 60.113(a)(2) proscribe that the site for a geologic repository possesses the property of pre-emplacement groundwater travel time (GWTT) along the fastest pathway from the disturbed zone to the accessible environment of less than 1000 years (or other criteria chosen by the Commission (10 CFR 60.113(b)). Since there is not yet an unambiguous definition of GWTT, four distinct liquid travel times have been defined for each vector for the present study:

- *Fastest* -- the minimum time for the transport of a non-diffusing particle along the fastest combination of possible matrix and fracture pathways in any of the seven flow columns representing the repository.
- *Most flux* -- the travel time through the pathway associated with the greatest flux from the repository to the accessible environment.
- *Flux averaged* -- the average travel time for all paths, weighted by the flux in each path.
- *Averaged* -- the average travel time for all paths, irrespective of the flux in each path.

For the purpose of IPA Phase 2, only liquid releases were included in this analysis; releases of gaseous ^{14}C were completely insensitive to liquid travel time. Carbon-14 was the major contributor to the normalized releases, therefore the inclusion of gaseous releases would have further masked the sensitivity of normalized release to travel time. Figure 9-10a shows the scatter plot of liquid travel time vs. normalized liquid release for each of the four definitions of travel time listed above. Fastest travel time and most flux travel time are similarly distributed with travel times controlled by fracture flow clustered at the short time end and travel times controlled by matrix flow at the long time end. Also, similarly distributed are average travel time and flux averaged travel time. The fact that the fastest travel times

Figure 9-10a Scatter plots of liquid travel time.

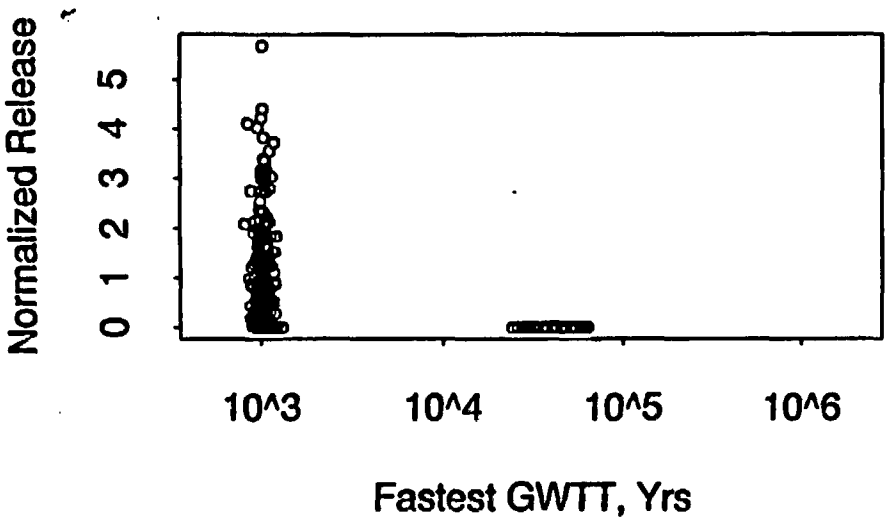

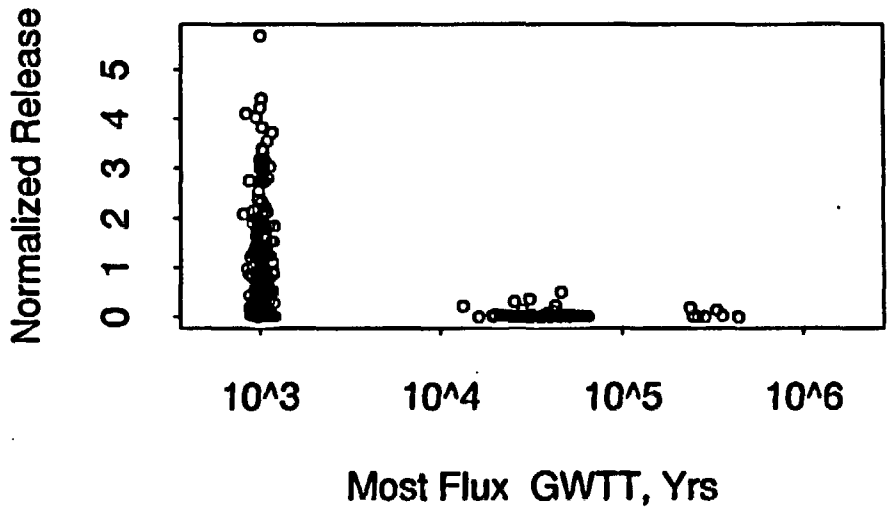

DEMONSTRATION PLOT ONLY, DOES NOT REPRESENT
EXPECTED REPOSITORY PERFORMANCE

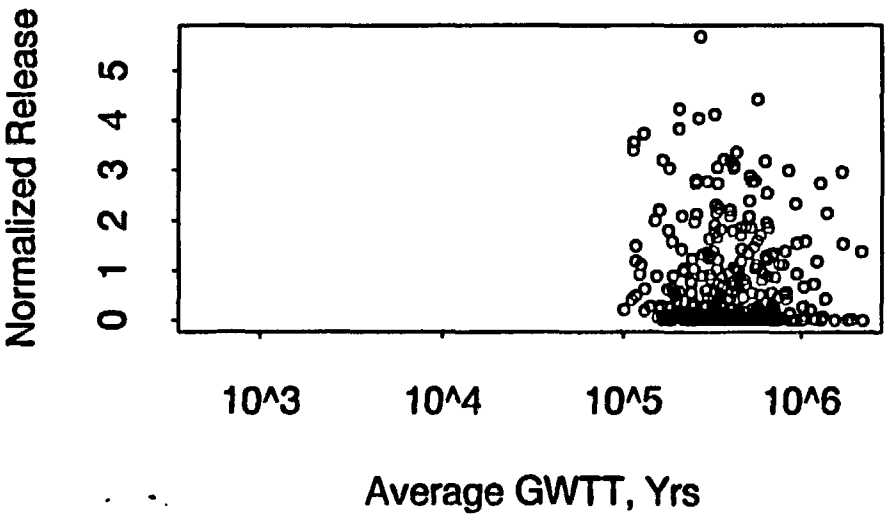

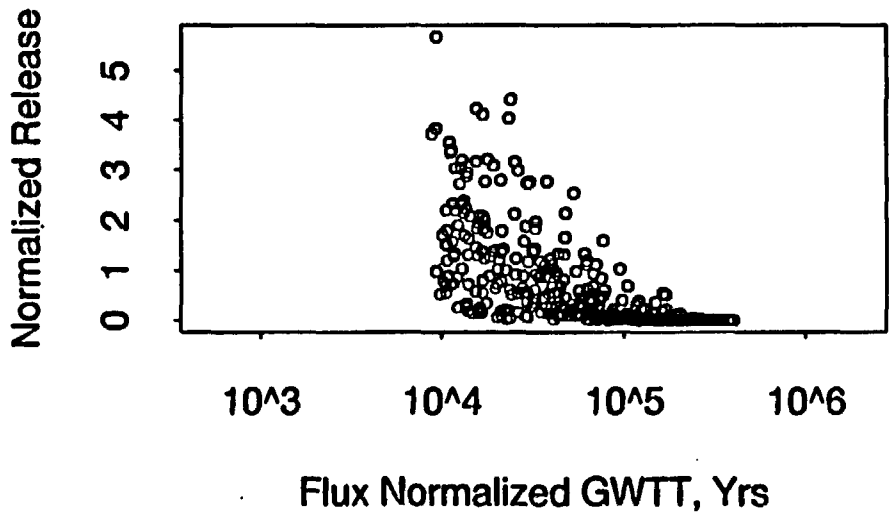

and most flux travel times are clustered around 1,000 years for cases controlled by fracture flow is an aspect of the site and the models chosen. Correlation coefficients were also calculated for the relationship between normalized liquid release and travel time for the four definitions. The flux normalized travel time had the highest coefficient correlation (-.52), followed by most flux (-.23), fastest (-.17), and average (-.05).

Figure 9-10b shows the sensitivity of the CCDF of liquid release in the base case scenario to excluding all or portions of cases with some fracture flow. As expected, excluding all cases involving a fast path to the accessible environment reduces liquid releases to very small amounts. Excluding, some of the fast path cases by using a criterion of 1,000 or 1,100 years does not have a significant effect on the CCDF even though a large portion of the fast path cases are being removed.

9.5.2 Effect of Release Rate from the EBS

The NRC regulations set forth in 10 CFR 60.113(a)(1)(ii)(B) specify that the release rate of any radionuclides from the engineered barrier system (EBS) should be 10^{-5}/year or less of the 1000 year inventory. Figure 9-11 shows that the CCDF for the base case scenario responds mildly to screening out the vectors that had release rates greater than 10^{-5}/year of the 1000 year inventory and greater than 0.1 percent of the calculated total release rate limit.

9.5.3 Effect of Waste Package Lifetime

Figure 9-12a shows the distribution of waste package failure time for the base case scenario. Figure 9-12b shows the CCDF sensitivity to screening for waste package lifetime (other than initial failures) which are less than 300 or 1000 years, as specified in 10 CFR 60.113(a)(1)(ii)(A). Long waste package lifetimes substantially decrease the release. Much of this benefit is derived from the suppression of releases of ^{14}C from early failures of containers, during the time when the containers are hot and gaseous travel times are shortest. Figure 9-12c shows the CCDF sensitivity plot for the same case, but for gaseous releases only. Figure 9-12d shows a scatterplot for all vectors of gaseous ^{14}C release to the accessible environment as a function of minimum failure time. There is a clear trend of high gaseous releases for short waste package lifetimes.

The effect of waste package failure time on compliance with the NRC release rate criterion was also investigated. Figure 9-12e is a scatter plot of fraction of the 1000-year inventory being released through the engineered barrier system (EBS), for dissolved radionuclides (including ^{14}C) versus the time of the maximum release for four selected radionuclides. The bi-modal nature of the plots for three of the radionuclides is caused by the large differences in cooling time (and therefore time-of-container failure) for different parts of the geologic repository. There does not appear to be any significant relationship between time of release and EBS release rate of dissolved radionuclides. Americium-241 has a relatively short half-life and is not a daughter of any of the other radionuclides in the list, and therefore does not display a bi-modal distribution. Although not plotted, one would expect that short failure times would also be related to higher releases of gaseous ^{14}C because of the dependence of the release model on temperature.

9.5.4 Effects of the Performance of All Natural and Engineered Barriers

Figure 9-13 shows the CCDFs for total liquid and gas cumulative releases in the base case scenario, with

Figure 9-10b CCDF sensitivity plot for "fastest" liquid travel time.

Fig 8-106

DEMONSTRATION PLOT ONLY, DOES NOT REPRESENT
EXPECTED REPOSITORY PERFORMANCE

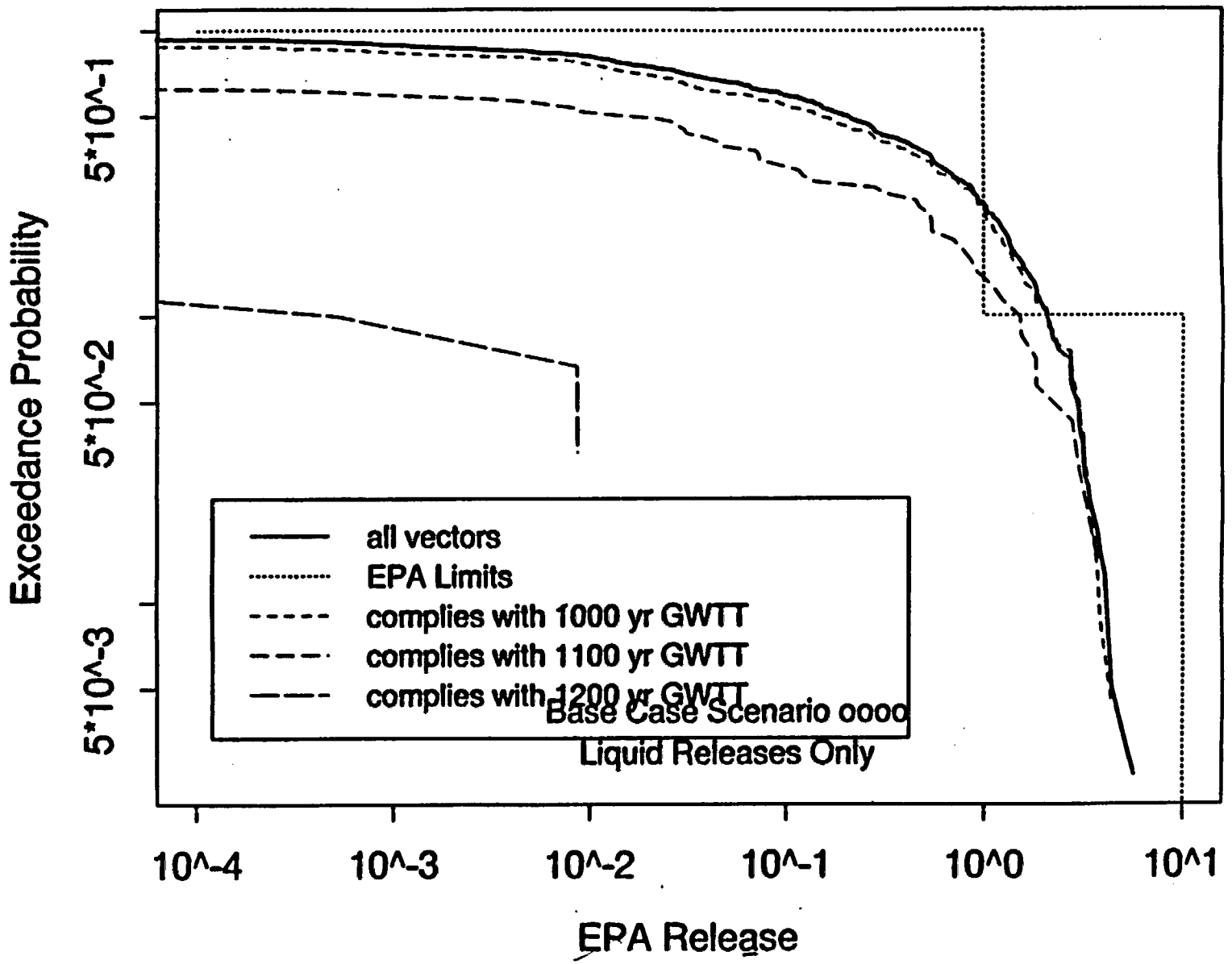

Figure 9-11. CCDF sensitivity plot for release rate from EBS.

Figure 8-11

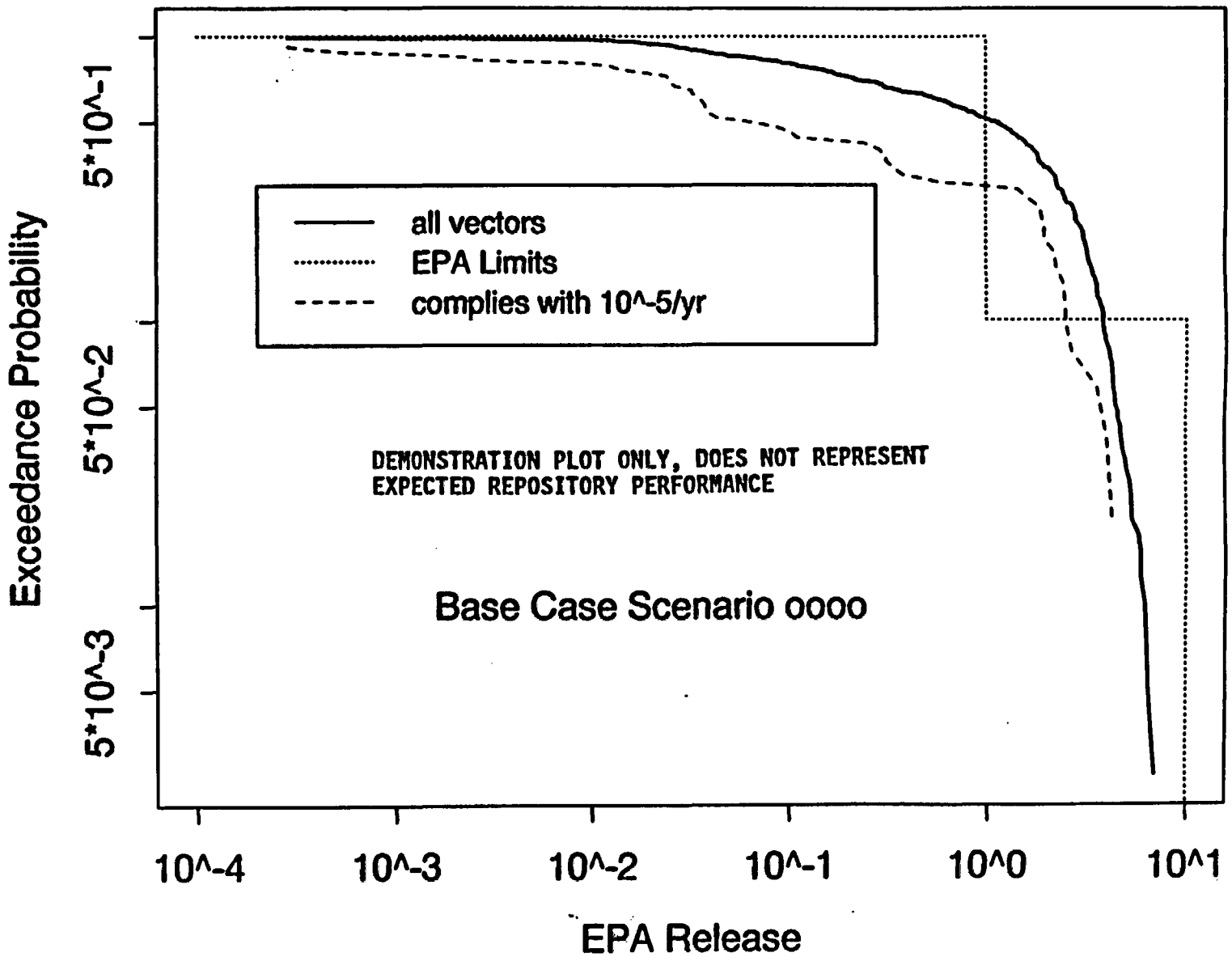
Exceedance Probability
5*10^-1
5*10^-2
5*10^-3
all vectors
EPA Limits
complies with 10^-5/yr
DEMONSTRATION PLOT ONLY, DOES NOT REPRESENT
EXPECTED REPOSITORY PERFORMANCE
Base Case Scenario oooo
10^-4
10^-3
10^-2
10^-1
10^0
10^1
EPA Release

Figure 9-12a. Waste package failure times for base case.

Fig. 8-12a

Corrosions for whole repository/oooo

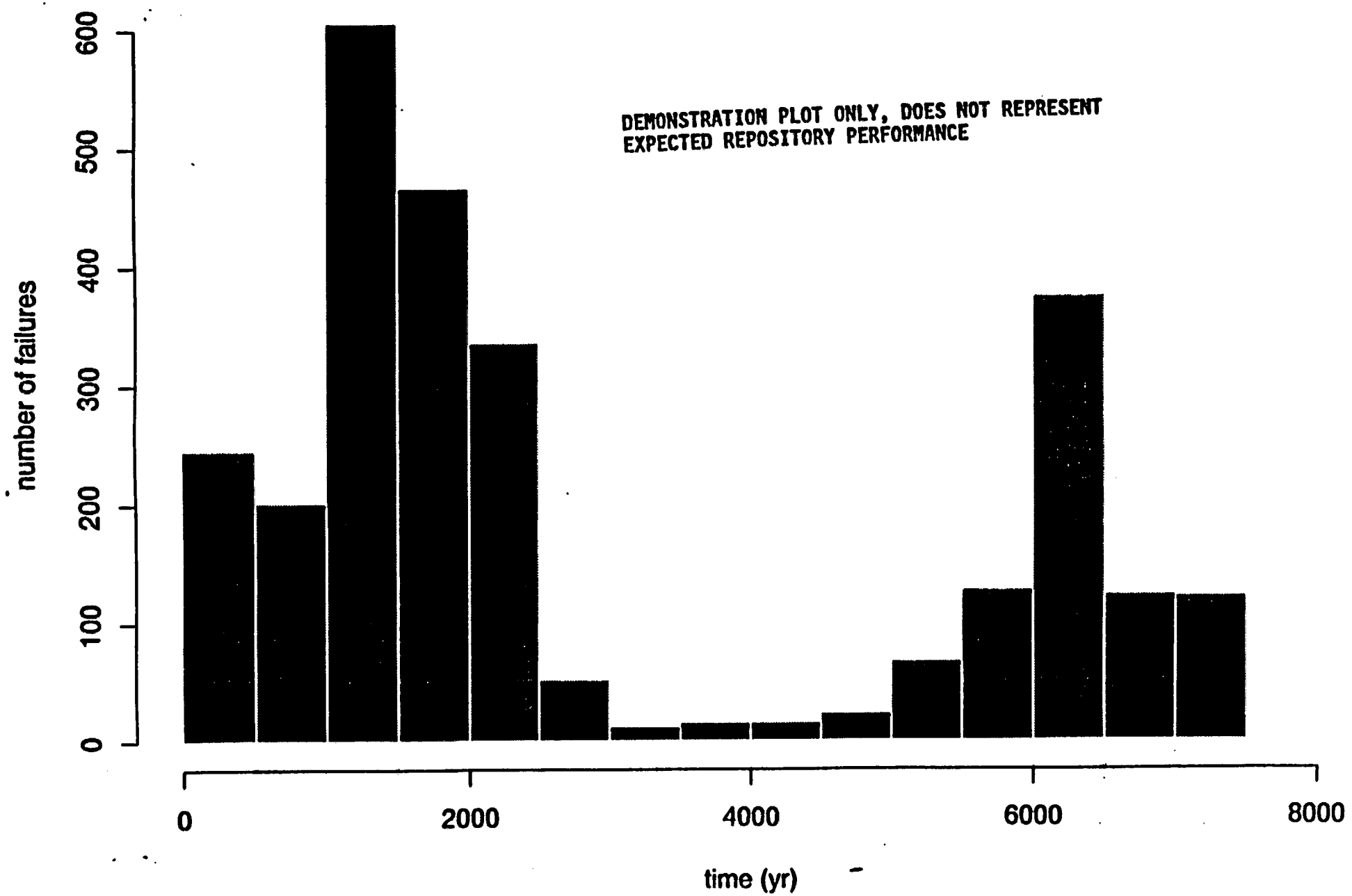

Figure 9-12b. CCDF sensitivity plot for waste package failure times for base case.

Fig 8.-12b
(Cont'd 1985

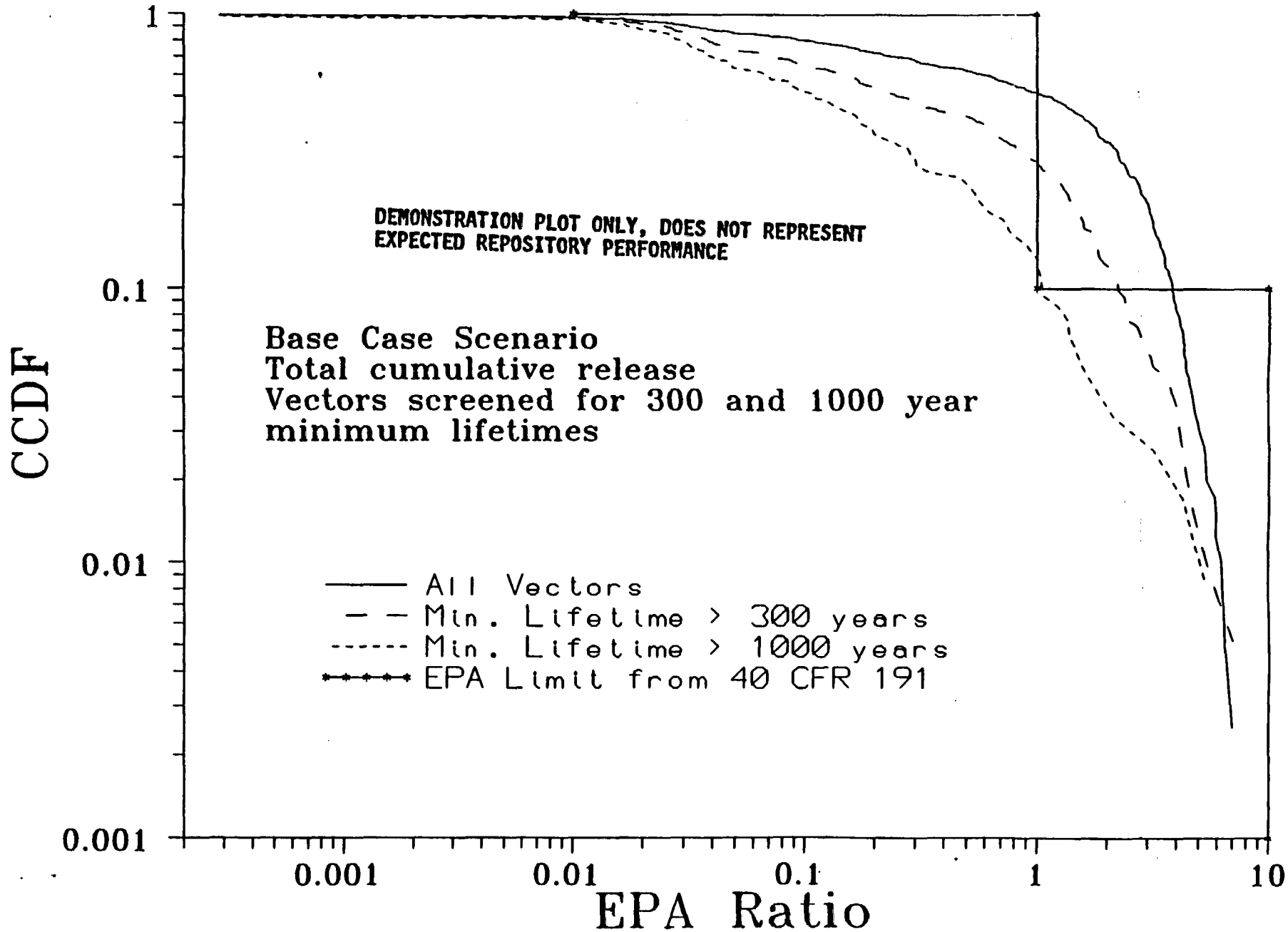

Figure 9-12c. CCDF sensitivity plot for waste package failure times for base case (gaseous release only).

Figure 8-14c
Gas only

DEMONSTRATION PLOT ONLY, DOES NOT REPRESENT
EXPECTED REPOSITORY PERFORMANCE

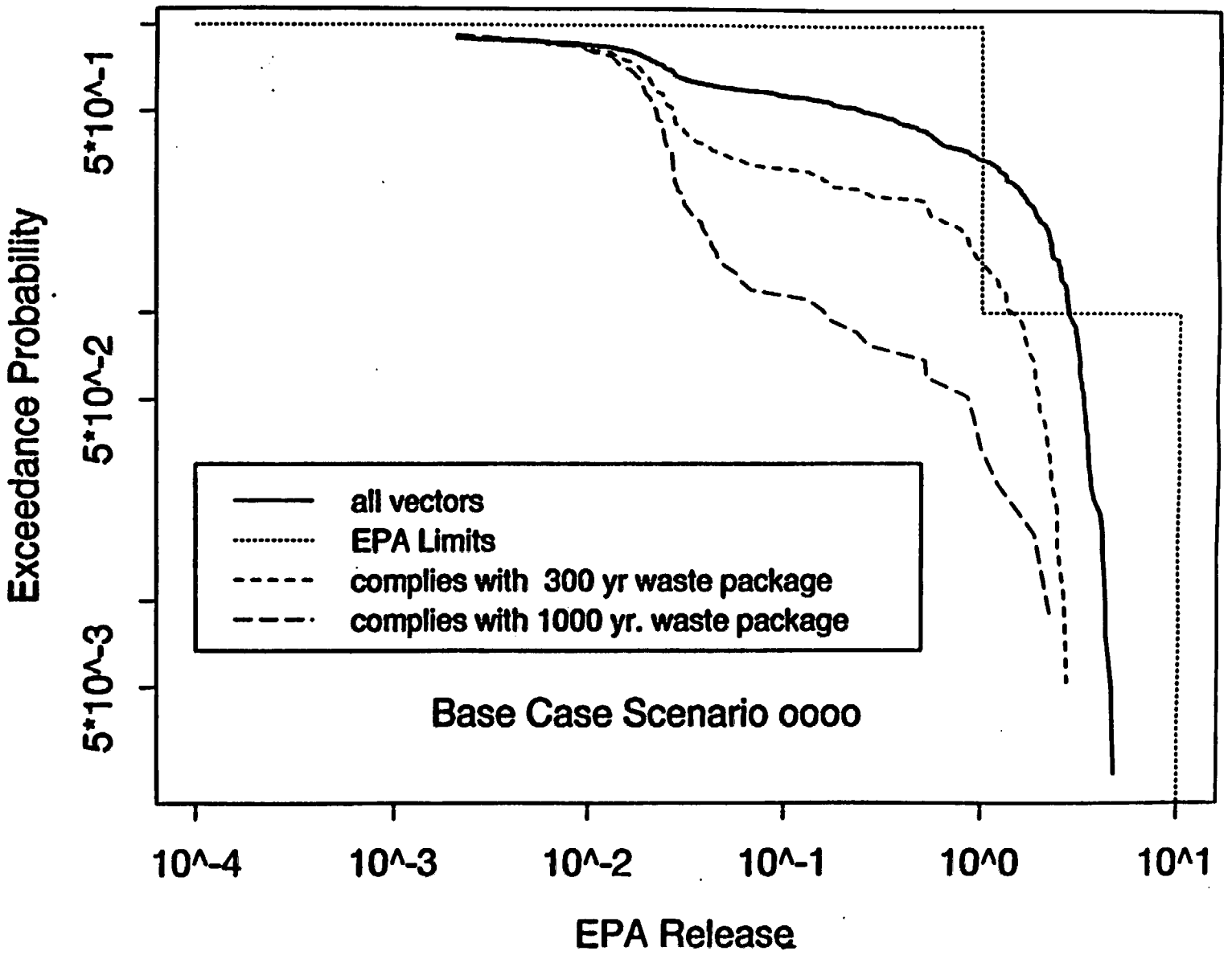

Figure 9-12d. Scatter Plots of Releases to Environment vs. Waste Package Failure Times For Base Case.

8-12d

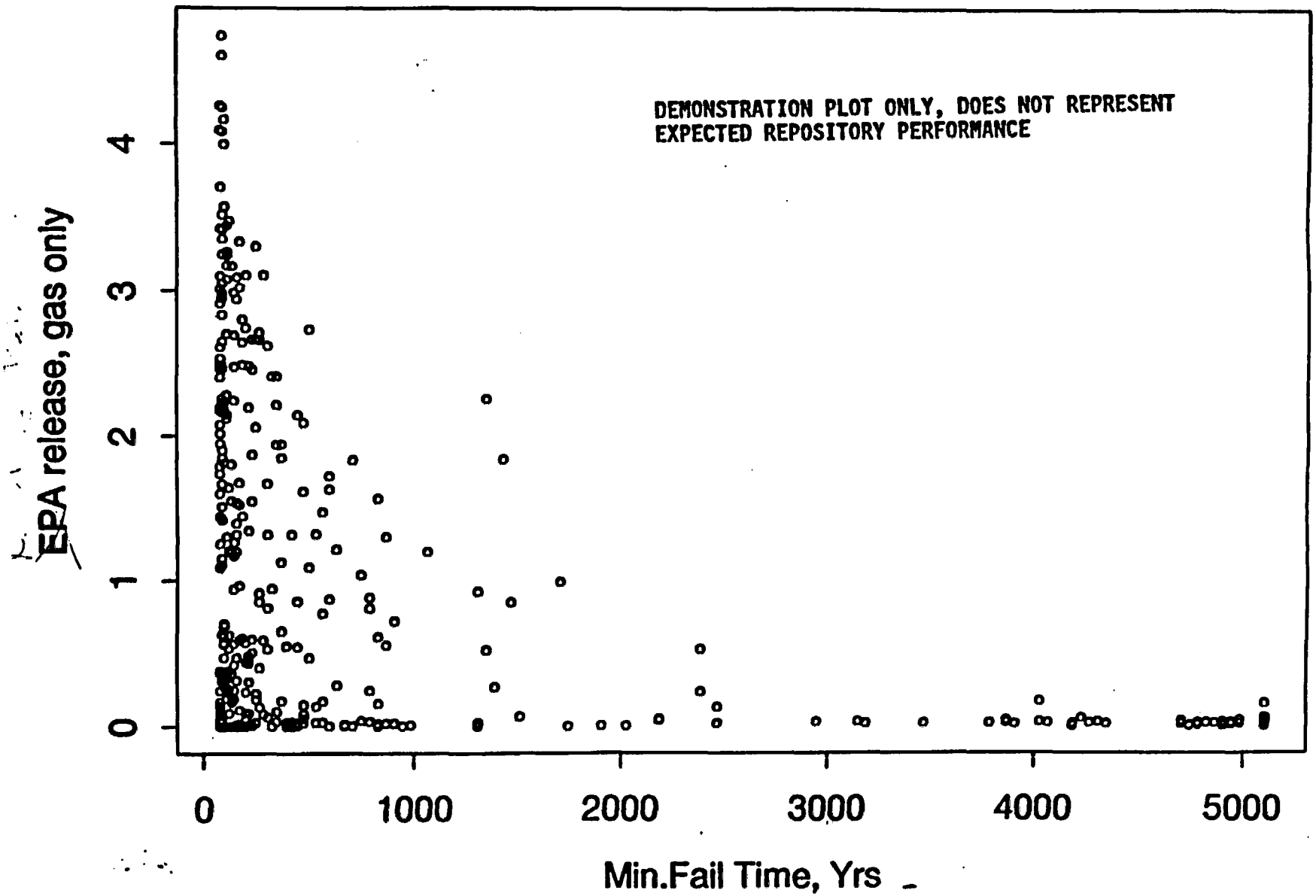
DEMONSTRATION PLOT ONLY, DOES NOT REPRESENT
EXPECTED REPOSITORY PERFORMANCE
EPA release, gas only
0
1
2
3
4
0
1000
2000
3000
4000
5000
Min.Fail Time, Yrs

Figure 9-12e. Scatterplots of EBS release rates vs. time of release for base case.

8-12 c

Fractional Releases vs. Time/Scenario oooo

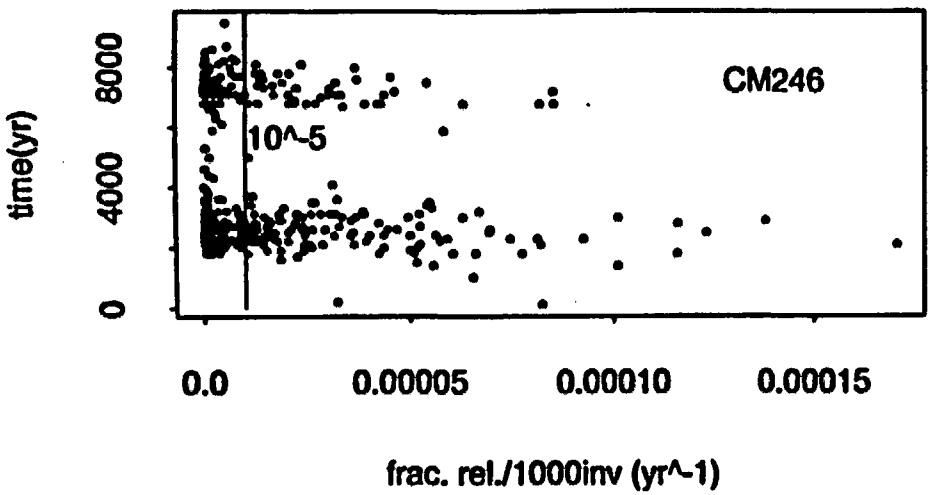

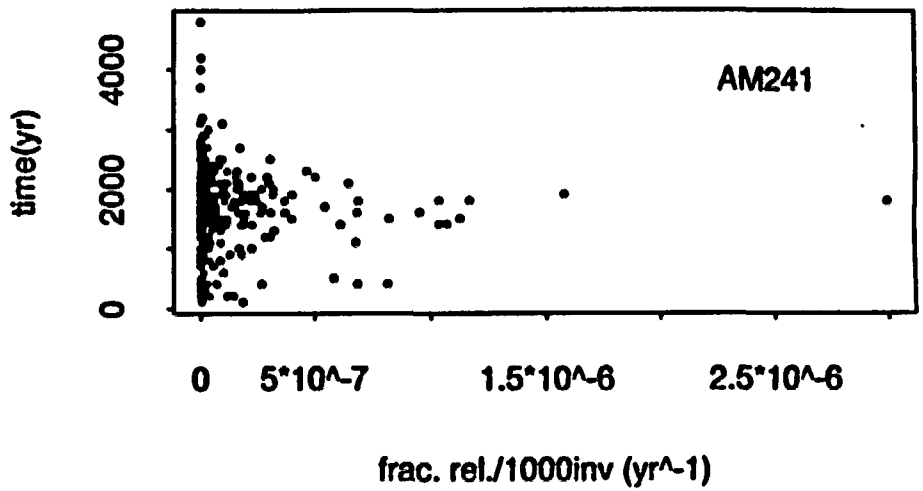

DEMONSTRATION PLOT ONLY, DOES NOT REPRESENT
EXPECTED REPOSITORY PERFORMANCE

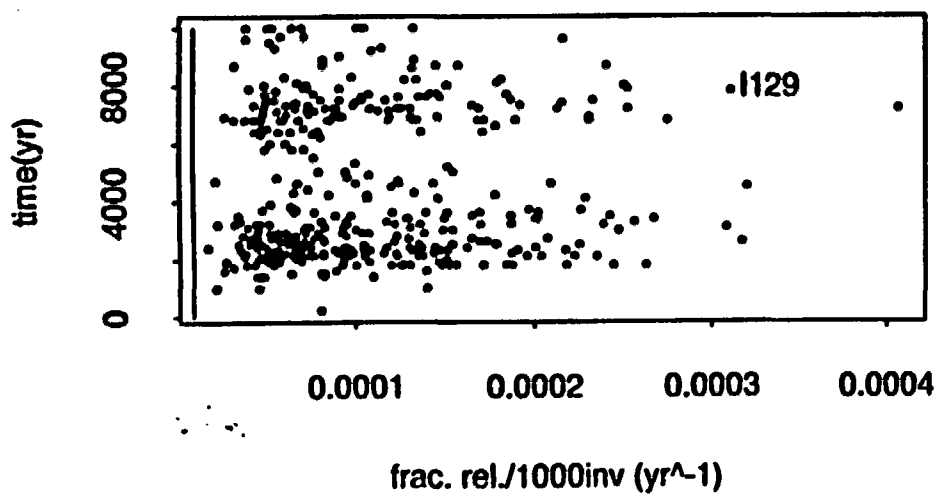

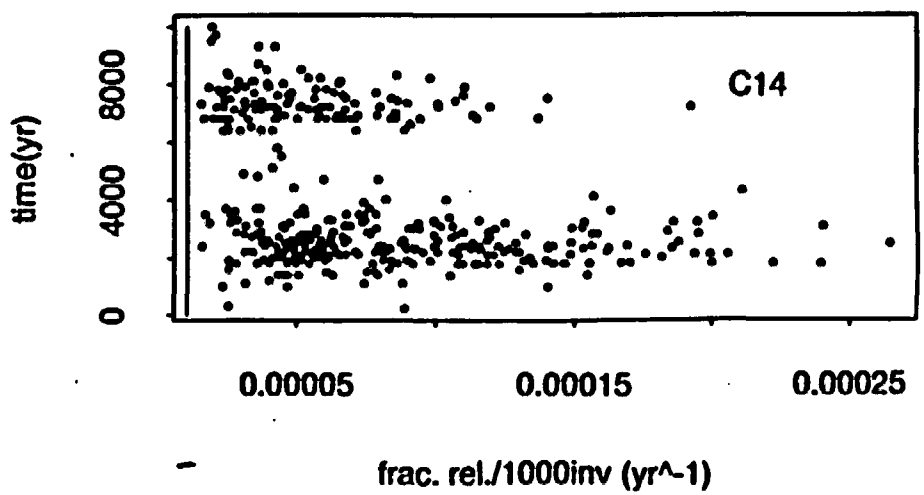

Figure 9-13. CCDF sensitivity plot for all NRC 10 CFR 60 subsystem requirements.

#13

DEMONSTRATION PLOT ONLY, DOES NOT REPRESENT
EXPECTED REPOSITORY PERFORMANCE

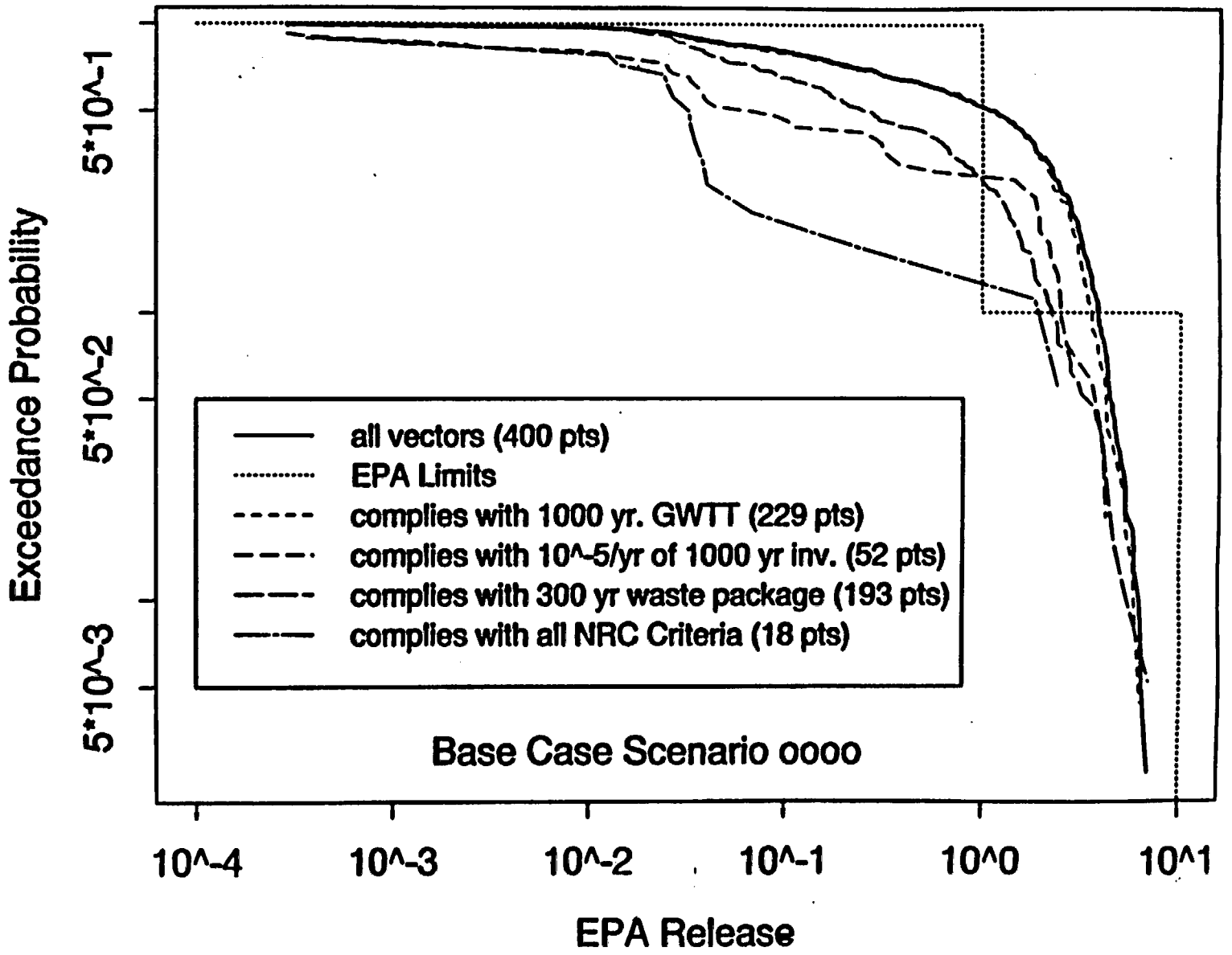

the effects of all natural and engineered barriers separately and in unison. Screening the vectors on the basis of barrier performance leads to a CCDF considerably better (in terms of compliance) than the unscreened vectors. Note that only 18 of the 400 vectors "passed" the screening tests, so the CCDF might not be statistically convergent.

9.6 ILLUSTRATION OF INDIVIDUAL ANNUAL DOSE CALCULATION

M. Rose Byrne

In IPA Phase 2, two types of average annual individual ingestion doses (rems/year) were derived from the 10,000-year cumulative population doses calculated by *DITTY*: (1) a crude estimate of dose for an individual member of the farm family who obtains his/her only source of drinking water from the contaminated well discussed in Chapter 7; and (2) a crude estimate of dose for the 177 individuals who reside within 100 kilometers of Yucca Mountain and who eat contaminated beef (whose only source of food was vegetation irrigated with the contaminated well water). Estimates of these individual doses are presented as histograms in Figure 9-14.

The doses in Figure 9-14 should not be construed as accurate estimates of individual annual doses at the site at Yucca Mountain, Nevada. They were included in this report only to illustrate some of the statistical techniques available to the NRC staff for use in future performance assessments. The method used to calculate individual doses in Figure 9-14 is based on the incorrect assumption that the release rate of any single radionuclide into water or beef remains approximately constant throughout the entire 10,000-year period of exposure. Since the times of release of radionuclides from the repository were random (as determined by LHS sampling), and the concentrations in the accessible environment because of these releases are generally pulses or step functions, this assumption is not appropriate. The crude individual dose values in Figure 9-14 therefore underestimate the "peak" individual dose values by an unknown amount.

The doses in Figure 9-14 were derived as follows. For any scenario class, each of the 400 vectors obtained from parameter distributions by LHS sampling was used to generate a corresponding 10,000-year population dose. The 400 dose values plotted in Figure 9-14 correspond to the set of 400 vectors associated with a scenario class in IPA Phase 2. For each vector, the fraction of 10,000-year dose calculated by *DITTY*, which was caused either by ingestion of contaminated beef or contaminated drinking water, was divided by 10,000 years (the exposure period) and either by 3 or 177 (the number of members in the family or the number of beef eaters) to obtain the very crude estimates of the individual doses in rems/year. The doses caused by the inhalation of airborne radioactivity by the 22,200 individuals (those who reside within 100 kilometers of the repository) were of the order of millirems over the 10,000-year exposure period. Since the individual doses caused by inhalation were negligible compared with the individual doses caused by ingestion of water and beef, they were not included in the histograms of Figure 9-14.

In future phases of IPA, more appropriate computer codes (e.g., *GENII*; Napier, *et al.*, 1988) may be required to obtain significantly better estimates of these individual annual doses. In addition, the transport modules will have to supply time-varying concentration data to the dose modules. In future performance assessments, the NRC staff may also need to devise a strategy to relate distributions of individual doses

Figure 9-14. Illustration of annual individual dose calculation.

DEMONSTRATION PLOT ONLY, DOES NOT REPRESENT
EXPECTED REPOSITORY PERFORMANCE

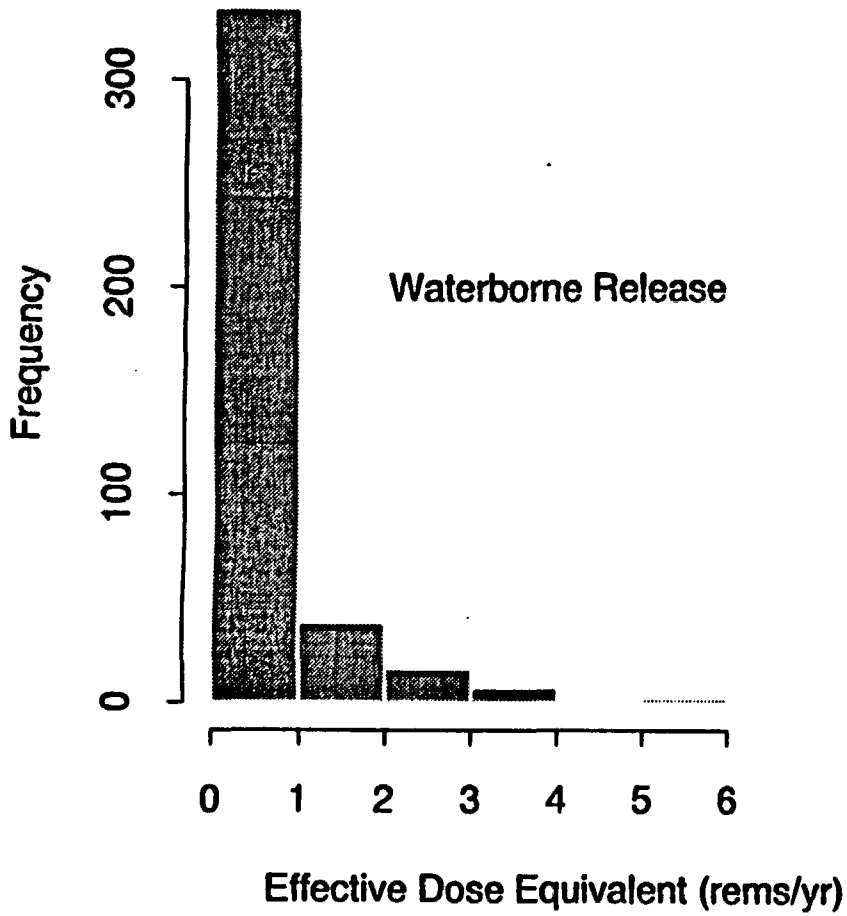

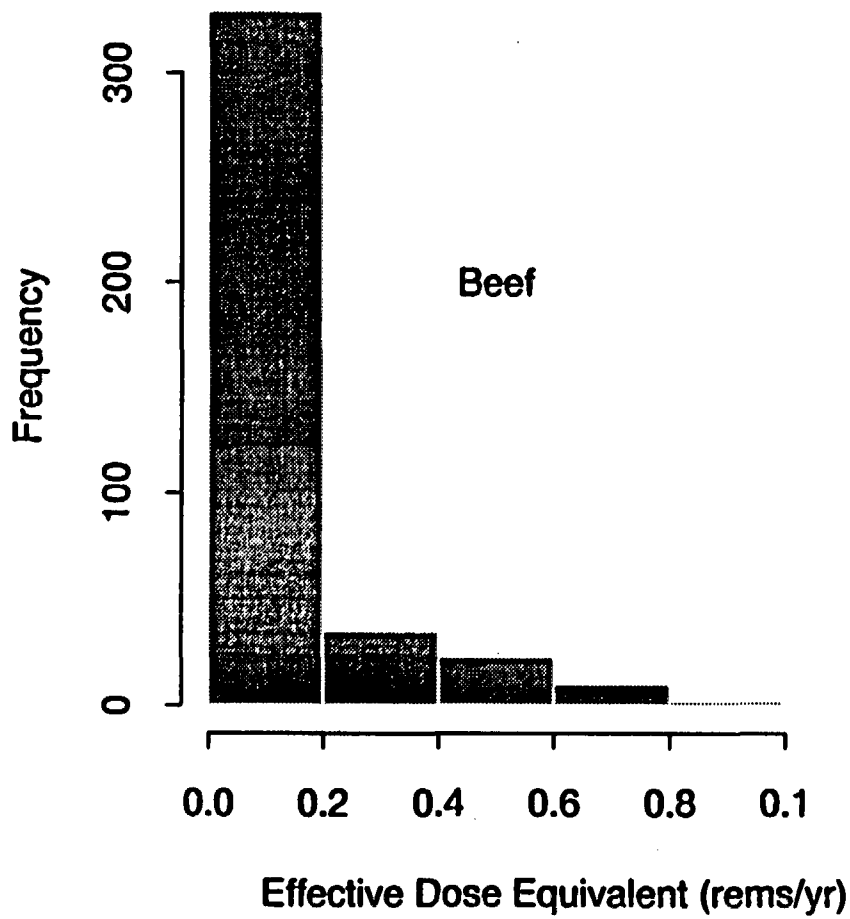

obtained in a probabilistic performance assessment (such as those illustrated in Figure 9-14) to a deterministic individual dose standard such as that proposed in 40 CFR 191.15 (58 *FR* 7935; EPA, 1993).

9.7 SUMMARY AND CONCLUSIONS

In this chapter, the results of the TSPA analyses were presented in terms of CCDFs, conditional CCDFs, single-vector CCDFs, scatter plots, and screened conditional CCDFs. Although the graphs were presented for demonstration purposes only, many of the representations were found to be especially useful for examining some specific aspects of the analyses. The scenario plots, for example, have proven to be a useful tool for evaluating the effect of disruptive event scenarios on individual vectors. Also, scenario-conditional CCDFs and single-vector CCDF plots ("hair diagrams") proved to be useful for displaying the results of variable uncertainty and scenario probability assumptions.

The difference between CCDFs of releases in the IPA Phase 1 and Phase 2 analyses was primarily caused by the greatly increased probability of the pluvial-climate scenario class in Phase 2, and the addition of the gas pathway for ^{14}C migration in Phase 2.

The relationship between the performance of the natural barrier as measured by liquid travel time and the EPA release criterion depends on what definition of liquid travel time is used. When liquid travel time is defined along the "fastest" pathway or the "most flux pathway", there is a bi-modal distribution because of the sharp distinction between matrix and fracture controlled flow. When travel time is "averaged" or "flux-normalized" this bi-modal distribution does not occur. Correlation analysis showed a significant relationship between flux-normalized travel time and normalized release. For an averaged liquid travel time there was almost no correlation. Certainly, the type of flow (fracture or matrix) that is strongly influenced by the sampled infiltration rate, appears to be the primary factor in reducing water-borne radionuclide movement to the accessible environment.

Little correlation was shown between the fractional release rate performance measure and the normalized release. Meeting the NRC release-rate criterion, alone, did not guarantee a normalized release less than 1. We conclude that more work is necessary to evaluate the relationship of the NRC EBS release-rate criterion to total system performance, as well as the feasibility of repository designs to meet the criterion.

Waste package lifetime appeared to have a significant effect on the normalized release for the liquid and gaseous components. Early canister failures were generally found to result in large ^{14}C releases to the accessible environment, primarily because of enhanced transport from large thermal gradients, and increased rates of $^{14}CO_2$ generation at higher temperatures. Significant sensitivity of releases to waste package failure times was observed in the 300- to 1000-year range. The effect of release time (a function of waste package lifetime) on compliance with the NRC EBS release-rate criterion, however, did not appear to be significant.

The effect of compliance with all of the NRC subsystem performance requirements on meeting the EPA release limit must be considered inconclusive because of the small number of realizations that met all

three criteria. Future analyses using selected ranges of sampled values and more realistic (less conservative) models may provide more definitive insights.

The individual dose calculation, while illustrative for the sake of comparison, is neither conservative nor accurate. Significant improvement in all phases of the performance assessment will be required if individual dose is to be calculated for regulatory purposes.

10. CONCLUSIONS AND RECOMMENDATIONS

10.1 INTRODUCTION

As noted in Chapter 1, a major goal of the IPA effort is to develop the necessary knowledge, tools, and methodologies to provide a basis for the NRC staff to evaluate the adequacy of DOE's site characterization program in the context of integrated repository performance as well as for reviewing the performance assessment in a repository license application. Further development of these tools and procedures is planned in future IPA iterations. In reviewing the results of Phase 2, the staff evaluated the adequacy of the methodology and the adequacy of the scientific bases used for these analyses. This evaluation is discussed in Section 10.2.

The staff gained insights from developing and evaluating the system code computational modules, performing the auxiliary analyses, and performing the sensitivity and uncertainty analyses on the results of the Phase 2 IPA. These insights include the relative importance of various site characteristics, design features, and repository processes to repository performance. Insights gained from performance assessment results (and limited by the accuracy of the models used) include evaluation of the relationships between the performance of natural and engineered barriers and performance of the repository, and evaluation of dose and release estimates and their relationship to scenario class and pathway. Insights and conclusions are discussed in Section 10.3.

Section 10.4 discusses additional research, modeling improvements and supporting analyses that will be needed to improve the methodology and scientific basis of future performance assessments. In Section 10.4.1, necessary research falling under the responsibility of DOE or its contractors has also been included. In some cases it will be necessary for NRC as well as DOE to pursue a more thorough understanding of the scientific bases of the sub-system models as well as improvements to the codes which incorporate the models so that NRC can evaluate critical DOE assumptions, conceptual descriptions, and mathematical representations of repository performance.

10.2 EVALUATION OF IPA PHASE 2 METHODOLOGY AND SCIENTIFIC BASES FOR ANALYSES

10.2.1 Adequacy of Methodology

The methodology evaluated, which is described in previous chapters, includes the simulation structure and treatment of uncertainty, scenario analysis, consequence analysis, the calculation of complementary cumulative distribution functions (CCDFs) for the normalized release and dose, and the use of auxiliary analyses to support model assumptions. An objective of IPA Phase 2 was to evaluate particular aspects of the performance assessment methodology, developed and transferred to the NRC by the Sandia National Laboratories (SNL), including the models and codes for flow and transport in partially saturated fractured rock (i.e., *DCM3D* -- flow; *NEFTRAN II* -- radionuclide chain transport) and the scenario analysis methodology. The purpose of this section is to discuss the adequacy of various aspects of the IPA Phase 2 performance assessment methodology including that developed by SNL.

The Monte Carlo simulation of multiple vectors or realizations, used in IPA Phase 2, is a common approach to uncertainty analysis, and was used in the IPA Phase 1 study and other recent studies such

as the Sandia performance assessment for the Waste Isolation Pilot Plant (WIPP) (Helton *et al.*, 1991), the Sandia performance assessment for Yucca Mountain (Barnard *et al.*, 1991), and the Pacific Northwest Laboratory (PNL) performance assessment for Yucca Mountain (Eslinger *et al.*, 1993). This procedure allows the propagation of parameter uncertainty through a series of linked models. Model uncertainty and uncertainty resulting from the spatial variability of the parameters, however, are not reflected directly in the results (although some of these uncertainties have been represented by input parameter variability).

The SNL scenario selection methodology (Cranwell *et al.*, 1990), whose modification and implementation was described in Chapter 3, provided an adequate basis for the staff's scenario analysis in IPA Phase 2. Sixteen mutually exclusive scenario classes, with associated estimated probabilities, were generated from an initial list of 17 potentially disruptive events and processes, of which 4 events and processes remained after screening for combination into scenario classes. These 16 scenario classes were provided for incorporation in the consequence analysis. Definition of repository system boundaries for the analysis kept the number of scenarios requiring evaluation to a tractable number.

The consequence models, described in Chapters 4-6, represent a limited attempt to estimate, for the most part using mechanistic models, the performance of the repository under selected scenario classes for each sampled realization. The increasingly mechanistic nature of the consequence models is considered to be a positive improvement over IPA Phase 1, because it has and will allow in future developments, more representative and realistic coupling between processes, and because the use of mechanistic models allows a more direct and transparent identification of needed information and data. The IPA Phase 2 models have not been run for time-varying boundary conditions (e.g., time-varying percolation flux through the repository for source term and dissolved transport models). However, some of the models allow for transient conditions caused by repository heat, (e.g., gas flux for ^{14}C transport) which is a function of time. Changing near-field temperatures caused by repository heat also influence the start of waste package corrosion and fuel alteration rates. Changing far-field temperatures influence gas transport. An alternative to this limited dynamic approach may be to employ stochastic time series generation of environmental processes such as that employed in a performance assessment in the United Kingdom (HMIP DOE, 1993). Also, in the IPA Phase 2 consequence models, limitations in site characterization data and excessively long computer code run times required the use of one and two dimensional transport models where a full three-dimensional, transient approach may have been more appropriate. While 3-dimensional models may remain impractical to include directly in the IPA evaluations, they can be used to develop abstracted codes.

The calculation of CCDFs, described in Chapter 9, was based on the assumption of equal probability for each realization determined for a scenario class. There were three presentations of CCDFs in IPA Phase 2: (1) conditional CCDF curves for each scenario class representing the parameter uncertainty; (2) composite or total CCDF curves representing all scenario classes; and (3) "hair diagrams", which are CCDF curves for multiple parameter vectors, each representing all scenario classes. The conditional CCDFs present repository behavior for each scenario class. They are combined to form the composite or total CCDF by weighting each by its scenario probability. The "hair diagram" presents the same information in a different way, keeping separate the scenario and parametric probabilities. For that reason, the extremes of system behavior may be better demonstrated with the hair CCDFs. For example the effects of extreme parametric values can be displayed for both high probability events (pluvial climate) and low probability events (volcanism). The mean of all of the hair CCDFs gives the same composite or total CCDF that would be calculated by combining the scenario CCDFs.

A comparison between the CCDF of cumulative radionuclide release resulting from the Phase 2 analysis and the CCDF computed by the earlier Phase 1 analysis demonstrated several significant differences. Much of the difference could be explained by the incorporation of the gas transport pathway in Phase 2 and the assignment of a higher probability of occurrence for the pluvial event. Similar comparisons in future Phases of IPA should be easier and more informative because comparisons are expected to be made after each incremental change rather then only at the completion of major revisions in the TSPA.

Auxiliary analyses are an important part of the NRC IPA methodology. Auxiliary analyses were used for development of the abstracted models described in Chapters 4 and 5 from more sophisticated models, to synthesize parameter values and distributions from more fundamental data, and to place the results of the analyses in perspective. The auxiliary analyses were used to set some constant parameters such as water level during the pluvial climate event, geochemical parameters for variou strata and radionuclides, and to determine the one-dimensional flow path characteristics for the liquid flow and transport computations. The auxiliary analyses proved to be indespensable and integral element of the staff IPA effort.

The use of the DCM3D and NEFTRAN II computer programs proved to be useful for implementing the conceptual models for liquid flow and transport of radionuclides, respectively. DCM3D was not used directly in the system code but was used principally to partition the groundwater flow between the fracture and matrix systems for input to NEFTRAN II. The transport of radionuclides was simulated using NEFTRAN II which accounted for element specific retardation, radioactive decay, and generation of radioactive progeny. This simple representation kept the fracture and matrix flow systems separate. More complex representations may require features of the computer programs not utilized in the current analysis (e.g., transient flow fields, matrix diffusion, and 3-dimensional models) or computer programs that represent additional processes (e.g., multi-phase flow).

Overall, the methodology provides a structured, analytical approach for estimating performance of a HLW repository. Various aspects of the methodology require improvement, such as consequence models, and the estimation of scenario probabilities as discussed in Section 10.4.

10.2.2 Adequacy of Scientific Basis for the IPA Phase 2 Analyses

For the purposes of this discussion, the scientific basis for analysis was considered to be published information about the site and the proposed repository design, published research conducted by DOE/Yucca Mountain Project Office (and its predecessors) and its contractors, and NRC sponsored research. Broader scientific and technical literature including published performance assessments, such as that performed for the WIPP project (Helton *et al.*, 1991), was used to supplement this information.

The scientific basis for analysis is improving through site characterization activities and research. However, the existing scientific basis is far from adequate to allow an accurate assessment of compliance with any of the applicable performance objectives with reasonable assurance. The paucity of data about the site is probably the greatest inadequacy. For example, the state of site characterization at the time these analyses were performed did not support a consensus among hydrologists about conceptual models of water movement through Yucca Mountain nor the appropriate paradigm for modeling transport of radionuclides. Far-field geochemistry, especially in its application to transport by fracture flow, is another area where conservative approximations have been used in the IPA Phase 2 analysis to account

for uncertainty. In this analysis, there was assumed conservatively to be no retardation in the fractures. Credible models of retardation processes, especially in fractures, would reduce the level of conservatism for this process.

The NRC staff has modeled the SCP repository design to the extent practical although we are aware of proposed design changes. Because of the preliminary nature of the design, many of the calculations have been performed as conservative or bounding analyses. Examples of such analyses are the seismic failure model for the waste packagess, the waste package corrosion model and the waste dissolution model. To the extent practicable, the SCP design has been used as a basis for modeling. Many aspects of the repository design are expected to change and the waste package design is likely to change significantly. Changes in placement configuration such as from vertical to horizontal will affect the waste dissolution and release models. Changes to thermal loading will affect the near-field hydrology of the waste packages and the circulation of rock gas.

10.2.3 Conclusions Regarding IPA Phase 2 Methodology and Analyses

The methodology can and must be improved as more data become available and the understanding of the site matures. However, we consider the present methodology suitable to gain insight into the significance of many of the germane parameters and processes and to gain insights regarding model development, repository performance, research and technical assistance needs.– However, the data and scientific understanding of the site are not sufficient at the current time to predict repository performance with certainty. Furthermore, several areas of modeling need imporovement in order to have confidence in the estimates of performance. The computed CCDFs presented in this report should not be taken to be indicative of actual repository system performance.

10.3 INSIGHTS AND CONCLUSIONS FROM IPA PHASE 2

10.3.1 Significant Insights and Conclusions From Model Development and From the Sensitivity and Uncertainty Analyses

The purpose of this section is to discuss insights identified through model development and the sensitivity and uncertainty analysis that have a significant effect on the results of the performance assessment. Most of these insights at this stage of the IPA process deal with site aspects, repository design, and repository processes.

As noted in Chapter 4, two features of the site which appear to strongly influence the results of the performance assessment are: (1) the rock media are unsaturated and therefore have the potential for advective transport of gas upward to the atmosphere; and (2) the rock media are fractured and have the potential for fast liquid pathways for radionuclide transport to the water table and beyond. The quantitative effects of both these features have been relatively difficult to model in a consistent manner. For example, permeability and porosity for flow through fractures in the dual porosity model for the repository cross section stratigraphy were estimated from fracture aperture widths and the number of fractures per unit area, where as permeability and porosity for the matrix were based on core analysis. Both of these data types are based on local (small scale) observations and need to be supplemented by data collected at a larger scale.

From the regression analyses for the base case scenario and other scenario classes not involving pluvial climate, infiltration rate was found to be the most important sampled parameter. There is strong correlation at low to moderate infiltration rates (base case) and weaker correlation at the high infiltration rates (pluvial case). In the former case, there was both matrix flow and fracture flow, but in the latter case, the flow was predominately in fractures. Under conditions of significant fracture flow, radionuclide travel times tended to be low, with relatively little decay. Figure 10-1 shows a significant decrease of liquid radionuclide releases for the base case CCDF when vectors with infiltration rates greater than 1 or 2 mm/year were eliminated from the CCDF.

Although the flux of liquid water through the repository depends on the parameters: infiltration, hydraulic conductivity and porosity, performance correlates most strongly to infiltration. The saturated hydraulic conductivity and porosity vary from layer to layer for each vector, and are assumed to be uncorrelated. There is only one value of infiltration per vector for all layers, however. Since in the one-dimensional representation of unsaturated flow, infiltrating water must pass through all layers, the sensitivity to the value of hydraulic conductivity or porosity of any single layer is reduced.

A number of model simplifications (e.g., one-dimensional flow paths, permeability ranges, and sub-areas for the total repository area) were used to abstract the three-dimensional problem and allow analysis of the uncertainties with reasonable computer execution times for the Phase 2 analysis. However, the proposed repository is a transient, 3-dimensional, partially saturated system with significant air and water vapor movement in a fractured, porous medium, complicated by potentially significant heat transfer and the associated flows of gas and liquid. How these phenomena can be approximated by simplifying assumptions and still provide an adequate representation for the calculation of system performance is poorly understood at this time and needs further investigation.

The Phase 2 analysis conservatively assumed that there was no retardation in the fractures and did not consider the process of matrix diffusion in the modeling. Future iterations need to evaluate the nature and magnitude of the conservatism of these assumptions and the relationship of fracture coatings to geochemical processes.

The design of the waste package container and its emplacement configuration is expected to have a strong influence on repository performance. As discussed in Section 10.2.2, the design of the waste package will greatly affect waste package failure times and release mechanisms. Phase 2 analyses had varying degrees of ability to treat design details; e.g., *SOTEC* was based on vertically emplaced waste packages, with no option for horizontal emplacement. *DRILLO* had the option for horizontal emplacement, but it was not used. Various options for treating the configuration of the waste package will probably need to be incorporated in some of the modules of the system code.

The corrosion related parameters that showed strong correlation with performance were the (electrochemical) potentials for pitting and crevice corrosion, and the active corrosion rate. Corrosion affects the time of waste package failure under static and seismic conditions. Dissolution-related parameters include the fuel alteration rate and solubilities of radionuclides. Other factors found to be important control the interaction of water with the waste package and influence whether and how water contacts the waste.

Failure of the waste packages by corrosion and transport of dissolved radionuclides from the waste

Figure 10-1 - CCDF for Dissolved Radionuclides, Base Case.
Vectors screened for less than 1 or 2 mm/yr infiltration.

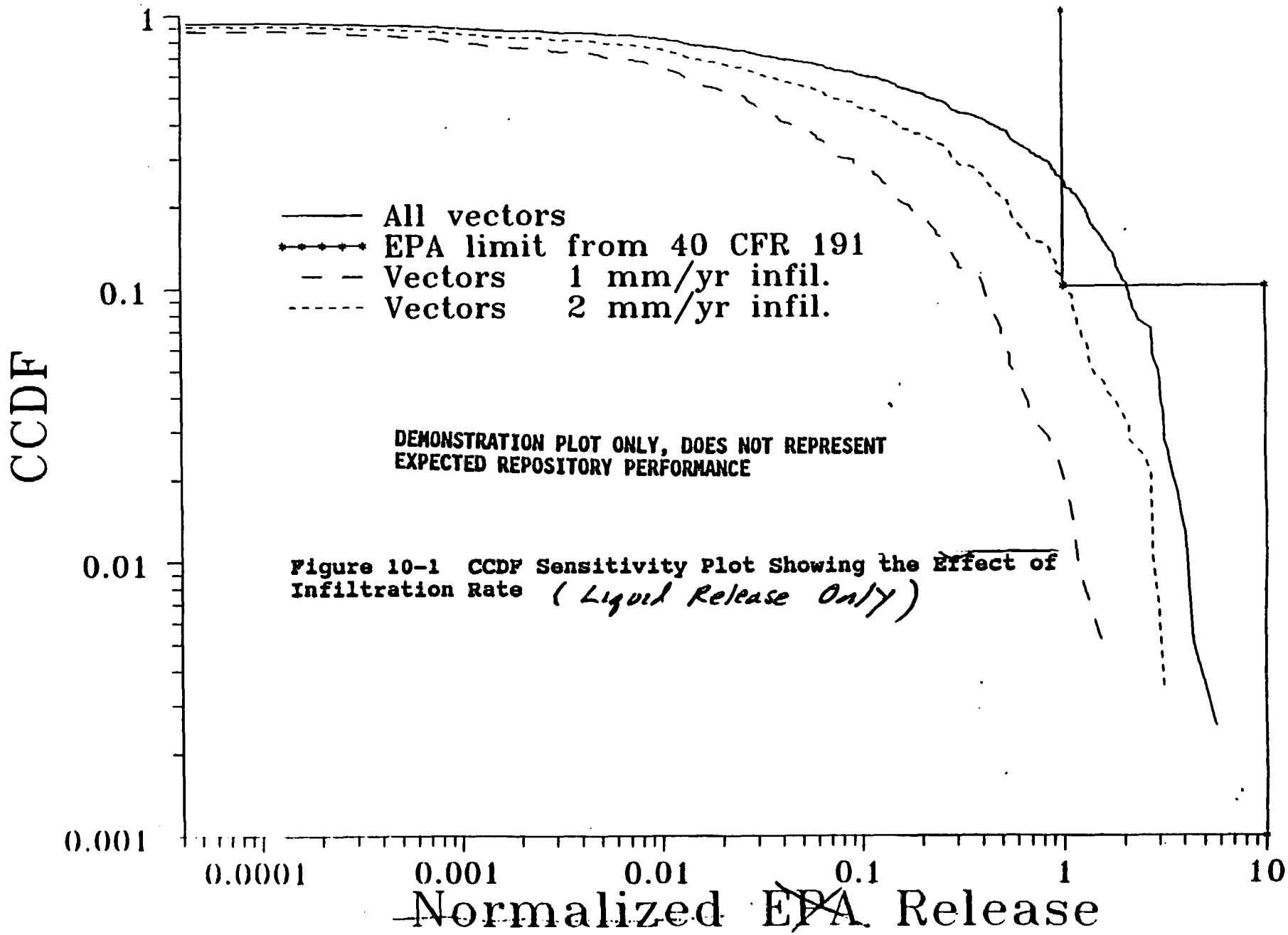

Figure 10-1 CCDF Sensitivity Plot Showing the Effect of Infiltration Rate (Liquid Release Only)

package are expected to depend on contact with liquid water. In IPA Phase 2, waste packages were assumed to remain dry until their surface temperature dropped below the boiling point, and came into contact with liquid water from dripping fractures and wet rock. Future models need the ability to consider plausible rewetting mechanisms for dry rock, the possible influx of liquid water such as dripping fractures, condensation of water vapor on waste package surfaces because of capillary and solution effects, rise in the water table, and water reflux driven by repository or geothermal heat.

Repository heat load is a design parameter which has the potential to significantly affect performance. The present analysis is based on the assumption of a hot repository with a design power loading of 57 kilowatts per acre. This loading results in a strong thermally induced gas flow when typical hydrologic properties are assumed for the rock strata as shown in Section 4.3. This loading is assumed to cause a period of dryness for the waste packages; that is, there is a period for which the temperature of the rock surrounding any particular waste package will be above the boiling point of water, assumed to protect it from corrosion. Temperature also affects corrosion rates and the rate of oxidation of spent nuclear fuel. Hence, the overall sensitivity of the TSPA to any particular loading is not clear at this point because only one loading was assumed for all simulations. A parametric study of repository thermal loading may provide additional insights in future phases.

Gas transport parameters were also identified to be important. Parameters identified are the gas permeability and retardation coefficient for ^{14}C in the Topopah Spring Unit. The gas transport of ^{14}C will be complicated by variations in moisture in the transport medium and gas flow due to the heat of the decaying nuclear waste as well as chemical processes leading to retardation of carbon. Geochemical modeling of ^{14}C transport demonstrated a retardation factor of approximately 30 to 40 due primarily to transfer of carbon between the CO_2 in the gas phase and dissolved carbonate and bicarbonate in the liquid phase. Some ^{14}C might be trapped temporarily in precipitating calcite during the period when temperatures are rising, and released from the calcite as it redissolves as temperatures fall. Although not modeled in IPA Phase 2, percolation of moisture and its effect on the upward movement of vapor may tend to reduce ^{14}C releases during pluvial periods possibly reducing the sensitivity of total normalized release to percolation rate.

Seismicity and volcanism caused large releases compared to the undisturbed (base) case, but did not appear to have a significant effect on the total CCDF. However, more realistic modeling of infiltration, corrosion, seismicity and magmatism could significantly change the importance of disruptive effects relative to one another as well as their influence on the total CCDF. For example, a more detailed study of magmatism may include changing groundwater chemistry and accelerating the corrosion of nearby waste packages.

Several potentially volatile compounds of ^{99}Tc, ^{79}Se, and ^{129}I will be present in spent nuclear fuel. Conservative estimates of gaseous releases of these radionuclides during volcanism and normal operations demonstrated relatively insignificant impacts, so this potential phenomenon was given a low priority for the Phase 2 study.

10.3.2 Insights and Conclusions Regarding System and Subsystem Performance

This section presents repository performance in terms of factors related to the behavior of the engineered

and natural barriers. In IPA Phase 2 the factors investigated were the integrity of the waste packages, the rate of release of radionuclides from the engineered barrier and the travel time of water through the geosphere. One of the primary goals of IPA is to give insight to the effectiveness and ability to implement the regulations applicable to the repository. The regulations in 10 CFR 60.113 address three "subsystem performance factors", namely liquid travel time, Substantially Complete Containment (SCC) and release rate from the Engineered Barrier System (EBS). The results presented in this section portray the total system performance in terms of our understanding of the primary factors of waste containment. The calculations are not for the purpose of directly drawing a comparison between total system performance in terms of normalized release or dose and the subsystem performance measure. There are primarily two reasons for this distinction: (1) The subsystem performance measures are supposed to be independent requirements assuring a minimal performance of each of the multiple barriers in a repository, unrelated to the total system performance; and (2) The characterizations of liquid travel time, SCC and EBS release rate used in IPA Phase 2 are crude and incomplete, and do not exactly conform to the definitions of those quantities in 10 CFR 60. For example, travel time as used here does not include the concept of the disturbed zone and is for post emplacement rather than pre-emplacement conditions. Furthermore, travel time calculated in *FLOWMOD* is an abstraction based on the fastest combination of possible fracture and matrix pathways, and does not correspond to a realistic flow path. Nevertheless, the following comparisons shed light on the importance of the engineered and natural barriers to the total system performance.

CCDFs have been drawn by "screening out" vectors that did not meet a given criterion. The screened CCDFs used with the barriers' performance showed waste package lifetime to have a significant effect on the normalized release for liquid and gaseous source term components in the 300 year to 1,000 year range. Early waste package failures were generally found to result in large ^{14}C releases to the accessible environment, primarily because of enhanced transport from large thermal gradients, and increased rates of $^{14}CO_2$ generation at higher temperatures. The relationship between liquid travel time and the EPA release criterion was strong, for flux weighted liquid travel time. However, travel times calculated as a result of averaging or flux weighting subarea travel times were generally in excess of 10,000 years. The relationship between "fastest" travel times from among the 7 repository subareas and the normalized release was most significant when used as a factor to determine the presence or absence of fracture controlled flow.

Release of ^{14}C through the gaseous pathway contributed significantly to the normalized release while not affecting significantly the effective dose equivalent estimate. This is probably because the normalized release limit for ^{14}C is related to the world-wide circulation of ^{14}C and the resulting dose, while the dose calculation in this study is limited to the assumed population in a circular area of 50 km radius.

The 10,000 year median collective dose for the fully disturbed case was approximately an order of magnitude greater than the corresponding dose for the base case scenario. For the normalized release, the median (i.e., 50% probability) of the fully disturbed case was about 5 times the median of the base case. For both dose and normalized release at the median probability, the most important disturbing event is pluvial climate and the resulting increase in percolation rate. The contributions by the ingestion pathway dominated the collective doses from both scenarios. The average annual dose to an individual in the region from inhalation was negligible compared to that from ingestion of contaminated drinking

water and locally-grown contaminated food. In scenario classes involving magmatism, order of magnitude increases over the base case dose resulted from direct releases to the surface during an extrusive magmatic events. The same type of event increased the normalized release by about a factor of four. The radionuclides which made the largest contributions to population dose (cumulated over 10,000 years) were ^{94}Nb, ^{210}Pb, ^{243}Am, and ^{237}Np.

10.4 RECOMMENDATIONS

10.4.1 Recommendations for Additional Scientific Input

Based on the insights and conclusions described above as well as recommendations identified in the Phase 1 report, there is a need for continuing research by both the NRC and the DOE in the general areas of hydrology and geochemistry, waste and waste package materials, repository hydrothermal effects, and probabilities and effects of disruptive events. The ability to identify research needs from the work performed in IPA Phase 2 is limited by the lack of sophistication of the models and paucity of data. When site characterization results are adequate to allow detailed modeling of hydrologic characteristics for different scales, ongoing research in scale effects will prove useful. The same is expected to be true of advanced corrosion and waste dissolution topics, shaft and borehole sealing, natural analogs, and seismic research. Hence there is a significant amount of research being pursued that will eventually support performance assessment but can not be directly justified by insights and conclusions from the present analysis.

Fracture-matrix interactions - Considerable research in hydrology will need to be directed at achieving a better understanding of fracture-matrix interactions. Flow in fractured or fractured-porous media can be represented in several ways: (1) *discrete fracture models* which represent flow explicitly in discrete channels and in the porous matrix, (2) *equivalent continuum models* which represent the averaging of the matrix and fracture system into an equivalent porous medium, and (3) *dual-continuum models* which treat the matrix and fracture as separate but interacting continua. Experimental information for fracture-matrix interactions is scarce and is needed to provide insights on the applicability of these approaches. DOE will need to provide detailed characterization of the fracture properties in the repository horizon as a minimum, for examination of near-field hydrothermal effects; and to a degree sufficient to determine percolation, liquid transport, and/or vapor transport properties through the rest of the Yucca Mountain repository area. Field measurement of gas flow rates and determination of Yucca Mountain pneumatic properties by DOE will need to be continued for adequate modeling of gas transport.

Regional Hydrology - Further research will also be required in the area of regional hydrology to determine maximum water levels and boundary conditions for site hydrologic modeling especially for disruptive consequences. DOE should investigate the steep gradient near the site because of the possible influence on future site groundwater elevations.

Percolation - DOE will need to continue the field measurement of deep percolation and its correlation with precipitation. NRC should explore the possible use of such correlations with expert elicitation information in climatology to determine ranges of percolation rates as a function of climatological assumptions. The development of a more sophisticated climate model should also be pursued.

Geochemical Models - NRC and DOE research in geochemistry including laboratory studies, field studies, and natural analogs must continue to provide adequate verification of present geochemical models or, if required, the bases for alternative models. Research in this area should emphasise flow through fractures because of the importance demonstrated for fracture flow. Further research in gas transport geochemistry should also be undertaken to determine if there are significant barriers to $^{14}CO_2$ release in the geosphere.

Corrosion Models - DOE should continue to collect data on the corrosion of waste container materials. Both NRC and DOE research in corrosion should be directed at obtaining a better understanding of the corrosion mechanism and how corrosion is likely to progress under conditions of high humidity or in contact with water of high ionic strength. In addition, models to determine accurately the contact of the waste form with liquid water will be highly design-specific to the repository concept finally adopted. Much of this work is expected to stem from confirmatory laboratory-scale and field heater tests used to validate mathematical models of two-phase heat and mass transfer. Since the experimental data must be necessarily of short duration and small scale relative to those of the repository, reliable mathematical models may be the only way to extrapolate results to greater times and distances. In this regard, the basis for the development of these models will rely on a mechanistic understanding of the processes and events related to the waste package's interaction with its environment. NRC needs to pursue an independent understanding of these processes to evaluate DOE's assumptions. DOE will need to continue characterization of the spent fuel waste form (inventories and dissolution rates) as these control the source term.

Magmatism - Additional geologic information is needed regarding volcanic processes to improve the probability estimates of the magmatic scenario. This information includes determining the role of volatiles in driving magma ascent, the importance of multiple dike intrusions, and the role of pre-existing geologic structure. The effects of uncertainty in geochronological data should also be evaluated. Additional improvements may also have to be made regarding magma interaction with water. NRC should develop an independent understanding in this area.

10.4.2 Recommendations Regarding Modeling Improvements and Supporting Analyses in NRC's Iterative Performance Assessment Activities

The following recommendations are listed by chapter and include recommendations for modeling improvements and additional analyses based on conclusions in the chapters and include recommendations from the Phase 1 report that have not yet been implemented. Some of these recommendations parallel those of section 10.4.1, but emphasize analysis rather than research.

10.4.2.1 System Code

(1) *Software Quality Assurance requirements need more prominence in module development* -- There were a number of difficulties encountered during the development of the Phase 2 modules and their integration into the system code. Many of the problems could probably be traced to a lack of documented module designs, lack of module integration designs, and lack of documented module testing. The system code and its computer modules need to be developed under a more consistent environment, incorporating aspects of modern code development such as object-oriented design and principles of software quality assurance. The computational platform should

be standardized to employ UNIX tools for software development and debugging. Requirements for individual code modules should be specified in advance of integrating them into the system code. There should be careful attention to interfaces among modules and the system code.

(2) *Future developments of the TPA will require more model abstraction and efficient computing techniques* --The computational requirements of modules can be prohibitive, and significant simplifications were required in order to achieve acceptably low execution costs. We recommend more attention to abstracting the complicated phenomena in order to achieve efficient computational modules, and examination of the feasibility of applying high performance computing procedures including massively parallel computers and advanced computational methods (e.g., adaptive grids, domain decomposition, and efficient matrix solvers).

(3) *The TPA system code must be easily ungraded* -- We recommend that the TPA system code be considered a dynamic entity, to be upgraded in future IPA iterations. Possible upgrades include: addition of new modules, changed scope of current modules, centralized use of databases, uniform interfaces between modules, and uniform coding practices among modules.

10.4.2.2 Scenario Analysis

1. *Staff judgments in screening the initial set of Events and Processes (EPs) should be reassessed using appropriate mathematical models and numerical codes, as recommended by Cranwell et al. (1990)*-- This could lead to the assignment of different probabilities to the EPs and result in a different outcome to the screening.

2. *Future work should investigate methods for generating individual scenarios "representative" of the scenario classes to which they belong* -- The approach taken in the IPA Phase 2 scenario analysis generated scenario classes (i.e., unique combinations of events or processes without regard to the order in which they occur). Generating representative events would likely involve the need to "partition" the individual scenario classes into appropriate subevents or subprocesses and then examining various combinations.

3. *Obtain geoscience input for modeling faulting, uplift, and subsidence at Yucca Mountain* -- In the IPA Phase 2 scenario analysis, the vibratory ground motion from local faulting was combined with seismicity. Regional uplift and subsidence were considered to have negligible consequences in the screening analysis, and no attempt was made to model these events. In future IPA iterations, all of these events will be modeled, probably in auxiliary analyses, to make a determination about whether they should be included.

10.4.2.3 Flow and Transport

1. *Examine modeling issues affecting percolation* -- Conceptual model assumptions with respect to percolation should have a major effect on water flux through a repository located in the unsaturated zone. Issues which can be investigated with auxiliary analyses include the relationship between highly transient rainfall and percolation estimates, the effect of topographic lows and fault zones as sources of increased recharge, how spatial variability in hydrologic parameters affect percolation, and the effect of fracture imbibition on percolation.

2. *Examine modeling assumptions affecting fracture-matrix interaction* -- Modeling assumptions regarding the interaction between matrix and fractures are very important due to differences in fluid velocities and retardation of the two flow systems. Auxilary analyses could improve the understanding of conceptual modeling assumptions regarding small scale interactions at the fracture-matrix interface (e.g., detailed simulations to examine the equilibration of pressure between the fracture and matrix considering transient conditions and the effects of mineral coatings on fracture surfaces) and large scale effects concerning the flow field within a hydrogeologic unit (e.g., examine how the small scale effects propagate through a geologic unit). These further analyses can be used to modify current IPA models and revise parametric ranges.

3. *Examine hydrogeologic features and heterogeneity that could allow a "short circuit" through the unsaturated zone* -- The Phase 2 flow and transport analyses assumed that fluid flow and radionuclide transport could be represented as one-dimensional stream tubes for each of the hydrogeologic units. Two- and three-dimensional analyses could investigate the impact of fault zones and perched water on pathways through the unsaturated zone. If the impact is of sufficient magnitude, then additional pathways could be added to the flow and transport analysis in future iterations.

4. *Examine the coupling of water in the gaseous and liquid phases* -- The model of the repository is highly idealized. The prototype is transient, 3-dimensional, partially saturated flow with significant air and water vapor movement in a fractured, porous medium complicated by potentially significant heat transfer and the associated flows of gas and liquid affecting the redistribution of moisture. Abstracted models need to be tested through simulation, comparing the results to those of the more complete model developed in the auxilary analyses, which includes the coupling of water movement in the liquid and gaseous phases under non-isothermal conditions. Simulation efforts could examine the variation in moisture contents and fluid flux through the repository due to vapor movement and condensation (this effect would be especially pronounced during the thermal phase of the repository).

5. *Examine refinements in the saturated zone modeling to improve concentration estimates for dose calculations* -- The calculation of dose requires a determination of the radionuclide concentration. The concentration determination requires consideration of flow and dispersion in the saturated zone which is not normally required for the calculation of time-integrated discharge (normalized release) for comparison with the EPA standard.

6. *Access the usefulness of additional intermediate calculations for understanding the flow and transport results* -- The Phase 2 analyses performance measures were integrated discharge and radionuclide dose. These results are often difficult to explain in the absence of other information on modeling results for individual modules (e.g., fluid flux or water velocity for the ground-water pathway, and release rates for the source term module). It would be beneficial to further examine the modeling approaches and identify intermediate calculations that could be performed to provide further insights on model and system performance.

7. *Evaluate the importance of thermally- and barometrically-driven air flow on performance* -- In IPA Phase 2, thermal gradient driven gas transport was incorporated in the calculation of the CCDF. Other pneumatic effects such as barometric pumping should be considered in future

iterations of IPA.

10.4.2.4 Source Term

1. *The models in SOTEC will have to be modified in response to the current waste disposal concepts that differ from the SCP design assumed for the IPA Phase 2.* IPA Phase 2 was based on the waste package concept described in the Yucca Mountain Site Characterization Plan of single-walled packages placed vertically in boreholes, with an air gap between the container and the surrounding rock. The current models will have to be modified as DOE progresses in site characterization and makes decisions about its thermal loading strategy, waste package design, waste package materials, and additional engineered barriers.

2. *Develop more mechanistic models for waste package corrosion* --The present version of *SOTEC* used in IPA Phase 2 considered simplified models for corrosion. Needed improvements to *SOTEC* include codes abstracted from complex physics-based models, including a mechanistic model for initiation and propagation of localized corrosion, taking into account the geochemical environment and mechanical stresses.

3. *Improve models for the effects of heat* -- The present temperature model uses a semianalytical approach for conduction-only. More realistic models could take heat and mass transfer in two-phase flow into account to better estimate the temperature in the near field and the transfer of liquid water and water vapor (Buscheck, 1993), inputs needed to predict the onset of corrosion and the interaction of liquid water with the waste.

4. *Take spatial and temporal variability into account in source term models* --IPA Phase 2 began to explore ensemble averages of the temporally and spatially varying environmental parameters that should be used in order to represent a large number of waste packages with relatively few calculations. Improved source term models should also take the variability of the properties of the fuel into account either explicitly or by defining effective input parameters that capture the variability without making the models too complex for total system performance assessments.

5. *Improve models for the release of gaseous ^{14}C* -- The IPA Phase 2 model considers the release of gaseous $^{14}CO_2$ emanating from the waste, based on steady state diffusion of oxygen and $^{14}CO_2$. Failure to include the transient diffusion of oxygen evident from the data could lead to inaccurate predictions of conversion rates at low temperatures. The model could be improved by considering transient diffusion. Also, the present implementation of the model for the release of gaseous ^{14}C mixes the contribution from the seven repository zones for use in the two-dimensional gas flow model. The model should be revised to take into account variations in release rate for each zone.

6. *Consider modes of waste package failure other than corrosion*-- Waste packages might also fail from mechanisms other than corrosion such as seismic shaking, volcanism, and inadvertent human intrusion. While IPA Phase 2 considered failure by drilling, volcanism and seismicity, the models were highly simplified. Models for failure by volcanism might take into account mechanisms of interaction between magma and the waste packages; e.g., corrosive gases and

viscous forces. Improved models for human intrusion might consider the site-specific likelihood for drilling, shear forces from drilling fluids, and mechanisms that could bring radioactive material to the surface. These disruptive events could also have a significant effect on the other aspects of the repository performance. Analytical expressions for buckling are only available for simplified geometries and loading conditions with static loads. A buckling model for a complex geometry and multiple and transient loads would require a complicated and computationally intensive simulation unsuited for IPA. Once the engineering design has been finalized, the structural failure of the waste packages from dynamic and other forces could be analyzed deterministically by numerical and experimental techniques and abstracted for IPA. These analyses would include the possible impact of mechanical fatigue of the waste packages from recurrent, low-intensity seismic activity. Improved models of seismic failure might take into account the range of frequencies of earth motion, and realistic dynamic modes of the waste packages.

7. *Improve model for the dissolution of radionuclides from the waste form* -- The chemistry within the waste package was treated in a highly simplified manner in IPA Phase 2. The model could be improved by taking into account the formation and subsequent transport of colloids, speciation of the elements released to the water, the contribution of minerals from the groundwater and structural materials in the waste package, the changing temperature, and other factors such as ionizing radiation.

8. *Improve model for transport of radionuclides from the waste package* -- Mass transfer out of the waste package by flowing water and diffusion was included in IPA Phase 2, based on the SCP conceptual waste package. The transport model, in conjunction with the waste form dissolution model, should consider the rates that water contacts and enters the waste package, interacts with the waste form, and transports radionuclides from the waste package by both advection and diffusion. The model should recognize that the suite of waste packages will represent a broad range of varying stages of degradation, with some completely intact and others significantly degraded from both anticipated and unanticipated processes and events. These conditions are progressive over the 10,000 year period of interest. Although conservatively neglected in *SOTEC*, the model could include recognition that degraded waste packages, including failed fuel (e.g., defective cladding), can still contribute to the isolation or controlled release of radionuclides.

9. *Include models for other waste forms* --The NRC staff's first two IPAs focussed on evaluating the performance of waste packages for spent fuel. In future IPAs, the staff should develop a source term model for the expected inventory of glass waste packages with special consideration to the kinetics of glass dissolution, formation of secondary silicate mineral, colloid formation and mass transport of radionuclides. Further, waste forms other than LWR spent fuel and defense-related glass may ultimately need to be considered if they are determined to be potentially significant sources. These may include any transuranic or greater-than-Class-C wastes.

10.4.2.5 Disruptive Consequence Modules

1. *Consolidate Calculations of Radionuclide Inventory in the Drilling Model* --The drilling code calculates inventory using the Bateman equations and determines the inventory for the time of the earliest drilling event. Greater efficiency may have been attainable by calculating the evolution of the inventory one time only. The inventory could then be moved from one bin to another as needed, rather than having this calculation repeated in several different modules. Having a unified list of inventories would provide more information on the migration of the nuclides through the geosphere and make accounting simpler for radionuclides that migrate through both liquid and gaseous pathways.

2. *Allow multiple waste package failure times in the drilling model* -- The effects of the number of drilling events are predicted to be small relative to the other releases calculated in Phase 2, in part because drilling affects only a small number of waste packages. However, for cases where there is both drilling combined with volcanism or seismicity, the source term model predicts all failures occur at the earliest time for any event. This simplifying modeling assumption could lead incorrectly to predictions of large total releases, when a later disruption (volcanic or seismic event) causes widespread failure of waste packages. The drilling code and source term code (SOTEC) should be modified to allow multiple waste package at different times within the same run.

3. *Reduce the number of variables and tie the sampled parameters to the extent of drilling activity in the drilling model* - The drilling model required 92 sampled parameters to determine whether, where and when there was a strike on a waste package. The model should be simplified to require fewer sampled parameters that would be more meaningful in the sensitivity and uncertainty analysis.

4. *Surface releases should be based on site specific mechanisms* - While IPA Phase 2 considered failure by drilling, volcanism and seismicity, the models were highly simplified. Future models might consider the site-specific likelihood for drilling, shear forces from drilling fluids, and mechanisms that could bring radioactive material to the surface.

10.4.2.6 Dose Assessment

1. *Improve the DITTY Dose Assessment Model* -- The results of dose assessments should be evaluated as functions of radionuclide type and exposure pathway. In addition, the dose conversion factors used in IPA Phase 2 should be re-calculated to obtain a more accurate estimate of population doses for long-lived radionuclides (as discussed in Section 7.6). Also, the model parameters currently used in *DITTY* must be verified as being applicable to the Yucca Mountain site.

2. *Evaluate Other Dose Assessment Computer Codes* -- Codes which should be evaluated include codes for estimating long-term individual and collective exposures, atmospheric dispersion models, and demographic models. Methods employed by international organizations for calculation of doses into the far future (e.g. BIOMOVS and NEA) should be evaluated. The 1990 recommendations of the ICRP should be incorporated into the codes if adopted by the NRC.

3. *Apply the statistical sensitivity and uncertainty methodology developed in IPA Phase 2 for the geosphere models to the dose assessment models* -- Sensitivity and uncertainty analyses can be used to identify the most important dose assessment parameters and the sensitivity of the dose estimate to these parameters.

10.4.2.7 Sensitivity and Uncertainty Analysis

1. *Sensitivity and uncertainty analysis should explore the use of dimensional analysis to form factors based on combinations of other parameters* -- Dimensional analysis is a useful technique for determining the functional relationships among variables. Principles of dimensional analysis might be applied for the purpose of simplifying the repository system, with its hundreds of independent parameters, into an equivalent system with fewer parameters. These dimensionless factors would make the task of analyzing the system and determining important parameters simpler.

2. *Importance sampling techniques such as the limit state approach should be evaluated* -- The Limit State Approach, discussed in Section 8.4, has the potential for easing the computational burden experienced in the Phase 2 study by reducing the number of vectors needed to construct the CCDFs and perform the sensitivity analyses. This approach should be evaluated further on the full repository system model. However, as presently implemented, the limit state approach cannot deal with hundreds of independent parameters. The number of independent variables analyzed by the limit state approach must be reduced, either by selecting the most important parameters by stepwise regression analysis, or combining parameters into groups.

3. *A method of directly obtaining CCDF sensitivity to individual parameters should be developed* -- Sensitivity analyses have been developed to determine the effect of changes in the input parameters of the models on scaler measures of repository performance such as cumulative release and effective dose equivalents. Some effort should be directed at developing a robust method for evaluating system sensitivity for a probabilistic performance measure, e.g., the CCDF.

11 REFERENCES

Chapter 1. Introduction

Bath, G.D. and C.E. Jahren, "Interpretations of Magnetic Anomalies at a Potential Repository Site Located in the Yucca Mountain Area, Nevada Test Site," U.S. Geological Survey, Open File Report, OFR-84-120, 1984

Codell, R.M., *et al.*, "Initial Demonstration of the NRC's Capability to Conduct a Performance Assessment for a High-Level Waste Repository," Nuclear Regulatory Commission, NUREG-1327, May 1992.

Cranwell, R.M., "Risk Methodology for Geologic Disposal of Radioactive Waste: Scenario Selection Procedure," Nuclear Regulatory Commssion, NUREG/CR-1667, month 1990.

dePolo, C.M., "The Maximum Background Earthquake for the Basin and Range Province, Western North America," Nevada Bureau of Mines and Geology, in press.

Napier, B.A, R.A. Peloquin, D.L. Streng, J.V., and J.V. Ramschell, "GENII: The Hanford Environmental Radiation Dosimetry Software System," Richland, Washington, Pacific Northwest Laboratory, PNL-6584, 3 vols., December 1988. [Prepared for the U.S. Department of Energy.]

Nuclear Regulatory Commission, "Draft License Application Review Plan for the Review of a License Application for a Geologic Repository for Spent Nuclear Fuel and High-Level Radioactive Waste, Yucca Mountain Site, Nevada," Office of Nuclear Material Safety and Safeguards, NUREG-1323, in press.

O'Neill, J.M., J.W. Whitney, and M.R. Hudson, "Photogeologic and Kinematic Analysis of Lineaments at Yucca Mountain, Nevada: Implications for Strike-Slip Faulting and Oroclinal Bending," U.S. Geological Survey, Open File Report, OFR-91-623, 1992.

Sagar, B., R.B. Codell, J. Walton, and R. Janetzke, "SOTEC: A Source Term Code for High-Level Geologic Repositories -- User's Manual (Version 1.0)," San Antonio, Texas, Center for Nuclear Waste Regulatory Analyses, CNWRA 92-009, July 1992. [Prepared for the Nuclear Regulatory Commission.]

Silling, S.A., "Final Technical Position on Documentation of Computer Codes for High-Level Waste Management," Nuclear Regulatory Commission, NUREG-0856, June 1983.

Spengler, R.W., "Resolution of the Stratigraphic and Structural Settings and Mineral Resource Potential of Yucca Mountain," Presentation at U.S. Department of Energy/Nuclear Regulatory Commission Technical Exchange on Geophysics Integration, Las Vegas, Nevada, June 8, 1993.

U.S. Department of Energy, "Site Characterization Plan Overview, Yucca Mountain Site, Nevada Research and Development Area, Nevada," Nevada Operations Office/Yucca Mountain Project Office, Nevada, DOE/RW-0198, December 1988.

Whitney, J.W., "Integration of the Geophysical Studies with Activities in the Tectonics Program," Presentation at U.S. Department of Energy/Nuclear Regulatory Commission Technical Exchange on Geophysics Integration, Las Vegas, Nevada, June 8, 1993.

Chapter 2. Total-System Performance Assessment Computer Code

Amtec Engineering, Inc., "TECPLOT User's Manual: Interactive Plotting for scientists and Engineers (Version 4.0)," Bellevue, Washington, month 1984.

Codell, R.M., *et al.*, "Initial Demonstration of the NRC's Capability to Conduct a Performance Assessment for a High-Level Waste Repository," Nuclear Regulatory Commission, NUREG-1327, May 1992.

Iman, R.L., and M.J. Shortencarier, "A FORTRAN 77 Program and User's Guide for the Generation of Latin Hypercube and Random Samples for Use in Computer Models," Nuclear Regulatory Commission, NUREG/CR-3624 (SAND 83-2365), month 1984. [Prepared by the Sandia National Laboratories.]

Janetzke, R., and B. Sagar, "preFOR: A Pre-Processor for FORTRAN Files: User's Manual," San Antonio, Texas, Center for Nuclear Waste Regulatory Analyses, CNWRA 91-003, month 1991a. [Prepared for the Nuclear Regulatory Commission.]

Janetzke, R., and B. Sagar, "RDFREE: A FORTRAN Utility for Format Free Input: User's Guide," San Antonio, Texas, Center for Nuclear Waste Regulatory Analyses, CNWRA 91-005, month 1991b. [Prepared for the Nuclear Regulatory Commission.]

Longsine, D.E., E.J. Bonano, and C.P. Harlan, "User's Manual for the NEFTRAN Computer Code," Nuclear Regulatory Commission, NUREG/CR-4766 (SAND86-2405), month 1987. [Prepared by the Sandia National Laboratories.]

Margulies, T., L.E. Lancaster, N.A. Eisenberg, and L.R. Abramson, "Probability Analysis of Magma Scenarios for Assessing Geologic Waste Repository Performance," *Proceedings American Society of Mechanical Engineers Winter Meeting*, Anaheim, California, November 8-13, 1992, pp. .

Napier, B.A, R.A. Peloquin, D.L. Streng, J.V., and J.V. Ramschell, "GENII: The Hanford Environmental Radiation Dosimetry Software System," Richland, Washington, Pacific Northwest Laboratory, PNL-6584, 3 vols., December 1988. [Prepared for the U.S. Department of Energy.]

Sagar, B., R.B. Codell, J. Walton, and R. Janetzke, "SOTEC: A Source Term Code for High-Level Geologic Repositories -- User's Manual (Version 1.0)," San Antonio, Texas, Center for Nuclear Waste Regulatory Analyses, CNWRA 92-009, July 1992. [Prepared for the Nuclear Regulatory Commission.]

Sagar, B., and R. Janetzke, "Total System Performance Assessment Computer Code: Description of Executive Module (Version 2.0)," San Antonio, Texas, Center for Nuclear Waste Regulatory Analyses, CNWRA 91-009, August 1993. [Prepared for the Nuclear Regulatory Commission.]

Sagar, B., and R. Janetzke, "Total System Performance Assessment Computer Code: Description of Executive Module," San Antonio, Texas, Center for Nuclear Waste Regulatory Analyses, CNWRA 91-009, month 1991. [Prepared for the Nuclear Regulatory Commission.]

Updegraff, C.D., C.E. Lee, and D.P. Gallegos, "DCM3D: A Dual-Continuum, Three-Dimensional, Ground-Water Flow Code for Unsaturated, Fractured, Porous Media," Nuclear Regulatory Commission, NUREG/CR-5536, month 1991.

Chapter 3. Scenario Analyses

Algermissen, S.T., *et al.*, "Probabilistic Estimates of Maximum Acceleration and Velocity in Rock in the Contiguous United States," U.S. Geological Survey, Open File Report, USGS OFR 82-1033, 1982.

Andersson, J., *et al.*, "The Joint SKI/SKB Scenario Development Project," Stockholm, Sweden, Statens Kärnkraftinspektion (SKI), SKI Technical Report 89:14, December 1989.

Apostolakis, G., *et al.*, "Techniques for Determining Probabilities of Events and Processes Affecting the Performance of Geologic Repositories: Suggested Approaches," Nuclear Regulatory Commission, NUREG/CR-3964 (SAND86-0196), Vol. 2, June 1991. [Prepared by the Sandia National Laboratories.]

Benson, L.V. and P.W. McKinley, "Chemical Composition of Groundwater in the Yucca Mountain Area, Nevada, 1971-1984," U.S. Geological Survey, Open File Report, USGS OFR-85-484, 1985.

Bernreuter, D.L., *et al.*, "Seismic Hazard Characterization of 69 Nuclear Power Plant Sites East of the Rocky Mountains: Methodology, Input Data and Comparison of Previous Results for Ten Sites," Nuclear Regulatory Commission, NUREG/CR-5250, Vols. 1-8, January 1989. [Prepared by the Lawrence Livermore National Laboratory.]

Bonano, E.J., *et al.*, "Demonstration of a Performance Assessment Methodology for High-Level Radioactive Waste Disposal in Basalt Formations," Nuclear Regulatory Commission, NUREG/CR-4759, June 1989. [Prepared by the Sandia National Laboratories.]

Bonano, E.J., *et al.*, "Elicitation and Use of Expert Judgment in Performance Assessment for High-Level Radioactive Waste Repositories," Nuclear Regulatory Commission, NUREG/CR-5411 (SAND89-1821), May 1990. [Prepared by the Sandia National Laboratories.]

Brune, J.N., W. Nicks, and A. Aburto, "Microearthquakes at Yucca Mountain, Nevada," *Bulletin Seisological Society of America*, 82:164-174 [1992].

Campbell, K.W., "A Preliminary Methodology for the Regional Zonation of Peak Ground Acceleration," National Science Foundation, *et al.*, *Proceedings of the Third International Earthquake Microzonation Conference*, Seattle, Washington, June 28 - July 1, 1982, Vol. 1, pp. 365-376 [1982].

Carrigan, C.R., *et al.*, "Potential for Water-table Excursions Induced by Seismic Events at Yucca Mountain, Nevada," *Geology*, 19:1157-1160 [1991].

Champion, D.E., "Volcanic Episodes near Yucca Mountain as Determined by Paleomagnetic Studies at Lathrop Wells, Crater Flat, and Sleeping Butte, Nevada," in *Proceedings of the International Topical Meeting: High Level Radioactive Waste Management, April 8-12, 1990,* American Nuclear Society/American Society of Civil Engineers, Las Vegas, Nevada, pp. 61-67 [1990].

Codell, R., *et al.*, "Initial Demonstration of the NRC's Capability to Conduct a Performance Assessment for a High-Level Waste Repository," Office of Nuclear Material Safety and Safeguards/Office of Nuclear Regulatory Research, NUREG-1327, May 1992.

Connor, C.B, and B.E. Hill, "Volcanism Research in NRC High Level Radioactive Waste Research at CNWRA, January - June, 1993," CNWRA 93-01S, Center for Nuclear Waste Regulatory Analyses, San Antonio, TX, pp. 10-6 to 10-14, 1993.

Cornell, C.A., "Engineering Seismic Risk Analysis," *Bulletin Seisological Society of America*, 58:1583-1606 [1968].

Cornell, C.A., "Probabilistic Analysis of Damage to Structure Under Seismic Loads, in Dynamic Waves," Chapter 27 in *Civil Engineering*, edited by D.A. Howells, I.P. Haily, and C. Taylor, Wiley Interscience, 1971.

Cranwell, R.M., "Risk Methodology for Geologic Disposal of Radioactive Waste: Scenario Selection Procedure," Nuclear Regulatory Commssion, NUREG/CR-1667, April 1990. [Prepared by the Sandia National Laboratories.]

Crowe, B.M., *et al.*, "Calculation of the Probability of Volcanic Disruption of a High-Level Radioactive Waste Repository within Southern Nevada, USA," *Radioactive Waste Management and the Nuclear Fuel Cycle*, 3(2):167-190, December 1982.

Crowe, B.M., et al., "Status of Volcanic Hazard Studies for the Nevada Nuclear Waste Storage Investigations," Los Alamos National Laboratory, LA-9325-MS, March 1983a.

Crowe, B.M., *et al.*, "Aspects of Potential Magmatic Disruption of a High-Level Radioactive Waste Repository in Southern Nevada," *Journal of Geology*, 91:259-276 [1983b].

Crowe, B.M. and F.V. Perry, "Volcanic Probability Calculation for the Yucca Mountain Site: Estimation of Volcanic Rates," in "Nuclear Waste Isolation in the Unsaturated Zone -- FOCUS '89, American Nuclear Society, *Proceedings of the Topical Meeting, September 17-21, 1989*, Las Vegas, Nevada, pp. 326-334 [1989].

Crowe, B.M., *et al.*, "Recurrence Models of Volcanic Events: Applications to Volcanic Risk Assessment,"in "High Level Radioactive Waste Management," American Nuclear Society/American Society of Civil Engineers, *Proceedings of the Third International Conference, April 12-16, 1992*, Las Vegas, Nevada, pp. 2344-2355 [1992].

DeWispelare, A.R., *et al.*, "Expert Elicitation of Future Climate in the Yucca Mountain Vicinity: Iterative Performance Assessment Phase 2.5," Center for Nuclear Waste Regulatory Analyses, CNWRA 93-016, August 1993. [Prepared for the U.S. Nuclear Regulatory Commission.]

Electric Power Research Institute (EPRI), "Seismic Hazard Methodology for the Central and Eastern United States," Vols. 1 and 2, Research Project Number P-101, 1986.

Electric Power Research Institute (EPRI), "Demonstration of a Risk-based Approach to High-Level Waste Repository Evaluation," EPRI NP-7057, 1990.

Garside, L.J. and J.H. Schilling, "Thermal Waters of Nevada," Nevada Bureau Mines, Geologic Bulletin 91, 1979.

Garside, L.J., *et al.*, "Oil and Gas Developments in Nevada," Nevada Bureau Mines, Geologic Bulletin 104, 1988.

Hanks, T.C. and Kanamori, "A Moment Magnitude Scale," *Journal of Geophysical Research*, 84:2348-2350 [1979].

Ho, C-H., "The Mathematical Model of Volcanism at Yucca Mountain," State of Nevada, Agency for Nuclear Projects/Nuclear Waste Project Office/Carson City, 1990. [Prepared by the University of Nevada, Las Vegas.]

Ho, C-H., *et al.*, "Eruptive Probability Calculation for the Yucca Mountain Site, USA: Statistical Estimation of Recurrence Rates," *Bulletin of Volcanology*," 54:50-56, 1991.

Ho, C-H, "Risk Assessment for the Yucca Mountain High-Level Nuclear Waste Repository Site: Estimation of Volcanic Disruption," *Mathematical Geology*," 24(4):347-364, 1992.

Hodgkinson, D.P. and T.J. Sumerling, "A Review of Approaches to Scenario Analysis for Repository Safety Assessment," paper presented at NEA Symposium on Safety Assessments for Repositories, Paris, France, 1989.

Howells, D.A., I.P. Haily and C. Taylor (eds), "Probabilistic Analysis of Damage to Structure Under Seismic Loads, in Dynamic Waves," in *Civil Engineering*, Wiley Interscience, 1971.

Hunter, R.L., "Preliminary Scenarios for the Release of Radioactive Waste From a Hypothetical Repository in Basalt of the Columbia Plateau," Nuclear Regulatory Commission, NUREG/CR-3353, October 1983. [Prepared by the Sandia National Laboratories.]

Hunter, R.L. and Mann, C.J., Chapter 3 "Climatology" in "Techniques for Determining Probabilities of Events and Processes Affecting the Performance of Geologic Repositories: Literature Review," Nuclear Regulatory Commission, NUREG/CR-3964, Vol. 1, June 1989. [Prepared by the Sandia National Laboratories.]

International Atomic Energy Agency, "Safety Assessment for the Underground Disposal of Radioactive Wastes," International Atomic Energy Agency, Vienna, Austria, Safety Series No. 56, 1981.

Margulies, T., *et al.*, "Probabilistic Analysis of Magma Scenarios for Assessing Geologic Waste Repository Performance," American Society of Mechanical Engineers, Winter Annual Meeting, Anahiem, CA: New York, NY. American Society of Mechanical Engineers, 1992.

McBirney, A.R., "Volcanology," Techniques for Determining Probabilities of Geologic Events and Processes, Studies in Mathematical Geology No. 4, R.L. Hunter and C.J. Mann, eds., New York: Oxford University Press, pp. 167-184, 1992.

McGuire, R.K., "Fortran Computer Program for Seismic Risk Analysis," U.S. Geological Survey, Open File Report, USGS OFR-76-67, 1976.

Meremonte, M.E., and A.M. Rogers, "Historical Catalog of Southern Great Basin Earthquakes 1868-1978," U.S. Geological Survey, Open File Report, USGS OFR-87-80, 1987.

Nevada Bureau of Mines & Geology, "Trace Element Associations in Mineral Deposits, Bare Mountain (Fluorine) Mining District, Southern Nye County, Nevada," State of Nevada, Report No. 39, 1984.

Raney, R. G., "Possible Effects of Surface and Underground Mining Proximal to a Closed High-Level Radioactive Waste Repository at Yucca Mountain, Nye County, Nevada," U.S. Bureau of Mines, 1990a. [Report to the Nuclear Regulatory Commission/Division of High-Level Waste Management.]

Raney, R.G., "Active Mines and Prospects Within a Thirty-Mile Radius of the Proposed High-level Repository Site at Yucca Mountain, Nye County, Nevada, Subsequent to January 1988 (As of July 1990)," U.S. Bureau of Mines, 1990b.

Ross, B., "A First Survey of Disruption Scenarios for a High-Level Waste Repository at Yucca Mountain, Nevada," Washington, D.C., Disposal Safety Incorporated, SAND85-7117, December 1987. [Prepared for the U.S. Department of Energy.]

SAIC, "Report of Early Site Suitability Evaluation of the Potential Repository Site at Yucca Mountain, Nevada," SAIC-91/8000, January 1992. [Prepared for the U.S. Department of Energy.]

Schweickert, R.A., "Evidence for a Concealed Dextral Strike-Slip Fault Beneath Crater Flat, Nevada," Geol. Soc. America, Abst. with Programs, Vol. 21, A90, 1989.

Scott, R.B., and J.G. Rosenbaum, "Evidence of Rotation about a Vertical Axis During Extension at Yucca Mountain, Southern Nevada (Abstract)," *EOS*, 67:16, April 22, 1986, p. 358.

Shaw, H.R., "Uniqueness of Volcanic Systems," U.S. Geological Survey, Professional Paper 1350, 1987.

Sheridan, M.F., "A Monte Carlo Technique to Estimate the Probability of Volcanic Dikes," in High Level Radioactive Waste Management," American Nuclear Society/American Society of Civil Engineers, *Proceedings of the Third International Conference, April 12-16, 1992*, Las Vegas, Nevada, pp. 2033-2038 [1992].

Smith, E.I. *et al.*, "The Area of Most Recent Volcanism Near Yucca Mountain, Nevada: Implications for Volcanic Risk Assessment," in *Proceedings of the International Topical Meeting: High Level Radioactive Waste Management, April 8-12, 1990*, American Nuclear Society/American Society of Civil Engineers, Las Vegas, Nevada, pp. 81-90 [1990].

Spaulding, W.G., "Vegetation and Climates of the Last 45,000 years in the Vicinity of the Nevada Test Site, South-Central, Nevada," U.S. Geological Survey Professional Paper 1329, 55 p., 1985.

State of Nevada, 1984, "Trace Element Association in Mineral Deposits, Bare Mountain (Flourine) Mining District, Southern Nye County, Nevada."

State of Nevada/Nevada Bureau of Mines, "Major Mines of Nevada, 1989," Geologic Special Publication No. 10, 1990.

State of Nevada/Department of Minerals, "Oil & Gas Permit Notices (Permit Numbers 605-607, issued December 14, 1990)," 1990.

Stephens, M.E. and B. Goodwin, "Systematic Scenario Analysis for the Post-Closure Assessment of the Canadian Concept for Nuclear Waste Disposal," Proceedings of the International Symposium Safety Assessment of Radioactive Waste, OECD/NEA, Paris, France, 1989.

Thornbury, W.D., *Regional Geomorphology of the United States*, John Wiley & Sons, New York, 609 p., 1967.

URS/John A. Blume & Associate, "Technical Basis and Parametric Study of Ground Motion and Surface Rupture Hazard Evaluations At Yucca Mountain, Nevada," SAND86-7013, September 1987. [Prepared for the U.S. Department of Energy.]

U.S. Department of Energy, "Site Characterization Plan Overview, Yucca Mountain Site, Nevada Research and Development Area, Nevada," Nevada Operations Office/Yucca Mountain Project Office, Nevada, DOE/RW-0198, December 1988a.

U.S. Department of Energy, "Site Characterization Plan, Yucca Mountain Site, Nevada Research and Development Area, Nevada," Nevada Operations Office/Yucca Mountain Project Office, Nevada, DOE/RW-0199, 9 Vols., December 1988b.

U.S. Environmental Protection Agency, "Environmental Standards for the Management of Spent Nuclear Fuel, High-Level and Transuranic Wastes [Final Rule]," *Federal Register*, vol. 50, no. 182, September 19, 1985, pp. 38066 - 38089.

U.S. Nuclear Regulatory Commission, "10 CFR Part 60, Disposal of High-Level Radioactive Wastes in Geologic Repositories: Conforming Amendments," *Federal Register*, vol. 51, no. 118, June 19, 1986, pp. 22288 - 22301.

Vaniman, D., *et al.*, "Variations in Authigenic Mineralogy and Sorptive Zeolite Abundance at Yucca Mountain, Nevada, Based on Studies of Drill Cores USW GU-3 and G-3," Los Alamos National Laboratory, LA-9707-MS, June 1984. [Prepared for the U.S. Department of Energy.]

Winograd, I.J. and B.J. Szabo, 1988, "Water-Table Decline in the South-Central Great Basin During the Quaternary: Implications for Toxic Waste Disposal," Chapter 13 in "Geologic and Hydrologic Investigations of a Potential Nuclear Waste Disposal Site at Yucca Mountain, Southern Nevada," M.D. Carr and J.C. Yount editors, USGS Bull. 1790, U.S. Geological Survey.

Yount, J.C., *et al.*, "Neotectonics of the Walker Lane, Pyramid Lake to Tonopah, Nevada - Part I," in *Crustal Evolution of the Great Basin and Sierra Nevada: Cordilleran/Rocky Mountain Section, Geological Society of America Guidebook*, edited by M.M. Lahren, J.H. Trexler, Jr., and C. Spinosa, Department of Geological Sciences, University of Nevada at Reno, pp. 383-408, 1993.

Chapter 4. Flow and Transport Module

Ababou R., "Approaches to Large Scale Unsaturated Flow on Heterogeneous, Stratified, and Fractured Geologic Media," Nuclear Regulatory Commission, NUREG/CR-5743, month 1991. [Prepared by the Center for Nuclear Waste Regulatory Analyses.]

Ababou, R., and A.C. Bagtzoglou, "BIGFLOW: A Numerical Code for Simulating Flow in Variably Saturated, Heterogeneous Geologic Media Theory and User's Manual," Nuclear Regulatory Commission, NUREG/CR-6028, month 1993. [Prepared by the Center for Nuclear Waste Regulatory Analyses.]

Ahola, M. and Sagar, B., "Regional Groundwater Modeling of the Saturated Zone in the Vicinity of Yucca Mountain, Nevada," San Antonio, Texas, Center for Nuclear Waste Regulatory Analyses, CNWRA 92-001, January 1992. [Prepared for the Nucelar Regulatory Commission.]

Bagtzoglou, A.C., R. Ababou, and B. Sagar, "Effects of Layering, Dipping Angle, and Faulting on Two-Dimensional Variably Saturated Flow (IPA Phase II)," Center for Nuclear Waste Regulatory Analyses, CNWRA92-004, month 1992. [Prepared for the Nucelar Regulatory Commission.]

Bagtzoglou, A.C., R. Ababou, B. Sagar, and M. Islam, "Effect of Some Common Geological Features on Two-Dimensional Variably Saturated Flow," *Scientific Basis for Nuclear Waste Management XVI*, 294:929-936 [1993].

Barnard, R.W. and H.A. Dockery, eds., "Technical Summary of the Performance Assessment Calculational Exercises for 1990 (PACE-90) Volume 1: 'Nominal Configuration' Hydrogeologic Parameters and Calculational Results," Sandia National Laboratories, Albuquerque, New Mexico, SAND90-2726, month 1992.

Benson, L.V., *et al.*, "Chemical Composition of Ground Water and the Locations of Permeable Zones in the Yucca Mountain Area, Nevada," U.S. Geological Survey, Open File Report, OFR-83-854, 1983.

Bentley, C.B., *et al.*, 1983, "Geohydrologic Data for Test Well USW H-5, Yucca Mountain Area, Nye County, Nevada," U.S. Geological Survey, Open File Report, OFR-83-853, 1983.

Blankennagel, R.K., "Hydraulic Testing Techniques of Deep Drill Holes at Pahute Mesa Nevada Test Site," U.S. Geological Survey, Open File Report, OFR-67-18, 1967.

Boyer A., "Computing Dirichlet Tessellations," *The Computer Journal*, 24:162-166 [1981].

Broxton, D. E., Warren, R. G., Hagan, R. C., and Luedemann, G., 1986, "Chemistry of diagenetically altered tuffs at a potential nuclear waste repository, Yucca Mountain, Nye County, Nevada," Los Alamos National Laboratory, LA-10802-MS, October 1986.

Buscheck, T.A., and J.J. Nitao, "Estimates of the Width of the Wetting Zone Along a Fracture Subjected to an Episodic Infiltration Event in Variably Saturated, Densely Welded Tuff, Lawrence Livermore National Laboratory, Livermore, California, UCID-21579, month 1988.

Celia, M.A., E.T. Bouloutas, and R.L. Zarba, "A General Mass-Conservative Numerical Solution for the Unsaturated Flow Equation," *Water Resources Research*, 26:1483-1496, [1990].

Chuang, Y., *et al.*, "Laboratory Analysis of Fluid Flow and Solute Transport Through a Variably Saturated Fracture Embedded in Porous Tuff," Nuclear Regulatory Commission, NUREG/CR-5482, month 1990.

Classen, H.C., "Water Quality and Physical Characteristics of Nevada Test Site Water-Supply Wells," U.S. Geological Survey, Open File Report, USGS-474-158, 1973.

Codell, R. *et al.*, "Initial Demonstration of the NRC's Capability to Conduct a Performance Assessment for a High-Level Waste Repository," Office of Nuclear Material Safety and Safeguards/Office of Nuclear Regulatory Research, NUREG-1327, May 1992.

Craig, R.W., *et al.*, "Geohydrologic Data For Test Well USW H-6, Yucca Mountain Area, Nye County, Nevada," U.S. Geological Survey, Open File Report, OFR-83-856, 1983.

Craig, R. W. and Robison, J.H., "Geohydrology of Rocks Penetrated by Test Well UE-25p#1, Yucca Mountain Area, Nye County, Nevada," U.S. Geological Survey, Water Resources Investigations, WRI-34-4248, 1984.

Craig, R.W. and K.A. Johnson, "Geohydrologic Data For Test Well UE-25p#1, Yucca Mountain Area, Nye County, Nevada," U.S. Geological Survey, Water Resources Investigations, OFR-84-450, 1984a.

Craig, R.W., "Geohydrology of Rocks Penetrated by Test Well USW H-6, Yucca Mountain, Nye County, Nevada," U.S. Geological Survey, Water Resources Investigations, WRI-89-4025, 1991.

Czarnecki, J.B., "Simulated Effects of Increased Recharge on the Ground-Water Flow System of Yucca Mountain and Vicinity, Nevada-California," U.S. Geological Survey, Water Resources Investigations, WRI-84-4344, 1984a.

Czarnecki, J.B., *et al.*, "Finite-Element Simulation of Ground-Water Flow in The Vicinity of Yucca Mountain, Nevada-California," U.S. Geological Survey, Water Resources Investigations, WRI-84-4349, 1984.

Drever, J.I., 1988, *The Geochemistry of Natural Waters*, Prentice Hall, Englewood Cliffs New Jersey.

Dudley, A.L., *et al.* "Total System Performance Assessment Code (TOSPAC), Volume 1: Physical and Mathematical Bases," Sandia National Laboratories, Albuquerque, New Mexico, SAND85-0002, month 1988.

Dykhuizen, R.C., "A New Coupling Term for Dual-Porosity Models," *Water Resources Research*, 26:351-356 [1990].

Freeze, R. A. and J.A. Cherry, *Groundwater*, Prentice Hall,Inc., Englewoood Cliffs, N.J, 1979.

Healey, "Borehole Gravity Meter Surveys in Drill Holes USW G-3, UE-25p#1, and UE-25c#1, Yucca Mountain Area, Nevada," U.S. Geological Survey, Open File Report, OFR-84-672, 1984.

Klaveter, E.A., and R.R. Peters, "Fluid Flow in a Fractured Rock Mass," Sandia National Laboratories, Albuquerque, New Mexico, SAND85-0855, month 1986.

Lahoud, R.G., *et al.*, "Geohydrology of Volcanic Tuff Penetrated by Test Well UE-25b#1, Yucca Mountain, Nye County, Nevada," U.S. Geological Survey, Water Resources Investigations, WRIR-84-4253, 1984.

Lobmeyer, D.H., *et al.*, "Geohydrologic Data for Test Well UE-25b#1, Nevada Test Site, Nye County, Nevada," U.S. Geological Survey, Open File Report, OFR-83-855, 1983.

Lobmeyer, D.H., "Geohydrology of Rocks Penetrated by Test Well USW G-4, Yucca Mountain, Nye County, Nevada," U.S. Geological Survey, Water Resources Investigations, WRIR-86-4015, 1986.

Mansure, A.J., and T.S. Ortiz, "Preliminary Evaluation of the Subsurface Area Available for a Potential Nuclear Waste Repository at Yucca Mountain," Sandia National Laboratories, Albuquerque, New Mexico, SAND85-0175, month 1984.

Massmann, J., and D.F. Farrier, "Effects of Atmospheric Pressures on Gas Transport in the Vadose Zone," *Water Resources Research*, 28:777-791 [1992].

Meijer, A., "Yucca Mountain Project Far-Field Sorption Studies and Data Needs," LA-11671-MS, 1990.

Montazer, P., and W.E. Wilson, "Conceptual Hydrologic Model of Flow in the Unsaturated Zone, Yucca Mountain, Nevada," U.S. Geological Survey, Water-Resources Investigations Report, WRI-84-4345, 1984.

Neuman, S.P., "Universal Scaling of Hydraulic Conductivities and Dispersivities in Geologic Media," *Water Resources Research*, 26:1749-1758 [1990].

Nienhuis, P. and Appelo, 1990, User Guide to PHREEQM: An adaptation of PHREEQE for use in a mixing cell flowtube.

Nitao, J.J., and T.A. Buscheck, "Infiltration of a Liquid Front in an Unsaturated, Fractured Porous Media," *Water Resources Research*, 27:2099-2112 [1991].

Olague, N.E. *et al.*, "User's Manual for the NEFTRAN II Computer Code," Nuclear Regulatory Commission, NUREG/CR-5618 (SAND90-2089), February 1991. [Prepared by the Sandia National Laboratories.]

Ortiz, T.S. *et al.*, "A Three-Dimensional Model of Reference Thermal/Mechanical and Hydrological Stratigraphy at Yucca Mountain, Southern Nevada, Sandia National Laboratories, Albuquerque, New Mexico, SAND84-1076, month 1985.

Pabalan, R. T., "Nonideality effects on the ion exchange behavior of the zeolite mineral clinoptilolite," *Mat. Res. Soc. Symp. Proc.*, 212:559-567 [1991].

Parsons, A.M., N.E. Olague, and D.P. Gallegos, "Conceptualization of a Hypothetical High-Level Nuclear Waste Repository Site in Unsaturated, Fractured Tuff," Nuclear Regulatory Commission, NUREG/CR-5495, month 1991.

Patrick, W.C., ed., "Report on Research Activities for Calendar Year 1990," Nuclear Regulatory Commission, NUREG/CR-5817, month 1991. [Prepared by the Center for Nuclear Waste Regulatory Analyses.]

Peters, R.R., *et al.*, "Fracture and Matrix Hydrologic Characteristics of Tuffaceous Materials from Yucca Mountain, Nye County, Nevada," Sandia National Laboratories, Albuquerque, New Mexico, SAND84-1471, month 1984.

Peters, R.R., J.H. Gauthier, and A.L. Dudley, "The Effect of Percolation Rate on Water-Travel Time in Deep, Partially Saturated Zones," Sandia National Laboratories, Albuquerque, New Mexico, SAND85-0854, month 1986.

Peters, C., A. Yang, I.C. Higgins, J.D., and Burger. P.A., "A preliminary study of the chemistry of pore water extracted from tuff by one-dimensional compression," Water-Rock Interaction, Kharaka & Maest (eds.), Balkema, Rotterdam, 1992.

Prindle, R.W. and P.L. Hopkins, "On Conditions and Parameters Important to Model Sensitivity for Unsaturated Flow Through Layered, Fractured Tuff: Results of Analyses for HYDROCOIN Level 3 Case 2," Sandia National Laboratories, Albuquerque, New Mexico, SAND89-0652, 1990.

Pruess, K., and Y.W. Tsang, "On Two-Phase Relative Permeability and Capillary Pressure of Rough-Walled Rock Fractures," Lawrence Berkeley Laboratory, Berkeley, California, LBL-27449, month 1989.

Pruess, K., J.S.Y. Wang, and Y.W. Tsang, "On Thermohydrologic Conditions Near High-Level Nuclear Wastes Emplaced in Partially Saturated Fractured Tuff 1. Simulation Studies With Explicit Consideration of Fracture Effects," *Water Resources Research*, 26:1235-1248, [1990].

Pruess, K., J.S.Y. Wang, and Y.W. Tsang, "On Thermohydrologic Conditions Near High-Level Nuclear Wastes Emplaced in Partially Saturated Fractured Tuff 2. Effective Continuum Approxomation," *Water Resources Research*, 26:1249-1261 [1990].

Pruess, K., J.S.Y. Wang, and Y.W. Tsang, "Effective Continuum Approximation for Modeling Fluid and Heat Flow in Fractured Porous Tuff," Sandia National Laboratories, Albuquerque, New Mexico, SAND86-7000, month 1988.

Reardon, E.J., "K_d's -- Can They Be Used to Describe Reversible Ion Sorption Reactions in Contaminant Migration?" *Groundwater*, 19:279-286 [1981].

Rush, F.E., *et al.*, "Geohydrologic and Drill-Hole Data for Test Well USW H-1, Adjacent to Nevada

Test Site, Nye County, Nevada," U.S. Geological Survey, Open File Report, OFR-83-141, 1983.

Rush, F.E., "Geohydrology of Test Well USW H-1, Yucca Mountain, Nye County, Nevada," U.S. Geological Survey, Water-Resources Investigations Report, WRIR-83-4032, 1984.

Scott, R.B., R.W. Spengler, S. Diehl, A.R. Lappin, and M.P. Chornak, "Geologic Character of Tuffs in the Unsaturated Zone at Yucca Mountain, Southern Nevada,"in J.W. Mercer, P.S.C. Rao, and I.W. Marine (eds.), *Role of the Unsaturated one in Radioacative and Hazardous Waste Disposal*, Ann Arbor Science Publishers, Ann Arbor, Mich. 1983, pp. 289-335.

Scott, R.B., and Bonk, J., "Preliminary Geologic Map of Yucca Mountain, Nye County, Nevada, With Geologic Sections," U.S. Geological Survey, Open File Report, OFR-84-494, 1984.

Scott, R.B.. "Stratigraphic and Structural Relations of Volcanic Rocks in Drill Holes USW GU-3 and USW G-3, Yucca Mountain, Nye County, Nevada," U.S. Geological Survey, Open File Report, OFR-84-491, 1984a.

Spengler, R.W., *et al.*, "Stratigraphy and Structure of Volcanic Rocks in Drill Hile USW-G1, Yucca Mountain, Nye County, Nevada," U.S. Geological Survey, Open File Report, OFR-81-1349, 1981.

Thomas, K., *Summary of Sorption Measurements Performed with Yucca Mountain, Nevada, Tuff Samples and Water from Well J-13*, LA-10960-MS, 1987.

Thordarson, W., "Geohydrologic Data and Test Results From Well J-13, Nevada Test Site, Nye County, Nevada," U.S. Geological Survey, Water-Resources Investigations Report, WRIR-83-4171, 1983.

Thordarson, W., *et al.*, "Geohydrology of Test Well USW H-3, Yucca Mountain, Nye County, Nevada," U.S. Geological Survey, Water-Resources Investigations Report, WRIR-84-4272, 1985.

Tsang, Y.W., and K. Pruess, "A Study of Thermally Induced Convection Near A High-Level Nuclear Waste Repository in Partially Saturated Fractured Tuff," *Water Resources Research*, 23:1958-1966 [1987].

Updegraff, C.D., C.E. Lee, and D.P. Gallegos, "DCM3D: A Dual-Continuum, Three-Dimensional, Ground-Water Flow Code for Unsaturated, Fractured, Porous Media," Nuclear Regulatory Commission, NUREG/CR-5536, month 1991.

U.S. Department of Energy, "Site Characterization Plan, Yucca Mountain Site, Nevada Research and Development Area, Nevada," Nevada Operations Office/Yucca Mountain Project Office, Nevada, DOE/RW-0199, 9 Vols., December 1988a.

DOE, 1988b

U.S. Department of Energy, "Site Characterization Plan Overview, Yucca Mountain Site, Nevada Research and Development Area, Nevada," Nevada Operations Office/Yucca Mountain Project Office, Nevada, DOE/RW-0198, December 1988c.

Weeks, E.P., "Effect of Topography on Gas Flow in Unsaturated Fractured Rock: Concepts and Observations," in Evans, D.D. and T.J. Nicholson, eds., *Flow and Transport Through Unsaturated Fractured Rock*, American Geophysical Union, Washington, D.C., Geophysical Monograph 42, pp. 165-170, 1987.

Whitfield, M.S., *et al.*, "Geohydrologic and Drill-Hole Data for Test Well USW H-4, Yucca Mountain, Nye County, Nevada," U.S. Geological Survey, Open File Report, OFR-84-449, 1984.

Whitfield, M.S., *et al.*, "Geohydrology of Rocks Penetrated by Test Well USW H-4, Yucca Mountain, Nye County, Nevada," U.S. Geological Survey, Water-Resources Investigations Report, WRIR-85-4030, 1985.

WoldeGabriel, G., Broxton, D.E., Bish, D.L., and Chipera, S.J., "Preliminary assessment of clinoptilolite K/Ar results from Yucca Mountain, Nevada, USA: A potential high-level radioactive waste repository site," in Kharaka & Maest (eds.), *Water-Rock Interaction*, Balkema, Rotterdam, 1992.

Chapter 5. Source Term Module

Altenhofen, M.K. and P.W. Eslinger, "Evaluation of near filed termal environmental conditions for a spent fuel repository in tuff", pp 402-409, High Level Radioactive Waste Management (1990), American Nuclear Society, La Grange Park Illinois

Bateman, H, 1910, "The solution of a system of differential equations occurring in the theory of radiactive transformation", Proceedings of the Cambridge Philosophical Society, 15:473

Bazant, Z.P. and L. Cedolin, 1991, Stability of Structures, Oxford University Press, New York

Carslaw, H.S., and J.C. Jaeger, *Conduction of Heat in Solids*, Oxford, England: Clarendon Press, 1959.

R. Codell, "Model for Release of Gaseous ^{14}C from Spent Fuel", *High Level Radioactive Waste Management*, April 26-30, 1993, Las Vegas Nevada, American Nuclear Society, La Grange Park, Illinois, 22 (1993).

Buscheck, T.A., and J.J. Nitao, "The Analysis of Repository-Heat-Driven Hydrothermal Flow at Yucca Mountain," Lawrence Livermore National Laboratory, *High Level Radioactive Waste Management, Proceedings of the Fourth Annual International Conference*, La Grange Park, IL: American Nuclear Society, Inc., 1993.

T.A. Buscheck, D.G. Wilder, and J.J. Nitao, "Large Scale In Situ Heater Tests for Hydrothermal Characterization at Yucca Mountain", *High Level Radioactive Waste Management*, April 26-30, 1993, Las Vegas Nevada, American Nuclear Society, La Grange Park, Illinois, 1854 (1993).

Einziger, R.E, and R. Kohli, "Low-temperature rupture behavior of Zircaloy-Clad pressurized water reactor spent fuel rods under dry storage conditions," *Nuclear Technology* 67:107-123 [1984].

Einziger, R.E. and R.E. Woodley, "Predicting spent fuel oxidation states in a tuff repository", HEDL-SA-3627, Westinghouse Hanford Company, April 1987

Einziger, R.E., and H.C. Buchanan, "Long-term, low-temperature oxidation of PWR spent fuel," Richland, Washington, Westinghouse Hanford Co, WHC-EP-0070, month 1988.

Einziger, R.E. 1991. *Effects of an Oxidizing Atmosphere in a Spent Fuel Packaging Facility*. Proceedings of FOCUS '91: American Nuclear Society: 88-99.

Einziger, R.E. "Evaluation of the Potential for Spent Fuel Oxidation Under Tuff Repository Conditions," Richland, Washington, Engineering Development Laboratory, HEDL-7452, month 1991.

Einziger, R.E., S.C. Marschman, and H.C. Buchanan, "Spent-fuel dry-bath oxidation testing. *Nuclear Technology*, 94:383-393 [1991].

Einziger, R.E., H.C. Buchanan, L.E. Thomas, and R.B. Stout. 1992. Oxidation of spent fuel in air at 75 and 195 C. *High-Level Radioactive Waste Management* 1449-1457.

Farmer, J.C., G.E. Gdowski, R.D. McCright, and H.S. Abluwablia, "Corrosion models for performance assessment of high-level radioactive-waste containers,' *Nuclear Engineering Design*, 129: 57-88 [1991].

Foster, A.R., and R.L. Wright, *Basic Nuclear Engineering (Third Edition)*, Boston, Massachusetts, Allyn and Bacon, 1977.

Gazarelli, F., D. Jorde, R. Manzel, "Review of PWR Fuel Rod Waterside Corrosion Behavior," Palo Alto, California, Electric Power Research Institute, month 1980.

Grambow, B., "Spent fuel dissolution and oxidation—An evaluation of literature data," Stokholm, Sweden, Swedish Nuclear Power Inspectorate, SKB Technical Report: 89-13, month 1989.

Henshall, G.A. 1991. *Stochastic models for predicting pitting corrosion damage of HLRW containers.* Proceedings of FOCUS'91. American Nuclear Society: 8.

Kubaschewski, O., and B.E. Hopkins, *Oxidation of Metals and Alloys,* London, England: Butterworth Publishers, ? 36, 1962.

Kopp, D., and H. Munzel, "Release of volatile carbon-14 containing products from Zircaloy. *Journal of Nuclear Materials*, 173: 1-6 [1990].

Johnson, G.L. and D.L. Montan, "Thermal calculations pertaining to a proposed Yucca Mountain nuclear waste repository", UCRL-ID-103534, Lawrence Livermore National Laboratory, February 1990

Lapidus, L., *Digital Computation for Chemical Engineers*, New York, New York, McGraw-Hill, 1962.

Macdonald, D.D., and M. Urquidi-Macdonald, "Thin-layer mixed-potential model for the corrosion of high-level nuclear waste canisters," *Corrosion*, 46(5): 380-390 [1990].

Nilson, R.H., E.W. Peterson, K.H. Lie, N.R. Burkhard, and H.R. Hearst, "Barometric pumping of contaminated gases through fractured permeable media", High Level Radioactive Waste Management, Las Vegas Nevada, 1991, American Nuclear Society, La Grange Park, Illinois, pp 861-868

O'Neal, W.C., D.W. Gregg, J.N. Hockman, E.W. Russell, and W. Stein, "Preclosure analysis of conceptual waste package designs for a nuclear waste repository in tuff," Livermore, California, Lawrence Livermore National Laboratory (LLNL), UCRL 53595, month 1984. [Prepared for the U.S. Department of Energy/Office of Civilian Radioactive Waste Management.]

Park, U.S., "Regulatory overview and recommendations on a repository's release of carbon-14," San Diego, California, Science Applications International Corp, January 1992. [Prepared for the U.S. Department of Energy/Office of Civilian Radioactive Waste Management.]

Pigford, Th.H., P.L. Chambré, W. Lee, "A Review of Near-Field Mass Transfer in Geologic Disposal Systems," *Radioactive Waste Management and the Nuclear Fuel Cycle* 16(3)(4) [1992].

Press, W.H., B.P. Flannery, S.A. Teukolsky, and W.T. Vettering, *Numerical Recipes*. New York, New

York, Cambridge University Press, 1989.

Ramirez, A.L. and D.G. Wilder, "Protoype engineered barrier system field tests", UCID-21640, Lawrence Livermore National Laboratory, 1991

Sagar, B., R.B. Codell, J. Walton, R.W. Janetzke, "SOTEC: A source term code for high-level nuclear waste geologic repositories - Users Manual: Version 1.0", CNWRA 92-009, Center for Nuclear Waste Regulatory Analyses

Sagar, B., and R.W. Janetzke, "Total System Performance Assessment Computer Code: Description of Executive Module," San Antonio, Texas, Center for Nuclear Waste Regulatory Analyses, CNWRA 91-009, month 1991. [Prepared for the Nuclear Regulatory Commission/Office of Nuclear material Safety and Safeguards.]

D.W. Shoesmith and S. Sunder, "The Prediction of Nuclear Fuel (UO_2) Dissolution Rates under Waste Disposal Conditions", *J. Nucl. Mat.* 190:, p. 20 (1992).

Smith, H.D., and D.L. Baldwin. 1989. *An investigation of thermal release of C-14 from PWR spent fuel cladding*. Proceedings of FOCUS '89. Las Vegas, Nevada: 46-49.

R. Stout, E. Kansa, H. Buchanan, R. Einziger, and L. Thomas, "Spent Fuel Waste Form Characteristics: Grain and Fragment Size Statistical Dependence for Oxidation Response", *High Level Radioactive Waste Management*, April 28-May 3, 1991, Las Vegas Nevada, American Nuclear Society, La Grange Park, Illinois, 103 (1991).

Stout, R.B., "Overview of spent fuel modeling concepts", presentation to Nuclear Waste Technical Review Board, Las Vegas Nevada, October 14-16, 1992

Thomas, L.E., O.D. Slagle, and R.E. Einziger," Nonuniform oxidation of LWR spent fuel in air," *Journal of Nuclear Material*, 184: 117-126 [1991].

U.S. Department of Energy, *Site Characterization Plan Overview, Yucca Mountain Site, Nevada Research and Development Area, Nevada*, Nevada Operations Office/Yucca Mountain Project Office, Nevada, DOE/RW-0198, (1988).

U.S. Department of Energy, *Integrated Data Base for 1992: U.S. Spent Fuel and Radioactive Waste Inventories, Projections and Characteristics*, Revision 8, RW-0006, U.S. Department of Energy, OCRWM (1992).

U.S. Department of Energy, *Site Characterization Progress Report, October 1, 1992 - March 31, 1993*, U.S. Department of Energy, DOE/RW-0423, Office of Civilian Radioactive Waste Management (1993).

Watson, M., and J. Postlethwaite, "Numerical simulation of crevice corrosion of stainless steel and nickel alloys in chloride solutions," *Corrosion*, 46(7): 522-530 [1990].

Williford, R.E. 1991. *Uncertainties in Container Failure Time Predictions*. Mat. Res. Soc. Symp.

Proc. 212: 335-342.

C.N. Wilson, *Results from NNWSI series 3 spent fuel dissolution tests*, Battelle Pacific Northwest Laboratories, Richland, Washington PNL-7071 (1990).

Van Konynenburg, R.A., C.F. Smith, H.W. Culham, and C.H. Otto, "Behavior of carbon-14 in waste packages for spent fuel in a repository in tuff," Livermore, California: Lawrence Livermore National Laboratory, UCRL-90855, November 1984.

R.A. Van Konynenburg, C.F. Smith, H.W. Culham, and H.D. Smith "Carbon-14 in Waste Packages for Spent Fuel in a Tuff Repository", *Material Research Society Proceedings, 84: p.* 185 (1987).

Van Konynenburg, R.A, "Carbon-14 in Waste Packages for Spent Fuel in a Tuff Repository," in *Scientific Basis for Nuclear Waste Management*, Materials Research Society 84: 185-196 [1987].

Van Konynenburg, R.A. 1991. *Gaseous Release of Carbon-14: Why the High-Level Waste Regulations Should be Changed.* Proceedings of the 1992 International High Level Waste Management Conference. Las Vegas Nevada: 313-319.

Van Konynenburg, R.A. personal communication 1992

WALTON 1993 (This reference has not been finalized yet. Lets ask Budhi before we go to press)

Wilson, C.N. "Results from NNWSI series 3 spent fuel dissolution tests," Richland, Washington, Battelle Pacific Northwest Laboratories, PNL-7071, month 1990.

Woodley, R.E., R.E. Einziger, and H.C. Buchanan, "Measurement of the oxidation of spent fuel between 140 and 225°C," *Nuclear Technology*, 85: 74-88 [1989].

P.A. Tempest, P.M. Tucker, J.W. Tyler, "Oxidation of UO_2 Fuel Pellets in Air at 503 and 543 °K Studied using X-ray Photoelectron Spectroscopy and X-ray Diffraction", *J. Nuclear Materials*, **151:**, p. 251 (1988) .

Chapter 6. Disruptive Consequence Analysis Module

Bazant, Z.P., and L. Cedolin, *Stability of Structures*, Oxford University Press, New York, New York,1991.

czarneki 1985

Connor, C.B., and B.E. Hill. 1993. *Volcanism Research, High-Level Radioactive Waste Research at CNWRA, January-June, 1993*. CNWRA 92-02S. San Antonio, TX: Center for Nuclear Waste Regulatory Analyses.

Connor, C.C., B.E. Hill, G.L. Stirewalt, and S.R. Young. "NRC High-Level Radioactive Waste Research at CNWRA, July 1 through December 31, 1992," Center for Nuclear Waste Regulatory Analyses, CNWRA 92-025, month 1993. [Prepared for the Nuclear Regulatory COmmission.]

Crisp, J.A., "Rates of Magma Emplacement and Volcanic Output," *Journal of Volcanology and Geothermal Research*, 20:177-211 [1984].

Crowe, B.M., M.E. Johnson, and R.J. Beckman, "Calculation of the Probability of Volcanic Disruption of a High-level Radioactive Waste Repository within Southern Nevada," *U.S. Radioactive Waste Management and the Nuclear Fuel Cycle*, 3:167-190 [1982].

crowe and perry 1989

Crowe, B.M., S. Self, D. Vaniman, R. Amos, and F. Perry, "Aspects of Potential Magmatic Disruptions of a High-Level Radioactive Waste Repository in Southern Nevada," *Journal of Geology*, 91:259-276 [1983].

Crowe, B.M. 1992. *Status of Probability Studies*. Panel on Structural Geology and Geoengineering Meeting on Volcanism. U.S. Nuclear Waste Technical Review Board, Sept. 14-16, 1992, Las Vegas, NV Meeting Notes.

Crowe, B.M., R. Picard, G.A. Valentine, and R.F. Perry. 1992. *Recurrence Models of Volcanic Events: Applications to Volcanic Risk Assessment*. Third Conference on Radioactive Waste Management, April 14-16, Las Vegas, NV: American Nuclear Society and American Society of Civil Engineers: 2344-2355.

ho 1990

Ho, C.-H. 1992. *Risk Assessment for the Yucca Mountain High-Level Nuclear Waste Repository Site: Estimation of Volcanic Disruption*. Panel on Structural Geology and Geoengineering Meeting on Volcanism. U.S. Nuclear Waste Technical Review Board, September 14-16, 1992, Las Vegas, NV Meeting Notes.

Ho, C.-H., E.I. Smith, D.L. Feurbach, and T.R. Naumann. 1991. Eruptive probability calculation for the Yucca Mountain site, USA: Statistical estimation of recurrence rates. *Bulletin of Volcanology* 54:50-56.

Lin, C.S., R.G. Baca, and R. Drake, "VOLCANO Code — A Module for Simulation of Magmatic Scenario Model Description and User Guide, Center for Nuclear Waste Regulatory Analyses, CNWRA 93-010. month 1993. [Prepared for the Nuclear Regulatory Commission.]

Margulies, T., L. Lancaster, N. Eisenberg, and L. Abramson, "Probability Analysis of Magma Scenarios for Assessing Geologic Waste Repository Performance," American Society of Mechanical Engineers, *Winter Annual Meeting*, Anaheim, CA, November 8-13, 1992.

Nakamura, K., "Volcanoes as Possible Indicators of Tectonic Stress Orientation: Principle and Proposal," *Journal of Volcanology and Geothermal Research*, 2:1-16 [1977].

Sagar, B., and R.W. Janetzke. 1993. *Total-System performance Assessment (TPA) Computer Code; Description of Executive Module, Version 2.0*. CNWRA 93-107. San Antonio, TX: Center for Nuclear Waste Regulatory Analyses.

Sheridan, M.F. 1992. A Monte Carlo technique to estimate the probability of volcanic dikes. *Proceedings of the Third International Conference on High-Level Radioactive Waste Management*. Las Vegas, NV: American Nuclear Society and American Society of Civil Engineers: 2033-2038.

Smith, E.I., T.R. Feuerbach, and J.E. Faulds. 1990. The area of most recent volcanism near Yucca Mountain, Nevada: Implications for volcanic risk assessment. High-Level Radioactive Waste Meeting. *Proceedings of the International Topical Meeting*. LaGrange Park, IL: American Nuclear Society 1:81-90.

Trapp, J.S. and P.S. Justus, "Regulatory Requirements to Address Issues Related to Volcanism and Magmatism: Code of Federal Regulations, Title 10, Part 60, Disposal of High-Level Radioactive Wastes in Geological Repositories. *Proceedings of the Third International Conference on High Level Radioactive Waste Management*: 2039-2046,. 1992.

Valentine, G.A., B.M. Crowe, and F.V. Perry. 1992. Physical Processes and Effects of Magmatism in the Yucca Mountain Region. *Proceedings of the Third International Conference on High-Level Radioactive Waste Management*. Las Vegas, NV: American Nuclear Society and American Society of Civil Engineers: 2014-2024.

Roark, R.J., and W.C. Young, *Formulas for Stress and Strain (Fifth Edition)*, New York, New York, McGraw-Hill Book Company, 1975. Table 35,

Chapter 7. Dose Assessment Module

Baes, C. F. III, R.D. Sharp, A.L. Sjoreen and R.W. Shor, "A Review and Analysis of Parameters for Assessing Transport of Environmentally Released Radionuclides through Agriculture, Oak Ridge, Tenn., Oak Ridge National Laboratory," ORNL-5786, 1984.

Biospheric Model Validation Study, "BIOMOVS II: Progress Report No. 2," Oxon, United Kingdom, INTERA, BIOMOVS II PR2 (Report IE2859-2), May 1992.

Charles, D. and G. M. Smith, "Conversion of Releases from the Geosphere to Estimates of Individual Doses to Man (Version 2)," Oxon, United Kingdom, INTERA, Report IM1802-10, July 1991.

Code of Federal Regulations, "Environmental Standards for the Management and Disposal of Spent Nuclear Fuel, High-Level and Transuranic Radioactive Wastes," Part 191, Chapter I, Title 40, "Protection of the Environment."

Code of Federal Regulations, "Standards for Protection Against Radiation," Part 20, Chapter I, Title 10, "Energy."

Czarnecki, J.B., "Simulated Water-Level Declines Caused by Withdrawls from Wells J-13 and J-12 Near Yucca Mountain, Nevada," U.S. Geological Survey, Open-File Report 91-478, 1992.

Doctor, P.G. *et al.*, "An Example Postclosure Risk Assessment Using the Potential Yucca Mountain Site," Richland, Washington, Pacific Northwest Laboratory, PNL-8081, May 1992. [Prepared for the U.S. Department of Energy.]

Federline, M.V., "Nuclear Regulatory Commission Staff Views on Environmental Standards for Disposal of High-Level Wastes," Unpublished Presentation to the National Academy of Sciences Committee on Technical Bases for Yucca Mountain Standards, May 27, 1993.

International Atomic Energy Agency, "Generic Models and Parameters for Assessing the Environmental Transfer of Radionuclides from Routine Releases, Exposures of Critical Groups: Procedures and Data," Vienna, Safety Series No. 57, 1982.

International Commission on Radiological Protection, "Reference Man: Anatomical, Physiological, and Metabolic Characteristics (Report of the Task Group on Reference Man)," Pergamon Press, Oxford, ICRP Publication 23, 1975.

International Commission on Radiological Protection, "Recommendations of the ICRP," *Annals of the ICRP*, vol. 1, no. 3, ICRP Publication 26, 1977.

International Commission on Radiological Protection, "Limits for Intakes of Radionuclides by Workers (Part 1)," *Annals of the ICRP*, vol. 2, nos. 3/4, ICRP Publication 30, 1979.

International Commission on Radiation Protection, "The Metabolism of Compounds of Plutonium and Other Actinides," Pergamon Press, New York, ICRP Publication 19, 1986.

International Commission on Radiological Protection, "Radiation Protection: 1990 Recommendations of the International Commission on Radiological Protection," *Annals of the ICRP*, vol. 21, nos. 1-3, ICRP Publication 60, 1990.

Kennedy, W.E., Jr. and D.L. Strenge, "Residual Radioacitive Contamination from Decommissioning, Technical Basis for Translating Contamination Levels to Annual Total Effective Dose Equivalent, Final Report," Nuclear Regulatory Commission, NUREG/CR-5512, 2 vols., October 1992. [Prepared by the Pacific Northwest Laboratory.]

Kocher, D.C., "Dose-Rate Conversion Factors for External Exposure to Photons and Electrons," Nuclear Regulatory Commission, NUREG/CR-1918, month 1981.

Leigh, C.D. *et al.*, "User's Guide for GENII-S: A Code for Statistical and Deterministic Simulation of Radiation doses to Humans from Radionuclides in the Environment," Albuquerque, Sandia National Laboratories, SAND 91-0561, April 1993.

Logan, S.E. *et al.*, "Parametric Studies of Radiological Consequences of Basaltic Volcanism," Albuquerque, Sandia National Laboratories, SAND 81-2375, April 1982. [Prepared for the U.S. Department of Energy.]

Mills, L., "Beginning Desert Gardening," University of Nevada Cooperative Extension, 1993.

Napier, B.A *et al.*, "GENII: The Hanford Environmental Radiation Dosimetry Software System, Volume 1: Conceptual Representation," Richland, Washington, Pacific Northwest Laboratory, PNL-6584, December 1988a. [Prepared for the U.S. Department of Energy.]

Napier, B.A *et al.*, "GENII: The Hanford Environmental Radiation Dosimetry Software System, Volume 2: Users' Manual," Richland, Washington, Pacific Northwest Laboratory, PNL-6584, December 1988b. [Prepared for the U.S. Department of Energy.]

Nevada Agricultural Statistics Service, "Nevada Agricultural Statistics: 1987-1988," Reno, Nevada, 1988.

Nuclear Regulatory Commission, "Standards for Protection Against Radiation [Final Rule]," *Federal Register*, vol. 56, no. 98, May 21, 1991, pp. 23360 - 23474.

U.S. Department of Commerce/Bureau of the Census, "1987 Census of Agriculture, Volume 1: Geographic Area Series, Part 28: Nevada State and County Data," Washington, D.C., AC87-A-28, June 1989.

U.S. Department of Commerce/National Oceanographic and Atmospheric Administration, "STAR Data for Desert Rock Station, Nevada (1986-1990)," Nashville, North Carolina, National Climatic Data Center, 1992.

U.S. Department of Energy, "Chapter 3, Hydrology," in "Site Characterization Plan, Yucca Mountain Site, Nevada Research and Development Area, Nevada," Office of Civilian Radioactive Waste Management, Nevada Operations Office/Yucca Mountain Project Office, Nevada, DOE/RW-0199, vol.II, Part A, December 1988.

U.S. Environmental Protection Agency, "Environmental Standards for the Management of Spent Nuclear Fuel, High-Level and Transuranic Wastes [Final Rule]," *Federal Register*, vol. 50, no. 182, September 19, 1985, pp. 38066 - 38089.

U.S. Environmental Protection Agency, "High-Level and Transuranic Radioactive Wastes: Background Information Document for Final Rule," Washington, D.C., Report 520/1-85-023, August 1985.

U.S. Environmental Protection Agency, "Limiting Values of Radionuclide Intake and Air Concentration and Dose Conversion Factors for Inhalation, Submersion and Ingestion," Washington, D.C., EPA-520/1-88-020, September 1988.

U.S. Environmental Protection Agency, "Environmental Radiation Protection Standards for the Management and Disposal of Spent Nuclear Fuel, High-Level and Transuranic Radioactive Wastes [Proposed Rule]," *Federal Register*, vol. 58, no. 26, February 10, 1993, pp. 7924 -7936.

Chapter 8. Sensitivity and Uncertainty Analysis Module

Baybutt, P., D.C. Cox, and R.E. Kurth, "Methodology for Uncertainty Analysis of Light Water Reactor Meltdown Accident Consequences," Topical Report prepared by the Battelle Columbus Laboratories for the Nuclear Regulatory Commission, month 1981.

Bowen, W.A. and C.A. Bennett, *Statistical Methods for Nuclear Material Management*, Nuclear Regulatory Commission, NUREG/CR-4604, March 1988.

Cochran, W.G., *Sampling Techniques*, John Wiley and Sons, 1963.

Codell, R. *et al.*, "Initial Demonstration of the NRC's Capability to Conduct a Performance Assessment for a High-Level Waste Repository," Office of Nuclear Material Safety and Safeguards/Office of Nuclear Regulatory Research, NUREG-1327, May 1992.

Draper, N.R. and H. Smith, *Applied Regression Analysis*, John Wiley and Sons, Inc. New York, 1966.

Gunst, R.F. and R.L. Mason, *Regression Analysis and its Application*, Marcel Dekker, Inc., New York, 1980.

Gureghian, A.B. Y.-T. Wu, B. Sagar, and R.B. Codell, "Sensitivity and Uncertainty Analyses Applied to One-Dimensional Radionuclide Transport in a Layered Fractured Rock," NUREG/CR-5917, December, 1992. [Prepared for the Nuclear Regulatory Commission.]

Helton, J.C., *SIAM Review*, vol 12, no.1 [1961].

Helton, J.C., J.W. Garner, R.D. McCurley, and D.K. Rudeen, "Sensitivity Analysis Techniques and Results for Performance Assessment at the Waste Isolation Pilot Plant," Sandia National Laboratories, SAND90-7103, March 1991.

Iman, R.L. and W.J. Conover, "The Use of Rank Transform in Regression," *Technometrics*, 21:499-509 [1979].

Iman, R.L., and J. Davenport, D. Zeigler, "Latin Hypercube Sampling (Program User's guide)," Sandia National Laboratories, SAND79-1473, month 1980.

Iman, R.L., and J.C. Helton, 1985, "A Comparison of Uncertainty and Sensitivity Analysis Techniques for Computer Models," Nuclear Regulatory Commission, NUREG/CR-3904, March 1985.

Intriligator, M.D. *Econometric Models, Techniques, and Applications*, Prentice-Hall, Englewood Cliffs, N.J., 1978.

McKay, M.D., "Interim Report on the Status of Research on Uncertainty Analysis of Computer Models," Prepared for U.S. Nuclear Regulatory Commission, month 1992.

Mallows, C.L., "Some comments on Cp," *Technometrics*, 15:661-675 [1973].

Mendenhall, W. and R.L. Schaeffer, *Mathematical Statisitcs with Applications*, Duxbury Press, North Scituate, Massachusetts, 1973.

Seitz, R.R., A.S. Rood, G.A. Harris, S.J. Maheras, M. Kotecki, "Sample Application of Sensitivity/Uncertainty Analysis Techniques to a Groundwater Transport Problem," Idaho National Engineering Laboratory, DOE/LLW-108, June 1991. [Prepared by EG&G Idaho, Inc., Idaho Falls, Idaho for the U.S. Department of Energy/Office of Civilian Radioactive Waste MAnagement.]

Sen, A. and M. Srivastava, *Regression Analysis -- Theory, Methods, and Applications*, Springer-Verlag, New York, 1990.

Tukey, J.W., *Exploratory Data Analysis*, Addison Wesley, Reading, MA, 1977.

Wapole, R.E., and R.H. Myers, *Probability and Statistics for Engineers and Scientists*, Macmillan Publishing Co., Inc., New York, NY., 1978.

Wu, Y.T., A.B. Gureghian, and R.B. Codell, "Sensitivity and Uncertainty Analysis Applied to One-dimensional Transport in a Layered Fractures Rock," San Antonio, Center for Nuclear Waste Regulatory Analysis, CNWRA92-002, March 1992,

Zimmerman, D.A., "A Review of Techniques for Propagating Data and Parameter Uncertainties in high-Level Radioactive Waste Performance Assessment Models," Nuclear Regulatory Commission, NUREG/CR 5393, March 1990.

Zimmerman, D.A., R.T. Hanson, and P.A. Davis, "A Comparison of Parameter Estimation and Sensitivity Analysis Techniques and Their Impact on the Uncertainty in Ground Water Flow Model Predictions," Nuclear Regulatory Commission, NUREG/CR-522, May 1991.

STA SCI 1992

Chapter 9. Analytical Results

Codell, R.M., *et al.*, "Initial Demonstration of the NRC's Capability to Conduct a Performance Assessment for a High-Level Waste Repository," Nuclear Regulatory Commission, NUREG-1327, May 1992.

Helton, J.C., J.W. Garner, R.D. McCurley, and D.K. Rudeen, "Sensitivity Analysis Techniques and Results for Performance Assessment at the Waste Isolation Pilot Plant," Sandia National Laboratories, SAND90-7103, March 1991. [Prepared for the U.S. Department of Energy/Office of Civilian Radioactive Waste MAnagement.]

Chapter 10. Tentative Conclusions

Barnard, R.W., M.L. Wilson, H.A. Dockery, J.W. Gauthier, P.G. Kaplan, R.R. Eaton, F.W. Bingham, and T.H. Robey, "TSPA: 1991 An Initial Total-System Performance Assessment for Yucca Mountain", Sandia National Laboratories, SAND91-2795, month 1991. [Prepared for the U.S. Department of Energy/Office of Civilian Radioactive Waste MAnagement.]

Eslinger, P.W., L.A. Doremus, D.W. Engel, T.B. Miley, M.T. Murphy, W.E. Nichols, M.D. White, D.W. Langford, and S.J. Ouderkirk, "Preliminary Total System Analysis of a Potential High-Level Nuclear Waste Repository at Yucca Mountain, Pacific Northwest Laboratory, PNL-8444, January 1993. [Prepared for the U.S. Department of Energy/Office of Civilian Radioactive Waste MAnagement.]

Gureghian, A.B., Y.T. Wu, B. Sagar, and R.B. Codell, "Sensitivity and Uncertainty Analyses Applied to One-Dimensional Radionuclide Transport in a Layered Fractured Rock, Volume 1: MULTFRAC -- Analytic Solutions and Local Sensitivities," Nuclear Regulatory Commission, NUREG/CR-5917, month 1992. [Prepared by the Center for Nuclear Waste Regulatory Analyses.]

Helton, J.C., J.W. Garner, R.D. McCurley, and D.K. Rudeen, "Sensitivity Analysis Techniques and Results for Performance Assessment at the Waste Isolation Pilot Plant", Sandia National Laboratories, SAND90-7103, month 1991. [Prepared for the U.S. Department of Energy/Office of Civilian Radioactive Waste Management.]

HMIP DOE, "A Trial Assessment of Underground Disposal of Radioactive Wastes Based on Probabilistic Risk Analysis", DOE Report No. DOE/HMIP/RR/92.042, January, 1993.

Wu, Y.T., A.B. Gureghian, B. Sagar, and R.B. Codell, "Sensitivity and Uncertainty Analyses Applied to One-Dimensional Radionuclide Transport in a Layered Fractured Rock -- Evaluation of the Limit State Approach," Nuclear Regulatory Commission, NUREG/CR 5917, month 19xx. [Prepared by the Center for Nuclear Waste Regulatory Analyses.]

APPENDIX A
LHS-Sampled Input Variables

The following is a list of variables used by the Total-System Performance Assessment computer code (including its modules) in the IPA Phase 2 demonstration. It includes constants that were considered as global variables. The list does not include variables or constants internal to a particular module. All dimensions are in meters-kilogram-years; open brackets ([ ]) are dimensionless variables. Variables that appear multiple times, such as *AKR( )*, are the same type of parameter, applied to a different repository subarea or stratigraphic unit.

The variables sampled for the base case *(oooo)* include those variables listed for the *C14*, *SOTEC*, and *FLOWMOD* modules. The variables sampled for the fully disturbed case *(csdv)* are those variables listed for the *C14*, *FLOWMOD*, *SOTEC*, *VOLCANO*, and *DRILLO* modules. The infiltration rate used for the fully disturbed case was the disturbed infiltration.

TYPE OF DISTIBUTION VALUE (OR RANGE IN VALUE)		*VARIABLE NAME*	*MODULE*	*VARIABLE DESCIPTION*	*BASIS FOR PARAMETER ASSIGNMENT*
CONSTANT 0.0		alpha	C14	gas dispersivity [m^2/yr]	
LOGNORMAL 6.5e-17	5.5e-15	AKR(1)	C14	fracture permeability of layer [m^2] (Tiva Canyon)	Klavetter, 1986 (+/- one order of magnitude of the reported value)
LOGNORMAL 1.6E-16	1.6e-14	AKR(2)	C14	fracture permeability of layer [m^2] (Paintbrush)	Klavetter, 1986 (+/- one order of magnitude of the reported value)
LOGNORMAL 3.24e-17	3.24e-15	AKR(3)	C14	fracture permeability of layer [m^2] (Topopah Spring)	Klavetter, 1986 (+/- one order of magnitude of the highest reported value)
LOGNORMAL 9.7E-17	9.7e-15	AKR(4)	C14	fracture permeability of layer [m^2] (Calico Hills, vitric)	Klavetter, 1986 (+/- one order of magnitude of the reported value)
LOGNORMAL 9.7E-17	9.7e-15	AKR(5)	C14	fracture permeability of layer [m^2] (Calico Hills, zeolitic)	Klavetter, 1986 (+/- one order of magnitude of the reported value)
CONSTANT 0.00014		pork(1)	C14	fracture porosity of layer [ ] (Tiva Canyon)	Klavetter, 1986 (reported value)
CONSTANT 0.000027		pork(2)	C14	fracture porosity of layer [ ] (Paintbush)	Klavetter, 1986 (reported value)
CONSTANT 0.000041		pork(3)	C14	fracture porosity of layer [ ] (Topopah Spring)	Klavetter, 1986 (reported value)
CONSTANT 0.000046		pork(4)	C14	fracture porosity of layer [ ] (Calico Hills, vitric)	Klavetter, 1986 (reported value)

TYPE OF DISTIBUTION VALUE (OR RANGE IN VALUE)		*VARIABLE NAME*	*MODULE*	*VARIABLE DESCIPTION*	*BASIS FOR PARAMETER ASSIGNMENT*
CONSTANT 0.000046		pork(5)	C14	fracture porosity of layer [ ] (Calico Hills, zeolitic)	Klavetter, 1986 (reported value)
UNIFORM 10.0	100.	retardk(1)	C14	retardation factor [ ] (Tiva Canyon)	
UNIFORM 10.0	100.	retardk(2)	C14	retardation factor [ ] (Paintbrush)	
UNIFORM 10.0	100.	retardk(3)	C14	retardation factor [ ] (Topopah Spring)	
UNIFORM 10.0	100.	retardk(4)	C14	retardation factor [ ] (Calico Hills, vitric)	
UNIFORM 10.0	100.	retardk(5)	C14	retardation factor [ ] (Calico Hills, zeolitic)	
LOGNORMAL 3.6e-19	1.2e-18	permm (1)	FLOWMOD	matrix permability [m^2] (Topopah Spring)	Peters, 1984 (reported range and correlation length considerations)
LOGNORMAL 3.9e-15	2.0e-14	permm (2)	FLOWMOD	matrix permability [m^2] (Calico Hills, vitric)	Peters, 1984 (reported range and correlation length considerations)
LOGNORMAL 1.3e-20	6.7e-19	permm (3)	FLOWMOD	matrix permeability [m^2] (Calico Hills, zeolitic)	Peters, 1984 (reported range and correlation length considerations)
LOGNORMAL 1.9e-16	9.6e-16	permm (4)	FLOWMOD	matrix permeability [m^2] (Prow Pass)	Peters, 1984 (reported range and correlation length considerations)
LOGNORMAL 5.1e-18	1.5e-17	permm (5)	FLOWMOD	matrix permeability [m^2] (Upper Crater Flat)	Peters, 1984 (reported range and correlation length considerations)
LOGNORMAL 3.5e-16	4.4e-16	permm (6)	FLOWMOD	matrix permeability [m^2] (Bullfrog)	Peters, 1984 (reported range and correlation length considerations)
LOGNORMAL 4.1e-18	1.6e-17	permm (7)	FLOWMOD	matrix permeability [m^2] (Middle Crater Flat)	assumed same as Upper Crater Flat

TYPE OF DISTIBUTION VALUE (OR RANGE IN VALUE)		VARIABLE NAME	MODULE	VARIABLE DESCIPTION	BASIS FOR PARAMETER ASSIGNMENT
LOGNORMAL 1.1e-16	1.9e-16	permf (1)	FLOWMOD	fracture permability [m^2] (Topopah Spring)	Klavetter, 1986 (reported range and correlation length considerations
LOGNORMAL 5.6e-16	1.2e-15	permf (2)	FLOWMOD	fracture permability [m^2] (Calico Hills, vitric)	Klavetter, 1986 (+/- 50 percent of reported value and correlation length considerations)
LOGNORMAL 6.2e-16	9.9e-16	permf (3)	FLOWMOD	fracture permeability [m^2] (Calico Hills, zeolitic)	Klavetter, 1986 (+/- 50 percent of reported value and correlation length considerations)
LOGNORMAL 3.9e-17	8.1e-17	permf (4)	FLOWMOD	fracture permeability [m^2] (Prow Pass)	Klavetter, 1986 (+/- 50 percent of reported value and correlation length considerations)
LOGNORMAL 6.7e-16	9.8e-16	permf (5)	FLOWMOD	fracture permeability [m^2] (Upper Crater Flat)	assumed same as Calico Hills
LOGNORMAL 4.9e-17	6.4e-17	permf (6)	FLOWMOD	fracture permeability [m^2] (Bullfrog)	assumed same as Prow Pass
LOGNORMAL 6.2e-16	9.9e-16	permf (7)	FLOWMOD	fracture permeability [m^2] (Middle Crater Flat)	assumed same as Calico Hills
UNIFORM 0.06	0.16	porm (1)	FLOWMOD	matrix porosity [ ] (Topopah Spring)	Peters, 1984 (reported range)
UNIFORM 0.330	0.560	porm (2)	FLOWMOD	matrix porosity [ ] (Calico Hills, vitric)	Peters, 1984 (+/- 25 percent of mean)
UNIFORM 0.20	0.33	porm (3)	FLOWMOD	matrix porosity [ ] (Calico Hills, zeolitic)	Peters, 1984 (+/- 25 percent of mean)
UNIFORM 0.24	0.40	porm (4)	FLOWMOD	matrix porosity [ ] (Prow Pass)	Peters, 1984 (+/- 25 percent of mean)
UNIFORM 0.18	0.30	porm (5)	FLOWMOD	matrix porosity [ ] (Upper Crater Flat)	Peters, 1984 (+/- 25 percent of mean)
UNIFORM 0.19	0.32	porm (6)	FLOWMOD	matrix porosity [ ] (Bullfrog)	Peters, 1984 (+/- 25 percent of mean)

TYPE OF DISTIBUTION VALUE (OR RANGE IN VALUE)	*VARIABLE NAME*	*MODULE*	*VARIABLE DESCIPTION*	*BASIS FOR PARAMETER ASSIGNMENT*
UNIFORM 0.18 0.30	porm (7)	FLOWMOD	matrix porosity [ ] (Middel Crater Flat)	assumed same as Upper Crater Flat or 25 +/- percent of mean)
CONSTANT 4.1e-5	porf (1)	FLOWMOD	fracture porosity [ ] (Topopah Spring)	Klavetter, 1986
CONSTANT 4.6e-5	porf (2)	FLOWMOD	fracture porosity [ ] (Calico Hills, vitric)	Klavetter, 1986
CONSTANT 4.6e-5	porf (3)	FLOWMOD	fracture porosity [ ] (Calico Hills, zeolitic)	Klavetter, 1986
CONSTANT 1.3e-5	porf (4)	FLOWMOD	fracture porosity [ ] (Prow Pass)	Klavetter, 1986
CONSTANT 4.6e-5	porf (5)	FLOWMOD	fracture porosity [ ] (Upper Crater Flat)	assumed same as Calico Hills
CONSTANT 1.3e-5	porf (6)	FLOWMOD	fracture porosity [ ] (Bullfrog)	assumed same as Prow Pass
CONSTANT 4.6e-5	porf (7)	FLOWMOD	fracture porosity [ ] (Middle Crater Flat)	assumed same as Calico Hills
UNIFORM 1.4 2.2	betam (1)	FLOWMOD	Beta, matrix [ ] (Topopah Spring)	Klavetter, 1986 (+/- 25 percent reported value)
UNIFORM 1.5 4.9	betam (2)	FLOWMOD	Beta, matrix [ ] (Calico Hills, vitric)	Klavetter, 1986 (+/- 25 percent of reported value) - lower bound replaced with reported low value in Peters, 1984
UNIFORM 1.2 3.3	betam (3)	FLOWMOD	Beta, matrix [ ] (Calico Hills, zeolitic)	Klavetter, 1986 (+/- 25 percent of reported value) - upper bound replaced with reported high value in Peters, 1984
UNIFORM 2.0 3.4	betam (4)	FLOWMOD	Beta, matrix [ ] (Prow Pass)	Klavetter, 1986 (+/- 25 percent of reported value) - upper bound replaced with reported high value in Peters, 1984

TYPE OF DISTIBUTION VALUE (OR RANGE IN VALUE)		VARIABLE NAME	MODULE	VARIABLE DESCIPTION	BASIS FOR PARAMETER ASSIGNMENT
UNIFORM 1.5	2.4	betam (5)	FLOWMOD	Beta, matrix [ ] (Upper Crater Flat)	Peters, 1984 (+/- 25 percent of mean)
UNIFORM 2.3	4.2	betam (6)	FLOWMOD	Beta, matrix [ ] (Bullfrog)	Peters, 1984 (reported range)
UNIFORM 1.5	2.4	betam (7)	FLOWMOD	Beta, matrix [ ] (Middle Crater Flat)	assumed same as Upper Crater Flat
UNIFORM 3.2	5.3	betaf (1)	FLOWMOD	Beta, fracture [ ] (Topopah Spring)	Klavetter, 1986 (+/- 25 percent of reported value)
UNIFORM 3.2	5.3	betaf (2)	FLOWMOD	Beta, fracture [ ] (Calico Hills, vitric)	Klavetter, 1986 (+/- 25 percent of reported value)
UNIFORM 3.2	5.3	betaf (3)	FLOWMOD	Beta, fracture [ ] (Calico Hills, zeolitic)	Klavetter, 1986 (+/- 25 percent of reported value)
UNIFORM 3.2	5.3	betaf (4)	FLOWMOD	Beta, fracture [ ] (Prow Pass)	Klavetter, 1986 (+/- 25 percent of reported value)
UNIFORM 3.2	5.3	betaf (5)	FLOWMOD	Beta, fracture [ ] (Upper Crater Flat)	assumed same as Calico Hills
UNIFORM 3.2	5.3	betaf (6)	FLOWMOD	Beta, fracture [ ] (Bullfrog)	assumed same as Prow Pass
UNIFORM 3.2	5.3	betaf (7)	FLOWMOD	Beta, fracture [ ] (Middle Crater Flat)	assumed same as Calico Hills
CONSTANT 0.0026		grad (1)	FLOWMOD	gradient in saturated zone [ ] (Topopah Spring)	based on elevation of water table at the Yucca Mountain site
CONSTANT 0.0026		grad (2)	FLOWMOD	gradient in saturated zone [ ] (Calico Hills, vitric)	based on elevation of water table at the Yucca Mountain site
CONSTANT 0.0026		grad (3)	FLOWMOD	gradient in saturated zone [ ] (Calico Hills, zeolitic)	based on elevation of water table at the Yucca Mountain site

TYPE OF DISTIBUTION VALUE (OR RANGE IN VALUE)		*VARIABLE NAME*	*MODULE*	*VARIABLE DESCIPTION*	*BASIS FOR PARAMETER ASSIGNMENT*
CONSTANT 0.0026		grad (4)	FLOWMOD	gradient in saturated zone [ ] (Prow Pass)	based on elevation of water table at the Yucca Mountain site
CONSTANT 0.0026		grad (5)	FLOWMOD	gradient in saturated zone [ ] (Upper Crater Flat)	based on elevation of water table at the Yucca Mountain site
CONSTANT 0.0026		grad (6)	FLOWMOD	gradient in saturated zone [ ] (Bullfrog)	based on elevation of water table at the Yucca Mountain site
CONSTANT 0.0026		grad (7)	FLOWMOD	gradient in saturated zone [ ] (Middle Crater Flat)	based on elevation of water table at the Yucca Mountain site
NORMAL 0.3	30.0	dispersion	FLOWMOD	dispersion length [m]	assumed
LOGUNIFORM 1.0e-4	5.0E-3	infiltration	FLOWMOD	infiltration rate (undisturbed) [m/yr]	assumed (similar to Phase 1; Codell, 1992)
LOGUNIFORM 5.0E-3	1.0e-2	infiltration (pluvial)	FLOWMOD	infiltration rate [m/yr] (pluvial conditions)	assumed (similar to Phase 1; Codell, 1992)
LOGUNIFORM 0.045	4.5	kdm (1)	FLOWMOD	Cm K_d [m^3/Kg] (Topopah Spring)	Codell, 1992 (+/- one order of magnitude of the mean of log of retradation factors from Phase 1)
LOGUNIFORM .328	32.8	kdm (2)	FLOWMOD	Cm K_d [m^3/Kg] (Calico Hills, vitric)	Codell, 1992 (+/- one order of magnitude of the mean of log of retardation factors from Phase 1)
LOGUNIFORM 0.166	16.6	kdm (3)	FLOWMOD	Cm K_d [m^3/Kg] (Calico Hills, zeolitic)	Codell, 1992 (+/- one order of magnitude of the mean of log of retardation factors from Phase 1)
LOGUNIFORM 0.116	11.6	kdm (4)	FLOWMOD	Cm K_d [m^3/Kg] (Prow Pass)	Codell, 1992 (+/- one order of magnitude of the mean of log of retardation factors from Phase 1)
LOGUNIFORM 0.132	13.2	kdm (5)	FLOWMOD	Cm K_d [m^3/Kg] (Upper Crater Flat)	Codell, 1992 (+/- one order of magnitude of the mean of log of retardation factors from Phase 1)
LOGUNIFORM 0.12	12.0	kdm (6)	FLOWMOD	Cm K_d [m^3/Kg] (Bullfrog)	Codell, 1992 (+/- one order of magnitude of the mean of log of retardation factors from Phase 1)

TYPE OF DISTIBUTION VALUE (OR RANGE IN VALUE)	*VARIABLE NAME*	*MODULE*	*VARIABLE DESCIPTION*	*BASIS FOR PARAMETER ASSIGNMENT*
LOGUNIFORM 0.132 13.2	kdm (7)	FLOWMOD	Cm K_d [m^3/Kg] (Middle Crater Flat)	Codell, 1992 (+/- one order of magnitude of the mean of log of retardation factors from Phase 1)
LOGUNIFORM 2.0E-5 2.0E-3	kdm (15)	FLOWMOD	U K_d [m^3/Kg] (Topopah Spring)	Meijer, 1990 (+/- one order of magnitude of log mean of reported values - wells UE25a1, G3, and J13)
LOGUNIFORM 0.002 0.2	kdm (16)	FLOWMOD	U K_d [m^3/Kg] (Calico Hills, vitric)	Meijer, 1990 (+/- one order of magnitude of the reported value - well G3)
LOGUNIFORM 0.0001 0.01	kdm (17)	FLOWMOD	U K_d [m^3/Kg] (Calico Hills, zeolitic)	Meijer, 1990 (+/- one order of magnitude of log mean of reported values - wells G1 and G2)
CONSTANT 0.0	kdm (18)	FLOWMOD	U K_d [m^3/Kg] (Prow Pass)	assumed to be zero
LOGUNIFORM 8.0E-5 8.0E-3	kdm (19)	FLOWMOD	U K_d [m^3/Kg] (Upper Crater Flat)	same retardation factor as Calico Hills zeolitic (allowances made for density and porosity)
LOGUNIFORM 0.0002 0.02	kdm (20)	FLOWMOD	U K_d [m^3/Kg] (Bullfrog)	Meijer, 1990 (+/- one order of magnitude of log mean of reported values - wells G1, J13, and UE25a1)
LOGUNIFORM 8.0E-5 8.0E-3	kdm (21)	FLOWMOD	U K_d [m^3/Kg] (Middle Crater Flat)	same retardation factor as Calico Hills zeolitic (allowances made for density and porosity)
LOGUNIFORM 0.081 8.1	kdm (22)	FLOWMOD	Am K_d [m^3/Kg] (Topopah Spring)	Meijer, 1990 (+/- one order of magnitude of log mean of reported values - wells J13, G3, and UE25a1)
LOGUNIFORM 0.081 8.1	kdm (23)	FLOWMOD	Am K_d [m^3/Kg] (Calico Hills, vitric)	assumed same K_d as Topopah Spring
LOGUNIFORM 0.17 17.0	kdm (24)	FLOWMOD	Am K_d [m^3/Kg] (Calico Hills, zeolitic)	Meijer, 1990 (+/- one order of magnitude of the reported value - well G2)
LOGUNIFORM 0.45 45.0	kdm (25)	FLOWMOD	Am K_d [m^3/Kg] (Prow Pass)	Meijer, 1990 (+/- one order of magnitude of log mean of reported values - wells G1 and UE25a1)

TYPE OF DISTIBUTION VALUE (OR RANGE IN VALUE)		VARIABLE NAME	MODULE	VARIABLE DESCIPTION	BASIS FOR PARAMETER ASSIGNMENT
LOGUNIFORM 0.136	13.6	kdm (26)	FLOWMOD	Am K_d [m^3/Kg] (Upper Crater Flat)	same retardation factor as Calico Hills zeolitic (allowances made for density and porosity)
LOGUNIFORM 0.014	1.4	kdm (27)	FLOWMOD	Am K_d [m^3/Kg] (Bullfrog)	Meijer, 1990 (+/- one order of magnitude of log mean of reported values - wells J13 and UE25a1)
LOGUNIFORM 0.136	13.6	kdm (28)	FLOWMOD	Am K_d [m^3/Kg] (Middle Crater Flat)	same retardation factor as Calico Hills zeolitic (allowances made for density and porosity)
LOGUNIFORM 0.00045	0.045	kdm (29)	FLOWMOD	^{237}Np K_d [m^3/Kg] (Topopah Spring)	Meijer, 1990 (+/- one order of magnitude of log mean of reported values - wells G3 and UE25a1)
LOGUNIFORM 0.00045	0.045	kdm (30)	FLOWMOD	^{237}Np K_d [m^3/Kg] (Calico Hills, vitric)	assumed same K_d as Topopah Spring
LOGUNIFORM 0.00027	0.027	kdm (31)	FLOWMOD	^{237}Np Kd [m^3/Kg] (Calico Hills, zeolitic)	Meijer, 1990 (+/- one order of magnitude of the reported value - well G2)
LOGUNIFORM 0.00051	0.051	kdm (32)	FLOWMOD	^{237}Np K_d [m^3/Kg] (Prow Pass)	Meijer, 1990 (+/- one order of magnitude of log mean of reported values - wells G1 and UE25a1)
LOGUNIFORM 0.00022	0.022	kdm (33)	FLOWMOD	^{237}Np K_d [m^3/Kg] (Upper Crater Flat)	same retardation factor as Calico Hills zeolitic (allowances made for density and porosity)
LOGUNIFORM 0.00051	0.051	kdm (34)	FLOWMOD	^{237}Np K_d [m^3/Kg] (Bullfrog)	assumed same K_d as Prow Pass
LOGUNIFORM 0.00022	0.022	kdm (35)	FLOWMOD	^{237}Np K_d [m^3/Kg] (Middle Crater Flat)	same retardation factor as Calico Hills zeolitic (allowances made for density and porosity)
LOGUNIFORM 0.017	1.7	kdm (8)	FLOWMOD	Pu K_d [m^3/Kg] (Topopah Spring)	Meijer, 1990 (+/- one order of magnitude of log mean of reported values - wells G3, J13, and UE25a1)
LOGUNIFORM 0.017	1.7	kdm (9)	FLOWMOD	Pu K_d [m^3/Kg] (Calico Hills, vitric)	assumed same K_d as Topopah Spring
LOGUNIFORM 0.0066	0.66	kdm (10)	FLOWMOD	Pu K_d [m^3/Kg] (Calico Hills, zeolitic)	Meijer, 1990 (+/- one order of magnitude of the reported value - well G2)

TYPE OF DISTIBUTION VALUE (OR RANGE IN VALUE)	*VARIABLE NAME*	*MODULE*	*VARIABLE DESCIPTION*	*BASIS FOR PARAMETER ASSIGNMENT*
LOGUNIFORM 0.013 1.3	kdm (11)	FLOWMOD	Pu K_d [m^3/Kg] (Prow Pass)	Meijer, 1990 (+/- one order of magnitude of log mean of reported values - wells G1 and UE25a1)
LOGUNIFORM 0.0053 0.53	kdm (12)	FLOWMOD	Pu K_d [m^3/Kg] (Upper Crater Flat)	same retardation factor as Calico Hills zeolitic (allowances made for density and porosity)
LOGUNIFORM 0.0094 0.94	kdm (13)	FLOWMOD	Pu K_d [m^3/Kg] (Bullfrog)	Meijer, 1990 (+/- one order of magnitude of log mean of reported values - wells J13 and UE25a1)
LOGUNIFORM 0.0053 0.53	kdm (14)	FLOWMOD	Pu K_d [m^3/Kg] (Middle Crater Flat)	same retardation factor as Calico Hills zeolitic (allowances made for density and porosity)
LOGUNIFORM 0.0048 0.48	kdm (36)	FLOWMOD	Th K_d [m^3/Kg] (Topopah Spring)	Codell, 1992 (+/- one order of magnitude of the mean of log of retardation factors from Phase 1)
LOGUNIFORM 0.034 3.4	kdm (37)	FLOWMOD	Th K_d [m^3/Kg] (Calico Hills, vitric)	Codell, 1992 (+/- one order of magnitude of the mean of log of retardation factors from Phase 1)
LOGUNIFORM 0.017 1.7	kdm (38)	FLOWMOD	Th K_d [m^3/Kg] (Calico Hills, zeolitic)	Codell, 1992 (+/- one order of magnitude of the mean of log of retardation factors from Phase 1)
LOGUNIFORM 0.012 1.2	kdm (39)	FLOWMOD	Th K_d [m^3/Kg] (Prow Pass)	Codell, 1992 (+/- one order of magnitude of the mean of log of retardation factors from Phase 1)
LOGUNIFORM 0.014 1.4	kdm (40)	FLOWMOD	Th K_d [m^3/Kg] (Upper Crater Flat)	Codell, 1992 (+/- one order of magnitude of the mean of log of retardation factors from Phase 1)
LOGUNIFORM 0.013 1.3	kdm(41)	FLOWMOD	Th K_d [m^3/Kg] (Bullfrog)	Codell, 1992 (+/- one order of magnitude of the mean of log of retardation factors from Phase 1)
LOGUNIFORM 0.014 1.4	kdm(42)	FLOWMOD	Th K_d [m^3/Kg] (Middle Crater Flat)	Codell, 1992 (+/- one order of magnitude of the mean of log of retardation factors from Phase 1)
LOGUNIFORM 0.15 15.0	kdm (43)	FLOWMOD	^{226}Ra K_d [m^3/Kg] (Topopah Spring)	Meijer, 1990 (+/- one order of magnitude of the reported value - well G1)
LOGUNIFORM 0.15 15.0	kdm (44)	FLOWMOD	^{226}Ra K_d [m^3/Kg] (Calico Hills, vitric)	assumed same K_d as Topopah Spring

TYPE OF DISTIBUTION VALUE (OR RANGE IN VALUE)		VARIABLE NAME	MODULE	VARIABLE DESCIPTION	BASIS FOR PARAMETER ASSIGNMENT
LOGUNIFORM 0.15	15.0	kdm (45)	FLOWMOD	^{226}Ra K_d [m^3/Kg] (Calico Hills, zeolitic)	assumed same K_d as Topopah Spring
LOGUNIFORM 0.15	15.0	kdm(46)	FLOWMOD	^{226}Ra K_d [m^3/Kg] (Prow Pass)	assumed same K_d as Topopah Spring
LOGUNIFORM 0.12	12.0	kdm (47)	FLOWMOD	^{226}Ra K_d [m^3/Kg] (Upper Crater Flat)	same retardation factor as Calico Hills zeolitic (allowances made for density and porosity)
LOGUNIFORM 0.5	50.0	kdm (48)	FLOWMOD	^{226}Ra K_d [m^3/Kg] (Bullfrog)	Meijer, 1990 (+/- one order of magnitude of log mean of reported values - well G1)
LOGUNIFORM 0.12	12.0	kdm (49)	FLOWMOD	^{226}Ra K_d [m^3/Kg] (Middle Crater Flat)	same retardation factor as Calico Hills zeolitic (allowances made for density and porosity)
LOGUNIFORM 0.00068	0.068	kdm (50)	FLOWMOD	^{210}Pb K_d [m^3/Kg] (Topopah Spring)	Codell, 1992 (+/- one order of magnitude of the mean of log of retardation factors from Phase 1)
LOGUNIFORM 0.0049	0.49	kdm (51)	FLOWMOD	^{210}Pb K_d [m^3/Kg] (Calico Hills, vitric)	Codell, 1992 (+/- one order of magnitude of the mean of log of retardation factors from Phase 1)
LOGUNIFORM 0.0025	0.25	kdm (52)	FLOWMOD	^{210}Pb K_d [m^3/Kg] (Calico Hills, zeolitic)	Codell, 1992 (+/- one order of magnitude of the mean of log of retardation factors from Phase 1)
LOGUNIFORM 0.0017	0.17	kdm (53)	FLOWMOD	^{210}Pb K_d [m^3/Kg] (Prow Pass)	Codell, 1992 (+/- one order of magnitude of the mean of log of retardation factors from Phase 1)
LOGUNIFORM 0.0020	0.20	kdm (54)	FLOWMOD	^{210}Pb K_d [m^3/Kg] (Upper Crater Flat)	Codell, 1992 (+/- one order of magnitude of the mean of log of retardation factors from Phase 1)
LOGUNIFORM 0.0018	0.18	kdm (55)	FLOWMOD	^{210}Pb K_d [m^3/Kg] (Bullfrog)	Codell, 1992 (+/- one order of magnitude of the mean of log of retardation factors from Phase 1)
LOGUNIFORM 0.0020	0.20	kdm (56)	FLOWMOD	^{210}Pb K_d [m^3/Kg] (Middle Crater Flat)	Codell, 1992 (+/- one order of magnitude of the mean of log of retardation factors from Phase 1)
LOGUNIFORM 0.036	3.6	kdm (57)	FLOWMOD	Cs K_d [m^3/Kg] (Topopah Spring)	Meijer, 1990 (+/- one order of magnitude of log mean of reported values - wells G1, G3, and UE25a1)

TYPE OF DISTIBUTION VALUE (OR RANGE IN VALUE)	VARIABLE NAME	MODULE	VARIABLE DESCIPTION	BASIS FOR PARAMETER ASSIGNMENT
LOGUNIFORM 0.024 2.4	kdm (58)	FLOWMOD	Cs K_d [m^3/Kg] (Calico Hills, vitric)	Meijer, 1990 (+/- one order of magnitude of log mean of reported values in Topopah Spring unit - well G3)
LOGUNIFORM 2.2 220.	kdm (59)	FLOWMOD	Cs K_d [m^3/Kg] (Calico Hills, zeolitic)	Meijer, 1990 (+/- one order of magnitude of log mean of reported values - wells G1 and G2)
LOGUNIFORM 0.22 22.0	kdm (60)	FLOWMOD	Cs K_d [m^3/Kg] (Prow Pass)	Meijer, 1990 (+/- one order of magnitude of log mean of reported values - wells G1, J13, and UE25a1)
LOGUNIFORM 1.76 176.0	kdm (61)	FLOWMOD	Cs K_d [m^3/Kg] (Upper Crater Flat)	same retardation factor as Calico Hills zeolitic (allowances made for density and porosity)
LOGUNIFORM 0.32 32.0	kdm (62)	FLOWMOD	Cs K_d [m^3/Kg] (Bullfrog)	Meijer, 1990 (+/- one order of magnitude of log mean of reported values - wells G1, J13, and UE25a1)
LOGUNIFORM 1.76 176.0	kdm (63)	FLOWMOD	Cs K_d [m^3/Kg] (Middle Crater Flat)	same retardation factor as Calico Hills zeolitic allowances made for density and porosity)
CONSTANT 0.0	kdm (64)	FLOWMOD	^{129}I K_d [m^3/Kg] (Topopah Spring)	assumed to be zero
CONSTANT 0.0	kdm (65)	FLOWMOD	^{129}I K_d [m^3/Kg] (Calico Hills, vitric)	assumed to be zero
CONSTANT 0.0	kdm (66)	FLOWMOD	^{129}I K_d [m^3/Kg] (Calico Hills, zeolitic)	assumed to be zero
CONSTANT 0.0	kdm(67)	FLOWMOD	^{129}I K_d [m^3/Kg] (Prow Pass)	assumed to be zero
CONSTANT 0.0	kdm(68)	FLOWMOD	^{129}I K_d [m^3/Kg] (Upper Crater Flat)	assumed to be zero
CONSTANT 0.0	kdm (69)	FLOWMOD	^{129}I K_d [m^3/Kg] (Bullfrog)	assumed to be zero

TYPE OF DISTIBUTION VALUE (OR RANGE IN VALUE)	*VARIABLE NAME*	*MODULE*	*VARIABLE DESCIPTION*	*BASIS FOR PARAMETER ASSIGNMENT*
CONSTANT 0.0	kdm (70)	FLOWMOD	^{129}I K_d [m^3/Kg] (Middle Crater Flat)	assumed to be zero
LOGUNIFORM 1.0E-6 1.0E-4	kdm (78)	FLOWMOD	^{99}Tc K_d [m^3/Kg] (Topopah Spring)	Meijer, 1990 (+/- one order of magnitude of log mean of reported values - wells G3 and UE25a1)
CONSTANT 0.0	kdm (79)	FLOWMOD	^{99}Tc K_d [m^3/Kg] (Calico Hills, vitric)	assumed to be zero
CONSTANT 0.0	kdm (80)	FLOWMOD	^{99}Tc K_d [m^3/Kg] (Calico Hills, zeolitic)	assumed to be zero
LOGUNIFORM 1.7E-5 1.7E-3	kdm (81)	FLOWMOD	^{99}Tc K_d [m^3/Kg] (Prow Pass)	Meijer, 1990 (+/- one order of magnitude of log mean of reported values - well J13)
CONSTANT 0.0	kdm (82)	FLOWMOD	^{99}Tc K_d [m^3/Kg] (Upper Crater Flat)	same retardation factor as Calico Hills zeolitic (allowances made for density and porosity)
LOGUNIFORM 0.00042 0.042	kdm (83)	FLOWMOD	^{99}Tc K_d [m^3/Kg] (Bullfrog)	Meijer, 1990 (+/- one order of magnitude of the reported value - well UE25a1)
CONSTANT 0.0	kdm (84)	FLOWMOD	^{99}Tc K_d [m^3/Kg] (Middle Crater Flat)	same as retardation factor as Calico Hills zeolitic (allowances made for density and porosity)
LOGUNIFORM 0.00037 0.037	kdm (99)	FLOWMOD	^{59}Ni K_d [m^3/Kg] (Topopah Spring)	Codell, 1992 (+/- one order of magnitude of the mean of log of retardation factors from Phase 1)
LOGUNIFORM 0.0027 0.27	kdm (100)	FLOWMOD	^{59}Ni K_d [m^3/Kg] (Calico Hills, vitric)	Codell, 1992 (+/- one order of magnitude of the mean of log of retardation factors from Phase 1)
LOGUNIFORM 0.0014 0.14	kdm (101)	FLOWMOD	^{59}Ni K_d [m^3/Kg] (Calico Hills, zeolitic)	Codell, 1992 (+/- one order of magnitude of the mean of log of retardation factors from Phase 1)
LOGUNIFORM 0.0009 0.09	kdm (102)	FLOWMOD	^{59}Ni K_d [m^3/Kg] (Prow Pass)	Codell, 1992 (+/- one order of magnitude of the mean of log of retardation factors from Phase 1)
LOGUNIFORM 0.0011 0.11	kdm (103)	FLOWMOD	^{59}Ni K_d [m^3/Kg] (Upper Crater Flat)	Codell, 1992 (+/- one order of magnitude of the mean of log of retardation factors from Phase 1)

TYPE OF DISTIBUTION VALUE (OR RANGE IN VALUE)	*VARIABLE NAME*	*MODULE*	*VARIABLE DESCIPTION*	*BASIS FOR PARAMETER ASSIGNMENT*
LOGUNIFORM 0.001 0.1	kdm (104)	FLOWMOD	^{59}Ni K_d [m^3/Kg] (Bullfrog)	Codell, 1992 (+/- one order of magnitude of the mean of log of retardation factors from Phase 1)
LOGUNIFORM 0.0011 0.11	kdm (105)	FLOWMOD	^{59}Ni K_d [m^3/Kg] (Middle Crater Flat)	Codell, 1992 (+/- one order of magnitude of the mean of log of retardation factors from Phase 1)
CONSTANT 0.0	kdm (106)	FLOWMOD	^{14}C K_d [m^3/Kg] (Topopah Spring)	assumed to be zero
CONSTANT 0.0	kdm (107)	FLOWMOD	^{14}C K_d [m^3/Kg] (Calico Hills, vitric)	assumed to be zero
CONSTANT 0.0	kdm (108)	FLOWMOD	^{14}C K_d [m^3/Kg] (Calico Hills, zeolitic)	assumed to be zero
CONSTANT 0.0	kdm (109)	FLOWMOD	^{14}C K_d [m^3/Kg] (Prow Pass)	assumed to be zero
CONSTANT 0.0	kdm (110)	FLOWMOD	^{14}C K_d [m^3/Kg] (Upper Crater Flat)	assumed to be zero
CONSTANT 0.0	kdm (111)	FLOWMOD	^{14}C K_d [m^3/Kg] (Bullfrog)	assumed to be zero
CONSTANT 0.0	kdm (112)	FLOWMOD	^{14}C K_d [m^3/Kg] (Middle Crater Flat)	assumed to be zero
LOGUNIFORM 0.00026 0.026	kdm (113)	FLOWMOD	^{79}Se K_d [m^3/Kg] (Topopah Spring)	Meijer, 1990 (+/- one order of magnitude of log mean of reported values - well G3)
LOGUNIFORM 0.0003 0.03	kdm (114)	FLOWMOD	^{79}Se K_d [m^3/Kg] (Calico Hills, vitric)	Meijer, 1990 (+/- one order of magnitude of the reported value - well G3)
LOGUNIFORM 0.00045 0.045	kdm (115)	FLOWMOD	^{79}Se K_d [m^3/Kg] (Calico Hills, zeolitic)	Meijer, 1990 (+/- one order of magnitude of log mean of reported values - wells G1 and G2)
LOGUNIFORM 0.00025 0.025	kdm (116)	FLOWMOD	^{79}Se K_d [m^3/Kg] (Prow Pass)	Meijer, 1990 (+/- one order of magnitude of the reported value - well G1)

TYPE OF DISTIBUTION VALUE (OR RANGE IN VALUE)	*VARIABLE NAME*	*MODULE*	*VARIABLE DESCIPTION*	*BASIS FOR PARAMETER ASSIGNMENT*
LOGUNIFORM 0.00036 0.036	kdm (117)	FLOWMOD	^{79}Se K_d [m^3/Kg] (Upper Crater Flat)	same retardation factor as Calico Hills zeolitic (allowances made for density and porosity)
LOGUNIFORM 0.0013 0.13	kdm (118)	FLOWMOD	^{79}Se K_d [m^3/Kg] (Bullfrog)	Meijer, 1990 (+/- one order of magnitude of log mean of reported values _ well G1)
LOGUNIFORM 0.00036 0.036	kdm (119)	FLOWMOD	^{79}Se K_d [m^3/Kg] (Middle Crater Flat)	same retardation factor as Calico Hills zeolitic (allowances made for density and porosity)
CONSTANT 0.0	kdm (120)	FLOWMOD	^{94}Nb K_d [m^3/Kg] (Topopah Spring)	assumed to be zero
CONSTANT 0.0	kdm (121)	FLOWMOD	^{94}Nb K_d [m^3/Kg] (Calico Hills, vitric)	assumed to be zero
CONSTANT 0.0	kdm (122)	FLOWMOD	^{94}Nb K_d [m^3/Kg] (Calico Hills, zeolitic)	assumed to be zero
CONSTANT 0.0	kdm (123)	FLOWMOD	^{94}Nb K_d [m^3/Kg] (Prow Pass)	assumed to be zero
CONSTANT 0.0	kdm (124)	FLOWMOD	^{94}Nb K_d [m^3/Kg] (Upper Crater Flat)	assumed to be zero
CONSTANT 0.0	kdm (125)	FLOWMOD	^{94}Nb K_d [m^3/Kg] (Bullfrog)	assumed to be zero
CONSTANT 0.0	kdm (126)	FLOWMOD	^{94}Nb K_d [m^3/Kg] (Middle Crater Flat)	assumed to be zero
LOGUNIFORM 0.0134 1.34	kdm (71)	FLOWMOD	^{126}Sn K_d [m^3/Kg] (Topopah Spring)	Codell, 1992 (+/- one order of magnitude of the mean of log of retardation factors from Phase 1)
LOGUNIFORM 0.097 9.7	kdm (72)	FLOWMOD	^{126}Sn K_d [m^3/Kg] (Calico Hills, vitric)	Codell, 1992 (+/- one order of magnitude of the mean of log of retardation factors from Phase 1)
LOGUNIFORM 0.049 4.9	kdm (73)	FLOWMOD	^{126}Sn K_d [m^3/Kg] (Calico Hills, zeolitic)	Codell, 1992 (+/- one order of magnitude of the mean of log of retardation factors from Phase 1)

TYPE OF DISTIBUTION VALUE (OR RANGE IN VALUE)	VARIABLE NAME	MODULE	VARIABLE DESCIPTION	BASIS FOR PARAMETER ASSIGNMENT
LOGUNIFORM 0.034 3.4	kdm (74)	FLOWMOD	^{126}Sn K_d [m^3/Kg] (Prow Pass)	Codell, 1992 (+/- one order of magnitude of the mean of log of retardation factors from Phase 1)
LOGUNIFORM 0.039 3.9	kdm (75)	FLOWMOD	^{126}Sn K_d [m^3/Kg] (Upper Crater Flat)	Codell, 1992 (+/- one order of magnitude of the mean of log of retardation factors from Phase 1)
LOGUNIFORM 0.035 3.5	kdm (76)	FLOWMOD	^{126}Sn K_d [m^3/Kg] (Bullfrog)	Codell, 1992 (+/- one order of magnitude of the mean of log of retardation factors from Phase 1)
LOGUNIFORM 0.039 3.9	kdm (77)	FLOWMOD	^{126}Sn K_d [m^3/Kg] (Middle Crater Flat)	Codell, 1992 (+/- one order of magnitude of the mean of log of retardation factors from Phase 1)
LOGUNIFORM 0.00048 0.048	kdm (85)	FLOWMOD	^{93}Zr K_d [m^3/Kg] (Topopah Spring)	Codell, 1992 (+/- one order of magnitude of the mean of log of retardation factors from Phase 1)
LOGUNIFORM 0.0034 0.34	kdm (86)	FLOWMOD	^{93}Zr K_d [m^3/Kg] (Calico Hills, vitric)	Codell, 1992 (+/- one order of magnitude of the mean of log of retardation factors from Phase 1)
LOGUNIFORM 0.0017 0.17	kdm (87)	FLOWMOD	^{93}Zr K_d [m^3/Kg] (Calico Hills, zeolitic)	Codell, 1992 (+/- one order of magnitude of the mean of log of retardation factors from Phase 1)
LOGUNIFORM 0.0012 0.12	kdm (88)	FLOWMOD	^{93}Zr K_d [m^3/Kg] (Prow Pass)	Codell, 1992 (+/- one order of magnitude of the mean of log of retardation factors from Phase 1)
LOGUNIFORM 0.0014 0.14	kdm (89)	FLOWMOD	^{93}Zr K_d [m^3/Kg] (Upper Crater Flat)	Codell, 1992 (+/- one order of magnitude of the mean of log of retardation factors from Phase 1)
LOGUNIFORM 0.0013 0.13	kdm (90)	FLOWMOD	^{93}Zr K_d [m^3/Kg] (Bullfrog)	Codell, 1992 (+/- one order of magnitude of the mean of log of retardation factors from Phase 1)
LOGUNIFORM 0.0014 0.14	kdm (91)	FLOWMOD	^{93}Zr K_d [m^3/Kg] (Middle Crater Flat)	Codell, 1992 (+/- one order of magnitude of the mean of log of retardation factors from Phase 1)
LOGUNIFORM 0.008 0.8	kdm (92)	FLOWMOD	^{90}Sr K_d [m^3/Kg] (Topopah Spring)	Meijer, 1990 (+/- one order of magnitude of log mean of reported values - wells G1, G3, and UE25a1)

TYPE OF DISTIBUTION	*VALUE (OR RANGE IN VALUE)*	*VARIABLE NAME*	*MODULE*	*VARIABLE DESCIPTION*	*BASIS FOR PARAMETER ASSIGNMENT*
LOGUNIFORM	0.0034 0.34	kdm (93)	FLOWMOD	^{90}Sr K_d [m^3/Kg] (Calico Hills, vitric) well G3)	Meijer, 1990 (+/- one order of magnitude of log mean of reported values in Topopah Spring unit -
LOGUNIFORM	0.89 89.0	kdm (94)	FLOWMOD	^{90}Sr K_d [m^3/Kg] (Calico Hills, zeolitic)	Meijer, 1990 (+/- one order of magnitude of log mean of reported values - wells G1 and G2)
LOGUNIFORM	0.045 4.5	kdm (95)	FLOWMOD	^{90}Sr K_d [m^3/Kg] (Prow Pass)	Meijer, 1990 (+/- one order of magnitude of log mean of reported values - wells G1, J13, and UE25a1)
LOGUNIFORM	0.71 71.0	kdm (96)	FLOWMOD	^{90}Sr K_d [m^3/Kg] (Upper Crater Flat)	same retardation factor as Calico Hills zeolitic (allowances made for density and porosity)
LOGUNIFORM	0.028 2.8	kdm (97)	FLOWMOD	^{90}Sr K_d [m^3/Kg] (Bullfrog)	Meijer, 1990 (+/- one order of magnitude of log mean of reported values - wells G1, J13, and UE25a1)
LOGUNIFORM	0.71 71.0	kdm (98)	FLOWMOD	^{90}Sr K_d [m^3/Kg] (Middle Crater Flat)	same retardation factor as Calico Hills zeolitic (allowances made for density and porosity)
UNIFORM	3.75E4 3.75E5	areao	FLOWMOD	area of discharge [m^2] determinations (see Table 4-9)	production zone thicknesses from field
UNIFORM	100. 150.	ecorr(1)	SOTEC	baseline corrosion potential [m/V]	
UNIFORM	-2. -.5	ecorr(2)	SOTEC	factor for temperature effect [ ]	
UNIFORM	-3.40 -3.	ecorr(3)	SOTEC	factor for temperature effect on ambient potential [ ]	
UNIFORM	100. 300.	ecorr(4)	SOTEC	factor for radiolysis effect [ ]	
UNIFORM	0.001 0.023	ecorr(5)	SOTEC	decay rate for gamma emitters [yr^{-1}]	

TYPE OF DISTIBUTION VALUE (OR RANGE IN VALUE)	VARIABLE NAME	MODULE	VARIABLE DESCIPTION	BASIS FOR PARAMETER ASSIGNMENT
UNIFORM 1000. 1500.	ecorr(6)	SOTEC	crevice corrosion potential [mV]	
UNIFORM 1000. 1500.	ecorr(7)	SOTEC	pitting corrosion potential [mV]	
LOGUNIFORM 1.e-5 0.001	ecorr(8)	SOTEC	rate for localized corrosion [m/yr]	
CONSTANT 1.e-7	carbon(1)	SOTEC	thickness of zirconium oxide [m]	
CONSTANT 1.e-5	carbon(2)	SOTEC	initial radius of UO_2 grain [m]	
CONSTANT 1.786e-2	carbon(3)	SOTEC	O_2 concentration outside of particle [Kg-mole/m^3]	
CONSTANT 37.	carbon(4)	SOTEC	density of UO_2 [Kg-mole/m^3]	
CONSTANT 5.256e-8	carbon(5)	SOTEC	reference diffusion, inner layer [m^2/yr]	
CONSTANT 3.942e-7	carbon(6)	SOTEC	reference diffusion, outer layer [m^2/yr]	
CONSTANT 32.	carbon(7)	SOTEC	activation energy [Kcal/g-mole]	
CONSTANT 473.	carbon(8)	SOTEC	reference temperature [°K]	
CONSTANT 3.	carbon(9)	SOTEC	moles of UO_2 per mole of O_2 [ ]	
CONSTANT 0.001	carbon(10)	SOTEC	radius of UO_2 fragment [m]	

TYPE OF DISTIBUTION VALUE (OR RANGE IN VALUE)	*VARIABLE NAME*	*MODULE*	*VARIABLE DESCIPTION*	*BASIS FOR PARAMETER ASSIGNMENT*
CONSTANT 6.1e-4	carbon(11)	SOTEC	thickness of cladding [m]	
CONSTANT 7.2e-4	carbon(12)	SOTEC	ci ^{14}C/Kg in UO_2 [ci/Kg]	
CONSTANT 4.89e-4	carbon(13)	SOTEC	ci ^{14}C/Kg in cladding [ci/Kg]	
CONSTANT 2.48e-5	carbon(14)	SOTEC	ci ^{14}C/Kg in ZrO_2 [ci/Kg]	
CONSTANT 6.2e-6	carbon(15)	SOTEC	ci ^{14}C/Kg in grain and gap [ci/Kg]	
LOGUNIFORM 1.0e-5 1.0e-3	forwar(1)	SOTEC	UO_2 alteration rate [1/yr] (repository subarea no. 1)	
LOGUNIFORM 1.0e-5 1.0e-3	forwar(2)	SOTEC	UO_2 alteration rate [1/yr] (repository subarea no. 2)	
LOGUNIFORM 1.0e-5 1.0e-3	forwar(3)	SOTEC	UO_2 alteration rate [1/yr] (repository subarea no. 3)	
LOGUNIFORM 1.0e-5 1.0e-3	forwar(4)	SOTEC	UO_2 alteration rate [1/yr] (repository subarea no. 4)	
LOGUNIFORM 1.0e-5 1.0e-3	forwar(5)	SOTEC	UO_2 alteration rate [1/yr] (repository subarea no. 5)	
LOGUNIFORM 1.0e-5 1.0e-3	forwar(6)	SOTEC	UO_2 alteration rate [1/yr] (repository subarea no. 6)	
LOGUNIFORM 1.0e-5 1.0e-3	forwar(7)	SOTEC	UO_2 alteration rate [1/yr] (repository subarea no. 7)	
UNIFORM 0.0 1.0	warea(1)	SOTEC	fraction of waste packages contacted [ ] (repository sub-area no. 1)	

TYPE OF DISTIBUTION VALUE (OR RANGE IN VALUE)		VARIABLE NAME	MODULE	VARIABLE DESCIPTION	BASIS FOR PARAMETER ASSIGNMENT
UNIFORM 0.0	1.0	warea(2)	SOTEC	fraction of waste packages contacted [ ] (repository sub-area no. 2)	
UNIFORM 0.0	1.0	warea(3)	SOTEC	fraction of waste packages contacted [ ] (repository sub-area no. 3)	
UNIFORM 0.0	1.0	warea(4)	SOTEC	fraction of waste packages contacted [ ] (repository sub-area no. 4)	
UNIFORM 0.0	1.0	warea(5)	SOTEC	fraction of waste packages contacted [ ] (repository sub-area no. 5)	
UNIFORM 0.0	1.0	warea(6)	SOTEC	fraction of waste packages contacted [ ] (repository sub-area no. 6)	
UNIFORM 0.0	1.0	warea(7)	SOTEC	fraction of waste packages contacted [ ] (repository sub-area no. 7)	
UNIFORM 0.08	0.2	rpor(1,1) packing(ep)	SOTEC	porosity in near field [ ] (repository sub-area no. 1)	
UNIFORM 0.08	0.2	rpor(2,1)	SOTEC	porosity in near field [ ] (repository sub-area no. 2)	
UNIFORM 0.08	0.2	rpor(3,1)	SOTEC	porosity in near field [ ] (repository sub-area no. 3)	
UNIFORM 0.08	0.2	rpor(4,1)	SOTEC	porosity in near field [ ] (repository sub-area no. 4)	
UNIFORM 0.08	0.2	rpor(5,1)	SOTEC	porosity in near field [ ] (repository sub-area no. 5)	
UNIFORM 0.08	0.2	rpor(6,1)	SOTEC	porosity in near field [ ] (repository sub-area no. 6)	
UNIFORM 0.08	0.2	rpor(7,1)	SOTEC	porosity in near field [ ] (repository sub-area no. 7)	

TYPE OF DISTIBUTION VALUE (OR RANGE IN VALUE)		VARIABLE NAME	MODULE	VARIABLE DESCIPTION	BASIS FOR PARAMETER ASSIGNMENT
LOGUNIFORM 5.7e-6	5.7e-3	rdiff(1,1)	SOTEC	diffusion coefficient in near field [m^2/yr] (layer No. 1)	
LOGUNIFORM 5.7e-6	5.7e-3	rdiff(1,2)	SOTEC	diffusion coefficient in near field [m^2/yr] (layer No. 1)	
LOGUNIFORM 5.7e-6	5.7e-4	rdiff(1,3)	SOTEC	diffusion coefficient in near field [m^2/yr] (layer No. 1)	
LOGUNIFORM 5.7e-6	5.7e-4	rdiff(1,4)	SOTEC	diffusion coefficient in near field [m^2/yr] (layer No. 1)	
UNIFORM 0.0	1.2	volmax(1)	SOTEC	maximum volume of water in waste package [m^3] (repository sub-area no. 1)	
UNIFORM 0.0	1.2	volmax(2)	SOTEC	maximum volume of water in waste package [m^3] (repository sub-area no. 2)	
UNIFORM 0.0	1.2	volmax(3)	SOTEC	maximum volume of water in waste package [m^3] (repository sub-area no. 3)	
UNIFORM 0.0	1.2	volmax(4)	SOTEC	maximum volume of water in waste package [m^3] (repository sub-area no. 4)	
UNIFORM 0.0	1.2	volmax(5)	SOTEC	maximum volume of water in waste package [m^3] (repository sub-area no. 5)	
UNIFORM 0.0	1.2	volmax(6)	SOTEC	maximum volume of water in waste package [m^3] (repository sub-area no. 6)	
UNIFORM 0.0	1.2	volmax(7)	SOTEC	maximum volume of water in waste package [m^3] (repository sub-area no. 7)	
LOGNORMAL 2.3	131.2	rde(1)	SOTEC	Cm retardation coefficient [ ]	
LOGNORMAL 1.003	1.325	rde(3)	SOTEC	U retardation coefficient [ ]	

TYPE OF DISTIBUTION VALUE (OR RANGE IN VALUE)		*VARIABLE NAME*	*MODULE*	*VARIABLE DESCIPTION*	*BASIS FOR PARAMETER ASSIGNMENT*
LOGNORMAL 2.79	165.4	rde(4)	SOTEC	Am retardation coefficient [ ]	
LOGNORMAL 1.008	1.81	rde(5)	SOTEC	Np retardation coefficient [ ]	
LOGNORMAL 1.3	33.6	rde(2)	SOTEC	Pu retardation coefficient [ ]	
LOGNORMAL 1.76	77.5	rde(6)	SOTEC	Th retardation coefficient [ ]	
LOGNORMAL 3.44	245.2	rde(7)	SOTEC	Ra retardation coefficient [ ]	
LOGNORMAL 1.39	40.07	rde(8)	SOTEC	Pb retardation coefficient [ ]	
LOGNORMAL 1.68	69.4	rde(9)	SOTEC	Cs retardation coefficient [ ]	
CONSTANT 1.0		rde(10)	SOTEC	I retardation coefficient [ ]	
LOGNORMAL 1.0002	1.016	rde(12)	SOTEC	Tc retardation coefficient [ ]	
LOGNORMAL 1.08	8.81	rde(15)	SOTEC	Ni retardation coefficient [ ]	
CONSTANT 1.0		rde(16)	SOTEC	C retardation coefficient [ ]	
LOGNORMAL 1.007	1.65	rde(17)	SOTEC	Se retardation coefficient [ ]	
CONSTANT 1.0		rde(18)	SOTEC	Nb retardation coefficient [ ]	

TYPE OF DISTIBUTION VALUE (OR RANGE IN VALUE)		VARIABLE NAME		MODULE	VARIABLE DESCIPTION	BASIS FOR PARAMETER ASSIGNMENT
CONSTANT 1.23	23.8	rde(11)		SOTEC	Sn retardation coefficient [ ]	
CONSTANT 1.39	40.1	rde(13)		SOTEC	Zr retardation coefficient [ ]	
CONSTANT 1.19	20.5	rde(14)		SOTEC	Sr retardation coefficient [ ]	
LOGUNIFORM 2.56e-7	5.e-4	sol(1)	CM	SOTEC	Cm solubility [Kg/m^3]	
LOGUNIFORM 4.e-8	3.e-5	sol(3)	U	SOTEC	U solubility [Kg/m^3]	
LOGUNIFORM 1.e-6	3.e-4	sol(4)	AM	SOTEC	Am solubility [Kg/m^3]	
LOGUNIFORM 1.4e-4	0.0237	sol(5)	NP	SOTEC	Np solubility [Kg/m^3]	
LOGUNIFORM 2.e-7	5.e-4	sol(2)	PU	SOTEC	Pu solubility [Kg/m^3]	
LOGUNIFORM 2.e-12	1.e-4	sol(6)	TH	SOTEC	Th solubility [Kg/m^3]	
LOGUNIFORM 9.e-6	9.e-5	sol(7)	RA	SOTEC	Ra solubility [Kg/m^3]	
LOGUNIFORM 2.1e-6	6.3e-4	sol(8)	PB	SOTEC	Pb solubility [Kg/m^3]	
CONSTANT 1.0		sol(9)	CS	SOTEC	Cs solubility [Kg/m^3]	
CONSTANT 1.0		sol(10)	I	SOTEC	I solubility [Kg/m^3]	

TYPE OF DISTIBUTION VALUE (OR RANGE IN VALUE)		VARIABLE NAME		MODULE	VARIABLE DESCIPTION	BASIS FOR PARAMETER ASSIGNMENT
CONSTANT 1.0		sol(12)	TC	SOTEC	Te solubility [Kg/m³]	
LOGUNIFORM 2.8e-7	1.7e-3	sol(15)	NI	SOTEC	Ni solubility [Kg/m³]	
CONSTANT 1.0		sol(16)	C	SOTEC	C solubility [Kg/m³]	
CONSTANT 1.0		sol(17)	SE	SOTEC	Se solubility [Kg/m³]	
CONSTANT 1.0		sol(18)	NB	SOTEC	Nb solubility [Kg/m³]	
CONSTANT 5.e-9	3.8e-6	sol(11)	SN	SOTEC	Sn solubility [Kg/m³]	
CONSTANT 4.e-9	2.e-7	sol(13)	ZR	SOTEC	Zr solubility [Kg/m³]	
CONSTANT 8.e-2		sol(14)	SR	SOTEC	Sr solubility [Kg/m³]	
UNIFORM 0.0	0.4	funnel(1)		SOTEC		
UNIFORM 0.0	0.4	funnel(2)		SOTEC		
UNIFORM 0.0	0.4	funnel(3)		SOTEC		
UNIFORM 0.0	0.4	funnel(4)		SOTEC		
UNIFORM 0.0	0.4	funnel(5)		SOTEC		

TYPE OF DISTIBUTION VALUE (OR RANGE IN VALUE)		*VARIABLE NAME*	*MODULE*	*VARIABLE DESCIPTION*	*BASIS FOR PARAMETER ASSIGNMENT*
UNIFORM 0.0	0.4	funnel(6)	SOTEC		
UNIFORM 0.0	0.4	funnel(7)	SOTEC		
UNIFORM 0.0	10000.	time	VOLCANO		
UNIIFORM 0.0	1.0	u1	VOLCANO	(dike(0.-.9)/cone(.9-1.)) [ ]	
UNIFORM 0.0	1.0	u2	VOLCANO	(dike X_o/cone $X_{___}$) [ ]	
UNIFORM 0.0	1.0	u3	VOLCANO	(dike X_o/cone $X_{___}$) [ ]	
UNIFORM 0.0	1.0	u4	VOLCANO	dike area [m^2]	
UNIFORM 0.0	1.0	u5	VOLCANO	dike length [m]	
UNIFORM 0.0	1.0	u6	VOLCANO	(dike angle wrt East) [ ]	
UNIFORM 0.0	1.0	u7	VOLCANO	cone radius [m]	
UNIFORM 0.0	1.0	u8	VOLCANO	cone area [m^2]	
NORMAL 3.5	27.5	number of holes	DRILLO [ ]		
UNIFORM 0.02	0.1	borehole radius	DRILLO [m]		

TYPE OF DISTIBUTION VALUE (OR RANGE IN VALUE)		*VARIABLE NAME*	*MODULE*	*VARIABLE DESCIPTION*	*BASIS FOR PARAMETER ASSIGNMENT*
UNIFORM 0.0	1.0	hit indicator(1)	DRILLO [ ]		
UNIFORM 0.0	1.0	hit indicator(2)	DRILLO [ ]		
UNIFORM 0.0	1.0	hit indicator(3)	DRILLO [ ]		
UNIFORM 0.0	1.0	hit indicator(4)	DRILLO [ ]		
UNIFORM 0.0	1.0	hit indicator(5)	DRILLO [ ]		
UNIFORM 0.0	1.0	hit indicator(6)	DRILLO [ ]		
UNIFORM 0.0	1.0	hit indicator(7)	DRILLO [ ]		
UNIFORM 0.0	1.0	hit indicator(8)	DRILLO [ ]		
UNIFORM 0.0	1.0	hit indicator(9)	DRILLO [ ]		
UNIFORM 0.0	1.0	hit indicator(10)	DRILLO [ ]		
UNIFORM 0.0	1.0	hit indicator(11)	DRILLO [ ]		
UNIFORM 0.0	1.0	hit indicator(12)	DRILLO [ ]		
UNIFORM 0.0	1.0	hit indicator(13)	DRILLO [ ]		

TYPE OF DISTIBUTION VALUE (OR RANGE IN VALUE)		VARIABLE NAME	MODULE	VARIABLE DESCIPTION	BASIS FOR PARAMETER ASSIGNMENT
UNIFORM		hit indicator(14)	DRILLO [ ]		
0.0	1.0				
UNIFORM		hit indicator(15)	DRILLO [ ]		
0.0	1.0				
UNIFORM		hit indicator(16)	DRILLO [ ]		
0.0	1.0				
UNIFORM		hit indicator(17)	DRILLO [ ]		
0.0	1.0				
UNIFORM		hit indicator(18)	DRILLO [ ]		
0.0	1.0				
UNIFORM		hit indicator(19)	DRILLO [ ]		
0.0	1.0				
UNIFORM		hit indicator(20)	DRILLO [ ]		
0.0	1.0				
UNIFORM		hit indicator(21)	DRILLO [ ]		
0.0	1.0				
UNIFORM		hit indicator(22)	DRILLO [ ]		
0.0	1.0				
UNIFORM		hit indicator(23)	DRILLO [ ]		
0.0	1.0				
UNIFORM		hit indicator(24)	DRILLO [ ]		
0.0	1.0				
UNIFORM		hit indicator(25)	DRILLO [ ]		
0.0	1.0				
UNIFORM		hit indicator(26)	DRILLO [ ]		
0.0	1.0				

TYPE OF DISTIBUTION VALUE (OR RANGE IN VALUE)		VARIABLE NAME	MODULE	VARIABLE DESCIPTION	BASIS FOR PARAMETER ASSIGNMENT
UNIFORM 0.0	1.0	hit indicator(27)	DRILLO [ ]		
UNIFORM 0.0	1.0	hit indicator(28)	DRILLO [ ]		
UNIFORM 0.0	1.0	hit indicator(29)	DRILLO [ ]		
UNIFORM 0.0	1.0	hit indicator(30)	DRILLO [ ]		
UNIFORM 100.0	9900.0	drill time(1)	DRILLO [ ]		
UNIFORM 100.0	9900.0	drill time(2)	DRILLO [yr]		
UNIFORM 100.0	9900.0	drill time(3)	DRILLO [yr]		
UNIFORM 100.0	9900.0	drill time(4)	DRILLO [yr]		
UNIFORM 100.0	9900.0	drill time(5)	DRILLO [yr]		
UNIFORM 100.0	9900.0	drill time(6)	DRILLO [yr]		
UNIFORM 100.0	9900.0	drill time(7)	DRILLO [yr]		
UNIFORM 100.0	9900.0	drill time(8)	DRILLO [yr]		
UNIFORM 100.0	9900.0	drill time(9)	DRILLO [yr]		

TYPE OF DISTIBUTION VALUE (OR RANGE IN VALUE)		VARIABLE NAME	MODULE	VARIABLE DESCIPTION	BASIS FOR PARAMETER ASSIGNMENT
UNIFORM 100.0	9900.0	drill time(10)	DRILLO [yr]		
UNIFORM 100.0	9900.0	drill time(11)	DRILLO [yr] #11		
UNIFORM 100.0	9900.0	drill time(12)	DRILLO [yr]		
UNIFORM 100.0	9900.0	drill time(13)	DRILLO [yr]		
UNIFORM 100.0	9900.0	drill time(14)	DRILLO [yr]		
UNIFORM 100.0	9900.0	drill time(15)	DRILLO [yr]		
UNIFORM 100.0	9900.0	drill time(16)	DRILLO [yr]		
UNIFORM 100.0	9900.0	drill time(17)	DRILLO [yr]		
UNIFORM 100.0	9900.0	drill time(18)	DRILLO [yr]		
UNIFORM 100.0	9900.0	drill time(19)	DRILLO [yr]		
UNIFORM 100.0	9900.0	drill time(20)	DRILLO [yr]		
UNIFORM 100.0	9900.0	drill time(21)	DRILLO [yr] #21		
UNIFORM 100.0	9900.0	drill time(22)	DRILLO [yr]		

TYPE OF DISTIBUTION	*VALUE (OR RANGE IN VALUE)*	*VARIABLE NAME*	*MODULE*	*VARIABLE DESCIPTION*	*BASIS FOR PARAMETER ASSIGNMENT*
UNIFORM		drill time(23)	DRILLO [yr]		
100.0	9900.0				
UNIFORM		drill time(24)	DRILLO [yr]		
100.0	9900.0				
UNIFORM		drill time(25)	DRILLO [yr]		
100.0	9900.0				
UNIFORM		drill time(26)	DRILLO [yr]		
100.0	9900.0				
UNIFORM		drill time(27)	DRILLO [yr]		
100.0	9900.0				
UNIFORM		drill time(28)	DRILLO [yr]		
100.0	9900.0				
UNIFORM		drill time(29)	DRILLO [yr]		
100.0	9900.0				
UNIFORM		drill time(30)	DRILLO [yr]		
100.0	9900.0				
UNIFORM		zone(1)	DRILLO [ ]		
.0	1.0				
UNIFORM		zone(2)	DRILLO [ ]		
.0	1.0				
UNIFORM		zone(3)	DRILLO [ ]		
.0	1.0				
UNIFORM		zone(4)	DRILLO [ ]		
.0	1.0				
UNIFORM		zone(5)	DRILLO [ ]		
.0	1.0				

TYPE OF DISTIBUTION VALUE (OR RANGE IN VALUE)		*VARIABLE NAME*	*MODULE*	*VARIABLE DESCIPTION*	*BASIS FOR PARAMETER ASSIGNMENT*
UNIFORM		zone(6)	DRILLO [ ]		
.0	1.0				
UNIFORM		zone(7)	DRILLO [ ]		
.0	1.0				
UNIFORM		zone(8)	DRILLO [ ]		
.0	1.0				
UNIFORM		zone(9)	DRILLO [ ]		
.0	1.0				
UNIFORM		zone(10)	DRILLO [ ]		
.0	1.0				
UNIFORM		zone(11)	DRILLO [ ]		
.0	1.0				
UNIFORM		zone(12)	DRILLO [ ]		
.0	1.0				
UNIFORM		zone(13)	DRILLO [ ]		
.0	1.0				
UNIFORM		zone(14)	DRILLO [ ]		
.0	1.0				
UNIFORM		zone(15)	DRILLO [ ]		
.0	1.0				
UNIFORM		zone(16)	DRILLO [ ]		
.0	1.0				
UNIFORM		zone(17)	DRILLO [ ]		
.0	1.0				
UNIFORM		zone(18)	DRILLO [ ]		
.0	1.0				

TYPE OF DISTIBUTION VALUE (OR RANGE IN VALUE)	*VARIABLE NAME*	*MODULE*	*VARIABLE DESCIPTION*	*BASIS FOR PARAMETER ASSIGNMENT*
UNIFORM .0 1.0	zone(19)	DRILLO [ ]		
UNIFORM .0 1.0	zone(20)	DRILLO [ ]		
UNIFORM .0 1.0	zone(21)	DRILLO [ ]		
UNIFORM .0 1.0	zone(22)	DRILLO [ ]		
UNIFORM .0 1.0	zone(23)	DRILLO [ ]		
UNIFORM .0 1.0	zone(24)	DRILLO [ ]		
UNIFORM .0 1.0	zone(25)	DRILLO [ ]		
UNIFORM .0 1.0	zone(26)	DRILLO [ ]		
UNIFORM .0 1.0	zone(27)	DRILLO [ ]		
UNIFORM .0 1.0	zone(28)	DRILLO [ ]		
UNIFORM .0 1.0	zone(29)	DRILLO [ ]		
UNIFORM .0 1.0	zone/seismic seed	DRILLO/SEISMO [ ]		

APPENDIX B

CONTENTS

		Page
B-1	Introduction	B-1
B-2	Table Information	B-1
B-3	References	B-4

TABLES

B-1	Hydrologic properties for hydrogeologic units at the Yucca Mountain site reported in modeling studies and experimental studies	B-6
B-2	Average sorption ratios from batch sorption experiments on crushed tuff for americium, plutonium, uranium, selenium, technetium, and neptunium	B-12
B-3	Average sorption ratios from batch sorption experiments on crushed tuff for strontium, cesium, barium, radium, cerium, and europium	B-14
B-4	Average (de)sorption ratios from batch sorption experiments on crushed tuff for strontium, cesium, barium, radium, cerium, and europium	B-16
B-5	Average (de)sorption ratios from batch sorption experiments on crushed tuff for americium, plutonium, uranium, technetium, and neptunium	B-18
B-6	Hydrogeologic parameteric values and ranges used for the ground-water pathway	B-20
B-7	Matrix K_d values, in cubic meters per kilogram, for selected radionuclides for the hydrogeologic units of interest	B-23

FIGURES

B-1	Location map for the zeolitic cross sections in Figures B-2, B-3, and B-4	B-25
B-2	Major zeolitic distributions, north-south cross section, shown as a dark pattern overlying the stratigraphic cross section of Scott and Bonk (1984)	B-26
B-3	Major clinoptilolite-mordenite distributions, northwest-southeast cross section	B-27
B-4	Major zeolite distributions, center to southeast cross section as depicted in Figure B-1	B-28

APPENDIX B
Hydrologic and Radionuclide Transport Data for the Ground-Water Pathway

T.J. McCartin/RES and J.W. Bradbury/NMSS

B-1 INTRODUCTION

Parametric values for use in hydrologic flow and radionuclide transport models were based, when possible, on information published for the Yucca Mountain site. Hydrologic information was based primarily on Peters (1984) and Klavetter (1986), whereas retardation information was based on Meijer (1990) and Thomas (1987). The following tables present the information used from these sources and the resulting ranges and distributions used in the current analysis:

Table	*Information*
B-1	Hydrologic information reported from experimental and modeling studies;
B-2 - B-5	Sorption information from batch experiments on crushed tuff;
B-6	Parametric values and ranges used to represent the ground-water pathway; and
B-7	K_d values.

B-2 TABLE INFORMATION

Table B-1 presents the hydrologic information from Peters and Klavetter, as well as parametric values used in modeling studies since the publication of the Peters report and information from the U.S. Department of Energy (DOE) Site Characterization Plan (SCP) (DOE, 1988). To assist the correlation to the Yucca Mountain site, the borehole at the site associated with the information taken from Peters (1984) is identified. Although the values reported from the various studies should only be interpreted based on the purpose for which the modeling was conducted, the values are presented to provide additional insights on differing interpretations of hydrologic properties of unsaturated tuff being examined. One obvious conclusion is that more information is available on, and more studies have concentrated on, the repository unit (Topopah Spring), than on other units present at Yucca Mountain.

Tables B-2 - B-5 present the information from Meijer (1990) used to develop the K_d values for individual hydrogeologic units present at Yucca Mountain (abbreviations used in Tables B-2 and B-3 and throughout the remainder of this appendix are as follows: the prefix *JA* indicates drill hole J-13; the prefix *YM* indicates drill hole UE25a-1; and the other abbreviations in the table are unambiguously labeled). A number of assumptions were used to derive the K_d values; therefore, a more detailed discussion of the interpretation and of the use of the data is given here. (The applicability of the K_d approach is not discussed here. See Section 4.4.2 for more information on the applicability of the K_d approach.)

As discussed in Section 4.2.4, the retardation coefficients for each hydrogeologic unit are calculated using the following equation:

$$R_f = 1.0 + \frac{\rho(1-n)}{\theta} \times K_d \quad , \qquad \text{(B-1)}$$

where:

Rf = retardation factor;
K_d = distribution coefficient;
θ = moisture content;
ρ = grain density; and
n = porosity.

The values for these parameters are specific to the five hydrogeologic units: Topopah Spring Member of the Paintbrush Tuff (Tpt); Calico Hills nonwelded vitric (CHnv); Calico Hills nonwelded zeolitic (CHnz); Prow Pass Member of the Crater Flat Tuff (Tcp); and Bullfrog Member of the Crater Flat Tuff (Tcb). Experimental values (see Tables B-2 - B-5) were used to determine mean K_d values for a specific hydrogeologic unit, while, for certain elements and hydrogeologic units without data, K_d values were assigned, based on chemical similarity to other measurements. When K_d values could still not be assigned, K_d values were taken from the IPA Phase 1 report (see Codell *et al.*, 1992, p. 56). Because a loguniform distribution is used to characterize the distribution of K_d, the average of the logs of the experimental values was used to calculate the mean value for the distribution. The range of the distribution was crudely estimated to be plus and minus one order of magnitude about the mean (the support for this assignment was derived from the 1988 SCP, where the range of K_d values for Sr and Cs varies over two orders of magnitude for different locations in drill hole G1). The K_d mean values, based on the Meijer and Thomas data, are:

Element	K_d (m^3/kg)				
	Tpt	*CHnv*	*CHnz*	*Tcp*	*Tcb*
Am	.810	.810	1.7	4.5	.140
Pu	.170	.170	.066	.130	.094
U	.0002	.020	.001	0.0	.002
Se	.0026	.003	.0045	.0025	.013
Tc	.000013	0.0	0.0	.00017	.0042
Np	.0045	.0045	.0027	.0051	.0051
Sr	.08	.034	8.9	.450	.280
Cs	.36	.24	22.0	2.2	3.2
Ba	1.2	.6	61.0	3.9	1.1
Ra	1.5	1.5	1.5	1.5	5.0
Th	.470				.340
Sn				.230	.660

A brief description of the procedure and assumptions used in determining the above K_d mean values are presented below:

Am The K_d in the Topopah Spring unit (Tpt) is a log average of the values from the wells J-13, G-3, and UE25a-1. The K_d in the Calico Hills nonwelded vitric unit (CHnv) is estimated to be the same as the Topopah Spring. Glassy units should have low sorption capability. The single measured K_d value in the Calico Hills nonwelded zeolitic unit (CHnz) is assumed to represent the mean. For the Prow Pass unit (Tcp), the K_d is again the log average of the values from wells G1 and UE25a-1. The K_d in the Bullfrog unit (Tcb) is the log average from the values for wells J-13 and UE25a-1.

Pu The K_d in the Topopah Spring unit is the log average of the values from the wells UE25a-1, G-3, and J-13. The K_d in the Calico Hills nonwelded vitric is estimated to be the same as the Topopah Spring unit. The single value reported for the Calico Hills nonwelded zeolitic is assumed to represent the mean. The Prow Pass unit K_d is the log average of the values from wells G-1 and UE25a-1. The Bullfrog unit K_d is the log average of the values from wells J-13 and UE25a-1.

U The K_d in the Topopah Spring unit is the log average of the values from wells UE25a-1, G-3, and J-13. The single value reported from well G-3 is assumed to represent the K_d in the Calico Hills nonwelded vitric unit. Figures B-1 through B-4 from the SCP (see DOE, 1988), illustrate where the zeolitic beds are located. The K_d value in the Calico Hills nonwelded zeolitic unit is a log average of the values from wells G-1 and G-2. The K_d in the Prow Pass unit is assumed to be zero, even though no data are available. The K_d in the Bullfrog unit is the log average of the values from wells G-1, J-13, and UE25a-1.

Se The K_d in the Topopah Spring unit is the log average of the values from well G-3. The single value reported from well G-3 is assumed to represent the mean value of the K_d in the Calico Hills nonwelded vitric unit. The K_d value in the Calico Hills nonwelded zeolitic is the average of the values from wells G-1 and G-2. The single value reported from well G-1 is assumed to represent the K_d in the Prow Pass unit. The K_d in the Bullfrog unit is the log average of the values from well G-1.

Tc The K_d in the Topopah Spring unit is the log average of the values from wells UE25a-1 and G-3. In the absence of information, the K_ds in the Calico Hills units are assumed to be zero. The K_d in the Prow Pass unit is the log average of the values from well J-13. The single value from well UE25a-1 is assumed to represent the mean of the K_d in the Bullfrog unit.

Np The K_d in the Topopah Spring unit is a log average of the values from the wells G-3 and UE25a-1. The K_d in the Calico Hills nonwelded vitric unit is estimated to be the same as the Topopah Spring unit. The single measured K_d value in the Calico Hills nonwelded zeolitic is assumed to represent the mean. For the Prow Pass, the K_d is the log average of the values from wells G1 and UE25a-1. The K_d in the Bullfrog unit is assumed to the same as the value in the Prow Pass.

Sr The K_d in the Topopah Spring unit is a log average of the values from the wells G-3, G-1, and UE25a-1. The K_d in the Calico Hills nonwelded vitric is based on the log average of the values from well G-3 for the Topopah Spring unit. The K_d value in the Calico Hills nonwelded zeolitic unit is the log average of the values from wells G-1 and G-2. For the Prow Pass unit the K_d is the log average of the values from wells G1, J-13, and UE25a-1. For the Bullfrog unit the K_d is the log average of the values from wells G1, J-13, and UE25a-1.

Cs The K_d in the Topopah Spring unit is a log average of the values from the wells G-3, G-1, and UE25a-1. The K_d in the Calico Hills nonwelded vitric unit is based on the log average of the values from well G-3 for the Topopah Spring unit. The K_d value in the Calico Hills nonwelded zeolitic unit is the log average of the values from wells G-1 and G-2. For the Prow Pass unit, the K_d is the log average of the values from wells G1, J-13, and UE25a-1. For the Bullfrog unit, the K_d is the log average of the values from wells G1, J-13, and UE25a-1.

Ba The K_d in the Topopah Spring unit is a log average of the values from the wells G-3, G-1, and UE25a-1. The K_d in the Calico Hills nonwelded vitric unit is based on the log average of the values from well G-3, for the Topopah Spring unit. The K_d value in the Calico Hills nonwelded zeolitic unit is the log average of the values from wells G-1 and G-2. For the Prow Pass unit, the K_d is the log average of the values from wells G1, J-13, and UE25a-1. For the Bullfrog unit, the K_d is the log average of the values from wells G1, J-13, and UE25a-1.

Ra The single value from well G-1 is assumed to represent the mean of the K_d for the Topopah Spring unit. The K_ds for the Calico Hills units and Prow Pass unit are assumed to be the same as the value used for the Topopah Spring unit. The K_d for the Bullfrog unit is the log average of the values from well G-1.

Th The K_d values are taken from Thomas (1987) for well G-1.

Sn The K_d values are taken from Thomas (1987) for well G-1.

The K_d in the fractures is assumed to be zero, because of the conceptualization that flow will be fast relative to the rates of the sorption reactions. This is the same approach as proposed in the SCP.

Table B-6 presents the distributions and the ranges used for representing the hydrologic parameters of the ground-water pathway. Table B-7 presents the K_d values used for each of the elements and hydrogeologic units used in the analysis.

B-3 REFERENCES

Barnard, R.W. and H.A. Dockery (eds.), "Technical Summary of the Performance Assessment Calculational Exercises for 1990 (PACE-90) Volume 1: 'Nominal Configuration' Hydrogeologic Parameters and Calculational Results," Sandia National Laboratories, SAND90-2726, 1992.

Codell, R. *et al.*, "Initial Demonstration of the NRC's Capability to Conduct a Performance Assessment for a High-Level Waste Repository," Nuclear Regulatory Commission, NUREG-1327, 1992.

Dudley, A.L. *et al.*, "Total System Performance Assessment Code (TOSPAC), Volume 1: Physical and Mathematical Bases," Sandia National Laboratories, SAND85-0002, 1988.

Klavetter, E.A., and R.R. Peters, "Fluid Flow in a Fractured Rock Mass," Sandia National Laboratories, SAND85-0855, 1986.

Meijer, A., "Yucca Mountain Project Far-Field Sorption Studies and Data Needs," Los Alamos National Laboratory, LA-11671-MS, 1990.

Nitao, J.J., and T.A. Buscheck, "Infiltration of a Liquid Front in an Unsaturated, Fractured Porous Media," *Water Resources Research*, 27(8):2099-2112 [1991].

Peters, R.R., *et al.*, "Fracture and Matrix Hydrologic Characteristics of Tuffaceous Materials from Yucca Mountain, Nye County, Nevada," Sandia National Laboratories, SAND84-1471, 1984.

Pruess, K., J.S.Y. Wang, and Y.W. Tsang, "On Thermohydrologic Conditions Near High-Level Nuclear Wastes Emplaced in Partially Saturated Fractured Tuff 1. Simulation Studies With Explicit Consideration of Fracture Effects," *Water Resources Research*, 26(6):1235-1248 [1990].

Thomas, K., "Summary of Sorption Measurements Performed with Yucca Mountain, Nevada, Tuff Samples and Water from Well J-13," Los Alamos National Laboratory, LA-10960-MS, 1987.

Tsang, Y.W., and K. Pruess, "A Study of Thermally Induced Convection Near a High-Level Nuclear Waste Repository in Partially Saturated Fractured Tuff," *Water Resources Research*, 23(10):1958-1966 [1987].

U.S. Department of Energy, "Site Characterization Plan Overview, Yucca Mountain Site, Nevada Research and Development Area, Nevada," Office of Civilian Radioactive Waste Management, DOE/RW-0198, December 1988.

Table B-1. Hydrologic properties for hydrogeologic units at the Yucca Mountain site reported in modeling studies and experimental studies (where appropriate borehole identification labels are provided after the reference).

TIVA CANYON (Welded, Devitrified)

Matrix Properties:

Hydrogeologic Unit/Reference	*Grain Density (kg/m^3)*	*Porosity*	*Residual Saturation*	*Saturation Conditions (m/yr)*	*Alpha (1/m)*	*Beta*
Peters (1984) [USW G4]	2,490	0.08	0.002	3.1E-4	8.2E-3	1.56
Peters (1984) [USW GU3]	2,480 - 2,490	0.09 - 0.15	0.014 - 0.160	2.2E-5 - 8.5E-5	3.9E-3 - 2.3E-2	1.51 - 2.13
Klavetter (1986)	2,490	0.08	0.002	3.1E-4	8.2E-3	1.56
Dudley (1988)	2,490	0.08	0.002	3.1E-4	8.2E-3	1.56

Fracture Properties:

Hydrogeologic Unit/Reference	*Fracture Aperture (microns)*	*Fracture Density ($1/m^3$)*	*Porosity*	*Residual Saturation*	*Fracture Conditions (m/yr)*	*Bulk Conditions (m/yr)*	*Alpha (1/m)*	*Beta*
Klavetter (1986)	6.7	20	1.4E-4	0.04	1.2E3	0.17	1.28	4.23
Dudley (1988)	6.7	20	1.4E-4	0.04	1.2E3	0.17	1.28	4.23

PAINTBRUSH (Non-welded, Vitric)

Matrix Properties:

Hydrogeologic Unit/Reference	*Grain Density (kg/m^3)*	*Porosity*	*Residual Saturation*	*Saturation Conditions (m/yr)*	*Alpha (1/m)*	*Beta*
Peters (1984) [USW G4]	2.450	0.65	0.105	75.6	1.6E-2	10.6
Peters (1984) [USW GU3]	2.350 - 2.440	0.40 - 0.59	0.084 - 0.114	11.0 - 50.4	1.1E-2 - 1.5E-2	2.53 - 8.88
Klavetter (1986)	2.350	0.40	0.100	12.3	1.5E-2	6.87
Dudley (1988)	2.350	0.40	0.100	12.3	1.5E-2	6.87

Table B-1 (continued)

PAINTBRUSH (Non-welded, Vitric)

Fracture Properties:

Hydrogeologic Unit/Reference	*Fracture Aperture (microns)*	*Fracture Density (1/m³)*	*Porosity*	*Residual Saturation*	*Fracture Conditions (m/yr)*	*Bulk Conditions (m/yr)*	*Alpha (1/m)*	*Beta*
Klavetter (1986)	27.0	1	2.7E-5	0.04	1.9E4	0.50	1.28	4.23
Dudley (1988)	27.0	1	2.7E-5	0.04	1.9E4	0.50	1.28	4.23

TOPOPAH SPRING (Welded, Devitrified)

Matrix Properties:

Hydrogeologic Unit/Reference	*Grain Density (kg/m³)*	*Porosity*	*Residual Saturation*	*Saturation Conditions (m/yr)*	*Alpha (1/m)*	*Beta*
Peters (1984) [USW G4]	2,470 - 2,580	0.06 - 1.16	0.058 - 0.120	4.1E-5 - 1.2E-3	2.6E-3 - 1.2E-2	1.56 - 2.12
Peters (1984) [USW GU3]	2,540	0.08	0.008	4.7E-5	1.2E-2	1.49
Klavetter (1986)	2,580	0.11	0.080	6.0E-4	5.7E-3	1.80
Tsang (1987)	2,580	0.11	0.080	6.0E-4	5.7E-3	1.80
Dudley (1988)	2,580	0.11	0.080	6.0E-4	5.7E-3	1.80
Pruess (1990)	2,550	0.10	9.6E-4	1.0E-2	7.0E-3	1.80
Nitao (1991)	---	0.20	0.080	6.0E-4	---	---
Barnard (1991)	2,500 - 2,570	0.06 - 0.12	0.0 - 0.15	1.6E-4 - 6.3E-4	4.0E-3 - 0.01	1.49 - 2.00
DOE (1988; Table 3-27)						
Lab data	---	0.04 - 0.33	---	1.1E-4 - 0.2	---	---
Field data	---	---	---	260.	---	---

Table B-1 (continued)

TOPOPAH SPRING (Welded, Devitrified)

Fracture Properties:

Hydrogeologic Unit/Reference	*Fracture Aperture (microns)*	*Fracture Density ($1/m^3$)*	*Porosity*	*Residual Saturation*	*Fracture Conditions (m/yr)*	*Bulk Conditions (m/yr)*	*Alpha (1/m)*	*Beta*
Peters (1984) [USW G4]	6 - 67	---	---	---	1.1E3 - 1.2E5			
Klavetter (1986)	4.3 - 5.1	8 - 40	4.1E-5 - 1.8E-4	0.04	5.0E2 - 6.9E2	0.02 - 0.10	1.28	4.23
Tsang (1987)	---	---	1.8E-3	0.04	---	5.5	---	4.23
Dudley (1988)	4.3 - 5.1	8 - 40	4.1E-5 - 1.8E-4	0.04	5.0E2 - 6.9E2	0.02 - 0.10	1.28	4.23
Pruess (1990)	64.15	4.5	2.9E-4	---	1.1E5	30.9	---	---
Nitao (1991)	90.	22	---	0.04	2.6E5	---	---	---
Barnard (1991)	6. - 20.	5 - 10	3.0E-5	0.04	1.3E3 - 1.3E4	3.8E-2 - 2.5	1.28	4.23

CALICO HILLS (Non-Welded, Vitric)

Matrix Properties:

Hydrogeologic Unit/Reference	*Grain Density (kg/m^3)*	*Porosity*	*Residual Saturation*	*Saturation Conditions (m/yr)*	*Alpha (1/m)*	*Beta*
Peters (1984) [USW GU3]	2,350 - 2,370	0.43 - 0.46	0.020 - 0.048	.82 - 9.1	1.0E-2 - 4.4E2	1.50 - 4.20
Klavetter (1986)	2,370	0.46	0.041	8.5	1.6E-2	3.87
Dudley (1988)	2,370	0.46	0.041	85	1.6E-2	3.87

Fracture Properties:

Hydrogeologic Unit/Reference	*Fracture Aperture (microns)*	*Fracture Density ($1/m^3$)*	*Porosity*	*Residual Saturation*	*Fracture Conditions (m/yr)*	*Bulk Conditions (m/yr)*	*Alpha (1/m)*	*Beta*
Peters (1984) [USW G4]	22	---	---	---	1.4E4			
Klavetter (1986)	15.5	3	4.6E-5	0.04	6.3E3	0.29	1.28	4.23
Dudley (1988)	15.5	3	4.6E-5	0.04	6.3E3	0.29	1.28	4.23

Table B-1 (continued)

CALICO HILLS (Non-Welded, Zeolitic)

Matrix Properties:

Hydrogeologic Unit/Reference	*Grain Density (kg/m^3)*	*Porosity*	*Residual Saturation*	*Saturation Conditions (m/yr)*	*Alpha (1/m)*	*Beta*
Peters (1984) [USW G4]	2,230 - 2,380	0.22 - 0.30	0.037 - 0.215	7.6E-7 - 5.0E-3	6.0E-4 - 6.0E2	1.46 - 3.3.2
Klavetter (1986)	2,230	0.28	0.110	6.3E-4	3.1E-3	1.60
Dudley (1988)	2,230	0.28	0.110	6.3E-4	3.1E-3	1.60
Barnard (1991)	2,280 - 2,320	0.23 - 0.36	0.0 - 0.15	2.2E-4 - 6.3E-4	2.0E-3 - 5.0E-3	1.37 - 1.65
DOE (1988, Table 3-27)						
Lab data	---	0.20 - 0.34	---	1.5E-3 - 0.11	---	---
Field data	---	---	---	180.	---	---

Fracture Properties:

Hydrogeologic Unit/Reference	*Fracture Aperture (microns)*	*Fracture Density ($1/m^3$)*	*Porosity*	*Residual Saturation*	*Fracture Conditions (m/yr)*	*Bulk Conditions (m/yr)*	*Alpha (1/m)*	*Beta*
Peters (1984) [USW G4]	6 - 31	---	---	---	9.8E2 - 2.5E4			
Klavetter (1986)	15.5	3	4.6E-5	0.04	6.3E3	0.29	1.28	4.23
Dudley (1988)	15.5	3	4.6E-5	0.04	6.3E3	0.29	1.28	4.23
Barnard (1991)	6.0	3	1.8E-5	0.04	9.4E2	0.02	1.28	4.23

Table B-1 (continued)

PROW PASS (Welded, Devitrified)

Matrix Properties:

Hydrogeologic Unit/Reference	*Grain Density (kg/m³)*	*Porosity*	*Residual Saturation*	*Saturation Conditions (m/yr)*	*Alpha (1/m)*	*Beta*
Peters (1984) [USW G4]	2,590	0.24	0.066	5.0E-2 - 4.4E-1	1.4E-2	2.64
Peters (1984) [USW GU3]	2,570 - 2,580	0.32 - 0.39	0.018 - 0.066	4.1E-2 - 2.2E-1	1.4E-2 - 3.1E-2	2.96 - 3.44
Klavetter (1986)	2,590	0.24	0.066	0.14	1.4E-2	2.64
Dudley (1988)	2,590	0.24	0.066	0.14	1.4E-2	2.64
Barnard (1991)	2,590	0.25	0.05	0.06 - 1.6	1.0E-2	2.7
DOE (1988, Table 3-27)						
Lab data	---	0.10 - 0.30	---	2.2E-4 - 0.36	---	---
Field data	---	---	---	36.0 - 5.3E2	---	---

Fracture Properties:

Hydrogeologic Unit/Reference	*Fracture Aperture (microns)*	*Fracture Density (1/m³)*	*Porosity*	*Residual Saturation*	*Fracture Conditions (m/yr)*	*Bulk Conditions (m/yr)*	*Alpha (1/m)*	*Beta*
Klavetter (1986)	4.16	3	1.3E-5	0.04	4.4E2	0.02	1.28	4.23
Dudley (1988)	4.16	3	1.3E-5	0.04	4.4E2	5.7E-3	1.28	4.23
Barnard (1991)	20.	3	6.0E-5	0.04	1.3E4	0.8	1.28	4.23

Table B-1 (continued)

Matrix Properties:

Hydrogeologic Unit/Reference	*Grain Density (kg/m^3)*	*Porosity*	*Residual Saturation*	*Saturation Conditions (m/yr)*	*Alpha (1/m)*	*Beta*
UPPER CRATER FLAT (Non-Welded, Zeolitic)						
Peters (1984) [USW G4]	2,240 - 2,290	0.19 - 0.29	0.135 - 0.322	6.3E-4 - 1.4E-2	3.2E-3 - 4.5E-3	1.87 - 2.02
BULLFROG (Welded, Devitrified)						
Peters (1984) [USW G4]	2,620 -2,630	0.24 - 0.27	0.056 -0.061	7.2E-2 - 2.0E-1	1.1E-2 - 2.9E-2	2.26 - 4.15
DOE (1988, Table 3-27)						
Lab data	---	0.17 - 0.34	---	1.1E-2 - 0.36	---	---
Field data	---	---	---	2.2 - 8.4E2	---	---
TRAM (Non-Welded)						
DOE (1988, Table 3-27)						
Lab data	---	0.18 - 0.26	---	1.5E-3 - 0.15	---	---
Field data	---	---	---	2.5E-3 - 2.9E2	---	---

Table B-2. Average sorption ratios (distribution coefficients) from batch sorption experiments on crushed tuff for americium, plutonium, uranium, selenium, technetium, and neptunium (Meijer, 1990). (The sorption ratio in parentheses represents the standard deviation of the mean.)

Unit	*Sample*	*Depth (ft)*	*Sorption Ratios (ml/g)*					
			Am	*Pu*	*U*	*Se*	*Tc*	*Np*
Pah Canyon (Tpp)	G2-547	547	13,000 (110)	1200 (120)	9.4 (0.1)	2 (2)	0	
	G2-723	723	890,000 (49,000)	>4500	2.4 (0.6)	19 (2)	0	
	GU3-433	433	3400 (200)	330 (60)	0	15 (3)	0	7.9 (0.1)
	GU3-855	855			10 (0.7)	10 (0.4)		
	GU3-916	916		250 (25)			0.72 (0.2)	4.9 (1)
Topopah Spring (Tpt)	YM-22	848	1200 (130)	64 (20)	1.8 (0.2)		0.3 (0.14)	7.0 (1.0)
	GU3-1203	1203	1100 (120)	360 (40)	0	1 (1)	0	2.7 (0.1)
	GU3-1301	1301	1800 (160)	290 (40)	0	7 (2)	0.03 (0.001)	5.0 (0.1)
	JA-18	1420	180 (30)	120 (20)	2.5 (0.4)			
Calico Hills, tuffaceous beds (Tht)	G1-1436	1436			10 (2)	10 (3)		
	G2-1952	1952	1700 (70)	66 (6)	0	2 (1)		2.7 (0.1)
	GU3-1436	1436			20 (2)	3		
bedded tuff (bt)	GU3-1531	1531			54 (9)	5 (1)		
	YM-38	1504	14,600 (1000)	140 (30)	5.3 (0.2)			11.0

Table B-2 (continued)

Unit	Sample	Depth (ft)	Sorption Ratios (ml/g)					
			Am	Pu	U	Se	Tc	Np
Prow Pass (Tcp)	G1-1883	1883	4700 (300)	77 (11)				6.4
	G1-1982	1982				2.5		2.4
	YM-48	2114					0.15 (0.02)	
	YM-49	2221	4300 (1400)	230 (50)			0.21 (0.02)	9 (3)
Bullfrog (Tcb)	G1-2233	2233			5	10		
	G1-2289	2289			2.5	9 (1)		
	YM-54	2491	153 (6)	80 (20)	1.3 (0.3)		4.2 (0.5)	
	G1-2363	2363			0	25 (5)		
	JA-32	2533	130 (30)	110	2.2 (0.9)			
Tram (Tct)	G1-2840	2840			0.5	3.1		
	G1-2901	2901			4.3	5.5		
	G1-3116	3116			3.7	3.3		
	JA-37	3497	28,000 (10,000)	400 (70)	4.6 (0.3)			22
bedded tuff (Tba)	G2-3933	3933	6600 (400)	1600 (30)	0		0.1 (0.06)	

Table B-3. Average sorption ratios (distribution coefficients) from batch sorption experiments on crushed tuff for strontium, cesium, barium, radium, cerium, and europium (Meijer, 1990). (The sorption ratio in parentheses represents the standard deviation of the mean.)

Unit	*Sample*	*Depth (ft)*	*Sorption Ratios (ml/g)*					
			Sr	*Cs*	*Ba*	*Ra*	*Ce*	*Eu*
Tiva Canyon (Tpc)	JA-8	606	270 (5)	2700 (400)	435 (15)			2100 (300)
	YM-5	251	280 (80)	5800 (800)	1100 (200)		450,000 (240,000)	2,300,000 (40,000)
Pah Canyon (Tpp)	G2-547	547	265 (10)	13,300 (1500)	3490 (30)			340 (30)
	G2-723	723	290 (40)	4100 (600)	3500 (400)			>10,000
	GU3-433	433	45 (9)	630 (20)	810 (100)			100 (14)
Topopah Spring (Tpt)	YM-22	848	53 (4)	290 (30)	900 (30)		1270 (40)	1390 (110)
	GU3-1203	1203	42 (1)	350 (30)	640 (40)			190 (2)
	G1-1292	1292	200 (6)	430 (28)	2100 (300)	1500 (100)	66 (8)	140 (14)
	GU3-1301	1301	28 (4)	160 (40)	570 (60)			45 (12)
	YM-30	1264	260 (80)	855 (5)	3400 (1500)		230,000 (100,000)	160,000 (50,000)
	JA-18	1420	17,000 (3000)	16,000 (1000)	38,000 (18,000)		2800 (1400)	1400 (200)
Calico Hills, tuffaceous beds (Tht)	G1-1436	1436	36,000 (3000)	7800 (500)	150,000 (24,000)		59,000 (7000)	30,000 (2000)
	G2-1952	1952	2200 (400)	63,300 (1100)	25,000 (4000)			89 (14)
Prow Pass (Tcp)	G1-1854	1854	60,000 (14,000)	13,000 (2000)	45,000 (7000)			15,000
	YM-45	1930	195 (14)	520 (90)	1200 (100)		730 (100)	1600 (200)
	G1-1883	1883	22 (0.2)	187 (3)	183 (12)		1420 (20)	
	YM-46	2002	190 (60)	840 (6)	14,000 (6000)		310,000 (110,000)	307,000 (110,000)
	G1-1982	1982	55 (4)	1120 (110)	700 (50)		560 (40)	970 (150)
	YM-48	2114	2100 (400)	9000 (4000)	18,000 (6000)		1400 (500)	2200 (500)
	YM-49	2221	3200 (300)	36,000 (3000)	42,000 (8000)		550 (100)	1200 (100)
	JA-26	1995	95 (35)	1500 (600)	800 (300)			

Table B-3 (continued)

Unit	Sample	Depth (ft)	Sorption Ratios (ml/g)					
			Sr	Cs	Ba	Ra	Ce	Eu
bedded tuff (bt)	YM-38	1504	17,000 (2000)	13,000 (2000)	100,000 (10,000)		760 (140)	1600 (200)
	YM-42	1824	3900 (600)	17,000 (1000)	94,000 (14,000)		49,900 (7000)	52,000 (4000)
Bullfrog (Tcb)	JA-28	2001	94 (20)	1640 (210)	820 (50)			2100(1000)
	G1-2233	2233	48,000 (3000)	13,500 (800)	250,000 (30,000)		1400 (300)	900 (200)
	G1-2289	2289	7300 (500)	37,000 (13,000)	66,000 (9000)	46,000 (20,000)		797 (10)
	YM-54	2491	62 (12)	180 (40)	400 (150)		150 (40)	470 (40)
	G1-2333	2333	180 (20)	1400 (130)	1500 (200)			2300 (400)
	G1-2363	2363	64 (3)	470 (40)	235 (9)	540 (60)		730 (50)
	G1-2410	2410	169 (1)	1250 (50)	1780			440 (80)
	JA-32	2533	57 (3)	123 (4)	380 (30)		82 (14)	90 (20)
	G1-2476	2476	41 (1)	700 (40)	385 (11)			3200 (100)
Tram (Tct)	G1-2698	2698	42,000 (3000)	7700 (400)	63,000 (5000)		240 (30)	200 (30)
	G1-2840	2840	860 (1)	2200 (200)	2070 (70)			4900 (400)
	G1-2854	2854	94 (1)	1080 (120)	1000 (50)			1300 (200)
	G1-2901	2901	68 (1)	1290 (110)	1600 (200)		42,000 (3000)	160,000 (50,000)
	G1-3116	3116	2400 (17)	6600 (500)	12,000 (4000)		100 (10)	760 (60)
	JA-37	3497	287 (14)	610 (40)	760 (150)			6000 (800)
older tuffs (Tl)	G1-3658	3658	13,000 (0)	4950 (50)	13,500 (500)		1000 (200)	530 (40)
bedded tuff (Tba)	G2-3933	3923	240 (60)	2500 (1000)	1700 (500)			1500 (700)

Table B-4. Average (de)sorption ratios (distribution coefficients) from batch sorption experiments on crushed tuff for strontium, cesium, barium, radium, cerium, and europium (Meijer, 1990). (The sorption ratio in parentheses represents the standard deviation of the mean.)

Unit	*Sample*	*Depth (ft)*	*(De)Sorption Ratios (ml/g)*				
			Sr	*Cs*	*Ba*	*Ce*	*Eu*
Tiva Canyon (Tpc)	JA-8	606	311 (3)	4600 (400)	480 (50)		10,000 (3000)
	YM-5	251	320 (30)	8900 (600)	1200 (120)	31,000 (30,000)	36,000 (14,000)
Pah Canyon (Tpp)	G2-547	547	210 (10)	8700 (550)	2900 (200)		1700 (600)
	G2-723	723	330 (4)	4300 (4)	4200 (10)		> 10,000
	GU3-433	433	40 (10)	520 (20)	460 (20)		140 (10)
Topopah Spring (Tpt)	YM-22	848	59 (2)	365 (7)	830 (100)	6500 (800)	3500 (200)
	GU3-1203	1203	47 (1)	340 (10)	720 (30)		650 (50)
	G1-1292	1292	120 (5)	510 (20)	1500 (100)	600 (200)	600 (70)
	GU3-1301	1301	80 (20)	185 (20)	675 (60)		100 (20)
	YM-30	1264	210 (30)	1500 (100)	3100 (600)	170,000 (15,000)	11,000 (700)
	JA-18	1420	15,000 (2000)	17,500 (700)	280,000 (50,000)	1600 (500)	2400 (300)
Calico Hills, tuffaceous beds (Tht)	G1-1436	1436	87,000 (12,000)	24,000 (2000)	340,000 (90,000)	6700 (600)	5300 (600)
	G2-1952	1952	4200 (200)	46,000 (1400)	40,000 (1000)		1600 (200)
	YM-38	1540	22,000	13,000	260,000	2600	7300
	YM-42	1842	4100 (1000)	21,000 (2000)	90,000	44,000 (5000)	64,000 (3000)
older tuffs (Tl)	G1-3658	3658	12,000 (3000)	12,000 (2000)	10,000 (4000)	9000 (4000)	9000 (3000)

Table B-4 (continued)

Unit	Sample	Depth (ft)	(De)Sorption Ratios (ml/g)				
			Sr	Cs	Ba	Ce	Eu
Prow Pass (Tcp)	G1-1854	1854	72,000 (13,000)	14,000 (2000)	150,000 (40,000)		4800 (700)
	YM-45	1930	210 (20)	620 (110)	1310 (60)	5800 (600)	7300 (900)
	G1-1883	1883	59 (1)	430 (4)	440 (10)	2200 (100)	1350 (50)
	YM-46	2002	260 (20)	1800 (300)	210,000 (3000)	300,000 (50,000)	31,000 (2000)
	G1-1982	1982	322 (8)	2300 (200)	2780 (120)	7000 (800)	6370 (130)
	YM-48	2114	2700 (200)	27,000 (4000)	34,000 (7000)	128,000 (300)	8100 (1200)
	YM-49	2221	4400 (100)	39,000 (1000)	65,000 (7000)	1040 (40)	2100 (500)
	JA-26	1995	39 (3)	1580 (90)	450 (13)		2900 (200)
Bullfrog (Tcb)	JA-28	2001	114 (3)	2400 (100)	1160 (20)		12,300 (500)
	G1-2233	2233	90,000 (40,000)	23,000 (6000)	240,000 (80,000)	20,000 (13,000)	5000 (2000)
	YM-54	2491	97 (9)	310 (20)	660 (20)	1000 (200)	1840 (110)
	G1-2333	2333	140 (13)	1230 (100)	1460 (130)		9900 (1200)
	G1-2363	2363	150 (6)	1200 (30)	820 (20)	130,000 (6000)	6100 (200)
	G1-2410	2410	140 (14)	1120 (100)	1760 (150)		6000 (3000)
	JA-32	2533	53 (3)	175 (11)	490 (40)	530 (120)	850 (130)
	G1-2476	2476	200 (40)	1520 (0)			
Tram (Tct)	G1-2698	2698	210,000 (50,000)	17,000 (1100)	190,000 (80,000)	2000 (400)	
	G1-2840	2840	1540 (4)	2300 (130)	2500 (200)		9000 (1100)
	G1-2854	2854	96 (1)	1160 (20)	1330 (0)		5000 (200)
	G1-2901	2901	67 (1)	1380 (30)	1980 (30)	39,000 (1000)	210,000 (50,000)
	G1-3116	3116	24,000 (13,000)	11,000 (3000)	160,000 (80,000)	3000 (1000)	8000 (3000)
	JA-37	3497	312 (9)	850 (50)	920 (40)		11,000 (2000)
bedded tuff (Tba)	G2-3933	3933	140 (20)	1400 (350)	1100 (200)		3000 (1100)

Table B-5. Average (de)sorption ratios (distribution coefficients) from batch sorption experiments on crushed tuff for americium, plutonium, uranium, technetium, and neptunium (Meijer, 1990). (The sorption ratio in parentheses represents the standard deviation of the mean.)

Unit	*Sample*	*Depth (ft)*	*(De)Sorption Ratios (ml/g)*				
			Am	*Pu*	*U*	*Tc*	*Np*
Pah Canyon (Tpp)	G2-547	547	17,000 (1400)	1200 (170)			
	G2-723	723	2.8×10^6 (26,000)	>4700			
	GU3-433	433	9300 (1780)	920 (40)			
Topopah Spring (Tpt)	YM-22	848	2500 (400)	1330 (140)	5 (2)	1.2 (0.3)	33 (5)
	GU3-1203	1203	1300 (200)	920 (15)			
	G1-1292	1292				0	
	GU3-1301	1301	2500 (600)	1300 (460)			
	JA-18	1420	1100 (300)	350 (140)	9.4 (1.4)		
Calico Hills, tuffaceous beds (Tht)	G2-1952	1952	5800 (1100)	350 (45)			15 (2)
	YM-38	1540	7100 (1200)	1600 (300)	14.8 (1.0)		24 (2)
Prow Pass (Tcp)	G1-1883	1883	7200 (900)	890 (60)			36 (10)
	G1-1982	1982			4.1		
	YM-48	2114				1.6 (0.2)	
	YM-49	2221	3400 (400)	720 (90)		2.0 (0.3)	12 (4)

Table B-5 (continued)

Unit	*Sample*	*Depth (ft)*	*(De)Sorption Ratios (ml/g)*				
			Am	*Pu*	*U*	*Tc*	*Np*
Bullfrog (Tcb)	G1-2233	2233			8 (2)		
	YM-54	2491	550 (80)	720 (40)	12 (8)		
	JA-32	2533	2200 (600)		8 (2)		
	G1-2476	2476			1.5 (0.2)		
Tram (Tct)	G1-3116	3116			1.7 (0.3)		
	JA-37	3497	32,000 (10,000)	1400 (300)	9.9 (0.4)		170 (50)
bedded tuff (Tba)	G2-3933	3933	12,000 (410)	530 (130)		0	

Table B-6. Hydrogeologic parameteric values and ranges used for the ground-water pathway

Distribution	*Range*		*Description*
Porosity of Matrix			
uniform	.06 - .16		Topopah Spring, welded
uniform	.33 - .56		Calico Hills, non-welded vitric
uniform	.20 - .33		Calico Hills, non-welded zeolitic
uniform	.24 - .40		Prow Pass, welded
uniform	.18 - .30		Upper and Middle Crater Flat, non-welded
uniform	.19 - .32		Bullfrog, welded
Saturated Conductivity (mm/yr) and Permeability [m²] of Matrix			
lognormal	0.11 - 36.	[3.6E-19 - 1.2E-18]	Topopah Spring, welded
lognormal	1.2E2 - 6.1E3	[3.9E-15 - 2.0E-14]	Calico Hills, non-welded vitric
lognormal	0.004 - .20	[1.3E-20 - 7E-19]	Calico Hills, non-welded zeolitic
lognormal	58. - 300.	[1.9E-16 - 9.6E-16]	Prow Pass, welded
lognormal	1.6 - 4.6	[5.1E-18 - 1.5E-17]	Upper Crater Flat, non-welded
lognormal	110. - 140.	[3.5E-16 - 4.4E-16]	Bullfrog, welded
lognormal	1.3 - 4.8	[4.1E-18 - 1.6E-17]	Middle Crater Flat, non-welded
lognormal	130. - 160.	[4.3E-16 - 5.1E-16]	Tiva Canyon, welded
lognormal	380. - 470.	[1.2E-15 - 1.5E-15]	Paintbrush, non-welded
van Genuchten Alpha Parameter, for Matrix (1/m)			
constant	.006		Topopah Spring, welded
constant	.016		Calico Hills, non-welded vitric
constant	.003		Calico Hills, non-welded zeolitic
constant	.014		Prow Pass, welded
constant	.004		Upper and Middle Crater Flat, non-welded
constant	.02		Bullfrog, welded
van Genuchten Beta Parameter, for Matrix			
uniform	1.4 - 2.2		Topopah Spring, welded
uniform	1.5 - 4.9		Calico Hills, non-welded vitric
uniform	1.2 - 3.3		Calico Hills, non-welded zeolitic
uniform	2.0 - 3.4		Prow Pass, welded
uniform	1.5 - 2.4		Upper and Middle Crater Flat, non-welded
uniform	2.3 - 4.2		Bullfrog, welded
Grain Density for Matrix (kg/m³)			
constant	2580		Topopah Spring, welded
constant	2370		Calico Hills, non-welded vitric
constant	2230		Calico Hills, non-welded zeolitic
constant	2590		Prow Pass, welded
constant	2270		Upper and Middle Crater Flat, non-welded
constant	2630		Bullfrog, welded

Table B-6 (continued)

Distribution	*Range*		*Description*
Porosity of Fracture			
constant	1.4E-4		Tiva Canyon, welded
constant	2.7E-5		Paintbrush, non-welded
constant	4.1E-5		Topopah Spring, welded
constant	4.6E-5		Calico Hills, non-welded vitric
constant	4.6E-5		Calico Hills, non-welded zeolitic
constant	1.3E-5		Prow Pass, welded
constant	4.6E-5		Upper and Middle Crater Flat, non-welded[1]
constant	1.3E-5		Bullfrog, welded[2]
Saturated Conductivity (mm/yr) and Permeability [m^2] of Fractures			
lognormal	34. - 59.	[1.1E-16 - 1.9E-16]	Topopah Spring, welded
lognormal	170. - 370.	[5.6E-16 - 1.2E-15]	Calico Hills, non-welded vitric
lognormal	190. - 310.	[6.2E-16 - 9.9E-16]	Calico Hills, non-welded zeolitic
lognormal	12. - 25.	[3.9E-17 - 8.1E-17]	Prow Pass, welded
lognormal	210. - 300.	[6.7E-16 - 9.8E-16]	Upper and Middle Crater Flat, non-welded[1]
lognormal	15. - 20.	[4.9E-17 - 6.4E-17]	Bullfrog, welded[2]
van Genuchten Alpha Parameter, for Fracture (1/m)			
constant	1.3		Tiva Canyon, welded
constant	1.3		Paintbrush non-welded
constant	1.3		Topopah Spring, welded
constant	1.3		Calico Hills, non-welded vitric
constant	1.3		Calico Hills, non-welded zeolitic
constant	1.3		Prow Pass, welded
constant	1.3		Upper and Middle Crater Flat, non-welded
constant	1.3		Bullfrog, welded
van Genuchten Beta Parameter, for Fracture			
uniform	3.2 - 5.3		Tiva Canyon, welded
uniform	3.2 - 5.3		Paintbrush non-welded
uniform	3.2 - 5.3		Topopah Spring, welded
uniform	3.2 - 5.3		Calico Hills, non-welded vitric
uniform	3.2 - 5.3		Calico Hills, non-welded zeolitic
uniform	3.2 - 5.3		Prow Pass, welded
uniform	3.2 - 5.3		Upper and Middle Crater Flat, non-welded
uniform	3.2 - 5.3		Bullfrog, welded

[1] Values are representative of Calico Hills.

[2] Values are representative of Prow Pass.

Table B-6 (continued)

Distribution	*Range*	*Description*
Infiltration Rate (mm/yr)		
loguniform	0.1 - 5.0	base case
loguniform	5.0 - 10.	pluvial case
Dispersivity (m)		
normal	.3 - 30.	dispersivity for all units
Discharge Area (m^2)		
uniform	3.75E4 - 3.75E5	discharge area for all regions

Table B-7. Matrix K_d values, in cubic meters per kilogram, for selected radionuclides for the hydrogeologic units of interest (suggested ranges are assumed to +/- one order of magnitude, a loguniform distribution is assumed for all). Where no values are present, a K_d of zero is assumed. (Values in parentheses are derived from NUREG-1327.)

Element	*Hydrogeologic Unit*					
	Topopah Spring	*Calico Hills*		*Prow Pass*	*Upper and Middle Crater Flat* [1]	*Bull Frog*
		vitric	*zeolitic*			
Cm	(0.45)	(3.28)	(1.66)	(1.16)	(1.32)	(1.20)
Pu	0.17	0.17	0.066	0.13	0.053	0.094
U	0.0002	0.02	0.001	----	0.0008	0.002
Am	0.81	0.81	1.7	4.5	1.36	0.14
Np	0.0045	0.0045	0.0027	0.0051	0.0022	0.0051
Th	(0.048)	(0.34)	(0.17)	(0.12)	(0.14)	(0.13)
Ra	1.5	1.5	1.5	1.5	1.2	5.0
Pb	(0.0068)	(0.049)	(0.025)	(0.017)	(0.020)	(0.018)
Cs	0.36	0.24	22.0	2.2	17.6	3.2
I	----	----	----	----	----	----
Sn	(0.134)	(0.97)	(0.49)	(0.34)	(0.39)	(0.35)
Tc	0.00001	----	----	0.00017	----	0.0042

[1] Values determined are based on Calico Hills zeolitic values and allowances are made for differences in porosity and density.

Table B-7 (continued)

Element	*Hydrogeologic Unit*					
	Topopah Spring	*Calico Hills*		*Prow Pass*	*Upper and Middle Crater Flat* [1]	*Bullfrog*
		vitric	*zeolitic*			
Zr	(0.0048)	(0.034)	(0.017)	(0.012)	(0.014)	(0.013)
Sr	0.08	0.034	8.9	0.45	7.1	0.28
Ni	(0.0037)	(0.027)	(0.014)	(0.009)	(0.011)	(0.010)
C	----	----	----	----	----	----
Se	0.0026	0.003	0.0045	0.0025	0.0036	0.013
Nb	----	----	----	----	----	----

[1] Values determined are based on Calico Hills zeolitic values.and allowances are made for differences in porosity and density.

Figure B-1. Location map for the zeolitic cross sections in Figures B-2, B-3, and B-4. This figure and the stratigraphy shown in Figures B-2 and B-4 are based on Scott and Bonk (1984). (Taken from DOE, 1988, p. 4-22.)

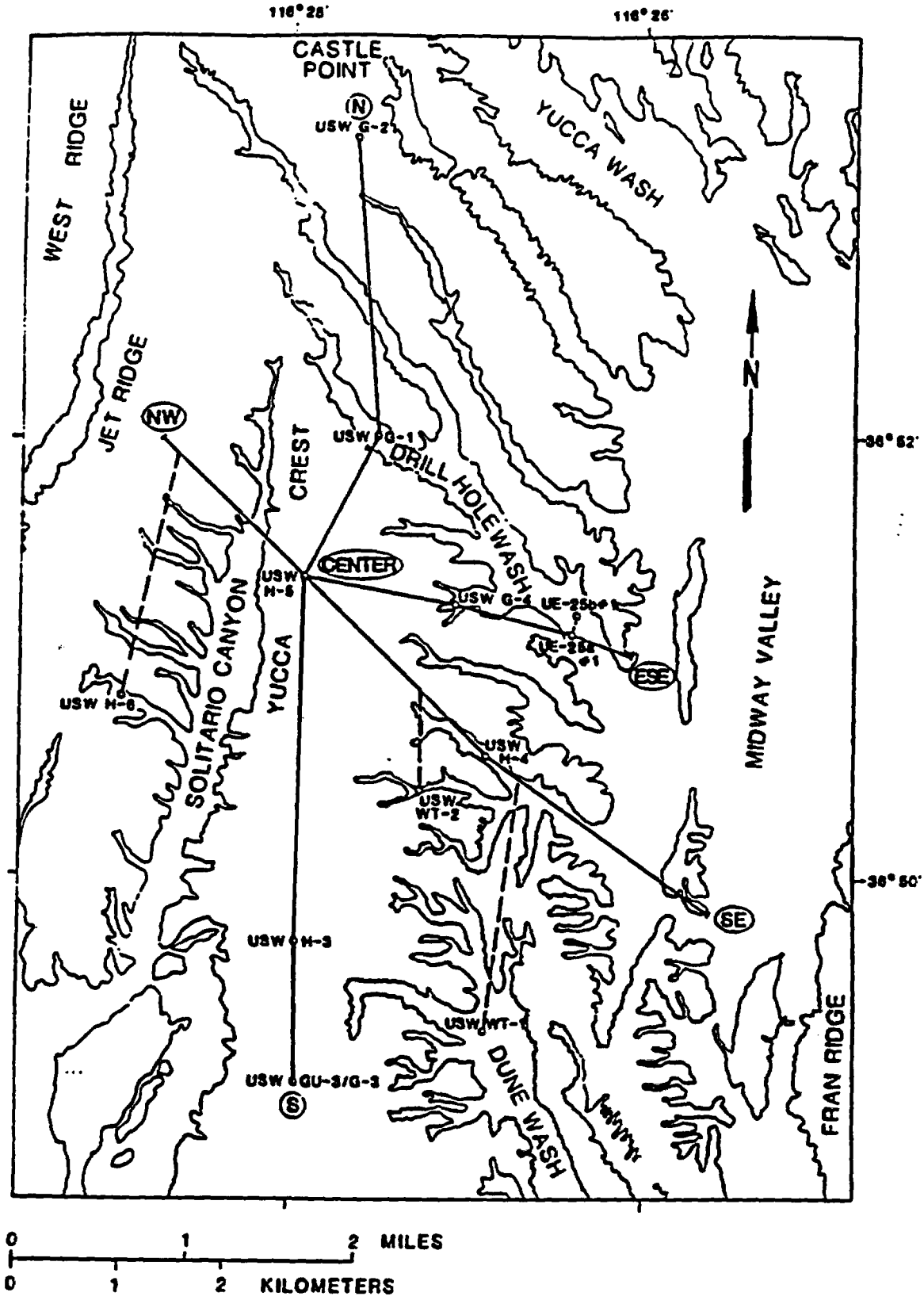

Figure 8-1. Location map for the zeolite cross sections in Figures 4-5, 4-6, and 4-7. This figure and the stratigraphy shown in Figures ~~[illegible]~~ and ~~[illegible]~~ are based on Scott and Bonk (1984).

8-2 8-3

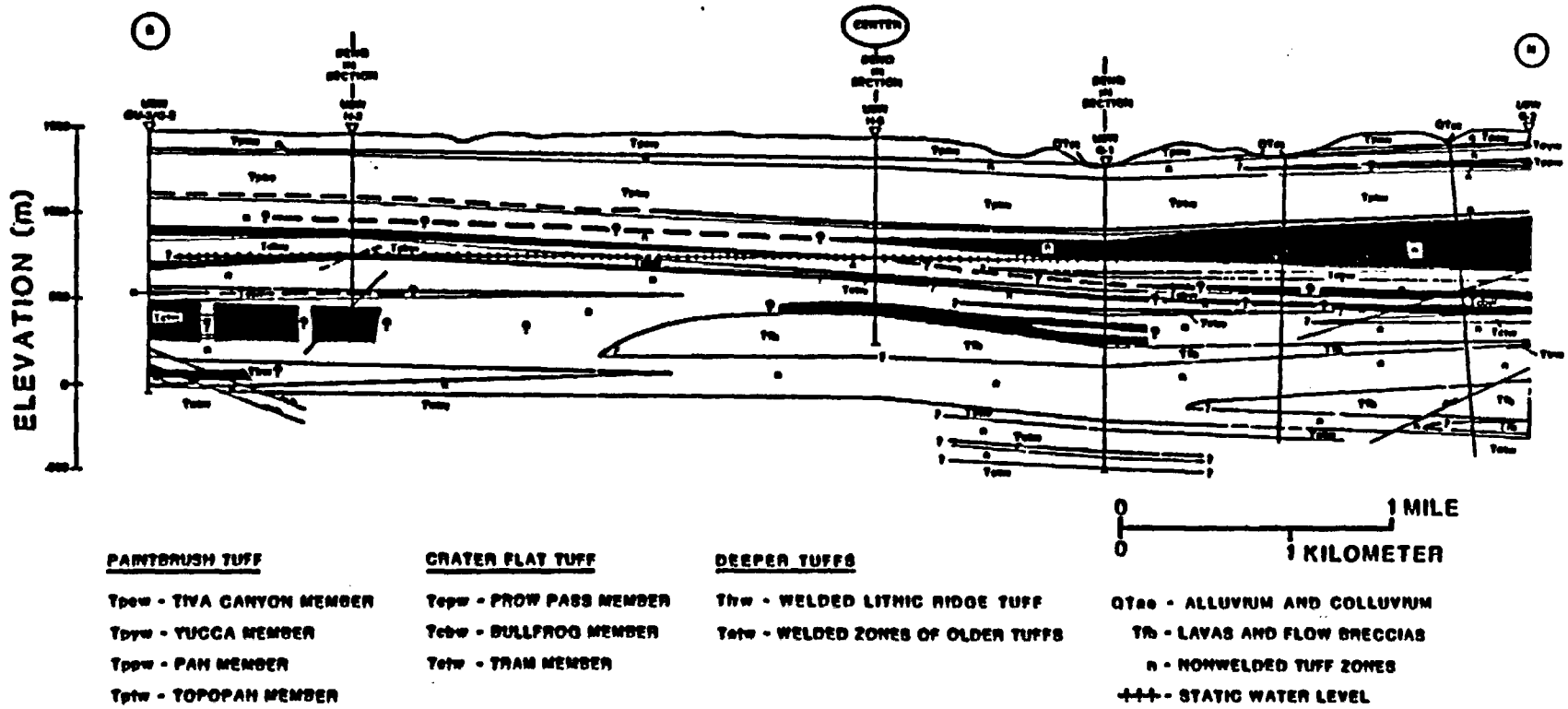

B-1

Figure B-2. Major zeolite distributions (Bish and Vaniman, 1985), north-south cross section, shown as a dark pattern overlying the stratigraphic cross section of Scott and Bonk (1984). Location of cross section is shown on Figure 4-4. Unit designations follow the usage of Scott and Bonk (1984). Tpcw, Tpyw, Tppw, and Tptw represent the welded zones of the Tiva Canyon, Yucca Mountain, Pah Canyon, and Topopah Spring members of the Paintbrush Tuff; Tcpw, Tcbw, and Tctw represent the welded zones of the Prow Pass, Bullfrog, and Tram members of the Crater Flat Tuff; Tfb represents lavas and flow breccias; the Totw represents the welded zones of older tuffs. The symbol n is used for all nonwelded tuff zones. The subhorizontal barred line indicates the water table as inferred from static water levels in the drillholes.

Figure B-3. Major clinoptilolite-mordenite distributions (Bish and Vaniman, 1985), northwest-southeast cross section. Location of cross section is shown on Figure B-1. Information on drillhole USW H-5 below 760 meters is from Bentley *et al.* (1983) and information on the central part of the drillhole USW H-6 is from Craig *et al.* (1983). (Taken from DOE 1988, p. 4-25.)

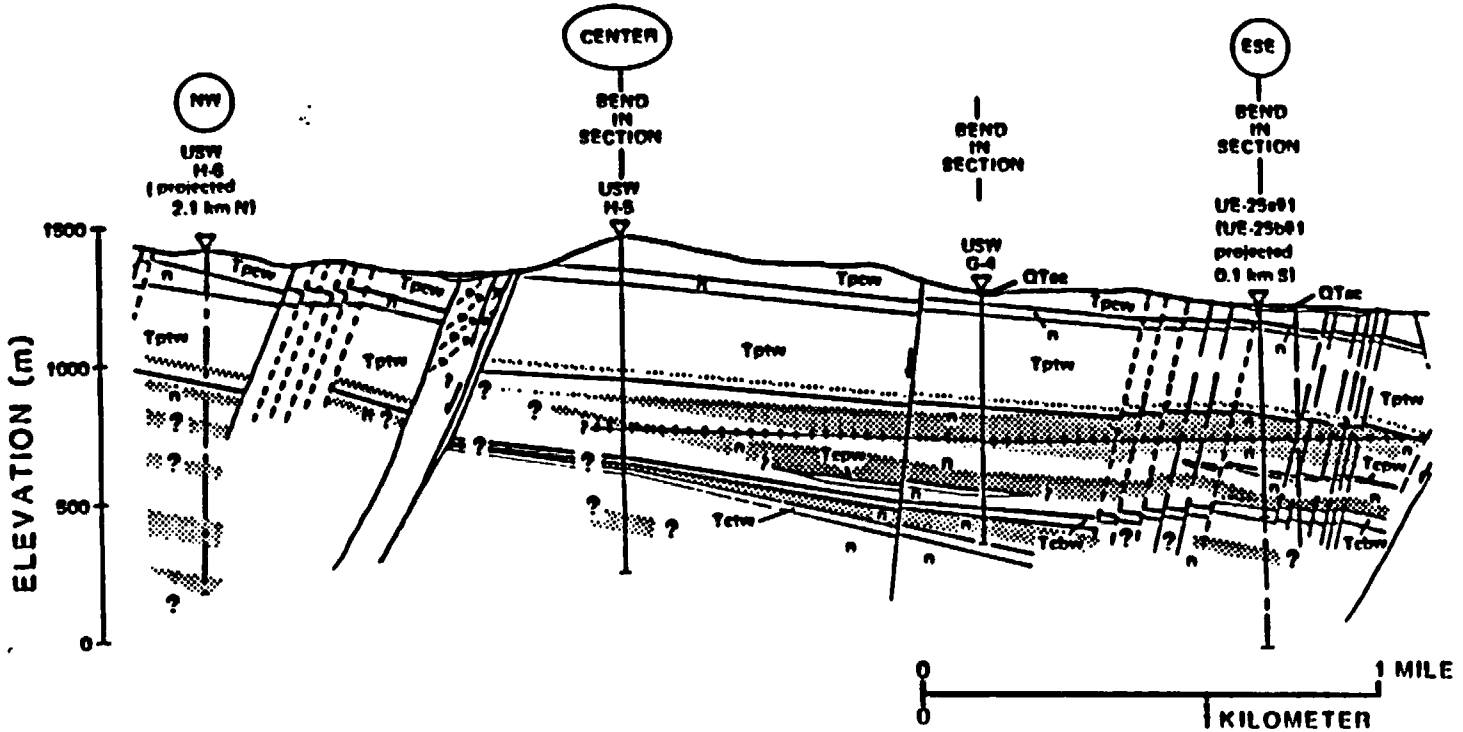

Figure B-3 Major clinoptilolite-mordenite distributions (Bish and Vaniman, 1985), northwest-southeast cross section. Location of cross section is shown on Figure B-1. Information on drillhole USW H-5 below 760 m is from Bentley et al. (1983), and information on the central part of the drillhole USW H-6 is from Craig et al. (1983)

Figure B-4. Major zeolite distributions (Bish and Vaniman, 1985), center to southeast cross section as depicted in Figure B-1. (Taken from DOE, 1988, p. 4-26.)

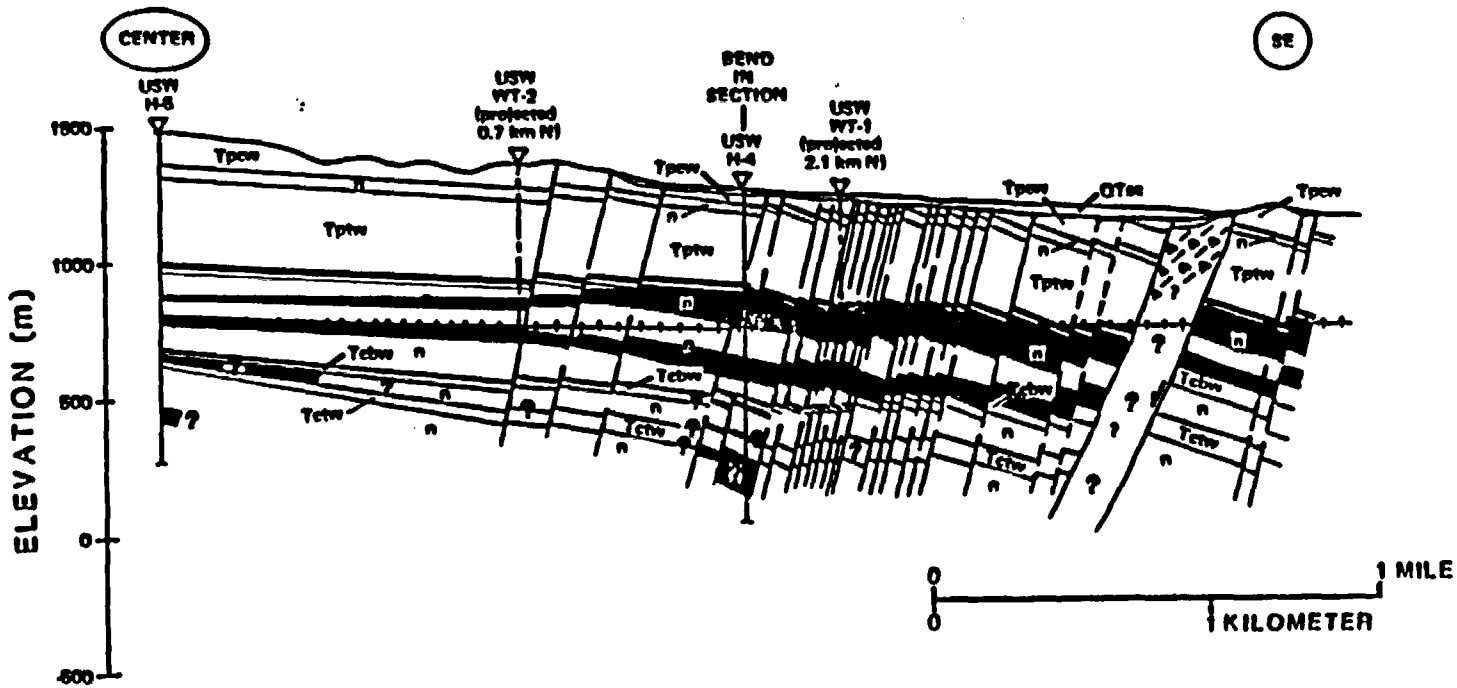

PAINTBRUSH TUFF

Tpcw - TIVA CANYON MEMBER

Tptw - TOPOPAH MEMBER

CRATER FLAT TUFF

Tcbw - BULLFROG MEMBER

Tctw - TRAM MEMBER

QTsc - ALLUVIUM AND COLLUVIUM

n - NONWELDED TUFF ZONES

+++ - STATIC WATER LEVEL

Figure 8-4. Major zeolite distributions (Bish and Vaniman, 1985), center to southeast cross section (Figure 8-1).

APPENDIX C

CONTENTS

		Page
C-1.	Task Objective	C-1
C-2.	Introduction	C-1
C-3.	Test Problem No. 1: Comparison with the Staff's Own Analytical Solution	C-1
C-3.1.	Problem Description	C-2
C-3.2.	Comparison of Results	C-2
C-4.	Test Problem No. 2: Two-Dimensional Flow on a Saturated-Unsaturated Region	C-4
C-4.1.	Problem Description	C-4
C-4.2.	Comparison of Results	C-6
C-5.	Test Problem No. 3: Simulation of Jornada Trench Experiment	C-6
C-5.1.	Problem Description	C-6
C-5.2.	Comparison of Results	C-11
C-6.	Test Problem No. 4: 2D Flow Through Fractured Rock	C-11
C-6.1.	Problem Description	C-11
C-6.2.	Comparison of Results	C-22
C-7.	Summary and Conclusions	C-25
C-8.	References	C-32

TABLES

C-1	Van Genuchten Soil Parameters	C-12
C-2	Coordinates of the Numbered Points in Figure C-7	C-16
C-3	Base Case Material Properties Used for the Hydrologic Units, as Depicted by Letters in Figure C-7	C-18
C-4	Material Properties Used in Modification	C-21
C-5	*DCM3D* Vertical Discretization Information	C-21
C-6	Transfer Factors Used for the Units Identified in Figure C-7 and Using Equation (C-8)	C-22

FIGURES

C-1. Comparison of *DCM3D* Results with a Quasi-Analytic Solution of a Vertical Infiltration Problem at t = 2 Hours C-3

C-2. Definition sketch for Test Problem 2 . . . . . C-5

C-3. *DCM3D* Pressure-Head Contour for a Two-Dimensional, Saturated-Unsaturated Problem . C-7

C-4. Comparison of Moisture Contents from *DCM3D* and *PORFLO3*, for Test Problem 2 . . . C-8

C-5. Definition Sketch for the Jornada Trench Experiment C-9

C-6. Comparison of *DCM3D* and *PORFLO-3* Results for the Jornada Trench Experiment . . . C-13

C-7. Moisture Content Results for Test BT-2 . . . . . C-14

C-8. Two-Dimensional Base-Case Stratigraphy C-15

C-9. Particle Paths Based on the *NORIA* Simulation C-23

C-10. Spatial Distribution of Flux at the Repository, Based on the *NORIA* Simulation Condition Values C-24

C-11. Particle Paths, Based on the *DCM3D* Simulation, Using a Composite Curve C-26

C-12. Spatial Distribution of Flux, Based on the *DCM3D* Simulation, Using the Composite Curves C-27

C-13. Particle Paths in the Matrix, Based on *DCM3D* Simulations, Using the Dual-Porosity Model C-28

C-14. Particle Paths in the Fracture, Based on *DCM3D* Simulations, Using the Dual-Porosity Model C-29

C-15. Spatial Distribution of Flux in the Matrix, Based on the *DCM3D* Simulation, Using the Dual-Porosity Model C-30

APPENDIX C
EVALUATION OF SNL TECHNOLOGY: TESTING OF THE DCM3D COMPUTER CODE

B. Sagar/CNWRA, L. Tweedy/SwRI, T.J. McCartin/RES, and
A.B. Gureghian/CNWRA

C-1. TASK OBJECTIVE

The objective of this auxiliary analysis is to evaluate the performance assessment technology developed by Sandia National Laboratories (SNL) for the Nuclear Regulatory Commission (NRC). SNL was the prime NRC contractor for performance assessment from the mid-seventies to 1990, when this technology was transferred to the Center for Nuclear Waste Regulatory Analyses (CNWRA). The SNL-developed computer code *DCM3D*, a three-dimensional (3D) dual-porosity saturated-unsaturated flow code, is of special interest for potential application to an unsaturated site like Yucca Mountain. This code was evaluated at CNWRA and at NRC, to determine how well it would perform as a flow simulator for use in assessing the performance of the total system.

C-2. INTRODUCTION

The *DCM3D* code evaluation work began with a review of literature on modeling of partially saturated flow (reported in the CNWRA's *First Annual Research Report* (see Gureghian and Sagar, 1991)). A more comprehensive review on unsaturated flow has also been performed (Ababou, 1991). In Gureghian and Sagar (1991), preliminary tests consisting primarily of those problems provided by the author of the *DCM3D* computer code were reported. In this second and concluding part of the evaluation, problems not included in the code's *User's Manual* (see Updegraff *et al.*, 1991) have been solved. The document by Updegraff *et al.* also discusses the dual-porosity formulation implemented in *DCM3D* in sufficient detail; therefore, code theory is not discussed any further here.

All four test problems described below were extracted from the literature. Because modeling of flow through partially saturated fractured rock is of recent origin, most of the literature considers flow in unfractured soils. In addition, the concept of dual porosity in modeling flow through fractured rock has rarely been applied to unsaturated regimes; it is even more difficult to find problems in the literature related to this concept. As outlined in Gureghian and Sagar (1991), the major difficulty in applying the dual-porosity concept is the estimation of the fluid transfer term that couples the equations describing flow in the two media (matrix and fracture). This difficulty is also encountered in other approaches. For example, when fractures are treated as networks, the practical determination of hydraulic properties of such networks is a major unsolved problem. Nevertheless, the differences of the predicted flow fields need to be determined, using the dual-porosity concept and other approaches. The last problem, taken from the International Code Intercomparison study (known as HYDROCOIN) is an effort to evaluate the differences. Data for the first three test problems have been taken from Magnuson *et al.* (1990).

C-3. TEST PROBLEM NO. 1: COMPARISON WITH THE STAFF'S OWN ANALYTICAL SOLUTION

Comparison with an analytic solution for one-dimensional (1D) unsaturated flow in a horizontal soil column has been discussed by Updegraff *et al.* (1991), in the *User's Manual* of *DCM3D*. Here the staff has added a comparison with a quasi-analytic solution representing flow in a vertical column, so that the

effects of gravity on flow can be simulated. For a single-porosity homogeneous medium, the quasi-analytic solution was obtained by Philip (1957). This solution is available as a FORTRAN code – *INFIL* (see El-Kadi, 1987). The object of solving this problem was to assess the accuracy of *DCM3D* in determining the position of the wetting front in a soil undergoing vertical moisture infiltration.

C-3.1. Problem Description

In the test problems, the vertical soil column had a height of 15 centimeters. The finite difference grid was uniform, with a grid spacing of 0.075 centimeters; thus the domain had 200 grid points. The soil was Yolo light clay, with hydraulic properties given by Haverkamp *et al.* (1977) – Equation (C-1) and Equation (C-2), below. The curve-fitting parameters in Equation (C-1) were $\alpha = 739.0$ and $\beta = 4.0$, and those in Equation (C-2) were $A = 124.6$ and $B = 1.77$. The saturated hydraulic conductivity was taken to have a constant value of 0.04428 centimeters/hour. The saturated volumetric moisture content (or porosity) was 0.495, and the residual moisture content was 0.124. The relationship of moisture-content relationship to pressure-head is given by:

$$\theta(\psi) = \frac{\alpha(\theta_s - \theta_r)}{\alpha + [\ln|\Psi|]^\beta} + \theta_r \quad , \tag{C-1}$$

and the relationship of hydraulic conductivity to pressure-head is given by:

$$K(\Psi) = K_s \frac{A}{A + |\Psi|^B} \quad , \tag{C-2}$$

where:

θ	=	volumetric moisture content;
θ_s	=	saturated volumetric moisture content (porosity);
θ_r	=	residual moisture content;
K	=	unsaturated hydraulic conductivity (centimeters/hour);
K_s	=	saturated hydraulic conductivity (centimeters/hour);
Ψ	=	pressure head (centimeters); and
α, β, A, B	=	curve fitting parameters.

The characteristic curves described in Equation (C-1) and Equation (C-2) are not part of the *DCM3D* code. These were coded for this test.

Initially the domain had a uniform pressure-head distribution of -601.8 centimeters, which corresponded to a moisture content of 0.238. The pressure-head boundary condition at the bottom surface corresponded to the value of the initial condition. The pressure-head boundary condition at the top surface was set to -1 centimeters which corresponded to essentially full saturation.

C-3.2. Comparison of Results

DCM3D results were compared with the quasi-analytic solution of Philip generated by the *INFIL* code in Figure C-1. The comparison showed reasonable agreement between the two solutions. Regarding the minor discrepancies, the *INFIL* code had some numerical approximations (e.g., summation of series) of

Figure C-1. Comparison of *DCM3D* results with a quasi-analytic solution of a vertical infiltration problem at $t = 2$ hours.

Figure C-1. Comparison of DCM3D results with a quasi-analytic solution of a vertical infiltration problem at t = 2 hours

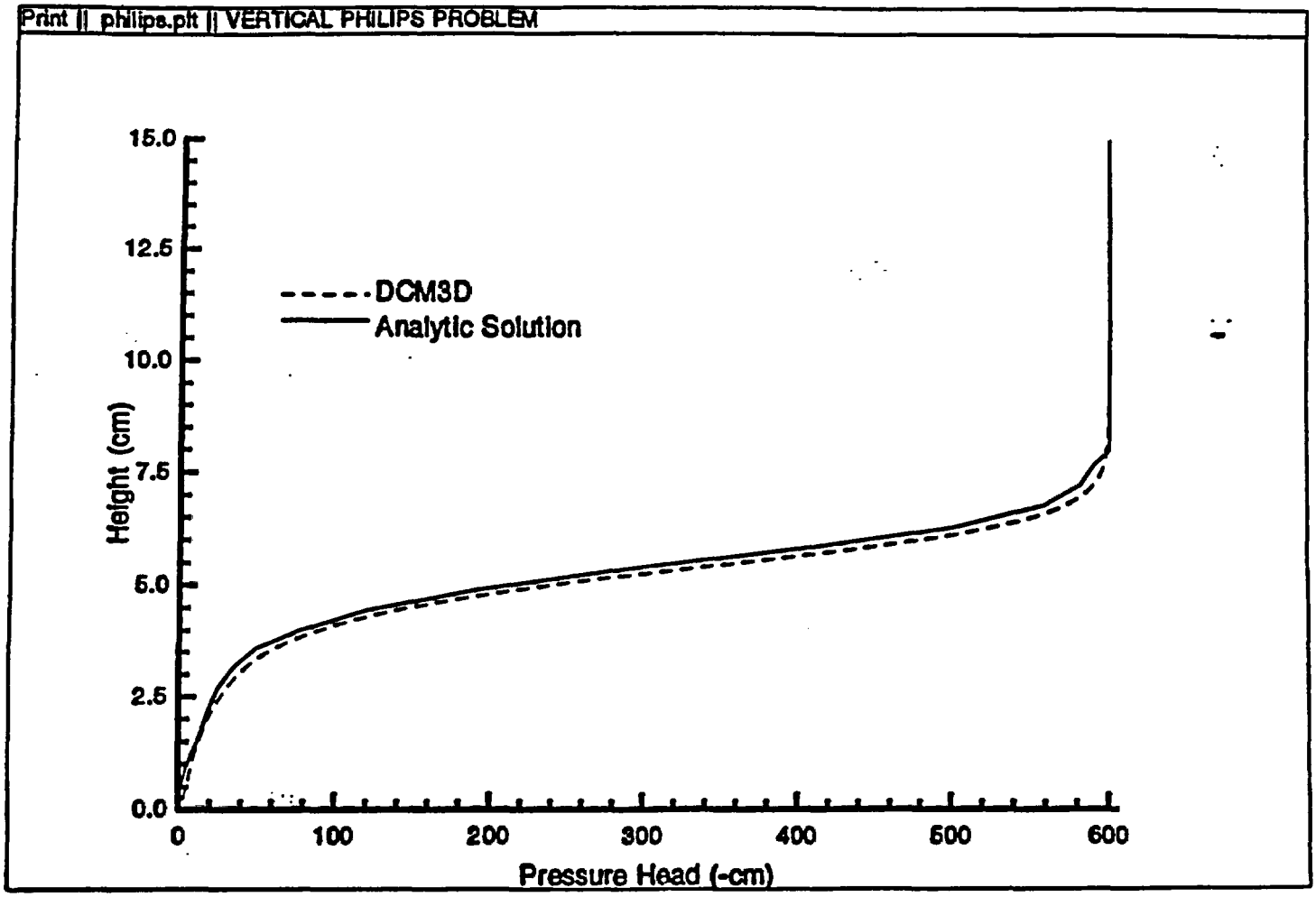

its own. Overall, the *DCM3D* was able to simulate the problem of one-dimensional vertical infiltration reasonably well.

To solve this problem, *DCM3D* used 1.24 CPU minutes on a VAX 8700 computer.

C-4. TEST PROBLEM NO. 2 (BENCHMARK): TWO-DIMENSIONAL (2D) FLOW ON A SATURATED-UNSATURATED REGION

This problem deals with 2D movement of moisture in a vertical cross-section of an unconfined aquifer, where the zone above the water table is under unsaturated-state conditions. Both the storativity and the hydraulic conductivity may be discontinuous (have a finite jump) at the water table. For example, the storage in the unsaturated zone is caused by change in moisture content caused by proximity to the water table and drainage (or filling) of pores; in the saturated zone, storage is primarily caused by compressibilities of the water and the medium. The objective of this test problem was to investigate the capability of *DCM3D* to deal with such changes in properties. The problem was solved in a transient mode for a long time to approximate steady-state conditions.

C-4.1. Problem Description

The physical domain was modeled as a 150-meters-wide by 35-meters-deep, vertical cross-section, as shown in Figure C-2. For the numerical solution, 30 evenly spaced nodes were placed in the x-direction. In the y-direction, a node spacing of 2 meters was used, from $y = 0$ to $y = 18$ meters. The y-direction model spacing was reduced to 1 meter after that. This led to 26 nodes in the y-direction for a total of 780 nodes. Initially, the water-table gradient was assumed to be constant and equal to 2/150. This slope was represented in the simulation by imposing hydrostatic fixed-head boundary conditions in the saturated parts of the two vertical boundaries. The water table itself was not an external boundary in this problem; that is, the water table was obtained as a part of the solution, except at the two external boundaries where it was fixed.

The hydraulic properties of the soil were those given by Huyakorn (1989). The saturated porosity was 0.25 and the saturated hydraulic conductivity was 750 meters/year.

The relationship of saturation to pressure-head is given by:

$$S = 0.25 + \frac{0.75}{1+(0.2\Psi)^2} \quad , \tag{C-3}$$

and the relationship of relative hydraulic-conductivity to pressure-head is given by:

$$K_r = [1+(0.2\Psi)^2]^{-4} \quad , \tag{C-4}$$

where:

S	=	degree of saturation;
K_r	=	relative hydraulic-conductivity; and
Ψ	=	pressure head.

Figure C-2. Definition sketch for Test Problem 2.

Figure C-2. Definition sketch for Test Problem 2

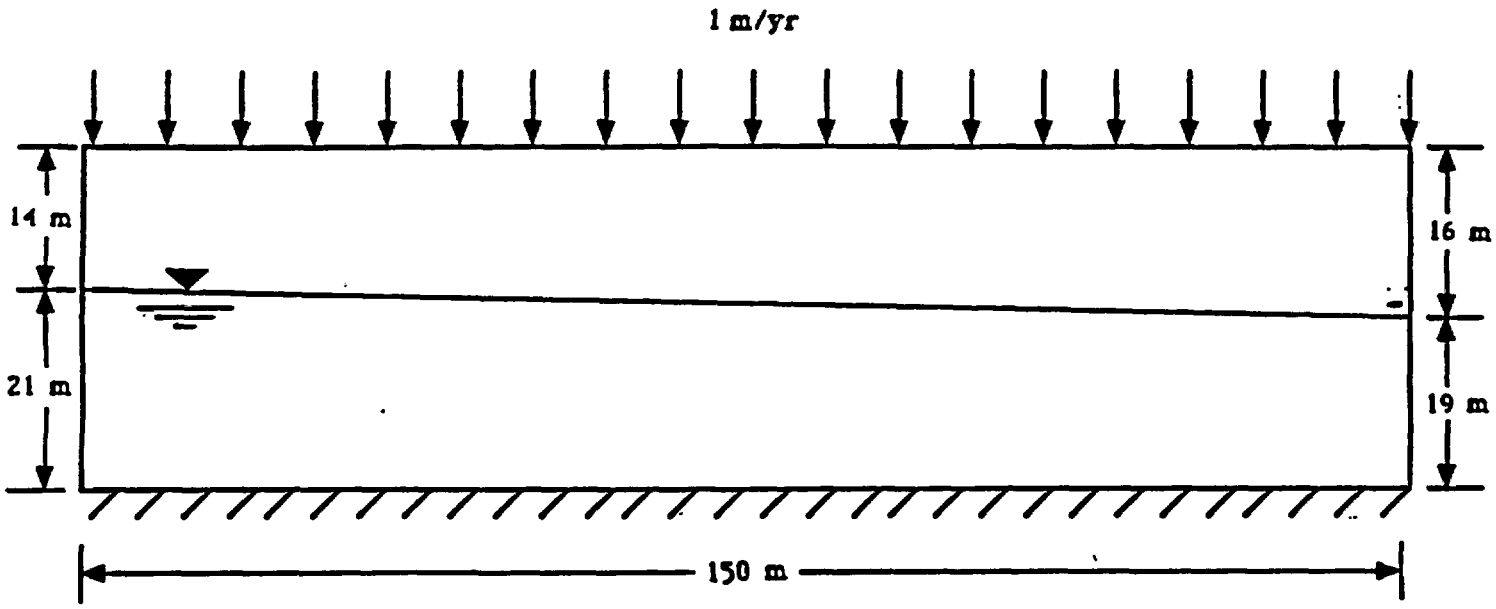

At the top boundary, infiltration was assumed to occur at a constant rate of 1 meter/year. The bottom boundary was assigned a no-flow boundary condition, as were the lateral boundaries of the model above the water table. Pressure heads were prescribed on both upstream and downstream parts of the saturated portion of the aquifer. When using *DCM3D*, either the thermodynamic pressure or the pressure head can be used (but not the total hydraulic head) as the dependent variable. This means that the lateral boundaries in the saturated region have to be assigned pressure heads that vary with elevation.

The initial conditions prescribed were inconsistent with the boundary conditions. The initial conditions were assigned as though there were a water table at a height of 18 meters. Pressure heads were assigned below 18 meters, according to the depth; and above 18 meters, a pressure head of -10 meters was assumed. However, because the problem had to be solved to a steady-state, the initial conditions were not so important.

This problem was solved by *DCM3D* and *PORFLO-3*, Version 1.0 (Runchal and Sagar, 1989; Sagar and Runchal, 1990), and results are compared below.

C-4.2. Comparison of Results

The *PORFLO-3* results for this problem were taken from the report by Magnuson *et al.* (1990) where these results were compared with those from *FEMWATER* (Yeh and Ward, 1979). In Figure C-3, steady-state pressure-head contours from *DCM3D* are plotted. *PORFLO-3* contours are not shown, as these are exactly the same as those for *DCM3D*, as shown in Figure C-3. Moisture-content profiles at a section 27.5 meters from the left boundary for *DCM3D*, and 30 meters for *PORFLO-3*, are compared in Figure C-4. The difference in locations of these sections is because of the two grid types used in the codes. *DCM3D* places the grid nodes in the middle of a cell, whereas *PORFLO-3* places the cell boundary in the middle of the grid nodes. Despite this difference, the moisture contents compare favorably.

To solve this problem, *DCM3D* used 3.1 CPU minutes on a VAX 8700 computer.

C-5. TEST PROBLEM NO. 3 (BENCHMARK): SIMULATION OF JORNADA TRENCH EXPERIMENT

The Jornada trench experiment is located northeast of Las Cruces, New Mexico, on the New Mexico State University College Ranch. Funded by NRC, this experiment is expressly designed for collected data that can be used in model validation. In the following example, simulation results are not compared with the measured data, but, rather with simulations by another code. Hence, even though the experimental conditions are used as the input data, this test is termed a benchmark (rather than a validation) exercise. A more detailed description of this experiment was provided in the CNWRA's *Quarterly Research Report* (see Sagar and Wittmeyer, 1991).

The Jornada test problem is conceptualized as a vertical 2D, multi-zone, unsaturated flow problem. Soil-hydraulic properties used in this test are based on those measured at the experimental site. This particular problem involves transient infiltration of water into an extremely dry, heterogeneous soil. Because of the initial dry conditions, the problem is highly nonlinear, and therefore is a good test for *DCM3D*.

C-5.1. Problem Description

The computational domain of this problem was divided into four zones, as shown in Figure C-5. A

Figure C-3. *DCM3D* Pressure-Head Contour for a Two-Dimensional, Saturated-Unsaturated Problem.

Figure C-3. DCM3D pressure-head contour for a two-dimensional, saturated-unsaturated problem (Test Problem 2)

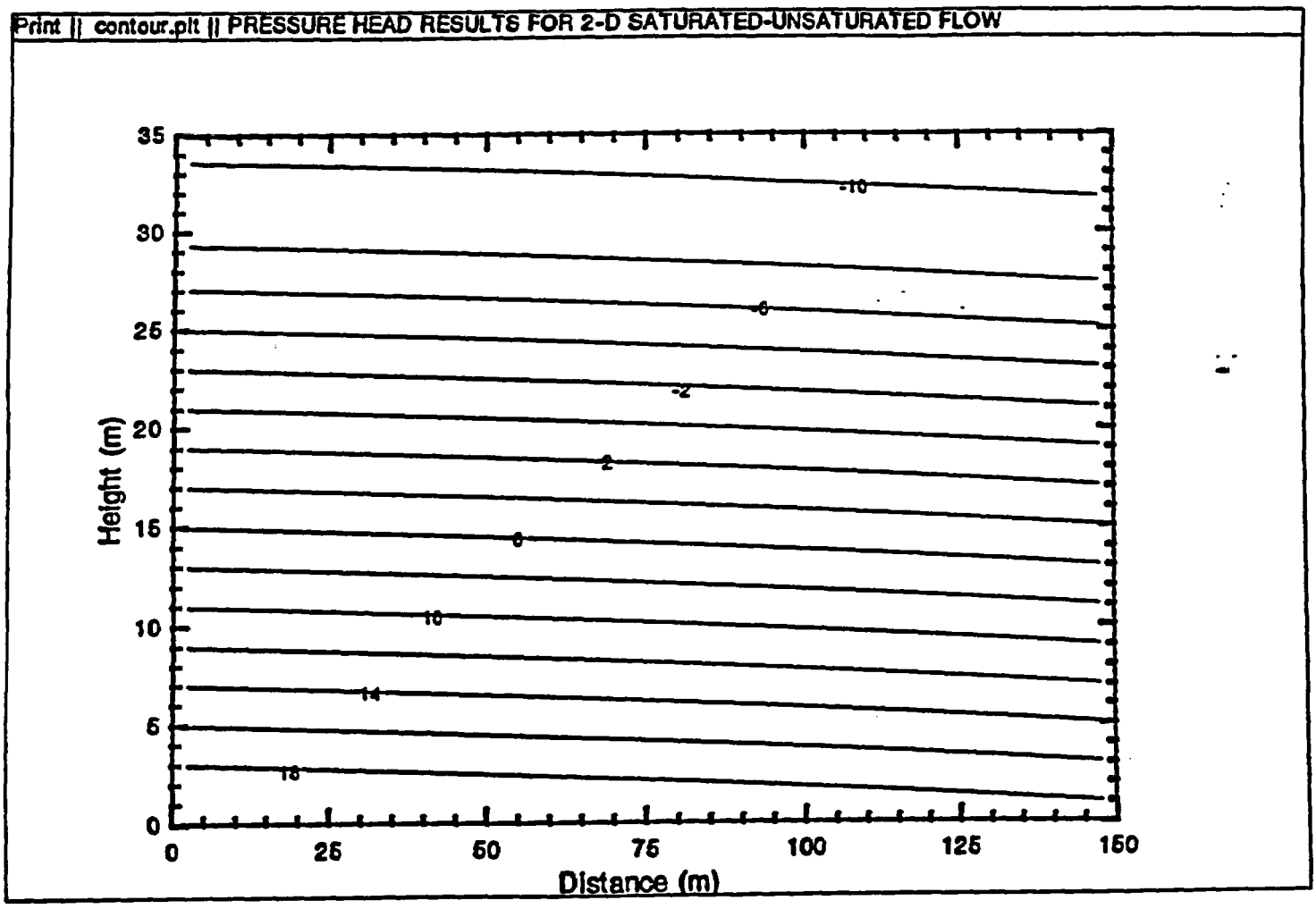

Figure C-4. Comparison of moisture contents from *DCM3D* and *PORFLO3*, for Test Problem No. 2.

Figure C-4. Comparison of moisture contents from DCM3D and PORFLO3 for Test Problem 2

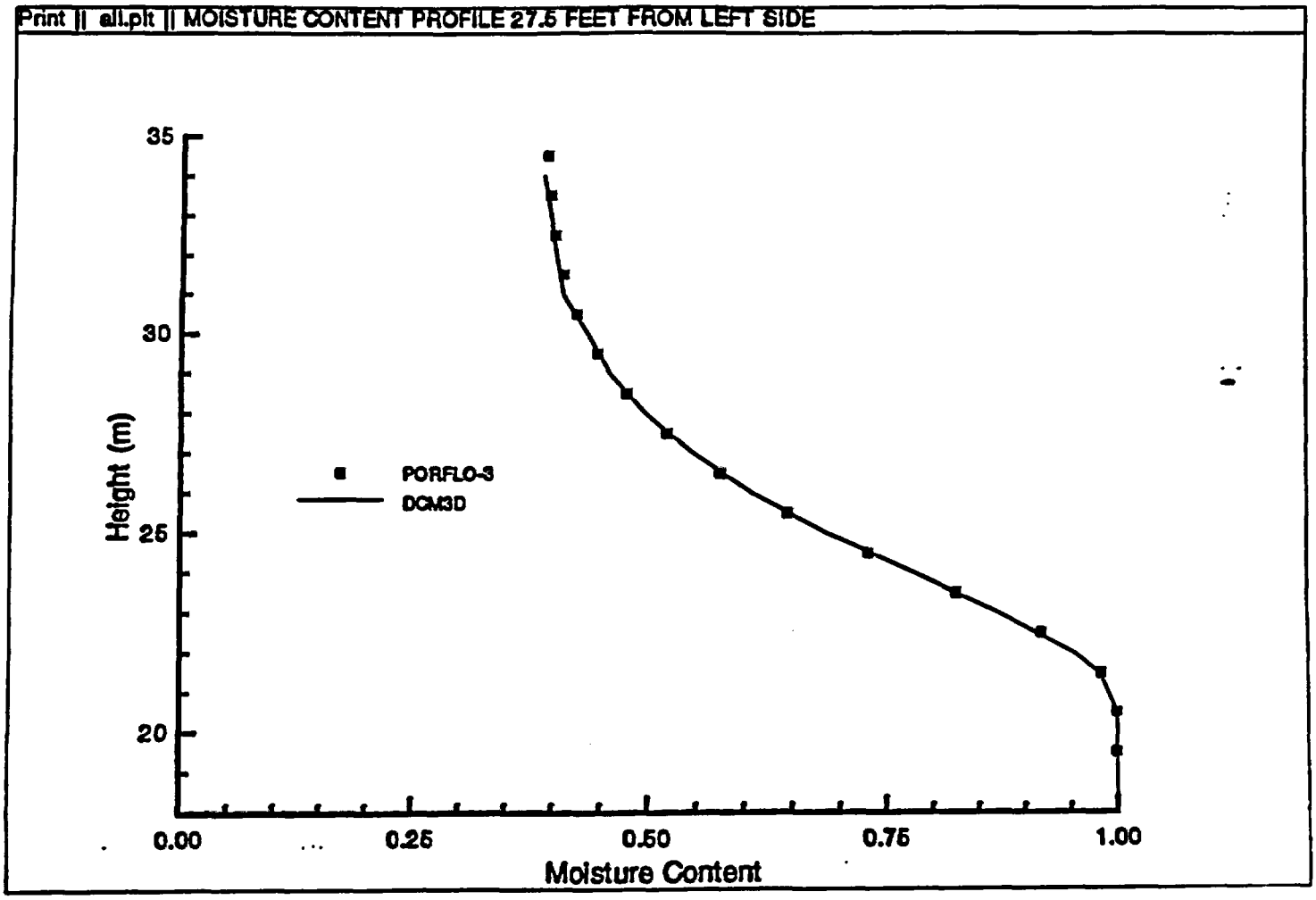

Figure C-5. Definition sketch for the Jornada Trench experiment (Test Problem No. 3).

Figure C-5. Definition sketch for the Jornada Trench experiment (Test Problem 3)

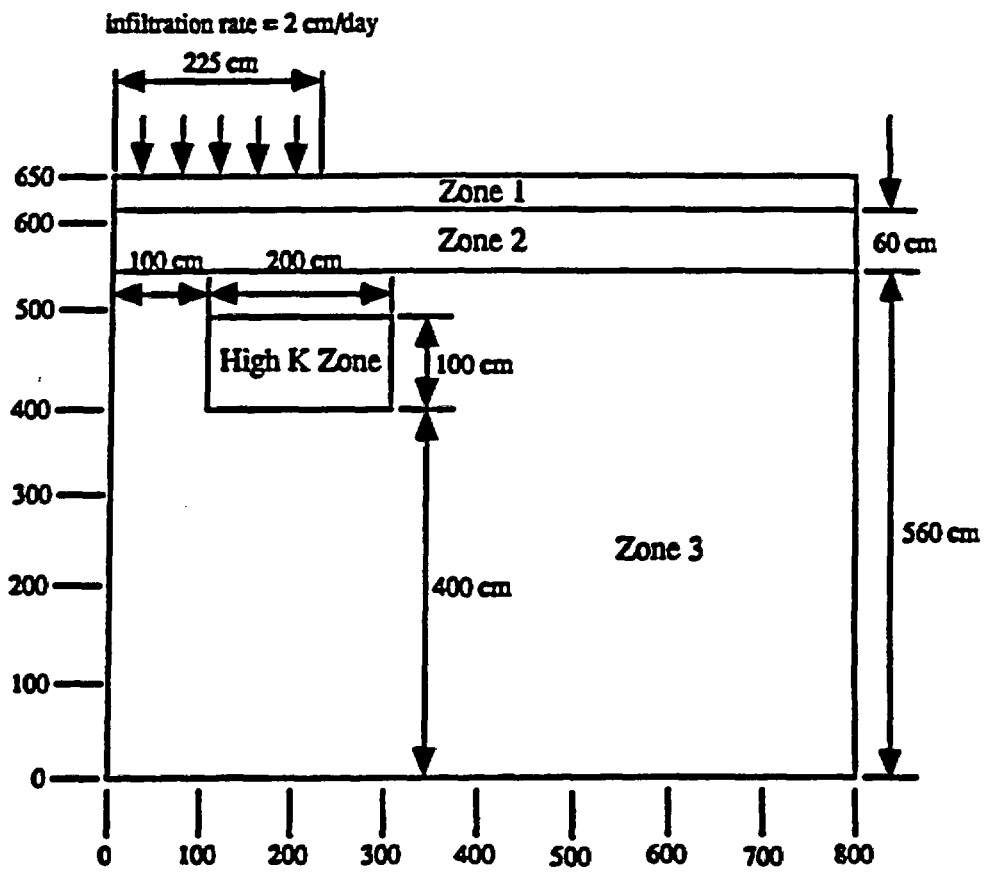

portion of the uppermost zone with a 225-centimeter width, measured from the top left hand corner of the domain of interest, was subjected to a water-infiltration rate of 2 centimeters/day (Figure C-5). The rest of the top surface was assumed to be impervious and was modeled as a no-flow boundary. In the experiment, the lateral boundary conditions were difficult to define, because the moisture content along the vertical boundaries would probably vary with time. For this test, the lateral boundaries were assumed to have zero flux crossing them. Such an assumption may cause errors (compared with the actually measured field conditions) unless the lateral boundaries are located at a great distance from the domain of interest. This problem with the lateral boundaries was not investigated further, because the interest here was to compare *DCM3D* results to results from another code. The bottom boundary was arbitrarily assumed to have zero flux. Again, it would probably be more accurate to either extend the domain to the water table, where a zero pressure-boundary condition can be assumed, or to impose a unit gradient (condition of gravity drainage). Using the first option would increase the domain size and consequently the computation time, whereas the second option is not available in *DCM3D*. Initially, the pressure head was assumed to be uniform throughout the entire domain at -734 centimeters.

The physical domain modeled was 800 centimeters by 650 centimeters. There were 56 nodes in the x-direction, and 47 nodes in the y-direction (total of 2632 nodes). From $x = 0$ centimeters to $x = 350$ centimeters, and $y = 350$ centimeters to $y = 650$ centimeters, grid spacing was 10 centimeters. From $x = 350$ centimeters to $x = 800$ centimeters, and from $y = 0$ centimeters to $y = 350$ centimeters, grid spacing was 25 centimeters.

The relationship of moisture content to pressure-head and the relationship of relative-permeability to moisture content are described by the van Genuchten (1980) equations as follows:

$$\theta = (\theta_s - \theta_r)\left(\frac{1}{1+(\alpha\Psi)^n}\right)^m + \theta_r \quad , \tag{C-5}$$

and

$$K_r = \sqrt{\theta_e}\left\{1-\left[1-(\theta_e)^{\frac{1}{m}}\right]^m\right\}^2 . \tag{C-6}$$

The variables are defined as follows:

θ	=	volumetric moisture content;
θ_r	=	residual moisture content;
θ_s	=	saturated moisture content;
Ψ	=	pressure head;
n	=	van Genuchten parameter;
m	=	van Genuchten parameter (= 1 - 1/n);
α	=	parameter;
K_r	=	relative hydraulic-conductivity.

The values of the input parameters for the four layers are given in Table C-1. The solver used was the *LSODES*, contained in *ODEPACK* (Hindmarsh, 1983). A relative convergence criterion of 1.0×10^{-5} and an absolute convergence criterion of 1.0×10^{-2} were imposed.

C-5.2. Comparison of Results

Again, *DCM3D* results were compared to *PORFLO-3* results taken from the report by Magnuson *et al.* (1990) in which *PORFLO-3* results were compared with the results from *FLASH* (Baca and Magnuson, 1992). Earlier, Smyth *et al.* (1989) used the same data for a test of *TRACER3D*, a code developed at Los Alamos Laboratories by Travis (1984).

The simulations were run in 30-day durations. The saturations at 30 days after the start of the moisture infiltration are shown in Figure C-6. The previous comparison of *PORFLO-3*, *FLASH*, and *TRACER3D* results are shown in Figure C-7. All four codes showed a pronounced effect of the high permeability zone on moisture distribution. For this complex problem, results of all the codes differed somewhat from each other. Figure C-7 indicates large differences between results (e.g. in advance of the wetting front) from *TRACER3D* and the other codes. The *DCM3D* results were reasonably close to those from *PORFLO-3* and *FLASH*.

DCM3D used 237 minutes of CPU time on a VAX 8700, while *PORFLO-3* used 5.95 minutes of INEL Cray CPU time. For the same problem, the CPU times for *TRACR3D* and *FLASH* were reported to be 5.79 Hanford CRAY minutes and 16.8 INEL CRAY minutes, respectively. Unfortunately, because of different computing environments, these execution times were not directly comparable.

C-6. TEST PROBLEM NO. 4: 2D FLOW THROUGH FRACTURED ROCK

The distinguishing feature of the *DCM3D* computer code is that it employs a dual-porosity conceptualization of the fractured porous medium, instead of an equivalent porous (single-porosity) medium or a fracture-network conceptualization. In the more common equivalent porous-medium approach, the characteristic curves for the rock matrix and the fractures are combined to form a composite characteristic curve. The composite curve assumes a rapid (with respect to the time scale of the flow being simulated) equilibration between the pressures of the fracture and matrix continua; and thus, the equilibration of pressure between the two continua is affected.

An important question is how different are the predicted flow fields for these two different conceptualizations. A convenient test case to explore this question was taken from the International Code Intercomparison study HYDROCOIN. The test case was based on a flow field associated with unsaturated-fractured tuff (Prindle, 1990). The HYDROCOIN test case was used here to examine the differences in the two conceptualizations, as well as to compare the *DCM3D* results with the HYDROCOIN results, to provide a measure of verification for *DCM3D*.

C-6.1. Problem Description

A complete description of the test case is provided in Prindle (1990). Only the information pertinent to the current simulations is provided here. The 2D cross-section was comprised of five layers, with a uniform dip of 6 degrees at unit interfaces (Figure C-8). Additionally, a repository location and a fault zone were defined for the test case. Material properties for the various layers were reproduced from the

Table C-1 Van Genuchten soil parameters

Zone	θ_s	θ_r	α (cm^{-1})	n	K_s
1	0.368	0.1020	0.0334	1.982	790.9
2	0.351	0.0985	0.0363	1.632	469.9
3	0.325	0.0859	0.0345	1.573	415.0
4	0.325	0.0859	0.0345	1.573	4150.0

Figure C-6. Comparison of *DCM3D* and *PORFLO-3* results (moisture contents) for the Jornada Trench experiment (Test Problem No. 3).

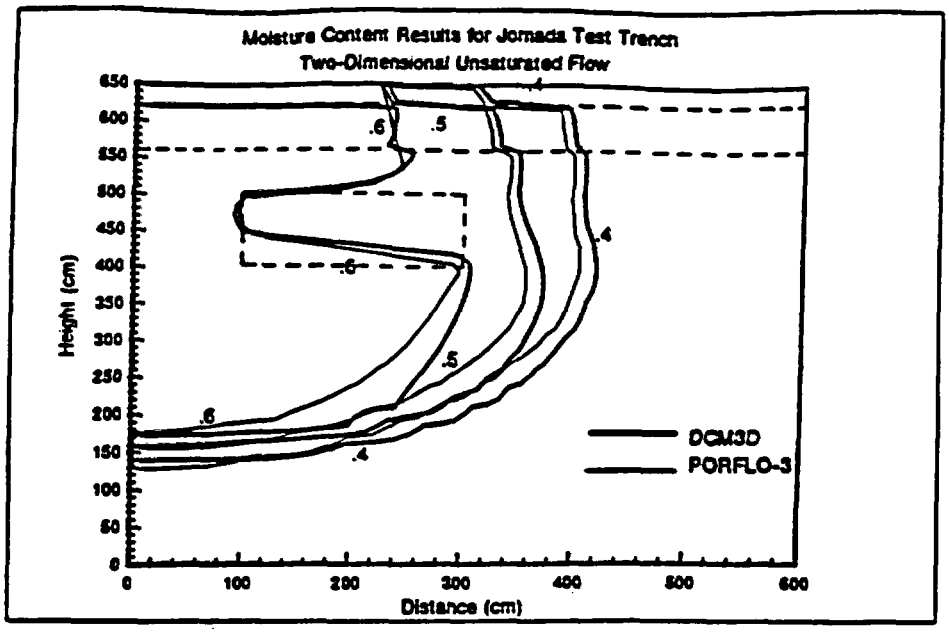

Figure C-6. Comparison of DCM3D and PORFLO-3 results (moisture contents) for the Jornada Trench experiment (Test Problem 3)

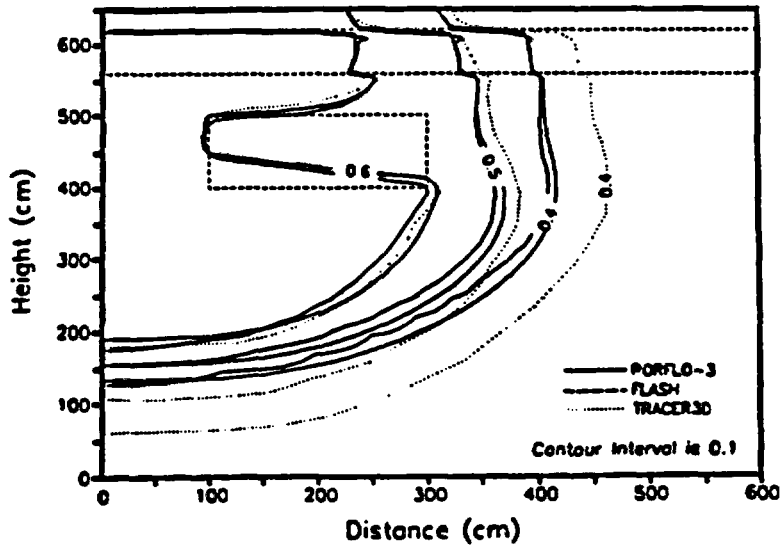

Figure C-7. Moisture content results for Test BT-2

Figure C-7. Moisture content results for Test BT-2.

Figure C-8. Two-dimensional base-case stratigraphy (see Table C-2 for coordinates of the numbered locations) (from Prindle, 1990).

Figure C-8. Two-dimensional base case stratigraphy (see Table 8-2 for coordinates of numbered locations) (Prindle, 1990)

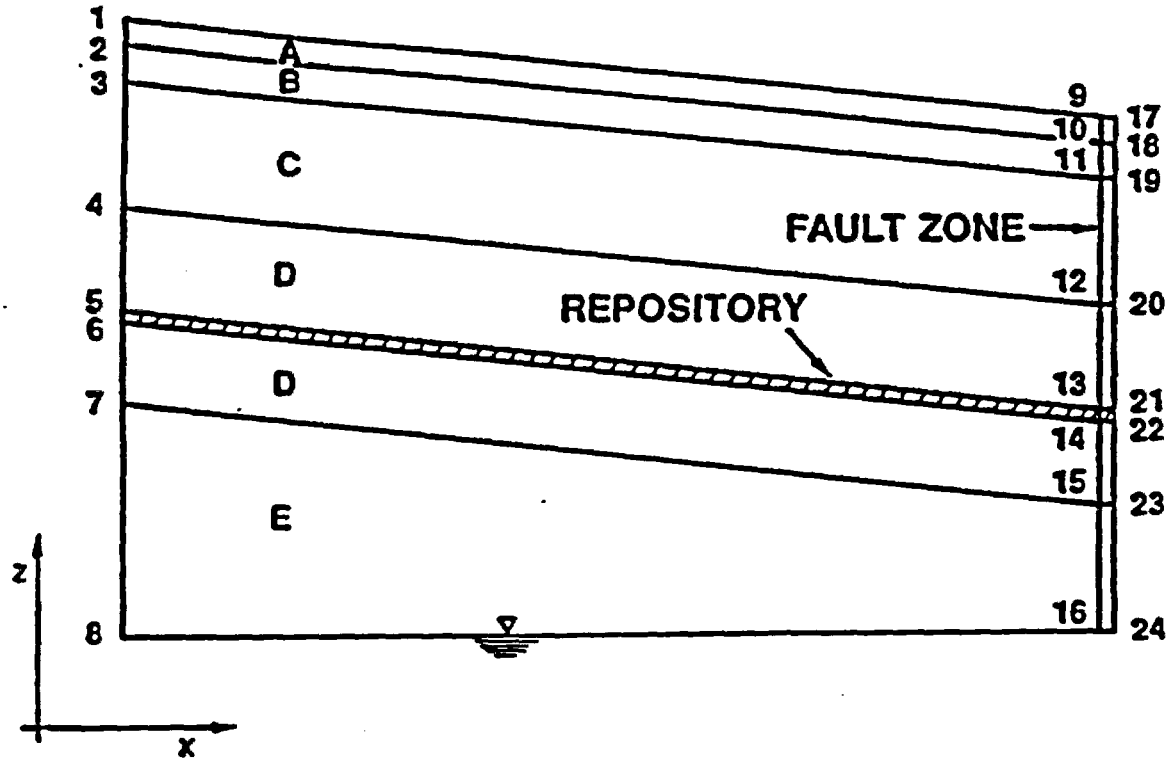

Table C-2

Coordinates of the numbered points in Figure C-7 (from Prindle, 1990).

Point	*Coordinates (meters)*		*Point*	*Coordinates (meters)*	
	x	*z*		*x*	*y*
1	0.0	635.5	13	1000.0	224.0
2	0.0	608.7	14	1000.0	219.5
3	0.0	570.6	15	1000.0	130.3
4	0.0	440.5	16	1000.0	0.0
5	0.0	329.1	17	1000.5	530.4
6	0.0	324.6	18	1000.5	503.6
7	0.0	235.4	19	1000.5	465.5
8	0.0	0.0	20	1000.5	335.4
9	1000.0	530.4	21	1000.5	224.0
10	1000.0	503.6	22	1000.5	219.5
11	1000.0	465.5	23	1000.5	130.3
12	1000.0	465.5	24	1000.5	0.0

Prindle report, in Table C-3.

The current simulations used modification 1, from the Prindle (1990) study. Modification 1 changed the original model description by not explicitly considering the fault zone and by modifying the rock properties, according to Table C-4. This modification was selected primarily because the beta parameter used for the van Genuchten equation was significantly lower (2.2 compared with 6.8) than the original value and was anticipated to lead to much shorter simulation times.

The finite difference grid for *DCM3D* was set up to provide the finest discretization in the vertical direction for the upper units (Table C-5) and a constant spacing in the horizontal direction. Rather than "stair-stepping" grid blocks at unit interfaces, the cross-sectional tilt was obtained by tilting gravity and increasing the depth to the water table by 100 meters (the depth to the water table was increased to decrease the affect of tilting the water-table boundary condition on the computational area of interest).

The tilting of gravity was considered to represent the problem description reasonably well, with the exception being near the side and bottom boundaries. Near the side boundaries, rather than a vertical boundary, the tilting of gravity causes the boundary to also appear slightly tilted. Near the bottom boundary, a significant flow is induced because of the tilting of gravity, which results in a gradient of 0.1. Despite these inaccuracies, the conceptualization was considered reasonable for examining flow diversion in the upper units (top 50 meters) and the spatial distribution of flow at the repository level (400 meters below the surface).

One additional parameter (the transfer term between matrix and fracture) was needed to perform the *DCM3D* simulations. The transfer term or factor, together with the gradient between the fracture and matrix controls the rate at which the fracture and matrix continua equilibrate. In the DCM3D *User's Manual* (Updegraff *et al.*, 1991), this parameter is defined by the following equation:

$$A = A_s \frac{k_s^m}{l} , \qquad \text{(C-7)}$$

where:

A	=	transfer factor;
k_s^m	=	matrix saturated permeability;
A_s	=	fracture specific surface area per unit volume; and
l	=	length parameter for gradient between fracture and matrix.

An attempt to determine the transfer factor in Equation (C-7), based on measurable quantities related to the fractures and matrix, was done by assuming that fractures were regularly spaced and planar and adopting a fracture-coating term. The fracture-coating term is used to represent a decrease (values less than 1) in transfer of water, resulting from a coating on the surface of the fracture, or an increase in transfer of water because of micro-fractures.

This conceptualization is represented by the following equation:

Table C-3

Base case material properties used for the hydrologic units, as depicted by letters in Figure C-7 (from Prindle, 1990).

Matrix Properties

Unit	*Porosity*	*Hydraulic Conductivity (meters/sec)*	*Residual Saturation*	*Van Genuchten Parameters*	
				Alpha (1/meter)	*Beta*
A	0.08 (.05 to .15)	9.7×10^{-12} (1×10^{-13} to 5×10^{-10})	0.002 (0. to .18)	.00821 (.003 to .024)	1.558 (1.3 to 2.4)
B	0.40 (.20 to .70)	3.9×10^{-7} (1×10^{-9} to 5×10^{-6})	0.100 (0. to .15)	.0015 (.001 to .031)	6.872 (1.2 to 15.)
C	0.11 (.05 to .20)	1.9×10^{-11} (1×10^{-13} to 5×10^{-10})	0.080 (0. to .23)	.00567 (.001 to .020)	1.798 (1.2 to 2.5)
D	0.11 (.05 to .20)	1.9×10^{-11} (1×10^{-13} to 5×10^{-9})	0.080 (0. to .32)	.00567 (.001 to .020)	1.798 (1.2 to 2.5)
Ev	0.46 (.30 to .55)	2.7×10^{-7} (1×10^{-13} to 5×10^{-6})	0.041 (0. to .25)	.0016 (.005 to .06)	3.872 (1.3 to 7.0)
Ez	0.26 (.20 to .45)	2.0×10^{-11} (1×10^{-14} to 5×10^{-10})	0.110 (0. to .30)	.00308 (.001 to .03)	1.602 (1.2 to 3.5)

Table C-3 (continued)

Individual Fracture Properties

Unit	*Fracture Aperture (Microns)*	*Fracture Hydraulic Conductivity (meters/s)*	*Fracture Density (No./meters^3)*	*Fracture Porosity*
A	6.74	3.8×10^{-5} (5×10^{-7} to 5×10^{-3})	20	1.4×10^{-4} (1×10^{-5} to .001)
B	27.0	6.1×10^{-4} (5×10^{-6} to 5×10^{-2})	1	2.7×10^{-5} (2×10^{-6} to 2×10^{-4})
C	5.13	2.2×10^{-5} (5×10^{-7} to 1×10^{-3})	8	4.1×10^{-5} (2×10^{-6} to 1×10^{-3})
D	4.55	1.7×10^{-5} (1×10^{-7} to 1×10^{-3})	40	1.8×10^{-4} (1×10^{-5} to 5×10^{-3})
Ev	15.5	2.0×10^{-4} (2×10^{-6} to 2×10^{-2})	3	4.6×10^{-5} (5×10^{-6} to 5×10^{-4})
Ez	15.5	2.0×10^{-4} (2×10^{-6} to 2×10^{-2})	3	4.6×10^{-5} (5×10^{-6} to 5×10^{-4})

Table C-3 (continued)

Bulk Fracture Properties

Unit	*Bulk Fracture Porosity*	*Hydraulic Conductivity (meters/sec)*	*Residual Saturation*	*van Genuchten Parameters*	
				Alpha(1/meter)	*Beta*
A	1.4×10^{-4} (1×10^{-5} to .001)	5.3×10^{-9} (5×10^{-12} to 5×10^{-6})	0.0395 (0. to .15)	1.285 (.2 to 6.0)	4.23 (1.2 to 7.0)
B	2.7×10^{-5} (2×10^{-6} to 2×10^{-4})	1.6×10^{-8} (1×10^{-11} to 1×10^{-5})	0.0395 (0. to .15)	1.285 (.2 to 6.0)	4.23 (1.2 to 7.0)
C	4.1×10^{-5} (2×10^{-6} to 1×10^{-3})	9.0×10^{-10} (1×10^{-12} to 1×10^{-6})	0.0395 (0. to .15)	1.285 (.2 to 6.0)	4.23 (1.2 to 7.0)
D	1.8×10^{-4} (1×10^{-5} to 5×10^{-3})	3.1×10^{-9} (1×10^{-12} to 1×10^{-6})	0.0395 (0. to .15)	1.285 (.2 to 6.0)	4.23 (1.2 to 7.0)
Ev	4.6×10^{-5} (5×10^{-6} to 5×10^{-4})	9.2×10^{-9} (1×10^{-11} to 1×10^{-5})	0.0395 (0. to .15)	1.285 (.2 to 6.0)	4.23 (1.2 to 7.0)
Ez	4.6×10^{-5} (5×10^{-6} to 5×10^{-4})	9.2×10^{-9} (1×10^{-11} to 1×10^{-5})	0.0395 (0. to .15)	1.285 (.2 to 6.0)	4.23 (1.2 to 7.0)

Table C-4 Material properties used in modification (from Prindle, 1990)

Property	*Unit B*	*Unit C*	*Unit D*
$K_{m,b}$	1.0×10^{-7}	8.0×10^{-11}	8.0×10^{-11}
α_m	0.010	0.015	0.015
β_m	2.2	1.6	1.6
$K_{f,b}$	3.6×10^{-6}	2.0×10^{-9}	3.1×10^{-9}
n_f	9.0×10^{-6}	9.0×10^{-5}	1.8×10^{-4}

Table C-5 *DCM3D* vertical discretization information. (Horizontal discretization is a constant spacing of 50 meters for 1000 meters.)

Finite Difference Row Indices	*Block Thickness (meters)*	*Depth (meters)*	*Unit*
1 - 35	10.0	705 - 400	Ez
36 - 55	10.0	400 - 200	D
56 - 60	10.0	200 - 150	C
61 - 63	8.0	150 - 126	C
64 - 65	6.0	126 - 114	C
66 - 67	4.0	114 - 106	C
68 - 70	2.0	106 - 100	C
71 - 100	1.0	100 - 70	C
101 - 140	1.0	70 - 30	B
141 - 170	1.0	30 - 0	A

$$A_r = 4\ C\ n^2\ (k_s^m)\ , \qquad \text{(C-8)}$$

where:

A_r	=	transfer factor, assuming regular-spaced planar fractures;
C	=	fracture-coating term;
n	=	number fractures per unit area; and
k_s^m	=	saturated permeability of the matrix.

Equation C-8, the parametric values presented in Table C-3, and a coating factor of 0.5 were used to determine the transfer terms (see Table C-6).

One objective of this analysis was to compare the results, assuming a composite curve, with those obtained by assuming a dual-continuum approach. It was considered advantageous to implement a composite curve approach within *DCM3D*, so as to use one input file for both conceptualizations. Modifications to *DCM3D* were made such that it would accept the composite characteristic curve as input.

C-6.2. Comparison of Results

Performance measures used for this analysis were: (1) particle paths starting along the upper boundary; and (2) the spatial distribution of water flux at the repository level. The HYDROCOIN results are taken from Prindle and are presented in Figures C-9 and C-10. These simulation results were obtained with the computer program called *NORIA* (Bixler, 1985).

Although CPU times for individual runs were not provided, Prindle reported that the 94 simulations required a combined 1300 hours of CPU time on a Cray X/MP 416.

The *DCM3D* results using the composite curve for representing the fracture/matrix continua are presented

Table C-6

Transfer factors used for the units identified in Figure C-7 and using Equation (C-8)

Unit	*Transfer Factor*
A	7.92×10^{-16}
B	2.04×10^{-14}
C	1.04×10^{-15}
D	2.61×10^{-14}
Ez	3.67×10^{-17}

Figure C-9. Particle paths based on the *NORIA* simulation (flux = 0.1 mm/yr) (from Prindle, 1990).

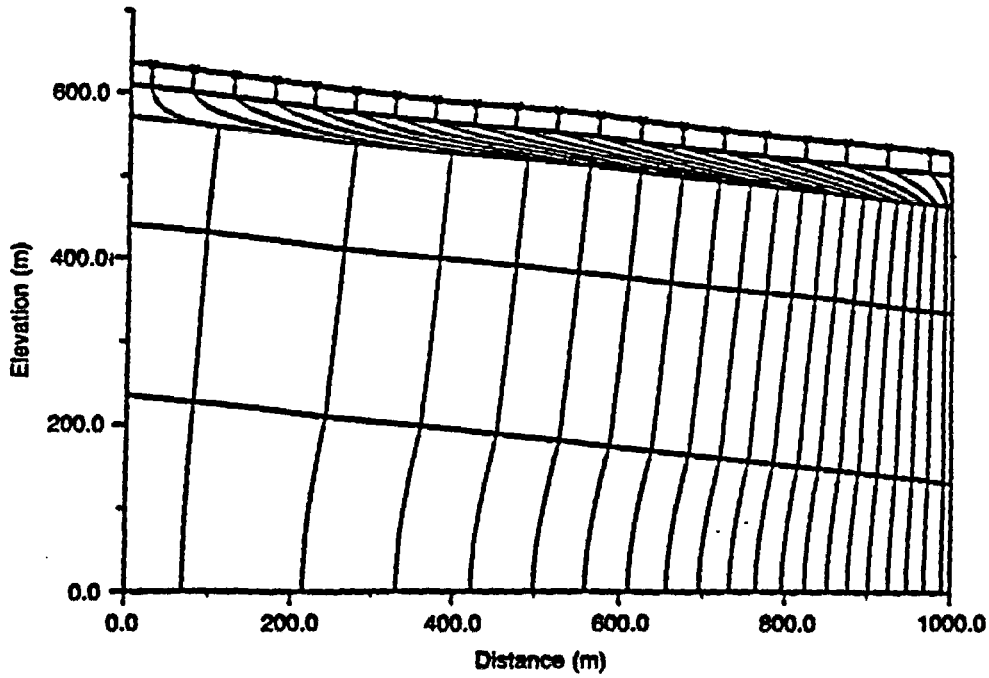
600.0
400.0
200.0
0.0
Elevation (m)
0.0
200.0
400.0
600.0
800.0
1000.0
Distance (m)

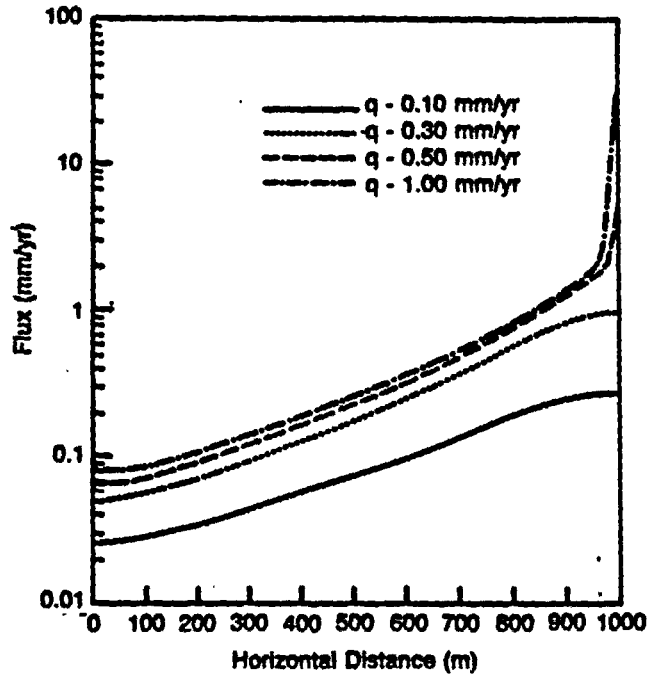
q - 0.10 mm/yr
q - 0.30 mm/yr
q - 0.50 mm/yr
q - 1.00 mm/yr
100
10
1
0.1
0.01
Flux (mm/yr)
0
100
200
300
400
500
600
700
800
900
1000
Horizontal Distance (m)

Figure C-10. Spatial distribution of flux at the repository, based on the *NORIA* simulation flux boundary condition values, as indicated by "*q*" (in the figure) (from Prindle, 1990).

in Figures C-11 and C-12. Ignoring some minor discrepancies due to boundary-condition differences, the results compare quite well with the *NORIA* results. This is not surprising because both programs utilize a composite curve conceptualization.

This simulation required approximately 50 minutes of CPU time on an IBM 3090 (for comparative purposes, the IBM is estimated to be 5 to 10 times slower than the Cray computer).

The *DCM3D* results using the dual-continuum approach are presented in Figures C-13, C-14, and C-15. As with the composite-curve results, the dual-continuum results compare reasonably well with the *NORIA* results. Although a somewhat significant discrepancy does exist near the bottom boundary, it can be attributed to the tilted bottom boundary and the fact that the simulation had not reached a steady state. *DCM3D* does not have a steady-state option, and the user is required to select a time sufficient to reach this point. For this simulation, a point in the middle of the domain rather than at the bottom boundary was used to determine steady-state conditions.

The fracture particle paths did not vary significantly from the matrix paths in the dual-continuum approach because of the isotropic conditions assumed for both matrix and fractures, the assumed connectivity of the fracture network, and the application of steady-state boundary conditions. Future work will consider anisotropic fracture conditions, high flux rates, and transient boundary conditions that could result in larger fracture flow (the current flux of 0.1 millimeters/year resulted in fracture flow at the repository level approximately 10 orders of magnitude lower than the matrix flow).

This simulation required approximately 8 hours of CPU time on the IBM 3090.

DCM3D results were generally in good agreement with the *NORIA* results. However, the dual-continuum versus the composite-curve approach needs to be examined further, to provide better insights into the differences in the models. Increased infiltration, anisotropic fracture properties, transient boundary conditions, and ranges of fracture-transfer terms should be used in future work. The current simulations, however, do provide a reasonable starting point for a departure into these more difficult simulations.

C-7. SUMMARY AND CONCLUSIONS

Four test problems of increasing complexity were solved, using the *DCM3D* computer code. In general, the code produced reasonable results for all of the four problems, indicating that the basic equations are correctly implemented in the computer code.

However, basic questions regarding the applicability of the dual-porosity approach for simulating partially saturated flow in fractured rock are not resolved by the testing discussed in this report. The main advantage of the dual-porosity approach is in its simplicity, obtained by lumping the fractures as a continuum superimposed over a matrix continuum. Thus, the geometric details of the fracture network need not be considered. Presumably, such an approach is capable of considering non-equilibrium pressure distribution between the fracture and rock continua. Conceptually, such a pressure non-equilibrium could occur when the flow field changes, for example during transient flow conditions, or at the interface between units with different fracture and matrix properties. This conceptual simplicity, however, introduces a parameter that represents, in a lumped fashion, the fluid interchange between the

Figure C-11. Particle paths, based on the *DCM3D* simulation, using a composite curve (flux = 0.1 mm/yr).

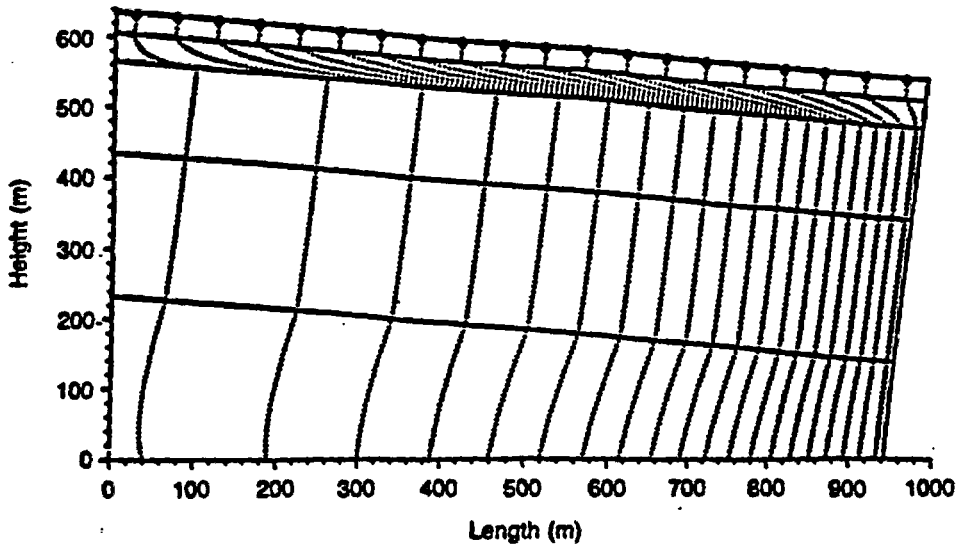
Height (m)
600
500
400
300
200
100
0
0
100
200
300
400
500
600
700
800
900
1000
Length (m)

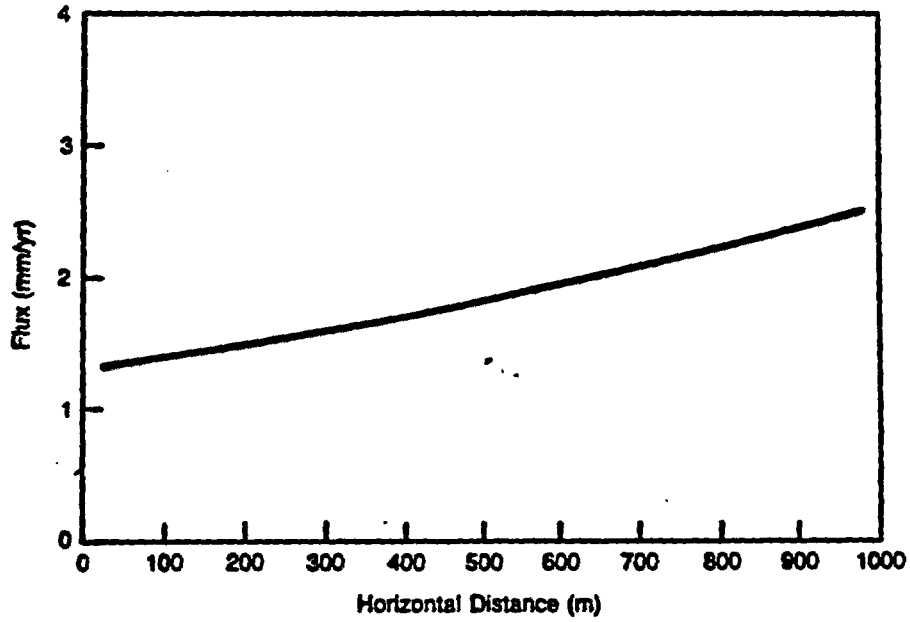
Flux (mm/yr)
4
3
2
1
0
0
100
200
300
400
500
600
700
800
900
1000
Horizontal Distance (m)

Figure C-12. Spatial distribution of flux, based on the *DCM3D* simulation, using the composite curves (flux = 0.1 mm/yr).

Figure C-13. Particle paths in the matrix, based on *DCM3D* simulations, using the dual-porosity model (flux = 0.1 mm/yr).

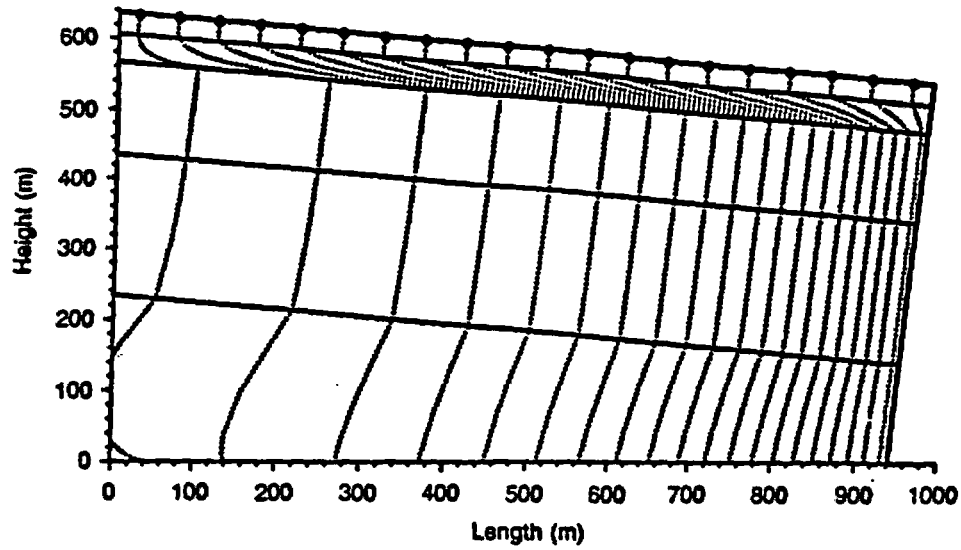
Height (m)
600
500
400
300
200
100
0
0
100
200
300
400
500
600
700
800
900
1000
Length (m)

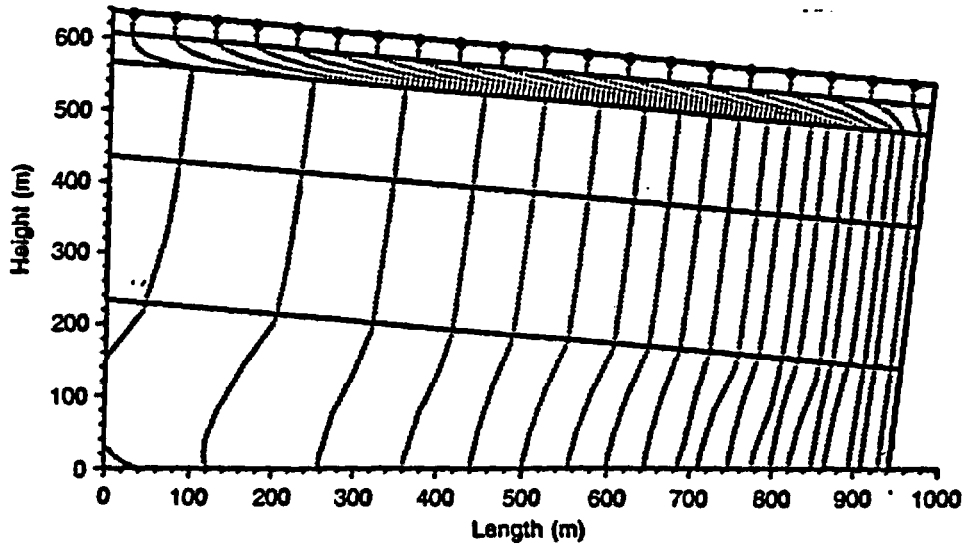
Height (m)
600
500
400
300
200
100
0
0
100
200
300
400
500
600
700
800
900
1000
Length (m)

Figure C-14. Particle paths in the fracture, based on *DCM3D* simulations, using the dual-porosity model (flux = 0.1 mm/yr).

Figure C-15. Spatial distribution of flux in the matrix, based on the *DCM3D* simulation, using the dual-porosity model (flux = 0.1 mm/yr).

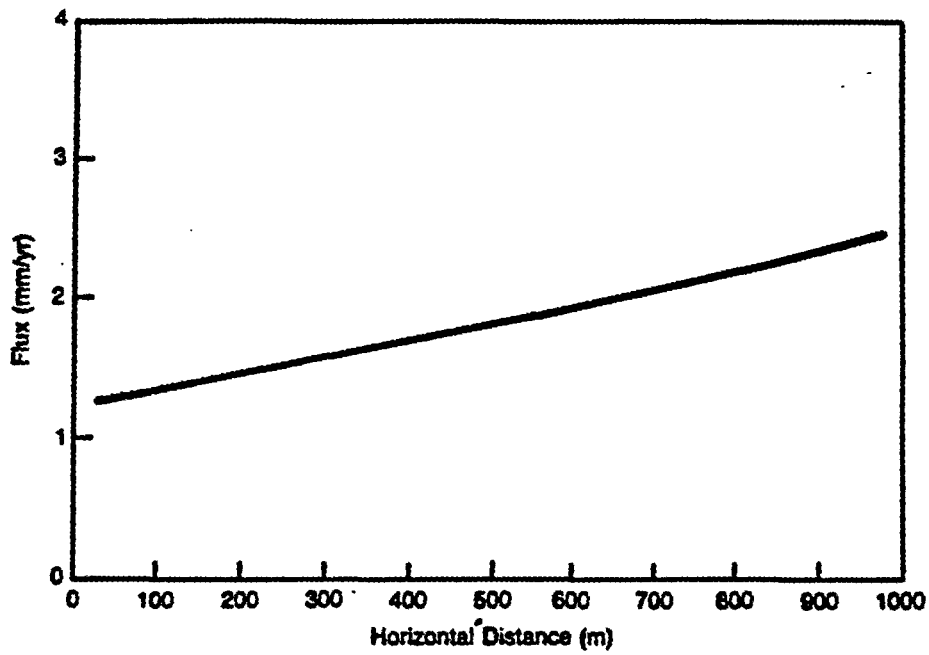
Flux (mm/yr)
0
1
2
3
4
0
100
200
300
400
500
600
700
800
900
1000
Horizontal Distance (m)

fracture and rock continua. The technical basis for this parameter (the transfer factor) and its relationship to measurable media properties need to be examined further. It should also be clear that the dual-porosity approach does not provide information on pressure distribution at the scale, for instance, of the fracture width. Again, this is because the fracture continuum has no definite location, but is continuously superimposed over the rock continua.

Similar problems are also attendant to other approaches to modeling partially saturated flow in fractured porous media. Use of a composite characteristic curve has the same disadvantage as the dual-porosity approach, in not distinguishing the distinct location and geometry of the fractures. In addition, this approach requires the assumption that locally (within a computational cell) the pressures in the fracture and the rock are instantaneously in equilibrium. However, computationally, the composite-curve approach is simpler and less time-consuming than the dual-porosity approach, because only a single governing equation needs to be solved. The fracture-network type of modeling requires not only detailed definition of the fracture topology, but also definition of its characteristic curves. Therefore, not only are the data needs multiplied, but the computation times become large. It may be that a mixed approach is appropriate, where the large faults that could control the flow system to a significant spatial scale (of the order of hundreds of meters) are represented as separate entities in the model, whereas the small fractures are dealt with as dual-porosity or composite curves.

As new users[1] of the *DCM3D* code, the IPA Phase 2 staff had difficulty in setting up the test problems. Some of the problems and recommendations are as follows:

- There is a need for experimental investigations of fracture-matrix interaction, to provide insight into applicability of the dual-porosity concept and the composite-curve approach.
- The idea of using an approach that combines features of the dual-porosity and fracture-network approaches should be investigated.
- The input structure, in general, is cumbersome; no comments are allowed, and the analyst has to input a great deal of inconsequential quantities. The input can certainly be improved to compress the input files and make these more readable.
- The options for the medium characteristic curves are too limited; at least one option allowing the input of a characteristic curve in a table format should be added.
- Only rectangular coordinates are allowed; it should be a relatively minor matter to add the cylindrical coordinates.
- Steady-state option is not available, and this problem cannot be easily fixed.

---

[1] The authors of this report often ran into trouble while setting up the test problems previously discussed. When called upon, Mr. C. David Updegraff, developer of the *DCM3D* computer code, was gracious in providing advice. His help is gratefully acknowledged.

- It would be worthwhile to examine what modifications are required to implement a steady-state option and to make the input more user-friendly.
- The manner in which the gravity is introduced in the model is confusing.
- The switch from thermodynamic pressure to pressure head is not straightforward; it essentially requires 'fooling' the code, and total hydraulic head can not be used as a dependent variable, at all.

C-8. REFERENCES

Ababou, R., "Approaches to Large Scale Unsaturated Flow in Heterogeneous, Stratified, and Fractured Geologic Media," Nuclear Regulatory Commission, NUREG/CR-5743, Month 1991. [Prepared by the Center for Nuclear Waste Regulatory Analyses.]

Baca, R.G. and S.O. Magnuson, "FLASH -- A Finite Element Computer Code for Variably Saturated Flow," EG&G Idaho, EGG-GEO-10274, 1992.

Bixler, N.E, "NORIA -- A Finite Element Computer Program for Analyzing Water, Vapor, and Energy Transport in Porous Media," Sandia National Laboratory, SAND84-2057, MONTH 1985.

El-Kadi, A. I, "INFIL," LOCATION, Holcomb Research Institute/International Groundwater Modeling Center, 1987.

Gureghian, A.B. and B. Sagar, "Evaluation of DCM3D -- A Dual Continuum, 3-D Groundwater Flow Code for Unsaturated, Fractured, Porous Media," in Patrick, W.C. (ed.), *Report on Research Activities for Calendar Year 1990*, Center for Nuclear Waste Regulatory Analyses, CNWRA 90-01A, 1991.

Haverkamp, R., M. Vanclin, J. Touma, P. J. Wierenga, and G. Vachaud, "A Comparison of Numerical Simulation Models for One-Dimensional Infiltration," *Soil Sci. Soc. Am. J.* 41:285-294 [1977].

Hindmarsh, 1983.

Huyakorn, P.S., J.B. Kool, and J.B. Robertson, "VAM2D -- Variably Saturated Analysis Model in Two Dimensions," Nuclear Regulatory Commission, NUREG/CR-5352, month 1989.

Magnuson, S.O., R.G. Baca, and A. Jeff Sondrup, "Independent Verification and Benchmark Testing of the PORFLO-3 Computer Code, Version 1.0," EG&G Idaho, EGG-BG-9175, 1990.

Philip, J.R, "Numerical Solution of Equations of the Diffusion Type with Diffusivity Concentration-Dependent II," *Australian Journal of Physics*, 10:29-42 [1957].

Prindle, R.W., and P. Hopkins, "On Conditions and Parameters Important to Model Sensitivity for Unsaturated Flow Through Layered Fractured Tough; Results of Analyses for HYDROCOIN Level 3, Case 2," Sandia National Laboratories, SAND89-0652, month 1990.

Runchal, A.K., and B. Sagar, "PORFLO-3: A Mathematical Model for Fluid Flow, Heat and Mass Transport in Variably Saturated Geologic Media -- User's Manual, Version 1.0," Richland, Washington, Westinghouse Hanford Company, WHC-EP-0041, 1989.

Sagar, B., and A.K. Runchal, "PORFLO-3: A Mathematical Model for Fluid Flow, Heat and Mass Transport in Variably Saturated Geologic Media -- Theory and Numerical Methods, Version 1.0," Richland, Washington, Westinghouse Hanford Company, WHC-EP-0042, 1990.

Sagar, B., and G. Wittmeyer, "Phase 2 Interval Project: Las Cruces Trench Solute Transport Modeling study, Plot 2, Experiment A," in Patrick, W.C. (ed.), *Report on the Research Activities for the Quarter January 1 Through March 31, 1991*, Center for Nuclear Waste Regulatory Analyses, CNWRA 91-01Q, MONTH 1991.

Smyth, J.D., S.B. Yabusaki, and G.W. Gee, "Infiltration Evaluation Methodology - Letter Report 3: Selected Tests of Infiltration Using Two-Dimensional Numerical Models," Richland, Washington, Pacific Northwest Laboratory, 1989.

Travis, B. J., "TRACER3D: A Model of Flow and Transport in Porous-Fractured Media," Los Alamos National Laboratories, LA-9667-MS, 1984.

Updegraff, C.D., C.E. Lee, and D.P. Gallegos, "DCM3D: A Dual-Continuum, Three-Dimensional, Ground-Water Flow Code for Unsaturated, Fractured, Porous Media," Nuclear Regulatory Commission, NUREG/CR-5536, MONTH 1991. [Prepared by ....]

van Genuchten, M.T., "A Closed-Form Equation for Predicting the Hydraulic Conductivity of Unsaturated Soils," *Soil Science*, 44:892-898 [1980].

Yeh, G.T., and D. S. Ward, "FEMWATER: A Finite-Element Model of Water Flow through Saturated-Unsaturated Porous Media," Oak Ridge, Tennessee, Oak Ridge National Laboratory, 1979.

APPENDIX D

CONTENTS

		Page
D.1	Introduction	D-1
D.2	Background/Definition of Issues	D-2
D.3	Conclusions and Recommendations	D-25
D.4	References	D-31

FIGURES

D-1	Nonlinear Isotherms	D-4
D-2	Flushing Solution Concentration Versus Cell Number, Flushing Solution Solute Preferentially Sorbed, Equal Starting Concentrations of Flushing Solution Solute, Competing Cation and Sorbing Site	D-7
D-3	K_d Versus Cell Number for Flow-Through Ion Exchange Simulation Illustrated in Figure D-2	D-8
D-4	Sorption Isotherm Calculated from Flow-Though Ion Exchange Simulation Illustrated in Figure D-3 Showing Favorable Characteristics	D-10
D-5	Flushing Solution Concentration Versus Cell Number, Flushing Solution Solute Preferentially Sorbed, Effect of Doubling Starting Concentration of Flushing Solution Solute Relative to Competing Cation and Sorbing Site Concentrations	D-11
D-6	K_d Versus Cell Number for Flow-Through Ion Exchange Simulation Illustrated in Figure D-5	D-12
D-7	Concentration of Competing Cation Versus Cell Number for Flow-Through Ion Exchange Simulation Illustrated in Figure D-5	D-13
D-8	Flushing Solution Concentration Versus Cell Number, Flushing Solution Solute Preferentially Desorbed, Equal Starting Concentrations of Flushing Solution Solute, Competing Cation and Sorbing Site	D-14
D-9	K_d Versus Cell Number for Flow-Through Ion Exchange Simulation Illustrated in Figure D-8	D-16
D-10	Sorption Isotherm Calculated from Flow-Though Ion Exchange Simulation Illustrated in Figure D-8 Showing Unfavorable Characteristics	D-17

D-11 Flushing Solution Concentration Versus Cell Number, Flushing Solution Solute Preferentially Sorbed, Effect of Increasing Sorbing Site Concentration Relative to Starting Concentrations of Flushing Solution Solute and Competing Cation D-18

D-12 K_d Versus Cell Number for Flow-Through Ion Exchange Simulation Illustrated in Figure D-11 . . . . . D-19

D-13 Sorption Isotherm Calculated from Flow-Though Ion Exchange Simulation Illustrated in Figure D-11 Showing Favorable Characteristics D-20

D-14 Flushing Solution Concentration Versus Cell Number, Flushing Solution Solute Preferentially Desorbed, Effect of Increasing Sorbing Site Concentration Relative to Starting Concentrations of Flushing Solution Solute and Competing Cation D-21

D-15 K_d Versus Cell Number for Flow-Through Ion Exchange Simulation Illustrated in Figure D-14 . . . . . D-22

D-16 Sorption Isotherm Calculated from Flow-Though Ion Exchange Simulation Illustrated in Figure D-14 Showing Unfavorable Characteristics D-23

D-17 Flushing Solution Concentration Versus Cell Number, Flushing Solution Solute Preferentially Sorbed, Trace Starting Concentration of Flushing Solution Solute, Relative to Competing Cation and Sorbing Site Concentrations D-24

D-18 K_d Versus Cell Number for Flow-Through Ion Exchange Simulation Illustrated in Figure D-17 . . . . . D-26

D-19 Sorption Isotherm Calculated from Flow-Though Ion Exchange Simulation Illustrated in Figure D-17 Showing Linear Behavior D-27

D-20 Flushing Solution Concentration Versus Cell Number, Flushing Solution Solute Preferentially Desorbed, Trace Starting Concentration of Flushing Solution Solute, Relative to Competing Cation and Sorbing Site Concentrations D-28

D-21 K_d Versus Cell Number for Flow-Through Ion Exchange Simulation Illustrated in Figure D-20 . . . . . D-29

D-22 Sorption Isotherm Calculated from Flow-Though Ion Exchange Simulation Illustrated in Figure D-20 Showing Linear Behavior D-30

APPENDIX D
K_d Approximation Testing
J.W. Bradbury/HLWM

D.1. INTRODUCTION

The most widely accepted conceptualization for the release of radionuclides from a geologic repository for high-level radioactive waste (HLW) to the accessible environment involves groundwater that flows through the repository, interacts with the radioactive waste, and carries the resulting dissolved and/or suspended contaminants to the accessible environment. In traveling along the path from the repository to the accessible environment, these radionuclides can interact with solids. These interactions can include precipitation/dissolution and sorption/desorption. This auxiliary analysis will focus on sorption/desorption reactions. When associated with the solid as results from sorption reactions, the radionuclide is immobile. The length of time the radionuclide is associated with the immobile solid phase versus the time the radionuclide spends in the flowing groundwater affects the rate of radionuclide migration. The more time spent on the solid, the more retarded is the movement of the radionuclide relative to the groundwater flow rate. The retardation of radionuclides by interactions with the geologic medium can limit the amount of radionuclides reaching the accessible environment in 10,000 years, as required by the Nuclear Regulatory Commission's regulation.[1]

Retardation is a process ascribed to dynamic systems. Chromatographic theory, however, states that, given certain assumptions, parameters measured in static systems can be used to calculate retardation in dynamic systems. Traditionally, static, batch experiments are performed in which groundwater containing a radionuclide is brought into contact with solids expected to occur along the flowpath to the accessible environment. The radionuclide partitions itself between solid and liquid phases. After the experiment, the concentrations of radionuclide on the solid and in the liquid are measured. When sorption/desorption are the processes controlling radionuclide/solid interactions, the ratio of radionuclide concentration on the solid to that in the liquid is called the sorption coefficient, or K_d, and normally has units of Ml/g. The relationship of K_d to retardation is:

$$R_f = 1 + \rho\frac{K_d}{\theta}, \qquad \text{(D-1)}$$

where ρ is the bulk density, θ is the porosity, and R_f is the retardation factor, which is defined as the ratio of the velocity of the groundwater to that of the radionuclide. Freeze and Cherry (1979, p. 404) state that Equation (D-1) is valid when:

- The sorption reaction is fast and reversible; and

[1] The Energy Policy Act of 1992 (Public Law 102-486), dated October 24, 1992, directs the Nuclear Regulatory Commission to promulgate a rule, modifying 10 CFR Part 60 of its regulations, so that these regulations are consistent with EPA's public health and safety standards for protection of the public, from releases to the accessible environment, from radioactive materials stored or disposed of at Yucca Mountain, Nevada, consistent with the findings and recommendations made by the National Academy of Sciences, to EPA, on issues relating to the environmental standards governing the Yucca Mountain repository.

- The sorption isotherm is linear.

A sorption isotherm is the locus of points describing the concentration of radionuclide on the solid as a function of its concentration in the liquid. When the isotherm is linear, K_d is constant (i.e., independent of radionuclide concentration in the liquid.)

D.2. BACKGROUND/DEFINITION OF ISSUES

The Total-System Performance Assessment (TPA) computer code of the present NRC performance assessment effort uses the K_d approach in estimating retardation of radionuclides. The sources of the values of K_d used in the TPA computer code are Meijer (1990) and Thomas (1987). These K_ds are based on batch sorption tests, supported in some cases by corresponding flow-through column experiments performed by investigators from Los Alamos. The batch sorption tests use site-specific groundwater to which radionuclides have been added, and crushed solids expected to occur along the flowpath from the repository to the accessible environment.

In a system as complex as Yucca Mountain, it remains to be demonstrated that simplifications such as the K_d approach in estimating retardation are valid. This auxiliary analysis tests the requirement that the sorption isotherm needs to be linear to make Equation (D-1) valid. The method involves modeling sorption reactions in a one-dimensional flowing system. Two specific sorption reactions are ion exchange and surface complexation. This modeling exercise simulates ion exchange involving sodium and potassium. The reaction considered is:

$$K^+ + NaX = KX + Na^+, \qquad \text{(D-2)}$$

where X is the sorbing site on the solid. This simple system was chosen as a first attempt to investigate the affects of ion exchange on solute migration. Lacking thermodynamic data on site-specific components, this simple system can be viewed as an analog for the radionuclide-tuff reactions at Yucca Mountain. The computer code capable of simulating these processes is *PHREEQM*, for use in mixing cell flowtube simulations described by Appelo and Willemsen (1987). This code, an adaptation of *PHREEQE* (Parkhurst *et al.*, 1990) can simulate speciation and mass-transfer processes, including precipitation, and dissolution, plus it can simulate ion exchange reactions, one-dimensional flow and transport, diffusion, and dispersion in a porous media. The reaction written above describes the situation where a solution containing potassium flows through a porous medium initially loaded with sodium. The potassium dissolved in the aqueous phase displaces sodium on the solid and this solute-solid interaction retards the movement of potassium down the column relative to that of water. One could also imagine that the potassium represents a radionuclide and X represents sorbing site on the tuff.

Investigators involved in the Yucca Mountain geochemical program perform batch sorption tests to determine an isotherm. If the isotherm is linear, a retardation factor is calculated. Sometimes, additional characterization may be performed to establish the actual mechanism responsible for the sorption. In this auxiliary analysis, however, the sorption mechanism is already known. Simulation of a flow-through experiment produces elution curves that are retarded relative to the flow of water. Thus, retardation factors can be determined. Finally, K_d values and sorption isotherms can be generated by characterizing the partitioning of the sorbing species for all points along the column at

all times.

The mass-action equation corresponding to Equation (D-2) is:

$$K = \frac{[KX][Na^+]}{[K^+][NaX]}, \tag{D-3}$$

where K is the equilibrium constant for the reaction and brackets represent activities. For this reaction, K is 5 (an arbitrary value in the database used by *PHREEQM*). For this study, accurate values for thermodynamic constants for specific reactions are not required, as only general relationships among parameters and their effects on solute migration are investigated. In comparison, the exchange constant for the K^+ - Na^+ ion-exchange reaction involving clinoptilolite is 17.2 (Pabalan, 1991). If the reverse of Equation (D-2) is considered,

$$Na^+ + KX = K^+ + NaX, \tag{D-4}$$

where the equilibrium constant is 1/5.

Vermeulen *et al.* (1987) subdivide sorption reactions into various types, depending on the shape of the isotherm. Isotherms that are convex up are termed favorable (e.g., Figure D-1a) and those that are concave up are termed unfavorable (e.g., Figure D-1b). The terms favorable and unfavorable refer to the ability of a chromatographic process to separate species that are variably sorbed. A favorable sorption reaction would result in elution curves with constant-shaped fronts. These are also termed self-sharpening fronts. An unfavorable sorption reaction would result in elution curves with changing or spreading fronts. For an ion-exchange process, if the equilibrium constant is greater than 1, sorption processes favorable for chromatographic separation are present. If the equilibrium constant is less than 1, unfavorable conditions are present.

Some of the sorption isotherms using site-specific materials from Yucca Mountain are nonlinear (DOE, 1988, pp. 4-81 - 4-82). These isotherms have been fitted using a Freundlich formulation:

$$C_s = KC_l^n, \tag{D-5}$$

where C_s and C_l are concentrations on the solid and in the liquid, respectively, and K and n are empirical constants. When n is greater than 1, the isotherm is concave up, and when it is less than 1, it is convex up. For plutonium, n is 0.84 to 0.88, when YM-22 (welded tuff) is the solid substrate and 0.96 to 1.0, when YM-49 (partially zeolitized and vitric sample) is the solid. For strontium, cesium, barium, and europium, n ranges from 0.71 to 0.92, when the solid substrate is YM-22 (DOE, 1988. pp. 4-82). The isotherm for these elements is linear when the solid is zeolitized.

By simulating flow-through experiments involving ion exchange represented by Equations (D-2) and (D-4), both favorable and unfavorable elutions are modeled. The significance of these types of elutions to performance assessment can then be better appreciated.

Figure D-1. Nonlinear isotherms. (1a) Favorable isotherm; (1b) Unfavorable isotherm.

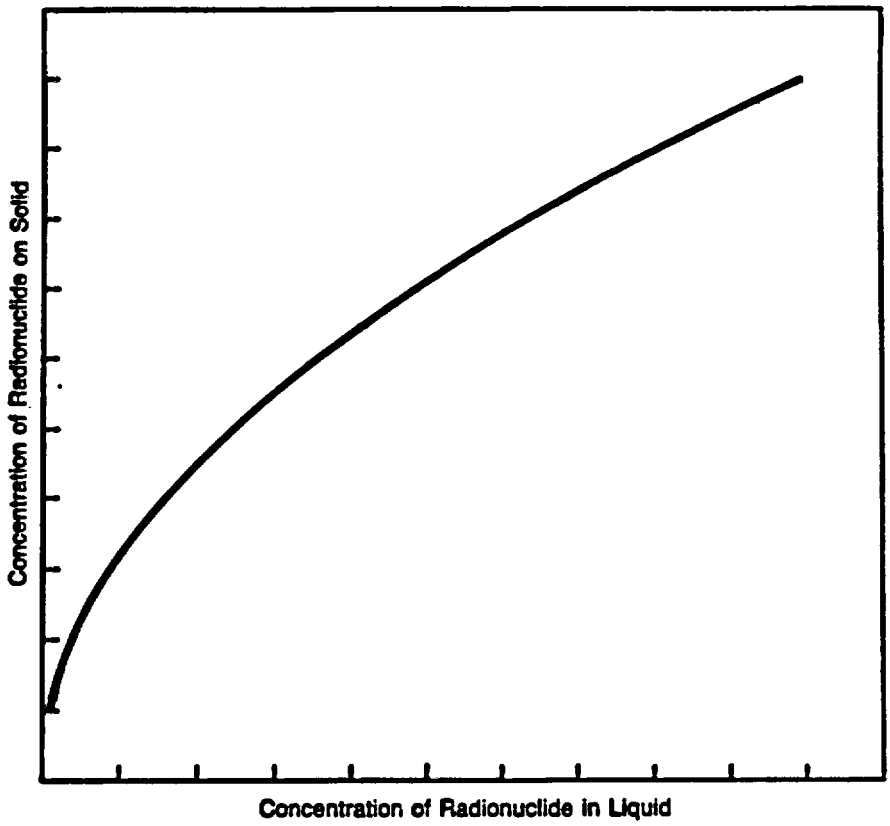
Concentration of Radionuclide on Solid
Concentration of Radionuclide in Liquid

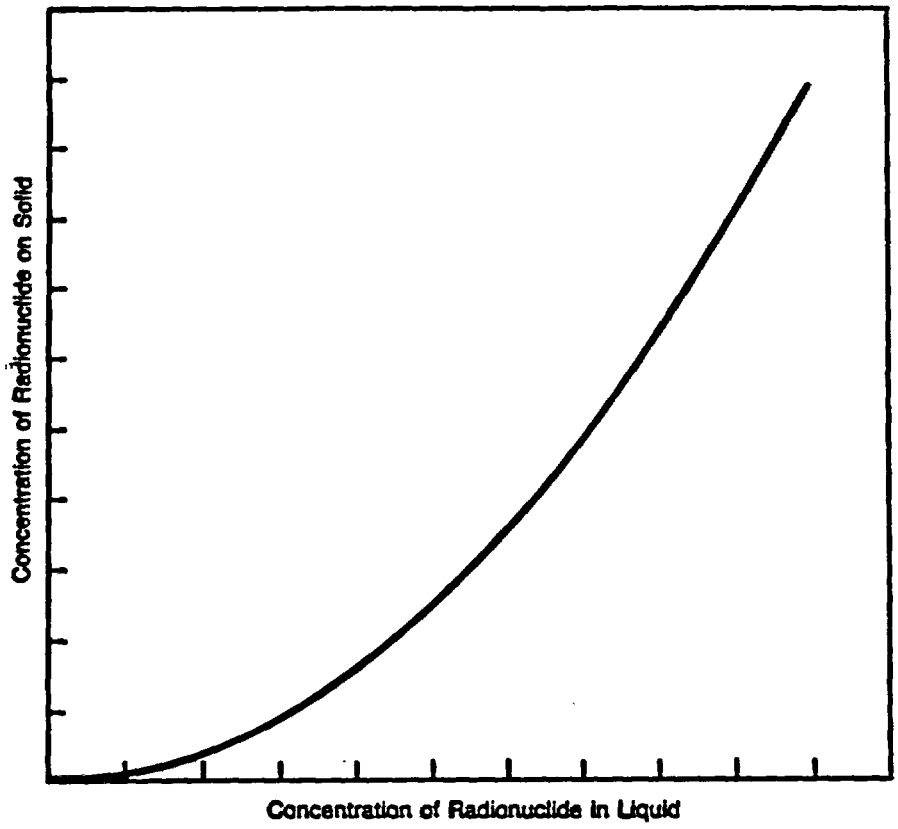
Concentration of Radionuclide on Solid
Concentration of Radionuclide in Liquid

Simulations

Conceptually, the column is divided into cells. Initially, the chemical constituents in each cell are reacted to equilibrium. The possible reactions include precipitation, dissolution, speciation, and ion exchange. Mixing is then simulated between adjacent cells. The mixing can be caused by both dispersion and diffusion. However, in the present study, it was decided arbitrarily that only dispersion be included in the simulation. Following mixing, the solutions in each cell are moved to the next cell downstream and re-equilibrated. The solution added to the column is called the flushing solution. Its composition remains constant throughout the simulation. Before adding the flushing solution, the compositions of both liquid and solid in the column are defined. The parameters that are varied in this study are the relative concentrations of competing species, and concentration of the sorbing site or complex, X^-.

The capability of a solid to sorb is commonly described in terms of cation-exchange capacity. The code, however, uses the concentration of the sorbing site, X^- (meq/L), which is related to the cation-exchange capacity by the relation:

$$X^-(meq/L) = \frac{CEC \times 1000}{100 \times \frac{\theta}{\rho}} , \qquad \text{(D-6)}$$

where *CEC* is the cation exchange capacity in meq per 100 grams soil, θ is the porosity, and ρ is the bulk density of the soil in kg/L.

Porosity is an input in the simulation and must remain constant along the length of the column, to maintain the constancy of masses of solution moving from cell to cell. The simulations involve only saturated hydrologic conditions. Porosity in these simulations has been set at 0.3, which lies within the range of porosities found at Yucca Mountain (see DOE, 1988, p. 3-192).

In the *PHREEQM* code, mixing between adjacent cells is calculated using the relation:

$$f = \frac{DISP(i) + DISP(i+1)}{L(i) + L(i+1)} + 4 \times DM \times \frac{DELTAT}{(L(i) + L(i+1))^2} , \qquad \text{(D-7)}$$

where f is the mixing factor, *DISP* is the dispersivity in meters, L is the length of the cell in meters, i represents the cell number, *DM* is the diffusivity in meters^2/second, *DELTAT* is the time for diffusion in seconds. The mixing factor is the percentage of a cell's dissolved contents that is transferred to an adjacent cell. Both upstream and downstream adjacent cells are involved in the mixing process. The code restricts $f < 0.33$ so that at least one-third of the original contents of a cell remain after a mixing simulation. All the factors on the right side of Equation (D-7) are inputs to the code. For this study, no diffusion is simulated, so the second term on the right side of Equation (D-7) is zero, and only the dispersion component of spreading is considered. All the simulations in this study have the same dispersivity.

The first simulation involves the elution of potassium through a column initially saturated with sodium. The initial concentrations are 1 meq/L of X^- and 1 meq/L of Na^+ on the solid, and 1 meq/L of Na^+ in the liquid in the column. A nonsorbing anion, NO_3^-, balances the charge in the liquid initially filling the column. The flushing solution contains 1 meq/L K^+ charge balanced by a nonsorbing anion. The column contains 20 cells. Figure D-2 illustrates the concentration of K^+ in the liquid phase along the column, for different amounts of flushing solution added. The flushing solution is added to the column at cell 1 and leaves the column after cell 20. The numbers associated with each concentration curve refer to the cell volumes of flushing solution added to the column, labelled "shifts" in the figure. Note that the flushing solution concentration curve or front corresponding to various shifts is of constant shape. The rounding of the front is due to dispersion modeled in this simulation. Each cell is 1-centimeter long and has an associated dispersivity of 2 mm (thus, f = 0.2). Apparently, this amount of dispersion does not affect the shape of the front as it migrates down the 20-centimeter column (i.e., the front does not spread with distance traveled). By defining only the porosity of the cells, only relative volumes of liquid to solid are fixed. Thus, actual amounts of flushing solution are not determined.

Figure D-2 can be used to determine the retardation factor for this simulation. One method for determining the retardation factor is to integrate under the concentration-cell number curve for a given number of shifts. The integration produces the total mass of K^+ in the aqueous phase. By dividing the total mass of K^+ added to the column for a given number of shifts by the total mass of K^+ in the aqueous phase, the retardation factor is obtained. This operation is comparable to converting the spreading front of the elution curve into a square front. For symmetrical fronts, another method for determining the retardation factor is to measure the distance K^+ travels down the column at the half height of its initial concentration. This point represents the center of mass of the migrating front. Note that at 20 shifts, the half height of the K^+ concentration (0.5 meq/L) is in cell 10. Thus, at this point the water has traveled all the way through the column, but K^+ has traveled only half the distance. Consequently, the retardation factor, R_f, is 2. From Equation (D-1), if ρ is assumed to be 2.5, the K_d is 0.12.

Each cell can be considered as a separate batch sorption test. The code calculates the partitioning of the ions between solid and liquid. Thus, it is possible to determine a K_d for K^+ for each cell and each shift. Figure D-3 is a plot of K_d versus cell number for various shifts. The K_d values range from 0.6 to 0.12 and are not constant for a particular cell (space), but change with the number of shifts (time). For example, cell 6 has a K_d of 0.6 at 4 shifts and 0.12 at 15 shifts. It should be noted that K^+ has reached cell 6 after only four shifts because of the dispersion where 20 percent of the dissolved contents of each cell is moved downstream per shift. Combined with information from Figure D-2, it is apparent that higher concentrations of K^+ in a particular cell correspond to the lower K_d value and vice versa. This observation provides an explanation for constant shape of the elution curve. Low concentrations lead high concentrations down the column. However, low concentrations correspond to high K_d values and so are slowed more than the high concentrations. The result is a front that maintains its steep concentration gradient.

The fact that this simulation produced a range of K_d values for particular cells raises an important issue, namely, what K_d value should be assigned to each cell? It is clear in this simulation that the appropriate K_d for use in Equation D-1 to determine retardation corresponds to the one measured at the highest flushing solution concentration. But, what if, as in the case of many of the radionuclides

Figure D-2. Flushing solution concentration versus cell number, flushing solution solute preferentially sorbed, equal starting concentrations of flushing solution solute, competing cation and sorbing site.

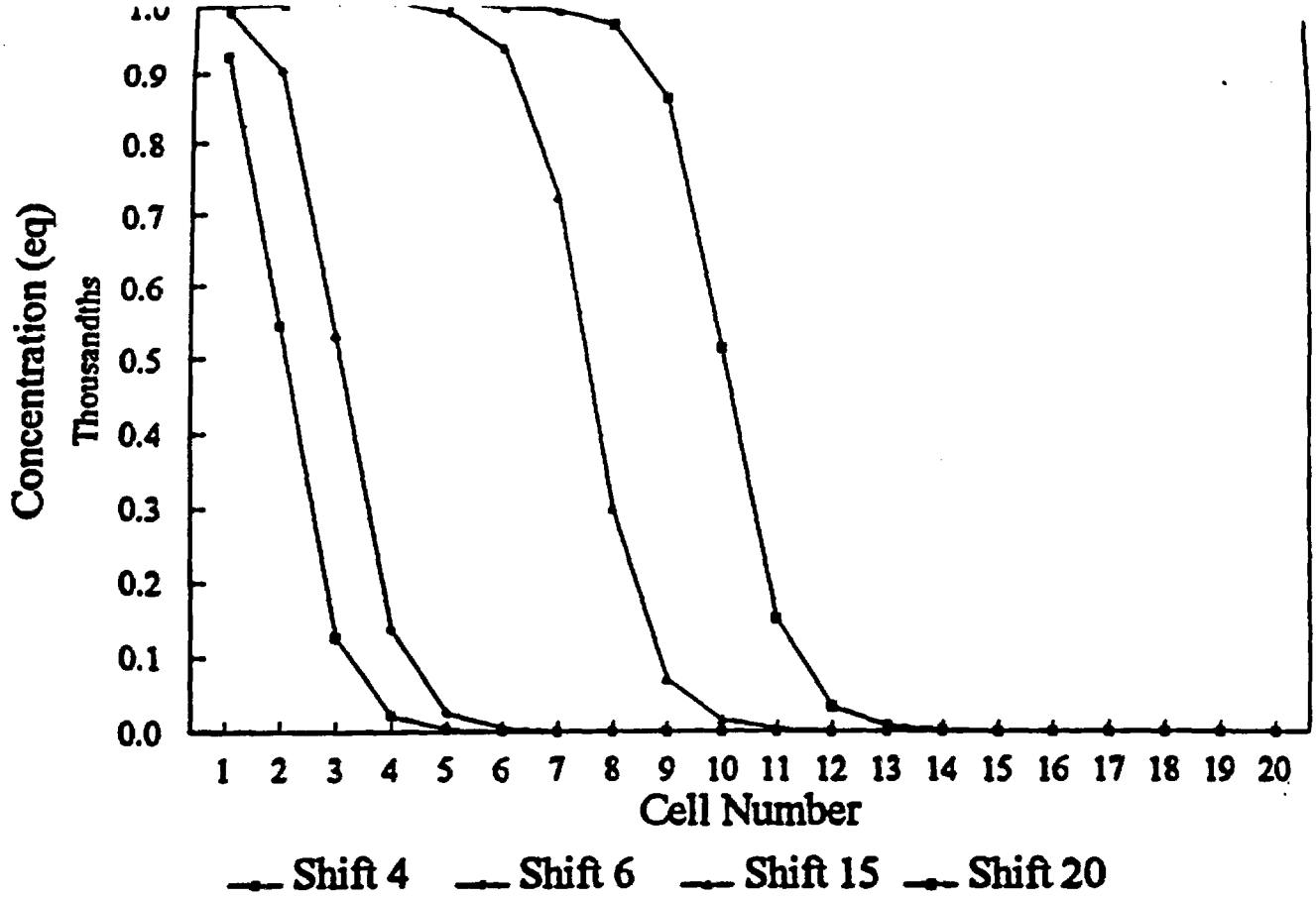

Column: solid, 1 meq/l X- 1 meq/l Na+; liquid, 1meq/l Na+
Flushing solution: 1meq/l K+

D2

Figure D-3. K_d versus cell number for flow-through ion exchange simulation illustrated in Figure D-2.

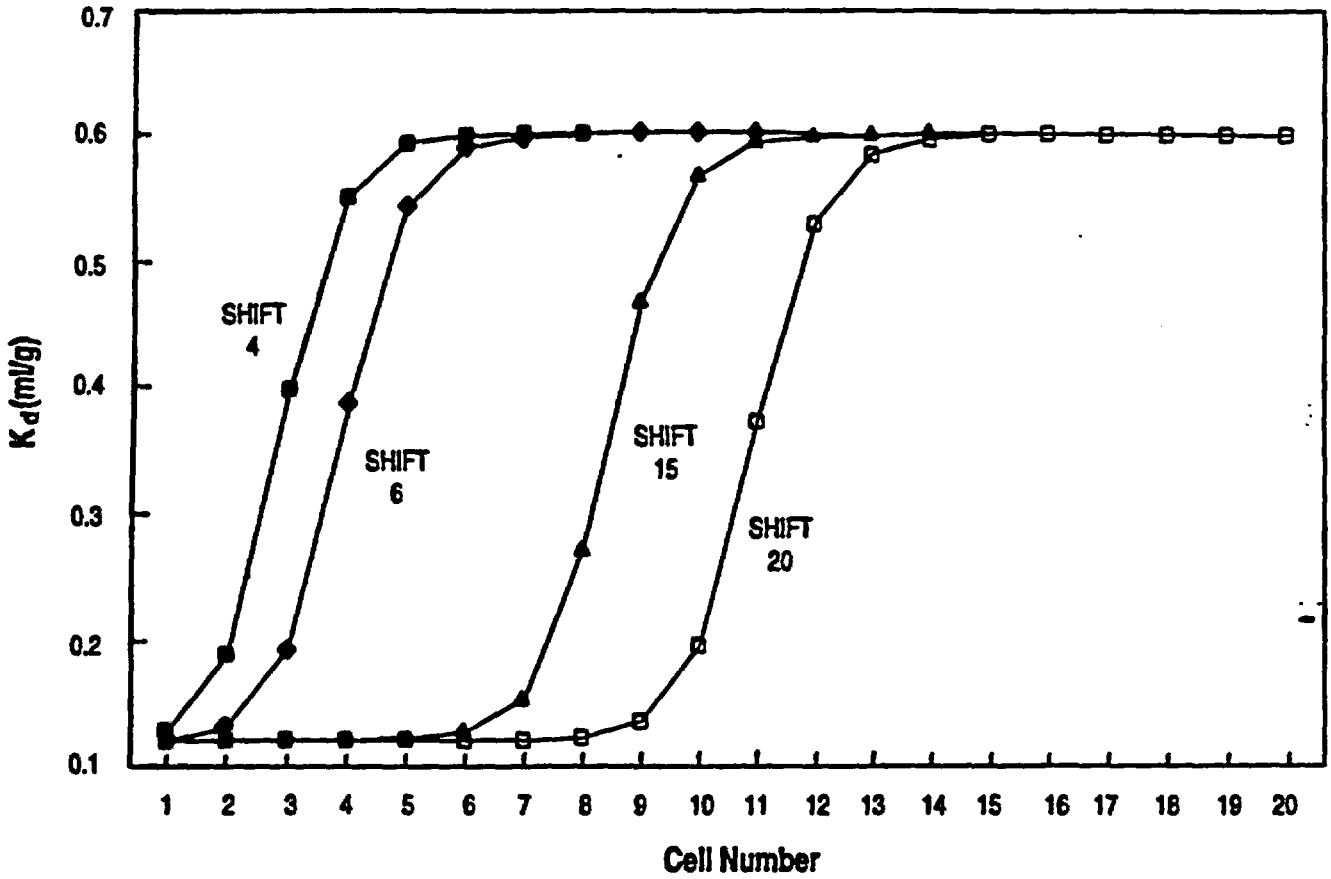
0.7
0.6
0.5
0.4
0.3
0.2
0.1
K_d(ml/g)
SHIFT 4
SHIFT 6
SHIFT 15
SHIFT 20
1 2 3 4 5 6 7 8 9 10 11 12 13 14 15 16 17 18 19 20
Cell Number

studied in the Yucca Mountain Project, only K_d values as a function of radionuclide concentration are determined for rock-water systems representing various locations in the repository block? Must not the radionuclide concentration at each location also be known in order to assign the appropriate K_d value? The approach to modelling radionuclide migration in the Yucca Mountain Project is to assume that K_d values are a function only of space and not time (Meijer, 1992). With this approach, a K_d value is chosen that is conservative relative to all K_d values, no matter what radionuclide concentration is present. However, it must be noted that Equation (D-5), describing the relation of radionuclide concentration on the solid to that in the liquid, has no formulation to limit the radionuclide concentration in the liquid. This limit must be supplied by additional information, such as solubilities.

From Figure D-2, it is evident that the concentrations of K^+ in a particular cell can vary from 0 to 1 meq/L depending on the number of shifts and the position of the cell. By plotting the concentration of K^+ on the solid in meq/g versus the concentration in the liquid for all cells and all shifts, the sorption isotherm can be generated. Figure D-4 is such a plot. This isotherm is convex up, and thus produces a front of constant shape, which is consistent with the description of Vermuelen, *et al.* (1987). The points on Figure D-4 could be fitted to a curve such as the Freundlich formulation (Equation (D-5)), but it is not necessary for this study.

Figure D-5 illustrates the effect of doubling the concentration of K^+ in the flushing solution while keeping all other parameters the same as in the first simulation. Here, for 20 shifts, or cell volumes added, the front measured at half concentration, falls between cell 12 and 13. This is comparable to a

K_d of 0.07. Figure D-6 shows K_d values versus cell number for this simulated elution. Unlike in Figure D-2, where the K_d values monotonically change from one extreme to the other for a given shift, these curves develop a bulge with more shifts. The bulge can be explained by rearranging Equation (D-3) to express K_d as:

$$\frac{[KX]}{[K^+]} = K_d = K * \frac{[NaX]}{[Na^+]}, \qquad \text{(D-8)}$$

where activities approximate concentrations. Since the equilibrium constant is fixed, the variation in K_d is caused by a variation in the concentrations of the sodium species. Figure D-7 shows the displacement of sodium on the solid by potassium in the flushing solution. As a result of the higher K^+ concentration, more Na^+ is displaced to the liquid in each cell downstream than was originally present (1 meq/L in liquid and 1 meq/L on solid). A wave of Na^+ develops with its crest increasing with the number of cell volumes added to the column. Thus, although the [NaX] varies smoothly from 0 to 1 meq/L down the column, the $[Na^+]$ goes through a maximum. This variation causes the bulge in the K_d values.

The ion-exchange reaction represented by Equation (D-4) involves the migration of sodium through a column initially saturated with potassium. With an equilibrium constant of 1/5, this simulation should result in the unfavorable condition of non-constant-shaped fronts. Figure D-8 illustrates the elution of 1 meq/L of Na^+ in the flushing solution through a column having 1 meq/L for both KX on the solid

Figure D-4. Sorption isotherm calculated from flow-though ion exchange simulation illustrated in Figure D-3 showing favorable characteristics.

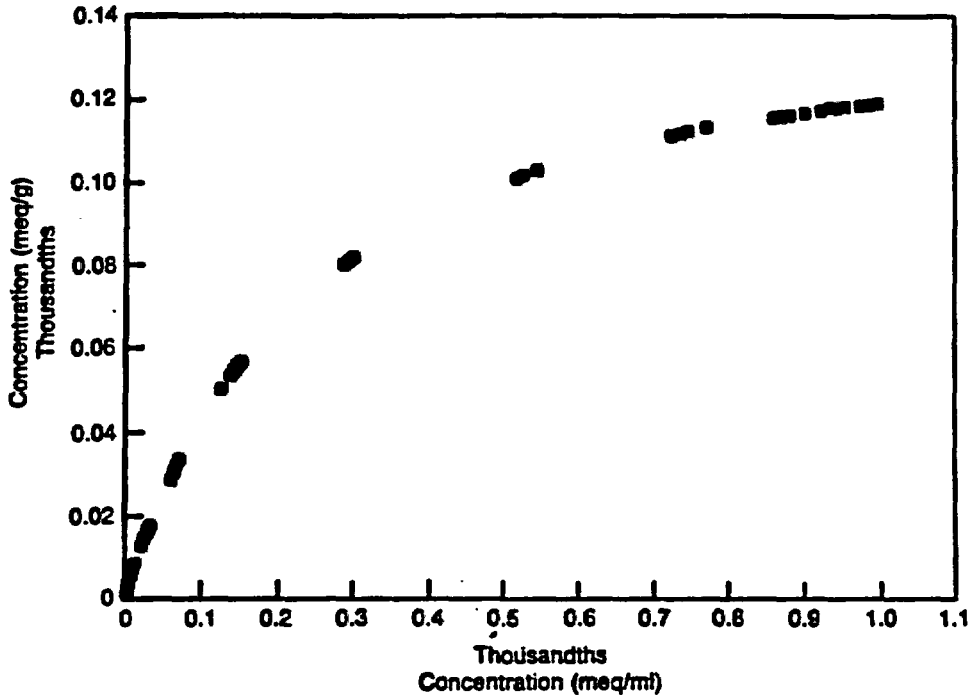
0.14
0.12
0.10
0.08
0.06
0.04
0.02
0
Concentration (meq/g)
Thousandths
0
0.1
0.2
0.3
0.4
0.5
0.6
0.7
0.8
0.9
1.0
1.1
Thousandths
Concentration (meq/ml)

Figure D-5. **Flushing solution concentration versus cell number, flushing solution solute preferentially sorbed, effect of doubling starting concentration of flushing solution solute relative to competing cation and sorbing site concentrations.**

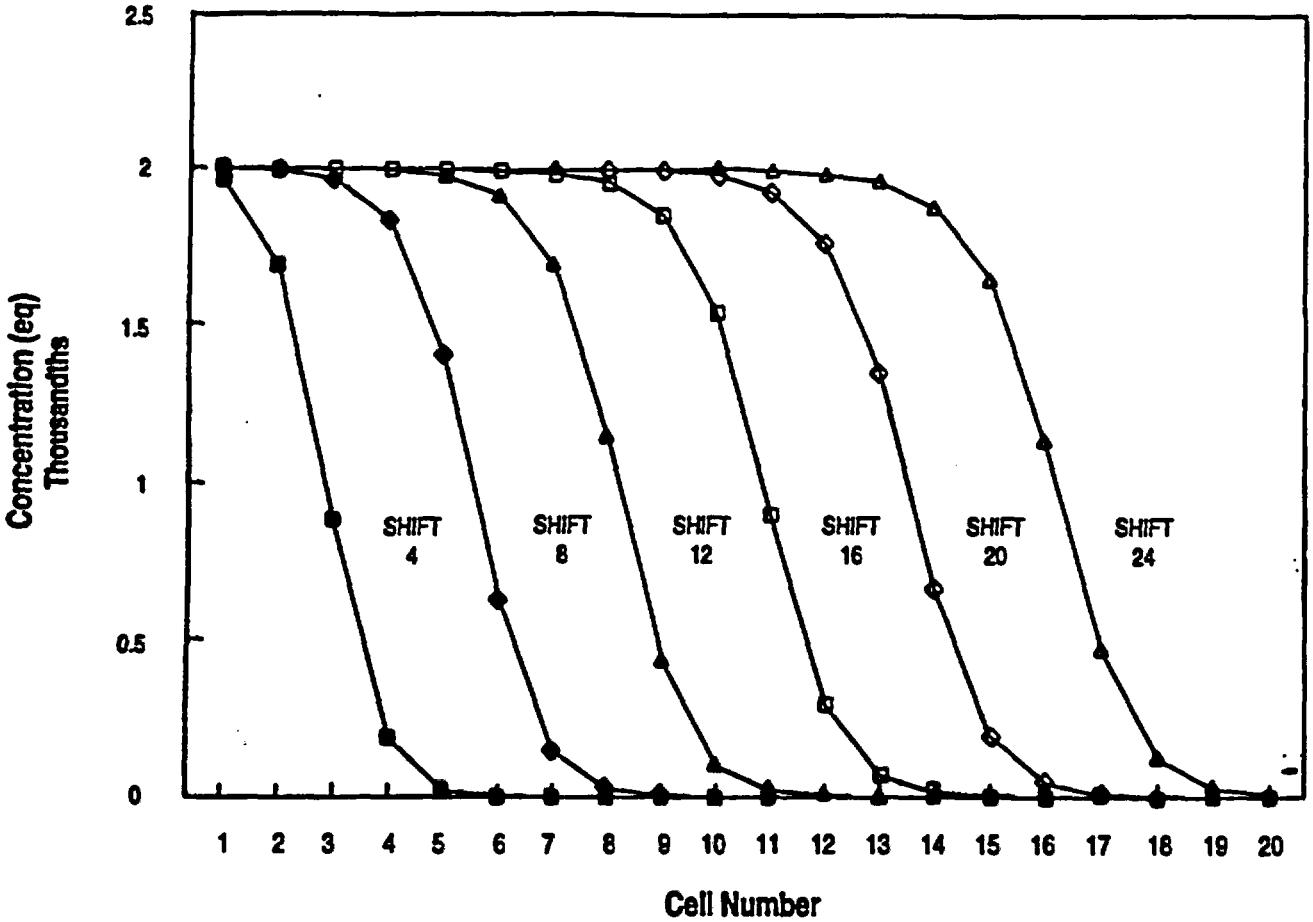
2.5
2
1.5
1
0.5
0
Concentration (eq)
Thousandths
SHIFT 4
SHIFT 8
SHIFT 12
SHIFT 16
SHIFT 20
SHIFT 24
1 2 3 4 5 6 7 8 9 10 11 12 13 14 15 16 17 18 19 20
Cell Number

Figure D-6. K_d versus cell number for flow-through ion exchange simulation illustrated in Figure D-5.

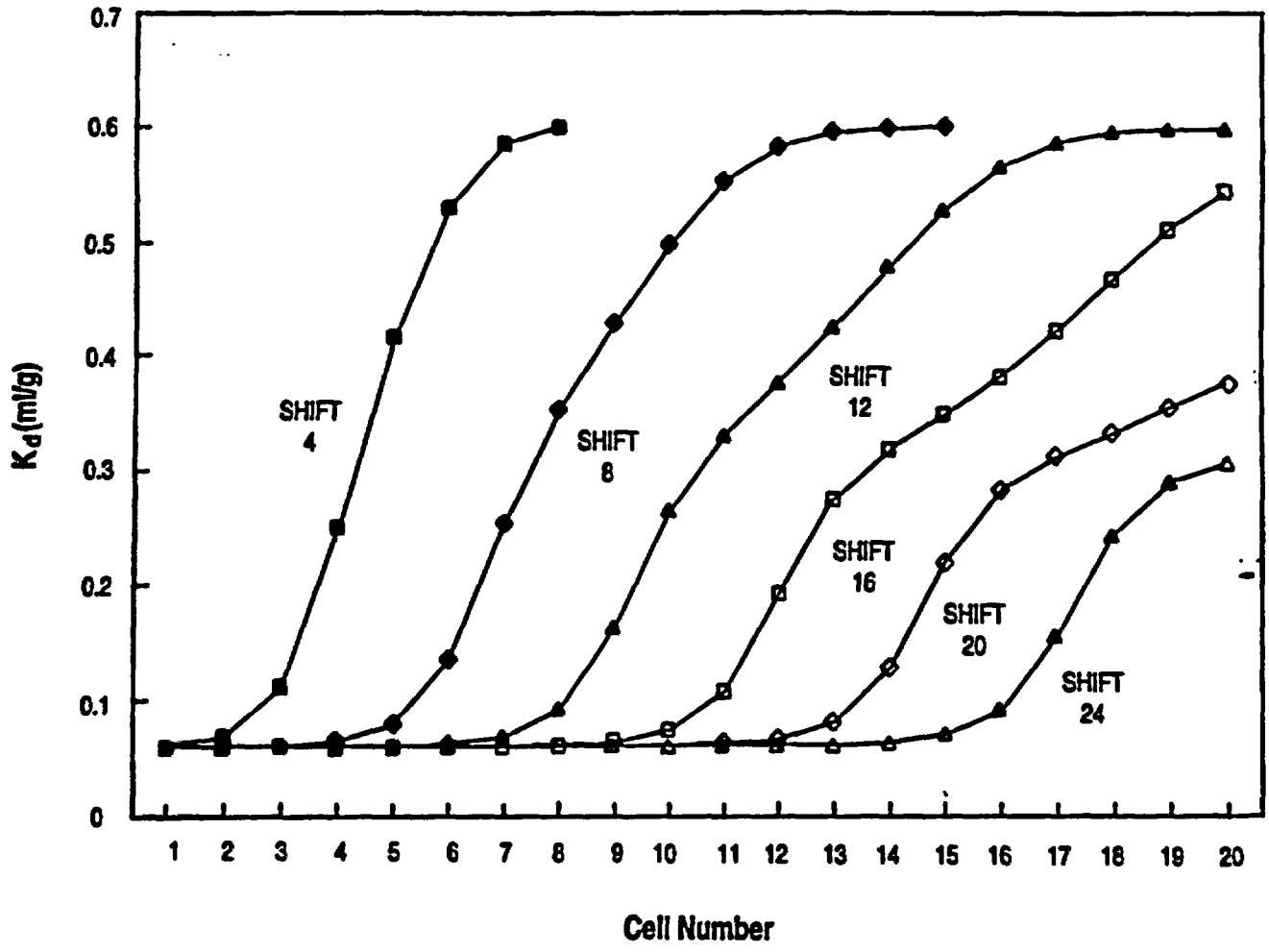
0.7
0.6
0.5
0.4
0.3
0.2
0.1
0
K_d(ml/g)
SHIFT 4
SHIFT 8
SHIFT 12
SHIFT 16
SHIFT 20
SHIFT 24
1 2 3 4 5 6 7 8 9 10 11 12 13 14 15 16 17 18 19 20
Cell Number

Figure D-7. Concentration of competing cation versus cell number for flow-through ion exchange simulation illustrated in Figure D-5.

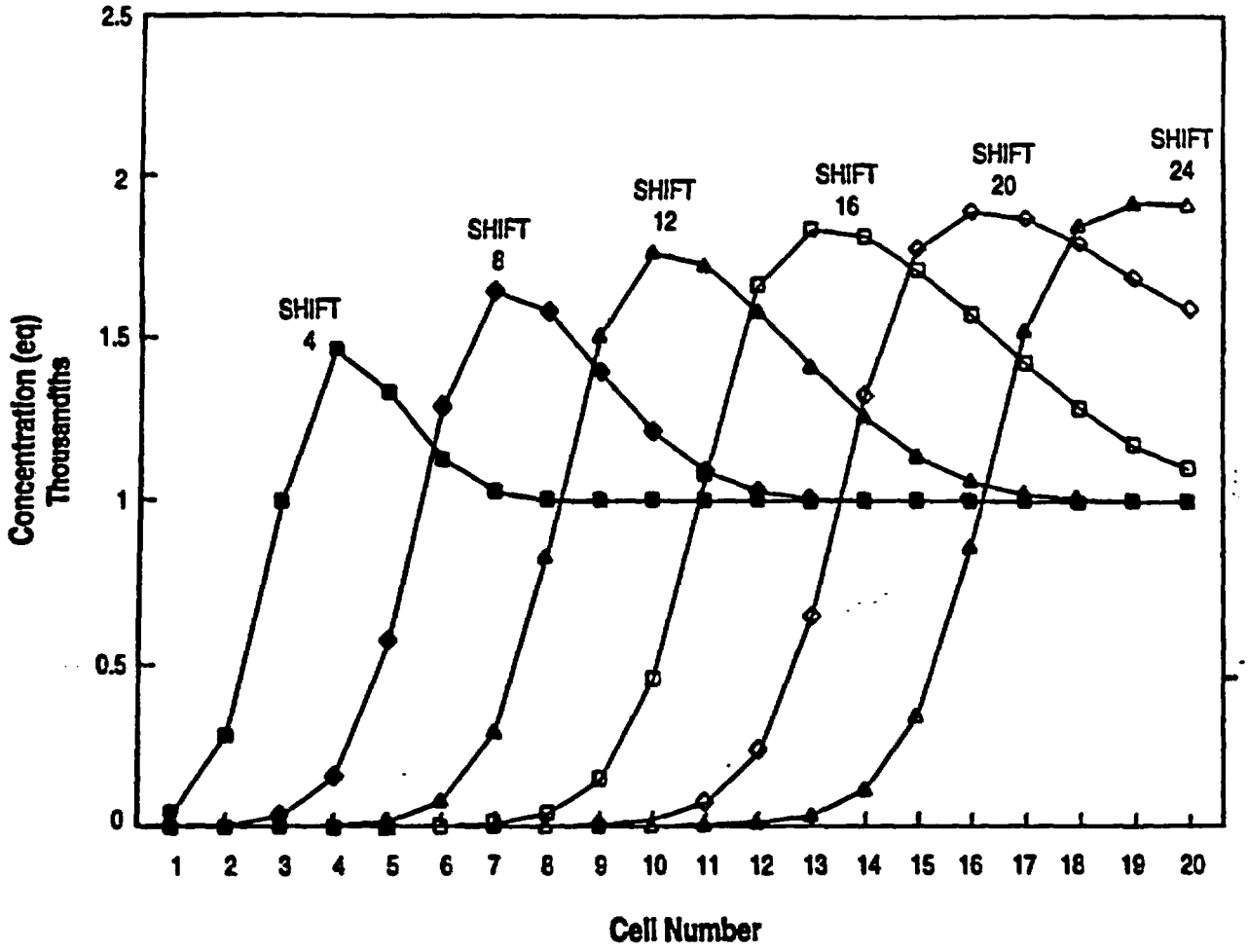
2.5
2
1.5
1
0.5
0
Concentration (eq)
Thousandths
SHIFT 4
SHIFT 8
SHIFT 12
SHIFT 16
SHIFT 20
SHIFT 24
1 2 3 4 5 6 7 8 9 10 11 12 13 14 15 16 17 18 19 20
Cell Number

Figure D-8. Flushing solution concentration versus cell number, flushing solution solute preferentially desorbed, equal starting concentrations of flushing solution solute, competing cation and sorbing site.

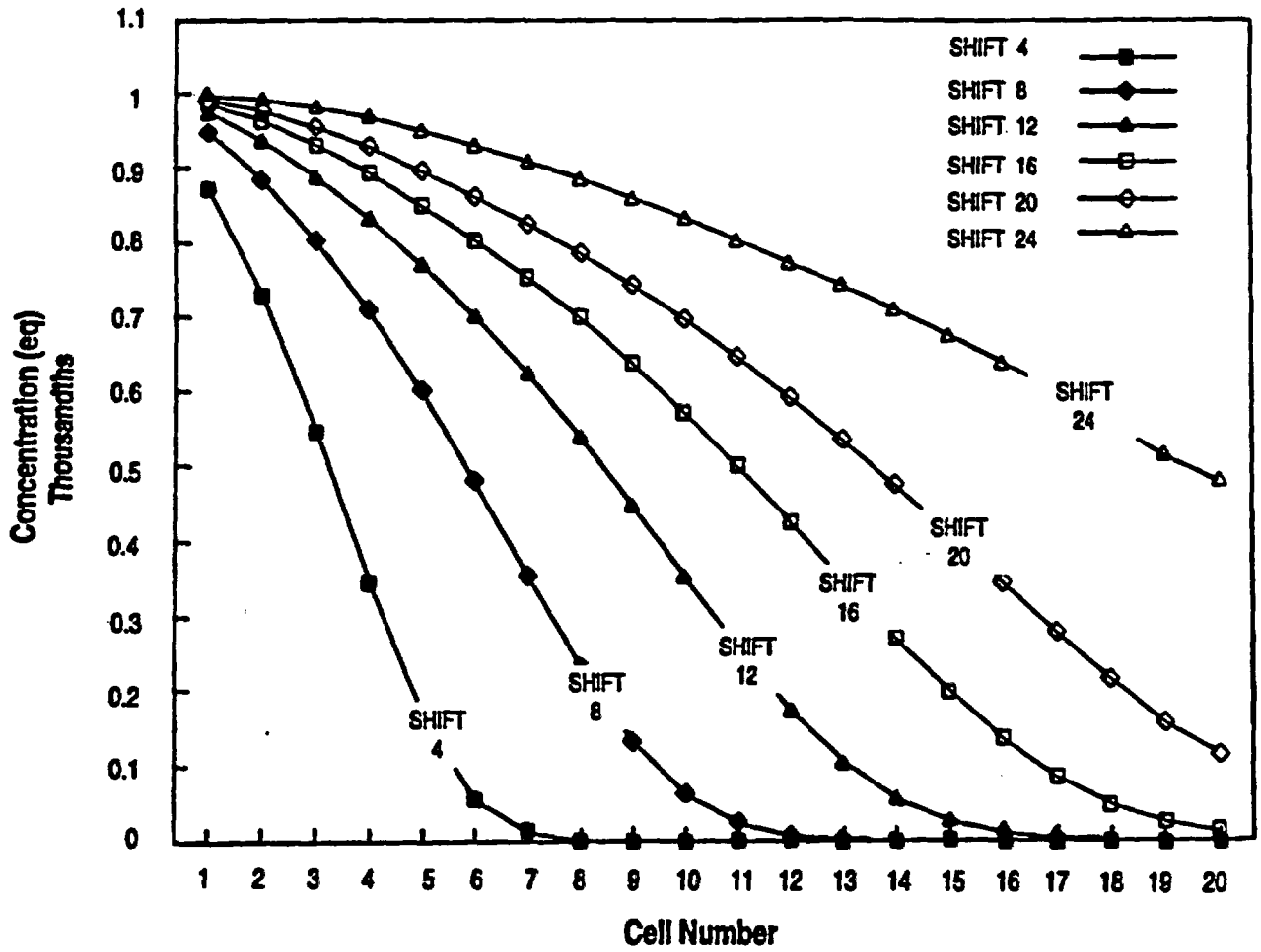
SHIFT 4
SHIFT 8
SHIFT 12
SHIFT 16
SHIFT 20
SHIFT 24
SHIFT 24
SHIFT 20
SHIFT 16
SHIFT 12
SHIFT 8
SHIFT 4
Concentration (eq)
Thousandths
Cell Number
1.1
1
0.9
0.8
0.7
0.6
0.5
0.4
0.3
0.2
0.1
0
1 2 3 4 5 6 7 8 9 10 11 12 13 14 15 16 17 18 19 20

and K^+ in solution. The curves representing various shifts definitely are not of constant shape. The retardation factor calculated for shift 16 is approximately 1.6. Unlike the favorable condition (Figure D-2) where, with a retardation factor of 2, no flushing solution solute was exiting the column even after 24 shifts, here significant flushing solution solute passes through the column at 20 shifts. Dispersivity for both favorable and unfavorable simulations is the same (2 millimeters). This simulation demonstrates that, in addition to the retardation factor, the shape of the curve is also important. Thus, with regard to Yucca Mountain, for a given retardation factor, the amount of radionuclide reaching the accessible environment depends on whether the ion exchange is favorable or not.

Figure D-9 shows K_d versus cell number for this simulation. Again the K_d values are not constant for a given cell. This graph does not have the same shape as Figure D-3, where the K_d values ranged between two extremes, with a retardation factor appropriately calculated from one of the K_d extremes. Here, the retardation factor corresponds to an intermediate K_d value. Figure D-10 is the sodium isotherm for this simulation. The curve is concave up, consistent with the unfavorable condition as described by Vermuelen *et al.* (1987).

The previous simulations involved 1 meq/L X^-. This amount of sorbing site is relatively small. For comparison, YM-22, a tuff sample from Yucca Mountain that has been used in many sorption experiments has a exchange capacity equivalent to 167 meq/L X^-. Elution simulations similar to the previous ones were performed with this higher sorbing site concentration. Figure D-11 shows the elution of 1 meq/L of K^+ through a column initially loaded with 167 meg/L NaX on the solid in contact with liquid containing 1 meq/L Na^+. As before, the flushing solution front maintains a steep concentration gradient. However, the migration of K^+ is greatly retarded. Note that it takes 800 shifts to move the half-height of the flushing solution to cell 5. The retardation factor is calculated to be approximately 133 corresponding to a K_d of 16. Figure D-12 is the K_d versus cell number plot showing the variation in K_d for each cell at different shifts. The corresponding isotherm in Figure D-13 is nonlinear and convex up.

Although, in Figure D-11 the front maintains a steep concentration gradient, it is evident that the front is not constant in shape. Apparently, the dispersion, which tends to spread the front, is competing against the favorable sorption (nonlinear convex up isotherm) which tends to sharpen the front. Since each shift involves the transfer of 20 percent of the constituents of the aqueous phase of one cell with an adjacent cell downstream, as calculated from Equation (D-7), with 800 shifts, dispersion becomes important in mobilizing the flushing solution solute.

Next, the elution of Na^+ through a column packed with YM-22 is simulated where 1 meq/L of Na^+ is added to a column initially loaded with 167 meg/L KX on the solid in contact with liquid containing 1 meq/L K^+. The spreading of the flushing solution front is evident in Figure D-14. Each cell has a range of K_d values, depending on the number of shifts or cell volumes that have been added to the column (Figure D-15). The sodium isotherm is nonlinear and concave up (Figure D-16).

For the simulations involving YM-22, the concentrations of sorbing ions are in trace amounts relative to the sorbing site concentration. However, the concentrations of the competing ions are initially equivalent. The simulation of elution of potassium in trace concentrations relative to the concentration of the competing ion is depicted in Figure D-17. Again, the shape of the flushing

Figure D-9. K_d versus cell number for flow-through ion exchange simulation illustrated in Figure D-8.

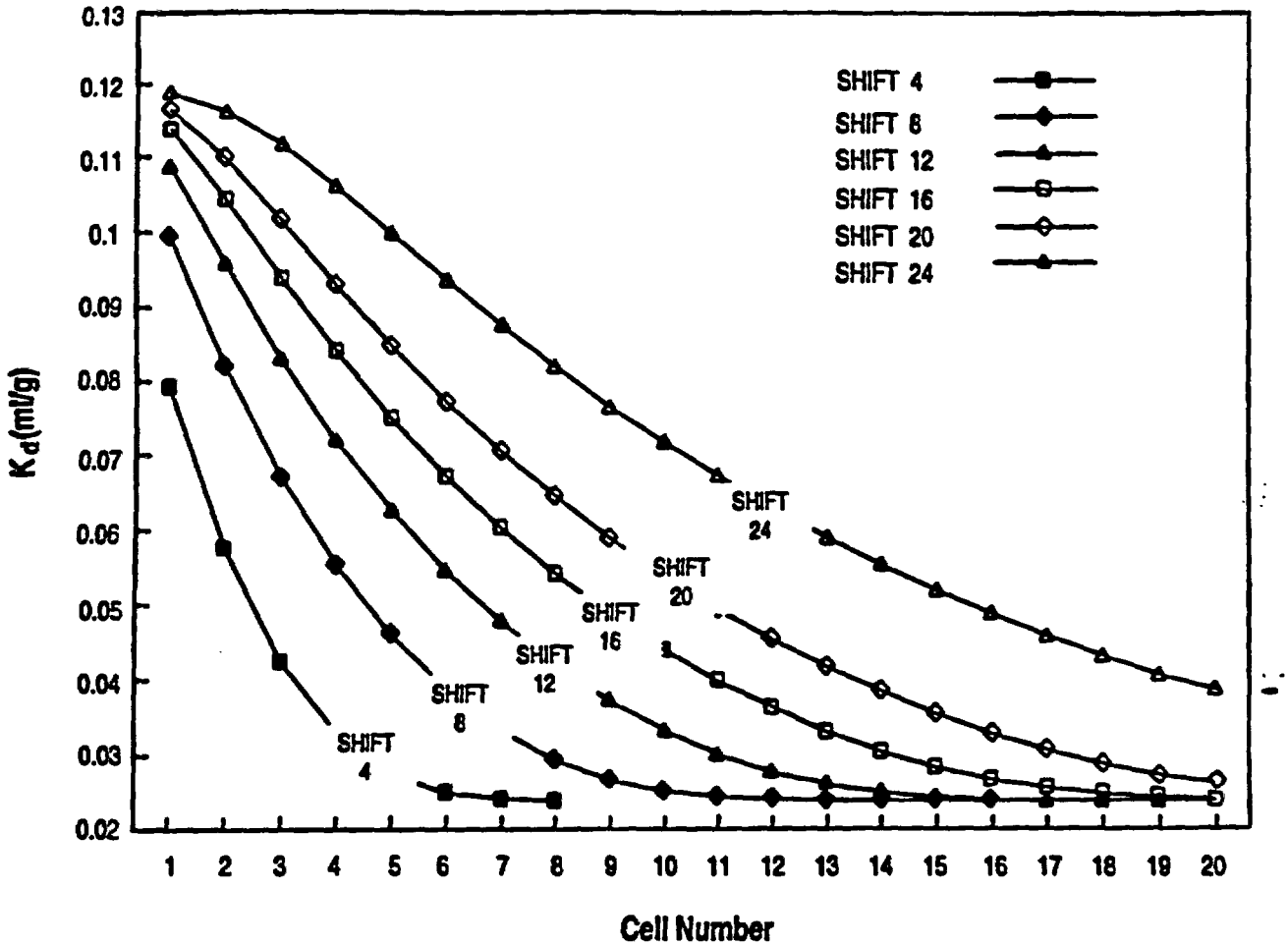
0.13
0.12
0.11
0.1
0.09
0.08
0.07
0.06
0.05
0.04
0.03
0.02
K_d(ml/g)
SHIFT 4
SHIFT 8
SHIFT 12
SHIFT 16
SHIFT 20
SHIFT 24
SHIFT 24
SHIFT 20
SHIFT 16
SHIFT 12
SHIFT 8
SHIFT 4
1 2 3 4 5 6 7 8 9 10 11 12 13 14 15 16 17 18 19 20
Cell Number

Figure D-10. Sorption isotherm calculated from flow-though ion exchange simulation illustrated in Figure D-8 showing unfavorable characteristics.

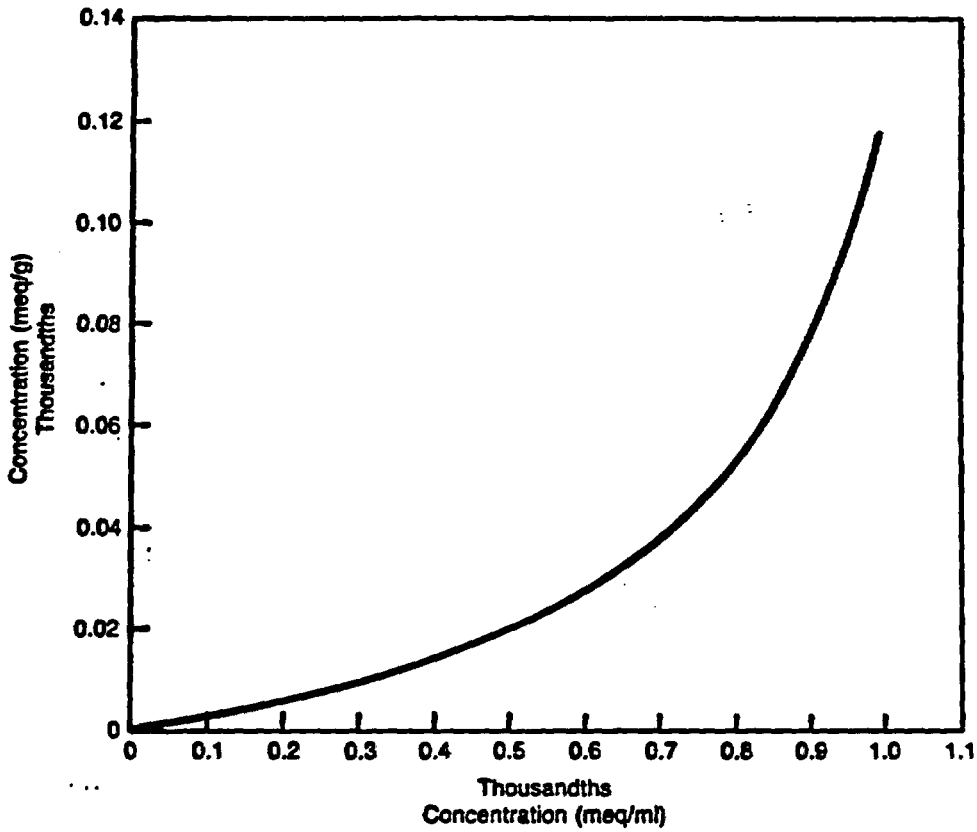
0.14
0.12
0.10
0.08
0.06
0.04
0.02
0
Concentration (meq/g)
Thousandths
0
0.1
0.2
0.3
0.4
0.5
0.6
0.7
0.8
0.9
1.0
1.1
Thousandths
Concentration (meq/ml)

Figure D-11. Flushing solution concentration versus cell number, flushing solution solute preferentially sorbed, effect of increasing sorbing site concentration relative to starting concentrations of flushing solution solute and competing cation.

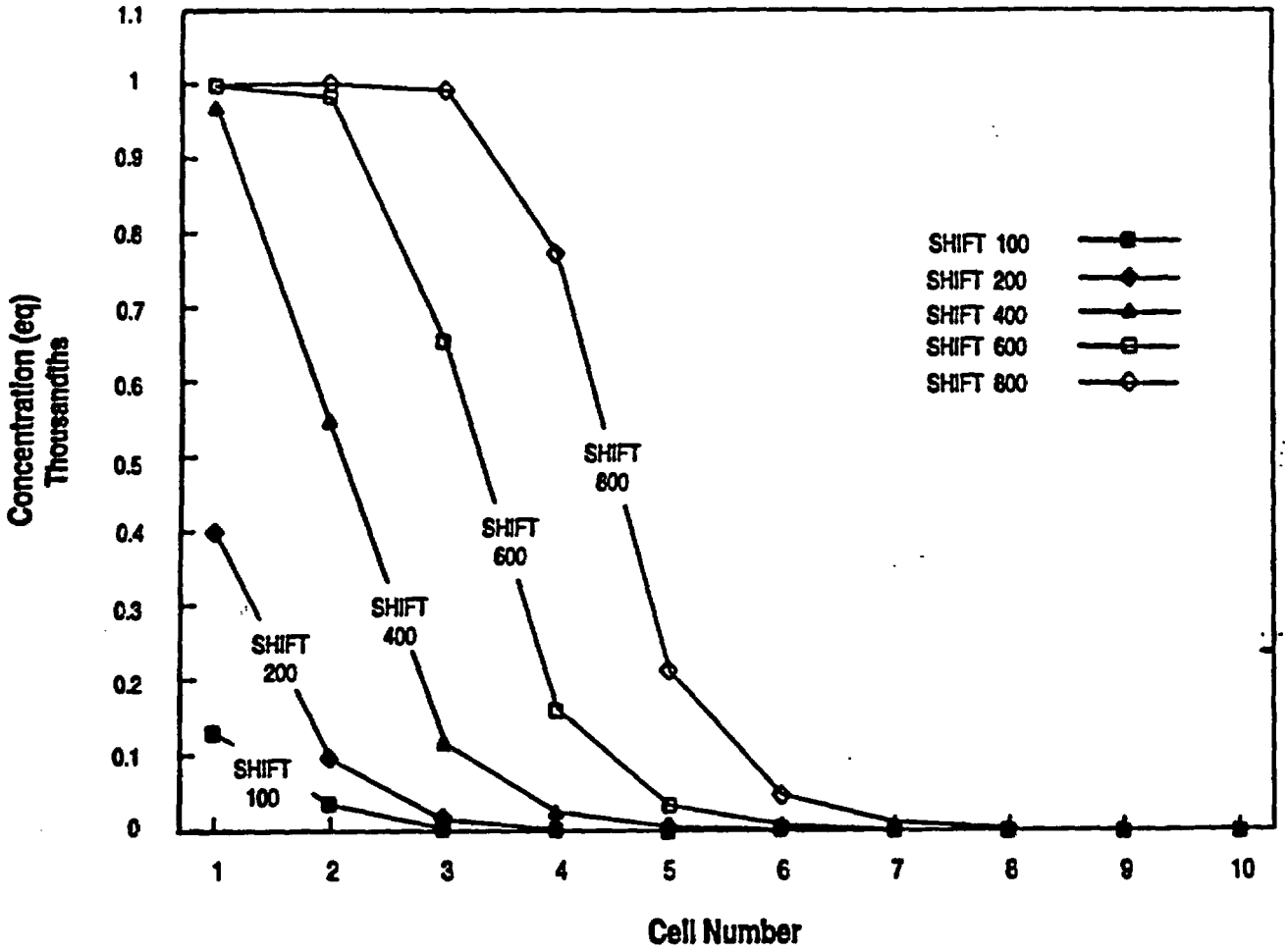
1.1
1
0.9
0.8
0.7
0.6
0.5
0.4
0.3
0.2
0.1
0
Concentration (eq)
Thousandths
1
2
3
4
5
6
7
8
9
10
Cell Number
SHIFT 100
SHIFT 200
SHIFT 400
SHIFT 600
SHIFT 800
SHIFT 100
SHIFT 200
SHIFT 400
SHIFT 600
SHIFT 800

Figure D-12. K_d versus cell number for flow-through ion exchange simulation illustrated in Figure D-11.

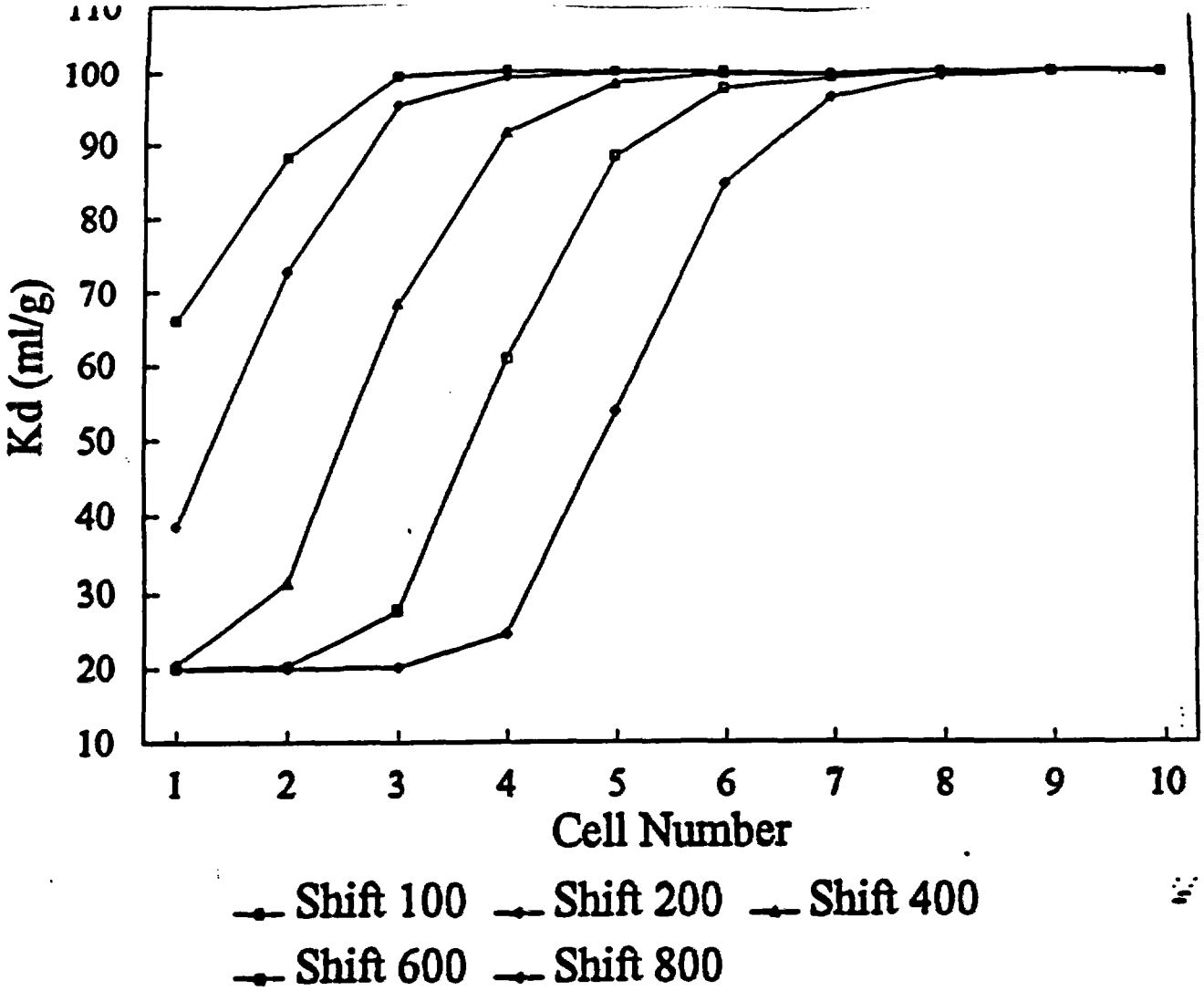

Column: solid, 167 meq/l X- 167 meq/l Na+; liquid, 1 meq/l Na+
Flushing solution: 1 meq/l K+

D12

Figure D-13. Sorption isotherm calculated from flow-though ion exchange simulation illustrated in Figure D-11 showing favorable characteristics.

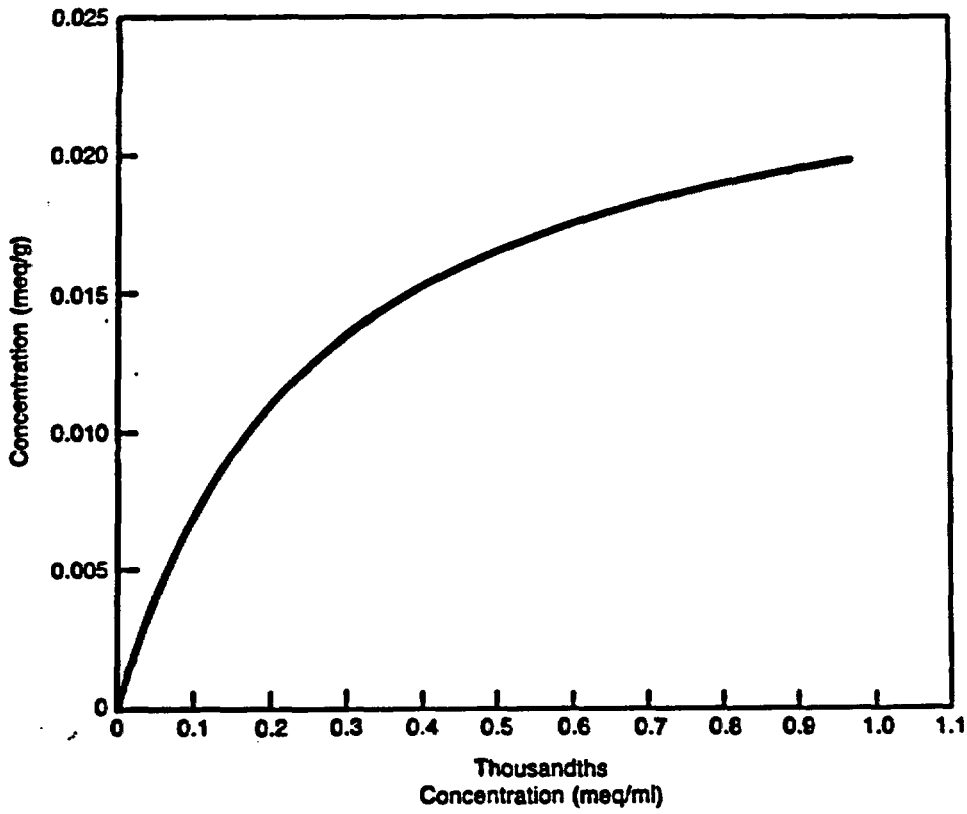
0.025
0.020
0.015
0.010
0.005
0
Concentration (meq/g)
0
0.1
0.2
0.3
0.4
0.5
0.6
0.7
0.8
0.9
1.0
1.1
Thousandths
Concentration (meq/ml)

Figure D-14. Flushing solution concentration versus cell number, flushing solution solute preferentially desorbed, effect of increasing sorbing site concentration relative to starting concentrations of flushing solution solute and competing cation.

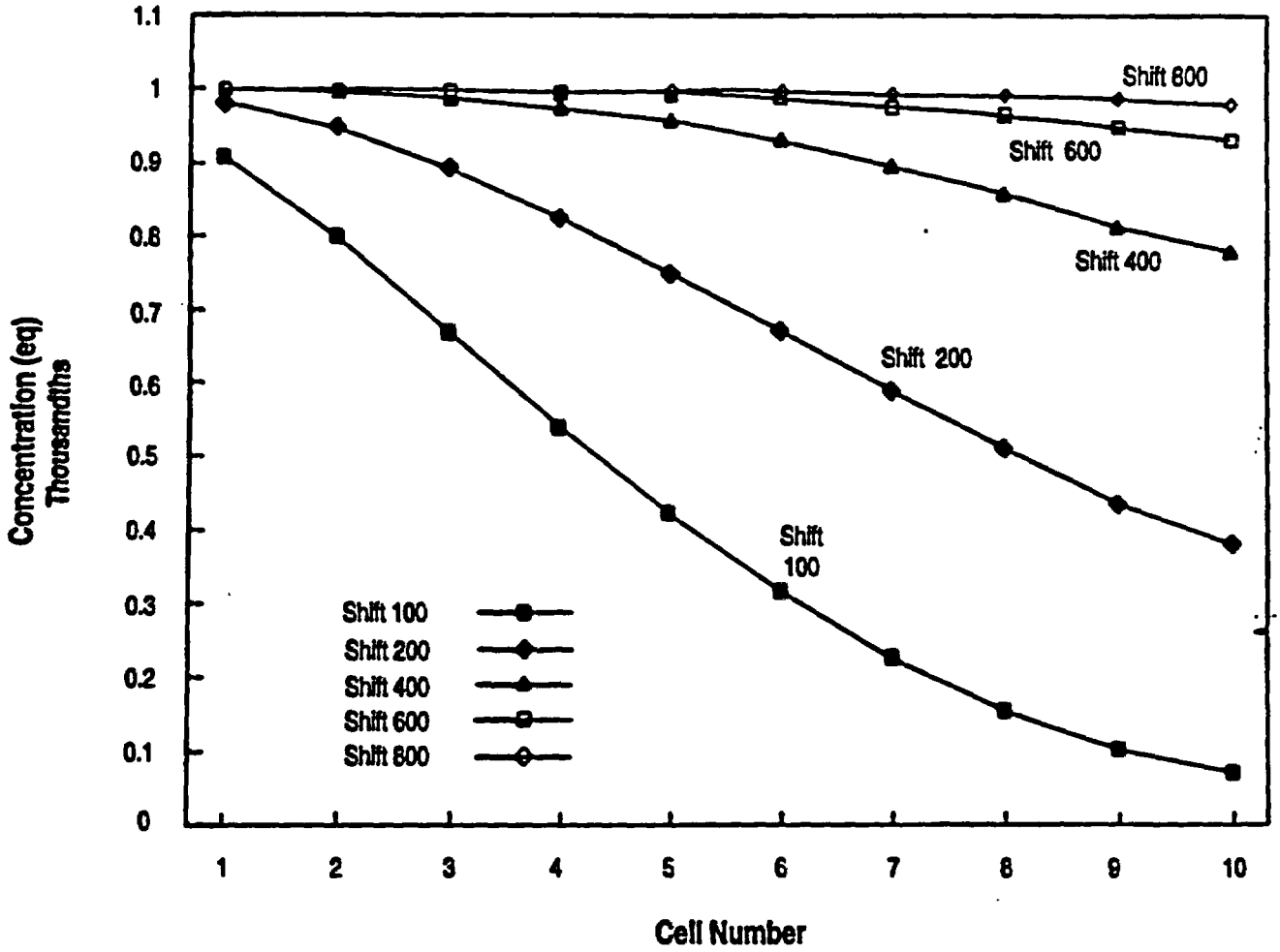
1.1
1
0.9
0.8
0.7
0.6
0.5
0.4
0.3
0.2
0.1
0
Concentration (eq)
Thousandths
1
2
3
4
5
6
7
8
9
10
Cell Number
Shift 800
Shift 600
Shift 400
Shift 200
Shift
100
Shift 100
Shift 200
Shift 400
Shift 600
Shift 800

Figure D-15. K_d versus cell number for flow-through ion exchange simulation illustrated in Figure D-14.

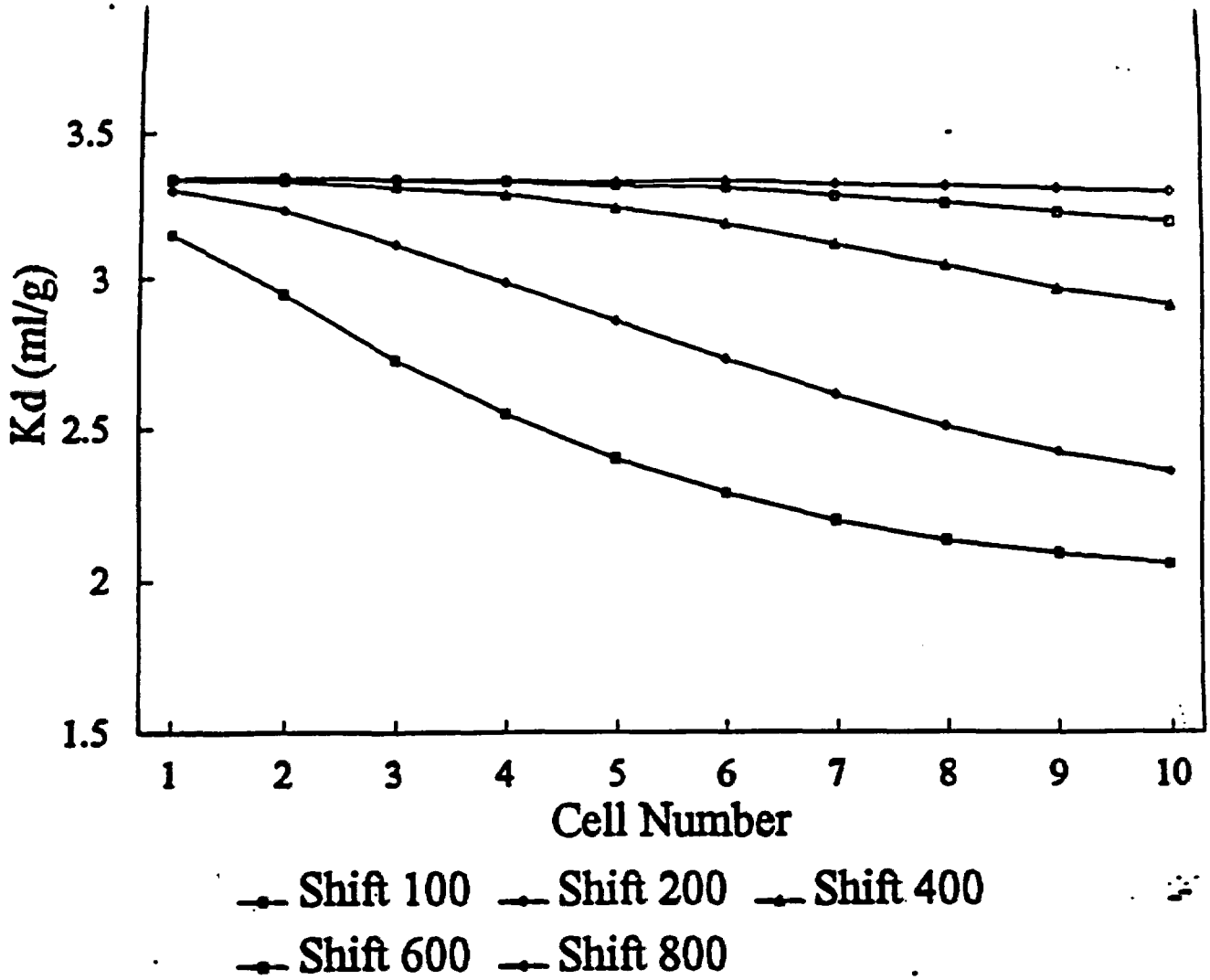

Column: solid, 167 meq/l X- 167 meq/l K+; liquid, 1 meq/l K+
Flushing solution: 1 meq/l Na+

D15

Figure D-16. Sorption isotherm calculated from flow-though ion exchange simulation illustrated in Figure D-14 showing unfavorable characteristics.

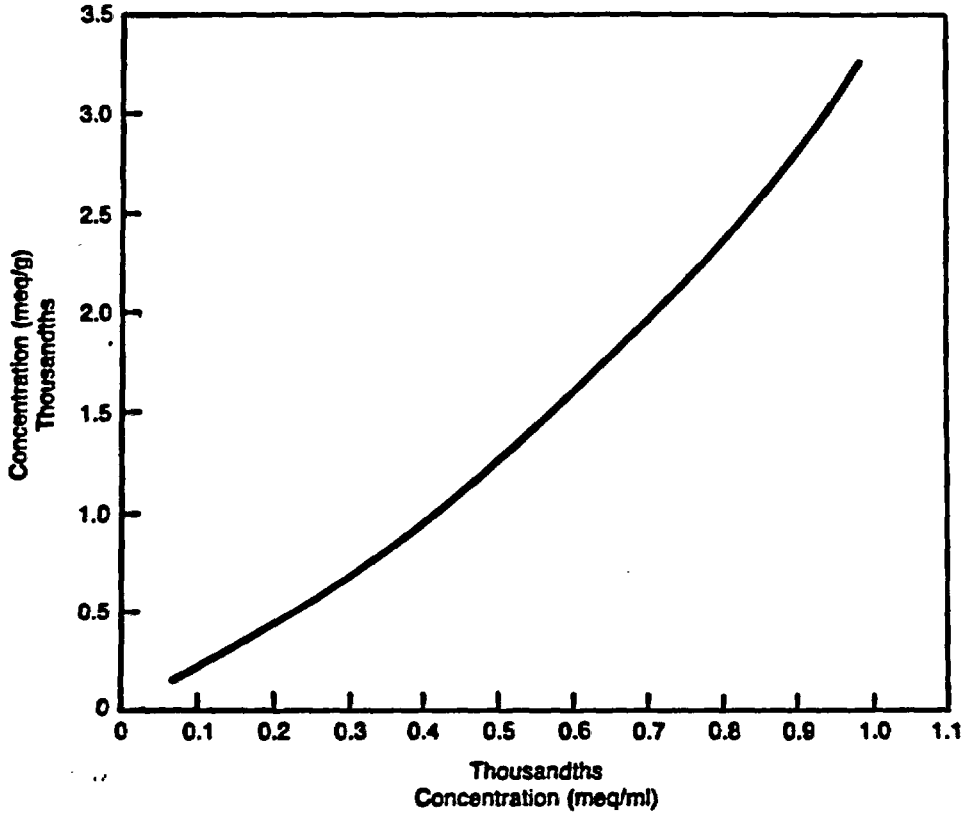
3.5
3.0
2.5
2.0
1.5
1.0
0.5
0
Concentration (meq/g)
Thousandths
0
0.1
0.2
0.3
0.4
0.5
0.6
0.7
0.8
0.9
1.0
1.1
Thousandths
Concentration (meq/ml)

Figure D-17. Flushing solution concentration versus cell number, flushing solution solute preferentially sorbed, trace starting concentration of flushing solution solute, relative to competing cation and sorbing site concentrations.

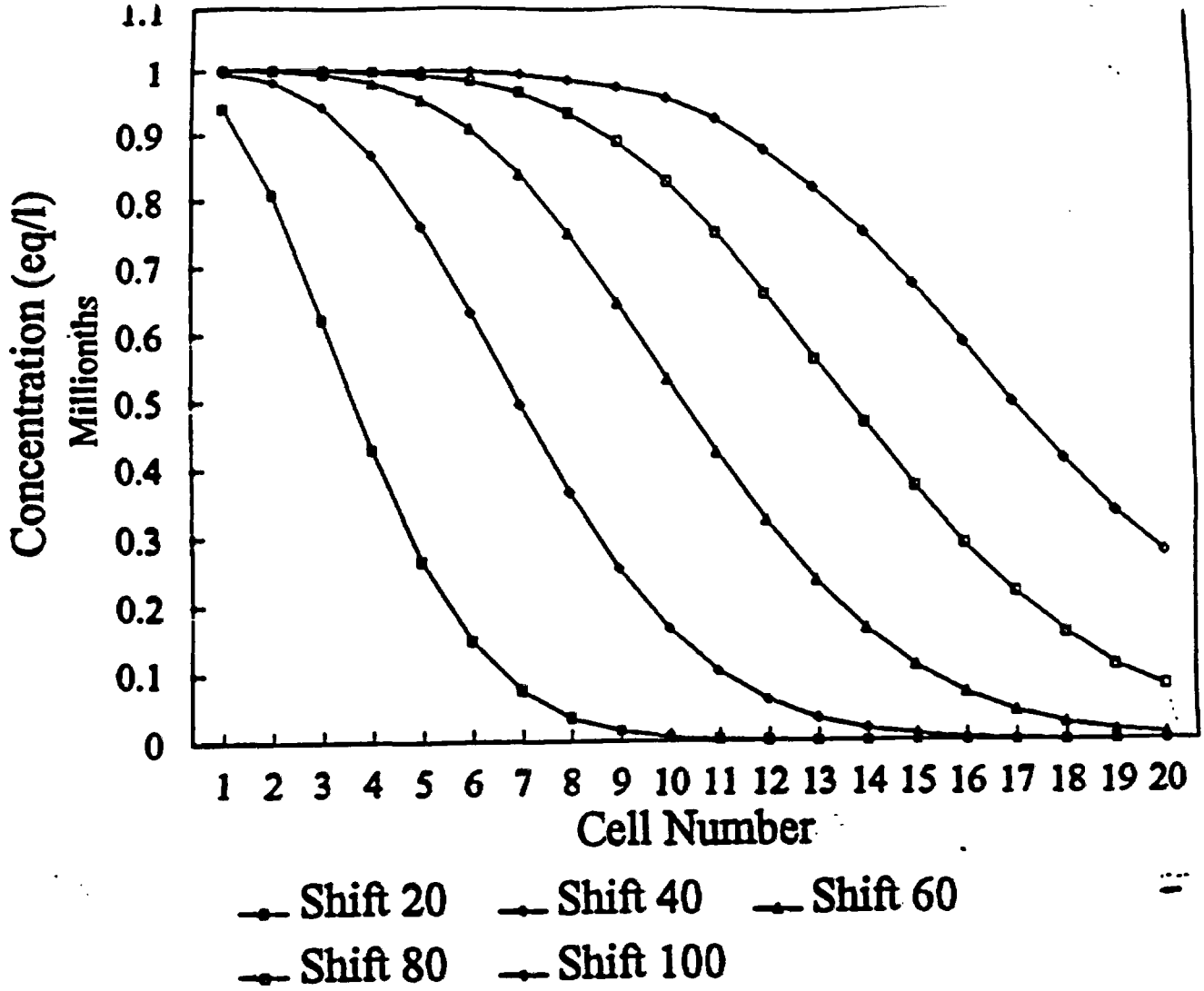

Column: solid, 1 meq/l X- 1 meq/l Na+; liquid, 1 meq/l Na+
Flushing solution: 0.001 meq/l K+

D17

solution front maintains a steep concentration gradient, but is not of constant shape. Dispersion has spread the front slightly, as it moves down the column. A retardation factor of 5.88 is determined (100 shifts/17 cells), from which a K_d of 0.59 is calculated. Figure D-18 illustrates that a single K_d value is associated with every cell. The corresponding isotherm is linear (Figure D-19).

It should be noted that the spreading of the front in Figure D-17, with only 100 shifts, is greater than the spreading of the front in Figure D-11, with 800 shifts. This is demonstrated by comparing the number of cells that correspond to the minimum and maximum flushing solution concentration. In Figure D-17, for 60 shifts, the spread is 18 cells (cell 20 contains the minimum concentration of K^+ and cell 2 contains the maximum); in Figure D-11, for 800 shifts, the spread is 7 cells (cell 10 contains the minimum concentration of K^+ and cell 3 contains the maximum). The difference in the degree of spreading between these two simulations must be caused by the differences in the shapes of the corresponding isotherms. Whereas the convex-up isotherm leads to greater retardation of the solute at lower concentrations, and thus a sharpening of the front and a tendency to compensate for dispersion, the linear isotherm lacks this characteristic.

The elution of sodium, which previously yielded a front that spread significantly, now is tested at trace amounts relative to the competing K^+ concentration. Figure D-20 shows the migration of Na^+ through a column initially loaded with K^+. Note that the spreading of the front is much reduced (compare with Figure D-14). The retardation factor is 1.18 (20 shifts/17 cells). The comparable K_d is 0.021. Figure D-21 illustrates that each cell has a constant K_d value. Finally, the isotherm is linear, as shown in Figure D-22. The spreading is caused by dispersion.

D.3. CONCLUSIONS AND RECOMMENDATIONS

The requirement that the sorption isotherm be linear so that Equation (D-1) is valid results in constant K_d values for each cell. However, the flushing-solution solute front is spread if dispersion occurs and thus is not of constant shape. A linear isotherm results from the condition in which the flushing solution solute is in trace amounts relative to the competing ions. Linear isotherms do not result from the condition where the flushing-solution solute concentration is in trace amounts, relative to the sorbing site but comparable to the concentration of the competing ion(s). When the isotherm is nonlinear and convex up, representing a favorable condition, the K_d value associated with the highest expected concentration of the flushing-solution solute can be used to determine the retardation factor from (D-1). This method is not possible when the isotherm is concave up.

Although dispersion tends to spread the flushing solution front, ion exchange, where the corresponding nonlinear sorption isotherm is convex up, tends to maintain a steep concentration gradient. On the other hand, ion exchange, where the corresponding nonlinear sorption isotherm is concave up, works in concert with dispersion to spread the front.

The information from this auxiliary analysis can be applied to the modeling of conditions and processes expected at Yucca Mountain. The assumption that all radionuclides will be in trace amounts relative to competing ions has not yet been proven. The waters at Yucca Mountain contain low concentrations of solute. Based on the solubility values from DOE's Site Characterization Plan (see DOE, 1988, pp. 4-100), uranium, neptunium, cesium, and technetium could be at concentration levels comparable to those in the uncontaminated waters. Furthermore, what constitutes a competing

Figure D-18. K_d versus cell number for flow-through ion exchange simulation illustrated in Figure D-17.

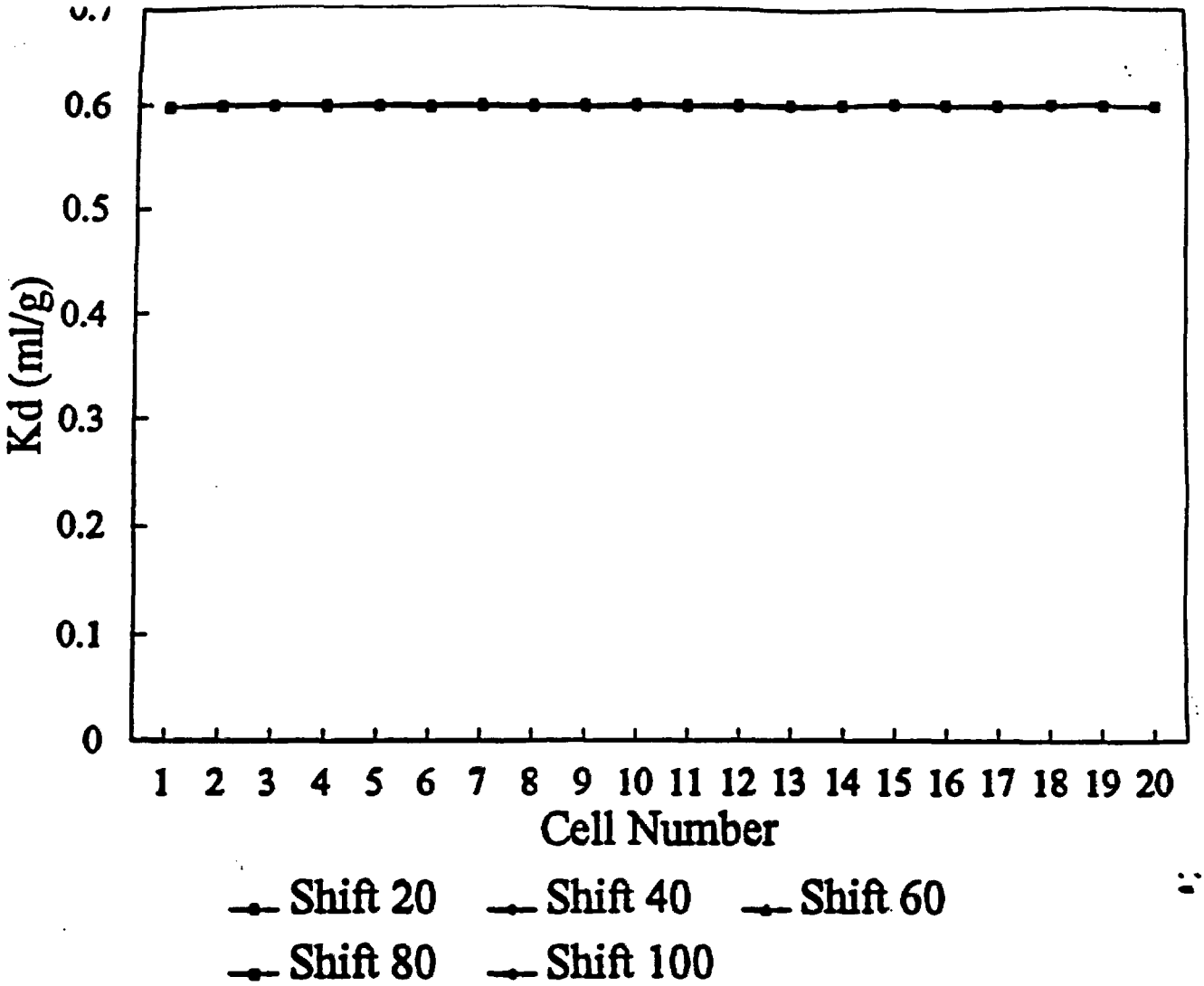

Column: solid, 1 meq/l X- 1 meq/l Na+; liquid, 1 meq/l Na+
Flushing solution:0.001 meq/l K+

D18

-18

Figure D-19. Sorption isotherm calculated from flow-though ion exchange simulation illustrated in Figure D-17 showing linear behavior.

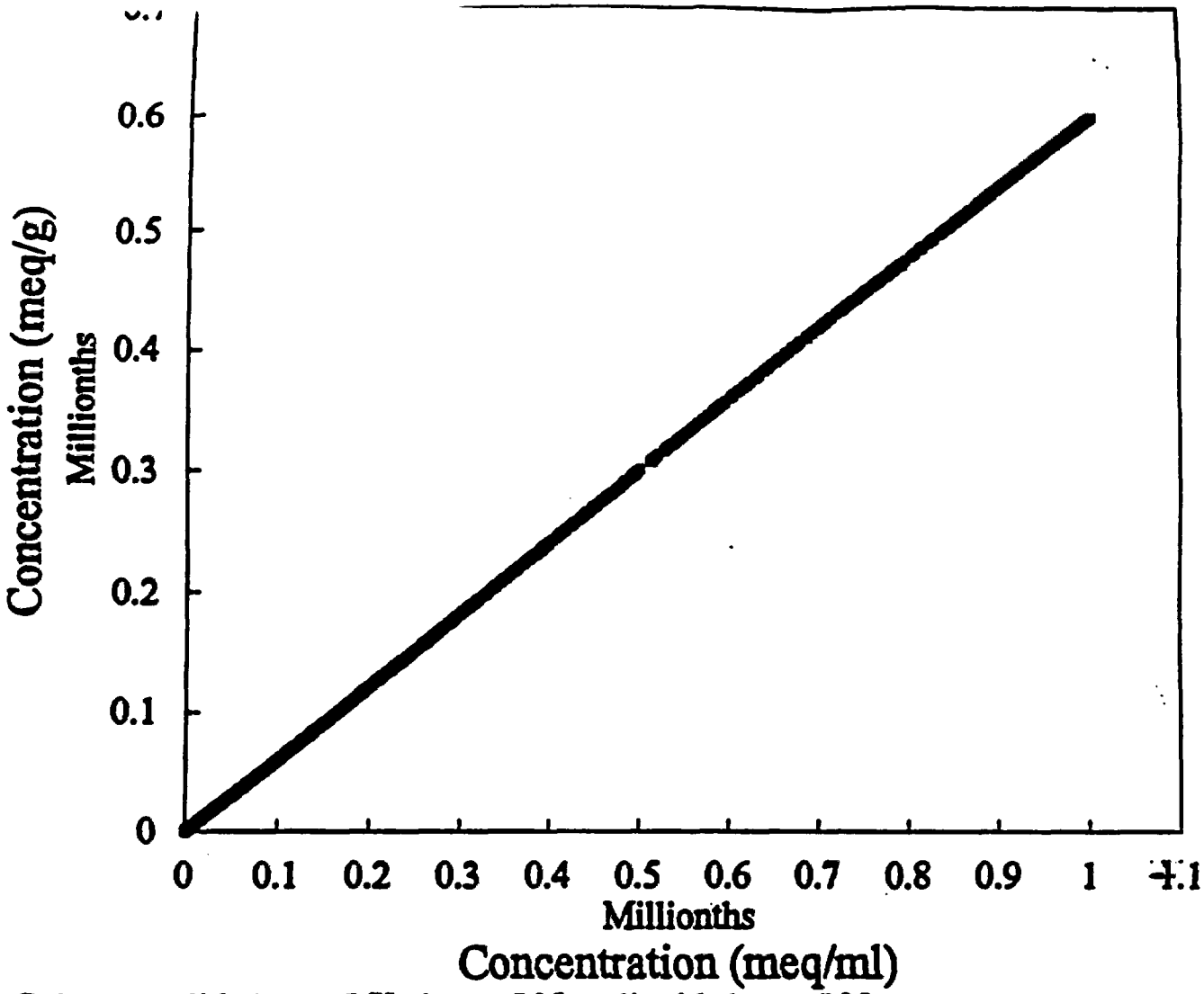

Column: solid, 1 meq/l X- 1 meq/l Na+; liquid, 1 meq/l Na+
Flushing solution: 0.001 meq/l K+

D19

Figure D-20. Flushing solution concentration versus cell number, flushing solution solute preferentially desorbed, trace starting concentration of flushing solution solute, relative to competing cation and sorbing site concentrations.

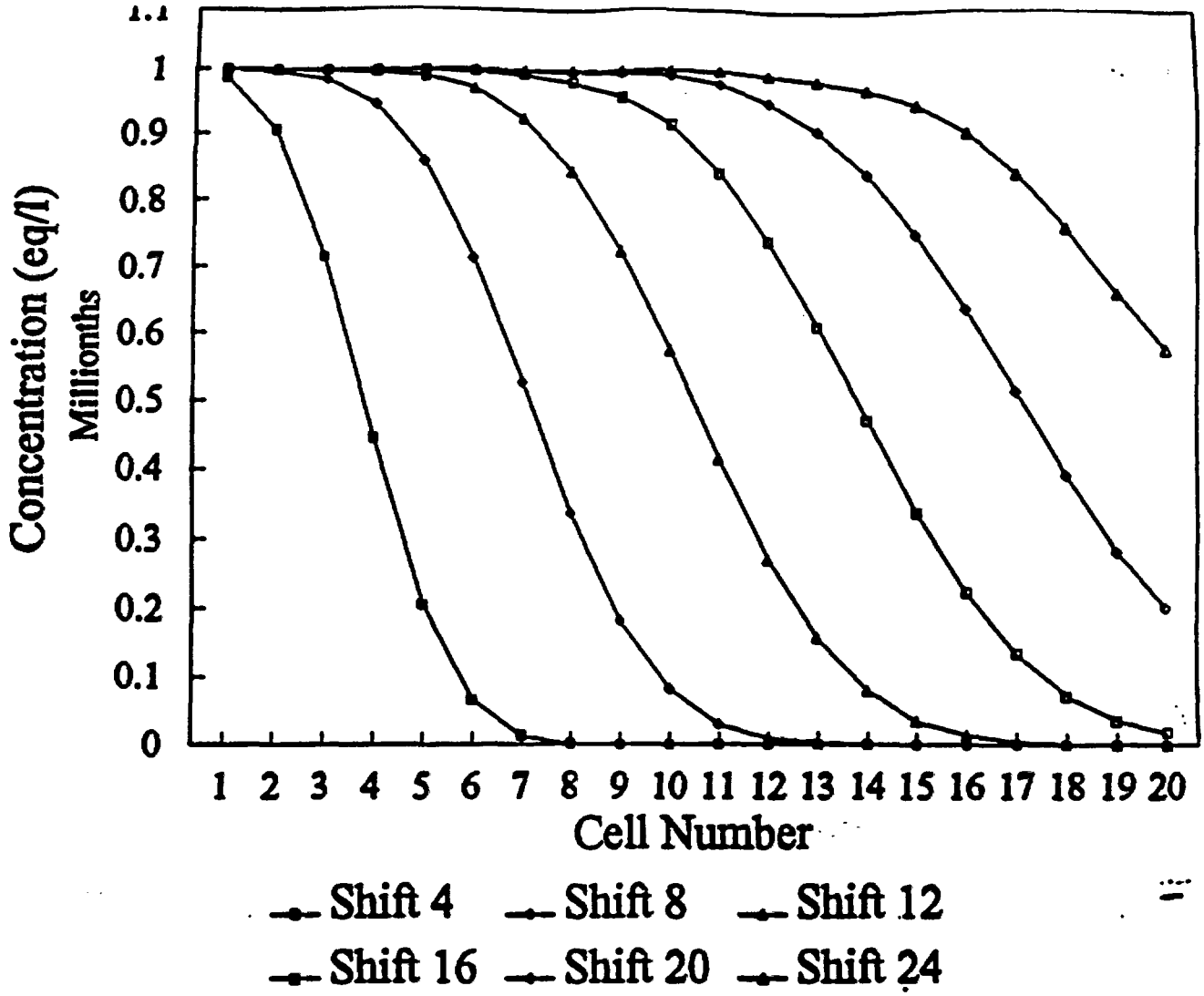

Column: solid, 1meq/l X- 1 meq/l K+; liquid, 1 meq/l K+
Flushing solution: 0.001 meq/l Na+

20

Figure D-21. K_d versus cell number for flow-through ion exchange simulation illustrated in Figure D-20.

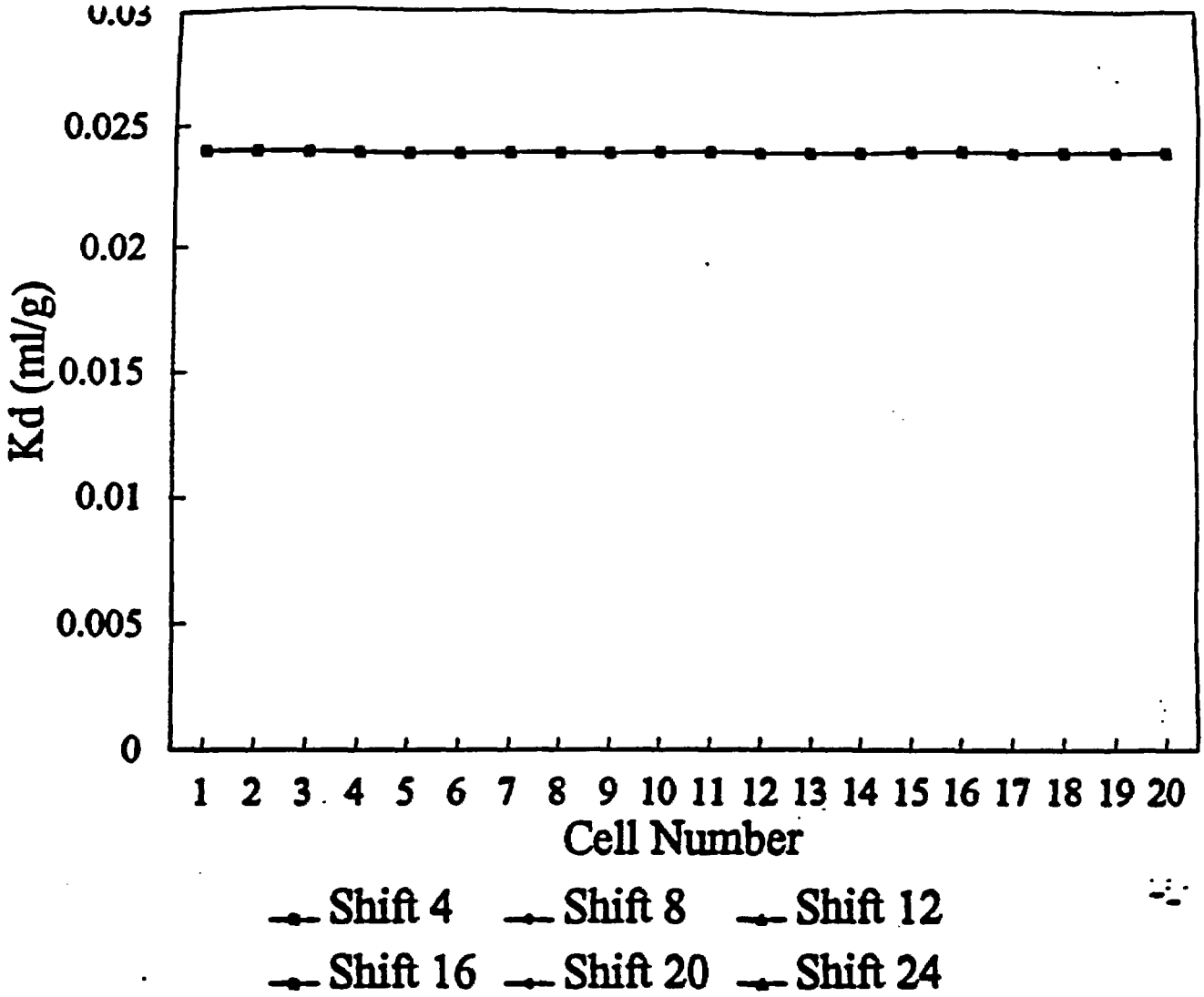

Column: solid, 1 meq/l X- 1 meq/l K+; liquid, 1 meq/l K+
Flushing solution: 0.001 meq/l Na+

D21

-21

Figure D-22. Sorption isotherm calculated from flow-though ion exchange simulation illustrated in Figure D-20 showing linear behavior.

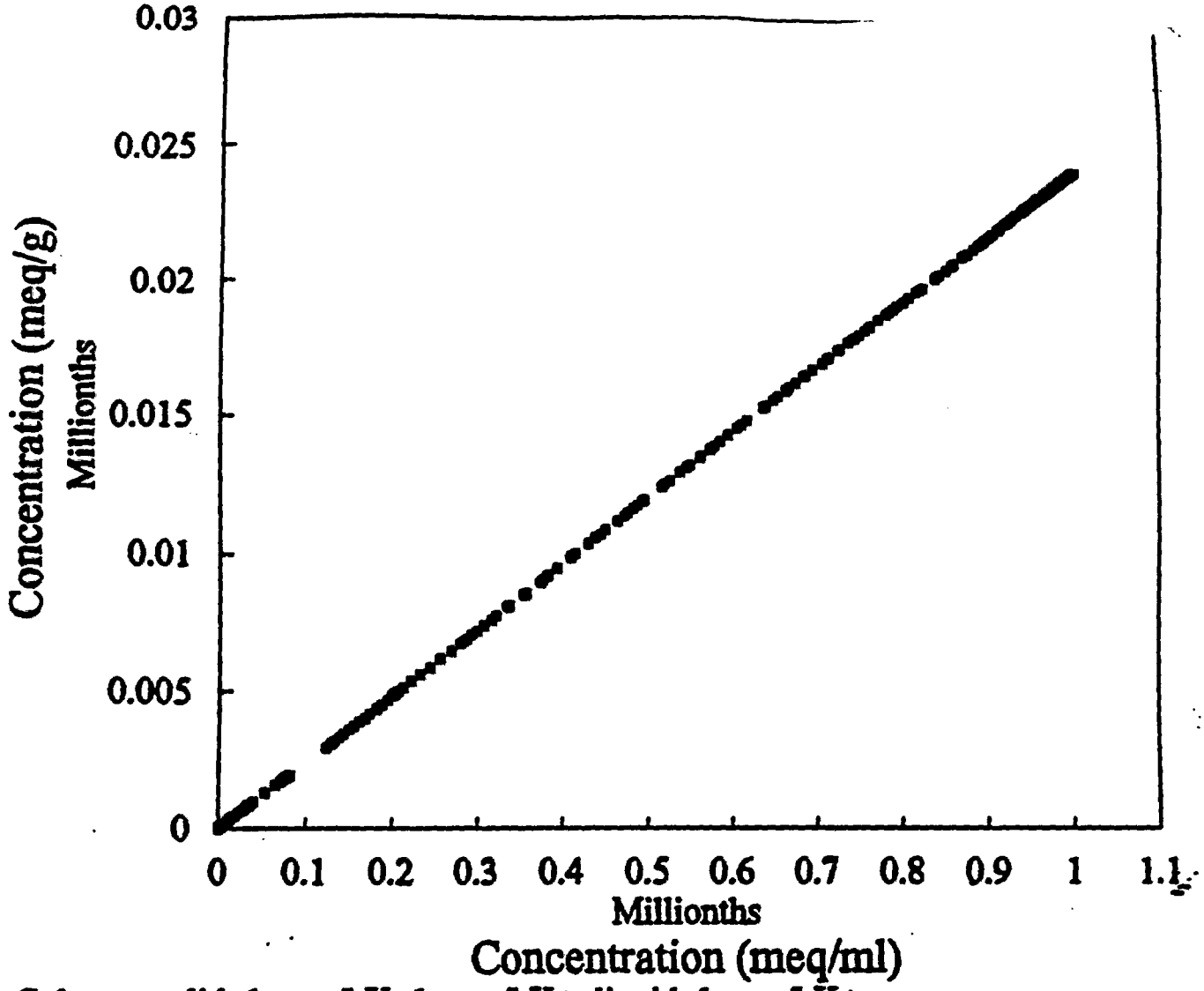

Column: solid, 1 meq/l X- 1 meq/l K+; liquid, 1 meq/l K+
Flushing solution: 0.001 meq/l Na+

D22

22

ion has not been established. Thus, in a solution with multiple species, the competing ion could be a major, minor, or trace constituent. Furthermore, at the low temperatures at Yucca Mountain, certain ion exchange reactions may be kinetically inhibited, thus allowing less thermodynamically favorable reactions to control the system. The questions concerning competing ions will have to be addressed by experimentation.

The simulations done in this auxiliary analysis involved the binary system Na-K. Consequently, changes in one component could affect the other, as shown when the two components were in comparable concentrations. When the one component was in trace amounts relative to the other, its addition to the system did not affect the other. This resulted in a linear isotherm, and constant K_d values along the column. However, Reardon (1981) has shown that variations in the concentrations of a major component can affect the partitioning (K_d) of a trace component. Thus, in a system as complex as Yucca Mountain, it is crucial that DOE demonstrate that the (competing constituent) chemistry of the farfield is relatively constant over the lifetime of the repository. Otherwise, the application of the K_d approach would not be technically defensible.

There are a number of aspects to modeling radionuclide transport that can be tested using *PHREEQM*. In future phases of the IPA effort, the modeling should concern the effect of charge of the competing ions on migration, changes in water saturation, and solid substrate heterogeneity. It is recommended that the database, *PHREEDA*, used by this code, be expanded to include radionuclide information.

D.4. REFERENCES

Appelo, C.A.T. and A. Willemsen, "Geochemical Calculations and Observations on Salt Water Intrusions, I., A Combined Geochemical/Mixing Cell Model," *Journal of Hydrology*, 94:313-330 [1987].

Freeze, R.A. and J.A. Cherry, *Groundwater*, Englewoood Cliffs, N.J, Prentice Hall, Inc., 1979.

Meijer, A., "Yucca Mountain Project Far-Field Sorption Studies and Data Needs," Los Alamos National Laboratory, LA-11671-MS, September, 1990.

Meijer, A., "A Strategy for the Derivation and Use of Sorption Coefficients in Performance Assessment Calculations for the Yucca Mountain Site," *Proceedings of the DOE/Yucca Mountain Site Characterization Project Radionuclide Adsorption Workshop, September 11-12, 1990*, Los Alamos National Laboratory, LA-12325-C, August 1992.

Nuclear Regulatory Commission, "Site Characterization Analysis of the Department of Energy's Site Characterization Plan, Yucca Mountain Site, Nevada," Office of Nuclear Material Safety and Safeguards, NUREG-1347, October 1989.

Pabalan, R. T., "Nonideality Effects on the Ion Exchange Behavior of the Zeolite Mineral Clinoptilolite," *Material Research Symposium Proceedings*, 212:559-567 [1991].

Parkhurst, D.L., D.C. Thorstenson, and L.N. Plummer, "PHREEQE: A Computer Program for Geochemical Calculations," U.S. Geological Survey, Water Research Investigations 80-96, 1990.

Plummer, L.N., E. Busenberg, P.D. Glynn, and A.E. Blum, "Dissolution of Aragonite-Strontionite Solid Solutions in Nonstoichiometric $Sr(HCO_3)_2$-$Ca(HCO_3)_2$-CO_2-H_20 Solutions," *Geochimica et Cosmochimica Acta*, 56:3045-3072 [1992].

Reardon, E.J., "Kd's -- Can They Be Used to Describe Reversible Ion Sorption Reactions in Contaminant Migration?," *Groundwater*, 19:279-286 [1981].

Thomas, K., "Summary of Sorption Measurements Performed with Yucca Mountain, Nevada, Tuff Samples and Water from Well J-13," Los Alamos National Laboratory, LA-10960-MS, December 1987.

U.S. Department of Energy, "Site Characterization Plan, Yucca Mountain Site, Nevada Research and Development Area, Nevada," Nevada Operations Office/Yucca Mountain Project Office, Nevada, 9 vols., DOE/RW-0199, December 1988.

Vermeulen, T., Le Van, M. D., Hiester, N. K., and G. Klein, "Adsorption and Ion Exchange" in *Perry's Handbook of Chemical Engineering*, McGraw-Hill, 1987.

APPENDIX E

CONTENTS

		Page
E-1	Introduction	E-1
E-2	Relevant Literature	E-2
E-3	Description of Analyses	E-3
E-4	Analyses Results	E-5
E-4.1	Regional Model Results	E-5
E-4.2	Subregional Model Results	E-7
E-5	Conclusions	E-11
E-6	References	E-14

TABLES

E-1	Hydraulic Conductivities for the Model	E-5

FIGURES

E-1	Regional and Subregional Models, for *PORFLOW*, Depicting Location of Recharge and Constant Head Discharge Areas	E-4
E-2	Regional Model for *PORFLOW* Depicting Boundary Conditions and Various Hydraulic Conductivity Zones	E-6
E-3	Simulated Hydraulic Head Distribution in the Vicinity of Yucca Mountain, Under Assumed Present-Day Conditions	E-8
E-4	Water Table Rise at Yucca Mountain and Forty Mile Wash as a Function of Recharge Rate	E-9
E-5	Water Table Rise at Yucca Mountain and Forty Mile Wash as a Result of Increasing the Permeability Through the Barriers North and Northeast of the Site	E-10
E-6	Impact of the Intrusion of a Single Volcanic Dike Oriented N15°E on the Groundwater Flow Field Directly Below the Repository	E-12
E-7	Maximum Water Table Rise at Potential Repository Site as a Function of Dike Orientation	E-13

E-8 Impact of the Intrusion of Multiple Volcanic Dikes on the Groundwater Flow Field Directly Below the Repository E-14

APPENDIX E
REGIONAL FLOW ANALYSIS

M.P. Ahola/CNWRA and B. Sagar/CNWRA

E-1 INTRODUCTION

Assessing the overall long-term performance of the proposed high-level radioactive waste (HLW) geologic repository at Yucca Mountain requires predictions of the impact of postulated disruptive events occurring over the 10,000-year isolation period of regulatory interest. Such predictions will usually be made through the use of computer modeling techniques. One area that has received much recent attention is the likelihood, in the future, of significant rises in the water table beneath Yucca Mountain, because of possible events such as seismic activity, increased precipitation over the region, volcanic intrusions, or changes to existing hydrogeologic barriers. Such events could lead to, for instance, a significant change in the groundwater travel time through the unsaturated zone beneath the repository horizon, because of alterations in the unsaturated pathway.

As one of the auxiliary analyses in Iterative Performance Assessment (IPA) Phase 2, it was decided to simulate the flow field in the saturated unconfined region that contains Yucca Mountain. The specific objective of this analysis is to study the fluctuations in the water table in response to postulated changes in recharge rates and other modifications in geohydrologic structures. The simulations were conducted both on a regional scale as well as a smaller scale, (i.e., the scale of Yucca Mountain). The regional-scale analysis provided the boundary conditions for the simulations of the saturated zone in the subregional model. A full discussion of this analysis and results is given in a recent report by Ahola and Sagar (1992).

Because of the limited objective of the analysis presented in this report, no attempt was made to estimate the probability of occurrence of such events mentioned above. Only data that were readily available from other published reports were used. Also, some parameter values were taken from other published reports (e.g., Rice, 1984; Waddell, 1982; and Czarnecki, 1985) without verifying their accuracy. Consequently, the analysis results should be considered as very preliminary and likely to change when more accurate field data are used in the simulations. Final analyses should also verify the accuracy of existing data taken from other published sources. In addition, evapotranspiration and modifications in surface runoff were not considered in this modeling effort.

The simulation results pertain to a two-dimensional (2-D) regional [about 250- by 250-kilometer] and subregional [50- by 50-kilometer area], and saturated groundwater flow analysis beneath Yucca Mountain and the surrounding area. For this application, *PORFLOW* (Runchal and Sagar, 1989; Sagar and Runchal, 1990), an integrated finite difference code, was modified (Version 1.11) to incorporate the free surface (water table) in a groundwater flow model. The model was set up in the *x-y* (horizontal) plane, and allowed for specification of recharge and discharge areas. An approximate model of the regional groundwater flow system around Yucca Mountain was first developed for the *PORFLOW* code. Once this was completed, various conditions were postulated, such as increasing the recharge to simulate future climatic changes that might take place in the geohydrologic basin containing Yucca Mountain.

E-2 RELEVANT LITERATURE

A brief summary of relevant literature pertinent to saturated zone modeling that was reviewed for this study follows. For this study, a comprehensive literature review of all hydrologic studies in the Yucca Mountain area was not conducted. A more detailed discussion of previous studies of the saturated-zone hydrology is given by Ahola and Sagar (1992), and can also be found in the U.S. Department of Energy's Site Characterization Plan (SCP) (see "Hydrology" (Chapter 3) in DOE, 1988). The purpose of this review was mainly to determine what other modeling studies were conducted to simulate the regional saturated hydrology, and to use the results and data (i.e., hydraulic conductivities and boundary conditions) from such studies for the *PORFLOW* analysis. These previous studies were more comprehensive in that their models were calibrated on measured heads. For this study, no model calibration was done; rather, parameter values from previous studies were adopted.

Waddell (1982) conducted flow modeling on a regional basis for the Nevada Test Site and vicinity. The main goals of his investigation were:

- To estimate fluxes for use in predictions of transport of radionuclides; and
- To study the effects of uncertainty in model parameters on these estimates.

Waddell (1982) used a horizontal 2-D finite-element model consisting of 685 nodes. The model encompassed an area approximately 175 by 175 kilometers, the boundaries of which were taken mainly along topographic highs to the north and east, and topographic lows to the southwest. For model calibration, a numerical parameter-estimation technique was used in which parameters such as transmissivities, groundwater sources, and sinks were derived throughout the modeled area such that the weighted sum of the squared residuals (observed head minus simulated head) was minimized. An iteration scheme was used to minimize the weighted sum of squared residuals by successive approximation to model parameters. It was generally found that absolute values of residuals were less than 30 meters.

Czarnecki and Waddell (1984) developed a smaller subregional horizontal finite-element model of the groundwater flow system in the vicinity of Yucca Mountain also using parameter estimation techniques. This model was formulated as a portion of the regional model conducted by Waddell (1982). Some of the boundaries for this subregional model were taken along groundwater barriers from the larger regional model. The remaining boundaries had either specified pressure heads or fluxes, which were calculated from the regional model. The purpose of this subregional model study was to gain a better understanding of the groundwater flow system beneath the Yucca Mountain area. Czarnecki (1985) used this same 2-D finite-element subregional model to assess the potential effects of changes in future climatic conditions on the groundwater system in the vicinity of Yucca Mountain. He found that the simulated position of the water table rose as much as 130 meters near the primary repository area at Yucca Mountain for a simulation involving a 100 percent increase in precipitation compared with current conditions. The average increase in recharge for the case of this 100 percent increase in annual precipitation was set at 15 times the modern-day recharge rate in all areas of his model. This water table rise was caused primarily by the increase in recharge, applied to Forty Mile Wash to the east of Yucca Mountain, by a factor of 15 times the baseline rate of 0.41 meters/year. For a factor of 10 increase in flux into the model, Czarnecki shows an increase in hydraulic head near Yucca Mountain of approximately 100 meters. Flooding on the primary repository area would require a water table rise of at least 300 meters.

Rice (1984) also developed a 2-D regional hydrologic model for the saturated flow system surrounding Yucca Mountain. A finite-difference grid consisting of 5600 nodes in the *x-y* plane was used for the simulations. The flow system was modeled under confined conditions, and only horizontal flow was allowed. Model calibration was accomplished by adjusting the transmissivities, within reasonable limits, to minimize the difference between the hydraulic heads simulated by the model and hydraulic heads measured at well locations. Results of simulated heads compared well with U.S. Geological Survey (USGS)-interpreted head distribution, based on well observations.

E-3 DESCRIPTION OF ANALYSES

Conceptual Models and Data: The conceptual models for these analyses consisted of both a regional model [approximately 250 by 250 kilometers], and a subregional model [50 by 50 kilometers], set up in the *x-y* (horizontal) plane, as shown in Figure E-1. Provision was made to allow for specification of recharge and discharge areas in the model. The primary recharge was assumed to occur on outcrops at higher elevations, as shown in Figure E-1. Current estimates of recharge in these areas range from approximately 7 to 200 millimeters/year, depending primarily on the land surface elevation, as given by Rice (1984). Although Figure E-1 shows only the general areas where recharge was applied, the specific values of recharge increased with elevation, with the highest values occurring in regions of snow accumulation. Discharge areas included Alkali Flats and the Furnace Creek Ranch, which were modeled as fixed head boundaries. Mathematical boundary conditions for the regional model consisted of both fixed pressures and no-flow boundaries; these boundary conditions were chosen to be consistent with the physical boundaries (Figure E-1). The regional and subregional models consisted of 13,161 and 18,225 finite difference computational cells, respectively. Each grid cell in the regional model was 2.5 kilometers on a side, encompassing an area of 6.25 kilometers^2. The grid cells for the subregional model ranged from 100 meters on a side near the center to 2.5 kilometers on a side near the outer edges. The boundary conditions for this model consisted only of fixed pressures that were obtained from the simulation results of the larger regional model. The hydrological data for the simulations were obtained from the review of previously published studies (Rice, 1984; Waddell, 1982; Waddell *et al.*, 1984; Czarnecki and Waddell, 1984; and Czarnecki, 1985).

The entire modeled region was divided into zones having one of eight possible values for the hydraulic conductivity as shown in Figure E-2 and listed in the following. These hydraulic conductivities varied over several orders of magnitude, and were estimated from transmissivity data published by Rice (1984). The model contains a low permeability zone north and northeast of Yucca Mountain indicated in Figure E-2 by Zones 1 and 2 (i.e., hatched regions in the area of Yucca Mountain and Yucca Flats) for simulating the present-day high hydraulic gradient at that location. The actual cause of the steep gradient is not yet fully known.

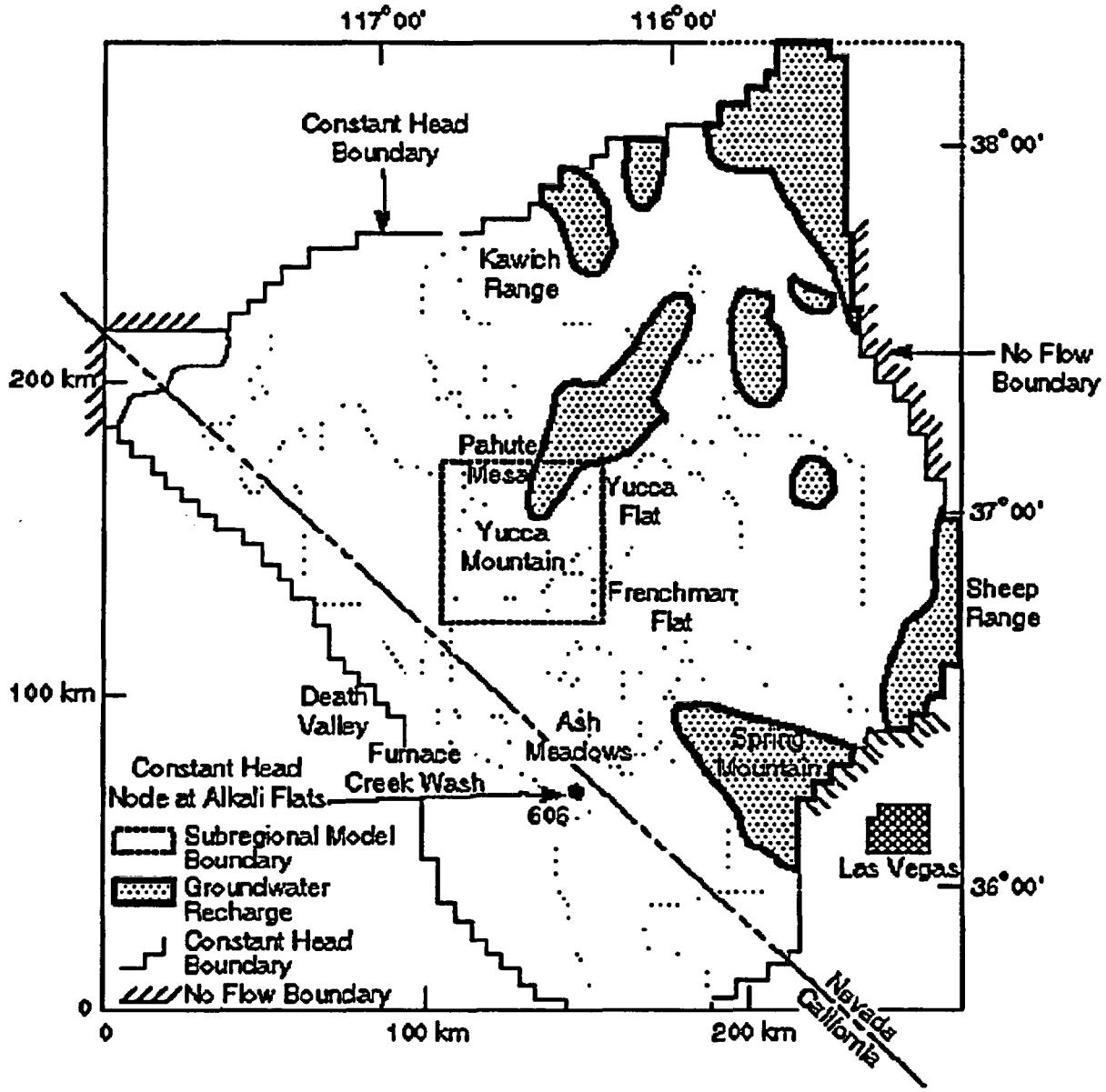

Figure E-1. Regional and subregional models, for PORFLOW, depicting location of recharge and constant head discharge areas (modified from Rice, 1984).

Table E-1. Hydraulic Conductivities for the Model

Zone Number	*Hydraulic Conductivity (meters/second*
1	5.80E-08
2	6.34E-07
3	3.49E-06
4	8.69E-06
5	3.47E-05
6	1.00E-04
7	6.00E-04
8	3.50E-03

To conduct the study, *PORFLOW* was modified (Version 1.11) to incorporate the free surface (water table) in a groundwater flow model. The free-surface boundary condition and approximations (e.g., Dupuit) used in the modifications to *PORFLOW* are described in Bear (1972). Ahola and Sagar (1992) provide a detailed discussion of the specific modifications to *PORFLOW*. In essence, the model allowed 2-D flow in the horizontal plane, with the height of the water table adjusted such that the water pressure along this boundary is just equal to zero.

E-4 ANALYSES RESULTS

E-4.1 Regional Model Results

For the regional analysis, a steady-state solution to the flow system was first obtained to represent the present-day conditions under normal precipitation and groundwater recharge. Figure E-3 shows a portion of the simulated regional water table in the area of interest under assumed modern-day recharge. Yucca Mountain is indicated by the small rectangular box in this figure and represents approximately two grid nodes in the regional model [250 by 250 kilometers] because of the 2.5 kilometer grid node spacing. Thus, on the Yucca Mountain scale, the regional model is quite coarse. Based on the simulation, one can see the steep hydraulic gradient to the north and northeast of Yucca Mountain, which is comparable to results obtained in previous studies. It should be noted, however, that no calibration of this model was conducted for this study. The results are based on the use of data published from previously calibrated models. Since the results appeared consistent with previous studies and our objective was to focus more on relative changes in the water table rather than on the absolute water table elevation itself, they were deemed acceptable for use as a base case or initial state for analyzing the effects of various postulated disruptive conditions.

One possible condition that could occur over the 10,000-year isolation period for a repository at Yucca Mountain would be increased precipitation and groundwater recharge throughout the region. Such groundwater recharge is thought to be greatest in the higher elevations where there is more precipitation and outcropping of the basement rock. Figure E-4 shows a relationship between increased recharge and

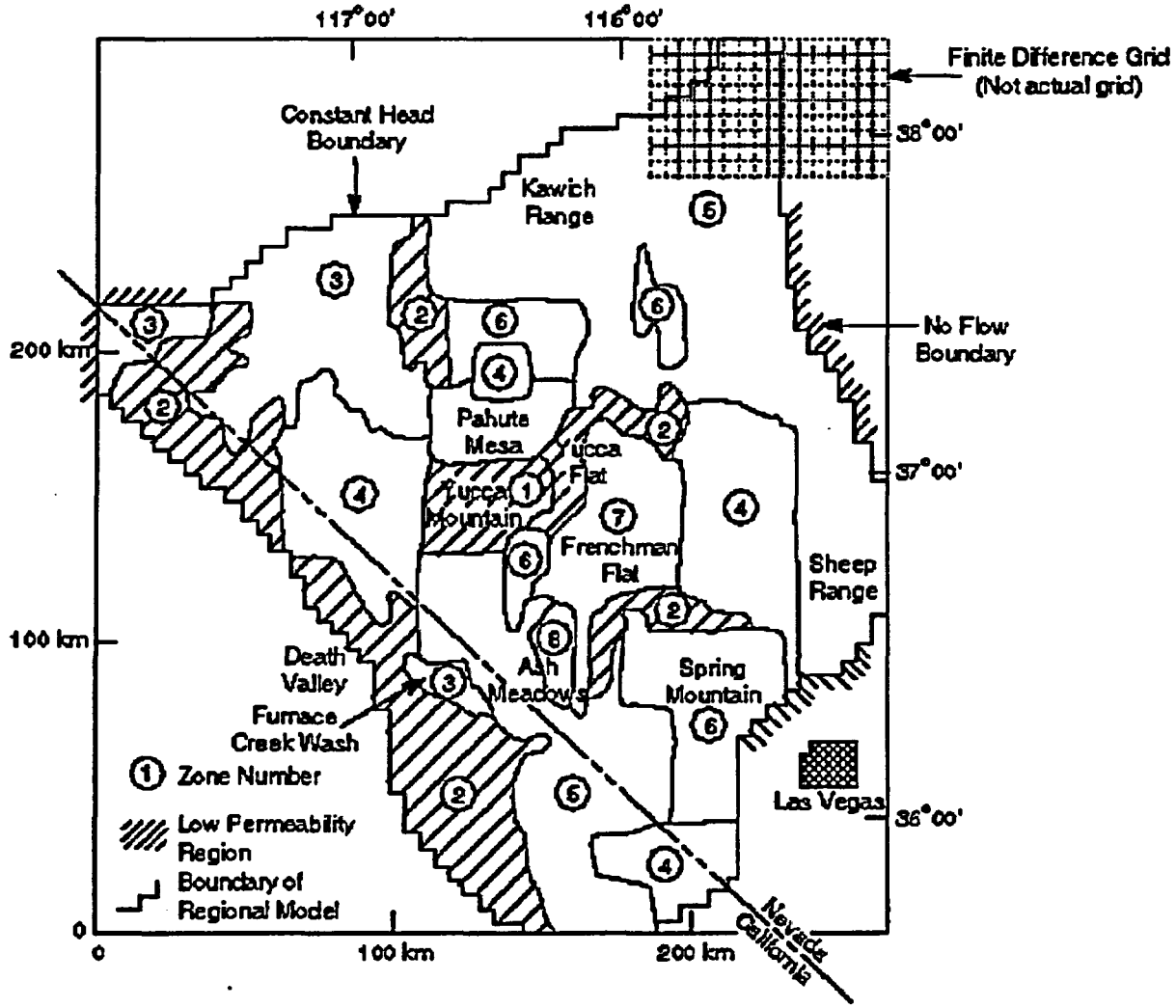

Figure E-2. Regional model for PORFLOW depicting boundary conditions and various hydraulic conductivity zones (modified form Rice, 1984).

water table rise at nodal points in the vicinity of Yucca Mountain and 5 kilometers to the east, at Forty Mile Wash. The numbers representing increase in recharge, as shown on the *x*-axis, are multipliers of the baseline (present-day) flux. The recharge is applied over those shaded regions indicated in Figure E-1. The results show a more or less linear relationship between the two parameters. In general, from the transient analysis, a larger increase in recharge resulted in a longer period of time in which the groundwater flow field reached steady state. For instance, the simulated water table configuration took approximately 400 years to equilibrate, when the recharge was increased 10 times, and 700 years to equilibrate when the recharge was increased 20 times. Czarnecki (1985) states that a 100 percent increase in annual precipitation over the region would correspond to an increase in groundwater recharge of approximately 15 times the present-day recharge rate. From Figure E-4, this would correspond to a water table rise at Yucca Mountain of approximately 65 meters. It is likely that a 100 percent increase in annual precipitation would be a conservative upper bound, based on geologic evidence at the site of past climatic conditions. Czarnecki (1985) found that, in addition, increasing the recharge into Forty Mile Wash above a small annual baseline recharge had a significant effect on the water table rise near Yucca Mountain, primarily because of its close proximity. It is conceivable that increased precipitation in the higher elevations would cause greater runoff into Forty Mile Wash, for example, and consequently greater recharge. The results shown in Figure E-4, however, assume no recharge into Forty Mile Wash.

As another potentially disruptive condition, it was postulated that future tectonic activity throughout the Basin and Range region could result in slip or opening of fractures through the areas north and northeast of Yucca Mountain, where large hydraulic gradients exist, and increase the flow toward Yucca Mountain. Although the exact cause is not well understood, it is thought that these large gradients may be because a low-permeability geologic unit has been juxtapositioned against a high-permeability unit, or perhaps that large lateral tectonic stresses within this region have closed existing north-south trending fractures. This condition was simulated in the regional model by increasing, to various degrees, the permeabilities through the previous low permeability regions just to the north (Zone 1) and northeast (Zone 2) of Yucca Mountain, as shown in Figure E-2.. The relationship between the increase in permeability through these two zones and the subsequent rise in the water table at nodal points near Yucca Mountain and Forty Mile Wash is shown in Figure E-5. The numbers along the *x*-axis represent multipliers of the assumed present-day permeabilities in the two zones directly north and northeast of the Yucca Mountain repository site. Figure E-5 shows that a fairly substantial rise in the water table can be expected for even a factor of 10 increase in the permeability of these two zones. If the permeability of these two zones is increased to a value representative of the hydraulic conductivity of Zone Number 7 (Table E-1), which is approximately 1000 times greater, the modeling results show a water table rise in the area of Forty Mile Wash of approximately 200 meters. In this case, the steep gradient north and northeast of Yucca Mountain no longer exists.

E-4.2Subregional Model Results

To study the impact of volcanic dike intrusions occurring directly beneath Yucca Mountain in more detail, an analysis was conducted using a smaller-scale subregional model. These dikes were assumed to be approximately 4 kilometers in length and to extend vertically through the saturated zone. For these simulations, the regional model was too coarse. The location of the subregional model is depicted by the dashed rectangular region in Figure E-1. The finite-difference grid encompassed an area of 50 by 50 kilometers. The grid cells were 100 meters on a side near the center of the mesh, where the volcanic dikes were assumed to be located. At the outer boundaries of the model, the largest grid cells were 2.5 kilometers on a side, which corresponded to the size of the grid cells for the regional model. The

Figure E-3. **Simulated hydraulic head distribution in the vicinity of Yucca Mountain, under assumed present-day conditions.**

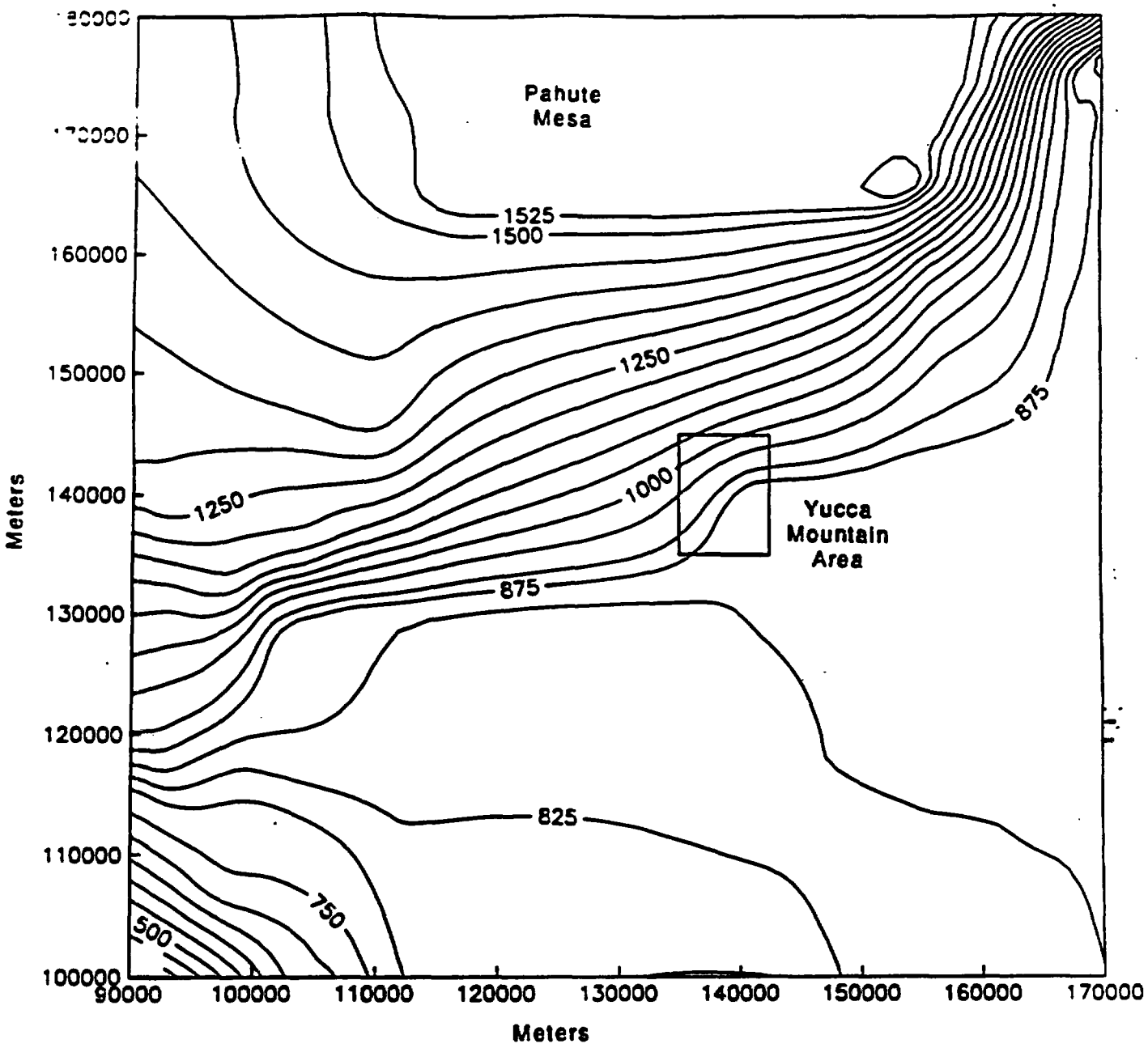

Simulated hydraulic head distribution in the vicinity of Yucca Mountain under assumed present-day conditions

Figure E-4. Water table rise at Yucca Mountain and Forty Mile Wash as a function of recharge rate.

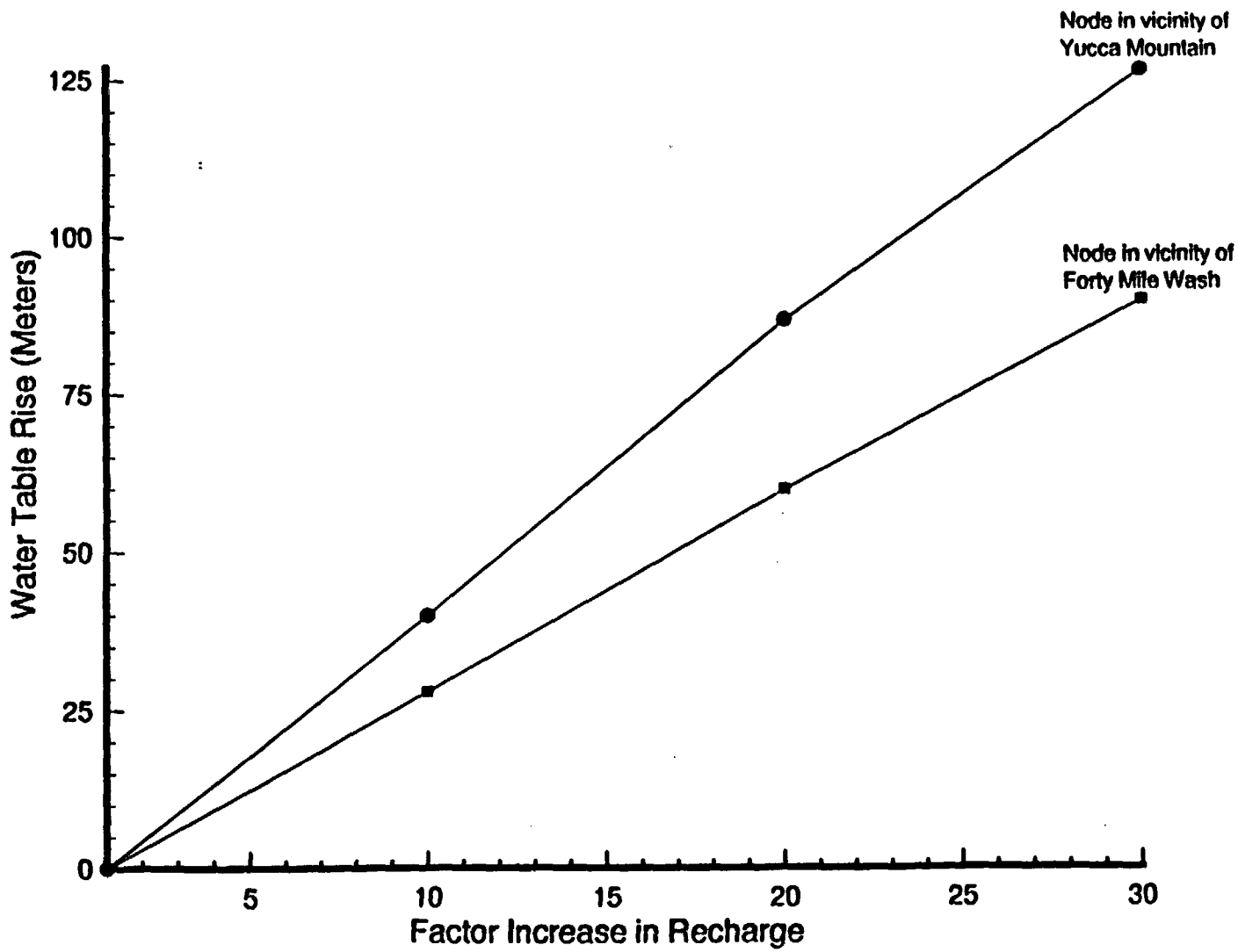

Water table rises at Yucca Mountain and Forty Mile Wash as a function of increased recharge rate

Figure E-5. **Water table rise at Yucca Mountain and Forty Mile Wash as a result of increasing the permeability through the barriers north and northeast of the site.**

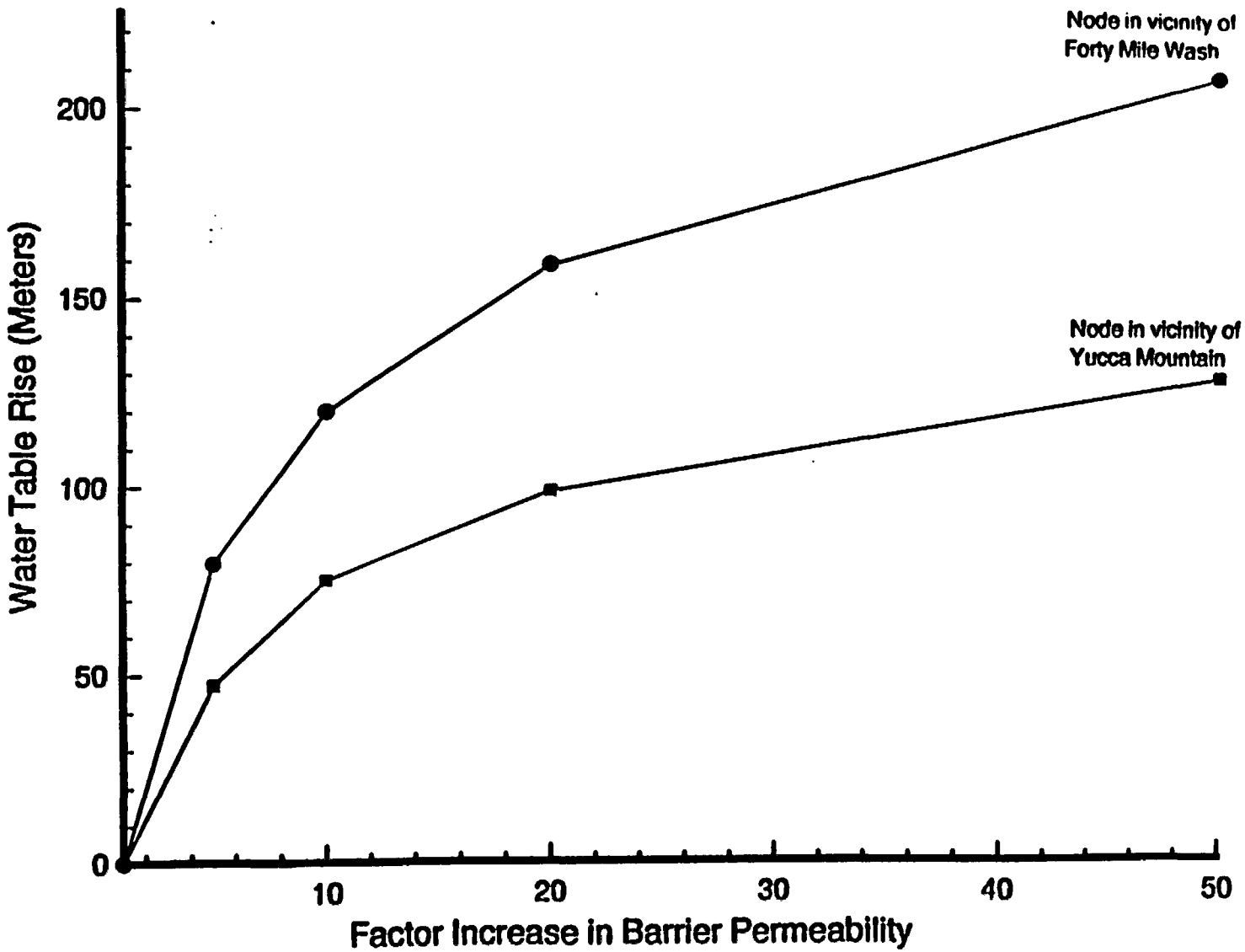

Water table rise at Yucca Mountain and Forty Mile Wash as a result of increasing the permeability through the barrier north and east of the site

boundary conditions along all four sides of this model consisted of fixed pressures obtained from corresponding nodes in the regional model. Linear interpolation was done to assign values of pressure to those additional nodes along the boundary of the subregional model as a result of refining the mesh. These fixed boundary pressures corresponded to the baseline (or current) water table configuration from the regional model.

No attempt was made to take into account the effect the temperature of the intruding dike might have on the saturated zone. The narrow dikes essentially acted as dams within the flow field, and were assumed to extend through the water table and well above any potential water table rise. They were created by specifying a very low permeability along lines one gridpoint in thickness and 4 kilometers in length. Figure E-6 shows the velocity vectors and several streamlines (dark solid lines) depicting the groundwater flow field directly beneath Yucca Mountain, for the case of a single dike oriented N15°E, where the north direction is to the top of the plot. Based on the existing fracture and faulting pattern at Yucca Mountain, it is believed that this could be a likely orientation for a possible dike intrusion. Figure E-6 shows that to the left of the dike, the flow field can be seen to be directed toward the south. Around the lower tip of the dike, some of the flow is directed back to the north. Without the presence of the dike, the flow through this area is primarily east and southeast. The small circle in this figure indicates the location where the maximum water table rise occurred, which in this case was 79 meters. Even though the groundwater travel time through the unsaturated zone would be somewhat decreased, the travel time in the saturated zone could be substantially increased, especially for the portion of the radionuclide inventory that entered the saturated zone on the left side of the dike. Figure E-7 shows the numerical simulation results for the water table rise at the repository site for various dike orientations. The figure suggests that a dike oriented roughly north to northeast would produce the maximum water table rise for a single dike intrusion.

Figure E-8 shows the intrusion of a second dike, which is perpendicular to the one shown in Figure E-6. This case was simulated because it is believed to be not uncommon for volcanic dikes to occur in pairs at more or less perpendicular orientations. Interestingly, Figure E-8 shows the dikes create stagnant pools of water which again may increase the length of the flow path in the saturated zone to the accessible environment. The maximum water table rise for this case of two perpendicular dikes was 103.4 meters.

E-5 CONCLUSIONS

A summary of the results from both a regional and subregional groundwater-flow analysis of the saturated zone surrounding Yucca Mountain, using the *PORFLOW* finite difference code, is presented. These results show the effects of various disruptive conditions on the water table elevations and resulting groundwater-flow directions near the proposed HLW repository. The results give an indication of what conditions would have a minimal impact on the saturated zone hydrology near the site, and those that would have a major impact. A rise in water table in the area of Forty Mile Wash was calculated to be greater than 200 meters, based on certain disruptive conditions simulated using the regional model. Because evapotranspiration and surface runoff were neglected, the actual rise would be less than calculated. In addition, the subregional model analysis showed a rise in the water table near the repository ranging from a few meters to as much as 103 meters, depending on the orientation of the simulated volcanic dikes.

The results presented here are meant to be preliminary and likely to change as site characterization studies

Figure E-6. Impact of the intrusion of a single volcanic dike oriented N15°E on the groundwater flow field directly below the repository.

Figure E-7. Maximum water table rise at potential repository site as a function of dike orientation.

Figure E-6. Impact of the intrusion of a single volcanic dike oriented N15°E on the groundwater flow field directly below the repository.

Figure E-7. Maximum water table rise at potential repository site as a function of dike orientation.

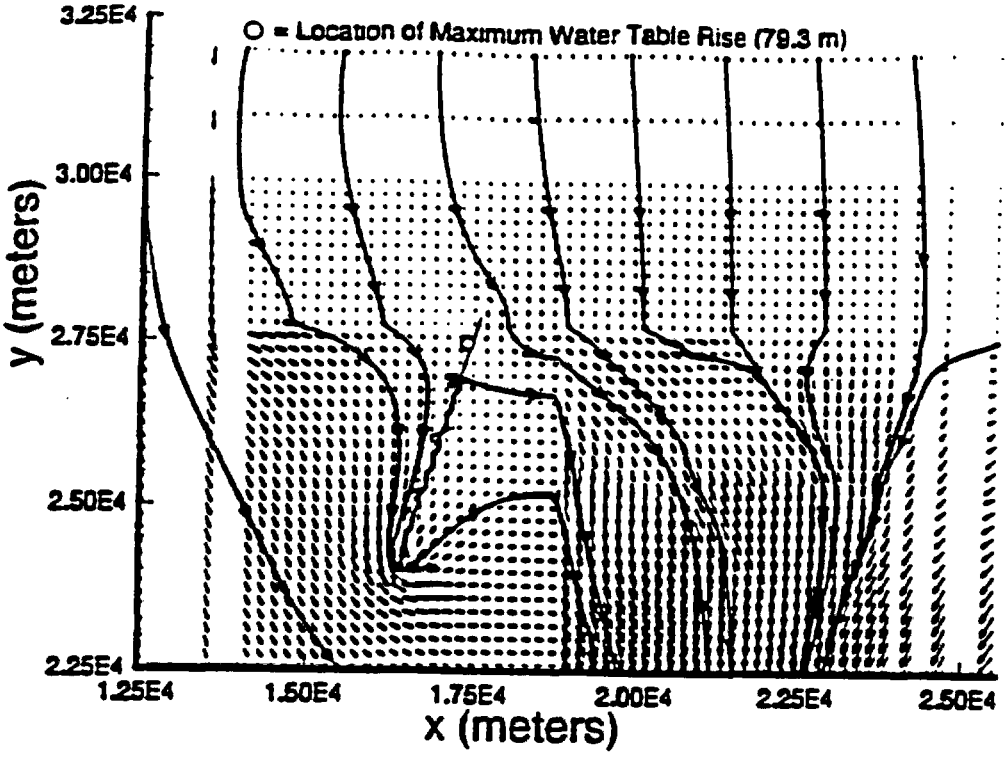

E6

~~Figure 4-6~~ Impact of the intrusion of a single volcanic dike oriented N15°E on the groundwater flow field directly below the repository. The straight line indicates the location of the dike.

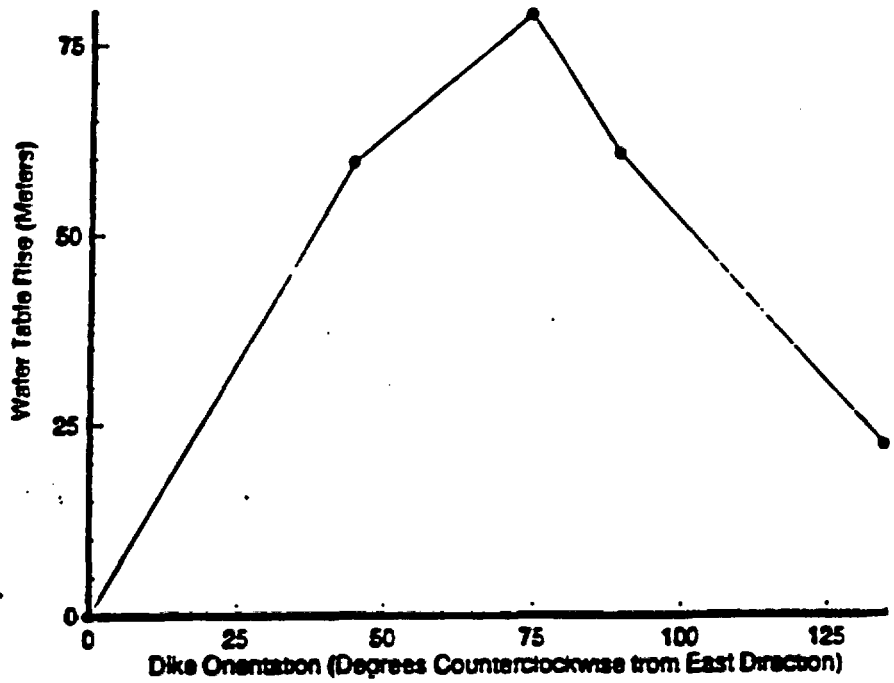

E7

~~Figure 4-7~~. Maximum water table rise at potential repository site as a function of dike orientation

Figure E-8. **Impact of the intrusion of multiple volcanic dikes on the groundwater flow field directly below the repository. The straight lines indicate the location of the dikes.**

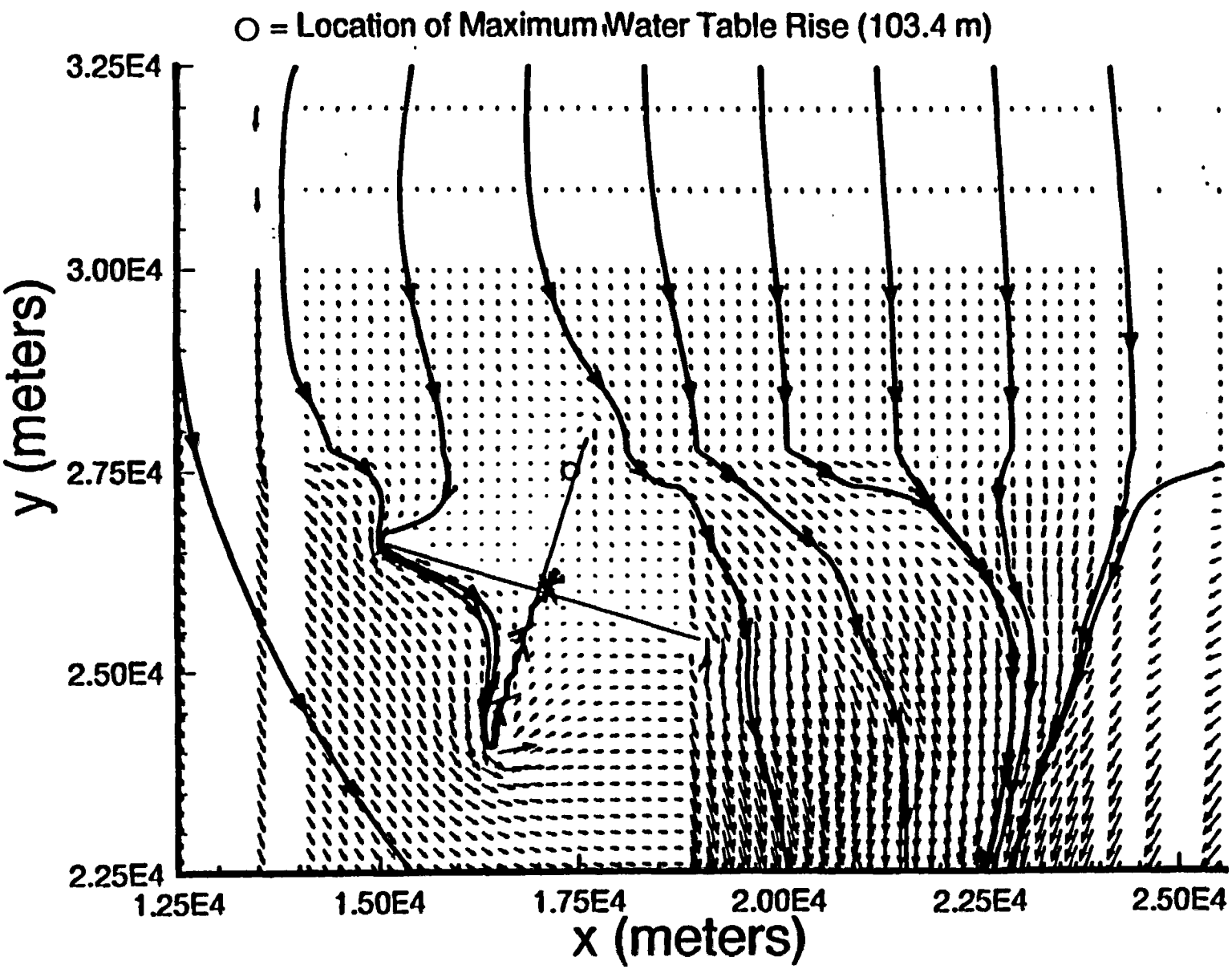

Impact of the intrusion of multiple volcanic dikes on the groundwater flow field directly below the repository

at Yucca Mountain provide more accurate hydrological parameters and better information on which disruptive conditions would be more likely to occur in the future. Also, some of the assumptions in this analysis could be improved in future studies. For instance, with respect to the high water table rises predicted, the formation of new discharge areas that such rises may cause was completely neglected.

E-6 REFERENCES

Ahola, M.P., and B. Sagar, "Regional Groundwater Modeling of the Saturated Zone in the Vicinity of Yucca Mountain, Nevada," Nuclear Regulatory Commission, NUREG/CR-5890, October 1992. [Prepared by the Center for Nuclear Waste Regulatory Analyses.]

Bear, J., *Dynamics of Fluids in Porous Media*, New York, Dover Publications, Inc., 1974.

Czarnecki, J.B., "Simulated Effects of Increased Recharge on the Groundwater Flow System of Yucca Mountain and Vicinity, Nevada-California," U.S. Geological Survey, Water-Resources Investigations Report, WRI-84-4344, 1985.

Czarnecki, J.B., and R.J. Waddell, "Finite-Element Simulation of Groundwater Flow in the Vicinity of Yucca Mountain, Nevada-California, "U.S. Geological Survey, Water Resources Investigations Report, WRI-84-4349, 1984.

Rice, W.A., "Preliminary Two-Dimensional Regional Hydrologic Model of Nevada Test Site and Vicinity," Sandia National Laboratories, SAND83-7466, 1984. [Prepared for the U.S. Department of Energy/Office of Civilian radioactive Waste Management.]

Runchal, A.K., and B. Sagar, "PORFLOW: A Mathematical Model for Fluid Flow, Heat, and Mass Transport in Variably Saturated Geologic Media (Users Manual - Version 1.0), Richland, WA, Westinghouse Hanford Company, WHC-EP-0041, 1989.

Sagar, B., and A.K. Runchal, "PORFLOW: A Mathematical Model for Fluid Flow, Heat, and Mass Transport in Variably Saturated Geologic Media -- Theory and Numerical Methods Version 1.0," Richland, WA, Westinghouse Hanford Company, WHC-EP-0042, 1990.

U.S. Department of Energy, "Site Characterization Plan, Yucca Mountain Site, Nevada Research and Development Area, Nevada," Nevada Operations Office/Yucca Mountain Project Office, Nevada, 9 vols., DOE/RW-0199, December 1988.

Waddell, R.K., "Two-Dimensional, Steady-State Model of Ground Water Flow, Nevada Test Site and Vicinity, Nevada-California," U.S. Geological Survey Water-Resources Investigations Report, WRI-82-4085, 1982.

Waddell, R.K., J.H. Robison, and R.K. Blankennagel, "Hydrology of Yucca Mountain and Vicinity, Nevada-California: Investigative Results Through Mid-1983," U.S. Geological Survey Water Resources Investigation Report, WRI-84-4267, 1984.

at Yucca Mountain provide more accurate hydrological parameters and better information on which disruptive conditions would be more likely to occur in the future. Also, some of the assumptions in this analysis could be improved in future studies. For instance, with respect to the high water table rises predicted, the formation of new discharge areas that such rises may cause was completely neglected.

E-6 REFERENCES

Ahola, M.P., and B. Sagar, "Regional Groundwater Modeling of the Saturated Zone in the Vicinity of Yucca Mountain, Nevada," Nuclear Regulatory Commission, NUREG/CR-5890, October 1992. [Prepared by the Center for Nuclear Waste Regulatory Analyses.]

Bear, J., *Dynamics of Fluids in Porous Media*, New York, Dover Publications, Inc., 1974.

Czarnecki, J.B., "Simulated Effects of Increased Recharge on the Groundwater Flow System of Yucca Mountain and Vicinity, Nevada-California," U.S. Geological Survey, Water-Resources Investigations Report, WRI-84-4344, 1985.

Czarnecki, J.B., and R.J. Waddell, "Finite-Element Simulation of Groundwater Flow in the Vicinity of Yucca Mountain, Nevada-California, "U.S. Geological Survey, Water Resources Investigations Report, WRI-84-4349, 1984.

Rice, W.A., "Preliminary Two-Dimensional Regional Hydrologic Model of Nevada Test Site and Vicinity," Sandia National Laboratories, SAND83-7466, 1984. [Prepared for the U.S. Department of Energy/Office of Civilian radioactive Waste Management.]

Runchal, A.K., and B. Sagar, "PORFLOW: A Mathematical Model for Fluid Flow, Heat, and Mass Transport in Variably Saturated Geologic Media (Users Manual - Version 1.0), Richland, WA, Westinghouse Hanford Company, WHC-EP-0041, 1989.

Sagar, B., and A.K. Runchal, "PORFLOW: A Mathematical Model for Fluid Flow, Heat, and Mass Transport in Variably Saturated Geologic Media -- Theory and Numerical Methods Version 1.0," Richland, WA, Westinghouse Hanford Company, WHC-EP-0042, 1990.

U.S. Department of Energy, "Site Characterization Plan, Yucca Mountain Site, Nevada Research and Development Area, Nevada," Nevada Operations Office/Yucca Mountain Project Office, Nevada, 9 vols., DOE/RW-0199, December 1988.

Waddell, R.K., "Two-Dimensional, Steady-State Model of Ground Water Flow, Nevada Test Site and Vicinity, Nevada-California," U.S. Geological Survey Water-Resources Investigations Report, WRI-82-4085, 1982.

Waddell, R.K., J.H. Robison, and R.K. Blankennagel, "Hydrology of Yucca Mountain and Vicinity, Nevada-California: Investigative Results Through Mid-1983," U.S. Geological Survey Water Resources Investigation Report, WRI-84-4267, 1984.

APPENDIX F

CONTENTS

Page

F-1. Introduction F-1

F-2. Description of Analyses F-2

F-3. Analyses Results and Discussion F-5

F-4. Conclusions F-9

F-5. References F-11

TABLES

F-1. Values of Spatially Variable Hydraulic Parameters F-4

FIGURES

F-1. Computational Grid F-3

F-2. Pressure Profiles for q_o = 1 millimeter/year F-6

F-3. Pressure Profiles for q_o = 50 millimeters/year F-7

F-4. Pressure Profiles for q_o = 50 millimeters/year and a Dip Angle of 6° F-8

F-5. *X-Z* Plane Flux Vector and Particle Plot F-10

APPENDIX F
EFFECTS OF STRATIFICATION, DIP OF STRATA, AND SUB-VERTICAL FAULTS

A.C. Bagtzoglou/CNWRA, R. Ababou/CNWRA, and B. Sagar/CNWRA

F-1. INTRODUCTION

This section presents results of unsaturated flow simulations undertaken as an auxiliary analysis for the Iterative Performance Assessment (IPA) Phase 2 project, one of the approaches adopted by the Nuclear Regulatory Commission (NRC) staff to develop repository license application review capabilities. The effects of common geological features on flow in a two-dimensional (2-D) domain, such as inclined stratification and vertical or near-vertical fault zones intersecting the strata, are of importance. In this work, numerical analysis is performed for a deep [approximately 530 meters] hard rock system. The *BIGFLOW* numerical code (Bagtzoglou *et al.*, 1992) is used in these simulations. Some of the data (i.e., the depth to water table, the number of primary geologic strata, their dip angle, and the existence of a fault zone) for the analysis were taken from the Yucca Mountain project reports (Scott and Bonk, 1984), but were adjusted to enhance the effects under study. In particular, extreme net infiltration rates [up to 50 millimeters/year] and hydraulic properties similar to the Calico Hills nonwelded, vitric (Chnv) unit were considered. Therefore, conclusions regarding the suitability of Yucca Mountain for the proposed geologic repository for high-level radioactive waste are not directly derivable from this analysis. Recognizing that there are no simple, natural initial-boundary conditions that can be used for the more complex problems, a method of successive approximation is implemented. This method uses solutions of auxiliary flow problems to set up pressure boundary conditions for the more complex problems. This is necessary because, in practice, no natural boundaries exist (or are adequately defined), especially in the lateral directions. The investigation is limited to three-dimensional (3-D) simulations in a vertical, thin slice, cross-section, with dipping strata intersected by a subvertical fault zone. The simulations are performed in a transient mode to study the manner in which the solutions of the flow equation approach steady state. A "wet," in terms of perceived net infiltration rates, hydro-climatic condition corresponding to a net annual infiltration rate of 50 millimeters/year is modeled. A hypothetical test problem is developed to study the effects of bedding, presence of a subvertical fault, and inclination of the beds.

The *BIGFLOW* simulation code accommodates 3-D transient or steady flow in saturated, or partially saturated, porous media with heterogeneous or spatially random hydrodynamic coefficients. For partially saturated flow, a mixed variable formulation of Richards' equation is used. That is:

$$\frac{\partial \theta(h,x)}{\partial t} = \nabla \left[K\,(h,x)\,(\nabla h + g) \right] \qquad \text{(F-1)}$$

where h is pressure head (meters), θ is volumetric water content (meters^3/meters^3), K is

hydraulic conductivity (meters/second), and g is the body force unit vector aligned with, and opposed to, the acceleration of gravity. The differential equations are discretized by an implicit finite difference scheme, two-point backward Euler in time, and seven-point centered in space. The spatial mesh is a regular rectangular lattice. The time step is generally variable and self-adjusted. The computational domain is a 3-D parallelepiped, whose coordinate system may be inclined at arbitrary angles with respect to the natural, horizontal-vertical coordinate system.

F-2. DESCRIPTION OF ANALYSES

The hydrogeologic properties in the unsaturated zone of Yucca Mountain, Nevada, were considered in order to represent, to some degree, the general features of the site in the simulations. Yucca Mountain consists of a series of North-trending fault-block ridges composed of strata of volcanic ash tuffs that generally have a regional dip of 5° to 7° to the East (Scott and Bonk, 1984). The proposed repository area is also bounded by steeply dipping faults or by fault zones, and is transected by a few normal faults. Therefore, it is important to study the effects of stratification, regional dipping, and fault zones on unsaturated water flow.

In the simulations presented herein, the computational domain is assumed to consist of five strata with approximately equal thicknesses spanning a total depth of 530 meters at which depth the water table is assumed to be located. The computational domain used in these simulations is based on a 3-D cartesian grid system. The axes of this system are aligned with East-West (x-axis), North-South (y-axis), and vertical (z-axis). The dimensions of the computational domain are 1230 meters, 80 meters, and 530 meters in the x-, y-, and z-directions, respectively. The domain is discretized into 29 by 5 by 54 nodes, comprising a total of 7830 nodes (Figure F-1).

The functional forms of pressure-dependent hydraulic conductivity and water content used herein are the exponential Gardner model for $K(h)$ and the van Genuchten model for $\theta(h)$. The exponential conductivity model is:

$$K(h) = K_s \exp\left[\alpha(h - h_b)\right] \qquad \text{if } h \le h_b$$

$$K(h) = K_s \qquad \text{if } h > h_b \tag{F-2}$$

where K_s is the saturated hydraulic conductivity, α is a characteristic inverse length scale or capillary diffusivity (Ababou, 1991), h is the pressure, and h_b is the air-entry pressure. The van Genuchten model for the retention curve is:

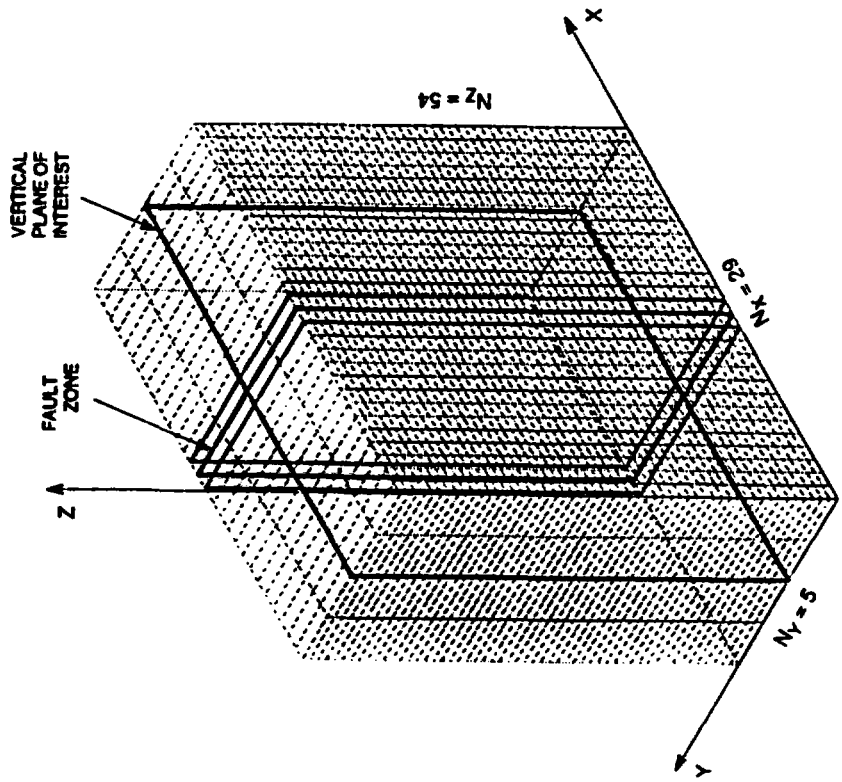

Figure F-1. Computational Grid.

$$\theta(h) = \theta_r + (\theta_s - \theta_r)\left[1 + (-\beta h)^n\right]^{-m} \tag{F-3}$$

where θ_s and θ_r are the saturated and residual moisture contents, respectively, β is a characteristic inverse length (similar to α in Equation (F-2)), and n and m are real exponents (dependent upon distribution of pore sizes) related by the Mualem constraint (Mualem, 1976).

All of the parameters in Equations (F-2) and (F-3) are, generally, spatially varying functions in all three dimensions. In the present work, however, they are assumed to be constant within a layer. Furthermore, the layer properties (K_s, α, h_b, and β) are assumed to be interchanging log-deviations around the geometric mean of each respective parameter [$\omega_G \exp(\pm\ \sigma_{\ln\omega})$], taken herein as representative of the Chnv unit. Thus, adjacent layers have a contrast in their hydraulic parameters equal to $\exp(2\sigma_{\ln\omega})$. The remaining matrix parameters are assumed to be constant in all strata, and are assigned typical values of the Chnv unit. Thus, θ_s = 44.11 percent, θ_r = 1.89 percent, n = 3.872, and m = 0.7417. The fault was arbitrarily modeled as a three-cell-wide, yz-planar zone located in the middle of the domain. The following table summarizes the hydraulic properties discussed above for the matrix layers and fault zone.

Table F-1. Values of Spatially Variable Hydraulic Parameters

Parameters	K_S *(m/d)*	α *(m^{-1})*	h_b *(m)*	β *(m^{-1})*
Geometric Mean ω_G	2.33×10^{-2}	2.2×10^{-2}	20	5×10^{-2}
Standard Deviation $\sigma_{\ln\omega}$	1.0	0.2	0.2	0.2
Fault Zone	9.32×10^{-1}	1.0×10^{-1}	10.417	9.6×10^{-2}

The values of these parameters, when substituted in Equation (F-2), yield different types of pressure-dependent curves *K(h)*. It is worthwhile noticing that the fault hydraulic conductivity is much greater than the matrix hydraulic conductivity near saturation, and remains higher for values of suction head up to about 50 meters. On the other hand, the fault becomes less conductive than the matrix for values of suction head significantly higher than 50 meters. The existence of a crossing point, where the fault becomes less permeable than the matrix, is of particular interest and, as will be shown later in this work, affects directly the overall behavior of the flow system. When parameter α_f is reduced threefold, a crossing point at a higher value of suction, ψ = 260 meters is attained. Note that, in terms of conductivities, this corresponds to a fault that is more like the porous matrix. Even though parameter β is varied from matrix to fault region, the remaining moisture retention curve properties are kept constant, causing the fault to desaturate at smaller suctions than the porous matrix.

The regional dip (6° to the East) results in an approximately 10 percent fraction of the body (gravity) force being parallel to the x-axis attached to the dipped domain. Finally, the net infiltration rate q_o is taken to vary from 0 to 50 millimeters/year. In particular, the low value $q_o = 0$ is used as a minimal base case, whereas the high value $q_o = 50$ millimeters/year accounts for potential occurrence of extreme infiltration conditions.

F-3. ANALYSES RESULTS AND DISCUSSION

Figure F-2 depicts the temporal variation of the vertical pressure head profile, at the central transect $y = 40$ meters, $x = 615$ meters, under a net infiltration rate of $q_o = 1$ millimeter/year. It can be seen that steady-state is obtained only after 250 years of simulation. It is also apparent that the steady state solution is much drier than the assumed (linear, but not hydrostatic) initial condition, deduced and modified from saturation values given by Montazer and Wilson (1984), emphasizing the need for consistent initial and boundary conditions discussed before. It can be observed, further, that the effect of stratification in hydraulic properties is felt only during the early times of simulation. However, because of the continuous influx of water from the top boundary, a nonhydrostatic pressure head profile is attained. The infiltration affects only the pressure profile in the coarse top layer. Finally, for the extremely wet case ($q_o = 50$ millimeters/year), the behavior of the flow system changes drastically. Steady state flow conditions are attained faster, that is, after only 100 years of simulation. Figure F-3 presents the temporal variation of the pressure head profile at the vertical transect ($y = 40$ meters, $x = 615$ meters). For this simulation, the initial condition is assumed to be hydrostatic. It is also worthwhile noticing that the effect of layering on pressure distribution appears to be almost insignificant for this flow rate, although the influence of the coarse top layer is still perceptible. Following a successive approximation methodology, the initial and boundary conditions for the simulations presented here are taken from the steady state results of less complex flow systems. Figure F-4 depicts results of a simulation with $q_o = 50$ millimeters/year, and a dip angle of 6° to the East, at time $t = 120$ years, at vertical transects at three different locations within the flow domain. The effects of infiltration are felt by a region having the same lateral extent as in the previous simulations (about 100 meters on either side of the fault). The infiltration "signal," however, is affecting a greater depth, down to almost 400 meters. It is also shown that the effects of dipping are minor (less than 5 meters of pressure head difference) for the conditions assumed in this analysis.

The high contrast in hydraulic properties between the matrix and fault zones renders the simulations extremely sensitive to the time step used. Choosing a $\Delta t_{max} = 365$ days, for example, resulted in a nonbinding constraint for the time step. Even though the actual time step had an upper envelope of $\Delta t \approx 20$ days, mass balance errors as high as 20 percent were observed. This resulted in solutions that were not able to reach steady state following an oscillatory pattern. When the lateral boundaries are set to no-flow (i.e., a 2-D system), the mass balance error causes slight fluctuations of the total discharge rate on the order of 2 percent. This is in contrast with the more pronounced fluctuations obtained for a system with the fault cutting

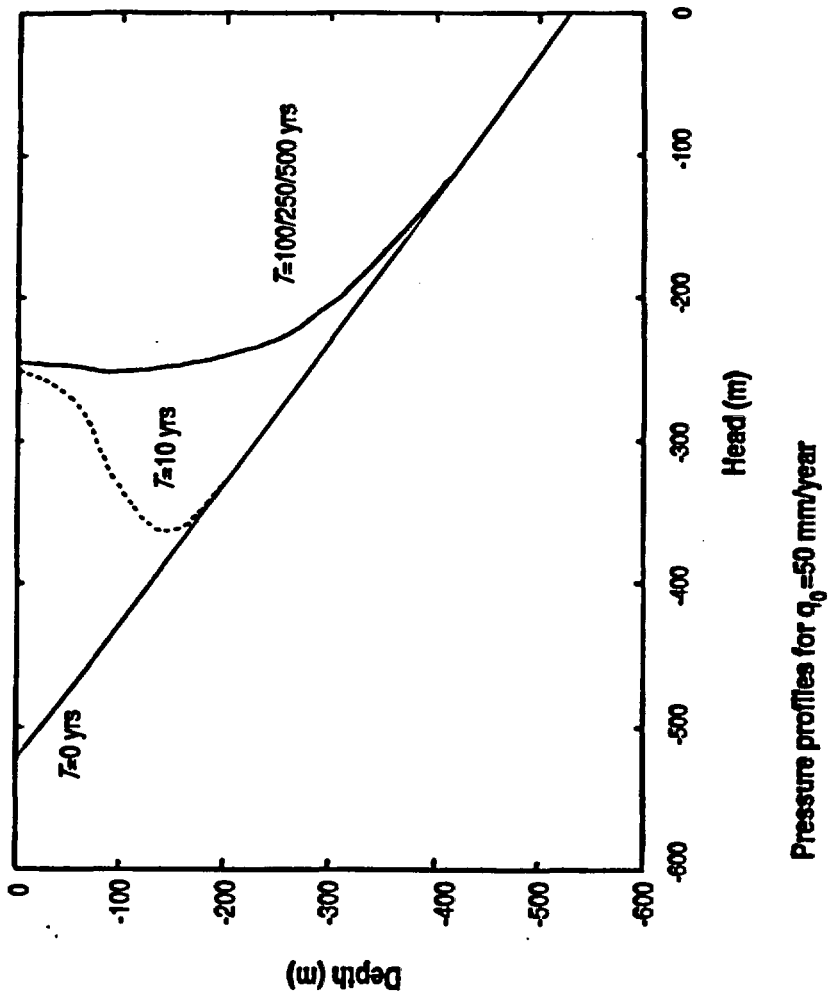

Figure F-3. Pressure Profiles for q_o = 50 mm/yr.

Figure F-4. Pressure Profiles for q_o = 50 mm/yr and a Dip Angle of 6°.

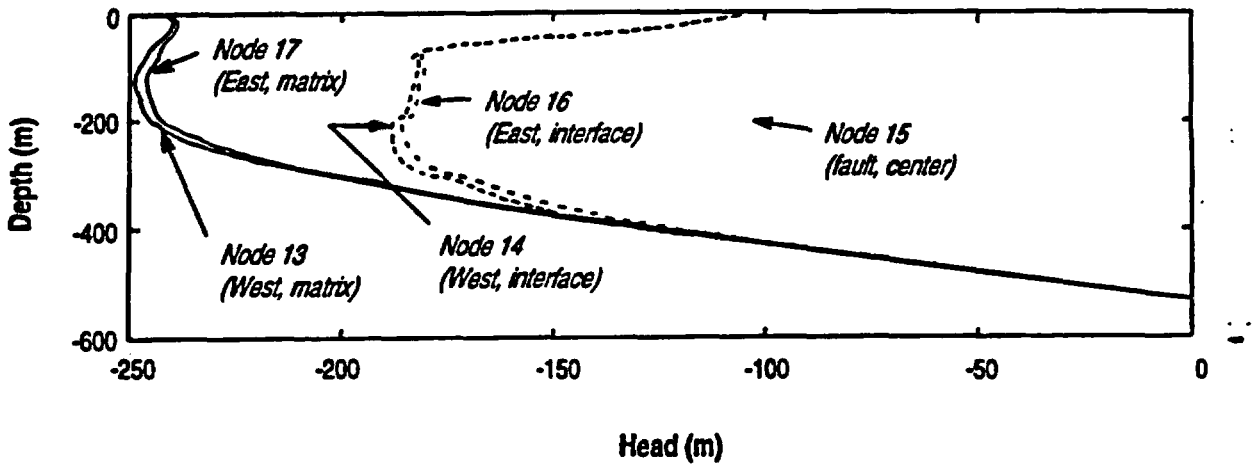
Node 17
(East, matrix)
Node 16
(East, interface)
Node 15
(fault, center)
Node 13
(West, matrix)
Node 14
(West, interface)
Depth (m)
0
-200
-400
-600
-250
-200
-150
-100
-50
0
Head (m)

Dirichlet boundaries. It was found that in order to obtain a well-behaved numerical solution, with clearly stable convergence to steady state, the time step had to be drastically reduced. When the maximum time step was decreased to Δt_{max} = 10 days, the mass balance plots indicated a complete elimination of large mass balance errors (except for early transients). The conclusion in this case is that, although the discrete-time system was unstable, the continuous-time system corresponding to a vanishingly small time step ($\Delta t \rightarrow 0$) is, in fact, stable and leads to a unique steady state solution as $t \rightarrow \infty$. While this phenomenon results from the discreetness (in time) of the numerical flow problem, it indicates a peculiar phenomenon related with the 3-D configuration of the faulted domain and with the direct connection between fault and permeable boundaries.

The steady state flow pattern in each case is best represented by 2-D vector plots of the unsaturated water velocity (or flux), and particle tracks depicting the locations of particles released in the steady flow system at selected points. These 2-D vector and particle tracks are shown in Figures F-5a and F-5b for the higher and milder property contrast case, respectively. Inspection of these figures clearly shows a significant effect of the contrast between slopes of the matrix/fault unsaturated conductivities. When the fault's conductivity slope is comparatively much larger than that of the matrix (α_m = 0.022 meters^{-1}, α_f = 0.10 meters^{-1}), higher fluxes were observed in the matrix. This results in a front that lags within the fault zone. Figure F-5(a) shows this effect for two lines of particles released at elevations 500 meters and 300 meters, respectively, and tracked for 1000 years. In this case, the maximum distance traveled in 1,000 years is approximately 67 meters. When the contrast is milder (α_m = 0.022 meters^{-1}, α_f = 0.035 meters^{-1}), the opposite behavior is observed. The fluxes within the fault zone are greater, but they point towards the matrix [Figure F-5(b)]. This creates a frontal shape that continuously expands outward from the fault zone. In this case, the maximum distance traveled in 1,000 years is 165 meters and more than 200 meters, for the two release planes, respectively. This important difference in behavior is because of the different values of the crossing-point suction in the two cases. Recall that the contrast between matrix and fault moisture retention curves was not changed. As a consequence, the steady state moisture patterns above the water table are almost identical for the two contrast cases studied. What is important to keep in mind is that the travel time of particles is sensitive to the unsaturated conductivity slope, even when the moisture retention curve is held constant.

F-4. CONCLUSIONS

A hypothetical test problem was developed in order to study the effect of bedding on flow, the presence of a subvertical fault zone, and the effect of inclination of the beds. A number of auxiliary tests were also conducted, using variations on these hypothetical data. There are some similarities between this hypothetical problem and the Yucca Mountain stratigraphy, but since all site properties are not used, these simulations are not representative of the Yucca Mountain flow conditions.

Figure F-5. *XZ* Plane Flux Vector and Particle Plot. F-5a: $\alpha_f = 0.1\ m^{-1}$. F-5b: $\alpha_f = 0.035\ m^{-1}$.

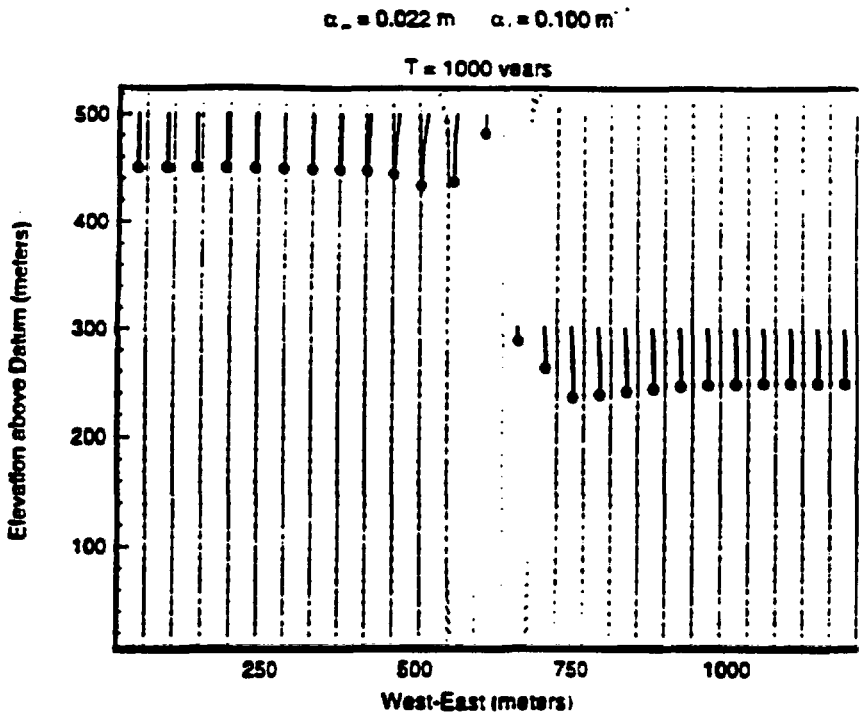

a)

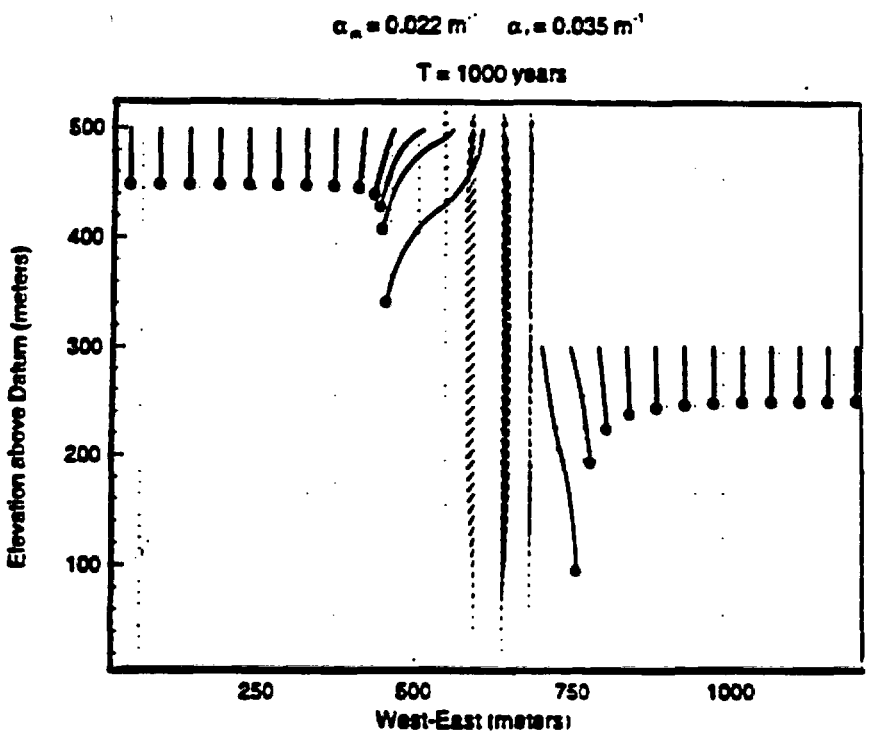

b)

Figure 4-13. XZ plane flux vector and particle plot: a) $\alpha_f = 0.1\ m^{-1}$; and b) $\alpha_f = 0.035\ m^{-1}$

Recognizing that there may not be natural initial-boundary conditions that can be used for the more complex problems, a method of successive approximation was implemented. This method uses solutions of auxiliary flow problems to set up pressure conditions for more complex problems. An oscillatory flow regime was observed at large times, that is, after initial transients died out. This was shown to be an effect of the discrete-time nature of the equations being solved, and was eliminated by using extremely small time steps ($\Delta t \rightarrow 0$). The techniques used to identify these effects relied on detailed plots of global mass balance in terms of instantaneous net discharge rate and instantaneous rate of change of total mass. Large Δt yielded oscillations for both 2-D and 3-D flow systems, but seemed more consequential in 3-D (fault-cutting pressure boundaries).

Based on the parameters used, and the simulations performed in this study, the following conclusions can be reached:

1. The effects of stratification are important only for low net infiltration rates and during the early parts of transient simulations.

2. A dip angle of 6° to the East has a minimal effect on the pressure head distributions (approximately 2 percent of the maximum pressure head difference).

3. The flow behavior (groundwater fluxes and travel times) of a system consisting of highly contrasted matrix and vertical fault properties is greatly influenced by the ratio of the slopes of the matrix and fault unsaturated hydraulic conductivity curves.

F-5. REFERENCES

Ababou R., "Approaches to Large Scale Unsaturated Flow on Heterogeneous, Stratified, and Fractured Geologic Media," Nuclear Regulatory Commission, NUREG/CR-5743, MONTH 1991. [Prepared by the Center for Nuclear Waste Regulatory Analyses.]

Bagtzoglou, A.C., R. Ababou, and A. Nedungadi, "BIGFLOW: A Multi-Dimensional Code for Flow in Heterogeneous and Variably Saturated Geologic Media (Theory and User's Manual -- Version 1.0), Center for Nuclear Waste Regulatory Analyses, CNWRA 92-026, MONTH 1992. [Prepared for the Nuclear Regulatory Commission.]

Montazer, P., and W.E. Wilson, "Conceptual Hydrologic Model of Flow in the Unsaturated Zone, Yucca Mountain, Nevada," U.S. Geological Survey, Water Resources Investigation Report, WRI-84-4345, 1984.

Mualem, Y., "A Catalogue of the Hydraulic properties of Unsaturated Soils," Haifa, Israel,, Technion Institute of Technology, Hydrodynamics and Hydraulic Laboratory, Research Project No. 442, 1976.

Scott, R.B., and Bonk, J., "Preliminary Geologic Map of Yucca Mountain with Geologic Sections, Nye County, Nevada," U.S. Geological Survey, Open-File Report, OFR-84-494, 1984.

APPENDIX G

CONTENTS

		Page
G-1.	Introduction	G-1
G-2.	Continuum Approaches	G-1
G-3.	Zero Transfer Simulation	G-3
G-4.	High Transfer Simulationm	G-4
G-5.	Simulation Comparing Single and Dual Continum Approaches	G-8
G-6.	Conclusions	G-8
G-7.	References	G-10

FIGURES

G-1	Contour Plot of Matric Potentials for Hypothetical Block of Topopah Spring Tuff Matrix and Fracture Continua After Simulating Two Weeks of Flow	G-5
G-2	Topopah Spring Welded Unit Fracture and Matrix Properties	G-6
G-3	Contour Plot of Matric Potentials for Hypothetical Block of Topopah Spring Tuff Matrix and Fracture Continua After Simulating Two Weeks of Flow	G-7
G-4	Contour Plot of Matric Potentials for Hypothetical Block of Topopah Spring Tuff Matrix and Fracture Continua After Simulating Two Weeks of Flow	G-9

APPENDIX G
EXPLORATION OF DUAL CONTINUUM FLOW MODELING CONCEPTS

W.H. Ford/NMSS

G-1. INTRODUCTION

In the development of the ground water flow and transport module, several different modeling approaches were attempted. One of the approaches required the staff to learn and experiment with *DCM3D*, a Dual-Continuum, Three[3]-Dimensional, Ground-Water Flow Code for Unsaturated, Fractured, Porous Media, described in Updegraff *et al.*, (1991). *DCM3D* is a recently developed computer code by Sandia National Laboratories for solving three-dimensional, ground-water flow problems in variably saturated, fractured porous media (Updegraff *et al.*, 1991). The code is based on a dual-continuum model with matrix media comprising one porous equivalent continuum and fractures the other. The continua are connected by a transfer term that is a function of the unsaturated permeability of the porous media.

G-2. CONTINUUM APPROACHES

It is attractive to use continuum codes to model ground-water flow at Yucca Mountain, because explicitly modeling individual fractures at the scale of Yucca Mountain at this time may not be possible. For example in the Yucca Mountain Site Characterization Plan (DOE, 1988; p. 3-173), it is stated that "No way is known to generate a complete set of fracture location and geometry data. Secondly, if the Topopah Spring welded unit has a mean fracture density of 20 fractures/meters^3 and has a mean thickness of 300 meters over the approximately 7×10^6 meters^2 area of the central Yucca Mountain block, then one would have to consider flow in approximately 4×10^{10} discrete fractures." This amount of detail would be too large to model at this time. Rather than explicitly modeling each fracture, continuum codes represent matrix and fractures as constituting either separate but overlapping continuum systems (Dual Continua Approaches) or as a single composite continuum system (Single Continua Approaches). It should be noted that these approaches assume matrix and fracture properties can be represented as spatial averages over rock mass volumes whose linear dimensions are very much smaller than the thickness of the hydrogeologic unit, but sufficiently large to include a representative, statistical sample of hydraulically connected fractures.

In modeling unsaturated flow conditions in soil, hydrologic properties are represented by characteristic curves, that describe moisture content and conductivity as a function of pressure head. In continuum approaches, rather than using a single characteristic curve to represent the unsaturated hydrologic properties of a single fracture, a single curve represents the hydrologic properties of large numbers of fractures. At present, two main types of

continua approaches are being used to model Yucca Mountain site unsaturated fracture and matrix ground-water flow; single continua and dual continua. Single continua approaches often use the same porosity values for both matrix and fractures and a single characteristic curve to represent matrix and bulk fracture-matrix hydrologic properties (Klavetter and Peters, 1986). In contrast, dual continuum models consist of two interconnected continua, with one continuum simulating flow through the rock matrix and the other simulating flow through large numbers of fractures. The two continua are connected by a fracture-matrix transfer term allowing water to flow between the fracture and matrix continua. This enables a dual continuum code to model the resistance to water movement between the matrix and fracture continua and may allow the code to simulate situations where a single continuum approach could experience code-convergence problems.

It may also be possible to simulate conceptual models with dual continuum codes that are not possible with single continuum codes. For example, in a single continuum model of unsaturated fracture and matrix ground-water flow, when water saturation in the matrix reaches a level where bulk fracture flow occurs, faster velocities are computed, but with no change in direction. Therefore, this approach assumes bulk fracture flow contains the same anisotropies as the matrix. However, individual fractures tend to be linear features with strong anisotropies. Therefore, for a single fracture it is reasonable to assume that irrespective of the flow direction in the matrix, flow in the fracture will be strongly influenced by the anisotropic properties of the fracture. Furthermore, when there are large numbers of fractures with similar linearities, a general fracture anisotropy may be created that is different from the rock matrix. This may be the case at Yucca Mountain, where faults and fractures are believed to be vertical or steeply dipping (DOE, 1988; pp. 3-175, 3-179, and 3-185; Barton, 1989). Use of a dual continuum code in this type of situation may be advantageous, because in a dual continuum code, different anisotropies can be assigned to both the matrix and fracture continua.

G-3. ZERO TRANSFER SIMULATION

The *DCM3D* computer model simulated a hypothetical two dimensional vertically placed block of tuff (20 meters by 48 meters). Initial simulations assigned Topopah Spring welded properties, obtained from Peters (1984), to the matrix and bulk fracture continua. Initial conditions of -2 meters matric potential were assigned to each grid node in both continua and no-flow boundary conditions were assigned to the two vertical sides of the block. A -2 meters of matric potential were assigned to the bottom boundary, and zero matric potential to the left one-quarter of the block top. This meant the code would simulate a wetting front moving down from the upper left side. Hydraulic conductivities for the matrix properties were isotropic and for the fracture continuum strongly anisotropic. In fact, fracture hydraulic conductivities were set to zero in the lateral direction, so that flow in the fracture continuum could only occur in the vertical direction. For the first run, the transfer coefficient was set to zero. This meant that no water could move between the two continua.

The objective of this exercise was to see if the code could successfully simulate a situation where the same boundary conditions would cause different flow directions in the two media, as a result of differences in their hydraulic conductivity anisotropies.

After 2 simulated weeks, two areas had formed in the block (Figure G-1): an area of wetting under the upper left one-quarter of the block and an area of dewatering (because of gravity) under the right side of the block. This result can be best understood in light of the characteristic curves used in the simulation (Figure G-2). The initial matric potential conditions of -2 meters meant that initial fracture continuum hydraulic conductivities were much lower than the matrix continuum. Therefore, the matrix dewatered faster than the fracture continuum. However, the zero matric potential upper boundary meant that under wetting conditions, the fracture continuum had a much higher hydraulic conductivity than the matrix. This caused the wetting front in the fracture continuum to move much faster than the matrix wetting front.

In the matrix continua, it can be seen that the wetting plume spreads both vertically and laterally. In the fracture continuum, which has no lateral hydraulic conductivity, water could only move vertically, forming a sharp wetting front down the left-hand side. Therefore, this run illustrates how the *DCM3D* code can be used to simulate separate flow directions in two different media.

G-4. HIGH TRANSFER SIMULATION

To see what would happen to flow directions if water were allowed to pass between the two media, the previous run was duplicated with a high-transfer coefficient. After two simulated weeks (Figure G-3) the matric potentials of both media were the same, because the high transfer coefficient allowed water to move rapidly between the two continua. This resulted in water moving from the wetter continuum to the dryer continuum until the matric potentials in both continua were equal. In other words, as a grid block in one continuum wets or drys, the corresponding grid block in the other continuum wets or drys.

In this simulation, the faster dewatering rate of the matrix continuum caused water to flow from the fracture continuum into the matrix continuum, resulting in much deeper dewatering of the fracture continuum, on the right half of the block. Additionally, the faster wetting of the fracture continuum caused water to flow from the fracture continuum into the matrix continuum, resulting in the formation of a much larger wetting front in the matrix continuum. It can also be observed that the wetting front in the fracture continuum moved laterally. However, when velocity outputs were inspected, the fracture continuum had a lateral flow velocity of zero. This was to be expected, since the lateral hydraulic conductivity of the fracture continuum had been set to zero. Consequently, for the water to move laterally in the fracture continuum, it first had to move into the matrix continuum, move laterally in the matrix continuum, and then move back into the fracture continuum. In

Figure G-1. Contour Plot of Matric Potentials for Hypothetical Block of Topopah Spring Tuff Matrix and Fracture Continua After Simulating Two Weeks of Flow. There is no Flow Between the Two Continua.

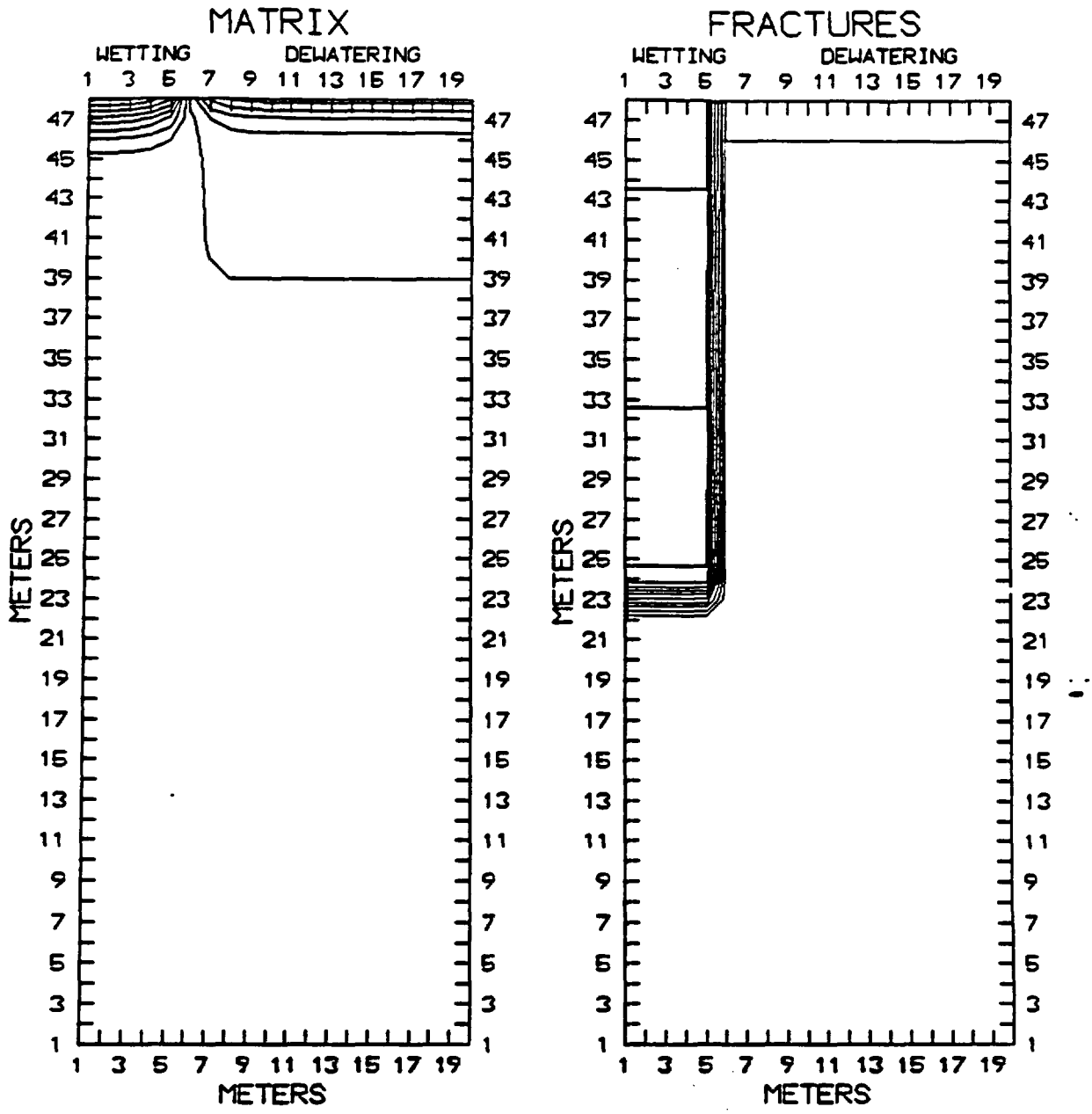

Figure 1: Contour Plot Of Matric Potentials For Hypothetical Block Of Topopah Springs Tuff Matrix And Fracture Continuum After Simulating 2 Weeks of Flow. There Is No Flow Between The Two Continua.

Figure G-2. Topopah Spring Welded Unit Fracture and Matrix Properties.

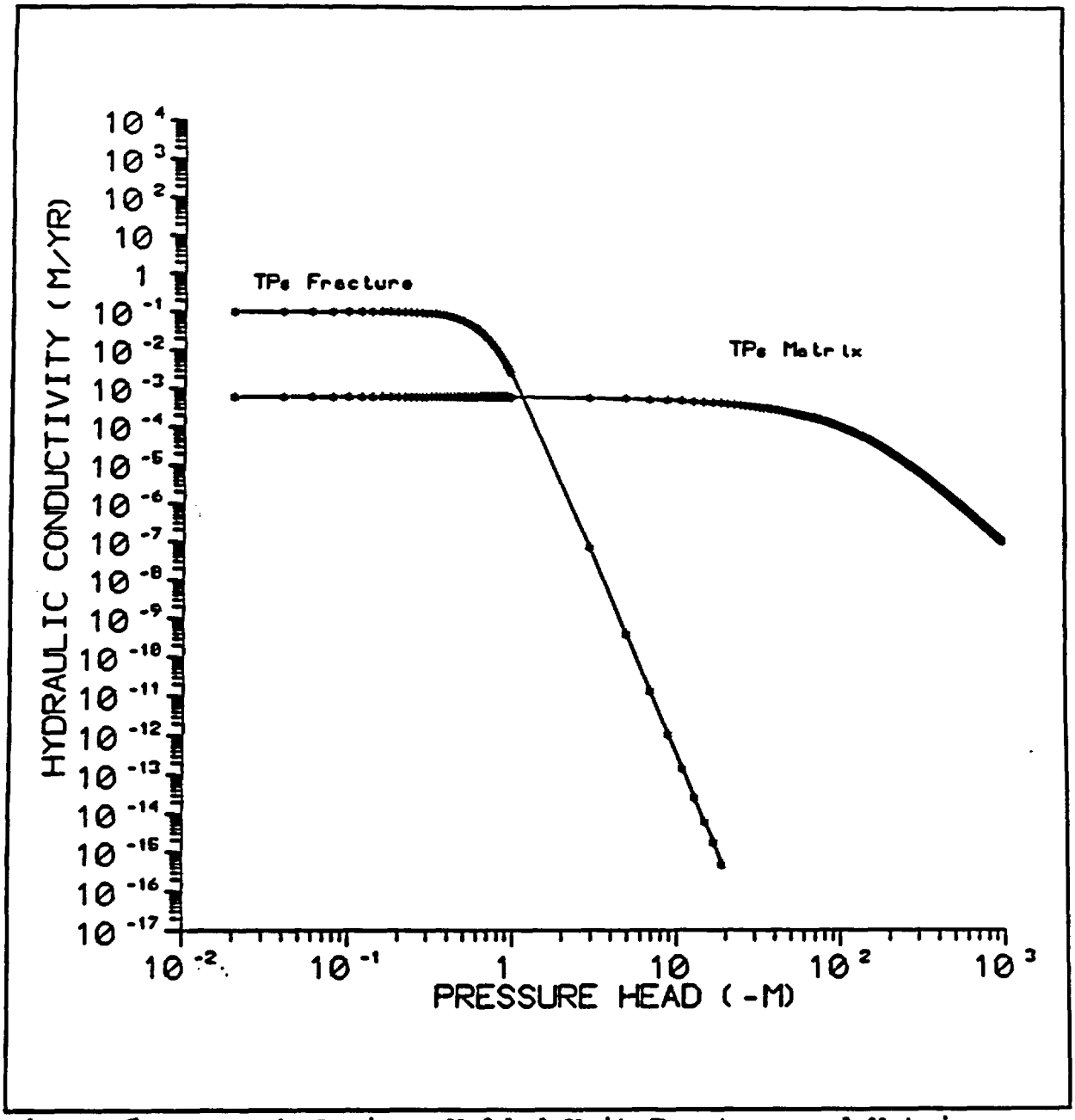

Figure 2: Topopah Springs Welded Unit Fracture and Matrix Properties.

Figure G-3. Contour Plot of Matric Potentials for Hypothetical Block of Topopah Spring Tuff Matrix and Fracture Continua After Simulating Two Weeks of Flow. Water Can Flow Between the Two Continua.

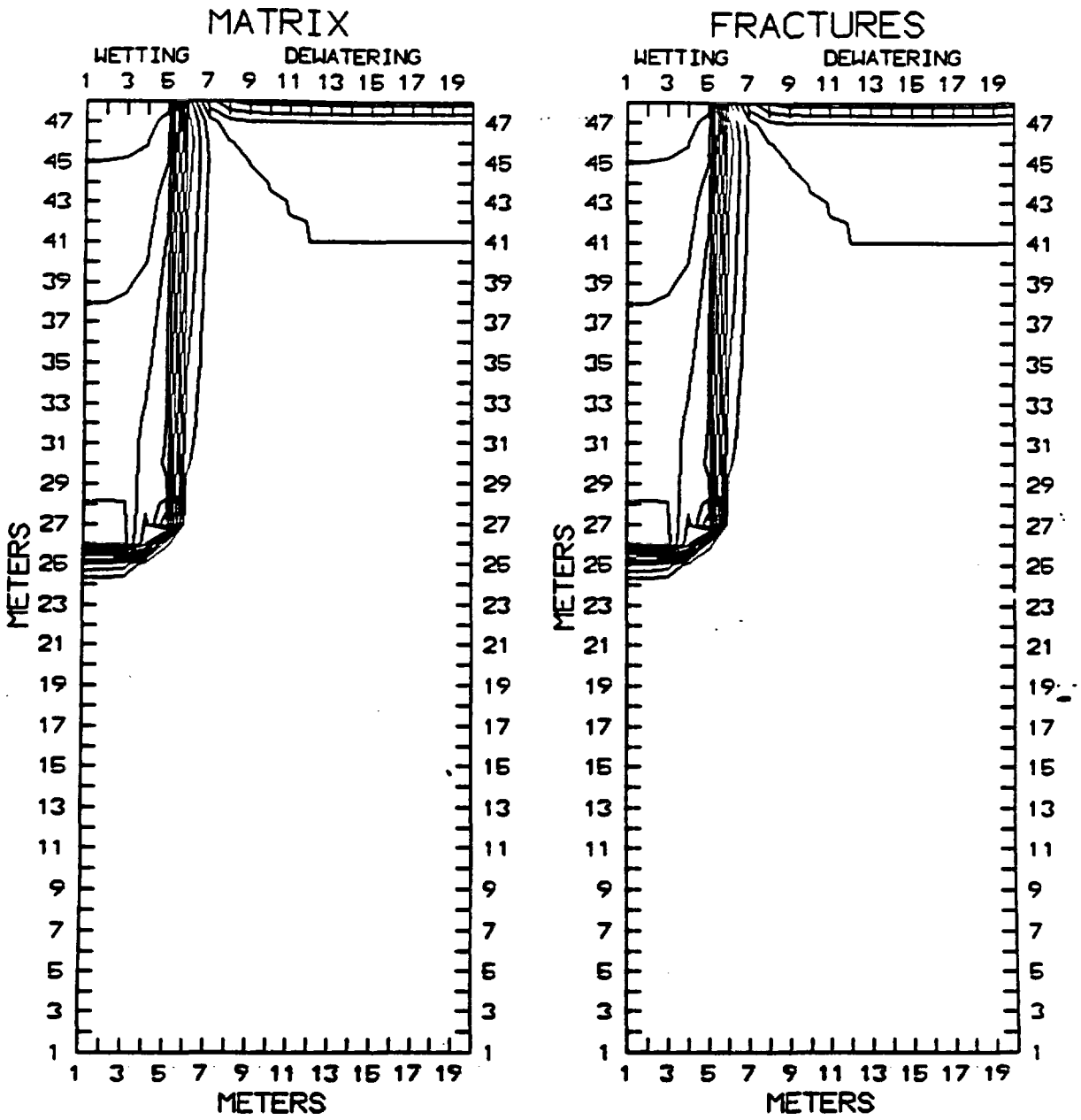

Figure 3: Contour Plot Of Matric Potentials For Hypothetical Block Of Topopah Springs Tuff Matrix And Fracture Continuum After Simulating 2 weeks of Flow. Water Can Flow Between The Two Continua.

nature, this would be analogous to flowing fractures wetting up the matrix, which, in turn, causes other fractures to flow. Therefore, an interpretation of model matric potentials, water contents, and velocities, which ignores water movement between the two continua, may be misleading about the rate and direction of fluid flow.

G-5. SIMULATION COMPARING SINGLE AND DUAL CONTINUUM APPROACHES

To further compare the single and dual continuum approaches, the *DCM3D* input was modified to make it simulate a single continuum approach. In a single continuum code, the combined matrix and fracture flow properties are assumed to have the same porosities and the same hydraulic conductivity anisotropies.

It was decided to make *DCM3D* mimic a single continuum code by assigning isotropic hydraulic conductivities to the fracture continuum, and to repeat the high transfer coefficient run. It was a little less clear what porosity values should be input. If a single porosity value were used for both the matrix and fracture continua, the simulation would contain a much higher total pore space than a single continuum approach would use. It was therefore decided to leave the porosity values the same as the previous high-transfer coefficient run. This meant that the matrix continuum had a porosity of 0.11 and that the fracture continuum, had a porosity of 1.8×10^{-4}. This was believed to be a reasonable compromise, since, in a single continuum approach, fracture flow is simulated when the pore space is nearly filled. The output from the previous dual continuum high-transfer run and the simulated single continuum run is compared in Figure G-4. This comparison shows that the lack of lateral fracture conductivity in the dual continuum simulation caused the wetting front to travel deeper, with less lateral spreading than the single continuum simulation.

G-5. CONCLUSIONS

These simulations demonstrate that the dual continuum code *DCM3D* can model flow in two continua with different anisotropies and that, depending on the problem to be modeled, it may produce significantly different answers than a single continuum code.

Comparison of Single and Dual Continuum Approaches.

Figure G-4. Contour Plot of Matric Potentials for Hypothetical Block of Topopah Spring Tuff Matrix and Fracture Continua After Simulating Two Weeks of Flow.

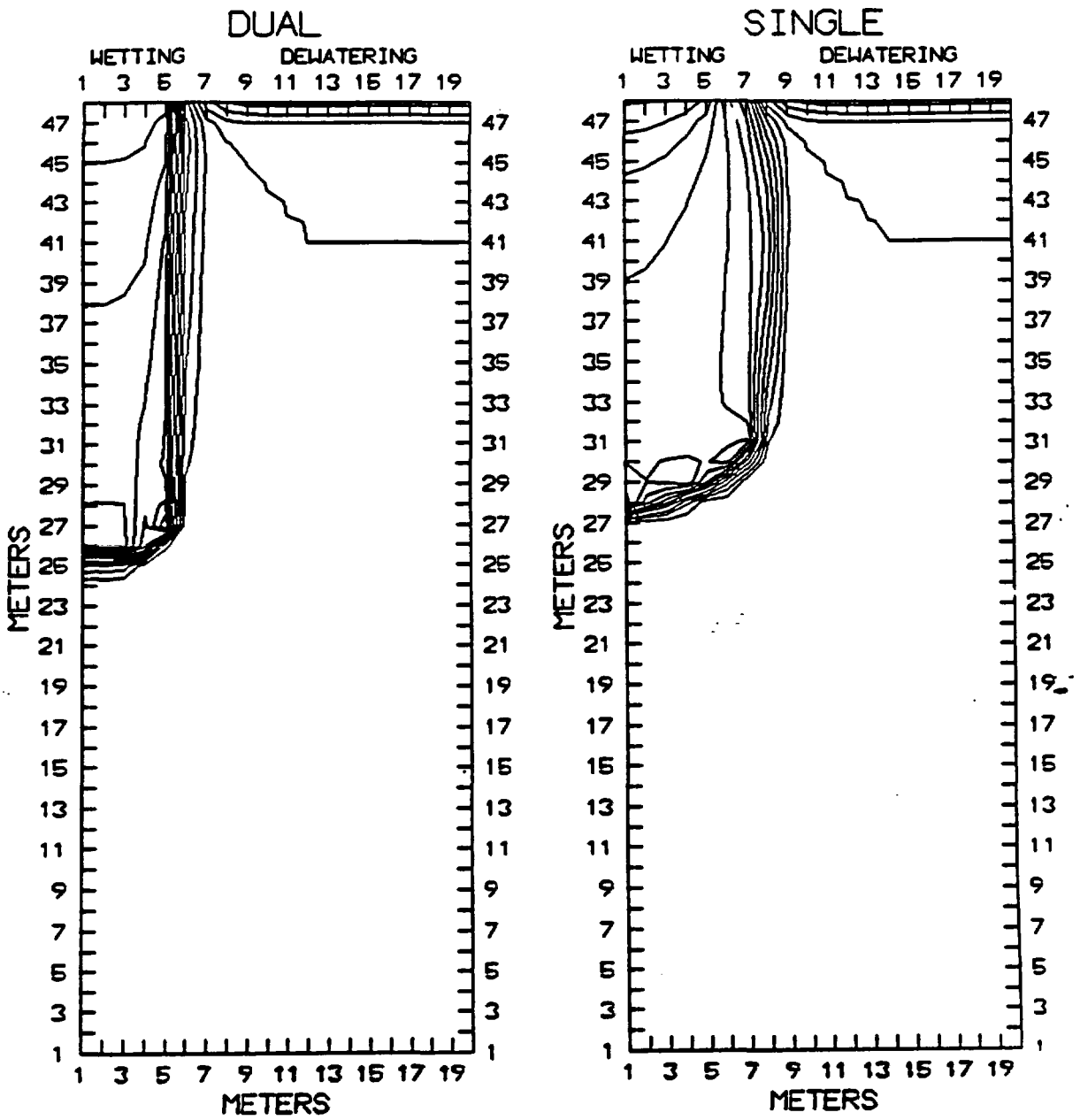

Figure 4: Contour Plot Of Matric Potentials For Hypothetical Block Of Topopah Springs Tuff After Simulating 2 weeks of Flow. Comparison of Single and Dual Continuum Approaches.

G-6. REFERENCES

Barton, C., W. Page, and T. Morgan, "Fractures in Outcrops in the Vicinity of Drill Hole USW G-4, Yucca Mountain, Nevada, Data Analysis and Compilation," U.S. Geological Survey, Open File Report, OFR-89-92, 1989.

Klavetter, E.A. and R.P. Peters, "Fluid Flow in a Fractured Rock Mass," Sandia national Laboratories, SAND85-0855, March 1986.

Updegraff, C.D., C.E. Lee, and D.P. Gallegos, "DCM3D: A Dual-Continuum, Three-Dimensional, Ground-Water Flow Code for Unsaturated, Fractured, Porous Media," NUREG/CR-5536, February 1991. [Prepared by the Sandia National Laboratories.]

U.S. Department of Energy, "Site Characterization Plan Overview, Yucca Mountain Site, Nevada Research and Development Area, Nevada," Office of Civilian Radioactive Waste management, DOE/RW-0198, December 1988.

APPENDIX H

CONTENTS

		Page
H-1	Introduction	H-1
H-2	Volatile Releases Resulting from the Intrusion of a Dike	H-1
H-3	Releases Under Normal Conditions	H-2
H-4	Mechanisms for the Release of Volatile Radionuclides from Failed Waste Packages	H-6
H-5	Transport of Volatile Radionuclides in the Geosphere	H-7
H-6	Conclusions	H-9
H-7	References	H-11

TABLES

H-1	Cumulative Releases for Selected Radionuclides	H-3
H-2	Vapor Pressure Estimates	H-5
H-3	Calculation of Volatile Releases at 100°C	H-10

FIGURES

H-1	Vapor Pressure of Several Radioactive Compounds	H-4
H-2	Down-Hole Pressure Variations at Bore-Hole USW-UZ-1	H-8

APPENDIX H
RELEASE AND TRANSPORT OF POTENTIALLY GASEOUS RADIONUCLIDES OTHER THAN ^{14}C DURING VOLCANISM AND NORMAL OPERATIONS

R.B. Codell/NMSS

H-1 INTRODUCTION

The Yucca Mountain site is unique among other proposed sites for the disposal of high-level radioactive waste because it would be constructed above the water table. One of the considerations at this site is radionuclide release from the waste package in the gas phase and possible transport as a gas to the atmosphere. Even if the gaseous release cannot escape to the atmosphere, it may serve as a source of contamination for the liquid pathway.

Several potentially volatile radionuclide compounds of ^{79}Se, ^{99}Tc, and ^{129}I have been identified in spent nuclear fuel (Lehrman, 1989; Park, 1991). The question of whether there is sufficient cause to consider the gaseous release and transport of these volatile radionuclides further has been addressed through a series of conservative calculations in the following sections. The direct release of the radioactive inventory by extrusive volcanism (i.e., the direct entrainment of the waste in magma brought to the surface of the earth) has been dealt with in Section 6.5. The present analysis is restricted to conditions of normal repository operation and intrusive volcanism that could potentially release volatile radionuclides from the waste package, but do not necessarily provide a mechanism for transport to the surface.

H-2 VOLATILE RELEASES RESULTING FROM THE INTRUSION OF A DIKE

To demonstrate the potential, caused by magmatic intrusion, for release of volatile radionuclides other than ^{14}C from the engineered barrier system, consider an example of a large dike through the middle of the Yucca Mountain site. The example considers only a single dike that intrudes into the repository and does not continue to flow. The dike is represented as an instantaneous vertical plane heat source with a heat content Q per unit area (but representing a dike of finite thickness). The staff calculated the maximum effect of the temperature increase at distances greater than half the assumed width of the dike, and compared the potential release of volatile radionuclides with present release limits, without specifying, at this point, a mechanistic model for the release of these components from the waste package. Although unlikely, the staff does not consider this example to be necessarily a "worst-case" situation. The example does not include the following phenomena that could lead to predictions of higher temperatures or releases:

- The formation of sills filling horizontal weakness in the rock or the repository drifts;
- Multiple dikes and sills;
- Long-term continuing eruptions;
- Heat transfer by convecting gas and water vapor; and
- Effect of corrosive volcanic gases on the waste form.

Assume for the purpose of this demonstration that a dike 10 meters in width and 3000 meters long intrudes through the middle of the repository, and that the waste packages are randomly spaced throughout the assumed site area of 5 kilometers^2. Assuming that the dike intrusion is instantaneous and does not continue to the surface, the maximum range of significant heating can be determined by assuming the dissipation of heat from an infinite plane source (Turcotte, 1982):

$$T - T_0 = \frac{Q}{2\rho C\sqrt{\pi\kappa t}} e^{-\frac{y^2}{4\kappa t}} \quad . \tag{H-1}$$

where:

ρ	=	density of the country rock
C	=	heat capacity of country rock
Q	=	instantaneous sensible and latent heat content of dike per unit area
κ	=	thermal diffusivity
y	=	distance from dike centerline
t	=	time
T_0	=	ambient temperature.

The maximum temperature at any distance y from the dike centerline is (Turcotte, 1982):

$$T_{max} = T_0 + \frac{Q}{\rho C y}\sqrt{\left(\frac{1}{2\pi e}\right)} \quad . \tag{H-2}$$

The time at which the maximum temperature occurs would be (Turcotte, 1982):

$$t_{max} = \frac{y^2}{2\kappa} \quad . \tag{H-3}$$

For the present example:

Q	=	5.44×10^9 Joules/meter^2
ρ	=	2640 kilograms/meter^3
C	=	687 Joules/kilogram - °K
κ	=	1.1×10^{-6} meters^2/second

With the above set of parameters, a maximum temperature increase of 10°K would extend only 78 meters from the dike centerline and would occur only about 0.13 years after dike penetration. The 100°K isotherm would extend a maximum of 7.8 meters from the centerline.

From the above analysis, the staff choose what were believed to be a very conservative maximum extent of thermal influence of the dike as 50 meters from the centerline and a 3000-meter linear extent covering

an area of 300,000 meters^2. The total repository area is approximately 5×10^6 meters^2, so the dike would affect approximately 6 percent of the waste packages. If it were conservatively assume that all of the volatile radionuclides other than ^{14}C were driven off by the excess heat (^{99}Tc, ^{79}Se, and ^{129}I) in the affected area, then the amounts in terms of the 10 CFR Part 40 cumulative release limits would be only 0.125 as summarized in Table H-1.

Table H-1
Cumulative Releases for Selected Radionuclides

Nuclide	*Inventory curies*	*.06 × Inventory*	*EPA[a] Limit for repository*	*EPA Ratio R*
^{129}I	2200	132	7000	0.019
^{79}Se	28300	1698	70000	0.024
^{99}Tc	915,000	54,900	700,000	0.078
Total	—	—	—	0.125

[a] U.S. Environmental Protection Agency (EPA)

H-3 RELEASES UNDER NORMAL CONDITIONS

Volatility of Radionuclides: Several sources of information for iodine, selenium, and technetium gave widely differing estimates of the vapor pressure. Figure H-1 shows the vapor pressure of several solid and aqueous phases of radionuclides that would occur in spent nuclear fuel, but the source of this information is unknown. Park (1991) reports values that are considerably lower. These values are shown in Table H-2.

The vapor pressure of Tc_2O_7 was also estimated from thermodynamic information:

$$Tc_2O_7(solid) \rightleftharpoons Tc_2O_7(gas)$$
$$\ln P = -\frac{\Delta G_R^0}{RT} \quad . \qquad \text{(H-4)}$$

The Gibbs free energy of reaction, $\Delta G^0_R = 47.1$ kilojoules/mole for the crystalline phase gives a vapor pressure for $Tc_2O_7 = 2.6 \times 10^{-7}$ atmospheres at 100°C and 6.3×10^{-6} atmospheres at 200°C (Phillips, 1988). Amorphous and hydroxide phases, however, could lead to considerably higher vapor pressures.

Figure H-1. Vapor pressure of several radioactive compounds (A. Lehrman, 1992).

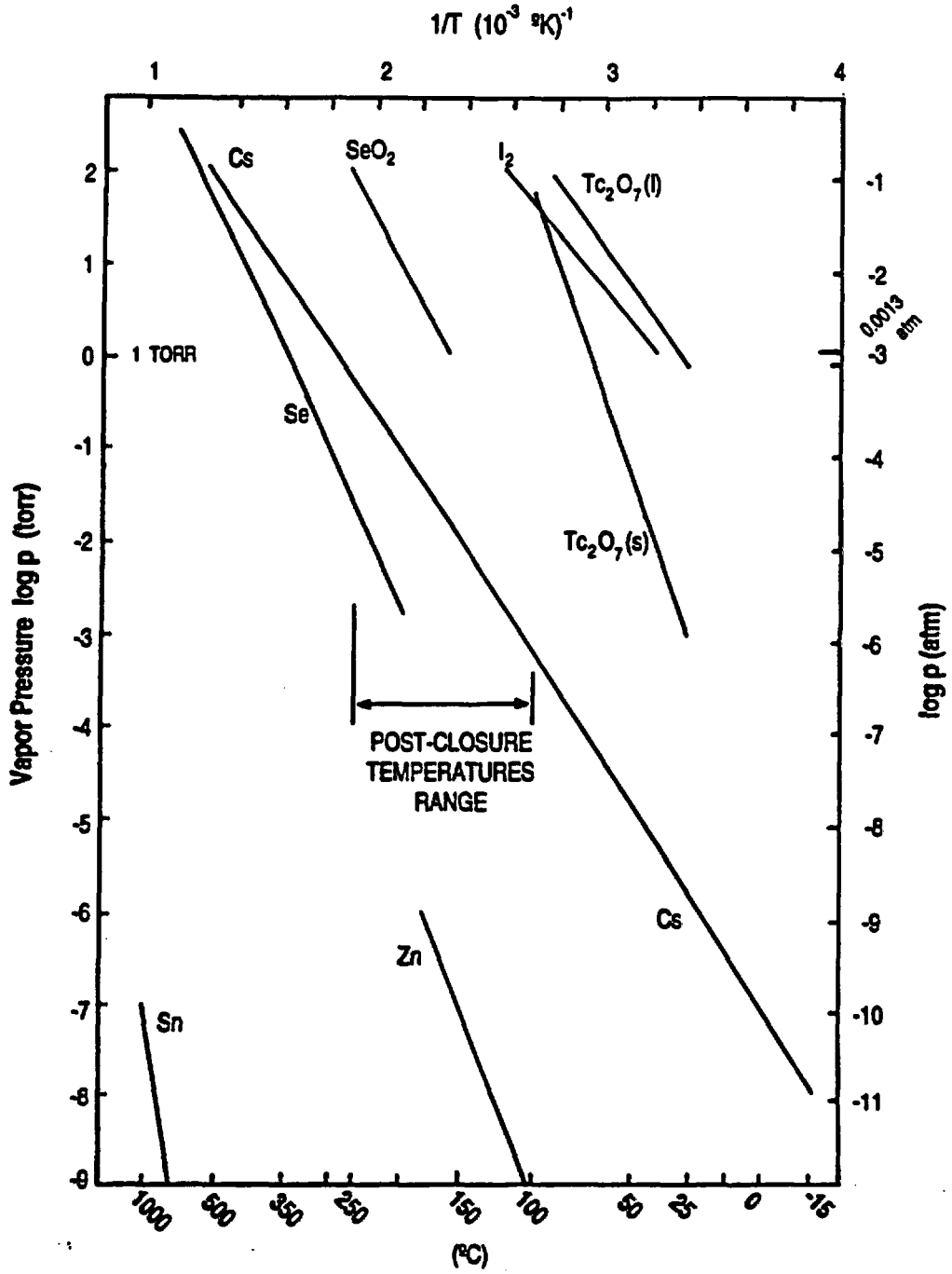
1/T (10^-3 °K)^-1
1
2
3
4
Vapor Pressure log p (torr)
2
1
0
-1
-2
-3
-4
-5
-6
-7
-8
-9
1 TORR
log p (atm)
-1
-2
-3
-4
-5
-6
-7
-8
-9
-10
-11
0.0013 atm
Cs
SeO2
I2
Tc2O7(l)
Se
Tc2O7(s)
POST-CLOSURE
TEMPERATURES
RANGE
Cs
Zn
Sn
1000
500
350
250
150
100
50
25
0
-15
(°C)

Table H-2
Vapor Pressure Estimates (from Park (1991) and Lehrman (1992))

Species	*P - atmospheres at 100°C*			*P - atmospheres at 200°C*		
	Park	*Lehrman*	*Equation 8.4*	*Park*	*Lehrman*	*Equation 8.4*
CO_2	>2000	—	—	12,000	—	—
I_2	0.06	0.01	—	3.7	16	—
SeO_2	0.00091	3E-5	—	0.054	0.02	—
Tc_2O_7	0.00012	0.3	2.6E-7	0.037	—	6.3E-6

The vapor pressures shown would be for pure phases only, and may be affected by the following phenomena:

- Most of the radionuclides would be tied up in the fuel matrix, although some might migrate to the surface of cracks and interstitial boundaries of the fuel:
- Some technetium is associated with highly resistant alloy particles in the fuel (Pearcy and Manaktala, 1992): and
- Much of the ^{129}I would probably be tied up with metallic fission products in the spent fuel, such as cesium and zinc (Park, 1991).

Rapid Release Fraction: Leaching experiments with spent nuclear fuel shows a rapid release fraction for technetium of about 1 percent of the total inventory, but much more modest releases, somewhat less than congruent, with respect to other radionuclides at later times (Wilson, 1990). There is a similar, but smaller, rapid release of ^{129}I from the same experiments of between 0.1 and 0.4 percent of the inventory. This result might indicate that some of the technetium migrated to the surfaces of cracks and grain boundaries, whereas the rest was tied up in the solid fuel. Releases of ^{79}Se were too small to measure.

Given the vapor pressures of technetium and iodine compounds, the rapid release fraction might be volatilized easily at normal operating temperatures in the repository. The effective vapor pressure of technetium, iodine, and selenium, within the matrix of the fuel, or tied up in metallic particles, would be lower than the pure phase vapor pressure. If the volatile components were ideal solid solutions, then Raoult's law would indicate that the vapor pressure P_j is proportional to the mole fraction of the component N_j and its individual vapor pressure P_j^* (Garrels, 1978):

$$P_j = P_j^* N_j \quad . \tag{H-5}$$

The mole fractions for ^{99}Tc, ^{79}Se, and ^{129}I, assuming the rest of the fuel is UO_2 are approximately 0.003, 0.0005, and 0.00003, respectively. If the volatile elements are solid solutions and if Raoult's law applies,

actual vapor pressures would be substantially lower than those for the pure phases. Additionally, the vapor pressures of volatile components might be limited by their slow diffusion from the interior of the solid to the surface.

H-4 MECHANISMS FOR THE RELEASE OF VOLATILE RADIONUCLIDES FROM FAILED WASTE PACKAGES

Within reasonable limits, the gases in the waste package can be considered to behave as an ideal gas and be governed by the relationship:

$$pV = nRT, \tag{H-6}$$

where:

P = pressure
V = void volume of waste package
R = universal gas constant
n = number of moles of gas
T = absolute temperature.

According to Equation (H-6), the number of moles of gas n in a container of volume V opened to the atmosphere would be directly proportional to P and inversely proportional to T. Volatile radionuclides can be released from a failed waste package by several processes, including venting of waste package pressure, molecular diffusion, and barometric pumping. Pressure within an intact waste package would depend on the initial pressure of the inert gas, release of pressurized gas within the fuel rods, partial pressure of the volatile components, and expansion of gas, because of the rise in temperature of the waste package. Upon waste package failure, the pressure would be vented, carrying with it any of the volatile radionuclides in the gas phase at that time. The fraction of the gas released $\Delta n/n_0$, assuming constant external pressure, would be:

$$\Delta \frac{n}{n_0} = \frac{\Delta(\frac{PV}{RT})}{(\frac{PV}{RT})_0} = 1 - \frac{T_0}{T'} \quad , \tag{H-7}$$

where T_0 = the initial temperature at which the waste package was sealed and T' = the temperature at which it fails. Assuming that the void space in a waste package V is 300 liters, and that the inert cover gas was initially charged to the waste package at 25°C (298°K) at one atmosphere, failure of the waste package at 100°C (373°K) would release only 1 - 298/373 = 0.25 of the waste package volume or 75 liters, according to Equation (H-7).

Although molecular diffusion might be a significant effect, barometric pumping is likely to be the most important mechanism for release of volatile radionuclides, in the long term. In this case, the change in the moles of gas in the waste package is proportional to the changes in the pressure. When atmospheric pressure drops, gas leaves the waste package, carrying with it the volatile components. In one complete

cycle of pressure change ΔP, the fraction of gas exchanges is:

$$\frac{\Delta n}{n_0} = \frac{\Delta P}{P_0} \quad . \tag{H-8}$$

Atmospheric pressure changes at the surface of the earth vary on several time scales. Small, rapid pressure changes occur because of local meteorological conditions. Larger and slower changes occur because of passing weather systems. Pressure fluctuations are smaller at depth because of the resistance to gas flow through the rock and the volume of gas held in the rock. Pressure fluctuations in the unsaturated zone at Yucca Mountain are shown in Figure H-2, indicating the damping of pressure with depth (Montazer, 1988). Although measurements of pressure fluctuations at the repository level are not available at Yucca Mountain, assume for the sake of this example that a 1 percent fully cyclic pressure change takes place 4 times per year at the repository level. This would lead to an exchange of air within the open waste package, according to the ideal gas law, of 0.04, or 12 liters of gas per year. Over 10,000 years, this gas flow would be 1.2×10^5 liters, far exceeding the initial pulse from pressure relief of the waste package.

H-5 TRANSPORT OF VOLATILE RADIONUCLIDES IN THE GEOSPHERE

The most significant volatile radionuclides other than ^{14}C, namely Tc_2O_7, SeO_2, And I_2, are highly reactive chemically and probably will strongly favor the water contained in the unsaturated rock rather than exist as gases in the geosphere (EPA, 1993). Experience with reactor emergency spray systems shows very high removal of iodine gas in slightly alkaline water. Yucca Mountain groundwater is alkaline, leading to the tentative conclusion that most of the iodine released as a gas would transfer to the liquid phase. Escape to the atmosphere, while likely for ^{14}C, is unlikely for the other volatile radionuclides.

Example: To demonstrate the likely maximum consequences of volatile releases of the potential gaseous radionuclides other than ^{14}C, consider the following bounding calculation. The main cause of waste package failure in the Iterative Performance assessment (IPA) Phase 2 assessment (Chapter 5) assumes that most of the waste packages will remain intact until their temperature has fallen below approximately 100°C. For the purpose of this conservative demonstration assume release of volatile radionuclides from a failed waste package under the following assumptions:

- Steady 100°C for a period of 10,000 years;
- The quick-release fractions of readily-volatilized radionuclides will be taken as 1 percent of the inventory for ^{99}Tc, 0.4 percent of the inventory for ^{129}I, and zero for ^{79}Se (Wilson, 1990);
- Vapor pressures for the pure substances at 100°C taken to be the largest values reported in Table H-2, of 0.06 atmospheres for ^{129}I, 0.00091 atmospheres for ^{79}Se, and 0.3 atmospheres for ^{99}Tc;
- The vapor pressures of the quick-release fractions are those of the pure phases;

Figure H-2. Down-hole pressure variations at bore-hole USW-UZ-1 (Montazer, 1988).

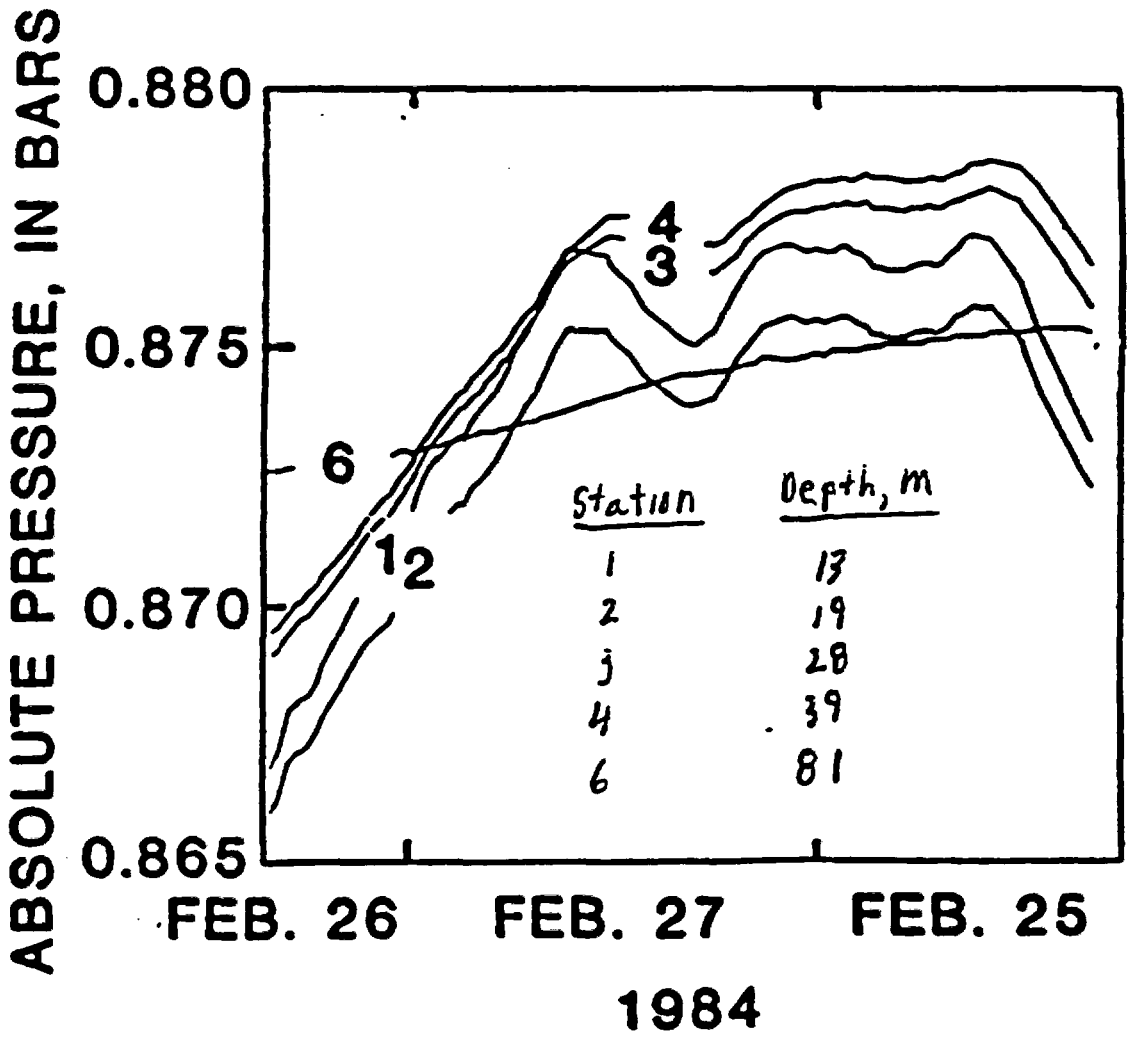
ABSOLUTE PRESSURE, IN BARS
0.880
0.875
0.870
0.865
FEB. 26
FEB. 27
FEB. 25
1984
4
3
6
1
2
Station
Depth, m
1
13
2
19
3
28
4
39
6
81

Figure H-2

- The remaining inventories have reduced vapor pressures according to Raoult's law and their mole fractions in the fuel (i.e., 0.003, 0.0005 and 0.00003 for ^{99}Tc, ^{79}Se, and ^{129}I respectively); and

- The gas exchange during the period is 12 liters/year per waste package.

Assuming no significant radioactive decay, the rate of loss from the quick-release fraction and the solid-solution fraction depends only on the partial pressure of each component and the flow rate of the gas. For the quick release fraction, the rate of release at one atmosphere total pressure would be:

$$R_q = \frac{P}{P_T} \times \frac{Q}{22.4} \times \frac{298}{T} \quad , \qquad \text{(H-9)}$$

where:

T = absolute temperature in $°K$
P = vapor pressure, atmospheres
P_t = total pressure, atmospheres
Q = flow rate out of waste package by barometric pumping, in liters per year
22.4 = the conversion for liters to gram moles at standard temperature and pressure
298°K = the standard temperature.

A similar expression is used for the rate of release of the volatile radionuclides contained in the matrix, except the vapor pressure is reduced by the mole fraction of the radionuclide in the solid solution. Calculations are summarized in Table H-3. The results of these calculation show that only the quick-release fraction of ^{99}Tc and ^{129}I would be volatilized within 10,000 years, and that overall release would be very small.

H-6 CONCLUSIONS

A series of conservative analyses demonstrate that the release of the potentially volatile radionuclides ^{79}Se, ^{99}Tc, and ^{129}I will not significantly add to the risk of the repository in terms of the EPA cumulative release limits. The first analysis demonstrated that even for a large volcanic intrusion, the effect of the additional heat would be of short duration and range, and would not affect a sufficient number of waste packages to release more than 12.5 percent of the combined EPA limits for those radionuclides. Even total release of the three radionuclides in question would have led to exceeding the EPA limit by a factor of about 2.

The second conservative analysis demonstrated that at temperatures likely to be encountered in the repository as a result of repository heat loads, only a small fraction of the volatile radionuclides could be vaporized and carried outside the waste packages. Furthermore, there is compelling evidence that, once released from the waste packages, the volatile radionuclides would strongly favor the water phase, and not be carried to the atmosphere as gases.

Table H-3
Calculation of Volatile Releases at 100°C

Radionuclide	*Inventory gm/moles per waste package*	*Quick-release fraction*[1]	*Vapor pressure at 100°C atm.*[2]	*Mole fraction in solid*	*Reduced vapor pressure atm.*[3]	*Fractional release (Quick)*[4]	Fractional release (solid)[5]	Fractional release (total)[6]
^{79}Se	7130	0	9.1E-4	5E-4	4.5E-7	0	2.7E-7	2.7E-7
^{99}Tc	7.6E5	0.01	0.3	0.003	9E-4	0.34	1.E-5	0.0034
^{129}I	1.34E5	0.004	0.06	3E-5	1.8E-6	0.98	1.2E-7	0.0039

[1] Based on Wilson (1990).

[2] Maximum values from Table F-1 in Appendix F.

[3] Assuming solid solution and Raoult's Law (Garrels, 1978).

[4] Fraction of quick-release radionuclide leaving the waste package in 10,000 years.

[5] Fraction of inventory in solid solution of UO_2 matrix leaving in 10,000 years.

[6] Fraction of total original inventory leaving waste form in 10,000 years.

H-7 REFERENCES

Garrels, R.M. and C.L. Christ, *Solutions, Minerals and Equilibria,* San Francisco, W.H. Freeman, Cooper and Co., 1978.

Lehrman, A. "Volatile Radionuclides: Limiting Concentrations and Transport Rates in an Unsaturated Rock Pore Space (Abstract), in *Migration '89,* 1989.

Montazer, P., E.P. Weeks, F. Thamir, S.N. Yard, and P.B. Hofrichter, "Monitoring the Vadose Zone in Fractured Tuff, Yucca Mountain, Nevada", *Groundwater Monitoring Review,* vol. VIII, no.2 [Spring 1988].

Park, U.S., "Gaseous and Semi-Volatile Radionuclides", Unpublished Presentation to the U.S. Nuclear Waste Technical Review Board, Denver Colorado, June 25-27, 1991.

Pearcy, E.W. and H.K. Manaktala, "Occurrence of Metallic Phases in Spent Nuclear Fuel: Significance for Source Term Predictions for High-Level Waste Disposal", in *High Level Radioactive Waste Management, Proceedings of the Third international Conference,* Las Vegas, Nevada, April 12-16, 1992, vol. 1, pp. 131-136.

Phillips, S.L., F.V. Hale, L.F. Silvester, and M.D. Siegal, "Thermodynamic Tables for Nuclear Waste Isolation", Nuclear Regulatory Commission, NUREG/CR-4864, June 1988.

Turcotte, D.L. and G. Schubert, *Geodynamics: Application of Continuum Physics to Geological Problems,* New York, J. Wiley and Sons, 1982.

Wilson, C.N., "Results from NNWSI Series 3 Spent Fuel Dissolution Tests", Pacific Northwest Laboratories, PNL-7071, 1990. [Prepared by the Battelle Memorial Institute.]

U.S. Environmental Protection Agency/Science Advisory Board, "An SAB Report: Review of Gaseous Release of Carbon-14", Washington D.C., EPA-SAB-RAC-93-010, April 1993.

APPENDIX I

CONTENTS

		Page
I-1	Introduction	I-1
I-2	Regional Setting Geohydrology	I-3
I-3	USGS Regional Model	I-4
I-3.1	*MODFE* Computer Code	I-4
I-3.2	Model Design	I-4
I-3.3	Model Boundaries	I-8
I-3.4	Aquifer Properties	I-8
I-3.5	Recharge and Discharge	I-11
I-3.6	Model Results	I-14
I-3.7	Model Sensitivity and Stability	I-14
I-4	Subsequent Work Related to the USGS Regional Model	I-17
I-4.1	Modeling of the Alkali Flat-Furnace Creek Ranch Subbasin	I-17
I-4.2	The Szymanski Hypothesis	I-19
I-4.3	Revised Conceptual Model	I-20
I-4.4	Site Characterization Study Plans	I-23
I-4.5	Data Needs to Improve Regional Model	I-23
I-5	Summary	I-28
I-6	References	I-29

TABLES

I-1	Hydraulic Conductivity Data	I-10
I-2	Hydraulic Conductivity Data and Recharge Data for Each Zone in Baseline Regional Model of Czarnecki	I-12

FIGURES

I-1	Locations of Regional and Subregional Modeled Areas, with Generalized Groundwater Flow Directions, and Generalized Geology	I-2
I-2	Location of Subregional Modeled Area and Nearby Geographic Features	I-6
I-3	Hydraulic head and Location of Measured Sites	I-7
I-4	Model Boundary Fluxes, Constant-Head Nodes, and Transmissivity Zones	I-9
I-5	Simulated Hydraulic Head for the Baseline-Condition Simulation	I-15
I-6	Baseline, Vertically Integrated Groundwater Flux Vectors at and in the Vicinity of the Primary Repository Area	I-16
I-7	Subregional Potentiometric Surface	I-21
I-8	Location map of Groundwater Subbasin	I-22

APPENDIX I
EVALUATION OF USGS GROUNDWATER MODELING FOR THE REGION THAT INCLUDES YUCCA MOUNTAIN

N.M. Coleman/NMSS

I-1 INTRODUCTION

This report describes the major groundwater modeling work that has been performed by the U.S. Geological Survey (USGS) for the region of southern Nevada. Emphasis will be placed on the evolution of the subregional model originally developed by Czarnecki and Waddell (1984). This report is an auxiliary analysis under the staff's Iterative Performance Assessment effort (IPA Phase 2). Through this program the staff is developing tools needed to review a license application for a potential high-level waste repository.

In the late 1970's the USGS began an appraisal of the Nevada Test Site for potential disposal sites for high-level nuclear wastes. This work included regional geologic and hydrologic investigations, and a regional groundwater flow model was developed by Waddell (1982). Waddell produced a two-dimensional (2-D), steady-state, finite element model that covered an area of about 18,000 kilometers^2. This model extended from the Pahranagat Range and Las Vegas Valley on the east to Pahute Mesa and Death Valley on the west (see Figure I-1). The model included the Yucca Mountain area and almost all of the Nevada Test Site.

Rice (1984) developed a preliminary finite difference model covering an even larger area, extending farther west and south than Waddell's (1982) model. One of the simplifying assumptions used was to simulate the flow system under confined conditions. Initial estimates of transmissivity were based on those obtained from the regional model of Waddell (1982). One of Rice's conclusions was that the model could be improved by calibrating it under unconfined conditions.

Following identification of the proposed Yucca Mountain site, Czarnecki and Waddell (1984) developed a subregional model within the hydrologic subbasin that includes the site. This model was derived using a parameter estimation procedure developed by Cooley (1977, 1979, 1982). Czarnecki (1985) later revised and improved this model to help develop smaller site-scale models of groundwater flow and transport for the Yucca Mountain site. He initially prepared a steady-state baseline model and revised it to simulate the geohydrologic effects of increased recharge in the region. A transient version of the model was later used to evaluate scenarios related to the large hydraulic gradient located north of Yucca Mountain (1990a). Czarnecki (1992) simulated future water level declines in response to various rates of groundwater withdrawals from wells J-13 and J-12.

Because of the importance of the USGS regional modeling work with respect to site characterization of the Yucca Mountain site, the NRC staff have acquired the subregional model

Figure I-1.

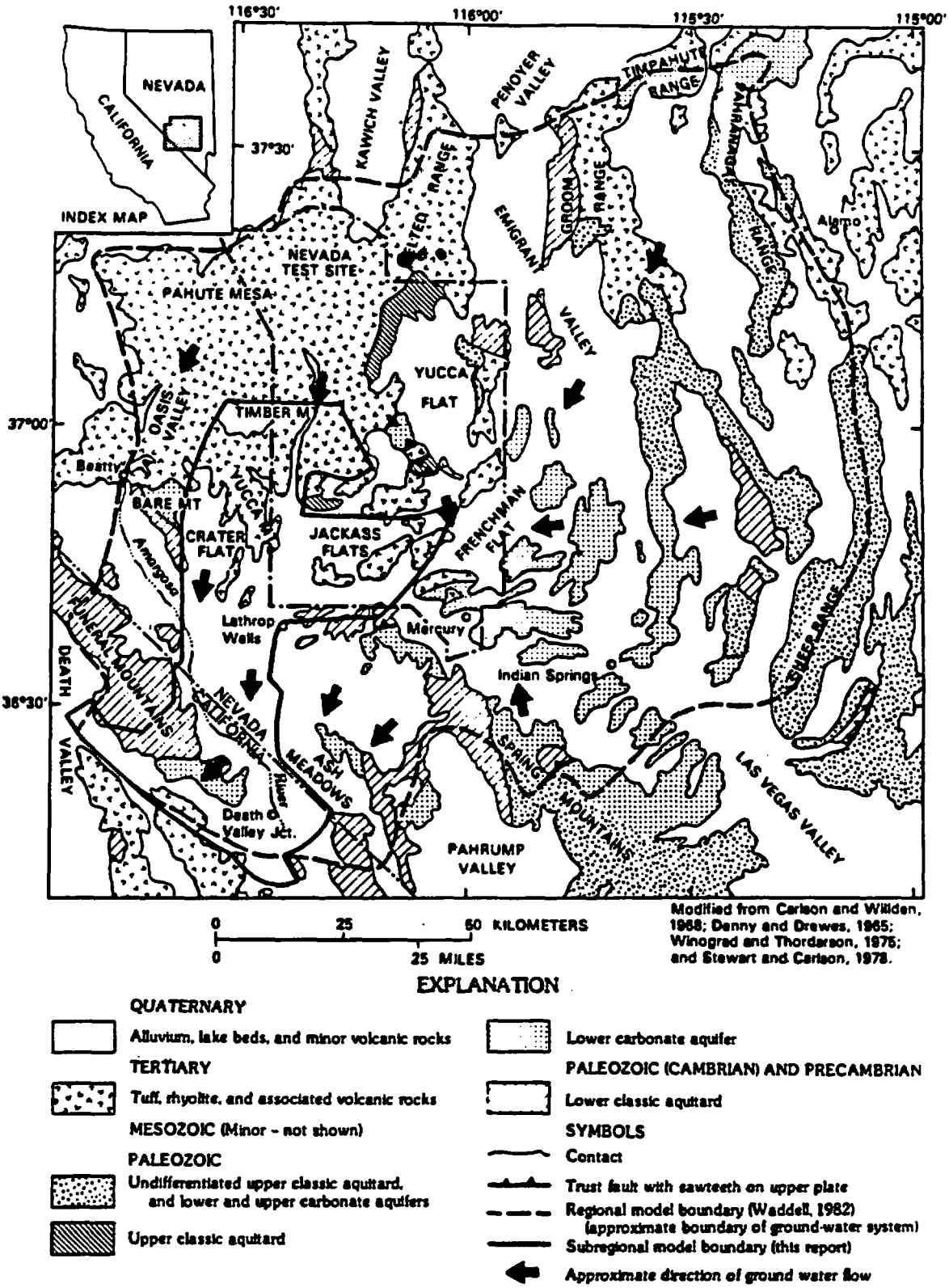

Figure I-1. - Locations of regional and subregional modeled areas, with generalized groundwater flow directions, and generalized geology (after Czarnecki and Waddell, 1984, p. 2).

of Czarnecki (1985) and the *MODFE* computer code. PC-based versions of the code and model have been prepared to facilitate evaluation by the staff.

This evaluation is provided below, and serves as an example of how the staff can directly obtain and evaluate numerical codes and models developed under DOE's high-level waste program. In this way the NRC staff can become more knowledgeable about codes and models during site characterization and prior to receipt of a potential license application.

I-2 REGIONAL SETTING GEOHYDROLOGY

All aspects of the geohydrologic setting must be considered when developing conceptual and numerical flow models for a site or region. The validity of a numerical model depends entirely on the validity of the conceptual model on which it is based. The conceptual flow model must reasonably represent climatic conditions, surface hydrology, hydrostratigraphy, aquifer coefficients, and recharge and discharge conditions. Chapter 3 ("Hydrology") of the Site Characterization Plan (SCP) (DOE, 1988) reports at length on past hydrogeologic work in southern Nevada. The data and interpretations contained in the SCP provide a basis for previous regional groundwater modeling efforts. The current review will not attempt to summarize the extensive information contained in the SCP. Instead, general geohydrologic conditions in the region will be described to place the regional flow modeling in perspective.

The Yucca Mountain site occurs in southern Nevada and has a climate that may be classified as mid-latitude desert. At nearby Yucca Flat the average annual precipitation for the period from 1962 to 1971 was 146 millimeters (DOE, 1988, p. 5-12). Greater amounts of precipitation occur in nearby zones of higher elevation. Annual average potential evapotranspiration greatly exceeds the average annual precipitation, ranging from about 1500 to 1700 millimeters/year (DOE, 1988, p. 3-8). There are no perennial streams in or near the Yucca Mountain area. The only perennial surface water in the region is associated with springs. However, many ephemeral stream channels are present, including those associated with the drainage systems of Forty Mile Wash and the Amargosa River. Runoff occurs at irregular intervals and magnitudes and is associated mainly with summer and winter storms. The estimated discharge for the 100-year flood along Forty Mile Wash is 340 meters^3/sec. (DOE, 1988, p. 3-21). Data on rainfall, runoff, and evaporation are inadequate to determine rainfall-runoff-recharge relationships (DOE, 1988, p. 3-9).

The Yucca Mountain site occurs within the Alkali Flat-Furnace Creek Ranch subbasin of the Death Valley groundwater basin. The subbasin is part of the Basin and Range physiographic province. The geology and structure of this province created the complex hydrogeologic conditions that exist within the subbasin. The regional hydrostratigraphic units within the subbasin are: (1) the valley fill aquifer; (2) volcanic rock aquifers and aquitards; (3) upper carbonate aquifer; (4) upper clastic aquitard; (5) lower carbonate aquifer; and (6) the lower clastic aquitard (DOE, 1988, p. 3-58). Yucca Mountain itself (and surrounding uplands) consists

of layered volcanic rocks of Tertiary age. In the vicinity of Yucca Mountain the water table occurs within these volcanic rocks. Deeper within the volcanic rocks, flow conditions may be confined or semi-confined. A much deeper, confined system exists within the lower carbonate aquifer that underlies the volcanics.

Most of the recharge within the subbasin is thought to occur in areas of higher elevation and correspondingly higher precipitation, located north of Yucca Mountain. A major proportion of recharge occurs in the winter and spring due to lower temperatures and evaporation rates. Recharge rates in lower elevation areas of the Amargosa Desert are unknown but are estimated to be very small. Czarnecki (1985) estimated recharge to be 0.7 millimeters/year for a zone of precipitation that includes Yucca Mountain. Principal discharge areas for the subbasin occur to the south at Franklin Lake Playa (*aka* Alkali Flat), with the closed basin of Death Valley serving as the ultimate discharge area for the region. Large areas of this valley occur at elevations below sea level.

I-3 USGS REGIONAL MODEL

I-3.1 MODFE Computer Code

The subregional groundwater model of Czarnecki (1985) was developed using the *MODFE* computer code (formerly known as *FEMOD*). Documentation for this code has been under development for many years, and has recently been published (Torak, 1992a, 1992b). Using this code, quasi-three-dimensional (3-D) models can be simulated with an areal, 2-D grid by assuming vertical integration of aquifer properties (over a specified depth) and recharge or discharge conditions. *MODFE* is a finite-element code, permitting external and internal boundaries with complex outlines to be represented. This is a definite advantage over finite-difference codes. Physical properties can be specified for individual nodes or for groups of nodes called zones.

MODFE is a modular code in the tradition of previous modular codes developed by the USGS. The modular nature of *MODFE* allows the user to tailor the source code to the problem at hand. For example, a code version for steady-state solutions can be built that excludes all those subroutines that relate only to transient problems. This greatly reduces the size of the compiled code and allows users to run the code even in the limited RAM environments of personal computers.

To reproduce Czarnecki's (1985) baseline results, the code version known as *NSSFE3* was used. This version incorporates steady-state, water table conditions and includes the ability to simulate non-linear vertical recharge and discharge. This latter capability was used to simulate evapotranspiration (ET), which is the principal discharge mechanism in southern Nevada.

I-3.2 Model Design

Czarnecki and Waddell (1984) constructed their numerical model based on what was known

about the Alkali Flat-Furnace Creek flow system in the early 1980's. The domain of this model covers an area of 6000 kilometers^2 and is a subset of Waddell's (1982) model domain (Figure I-1). Geographic features in the vicinity of the model are shown in Figure I-2. The Timber Mountain Caldera is located along the northern boundary and Death Valley occurs at the southwestern extremity of the model.

Czarnecki and Waddell (1984) prepared a horizontal 2-D mesh of 2245 nodes (comprising 4222 elements), with nodal coordinates being expressed as meters north and east of an arbitrary origin. The model mesh is more finely discretized in the vicinity of Yucca Mountain to accommodate the large hydraulic gradient that is present. The finer mesh would also have advantages if a transport model were to be developed to evaluate radionuclide migration near Yucca Mountain. Elements in the finer part of the mesh downgradient from the site have a representative length of about 800 meters, allowing for dispersivities as small as 80 meters (Czarnecki and Waddell, 1984). Model nodes were divided into 13 zones for the specification of areally distributed fluxes and transmissive properties. Transmissivity values were selected using numerical parameter estimation techniques developed by Cooley (1977, 1979). The method used is also known as the "inverse" approach, in which hydraulic head data are input to the parameter estimation model and a transmissivity "solution" is obtained. More than 90 values of hydraulic head were obtained from water levels in wells and springs. Data locations are shown in Figure I-3.

The northern boundary of the model consisted of a line of specified head nodes to represent the area near Timber Mountain. Zones of specified flux were used to represent discharge from the model at Franklin Lake Playa and Furnace Creek Ranch. Specified fluxes into the model were applied along Rock Valley, the western edge of the Amargosa Desert, the western edge of Ash Meadows, and along the northern boundary of Jackass Flat. A flux was also specified along Forty Mile Wash and at the high-ET location of Franklin Lake Playa. The flux values used in the model are not well known (Czarnecki and Waddell, 1984), but were intended to make the simulations more realistic by allowing flow into and out of the model in areas where springs exist, extensive ET is occurring, or where geologic conditions favor flow.

The steady-state solution ultimately arrived at by Czarnecki and Waddell (1984) through trial and error was a set of transmissivity zones and other parameters (lateral and areally distributed flux values) which reasonably represented the observed hydraulic head values. It is emphasized that the result of the calibration procedure is not unique and that different sets of parameters may fit the model equally well. Only geohydrologic experience and judgement can determine which solution is more likely, and to identify where additional field data need to be collected to improve reliability of the simulations.

Czarnecki (1985) used the same mesh described above, but the steady-state model was revised and improved by providing altitude data for each node and incorporating a routine to treat ET as a head-dependent function. The zonation and input parameters were also partly changed.

Figure I-2.

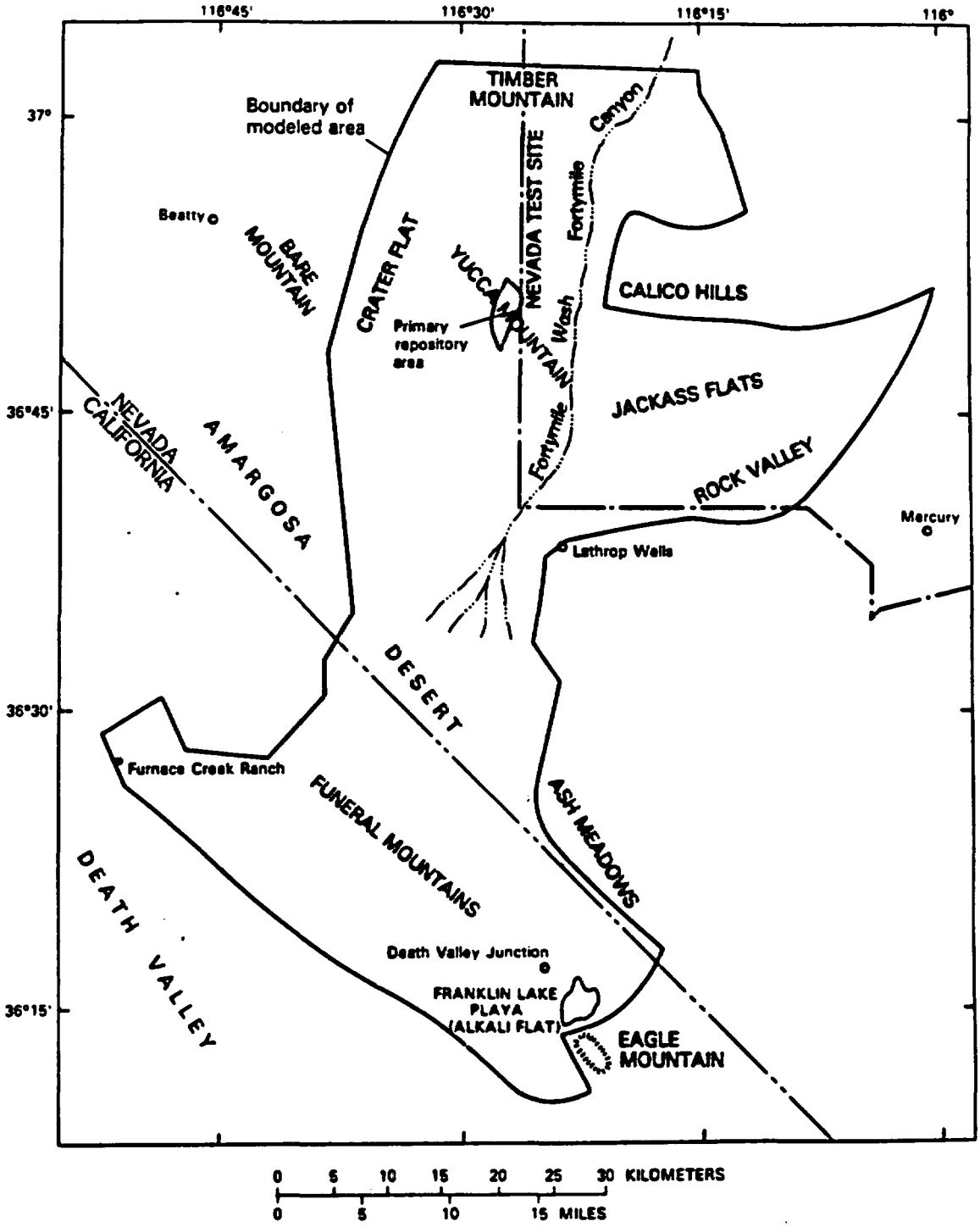

Figure I-2. - Location of subregional modeled area and nearby geographic features (after Czarnecki and Waddell, 1984, p. 6).

Figure I-3.

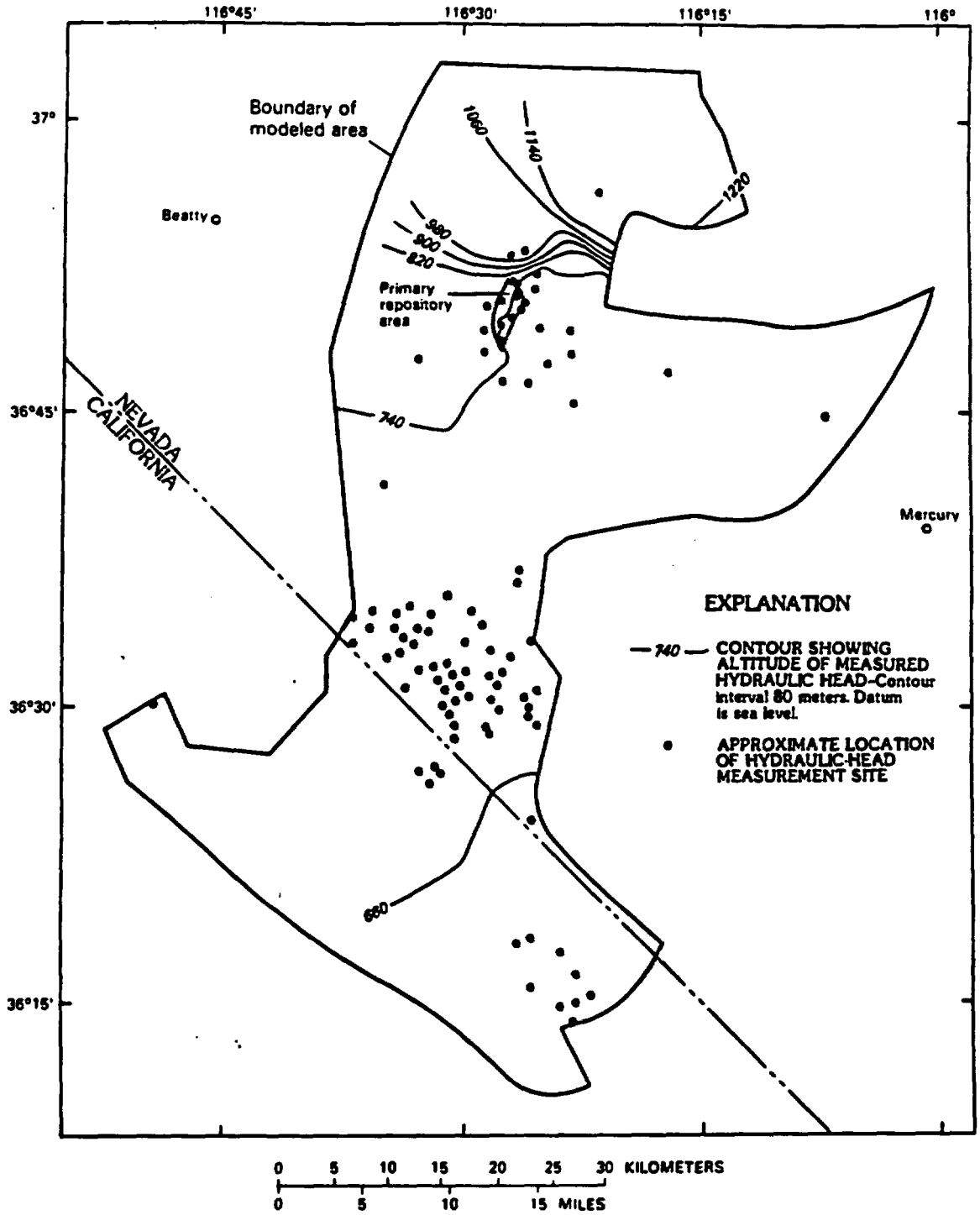

Figure I-3. - Hydraulic head and location of measurement sites (after Czarnecki and Waddell, 1984, p. 13).

Specified head nodes used in the parameter estimation model were replaced with specified flux boundaries. Specified head conditions were established at Furnace Creek and Alkali Flat, in place of prescribed flow conditions in the earlier model. An aquifer thickness of 1000 meters was assumed and transmissive properties were input as hydraulic conductivities. This constitutes Czarnecki's baseline model, which was subsequently modified to evaluate future groundwater scenarios (see section titled "Subsequent Work Related to the USGS Regional Model"). The following sub-sections provide details about the construction of Czarnecki's (1985) baseline model.

I-3.3 Model Boundaries

Czarnecki and Waddell (1984) point out that the boundaries of the Alkali Flat-Furnace Creek Ranch groundwater basin are not well known. They were estimated from potentiometric data, geology, locations of discharge areas, and hydrochemistry. Outer boundaries in the model were derived based on characteristics of the flow system that were assumed to exist. For example, no-flow boundaries were placed along the model edges where little or no input or output was expected to occur, or where flow was considered to be roughly parallel to the boundary itself. Head-dependent flux boundaries were defined for areas where flow was known or assumed to be occurring. Six zones of specified flux were defined to describe volumetric flow into the model domain along boundary segments. Figure I-4 represents these specified fluxes as a series of arrows. For example, based on hydraulic gradients and stratigraphy, flow must enter the subbasin along its northern boundary with the Timber Mountain area. Flow is also assumed to be entering the subbasin from the Calico Hills and Frenchman Flat, from the Ash Meadows area, and from the western Amargosa Desert. All other exterior boundaries of the model were assumed to represent no-flow (or parallel-flow) conditions.

An internal boundary was effectively created by assigning a low hydraulic conductivity value to the zone of high hydraulic gradient located north and northeast of Yucca Mountain. The resulting conductivity contrast diverts groundwater flux around the western portion of this zone and then east and southeast across the Yucca Mountain area.

I-3.4 Aquifer Properties

There is a general lack of hydraulic property data in the modeled region, although some field data exist in the vicinity of Yucca Mountain, the Nevada Test Site, and elsewhere. Much of the available transmissivity data were estimated from specific capacity data. The most transmissive unit in the region is the lower carbonate aquifer, which has transmissivity values as large as 10,000 m^2/d. All other aquifers have transmissivities that are more than an order of magnitude smaller (DOE, 1988, p. 3-68). Transmissivity for the valley-fill aquifer ranges from about 10 to 400 m^2/d.

Hydraulic properties of the volcanic tuffs that form and underlie Yucca Mountain are dominated by the degree of faulting and fracturing that is present, and on the rock properties that contribute to fracturing. Based on pumping tests at well J-13, Thordarson (1983) concluded that the

Figure I-4.

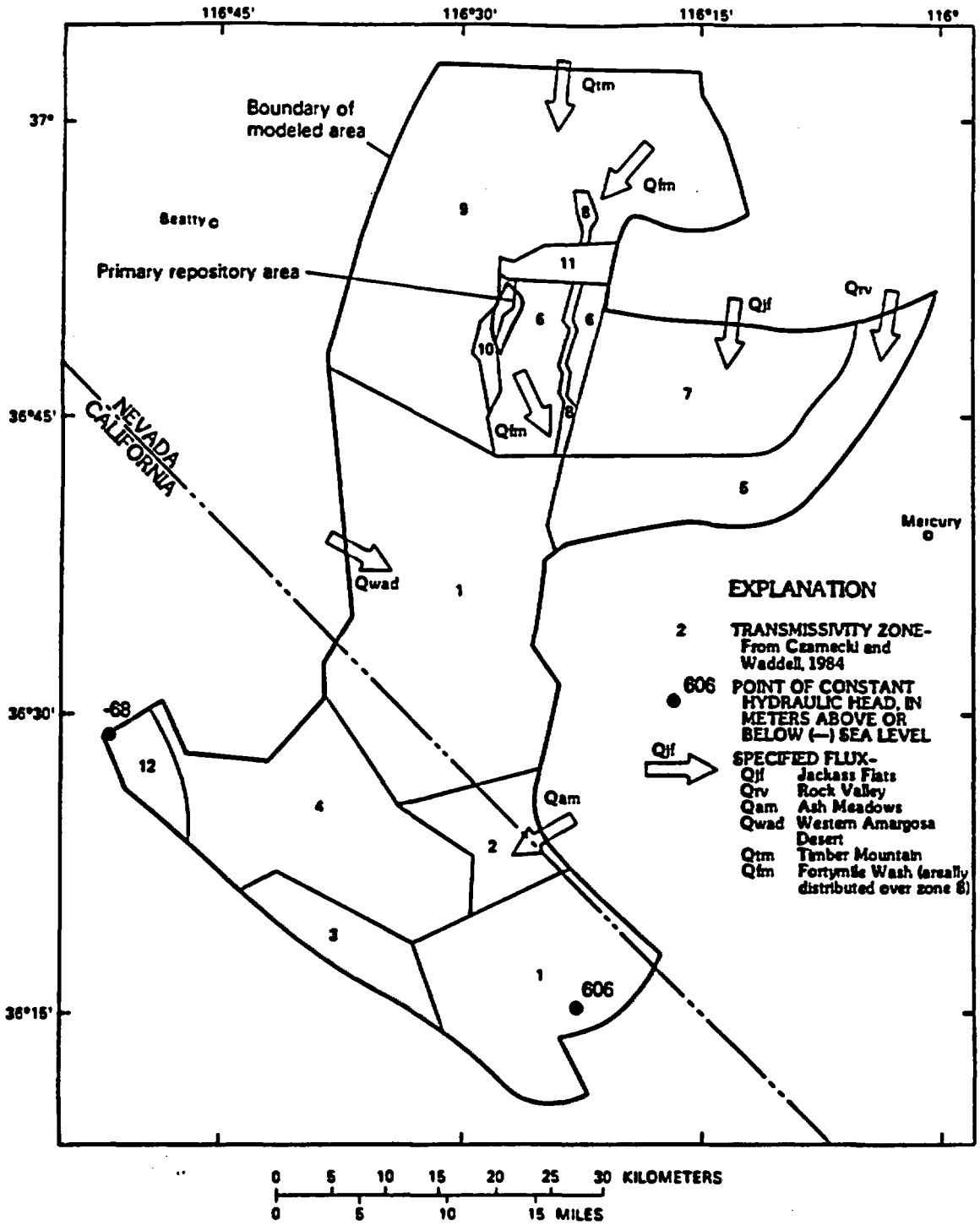

Figure I-4. - Model boundary fluxes, constant-head nodes, and transmissivity zones (after Czarnecki, 1985, p. 7).

Topopah Spring Member of the Paintbrush Tuff has a transmissivity of 120 m^2/d and a hydraulic conductivity of 1.0 m/d. This welded tuff unit, which is the proposed candidate horizon for a high-level waste repository, is unsaturated beneath Yucca Mountain. However, because the volcanic units dip toward the E-SE, it becomes saturated in the vicinity of J-13. Near Yucca Mountain this regional dip causes the top of the water table to occur in various volcanic units, including the Prow Pass and Bullfrog members of the Crater Flat Tuff, tuffaceous beds of the Calico Hills, and the Topopah Spring Member of the Paintbrush Tuff. Table I-1 gives average hydraulic conductivity data for these units in the vicinity of Yucca Mountain, as reported by DOE (1988).

Table I-1. Hydraulic Conductivity Data (from DOE, 1988, p. 3-182)

Stratigraphic Unit	*Well Number*	*Average Hydraulic Conductivity (m/d)*
Topopah Spring Member (Paintbrush Tuff)	J-13	0.7
Tuffaceous beds of Calico Hills	UE-25b#1	0.5
Prow Pass Member (Crater Flat Tuff)	USW H-1 USW H-4 UE-25b#1 UE-25p#1	1.1 to 1.4 0.2 to 0.8 0.4 0.1
Bullfrog Member (Crater Flat Tuff)	USW H-1 USW H-4 UE-25b#1 UE-25p#1	0.006 0.6 to 2.3 0.4 0.05

The hydraulic property data presented above are based on analyses that assume the aquifers to be porous media rather than fractured rock aquifers. An important part of the site characterization program will be to determine under what conditions such assumptions are acceptable. It is often acceptable to make such assumptions in regional modeling. However, at the smaller site scale it may be necessary to consider discrete flow paths within the fractured volcanic rock aquifer.

Czarnecki and Waddell (1984) developed zones of uniform transmissivity based on dominant lithologies considered to be present at the water table (e.g., alluvium, tuffs, carbonate rocks). Using transmissivity values obtained during the earlier parameter estimation modeling, Czarnecki (1985) estimated hydraulic conductivities by dividing the transmissivity values by an assumed

uniform saturated thickness of 1000 meters. The value of saturated thickness was estimated using borehole data from Yucca Mountain and the Amargosa Desert and using resistivity surveys conducted in the Amargosa Desert (Czarnecki, 1985).

Using the *MODFE* code, hydraulic property data are assigned to groups of finite-element nodes which comprise discrete zones. Czarnecki (1985) divided the model mesh into 12 zones of varying hydraulic conductivity and areal recharge (see Figure I-4). The general pattern of these zones was developed during the previous parameter estimation modeling (Czarnecki and Waddell, 1984). An important difference is that Czarnecki (1985) subdivided the Amargosa Desert into three distinct areas. Table I-2 shows that the 12 zones actually comprise 14 different combinations of hydraulic conductivity and areally distributed recharge. Values of hydraulic conductivity used in the model range from a high of 12.8 m/d for Rock Valley to a low of 0.004 m/d used to represent the zone of high hydraulic gradient located north and northeast of the Yucca Mountain Site. A value of 3.65 m/d was used to represent the area which includes Yucca Mountain and western Jackass Flat. This value of hydraulic conductivity is somewhat higher than the average values shown in Table I-1.

I-3.5 Recharge and Discharge

Recharge to the model (Czarnecki, 1985) occurs as a series of specified fluxes along the outer boundaries of the model. The locations of these fluxes are shown in Figure I-4. The other source of recharge to the model consists of steady-state, areally distributed recharge that is applied by zone. Values of areally distributed recharge were based on those estimated by Rush (1970). Rush (1970) estimated average annual groundwater recharge using the technique of Eakin *et al.* (1951). Table I-2 shows the amounts of recharge in millimeters/year for each zone. Four different values of recharge were applied, i.e., 0.0, 0.5, 2.0, and 410 millimeters/year. The largest recharge rate was applied along Forty Mile Wash, the value being obtained through trial and error during parameter estimation modeling (Czarnecki and Waddell, 1984).
Discharge from the model occurs in the vicinity of the constant head nodes at Furnace Creek Ranch and at Franklin Playa, which are located at the southeastern and southwestern extremities of the regional model. These areas are topographic lows, with the result that the assigned heads control discharge fluxes out of the model at these locations. The water table altitudes for these nodes were made to correspond to a depth of 5 meters below land surface to be consistent with the 5-meter extinction depth assigned to the routine to compute ET. A hydraulic head of -68 meters was specified for the vicinity of Furnace Creek Ranch. A head of 606 meters was specified for Franklin Lake Playa (aka Alkali Flat), a known discharge area with high rates of ET. In the baseline model of Czarnecki (1985), discharge from the model domain across specified head boundaries totaled 0.188 meters^3/sec.

Discharge also occurs as ET at model grid nodes where the simulated water table rises to less than 5 meters below land surface. No surface water is permitted to form in the model (i.e., springs or creeks). Wherever the simulated water table rises to the land surface, it is discharged entirely as ET.

Table I-2. Hydraulic Conductivity and Recharge Data for Zones in Baseline Regional Model of Czarnecki (1985).

Zone Number	*Hydraulic Conductivity (m/s)*	*Areally Distributed Recharge*			*Locale*
		(m/d)	*(m/s)*	*(mm/yr)*	
1	0.1691E-04	1.46	0.0	0.0	Amargosa Desert and Franklin Lake Playa
	0.1691E-04	1.46	0.1585E-10	0.5	Amargosa Desert (northern part)
2	0.1105E-04	0.955	0.0	0.0	Area west of Ash Meadows
3	0.1484E-05	0.128	0.1585E-10	0.5	Greenwater Range (western part)
4	0.1385E-05	0.120	0.0	0.0	Funeral Mtns.
5	0.1480E-03	12.8	0.0	0.0	Rock Valley (western part)
	0.1480E-03	12.8	0.1585E-10	0.5	Rock Valley (east) and Frenchman Flat
6	0.4229E-04	3.65	0.1585E-10	0.5	Yucca Mt. and western Jackass Flat (highly discretized)
7	0.4229E-04	3.65	0.1585E-10	0.5	Jackass Flat (eastern part)
8	0.4229E-04	3.65	0.1300E-07	410	Forty Mile Wash
9	0.1105E-05	0.095	0.6340E-10	2.0	Timber Mountain
	0.1105E-05	0.095	0.1585E-10	0.5	Crater Flat
10	0.9100E-06	0.079	0.1585E-10	0.5	Solitario Canyon and Yucca Mt.
11	0.4500E-07	0.0038	0.6340E-10	2.0	Zone NE of Yucca Mt. (with high hydraulic gradient)
12	0.2000E-05	0.173	0.0	0.0	Furnace Creek (Death Valley)

To treat ET in the model, a value for land surface altitude had to be assigned to each node. This information was used by the model subroutine that simulates ET as a non-linear vertical discharge per unit area. This was an important improvement introduced by Czarnecki (1985) over the previous version of this model (Czarnecki and Waddell, 1984), providing a reference altitude for each node to compare with computed water table altitudes. An "extinction" depth of 5 meters was assigned; this was considered the maximum depth from which bare-soil evaporation could occur. During a simulation, ET would occur whenever the simulated water level at a node rose to a depth of less than 5 meters. The ET coefficient used was 0.864 m/d per unit area at land surface. This very large ET rate was used to prevent the simulated water table from rising above the surface. It also removed water from the model area that might have left through runoff. The ET rate decreased linearly to zero at the extinction depth of 5 meters below land surface (Czarnecki, 1985). Thus, the maximum ET would occur for simulated heads at land surface, and all of the discharge would be treated as ET rather than allowing the creation of surface water bodies like springs and streams.

Discharge data are available for springs in the Furnace Creek Ranch area. Some of the springs occur several hundred m above the floor of Death Valley. Discharges in this area were estimated at 0.2 meters^3/sec. (Waddell, 1982). DOE (1988, Tables B-3 - B-5) lists data for more than 20 spring outlets (plus numerous seeps and phreatophyte areas) in the Furnace Creek area. For those springs for which discharge was determined, the combined discharge totals more than 0.15 meters^3/sec This is a minimum discharge because it does not include the many seeps and phreatophyte areas in the vicinity. Czarnecki and Waddell (1984) attribute a total discharge flux of 0.22 meters^3/sec. to the Furnace Creek Ranch area.

Walker and Eakin (1963) estimated discharge by ET from Franklin Lake Playa to be ~0.4 meters^3/sec. Czarnecki (1990b) estimated an average volumetric discharge rate of ~0.26 meters^3/sec. based on field studies at the playa (June 1983 to April 1984). Using Czarnecki's estimate, the ET discharge from this playa, when combined with estimated spring discharges in the region near Furnace Creek (~0.2 meters^3/sec., Waddell, 1982), yields a total discharge at these locations of about ~0.4 to ~0.5 meters^3/sec. This can be compared with the simulated steady-state discharges for these areas obtained using Czarnecki's (1985) model. The combined discharge across specified-head boundaries at Franklin Lake Playa and Furnace Creek Ranch is ~0.19 meters^3/sec. The nonlinear routine that calculates ET yields a discharge of ~0.27 meters^3/sec. The total simulated discharge occurring in the vicinity of Franklin Lake Playa and Furnace Creek Ranch is approximately ~0.46 meters^3/sec.

There is apparent agreement between the observed and simulated discharges in the southern part of the model. However, the estimated spring and ET discharges do not include groundwater underflow which may exit the subbasin in these areas. For example, a significant amount of discharge likely occurs through the alluvial sediments that underlie the Amargosa River. This river basin hydrologically connects the Amargosa Desert to Death Valley, even when no surface

water is flowing. The course of the ephemeral Amargosa River eventually descends into Death Valley, with a terminus at Badwater Basin (the lowest topographic basin in the U.S.). Some groundwater underflow may also occur beneath the Greenwater and Funeral Mountains via the Paleozoic carbonate aquifer. Further discussion about the discharges in the southern part of the model may be moot given the new conceptual model of flow that includes a possible flow divide in the Greenwater Range (see discussion later in this review).

Czarnecki and Waddell (1984) had previously determined that simulated rates of ET at Franklin Lake Playa had the largest effect (of all the model-boundary conditions) on estimated values for aquifer transmissivity at Yucca Mountain. Therefore, ET estimates for the playa had to be better defined. Czarnecki (1990b) documents an extensive program of field investigations at Franklin Lake Playa between June 1983 and April 1984. The playa shows extensive evidence of groundwater discharge. It is characterized by salt pan and porous surfaces, phreatophytes, very shallow groundwater, and upward vertical gradients that greatly exceed horizontal hydraulic gradients. In general, the ET rate depends on the types and density of phreatophytes, depth to the water table, groundwater salinity, soil-moisture properties, and climatic conditions (Czarnecki, 1990b). Czarnecki estimated rates of ET (centimeters/day) using various approaches, including energy-balance eddy correlation and analyses of temporal changes in soil-moisture content, temperature profiles, vertical gradients in the saturated zone, and others. He concluded that the eddy correlation technique gave the most reliable estimates for ET because it is the most direct method. Czarnecki reported an estimated ET range of 38 to 41 centimeters/year at Franklin Lake Playa for 1983-84.

I-3.6 Model Results

Czarnecki (1985) obtained a baseline, steady-state solution of simulated hydraulic heads for the subbasin (see Figure I-5). Compared to the solution from the parameter-estimation model of Czarnecki and Waddell (1984), the model results showed a decrease in the range of head residuals (-18.9 to +21.0 meters) and a reduced estimated sum-of-squared errors for observed-versus-calculated hydraulic heads (4101 meters^2). However, these comparisons may not have much meaning because the observed hydraulic head data are concentrated in areas that have small hydraulic gradients (e.g., the Amargosa Desert). Data are needed in areas where water table elevations change more rapidly (e.g., Furnace Creek area, and the region north and west of Yucca Mountain). Figure I-6 shows the vertically integrated groundwater flux vectors in the vicinity of the Yucca Mountain site for the baseline simulation.

I.3-7 Model Sensitivity and Stability

Modeling studies by Waddell (1982) and Czarnecki and Waddell (1984) showed recharge to be a highly sensitive element of their regional flow models. In particular, the recharge value applied to Forty Mile Wash had a strong influence over the simulated heads at nearby Yucca Mountain. The solution was also found to be very sensitive to the rate of ET at Franklin Lake Playa.

Figure 5

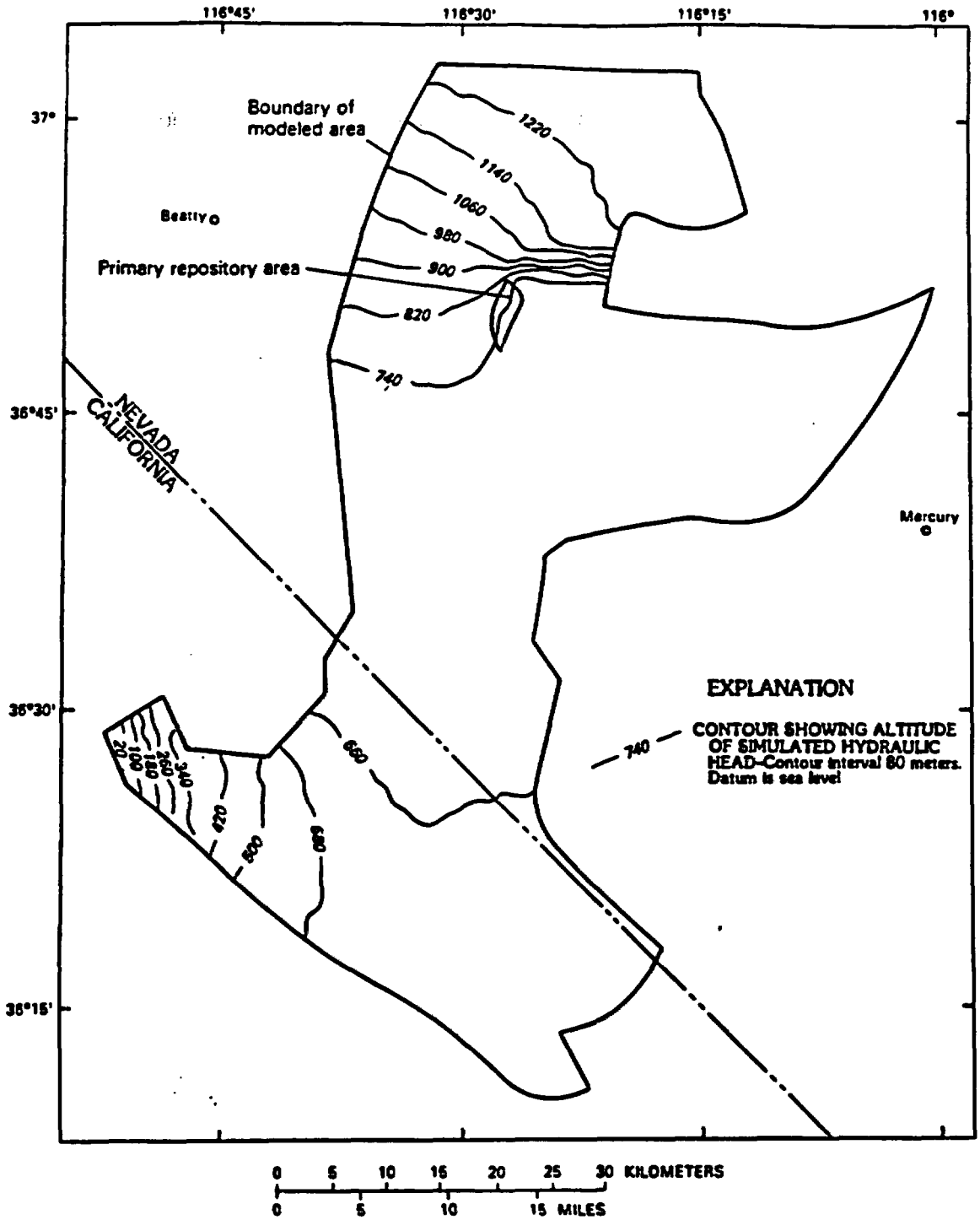

Figure I-5. - Simulated hydraulic head for the baseline-condition simulation (after Czarnecki, 1985, p. 10).

Figure 6

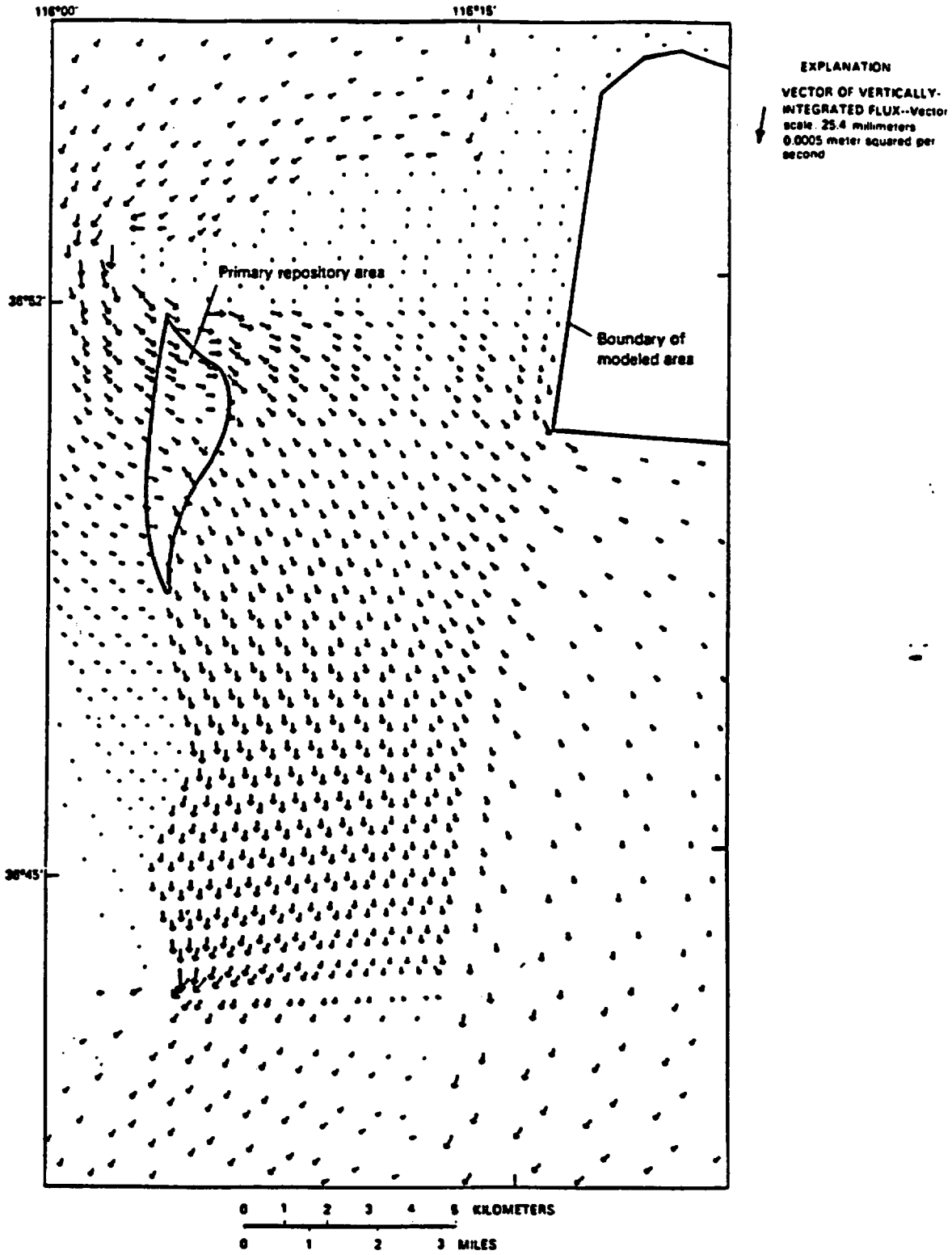

Figure I-6. - Baseline, vertically integrated groundwater flux vectors at and in vicinity of primary repository area (after Czarnecki, 1985, p. 29).

Czarnecki (1985) reported instability problems with the model that were probably caused by the nonlinear routine in *MODFE* that handles ET. It is known that nonlinear routines can cause instability problems in numerical solutions (Roache, 1973). Significant mass-balance errors resulted when extinction depths of less than 5 meters were specified. Discretization errors may be produced by the presence of obtuse angles within the triangular elements of the finite-element mesh (Torak, 1992a). The finite-element mesh prepared by Czarnecki and Waddell (1984) contains 4222 elements. The mesh was analyzed with a *BASIC* routine and found to contain almost 600 elements that include obtuse angles. For a more accurate numerical solution, all angles within the triangular elements should be acute.

In independent simulations, the NRC staff found that Czarnecki's modeling results could be reproduced using 386 and 486 personal computers equipped with *WEITEK* math coprocessors. Serious instability problems caused by round-off errors arose when running the model on computers equipped with another type of math coprocessor. The problem was corrected by specifying floating point double precision (DECLARE ALL REAL*8) in each subroutine of the *FORTRAN* source code. Of course, the use of double precision greatly increases the memory (RAM) required to run the model.

I-4 Subsequent Work Related to the USGS Regional Model

I-4.1 Modeling of the Alkali Flat-Furnace Creek Ranch Subbasin

Czarnecki (1985) investigated the possible effects on the water table of a wetter future climate. He revised the baseline model to simulate the effects of increased recharge in the region. Both recharge amounts and lateral fluxes were increased, resulting in water table rises at the Yucca Mountain site. Based on this model, Czarnecki (1985) concluded that a 100 percent increase in precipitation caused the simulated position of the water table at Yucca Mountain to rise as much as 130 meters. This degree of water table rise would not be enough to flood a hypothetical repository in the Topopah Spring Member of the Paintbrush Tuff. However, the simulated water table rise would greatly reduce the thickness of the unsaturated zone and would be sufficient to cause springs to form south and west of Timber mountain, along Forty Mile Wash, in the Amargosa Desert near Lathrop Wells and Franklin Lake Playa, and near Furnace Creek Ranch in Death Valley.

Czarnecki (1985) noted that the future water table rise due to a wetter climate (and increased recharge) may be exaggerated because surface water runoff was not permitted in the model. All discharges from the model occurred as either ET or lateral groundwater flow. However, it is noted that the future simulations were derived by revising a baseline model that had assumed zero modern-day recharge over large areas of the model domain. It is not yet known whether the recharge assumptions used in the baseline model are reasonable (see discussion under "Revised Conceptual Model").

There is evidence that the water table at Yucca Mountain was significantly higher in the past.

Marshall *et al.* (1993) describe strontium isotopic evidence for a higher water table at Yucca Mountain. They conclude that the water table may have been about 85 meters higher in the past. This degree of water table rise is of the same order of magnitude as that predicted by Czarnecki (1985) under wetter climatic conditions. This is significant with respect to performance of a potential repository. Any long-term rise of the water table over the next 10,000 years would reduce the thickness of the unsaturated zone beneath the repository. This portion of the unsaturated zone is considered the key barrier within the natural system.

There is also evidence that a perennial spring existed in Forty Mile Wash near Yucca Mountain approximately 47,000 years ago (Wisconsin glacial stage). Midden site FMC-7 is located about 13 kilometers northeast of Yucca Mountain adjacent to the canyon of Forty Mile Wash (Area 29, Nevada Test Site). The site occurs at an elevation of 1250 meters, about 60 meters above the floor of the canyon (National Research Council, 1992, p. 87). The midden site is north of the zone of high hydraulic gradient in an area where groundwater is presently much shallower than at Yucca Mountain. This is the only discovered evidence of a past discharge site relatively near Yucca Mountain. The National Research Council (1992, p. 86) concluded that there is "virtually no evidence in the glacial-age fossil record for an increase in average annual precipitation exceeding 40 percent of modern amounts."

Czarnecki developed a transient version of his model to investigate phenomena like the large hydraulic gradient located north of the site (Czarnecki, 1990a). In one scenario, a postulated hydrologic barrier was disrupted and large volumes of groundwater were released to flow southward. Such a scenario could arise due to faulting associated with an earthquake. This scenario caused a maximum rise of about 40 meters in the simulated water-level at Yucca Mountain (National Research Council, 1992, citing personal communication with J. Czarnecki).

Czarnecki (1992) simulated water level declines in the Yucca Mountain area in response to future groundwater withdrawals from wells J-13 and J-12, located about 7 kilometers southeast of the Yucca Mountain site. This work is very important because it represents a 10-year forecast of how future groundwater levels will be affected by human activities. This work supported a request from DOE to the State of Nevada for a permit to pump up to 5.7×10^{-3} meters^3/sec. from J-13. DOE requested the water to support site characterization work at Yucca Mountain over the next 10 years. Eight different pumping scenarios were analyzed using a transient version of Czarnecki's 1985 model and various combinations of withdrawal rates. Four of the scenarios involved pumping from a single well, while both wells were pumped in the other four scenarios. For each withdrawal rate, simulations were made with aquifer specific yields set at 0.001, 0.005, and 0.01. Czarnecki (1992) considered a specific yield of 0.01 to be the value that is best supported by available data. The most extreme scenario represented the combined maximum pumping capacities from both wells (8.771×10^{-2} meters^3/sec.) and assumed an aquifer specific yield of 0.001. This resulted in a drawdown of over 12.2 meters at both wells J-12 and J-13 at the end of the 10-year period. Under the same pumping conditions, and assuming a specific yield of 0.01, simulated drawdowns at J-13 and J-12 were

about 3.0 meters and varied from 1.8-2.4 meters at the Yucca Mountain site. The simulated drawdown for the anticipated withdrawal rate of 5.7×10^{-3} meters^3/sec. from well J-13 (based on a 10-year pumping period and a specific yield of 0.01) was 0.29 meters at J-13. The drawdown at the Yucca Mountain site would be about 0.2 meters. It is expected that one of the many scenarios analyzed by Czarnecki (1992) will be representative of actual groundwater withdrawals during site characterization, and can be used to test how well the regional model represents the flow system.

Oatfield and Czarnecki (1989) analyzed drillers' logs and data from geophysical surveys to identify areas in the Amargosa Desert that have relatively higher or lower transmissivities. They concluded, based on drillers' logs, that the thick alluvial deposits cannot easily be subdivided into correlative stratigraphic units. However, the drillers' logs suggested a trend of increasing consolidation of sediments from north to south. Hydrogeologic interpretation of a resistivity (vertical electric sounding) survey was complicated by a lack of information about aquifer properties and groundwater quality at depth. However, high resistivity values in the upper 75 meters of alluvium were interpreted to coincide with relatively fresh, shallow groundwater that may enter the Amargosa Desert via the Forty Mile Wash drainage system.

I-4.2 The Szymanski Hypothesis

Szymanski (1989) asserted that groundwater at Yucca Mountain had risen to repository level repeatedly in the past, primarily due to tectonic processes. A panel of the National Research Council (1992) evaluated the potential for future rises of the water table to occur at Yucca Mountain. The panel assessed the likelihood that the water table could rise to the height of the repository horizon by any plausible geological process, or whether such a rise had occurred in the past. The panel cited the previous work of Waddell and Czarnecki, and emphasized the importance of field evidence in establishing the presence of past discharge areas. Also, the hydrologic effects of some historic earthquakes were discussed. The panel did not reach any definitive conclusions about how high the water table might rise in response to earthquakes. However, they concluded that there is no evidence to support the assertion that the water table has periodically risen hundreds of m from deep within the earth. With respect to earthquakes, the panel (National Research Council, 1992, p. 128) concluded that "... while there are uncertainties in current interpretations because specific site data are not available, ... there is nevertheless sufficient confidence in the aseismicity of the site and in the inability of earthquakes to generate large water table changes at the site ... to warrant further characterization of the site to determine its suitability ..." The panel recommended that the Department of Energy conduct a literature search regarding the hydrologic effects of historic earthquakes, locally and worldwide, to determine the potential for large water table rises in response to the coupling of seismic and hydrologic systems.

The earthquake that occurred near Little Skull Mountain on June 29, 1992 (magnitude 5.6) caused only a minor, transient change in the water table at the Yucca Mountain site. The maximum fluctuation of the water table at the site was estimated at only 0.4 meters (O'Brien and

Tucci, 1992). The data were obtained from two wells instrumented to continuously monitor fluctuations in the water table and fluid-pressure in a deeper, isolated interval. Water table fluctuations of similar magnitude were caused by more distant and more powerful earthquakes. Two major earthquakes occurred in southern California on June 28, 1992. Both were about 300 kilometers from Yucca Mountain and were measured as having magnitudes of 7.5 (Landers) and 6.6 (Big Bear Lake). The Landers and Big Bear Lake quakes caused estimated water table fluctuations of 0.9 meters and 0.2 meters, respectively (O'Brien and Tucci, 1992).

I-4.3 Revised Conceptual Model

New ideas about regional flow in the subbasin were presented and documented by Czarnecki (1987, 1989) and Czarnecki and Wilson (1989). The previously-accepted conceptual model of the regional groundwater system assumed that flow beneath the central Amargosa Desert ultimately discharges from two major areas: Furnace Creek Ranch and Franklin Lake Playa. In the baseline model of Czarnecki (1985), zero recharge was assumed to be occurring over most of the subregion south of Yucca Mountain. New data were obtained by Czarnecki (1989) which led to an alternate conceptual model of subregional flow. Potentiometric data were obtained from mining property boreholes in the Greenwater Range (between Death Valley and the Amargosa Desert). These data show a water table altitude in that area of about 875 meters (Figure I-7), providing evidence of significant groundwater recharge and the probable presence of a groundwater flow divide beneath this range. The data suggest that flow divides beneath the Greenwater and Funeral Mountains may isolate the water table aquifer in the Amargosa Desert from the flow system in Death Valley. Geographic features of this area are illustrated in Figure I-8.

The inclusion of flow divides beneath the Greenwater and Funeral Mountains is a major revision of the conceptual model used to develop Czarnecki's regional flow model, in that the discharge area at Furnace Creek Ranch may be relatively isolated from the water table aquifer underlying the Amargosa Desert. Instead, Franklin Lake Playa may serve as the principal discharge area for the subregional water table flow system that includes Yucca Mountain, and discharge at Furnace Creek Ranch may be derived primarily from the confined carbonate aquifer. Winograd and Thordarson (1975) had previously suggested this possibility, based on the proximity of spring discharge to the lower carbonate aquifer and temperature and hydrochemical conditions (DOE, 1988, p. 3-79). A portion of the discharge at Furnace Creek Ranch may also be derived from recharge in the nearby mountains. To help confirm the new conceptual model, a number of wells would be needed to better define hydraulic heads in the groundwater divide areas north and east of Furnace Creek Ranch. DOE (1991a, p. 3.2-6) describes plans to drill new wells, including one planned for the eastern edge of the Funeral Mountains. Figure I-7 shows Czarnecki's proposed revision of the flow system with inferred water-level contours based on the data from the Greenwater Range and a principal discharge area at Franklin Lake Playa.

As discussed in Czarnecki and Wilson (1989), a revised conceptual model for the subbasin would include the following:

Figure I-7.

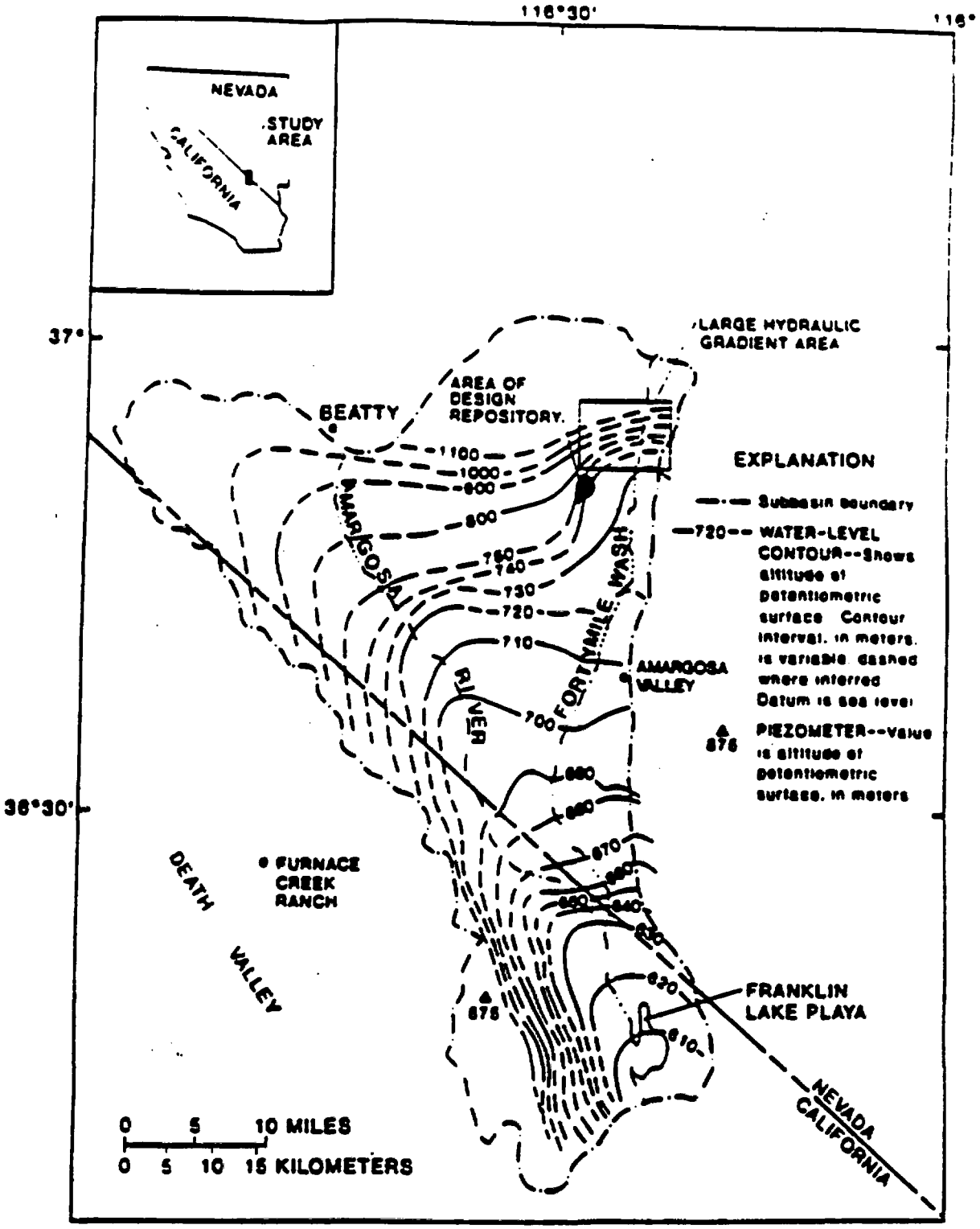

Figure I-7. - Subregional potentiometric surface (after DOE, 1991a, p. 1.2-7).

Figure I-8.

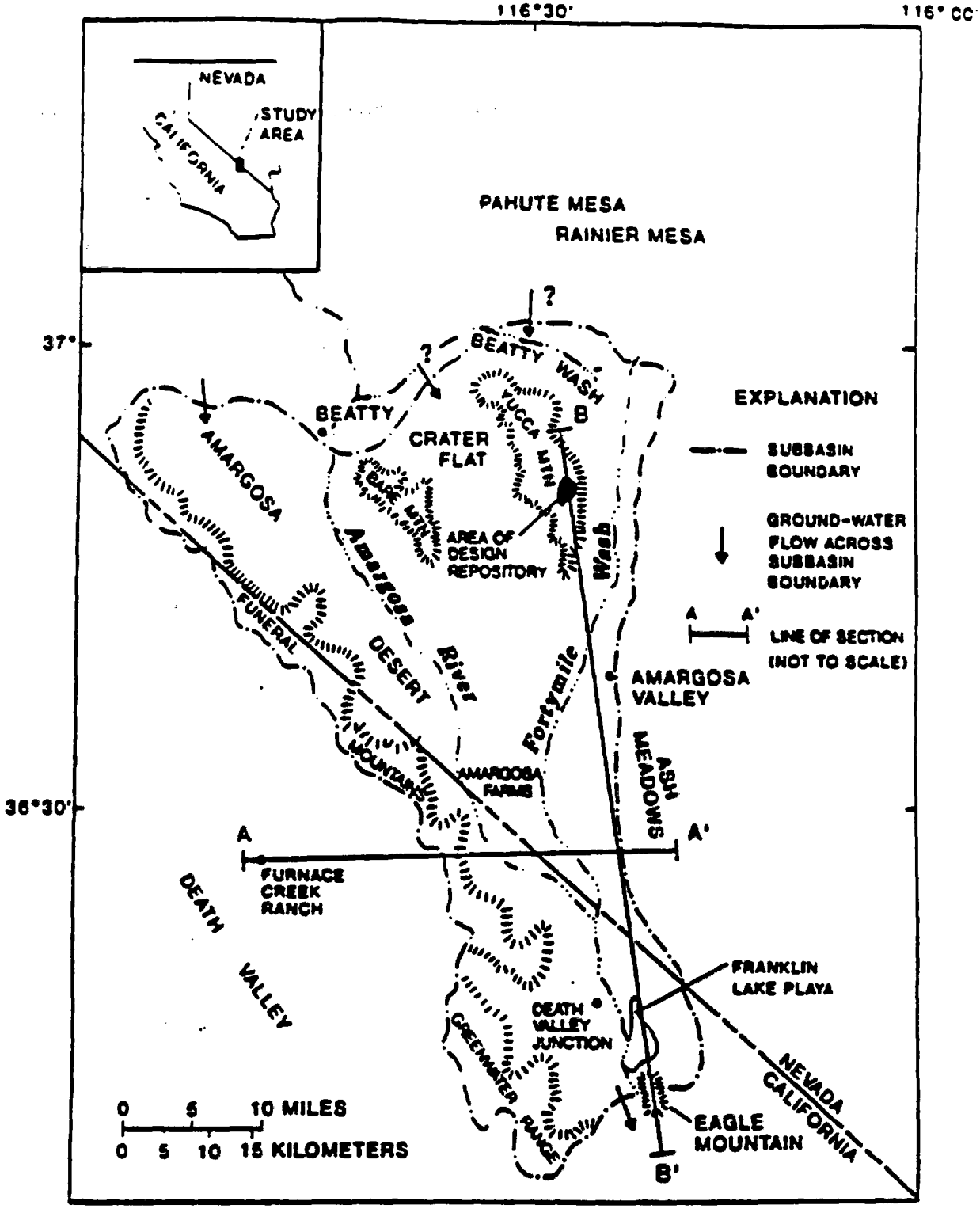

Figure I-8. - Location map of groundwater sub-basin (after DOE, 1991, p. 1.2-3).

- The presence of a regional Paleozoic carbonate aquifer which underlies the subbasin that includes Yucca Mountain;

- Upward flow originating from the carbonate aquifer occurs from great depths within the subbasin;

- Spring flow in Death Valley near Furnace Creek Ranch is from the carbonate aquifer, which forms a confined aquifer that is separate from the overlying water table system; and

- Some recharge to the groundwater system may be occurring even in arid areas such as the Funeral Mountains and the Greenwater Range.

The revised conceptual model is significant in that it would require less volumetric flow through the region that includes Yucca Mountain. Other conditions being equal, this means that simulated groundwater velocities would generally be less than in the original model. But it also suggests that the flow system may be more susceptible to future large-scale stresses such as extensive groundwater overdrafts.

I-4.4 Site Characterization Study Plans

In support of the Yucca Mountain project, the DOE has developed study plans that outline a program for characterizing and modeling the regional flow system. DOE (1991a) describes plans to characterize the regional groundwater flow system. The study "Regional Hydrologic Synthesis and Modeling" (DOE, 1992) will analyze regional groundwater data, formulate conceptual models of the regional flow system, and develop and calibrate numerical models. Other study plans, such as those involving climatology, geochemistry, and geology, are also related to the characterization and modeling of the groundwater system. Results of the regional modeling will be used to specify boundary conditions for site-scale models of the saturated zone at Yucca Mountain. Regional models will also be used to estimate changes in the regional (and local) groundwater system caused by future climatic conditions, human activities, and tectonic events. In this way the modeling results are intended to support site-scale evaluations of repository performance with respect to the NRC's criterion for groundwater travel time and the EPA standards under 40 CFR Part 191.

I-4.5 Data Needs to Improve Regional Model

Documentation of Well Data: Previous reports on regional modeling in the Yucca Mountain region do not provide sufficient information about wells and boreholes used to obtain hydraulic heads for model calibration. For example, Czarnecki and Waddell (1984) provide a table of hydraulic heads and a list of data sources. However, of the five data sources listed, only two are published reports, and only one of these (Walker and Eakin, 1963) lists tabular information about wells in the region. The Walker and Eakin (1963) reference is almost 30 years old and

presents well locations using township and range coordinates rather than the currently-used Nevada State plane coordinate system. The other published data source cited by Czarnecki and Waddell (1984) is Waddell (1982). This reference cites Thordarson and Robinson's (1971) inventory of over 6000 wells and springs within a 161-kilometer radius of the Nevada Test Site, but that reference is more than 20 years old. Because these references are decades old, the current status of the documented wells is unknown.

It is recognized that regional modeling studies rely heavily on existing data sources such as irrigation wells, farm and ranch wells, and mining exploration boreholes. These wells and boreholes were not designed for the scientific collection of groundwater data; therefore, details of their construction are usually not well documented. Nevertheless, they are indispensable for establishing long-term water-level changes and calibrating regional models, and known details about such data sources should be documented. Such wells and boreholes are generally privately owned and may become inaccessible to future investigators; therefore, they should be documented to the extent practicable.

Regional Evapotranspiration (ET) and Recharge: DOE (1991a) describes characterization of the regional groundwater flow system, and includes an activity titled "Evapotranspiration Studies." The objective of the activity is to estimate ET rates in the Amargosa Desert to provide data for regional and sub-regional models. Although the objective refers to the Amargosa Desert, the activity mainly emphasizes work at Franklin Lake Playa, a key discharge area. It is not clear how estimates of ET and recharge will be obtained for other areas in the regional model. In fact, Czarnecki (1985) assumed zero recharge for most of the area of the regional model that is south of Yucca Mountain.

Groundwater recharge rates are thought to be small over most of southern Nevada. More groundwater recharge is expected to occur in areas of higher elevation due to lower temperatures and greater annual precipitation. Some areas, such as Forty Mile Wash and other alluvial valleys, are capable of producing high recharge fluxes during infrequent, surface-water runoff events of large magnitude. In his steady-state, sub-regional model, Czarnecki (1985) used recharge rates ranging from 0.0 millimeters/year (Amargosa Desert, western Rock Valley, Franklin Lake Playa, Funeral Mountains) to 410 millimeters/year (Forty Mile Wash). Intermediate recharge rates of 0.5 and 2.0 millimeters/year were assigned to other areas, with Timber Mountain having a designated rate of 2.0 millimeters/year.

In most of Nevada, actual rates of ET are much less than the potential evapotranspiration (PET), which is the maximum amount that can occur under given meteorologic conditions. This is true because in many areas the only water available for ET is obtained from scanty precipitation. Franklin Lake Playa is an exception in that groundwater flows upward in this discharge area, producing a shallow water table and maximizing the amount of ET that can occur.

In sensitivity studies of the parameter estimation model of Czarnecki and Waddell (1984),

specified flux at the Franklin Lake Playa had the largest effect of all the specified fluxes on the estimate of hydraulic properties in the vicinity of Yucca Mountain. As a result of these sensitivity studies, Czarnecki (1990b) performed extensive fieldwork at the playa to evaluate various methods to estimate ET and to measure hydraulic gradients and aquifer properties (see previous discussion). Czarnecki (1990b) considered a range of 38 to 41 centimeters/year as the most reliable ET estimate at Franklin Lake for 1983-84. Although rates of ET can be estimated at given locations, to obtain volumetric fluxes it is necessary to estimate the area over which a given ET rate is occurring. This is difficult to accomplish in practice, and limits the accuracy of areal estimates of ET over various scales. For example, at Franklin Lake Playa the total area of shallow groundwater and relatively high ET is not well known.

There is a need to obtain improved estimates of ET and groundwater underflow at Franklin Lake Playa, especially in light of the alternate conceptual flow model presented in Czarnecki (1989) in which the playa area may act as the principal water table discharge area for the subbasin that includes Yucca Mountain. There is also a need for improved estimates of ET for other areas within the region in order to better estimate rates of deep percolation through the unsaturated zone to the water table. Such estimates are dominated by ET rates because the percentage of precipitation that returns to the atmosphere via ET greatly exceeds the percentage of rainfall that ultimately becomes groundwater recharge.

Hydraulic Heads: Although some aquifer property data exist in the modeled region, the regional model was calibrated primarily based on hydraulic heads. As shown in Figure I-3, wells in the USGS model are concentrated in three areas: (1) the Amargosa Desert; (2) the vicinity of Yucca Mountain; and (3) near Franklin Lake playa. For some key areas, well data are practically nonexistent. There are no wells along the northernmost boundary where a groundwater influx is assumed from the Timber Mountain caldera. Insufficient wells exist north of Yucca Mountain to define the extent and nature of a zone of high hydraulic gradient. This high gradient zone is the dominant feature in the potentiometric surface at the site. It is important to determine the source of this feature and its physical properties. This issue was raised by the NRC staff in Comment 20 of its Site Characterization Analysis (NRC, 1989, p. 4-25). DOE has specific plans to explore the high hydraulic gradient, which include the drilling of new wells. Wells WT-23 and WT-24 will be located at intermediate distances between two of the wells that currently define the high gradient, H-1 and I-1 (DOE, 1991b). Borehole UZ-14 is being drilled in Drill Hole Wash in 1993 and may also help to define the nature of the high gradient. It is being constructed near the existing borehole UZ-1, which encountered either extensive perched water or the water table itself. UZ-14 will clarify the groundwater conditions near UZ-1.

Wells are also lacking in the geologic transition zone that occurs between the volcanic terrane of Yucca Mountain and the Amargosa Desert. Wells are similarly lacking in the Funeral Mountains area, south of the Amargosa Desert. The head contours simulated by Czarnecki show a steepened gradient in the vicinity of Furnace Creek Ranch. This cannot be verified due to a

lack of wells, but it does correspond with a drop in elevation toward Death Valley. But most importantly, the preliminary information that indicates a flow divide may exist between Franklin Lake Playa and Furnace Creek Ranch, if confirmed, would require a reconfiguration of the model to properly reflect newly inferred subbasin boundaries.

Three-Dimensional Modeling: DOE (1992) describes plans to proceed with 3-D modeling of the regional groundwater system. Three-dimensional (multi-layer) numerical models can be useful tools for understanding the interactions between unconfined and confined aquifers. However, there must be sufficient potentiometric (and other hydrogeologic) data to reasonably define and calibrate a model to justify the use of 3-D techniques. In other words, to model in three spatial dimensions, supporting hydrogeologic data must be reasonably distributed in three dimensions.
(DOE, 1992) discusses previous regional modeling and indicates that a preliminary quasi-3-D model has already been developed, citing Sinton and Downey (written communication). This model consists of two layers, the lower of which represents the Paleozoic carbonate rocks. DOE (1992, page 3.4-1) states that "With the existing data base, use of more than two layers to represent the regional ground-water-flow system is not expected to be justified because of a sparsity of data on the 3-D hydrogeologic properties of the system."

It is not clear whether 3-D modeling of even two layers can be supported given that very little hydrologic information presently exists for the deep Paleozoic aquifer system (upper and lower carbonate aquifers). In the vicinity of Yucca Mountain, only one well (UE-25 p#1) penetrates Paleozoic carbonate rocks. At this location the carbonates are 1.2 kilometers deep, and have a hydraulic head that is about 19 meters higher than in the overlying zone. Although this is a significant upward gradient, it is not known whether it could significantly influence flow directions and magnitudes in the upper part of the saturated zone, more than 1000 m above the carbonates at the location of UE-25 p#1. Even within the tuffs that overlie the deep carbonate rocks, there are zones that are confined or semi-confined, illustrating the complexity of the saturated zone flow system. Without the necessary subsurface data, there may not be enough potentiometric or physical property data from the Paleozoic carbonates to adequately calibrate a 3-D model.

Data limitations are also discussed in the study plan to characterize the Yucca Mountain Regional Ground Water Flow System (DOE, 1991a). That is the key study plan under which data will be collected to support the regional groundwater modeling activities. DOE (1991a, p. 3.1-6) states that: "Little is known about the distribution of hydraulic head with depth within the flow system. Hydraulic-head data in the vertical dimension are critical for calibrating 3-D models of ground-water flow. At present, only a handful of points exist where hydraulic head has been determined at various depths."

DOE has identified additional wells to be drilled in the vicinity of Yucca Mountain that may penetrate the Paleozoic aquifer and would contribute to 3-D site models. They would not,

however, significantly add to regional well coverage. Wells proposed to be drilled in Crater Flat, near Lathrop Wells, and near the Funeral Mountains (DOE, 1991a) would improve the regional data base, but it is questionable whether the data would be sufficient to calibrate a 3-D model that includes the Paleozoic carbonates as a separate layer.

Downey *et al.* (1990) describe a conceptual groundwater model of the southern Nevada and Death Valley region. This conceptual model illustrates the geologic complexity of the region. Downey *et al.* criticize existing models of the Yucca Mountain region for being 2-D, and inadequate to represent long-term changes in the groundwater flow system. They state that existing models are based on limited head data, elevation and precipitation estimates, and simplified geology. Downey *et al.* (1990) advocate a 3-D approach for boundary selection and estimation to properly represent the groundwater system. Their approach to estimating unknown boundary conditions for the regional flow system includes six steps (Downey *et al.*, 1990, p. 725):

(1) Incorporate known boundary-conditions from playas in Death Valley and Ash Meadows;

(2) Use geological, pedological, geomorphological, botanical, and hydrological observations to develop initial boundary conditions for other boundaries;

(3) Test the initial conditions using steady-state and transient 3-D models;

(4) Back-calculate the boundary conditions for flux boundaries to the northwest, north, and east, thereby obtaining new, improved boundary-condition estimates;

(5) Compare calculated values with known data during calibration steps; and

(6) Adjust the model.

The apparent intent is to integrate all existing geologic, hydrologic, geophysical, and hydrochemical data for the Death Valley flow system using a Geographic Information System. DOE's intent is to synthesize all existing data into the best regional models that can be generated (DOE, 1993). Notwithstanding the recommendations of Downey *et al.* (1990), it is not clear whether their approach will, in practice, be greatly superior to or substantially different from past modeling efforts. Their recommended Step "2" basically says to incorporate more data from interdisciplinary sources. Obtaining more data will improve any model. The 3-D approach will require specification of hydrologic conditions within model layers and along the boundary between layers. Overall, it is not clear whether sufficient data exist or will become available to justify 3-D modeling, particularly for the Paleozoic carbonate aquifer. A

commitment to perform 3-D modeling will have to be accompanied by a commitment to obtain enough data to reasonably justify the 3-D approach.

Other Information Needs: Previous reports that document regional modeling do not include adequate information about how model boundaries were selected. It is recognized that the selection of boundaries for any model includes qualitative professional judgements about subsurface flow conditions. Future reports should present the general rationale used in constructing model boundaries. There is also a need to systematically incorporate hydrochemical data in the development and verification of conceptual models of regional flow. The data may provide insight about general recharge conditions, groundwater age, flowpaths, and inter-formational hydraulic communication.

I-5 SUMMARY

A number of key activities should be performed in the next few years to improve the regional modeling efforts. The DOE is planning a drilling and testing program to characterize the zone of high hydraulic gradient located north of the Yucca Mountain site. The results of that program could lead to significant changes in numerical models of the site and region. Also, the search should continue for additional evidence of past discharge areas in the currently dry water courses near Yucca Mountain, particularly Forty Mile Wash. This would provide further information about possible water table rises over the past several millennia.

Better estimates of present-day recharge over the site and region are needed to improve future estimates of recharge under varying climatic conditions. There is also a need for additional hydraulic conductivity data over the site and region. In particular, there are virtually no data on vertical hydraulic conductivities at the contacts of hydrostratigraphic units. Such data would be needed to support 3-D modeling. Currently available data may not be sufficient to justify the use of 3-D modeling on a regional scale. The DOE needs to determine whether the data are sufficient, and whether 3-D modeling will be required to adequately represent the regional flow system.

The work of Czarnecki and Waddell (1984), Czarnecki (1985, 1989, 1990a, 1990b), and Czarnecki and Wilson (1989) illustrates a methodical process for developing and improving numerical models of groundwater flow. An initial conceptual model was developed and parameter estimation techniques were applied to help construct a corresponding numerical model. Sensitivity studies were performed to determine where parameters needed to be refined. Most importantly, the search was continued for hydrologic data in areas where little information existed, leading to the discovery of new potentiometric data from the Greenwater Range. Based on this data, a new conceptual model of regional groundwater flow was developed which will guide future data collection and modeling work. Each of the above steps was documented through professional presentations and publications. In order to use the regional flow model to predict future conditions in the regional flow system, the model may need to be modified based

on the hydraulic head data from the Greenwater Range and other locations. Other changes may be needed based on results of ongoing site characterization work.

Finally, the work of Czarnecki (1992) represents an important 10-year forecast of how future groundwater levels will be affected by human activities. After 10 years of site characterization, it will be possible to see how well the regional model has predicted the perturbations caused by pumping at wells J-13 and J-12. It is expected that one of the many scenarios analyzed by Czarnecki will approximate actual groundwater withdrawals at the wellsites. This will provide a test of how well the regional model represents present-day conditions in the flow system near Yucca Mountain.

In closing, it is appropriate to consider remarks by Konikow and Bredehoeft (1992, p. 78,) in their commentary on model interpretation, validation, and use. They criticize use of the expressions "model validation" and "model verification" because they tend "to lend undue credibility to a process that ... is, in the end, inherently subjective." They prefer to describe the process using expressions such as model testing, model evaluation, model calibration, sensitivity testing, benchmarking, history matching, and parameter estimation. Konikow and Bredehoeft (1992, p. 82) consider that it is "naive to believe that we will somehow validate a computer model so that it will make accurate predictions of system responses far into the future." They note, however, that models "provide a tool for critical analysis. They are a means to organize our thinking, test ideas for their reasonableness, and indicate which are the sensitive parameters. They point the way for further investigation...They serve to sharpen our professional judgement. In the end, action concerning waste disposal will be a judgement; a professional judgement by the scientific community and a judgement by society."

I-6. REFERENCES

Cooley, R. L., "A Method of Estimating Parameters and Assessing Reliability for Models of Steady State Groundwater Flow, 1 -- Theory and Numerical Properties," *Water Resources Research,* 13:318-324 [1977].

Cooley, R. L., "A Method of Estimating Parameters and Assessing Reliability for Models of Steady State Groundwater Flow, 2 -- Application of Statistical Analysis," *Water Resources Research,* 15;603-617 [1979].

Cooley, R. L., "Incorporation of Prior Information on Parameters into Nonlinear Regression Groundwater Flow Models, 1 -- Theory," *Water Resources Research,* 18:965-976 [1982].

Czarnecki, J. B., "Simulated Effects of Increased Recharge on the Ground-Water Flow System of Yucca Mountain and Vicinity, Nevada-California," U.S. Geological Survey, Water-Resources Investigations Report 84-4344, 1985.

Czarnecki, J. B., "Should the Furnace Creek Ranch-Franklin Lake Playa Ground-Water Subbasin Simply be the Franklin Lake Playa Ground-Water Subbasin? [Abstract]," *EOS Transactions,* American Geophysical Union, 68:1292 [1987].

Czarnecki, J.B., "Characterization of the Subregional Ground-Water Flow system at Yucca Mountain and Vicinity, Nevada-California," *Radioactive Waste Management and the Nuclear Fuel Cycle,* 13:51-61 [1989].

Czarnecki, J. B., "Preliminary Simulations Related to a Large Horizontal Hydraulic Gradient at the North End of Yucca Mountain, Nevada [Abstract]," *Proceedings American Institute of Hydrology Spring Meeting,* Las Vegas, NV, March 12-16, 1990a.

Czarnecki, J.B., "Geohydrology and Evapotranspiration at Franklin Lake Playa, Inyo County, California," U.S. Geological Survey, Open-File Report 90-356, 1990b.

Czarnecki, J.B., "Simulated Water-Level Declines Caused by Withdrawals from Wells J-13 and J-12 Near Yucca Mountain, Nevada," U.S. Geological Survey, Open-File Report 91-478, 1992.

Czarnecki, J.B. and R.K. Waddell, "Finite-Element Simulation of Ground-Water Flow in the Vicinity of Yucca Mountain, Nevada-California," U.S. Geological Survey, Water-Resources Investigations Report 84-4349, 1984.

Czarnecki, J.B. and W.E. Wilson, Site Characterization and Conceptual Models of the Regional Ground-Water Flow System, Yucca Mountain and Vicinity, Nevada-California [Abstract]," *Proceedings of the Symposium on Waste Management -- Waste Management '89,* Tucson, Arizona, vol. 1, p. 473, 1989.

Downey, J.S., K.E. Kolm, and E.D. Gutentag, "Selection of Geohydrologic Boundaries for Ground-Water Flow Models, Yucca Mountain, Nevada," *Proceedings of the Symposium on Waste Management -- Waste Management '90,* Tucson, Arizona, pp.725-734, 1990.

Eakin, T. E., G. B. Maxey, T. W. Robinson, J. C. Fredericks, and O. J. Loeltz, "Contributions to the Hydrology of Eastern Nevada," Nevada Department of Conservation and Natural Resources Water Resources Bulletin 12, p. 14-16, 1951.

Konikow, L. F. and J. D. Bredehoeft, "Ground-Water Models Cannot Be Validated," *Advances in Water Resources,* 15:75-83, 1992.

Marshall, B.D., Z.E. Peterman, and J.S. Stuckless, "Strontium Isotopic Evidence for a Higher Water Table at Yucca Mountain," in *Proceedings of the Fourth Annual International Conference for High Level Radioactive Waste Management*, April 26-30, 1993, Vol. 2, pp. 1948-1952.

National Research Council, "Ground Water at Yucca Mountain: How High Can it Rise? -- Final Report of the Panel on Coupled Hydrologic Tectonic/Hydrothermal Systems at Yucca Mountain: Board on Radioactive Waste Management; Commission on Geosciences, Environment, and Resources," Washington, D.C., National Academy Press, April 1992.

Nuclear Regulatory Commission, "NRC Staff Site Characterization Analysis of the Department of Energy's Site Characterization Plan, Yucca Mountain Site, Nevada," Office of Nuclear Material Safety and Safeguards, NUREG-1347, August 1989.

Oatfield, W. J. and J. B. Czarnecki, "Hydrogeologic Inferences from Drillers' Logs and from Gravity and Resistivity Surveys in the Amargosa Desert, Southern Nevada," U.S. Geological Survey, Open-File Report 89-234, 1989.

O'Brien, G.M. and P. Tucci, "Earthquake-Induced Water-Level and Fluid-Pressure Fluctuations of Yucca Mountain, Nevada [Abstract]," *EOS Transactions*, American Geophysical Union, 73:157 [1992].

Rice, W. A., "Preliminary Two-Dimensional Regional Hydrologic Model of the Nevada Test Site and Vicinity, "Sandia National Laboratories, SAND83-7466, 1984. [Prepared by Pacific Northwest Laboratory, Richland, WA.]

Roache, P.J., *Computational Fluid Dynamics*, Albuquerque, NM, Hermosa Publishers, 1973.

Rush, F. E., "Regional Ground-water Systems in the Nevada Test site Area, Nye, Lincoln, and Clark Counties, Nevada," Nevada Department of Conservation and Natural Resources Water Resources Reconnaissance Series Report 54, p. 10-16, 1970.

Szymanski, J.S., "Conceptual Considerations of the Yucca Mountain Groundwater System with Special Emphasis on the Adequacy of this System to Accommodate a High-Level Nuclear Waste Repository," U.S. Department of Energy, Nevada Operations Office, Yucca Mountain Project Office, Las Vegas, Nevada, July 26, 1989.

Thordarson, W., "Geohydrologic Data and Test Results from Well J-13, Nevada Test Site, Nye County, Nevada," U.S. Geological Survey, Water-Resources Investigations Report, WRI-83-4171, 1983.

Thordarson, W. and B.P. Robinson, "Wells and Springs in California and Nevada Within 100 Miles of the Point 37 Deg. 15 Min. N., 116 Deg. 25 Min. W., on Nevada Test Site," U.S. Geological Survey, USGS-474-85, 1971.

Torak, L.J., "A Modular Finite-Element Model (MODFE) for Areal and Axisymmetric Ground-Water Flow-Problems, Part 1: Model Description and User's Manual," U.S. Geological Survey,

Open-File Report 90-194, 1992a.

Torak, L.J., "A Modular Finite-Element Model (MODFE) for Areal and Axisymmetric Ground-Water-Flow Problems, Part 3: Design Philosophy and Programming Details," U.S. Geological Survey, Open-File Report 91-471, 1992b.

U.S. Department of Energy, "Site Characterization Plan, Yucca Mountain Site, Nevada Research and Development Area, Nevada," Office of Civilian Radioactive Waste Management, Nevada Operations Office/Yucca Mountain Project Office, Nevada, DOE/RW-0199, 9 Vols., December 1988.

U.S. Department of Energy, "Characterization of the Yucca Mountain Regional Ground Water Flow System," Office of Civilian Radioactive Waste Management, Study Plan 8.3.1.2.1.3, Rev. 0, 1991a. [Prepared by the U.S. Geological Survey.]

U.S. Department of Energy, "Characterization of the Site Saturated-Zone Groundwater Flow System," Office of Civilian Radioactive Waste Management, Study Plan 8.3.1.2.3.1.1-6, Rev. 0, 1991b. [Prepared by the U.S. Geological Survey.]

U.S. Department of Energy, "Regional Hydrologic Synthesis and Modeling," Office of Civilian Radioactive Waste Management, Study Plan 8.3.1.2.1.4, Rev. 0, 1992. [Prepared by the U.S. Geological Survey.]

U.S. Department of Energy, "Letter from D. Shelor (DOE) to J. Holonich (NRC) transmitting DOE response to NRC's Phase II Review of Study Plan 8.3.1.2.1.4, Regional Hydrologic System Synthesis and Modeling," August 30, 1993.

Waddell, R.K., "Two-Dimensional, Steady-State Model of Ground-Water Flow, Nevada Test Site and Vicinity, Nevada-California," U.S. Geological Survey, Water Resources Investigations 82-4085, 1982.

Walker, G.E. and T.E. Eakin, "Geology and Ground Water of Amargosa Desert, Nevada-California," U.S. Geological Survey, Ground-Water Resources-Reconnaissance Series, Report 14, 1963.

Winograd and Thordarson, "Hydrogeologic and Hydrochemical Framework, South-Central Great Basin, Nevada-California, with Special Reference to the Nevada Test Site," U.S. Geological Survey Professional Paper 712-C, 1975.

APPENDIX J

CONTENTS

Page

J-1. Introduction J-1

J-2. Discussion J-1

J-3. Summary Observations/Conclusions from Runs J-5

J-4. References J-7

FIGURES

J-1 Location of geologic cross-section used to construct one dimensional *DCM3D* saturated flow simulations J-2

J-2 Geologic cross-section based on Wells H-4, UE25p#1, and J-13 . . . . . J-2

J-3 Plot of water table and computer run head elevations J-6

TABLES

J-1 Input Data for *DCM3D* One-Dimensional Simulations J-2

J-2 Output Data for *DCM3D* One-Dimensional Simulations J-3

APPENDIX J
MODELING SATURATED ZONE FLOW TO THE ACCESSIBLE ENVIRONMENT

W.H. Ford/NMSS

J-1. INTRODUCTION

In the development of the ground water flow and transport module, several different modeling approaches were attempted. One of the approaches used *DCM3D*, a Dual-Continuum, Three[3]-Dimensional, Ground-Water Flow Code for Unsaturated, Fractured, Porous Media (Updegraff, 1991). Using this code, a one-dimensional saturated zone flow model was built from a Yucca Mountain site geologic cross-section. The cross-section ran in a southeast direction from well H-4 to well J-13 (Figures J-1 and J-2) and was built using stratigraphic data and water-level data from wells H-4, UE25p#1, and J-13 (Thordarson, 1983; Whitfield; 1984, Craig, 1984; DOE, 1988; Czarnecki *et al.*, 1984). It should be noted that well H-4 is located at the proposed repository boundary and well J-13 is near the presently defined Accessible Environment Boundary. This means the cross-section passes through that portion of the saturated zone simulated by the performance assessment flow module.

J-2. DISCUSSION

Water levels and stratigraphic changes along the surface of the water table were used to construct a one-dimensional model of ground water flow. In building the model, some changes from the cross-section were made. The cross-section covers a length of 5582.1 meters, whereas the model covers a length of 5000 meters. Furthermore, the head elevation at well H-4 is 730.1 meters msl and at J-13, 728.1 meters msl. In the model, head elevations at well H-4 were set at 730 meters msl and at the other end of the model (5000 meters), head elevations were set at 728 meters msl. At the time, these changes were made for ease of input, with the result that model output could come close, but could never duplicate actual head elevations.

Saturated hydraulic conductivity and porosity values were varied, whereas, head values at both boundaries were fixed. A constant head boundary of 730 meters msl was assigned to the upgradient end and 728 meters to the down gradient end. Calico Hills nonwelded zeolitized unit properties were assigned from the up gradient end to 2310 meters and Topopah Spring welded unit properties were assigned from 2310 meters to the down gradient end at 5000 meters.

Saturated hydraulic conductivity and porosity data for the Calico Hills and Topopah Spring units were obtained from a variety of sources. Table J-1 contains saturated hydraulic conductivity and porosity inputs used in the runs. Run No. 1 used average matrix and porosity values and Run No. 2 used maximum matrix values. Run No. 3 used minimum

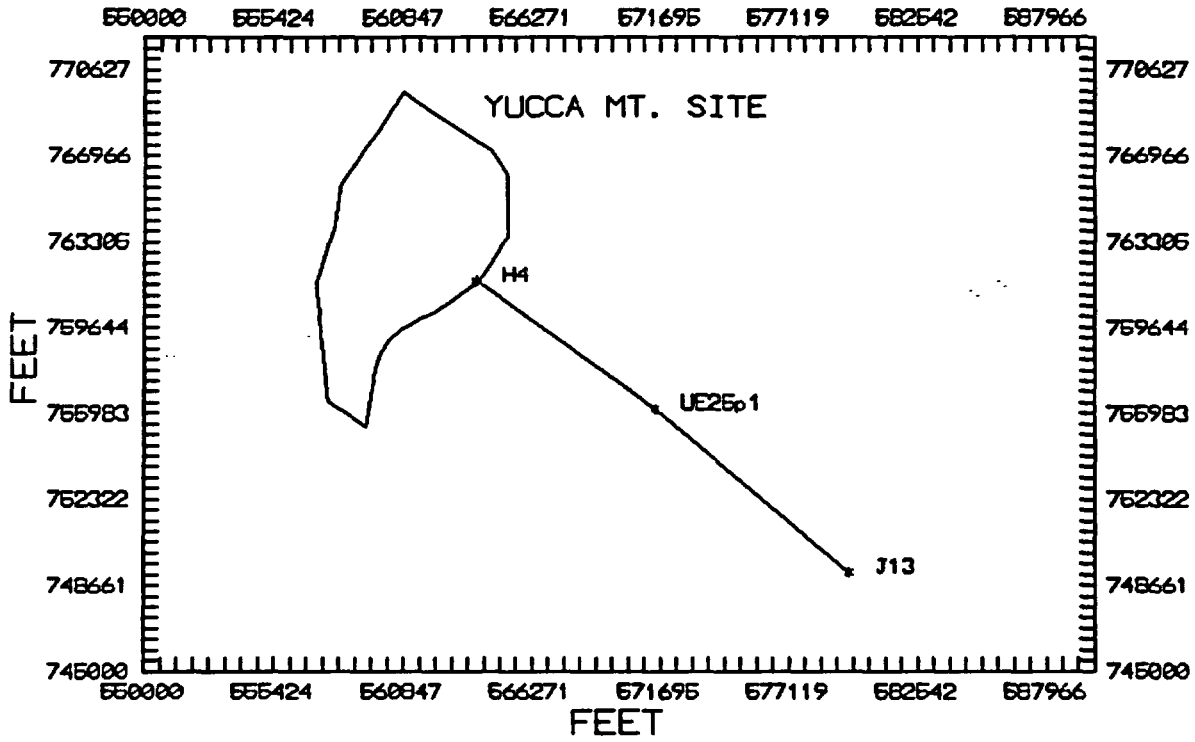

Figure J-1. Location of geologic cross-section used to construct one dimensional DCM3D saturated flow simulations.

Figure J-2. Geologic cross-section based on Wells H-4, UE25p#1, and J-13.

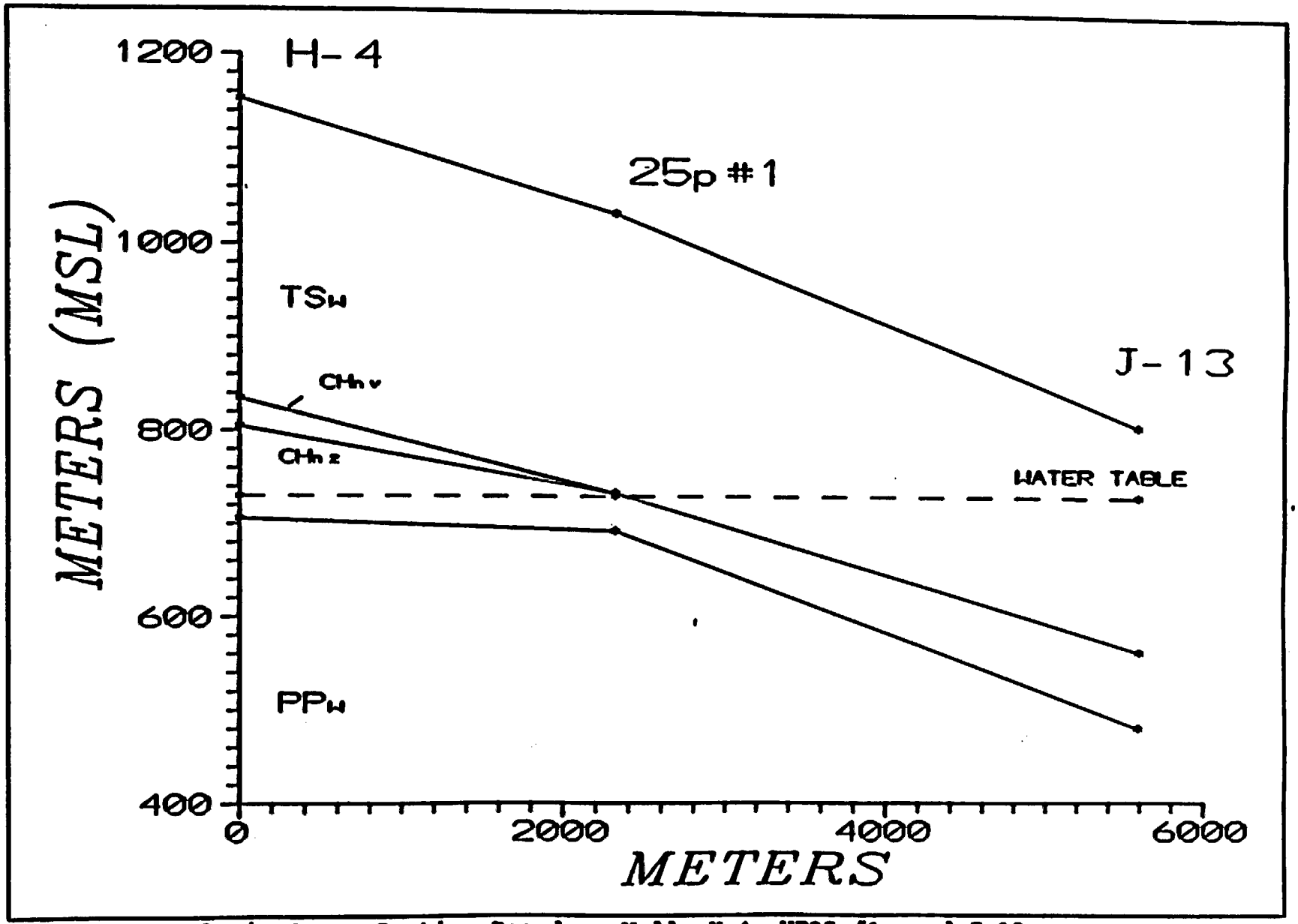

Figure 2: Geologic Cross Section Based on Wells H-4, UE25p#1, and J-13.

bulk fracture properties and Run No. 4 used maximum bulk fracture properties. Properties for Run nos. 1, 2, 3, and 4 were obtained from Peters (1984), Ababou (1991), Barnard (1991), and Dudley (1988). These runs reflect the hydrologic parameters of the Calico Hills and Topopah Spring units used in the iterative performance assessment simulations.

Table J-1
Input Data for *DCM3D* One-Dimensional Simulations

Run, No.	*Description*	*Topopah Spring*		*Calico Hills*	
		Ksat (m/yr.)	*Porosity*	*Ksat (m/yr.)*	*Porosity*
1	Average Matrix	6.0×10^{-4}	0.11	6.0×10^{-4}	0.28
2	Maximum Matrix	6.0×10^{-2}	0.11	6.0×10^{-2}	0.28
3	Minimum Fracture	3.0×10^{-4}	0.000021	3.0×10^{-3}	0.000046
4	Maximum Fracture	$3.0 \times 10^{+0}$	0.000041	$3.0 \times 10^{+0}$	0.000046
5	From Well Tests	$2.8 \times 10^{+2}$	0.000041	$2.0 \times 10^{+1}$	0.000046

Run No. 5 was constructed using average values from Yucca Mountain well tests (Lahoud *et al.*, 1984; Montazer, 1988; Thordarson, 1983). This run illustrates how saturated zone data may be used to help characterize the unsaturated zone (or vice versa). At Yucca Mountain, it may be difficult to determine bulk fracture saturated hydraulic conductivities in the unsaturated zone. However, within a few kilometers of the site, rock units in the Yucca Mountain unsaturated zone dip below the water table. If it is assumed that saturated hydraulic conductivities determined from well tests are representative of bulk fracture saturated hydraulic conductivities, well test data may be used to help determine parameters useful in unsaturated zone modeling.

At this time, well test data from the site are limited. Therefore, Run No. 5 used average saturated hydraulic conductivity values from just five wells; with two wells (J-13 and UE-25b#1), supplying much of the data. Furthermore, because porosity data were not available, the same porosity values as Run nos. 3 and 4 were used in Run No. 5.

Each simulation was run until it approached steady-state conditions. Table J-2 contains output from these runs. Output is presented in the form of average Darcy velocity, average seepage velocity, and flow time from one end of the simulation to the other (calculated from the seepage velocities).

J-3. SUMMARY OBSERVATIONS/CONCLUSIONS FROM RUNS

A number of interesting observations can be made from these runs:

(1) The slowest velocities and longest flow times were obtained from runs that used matrix properties. Seepage velocities were 1.3×10^{-6} and 1.6×10^{-5} meters/year, resulting in extremely long calculated flow times of 3180 million years and 31.7 million years. This indicates that in this model, matrix flow cannot readily transport radionuclides from the site.

(2) The fastest velocities and shortest flow times were obtained from runs that used hydrologic properties from well tests. The average seepage velocity was 473 meters/year and the calculated flow time was 10.6 years.

(3) Run No. 3 was constructed using minimum fracture flow properties with saturated hydraulic conductivities as low as the matrix property runs (Run Nos. 1 and 2). However, Run No. 3 produced faster flow velocities and shorter flow times than the matrix property runs, because of the small porosity values used in the Run No. 3 simulation. Since porosity values used in all the fracture property runs were hypothetically determined, they illustrate the importance of porosity in flow velocity calculations and the need to determine representative bulk fracture porosities during site characterization.

Table J-2
Output Data for *DCM3D* One-Dimensional Simulations

Run	Description	Average Darcy Velocity (m/yr.)	Average Seepage Velocity (m/yr.)	Flow Time (yrs.)
No. 1	Average Matrix	2.4×10^{-7}	1.3×10^{-6}	$3.81 \times 10^{+9}$
No. 2	Maximum Matrix	4.0×10^{-5}	1.6×10^{-5}	$3.17 \times 10^{+7}$
No. 3	Minimum Fracture	2.1×10^{-7}	4.8×10^{-3}	$1.05 \times 10^{+6}$
No. 4	Maximum Fracture	2.3×10^{-3}	54	92.4
No. 5	From Well Tests	2.0×10^{-2}	473	10.6

A plot of hydraulic heads for each of the runs was prepared to compare the results from each simulation to the cross-section water levels (see Figure J-3). The cross-section water table illustrates the low head gradient over this distance (2 meters). A change in the head gradient occurs at 2310 meters, which is where the hydrogeologic stratigraphy in the cross-section

FIGURE J-3. Plot of water table and computer run head elevations.

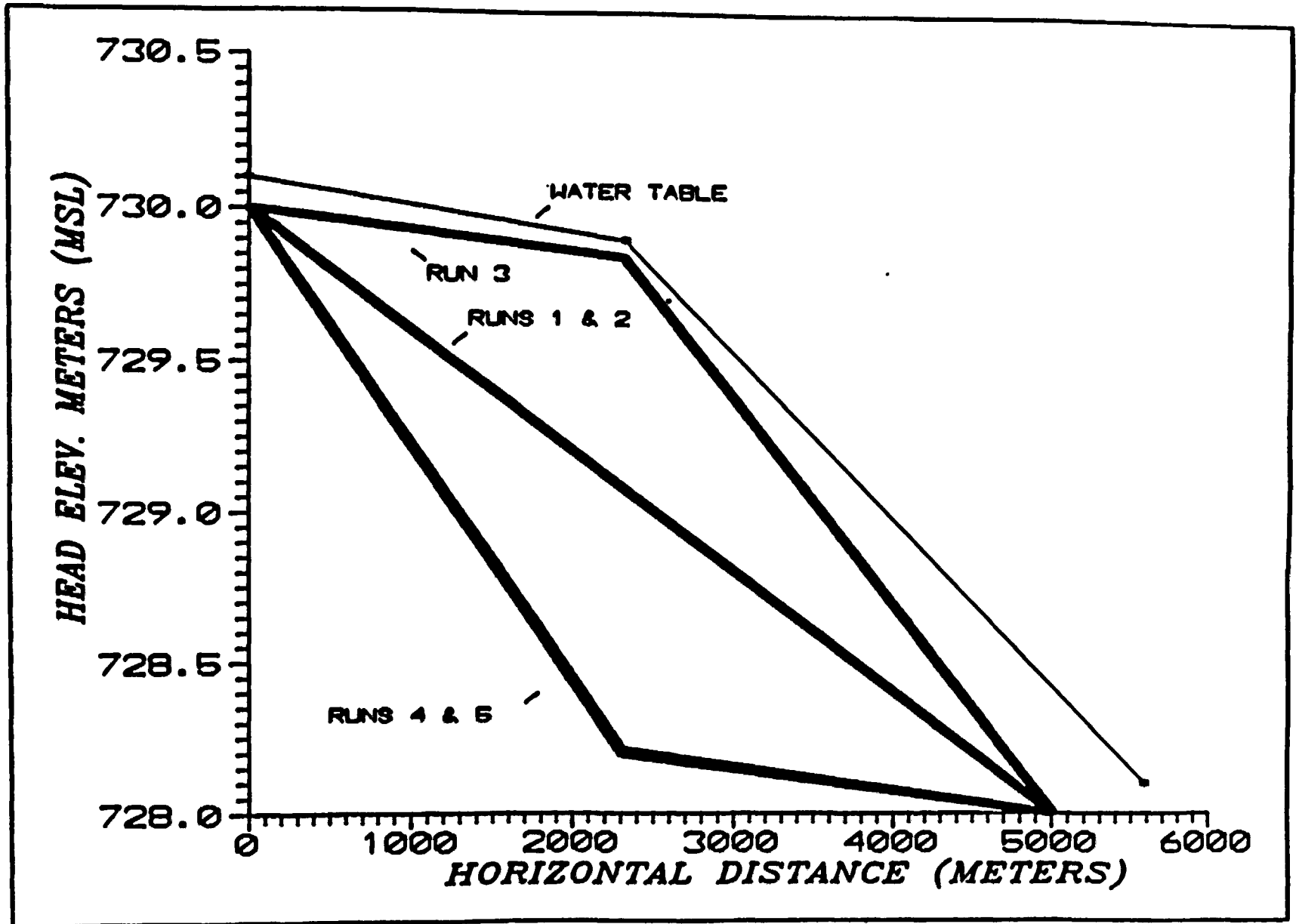

Figure 3: Plot of Water Table and Computer Run Head Elevations.

changes from the Calico Hills unit to the Topopah Spring unit. Run No. 3, using minimum bulk fracture values, produced the best match in heads. The staff recognizes that a match between predicted and actual heads does not prove that a model is correct. However, it does provide added confidence that the range of iterative performance assessment hydraulic conductivity values may be conservative (produce fast flow rates).

J-4. REFERENCES

Ababou, A.C., "Approaches to Large Scale Unsaturated Flow in Heterogenous, Stratified, and Fractured Geologic Media," Nuclear Regulatory Commission, NUREG/CR-5743, August 1991. [Prepared by the Center for Nuclear Waste Regulatory Analyses.]

Barnard, R.W., *et al,* "Technical Summary of the Performance Assessment Calculational Exercises for 1990 (PACE-90)", Volume 1, "Nominal Configuration Hydrogeologic Parameters and Calculational Results," Sandia National Laboratories, SAND90-2726, *MONTH* 1991. [Prepared for the U.S. Department of Energy/Office of Civilian Radioactive Waste Management.]

Craig, R.W. and Robison, J.H., "Geohydrology of Rocks Penetrated by Test Well UE-25p#1, Yucca Mountain Area, Nye County, Nevada," U.S. Geological Survey, Water Resources Investigations Report, WRI-34-4248, 1984.

Czarnecki, J.B., *et al.*, "Finite-Element Simulation of Ground-Water Flow in the Vicinity of Yucca Mountain, Nevada-California," U.S. Geological Survey, Water Resources Investigations Report, WRI-84-4349, 1984.

Dudley, A.L., "Total System Performance Assessment Code (TOSPAC)", Volume 1, "Physical and Mathematical Bases, Sandia National Laboratories," SAND85-0002, December 1988. [Prepared for the U.S. Department of Energy/Office of Civilian Radioactive Waste Management.]

Lahoud, D.H., *et al.*, "Geohydrology of Volcanic Tuff Penetrated by Test Well UE-25b#1, Yucca Mountain, Nye County, Nevada," U.S. Geological Survey, Water Resources Investigations Report, WRI-84-4253, 1984.

Montazer, P., *et al.*, "Monitoring The Vadose Zone in Fractured Tuff, Ground Water Monitoring Review", Spring, Vol. VIII, No. 2 [1988].

Peters, R.R., *et al.*, "Fracture and Matrix Hydrologic Characteristics of Tuffaceous Materials from Yucca Mountain, Nye County, Nevada," Sandia National Laboratories, SAND84-1471, December 1984.

Thordarson, W., "Geohydrologic Data and Test Results From Well J-13, Nevada Test Site, Nye County, Nevada," U.S. Geological Survey, Water Resources Investigations Report WRI-83-4171, 1983.

Updegraff, C.D., *et al.*, "DCM3D, A Dual-Continuum, Three-Dimensional, Ground-Water Flow Code for Unsaturated, Fractured, Porous Media," Nuclear regulatory Commission, NUREG/CR-5536, February 1991. [Prepared by the Sandia National Laboratories.]

U.S. Department of Energy, "Site Characterization Plan Overview, Yucca Mountain Site, Nevada Research and Development Area, Nevada," Office of Civilian Radioactive Waste Management, DOE/RW-0198, 9 vols., December 1988.

Whitfield, M.S., *et al.*, "Geohydrologic and Drill-Hole Data for Test Well USW H-4, Yucca Mountain, Nye County, Nevada," U.S. Geological Survey, Open File Report, OFR-84-449, 1984.

APPENDIX K

CONTENTS

		Page
K-1	Introduction	K-1
K-2	Geochemical Model	K-1
K-3	Total Carbon Transport Model	K-2
K-4	^{14}C Transport Model	K-3
K-5	Example	K-3
K-6	Conclusions	K-11
K-7	References	K-13

TABLES

K-1	Initial Conditions and Parameters	K-8

FIGURES

K-1	One-Dimensional Flow and Transport Model	K-4
K-2	Temperature in One-Dimensional Model as a Function of Time	K-5
K-3	Gas Flux as Function of Time Through Column	K-6
K-4	Water Saturation in Column as Function of Time	K-7
K-5	Carbon Content of Gas, Liquid and Solid Phases	K-9
K-6	^{14}C Content of Gas, Liquid and Solid Phases, with Scale Changes	K-10
K-7	Cumulative Release by 1500 Years as a Function of when ^{14}C was Released	K-11

APPENDIX K
GEOCHEMICAL MODEL FOR ^{14}C TRANSPORT IN UNSATURATED ROCK

R.B. Codell/NMSS and W.M. Murphy/CNWRA

K-1 INTRODUCTION

Under oxidizing conditions in a geologic repository, ^{14}C in high-level radioactive waste might be released as $^{14}CO_2$ (Light *et al.*, 1990). Any such gas escaping the engineered barrier will be incorporated in the existing carbon system of the geosphere, and be transported along with gaseous and dissolved carbon.

Several recent studies addressed ^{14}C gaseous transport at the Yucca Mountain repository environment using simplified models of geochemical retardation (Ampter and Ross, 1990; Light et al., 1990; and Knapp, 1990). Accurate modeling of ^{14}C transport requires coupling of relations between the source, heat flow, two-phase fluid flow, and the distribution of chemical species among solid *(s)*, liquid *(l)*, and gas *(g)* phases (Codell and Murphy, 1992). Interphase exchange of carbon could result in a significant retardation of released ^{14}C, thereby delaying its arrival at the accessible environment. This auxiliary analysis reports on a mechanistic model for the geochemical interaction of ^{14}C for a geologic repository in partially saturated rock.

The ^{14}C transport model consists of three parts:

(1) A geochemical model describing the state of all carbon species in a representative volume of rock;

(2) A flow and transport model for movement of total carbon through the system which consists of a number of connected volumes or "cells"; and

(3) A model of ^{14}C migration as a trace quantity in the general movement of total carbon.

K-2 GEOCHEMICAL MODEL

A carbon system geochemical model which incorporates all reactions of primary significance to ^{14}C transport in unsaturated fractured rock can be based on local chemical equilibrium and mass and charge conservation in a representative volume. Chemical reactions in the model comprise carbonate equilibria among aqueous *(aq)* species, dissociation of water, vapor-liquid equilibria for CO_2 and H_2O, and calcite dissolution and precipitation. In addition to the aqueous species in these equilibria, the present model includes Na^+ to represent other aqueous cations. The reactions represented in the present model are given next:

$$H_2O(l) + CO_2(aq) \rightleftarrows H^+ + HCO_3^- \quad \text{(K-1)}$$

$$HCO_3^- \rightleftarrows H^+ + CO_3^{2-} \quad \text{(K-2)}$$

$$H^+ + OH^- \rightleftarrows H_2O \quad \text{(K-3)}$$

$$CaCO_3(s) + H^+ \rightleftarrows Ca^{2+} + HCO_3^- \quad \text{(K-4)}$$

$$CO_2(g) = CO_2(aq) \quad \text{(K-5)}$$

Local charge balance in the model aqueous phase is represented by equating sums of aqueous cation and anion equivalents. Local mass conservations for carbon and calcium are maintained within each cell, and the mass of sodium is conserved in the aqueous phase.

Given the total masses of C, Ca and other species, mass of water, and the temperature, pore volume and pressure of each cell, the above relationships lead to a set of nonlinear algebraic equations that are solved simultaneously to characterize local equilibrium in each cell for each time step. Equilibrium constants for reactions 1 to 5 are functions of temperature only at one bar pressure. Activity coefficients are functions of ionic strength, and are generated from an extended Debye-Hückel equation. Calcite is permitted to precipitate or dissolve at equilibrium, and the model solution is undersaturated with respect to calcite in its absence . The partial pressure of CO_2 is calculated from the activity of aqueous CO_2, assuming ideal gas relations.

K-3 TOTAL CARBON TRANSPORT MODEL

The calculation of transport of total carbon through the modeled system is performed by sequential iteration in the following steps:

(1) Local chemical equilibrium is calculated in each cell at time t, using the geochemical model;

(2) Inputs and outputs to each cell are determined from an independent flow model for the next time step $t + \Delta t$. In the present model, only advective transport by gaseous flow is allowed. Therefore, the input of CO_2 to a cell is determined only by the partial pressure of CO_2 in the previous cell or upstream boundary and the flow of the transporting gas from that cell. Gaseous flow and condensation/evaporation of water are accounted for independently as part of the flow model and input to the chemical model; and

(3) Mass distributions are revised in the cells for time step $t + \Delta t$, using the geochemical model with updated temperature and liquid saturation states.

The carbon transport algorithm in the preceding steps simulates changes to the chemistry of each phase in the system, as a function of time and space. The carbon transport model determines the quantities of CO_2 gas moving through the system of cells, as well as the exchange rates of carbon between the various phases.

K-4 ^{14}C TRANSPORT MODEL

The ^{14}C transport model uses the state and evolution of total carbon speciation to simulate transport of trace amounts of ^{14}C through the system. ^{14}C is assumed to behave exactly in proportion to the total carbon, with no isotopic fractionation. However, radioactive decay removes ^{14}C from the solid, liquid, and gas inventories. The model assumes ^{14}C enters the system as an instantaneous pulse within a specified cell. ^{14}C is removed from the liquid/gas phases if calcite precipitates from solution. It re-enters the system if previously contaminated calcite dissolves. The model assumes that calcite dissolves first from the ^{14}C-contaminated calcite inventory before uncontaminated calcite redissolves. The model further assumes that the ^{14}C is distributed homogeneously within the contaminated calcite of each cell.

K-5 EXAMPLE

The present geochemical transport model has been applied to simplified examples, to demonstrate the range of possible phenomena associated with the release and transport of $^{14}CO_2$ in unsaturated fractured rock. The model system is a one-dimensional column of 145 cells, represented in Figure K-1, with constant hydraulic properties and cross section, passing through the center of a hypothetical repository plane, which is located at cell 55. Water, gas, and relevant mineral chemistries, as well as the geothermal gradient that resemble those factors observed at Yucca Mountain, are provided as initial conditions. The system chosen for the example was simple, so as not to confound the results of the geochemical transport model with other phenomena. For example, gas is assumed to flow in the upward direction only, even though thermal-hydraulic simulations indicate an initially outward gas flow in all directions from a heated repository in unsaturated tuff (Nitao, 1990). Additionally, there is no transport of ^{14}C by water flow or diffusion in gas or water.

Time-dependent temperature and gas flow used in the present example were generated from two-dimensional codes, developed by the U.S. Nuclear Regulatory Commission (NRC) staff for predicting air flow through Yucca Mountain. The NRC models are similar to those developed by Ampter and Ross (1990). Temperature, represented in Figure K-2, was calculated from a two-dimensional thermal conduction model that included the geothermal gradient. Gas flux, shown in Figure K-3, varied with time, but was uniform through the one-dimensional column.

Liquid saturation is shown in Figure K-4. The temperature and gas flow models did not include water saturation explicitly. Therefore, an approximate empirical model for saturation of the column was derived from the results of simulations of two-phase thermally induced circulation near repositories in tuff. The empirical model used in the example predicts that water saturation is 80 percent except within a zone of about 50 meters above and below the repository for a period of less than 2000 years.

Figure K-1. One-dimensional flow and transport model.

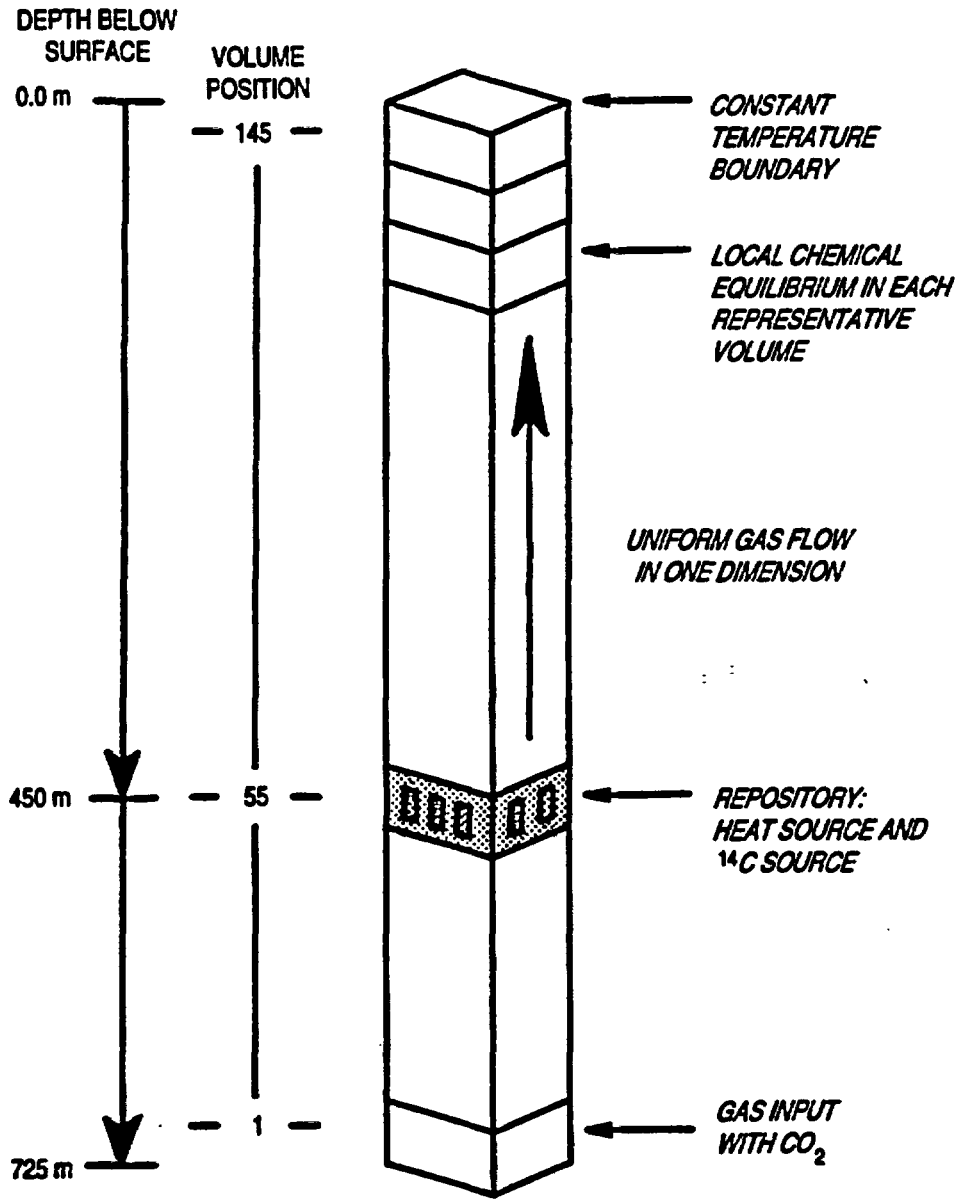
DEPTH BELOW SURFACE
VOLUME POSITION
0.0 m
145
CONSTANT TEMPERATURE BOUNDARY
LOCAL CHEMICAL EQUILIBRIUM IN EACH REPRESENTATIVE VOLUME
UNIFORM GAS FLOW IN ONE DIMENSION
450 m
55
REPOSITORY: HEAT SOURCE AND ^{14}C SOURCE
1
GAS INPUT WITH CO_2
725 m

Figure K-2. Temperature in one-dimensional model as a function of time.

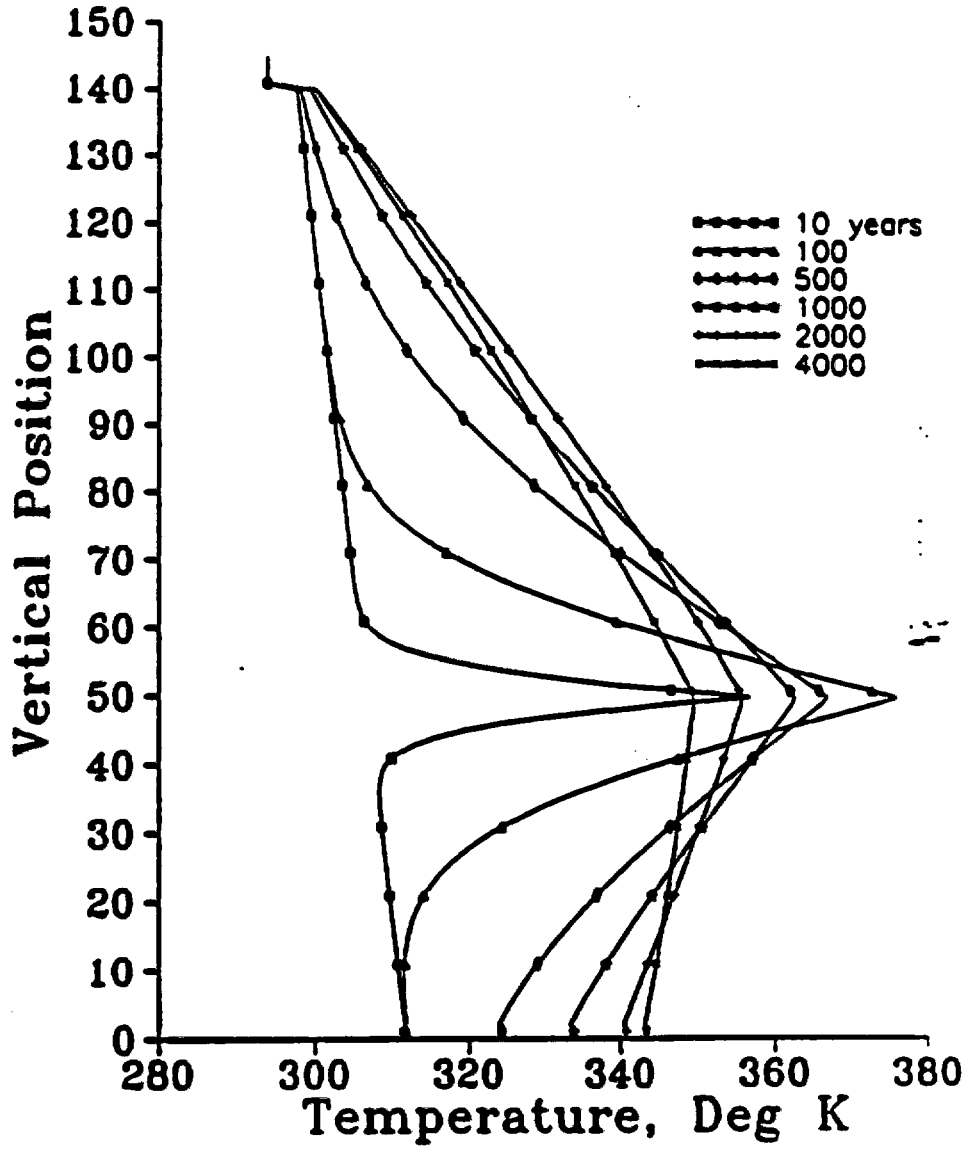
150
140
130
120
110
100
90
80
70
60
50
40
30
20
10
0
Vertical Position
280
300
320
340
360
380
Temperature, Deg K
10 years
100
500
1000
2000
4000

Figure K-3. Gas flux as function of time through column.

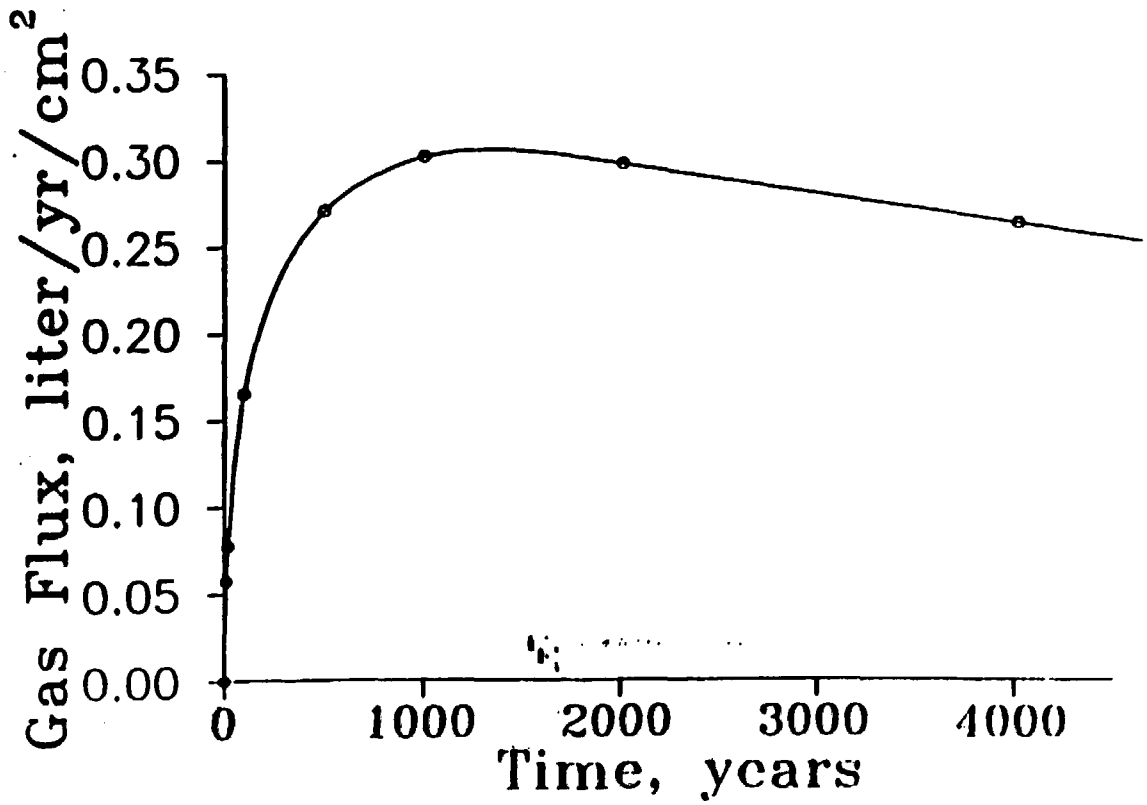
Gas Flux, liter/yr/cm^2
0.35
0.30
0.25
0.20
0.15
0.10
0.05
0.00
0
1000
2000
3000
4000
Time, years

Figure K-4. Water saturation in column as function of time.

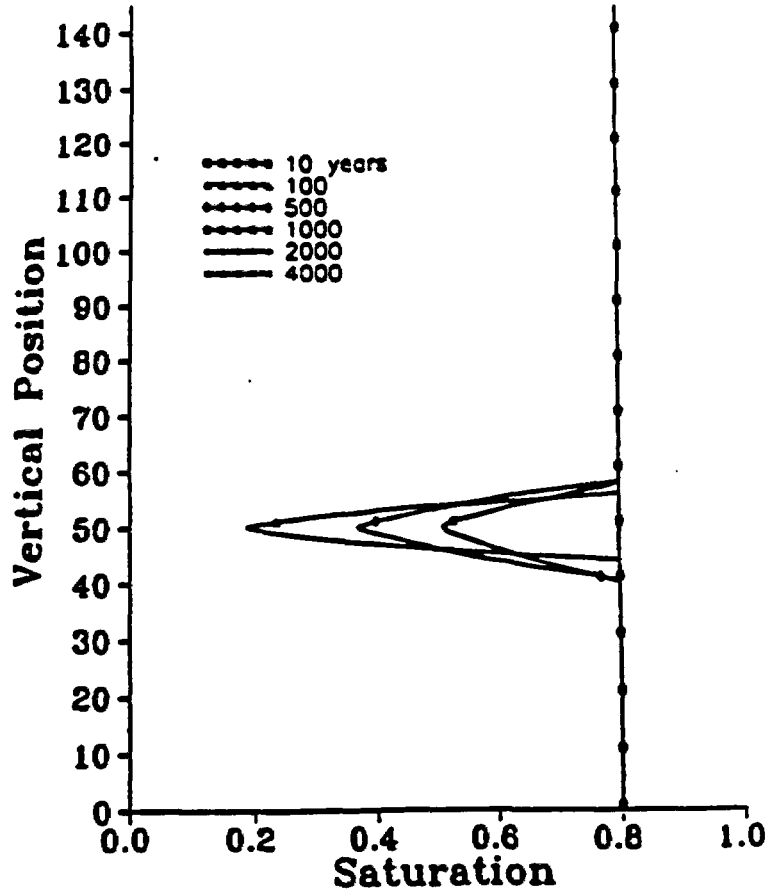

Figure 4 - Water Saturation for Example

Other initial conditions and parameters of the example system are given in the Table K-1. These conditions lead to an initial solution with Ph ≈ 7.2, moderately undersaturated with respect to calcite with the *Q/K* (saturation index/equilibrium constant) about 0.2, and partial pressures of CO_2 in the range 0.005 to 0.008 bar, depending on temperature.

Table K-1. Initial Conditions and Parameters

Parameter	*Value*
Cell Cross Section	12.5 centimeter^2
Cell Spacing	5 meters
Cell Volume	6250 centimeter^3
Porosity	0.2
Initial Saturation	0.8
Initial C/cell	0.00202 moles
Na/cell	0.001 moles
Ca/cell	0.0004 moles
CO_2 Input Gas	2.53×10^{-4} moles/liter

Results for the Carbon Model: Results for the carbon transport model are given in Figure K-5, which shows the distribution of carbon for each cell among the gas, liquid, and solid phases for various times after repository closure. Initially, the carbon content decreases in the liquid phase and increases in the solid and gas phases near the repository level. Just above the repository, however, the carbon content of the gas and liquid phases increases, a reflection of gas transport of the pulse of CO_2 initially volatilized from the liquid near the repository and transported. Increasing temperature, decreasing solvent mass, and increasing Ph because of CO_2 volatilization all promote calcite precipitation near the repository horizon.

At 500 years, the initially volatilized CO_2 pulse has been flushed out the top of the column. The calcite content continues to grow, spreading above and below the repository level, as temperature increases. At 2000 and 4000 years, the calcite progressively redissolves while the liquid content of carbon increases as the rock cools.

Results of ^{14}C Model: Figure K-6 shows the distribution of ^{14}C for each cell in the gas, liquid and solid phases, at various times for 10^{-6} ci of ^{14}C released 15 meters below the assumed repository plane at time zero. The ^{14}C was released below the repository plane to account for gas circulation expected near the repository, and allows interaction of the contaminant below as well as above the engineered barrier.

At 100 years, most of the ^{14}C has redistributed to the liquid phase. The liquid and gas inventories of ^{14}C have moved above the repository plane because of gas transport, even though the fraction of ^{14}C in the gas phase is small. The ^{14}C in the calcite remains fixed until calcite redissolves. At 500 years, the gas and liquid inventories of ^{14}C have moved further above the repository plane. Some of the calcite near

Figure K-5. Carbon content of gas, liquid and solid phases.

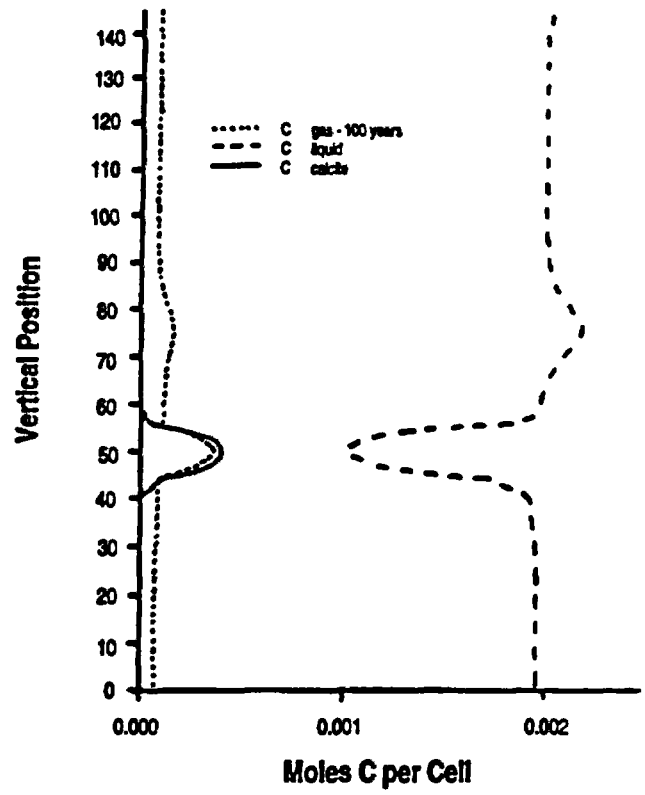
C gas - 100 years
C liquid
C calcite
Vertical Position
Moles C per Cell
0.000
0.001
0.002

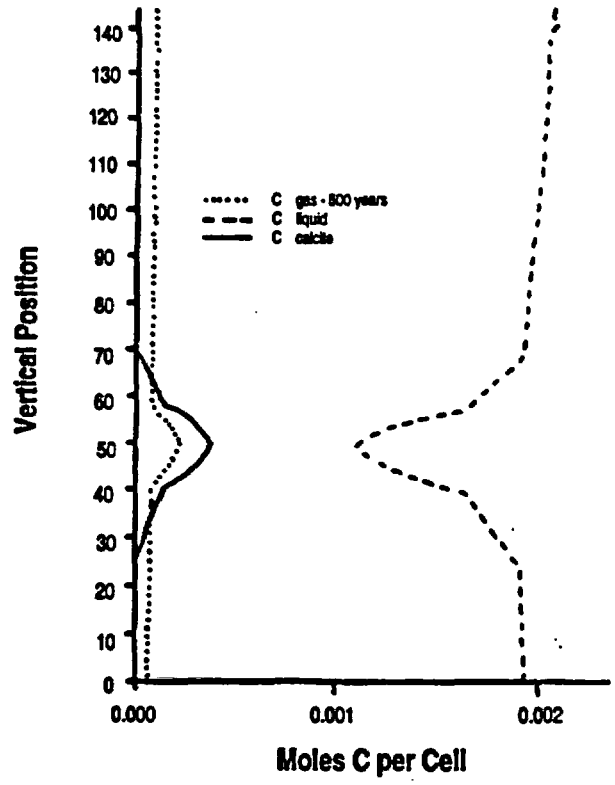
C gas - 500 years
C liquid
C calcite
Vertical Position
Moles C per Cell
0.000
0.001
0.002

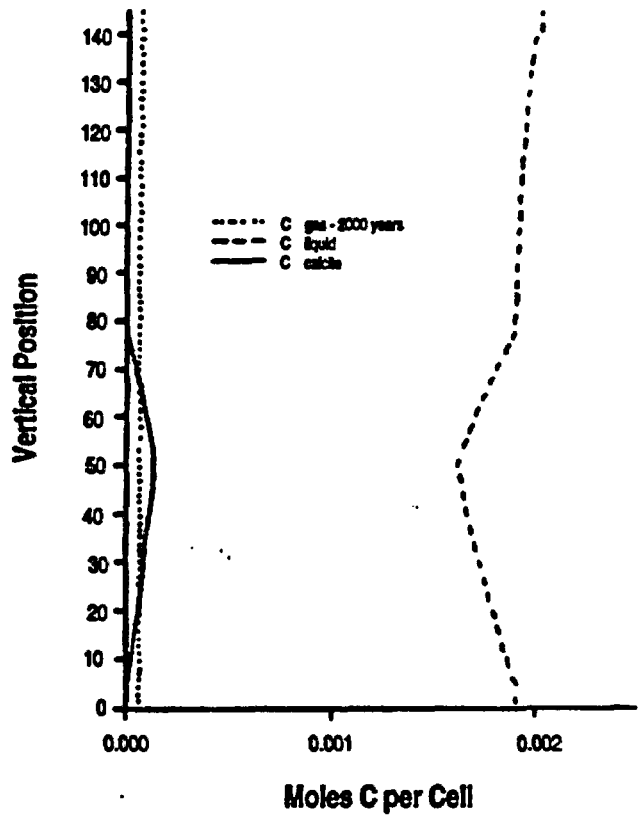
C gas - 2000 years
C liquid
C calcite
Vertical Position
Moles C per Cell
0.000
0.001
0.002

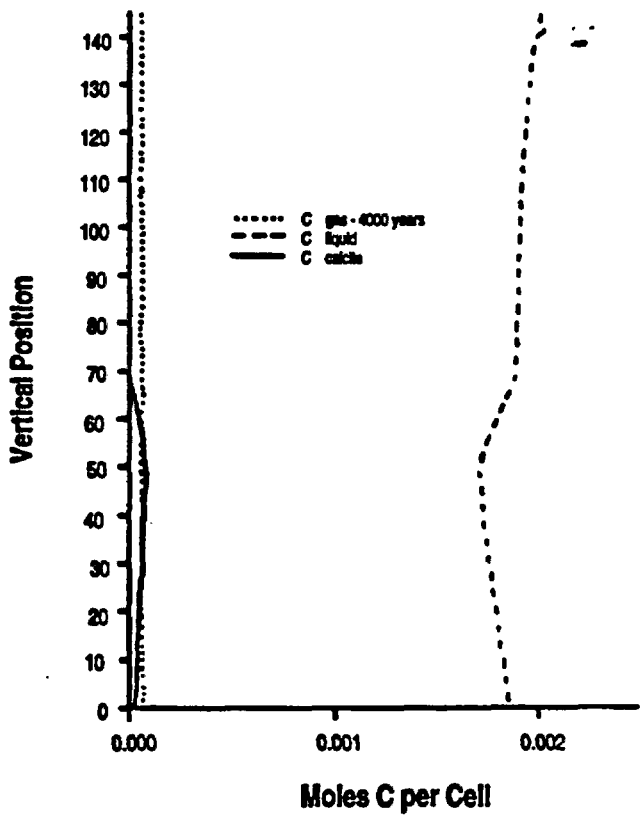
C gas - 4000 years
C liquid
C calcite
Vertical Position
Moles C per Cell
0.000
0.001
0.002

Figure K-6. ^{14}C content of gas, liquid and solid phases, with scale changes.

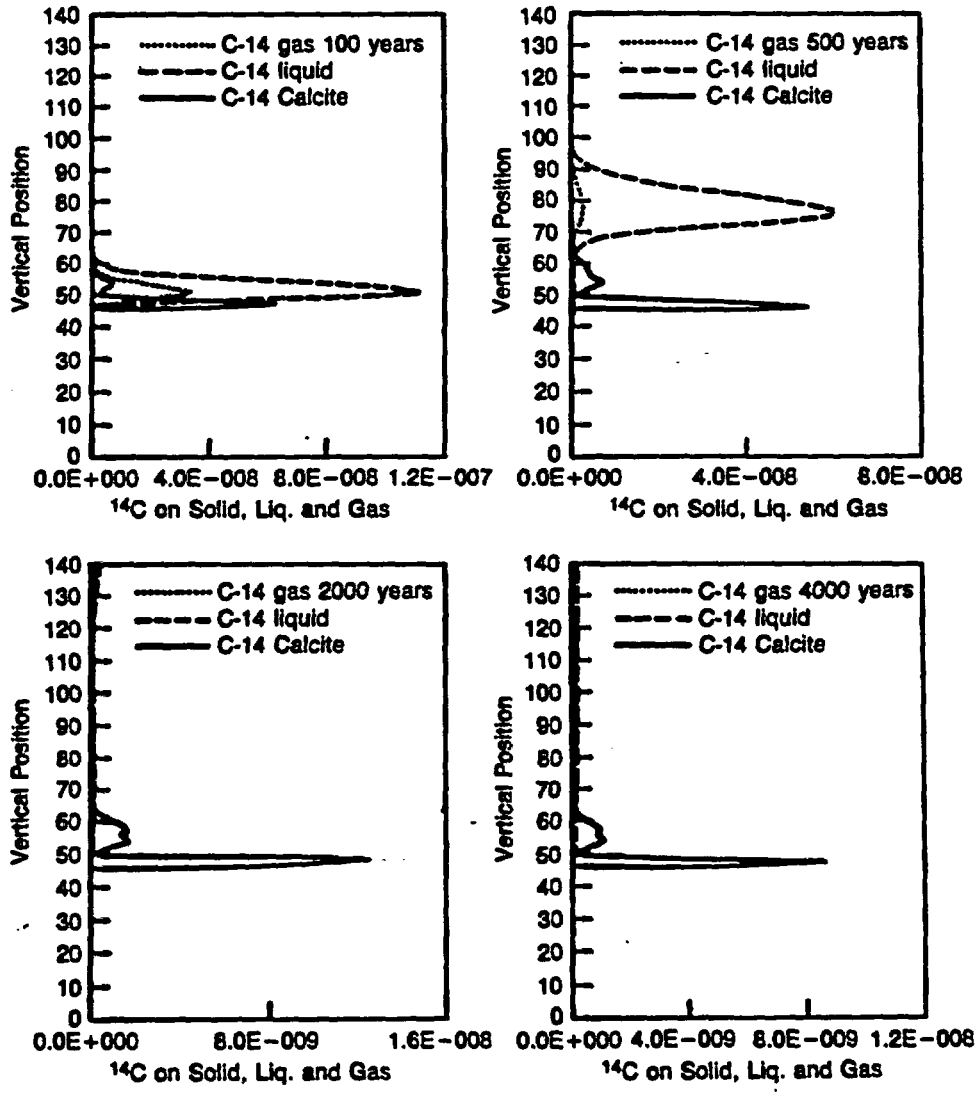
C-14 gas 100 years
C-14 liquid
C-14 Calcite
Vertical Position
0.0E+000 4.0E−008 8.0E−008 1.2E−007
14C on Solid, Liq. and Gas
C-14 gas 500 years
C-14 liquid
C-14 Calcite
Vertical Position
0.0E+000 4.0E−008 8.0E−008
14C on Solid, Liq. and Gas
C-14 gas 2000 years
C-14 liquid
C-14 Calcite
Vertical Position
0.0E+000 8.0E−009 1.6E−008
14C on Solid, Liq. and Gas
C-14 gas 4000 years
C-14 liquid
C-14 Calcite
Vertical Position
0.0E+000 4.0E−009 8.0E−009 1.2E−008
14C on Solid, Liq. and Gas

the repository plane redissolves, releasing its ^{14}C inventory, which in turn is partially captured by precipitating calcite further from the repository plane, where temperature continues to increase.

By 2000 years, nearly all ^{14}C is swept from the column, except that which remains trapped in the calcite. At this point in time, calcite is redissolving everywhere, so the contaminated calcite acts as a long-term source of ^{14}C to the system. Some of this residual ^{14}C remains even at 4000 years.

Dependence on Time of Release: The model predicts that calcite starts to precipitate shortly after repository closure and then redissolves. Therefore, the timing of the release of ^{14}C from the waste is important to its ultimate fate. ^{14}C released after most calcite has precipitated will not be removed from the liquid and gas phases as effectively as ^{14}C released during the period of active calcite precipitation. Figure K-7 shows the cumulative release over 1500 years from repository closure of ^{14}C past several points in the column as a function of time of ^{14}C release. This figure demonstrates the interesting phenomenon that ^{14}C released at early times can arrive at the end of the column after ^{14}C released at later times.

K-6 CONCLUSIONS

Numerical experiments with a flow and transport model that includes coupled nonisothermal geochemistry provide insights into the behavior of ^{14}C in an unsaturated geologic repository for nuclear waste. These experiments have been applied to a system resembling the proposed repository at Yucca Mountain, Nevada. Model results show a significant redistribution of autochthonous carbon among solid, liquid, and gas phases, even in areas remote from the repository plane. Carbon remains predominantly in the aqueous solution, in spite of the fact that near-field heating results in a reduction of liquid saturation, abundant calcite precipitation, and increased equilibrium fractionation of CO_2 into the gas phase.

Transport of ^{14}C released from the repository is generally retarded by a factor of approximately 30 to 40, because of immobilization in the liquid phase. In addition, ^{14}C released early during the period of solid calcite precipitation can be fixed for a long period before repository cooling leads to redissolution of the calcite.

Although simplified, the model demonstrates the complex nature of the geochemical processes affecting ^{14}C release. Results of the simulation depend strongly on model assumptions, and retardation of ^{14}C in the liquid or solid phases could be greater or smaller under different conditions of chemistry, hydrology, temperature, or gas flow. We contemplate coupling geochemistry and carbon transport models with more realistic two-or-three-dimensional treatments of heat and mass transfer near a repository in unsaturated tuff, which would include transport in the gas and liquid phases and allow for molecular diffusion.

Figure K-7. Cumulative release by 1500 years as a function of when ^{14}C was released

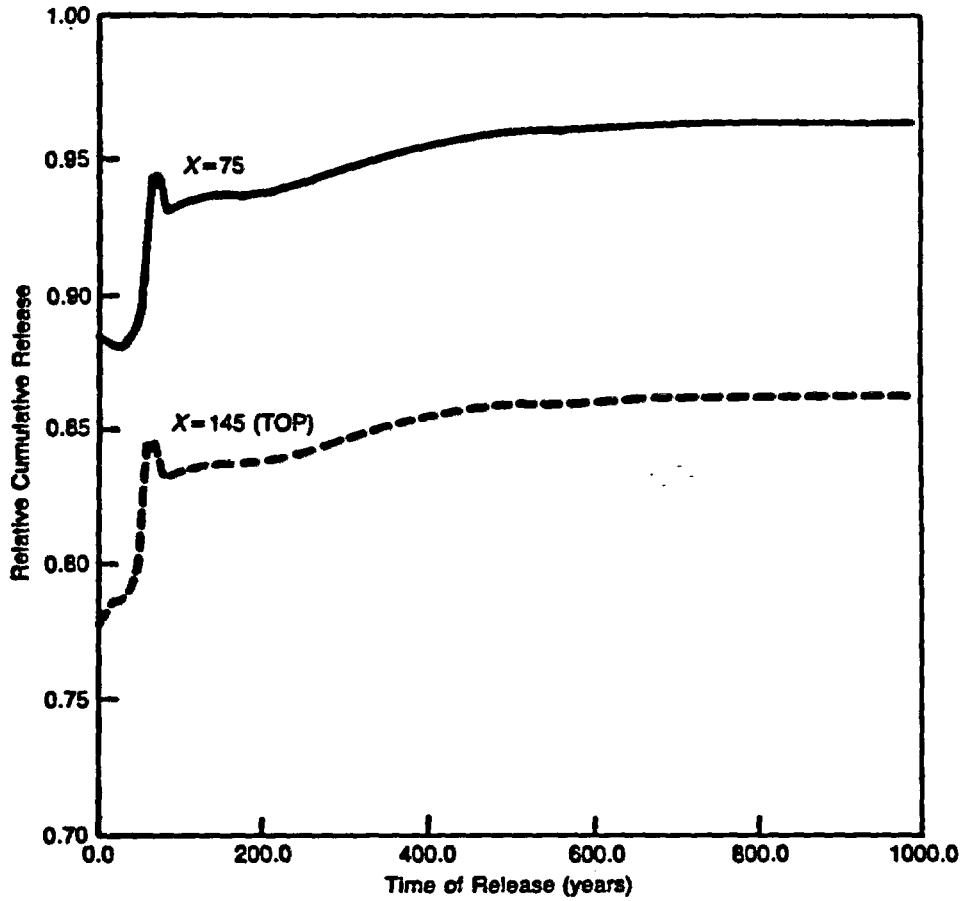
1.00
0.95
0.90
0.85
0.80
0.75
0.70
Relative Cumulative Release
X=75
X=145 (TOP)
0.0
200.0
400.0
600.0
800.0
1000.0
Time of Release (years)

K-7 REFERENCES

Ampter, S., and B. Ross, "Simulation of Gas Flow beneath Yucca Mountain, Nevada with a Model Based on Freshwater Head," *Proceedings of the Symposium on Waste Management*, Tucson, AZ, 2, 915, 1990.

Codell, R.B., and W.M. Murphy, "Geochemical Model for ^{14}C Transport in Unsaturated Rock," *Proceedings Third International Conference on High-level Radioactive Waste Management*, Las Vegas, 1992 pp. 1959-1965.

Knapp, R.B., "An Approximate Calculation of Advective Gas-Phase Transport of ^{14}C at Yucca Mountain, Nevada", *Journal of Contaminant Hydrology*, 5: [1990].

Light, W.B., T.H. Pigford, P.L. Chambre, and W.W.L. Lee "Analytical Models for C-14 Transport in a Partially Saturated, Fractured, Porous Media," American Nuclear Society, *Proceedings Nuclear Waste Isolation in the Unsaturated Zone -- FOCUS '89*, Lagrange Park, Illinois, 1990.

Nitao, J.J., "Numerical Modeling of the Thermal and Hydrological Environment Around a Nuclear Waste Package Using the Equivalent Continuum Approximation: Horizontal Emplacement," Lawrence Livermore National Laboratory, UCID-21444, 1990.

APPENDIX L

CONTENTS

		Page
L-1	Introduction	L-1
L-2	Background	L-1
L-3	Geochemical Code	L-2
L-4	Simulations	L-2
L-4.1	Effect of Ion Exchange on K/Ar Dating	L-2
L-4.2	Calculated Compositions of Water from the Unsaturated Zone	L-4
L-5	Results	L-4
L-5.1	Effect of Ion Exchange on K/Ar Dating	L-4
L-5.2	Calculated Compositions of Water from the Unsaturated Zone	L-4
L-6	Conclusions	L-8
L-7	References	L-14

FIGURES

L-1	Concentration of Exchangeable Cations in Solid vs. Distance Along Slow Path	L-5
L-2	Composition of Solution Passing Through Column	L-6
L-3	Ternary Diagram of Zeolite Composition to Liquid Composition in Well G-3 Saturated and Unsaturated Zones	L-7
L-4	Zeolite to Liquid Compositions for Well G-1	L-9
L-5	Zeolite to Liquid Compositions for Well G-2	L-10
L-6	Zeolite to Liquid Compositions for Well G-4	L-11
L-7	Zeolite to Liquid Compositions for Well H-3	L-12
L-8	Zeolite to Liquid Compositions for Well H-4	L-13

THE EXCHANGE OF MAJOR CATIONS IN YUCCA MOUNTAIN

H.M. Astwood/NMSS

L-1 INTRODUCTION

An important characteristic of Yucca Mountain, the proposed geologic repository for high-level radioactive waste, is the presence of zeolitic tuffs. Zeolites are crystalline, hydrated aluminosilicates, which are characterized by an ability to readily exchange cations with aqueous solutions. The presence of zeolites is seen as an important barrier to the migration of radionuclides to the accessible environment. This auxiliary analysis was designed to answer two questions related to the exchange of cations in Yucca Mountain.

The first question concerned the stability (i.e., constancy, of exchangeable cation composition) of zeolites. Using potassium/argon (K/Ar) dating techniques, WoldeGabriel *et al.* (1992) determined that the zeolites from drillholes in the Yucca Mountain vicinity range in age from 2 million years to 10 million years old. However, ion exchange involving potassium and sodium on zeolites has been shown to reach equilibrium in about 2 days (Pabalan, 1991). How, then, can a mineral that can alter within a couple of days exist for at least 2 million years? To answer that question, simulations were performed in which pore water, whose composition approximates that found at Yucca Mountain, percolates through site-specific zeolite layers for a period of approximately 150,000 years. The simulation was intended to represent the chemical reactions that would take place between the cations dissolved in the pore water and the cations sorbed onto zeolites. If, in the simulation, the K ions attached to the zeolites become mobile, there would be reason to doubt the zeolites could be accurately dated, using a K/Ar technique. If, however, the K is immobile, the K/Ar ratios would not be affected by ion-exchange reactions. This information is important to the siting of the repository, for it supports the conceptualization that the zeolites should remain stable for the lifetime of the repository and should act as a barrier for the release of radionuclides to the accessible environment.

The second question to be answered by this analysis involved the determination of pore water compositions from the unsaturated zone. Peters *et al.* (1992) describe methods of measuring pore water compositions from rocks of the unsaturated zone, plus the possible causes of changes in the compositions of the pore waters because of the method of extraction (compression). Given that ion-exchange reactions involving zeolites are fast (Pabalan, 1991), can we determine the chemical composition of pore water from the unsaturated zone, if the composition of the zeolite in direct contact with the pore water is known? If the answer is yes, then are there any significant spatial patterns of these compositions?

L-2 BACKGROUND

Ion exchange is a process by which ions in one phase displace ions in another phase. For example:

$$mA^{n+} + nBX_m = mAX_n + nB^{m+} , \qquad \text{(L-1)}$$

where A and B represent cations of charge n and m, respectively, and X represents the sorption site on the solid phase. The cation exchange capacity (CEC) and the quantity of major cations present in a system can strongly influence the exchange or distribution coefficient (K_d) of radionuclides, as shown

in the following equations:

$$Rn + NaX = RnX + Na \ , \tag{L-2}$$

$$K = \frac{[RnX][Na]}{[Rn][NaX]} \ , \tag{L-3}$$

$$K_d = K\frac{[NaX]}{[Na]} \ , \tag{L-4}$$

where *Rn* represents a radionuclide, K_d is the distribution of the radionuclide between the solid and the aqueous phase, *K* is the equilibrium constant, and brackets represent activities. The K_d of a specific nuclide in a specific environment is commonly used when describing sorptive properties. Since K_d is directly related to the cation content, an understanding of the major cation chemistry (Na^+, Ca^{2+} and K^+) is needed to fully understand the ability of Yucca Mountain to sorb radionuclides.

L-3 GEOCHEMICAL CODE

The simulations performed to address the first question in this auxiliary analysis concerning the validity of K/Ar dating relied on the geochemical modeling code *PHREEQM*, a code for use, in mixing cell flowtube simulations, described by Appelo and Willemsen (1987). *PHREEQM* (Ph-REdox-EQuilibrium-Mixing), a modification of *PHREEQE*, has the same capabilities of *PHREEQE*, plus it can simulate one-dimensional fluid flow, diffusion, dispersion, and ion exchange. *PHREEQE* (Ph-REdox-EQuilibrium-Equations) is based on an ion-pairing aqueous model and can calculate Ph, redox potential, and mass transfer as a function of reaction progress (Parkhurst *et al.*, 1980).

PHREEQM has the ability to simulate the flow of a solution through a multilayered heterogeneous column of porous material. Up to 10 layers, or a total of 100 cells, can be included in the simulated column. In each layer, equilibration with up to 10 minerals and reaction with up to 10 components can be simulated. Initial solid and liquid compositions in the column are input parameters of the code. Other input parameters are the length of each cell, the dispersivity associated with each cell, the porosity of any cell, the number of cell volumes of flushing solution added to the column, the composition of the flushing solution, the time allowed for diffusion/mixing of chemical constituents between adjacent cells, and the molecular diffusivity of elements in water.

Output includes composition of liquid, quantities of minerals precipitated or dissolved, and composition of solid ion exchanger in each cell for all timesteps. The output is presented in spreadsheet format, to facilitate the graphing of the results.

L-4 SIMULATIONS

L-4.1 Effect of Ion Exchange on K/Ar Dating

This analysis involved simulating the flow of site-specific groundwater, through site-specific porous

rock, at a site-specific rate. The simulation that was performed used mole fractions of Na, Ca+Mg, and K derived from the zeolite compositions reported by Broxton *et al.* (1986). In that study, the mole fractions of the exchangeable cations were determined for an extensive array of samples taken from boreholes in the vicinity of Yucca Mountain, in both the saturated and unsaturated zones. The zeolitic compositions vary both laterally and vertically. To simplify the simulation, a solid ion-exchanger composition was chosen that approximates the average composition of zeolites from the Topopah Spring member of the Paintbrush Tuff, where the proposed high-level radioactive waste repository is to be sited. The relative mole fractions for Ca+Mg, Na, and K were 33 percent, 19 percent, and 48 percent, respectively. The flushing solution composition in the simulation approximates that of the site-specific water from Peters *et al.* (1992). This site-specific water was extracted from pores, from several representative samples of tuff, by means of compression. Given that the zeolite compositions from Broxton *et al.* (1986) summed the concentrations of the exchangeable cations, Ca and Mg, the same was done for the liquid. The composition of the simulated water (flushing solution) was 3.10 moles/liter Ca+Mg, 1.83 moles/liter Na, and 8.03 moles/liter Cl. Other chemical constituents measured in the pore water from the squeezed rock but not included in this simulation, were HCO_3, SO_4, SiO_2, and Ph. These constituents have no effect on the reaction modeled.

The column through which water flowed in the simulation was divided into 100 cells. Each cell was 5 meters long. The whole column was then composed of 500 meters of the Paintbrush unit. The porosity of the column is assumed to be 0.3, which lies within the range of porosities found at Yucca Mountain.

The percolation flux of flushing solution through the column was set at 0.6 millimeters/year. This is comparable to moving the liquid from one cell to an adjacent cell downstream every 2500 years. This value approximates that derived from matrix potentials in USW UZ-1 (Montazer *et al.*, 1985). The range of estimates of percolation fluxes, however, extend from negative values (upward fluxes) to 100 mm/yr (Montazer and Wilson, 1984; and Montazer *et al.*, 1985). The dispersivity associated with each cell was arbitrarily set at 0.02 meters. Molecular diffusivity was 3 meters^2/100 years.

The CEC was set at 6667 meq/l. This value lies approximately halfway between the extremes of CEC's of rocks from Yucca Mountain (from Thomas, 1987). The three ion-exchange reactions modeled are:

$$NaX + K^+ = KX + Na^+ \quad ; \tag{L-5}$$

$$2Na^+ + CaX_2 = 2NaX + Ca^{2+} \; ; \tag{L-6}$$

$$2K^+ + CaX_2 = 2KX + Ca^{2+} \quad . \tag{L-7}$$

Equilibrium constants for Equations (L-5) and (L-6) were from Pabalan (1991). The equilibrium constant for Equation (L-7) was derived by multiplying Equation (L-5) by two and adding the result to Equation (L-6). In this simulation, ideal mixing was assumed in the solid phase. This assumption is most likely incorrect, as indicated by the experimental evidence of nonideality in the binary systems

Na-K and Na-Ca clinoptilolite (Pabalan, 1991). However, experimental studies on mixing in the solid phase of the ternary system Na-K-Ca clinoptilolite have yet to be performed, so the assumption of ideality in the solid phase was required.

L-4.2 Calculated Compositions of Water from the Unsaturated Zone

By using the compositions of clinoptilolites from the unsaturated zone of Yucca Mountain (Broxton *et al.*, 1986) and the equilibrium constants from Pabalan (1991) and this study for Equations (L-5) through (L-7), the relative concentrations of the exchangeable cations in the pore were calculated. Again, ideality of mixing in the solid was assumed. Activity coefficients for species in the liquid phase were derived from the Debye-Huckel formulation. However, the ionic strength of pore water in equilibrium with the zeolites is assumed to be constant and comparable to the extracted pore water from Peters *et al.* (1992). Consequently, the activity coefficients are likewise constant.

L-5 RESULTS

L-5.1 Effect of Ion Exchange on K/Ar Dating

Figure L-1 shows the concentration of exchangeable cations in the solid versus distance along flow path (represented as cell numbers). Cell 0 represents the top of the column; cell 100 represents the bottom of the column. The flushing solution is input into the top of the column at cell 0. The horizontal lines represent the chemical composition of the solid phase in the column after 60 shifts (cell volumes) or 150,000 years. The composition is relatively constant, except in the first few cells.

Figure L-2 represents the composition of the solution passing through the column after 60 shifts. The original water composition is shown on the *Y*-axis. This graph demonstrates that the composition of the pore water is dominated by the composition of the zeolites. Since the composition of the zeolites varies, it is reasonable to assume that the pore water chemistry will also vary, as the water percolates through the zeolites.

The results of this auxiliary analysis demonstrate that the K in the zeolites is relatively immobile. This is because of the large reservoir of K held in the zeolite versus the amount of exchangeable cations in the liquid. There simply are not enough cations in the pore water to exchange with the K on the zeolites, and therefore the K remains immobile. Consequently, the K/Ar technique for determining the age of the zeolites should not be affected by ion exchange, given the low concentrations of cations in the groundwater.

L-5.2 Calculated Compositions of Water from the Unsaturated Zone

The compositions of zeolites and ground waters in equilibrium with those zeolites were plotted on ternary diagrams using the code *GRAPHER*. The ternary diagrams illustrate the relative concentrations of sodium, potassium, and calcium and not the total concentrations. This representation for the liquid compositions is consistent with ternary representations of solid compositions in Broxton *et al.* (1986). Figure L-3 is a ternary diagram showing the relationship of the zeolite compositions to the liquid compositions, in equilibrium with those solids in Well G-4. This figure contains solid and liquid compositions from the unsaturated zone. The solid compositions have an average K content of 50 percent. However, the water in equilibrium with these solids contains very little potassium. The saturated zone information was not included in the graph, so the unsaturated zone information is more defined. Figure L-3 clearly demonstrates that the zeolites of the

Figure L-1. Concentration of exchangeable cations in solid vs. distance along slow path.

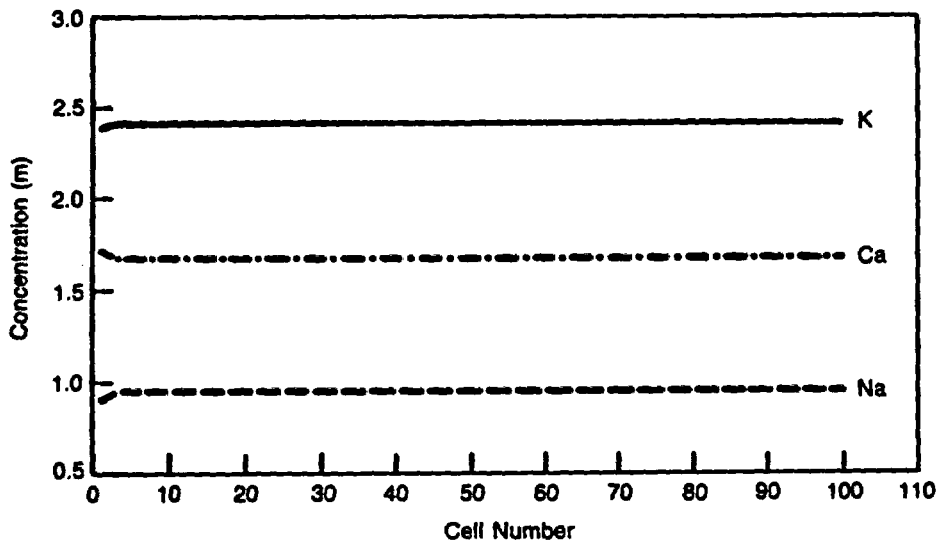
3.0
2.5
2.0
1.5
1.0
0.5
Concentration (m)
K
Ca
Na
0
10
20
30
40
50
60
70
80
90
100
110
Cell Number

Figure L-2. Composition of solution passing through column.

Figure L-2. Composition of solution passing through column.

Yucca Mountain Flow Simulation

Unsaturated Zone Liquid Composition

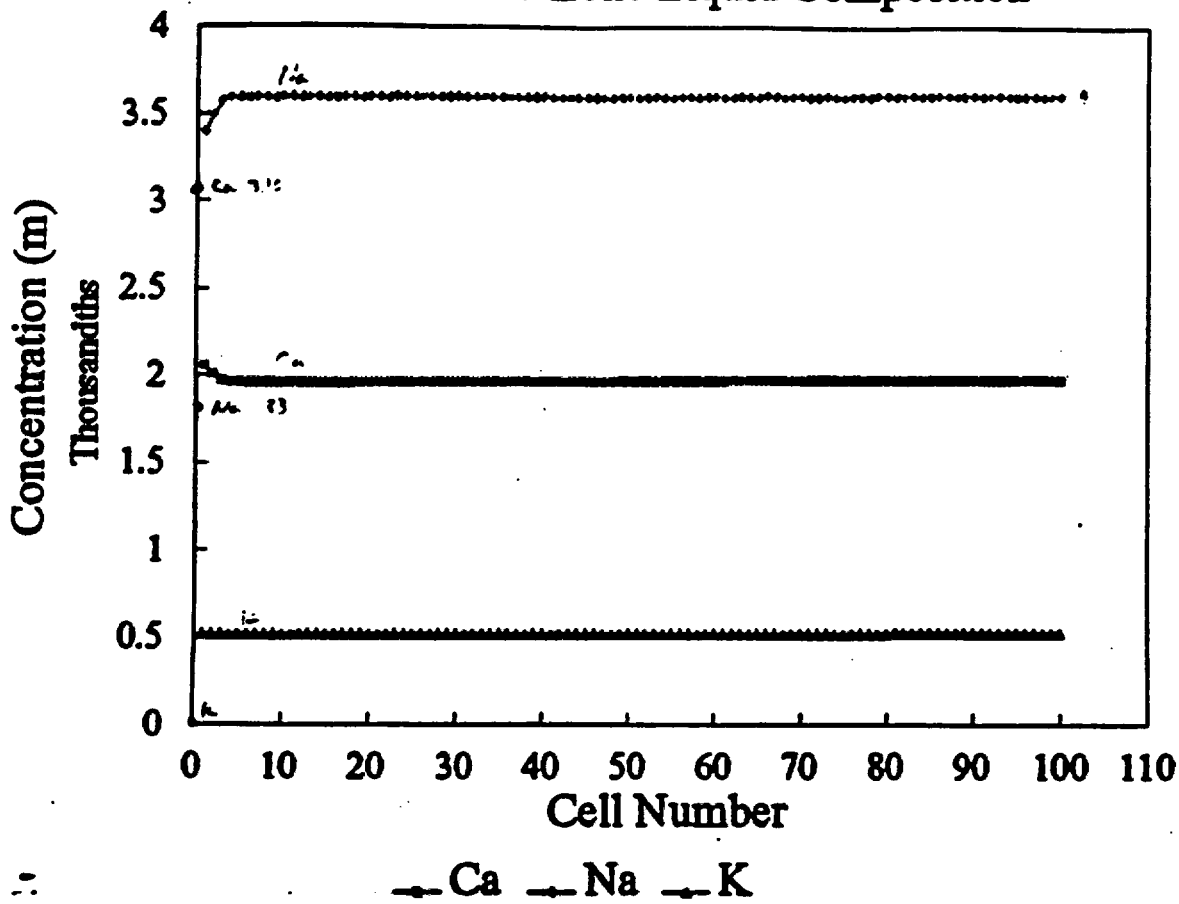

Shift 60 - Flushing solution = Yang water
Broxton zeolite composition

Figure 2

Figure L-3. Ternary diagram of zeolite composition to liquid composition in Well G-4 unsaturated zone.

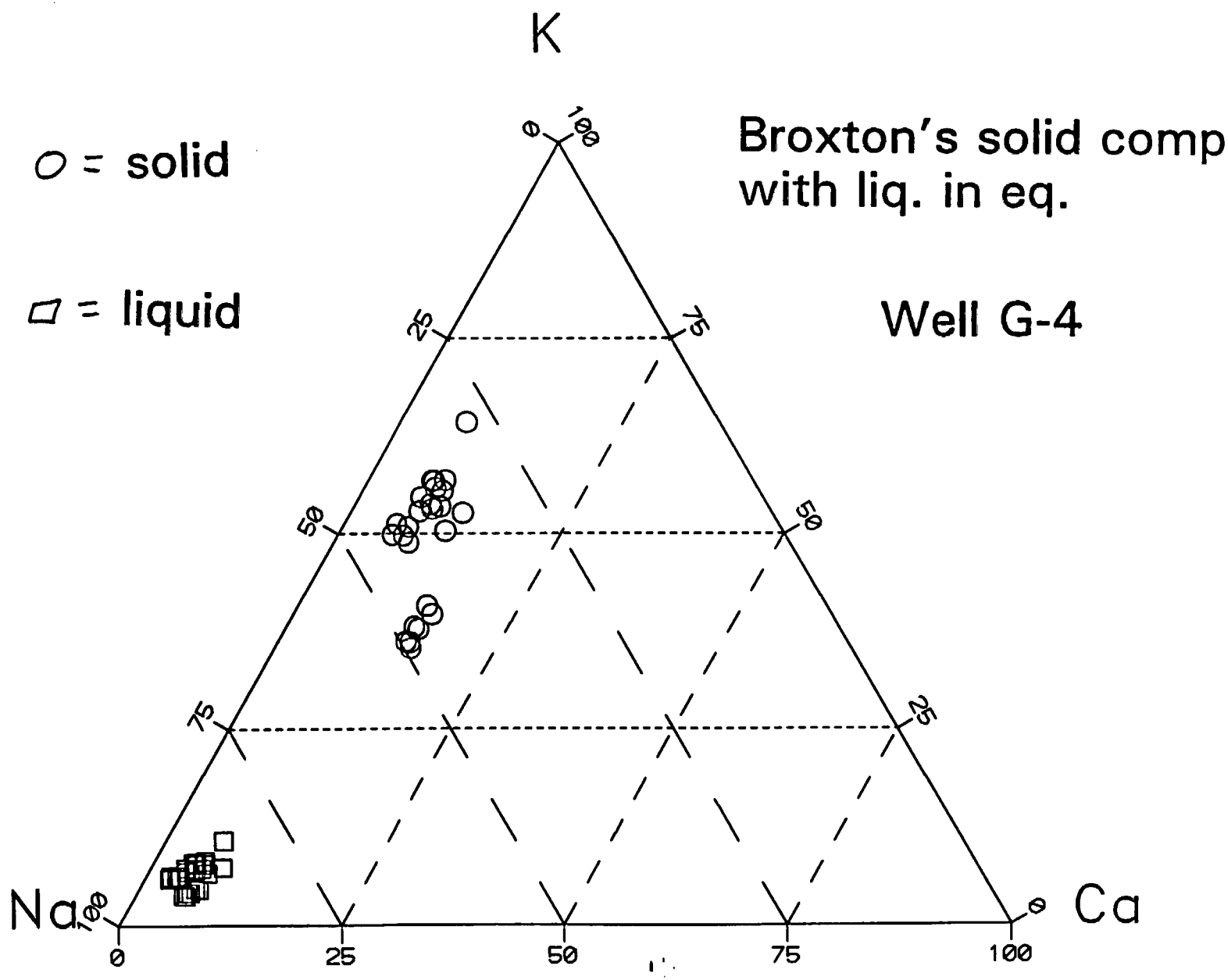
K
Na
Ca
0
25
50
75
100
○ = solid
▱ = liquid
Broxton's solid comp
with liq. in eq.
Well G-4

unsaturated zone are deficient in Na, where the pore water in equilibrium is Na-rich and K-deficient. The potassium concentrations of the unsaturated zone pore water measured by Peters *et al.* (1992) were suspect, and so were not reported. The potassium concentration measured in replicate samples varied, but generally was less than 10 ppm (Peters, personal communication, 1993).

Figures L-4 - L-8 illustrate the compositions of zeolites and coexisting ground waters in Wells G-1, G-2, G-3, H-3, and H-4. On Figure L-8, the composition of J-13 well water is plotted, as well as the composition of the water removed from Well USW-H4. The Na-rich composition of the water from USW-H4 is consistent with Na-K-rich zeolites analyzed from this well in the saturated zone. Establishing a comparable match with J-13 groundwater/zeolite is not apparent, possibly because of not knowing the depth from which the water comes.

L-6 CONCLUSIONS

In summary, this auxiliary analysis has produced valuable information on the exchange of the major cations in Yucca Mountain. The results indicate that the potassium associated with the zeolites is relatively immobile for the time period of these modeling runs. It also demonstrates the wide variation, in the pore water chemistry, which is possible in this environment. In addition, this analysis has shown that the chemical composition of the pore waters in contact with the solids in the unsaturated zone may be different from the composition of the water in the saturated zone. This is important for those who wish to do exchange experiments and require the solution and solids to be in equilibrium.

Figure L-4. Zeolite to liquid compositions for Well G-1.

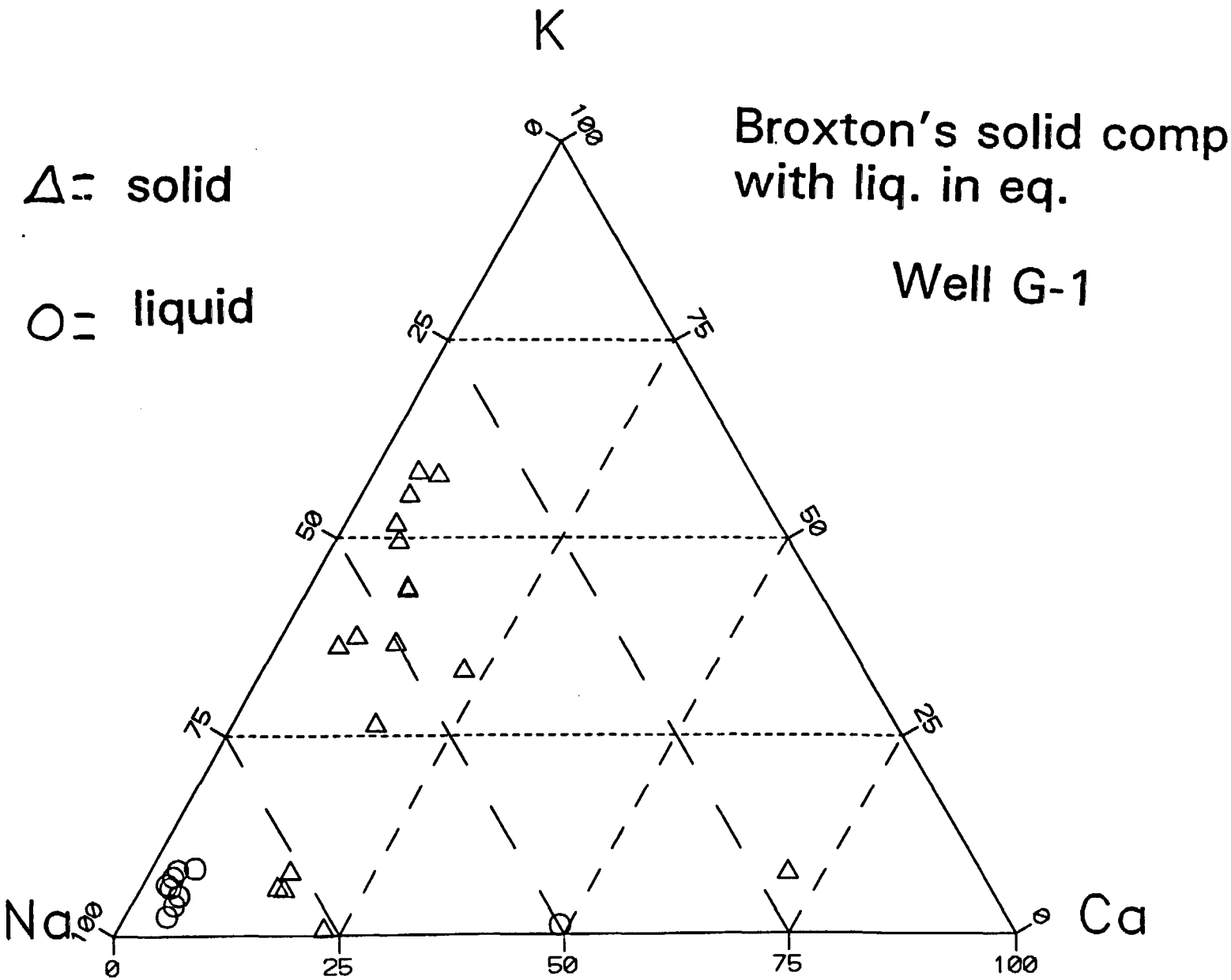
K
Broxton's solid comp
with liq. in eq.
Well G-1
Δ = solid
O = liquid
Na
Ca
0
25
50
75
100

Figure L-5. Zeolite to liquid compositions for Well G-2.

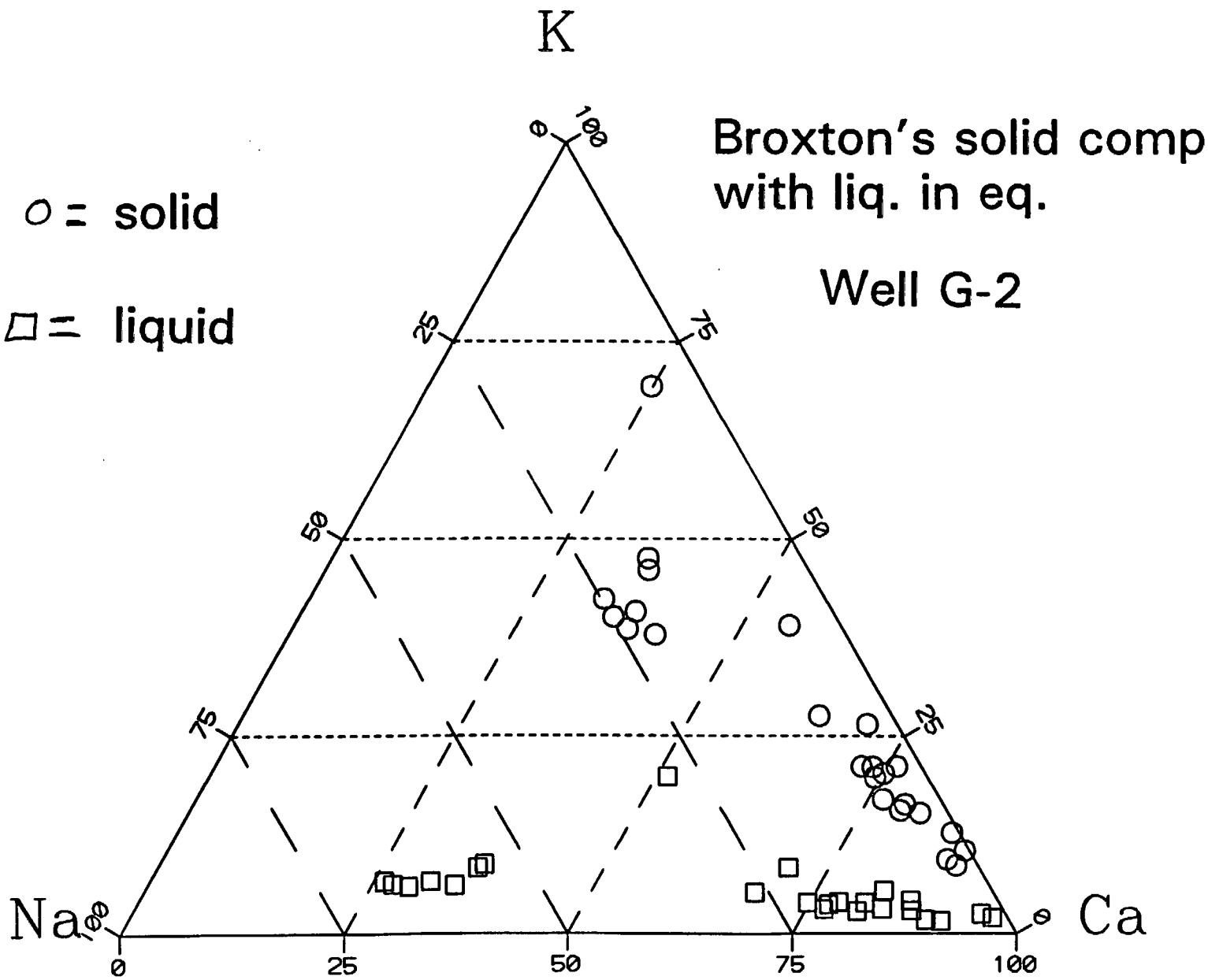
K
Na
Ca
0
25
50
75
100
○ = solid
□ = liquid
Broxton's solid comp
with liq. in eq.
Well G-2

Figure L-6. Zeolite to liquid compositions for Well G-3.

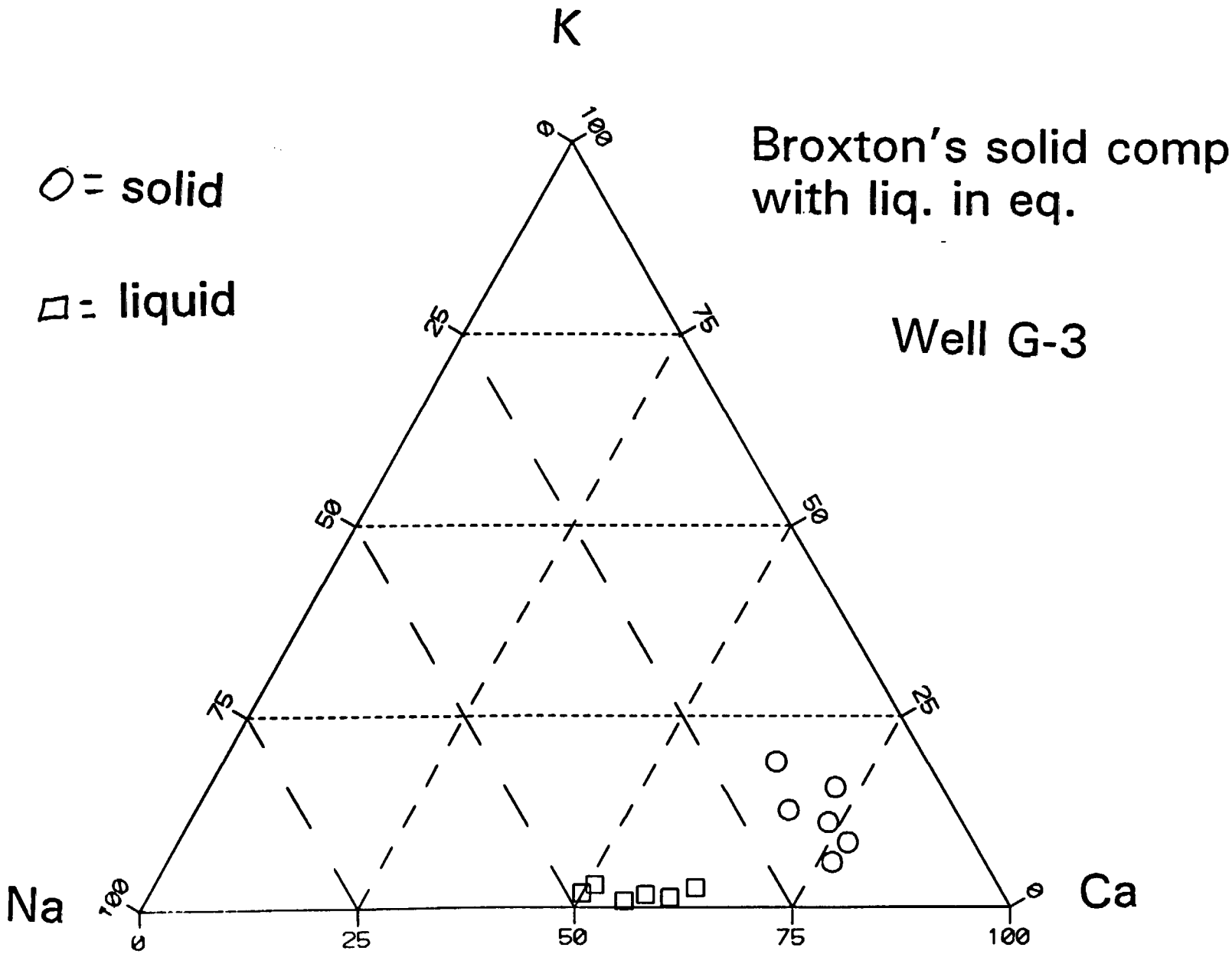
K
Na
Ca
O = solid
□ = liquid
Broxton's solid comp
with liq. in eq.
Well G-3
0
25
50
75
100

Figure L-7. Zeolite to liquid compositions for Well H-3.

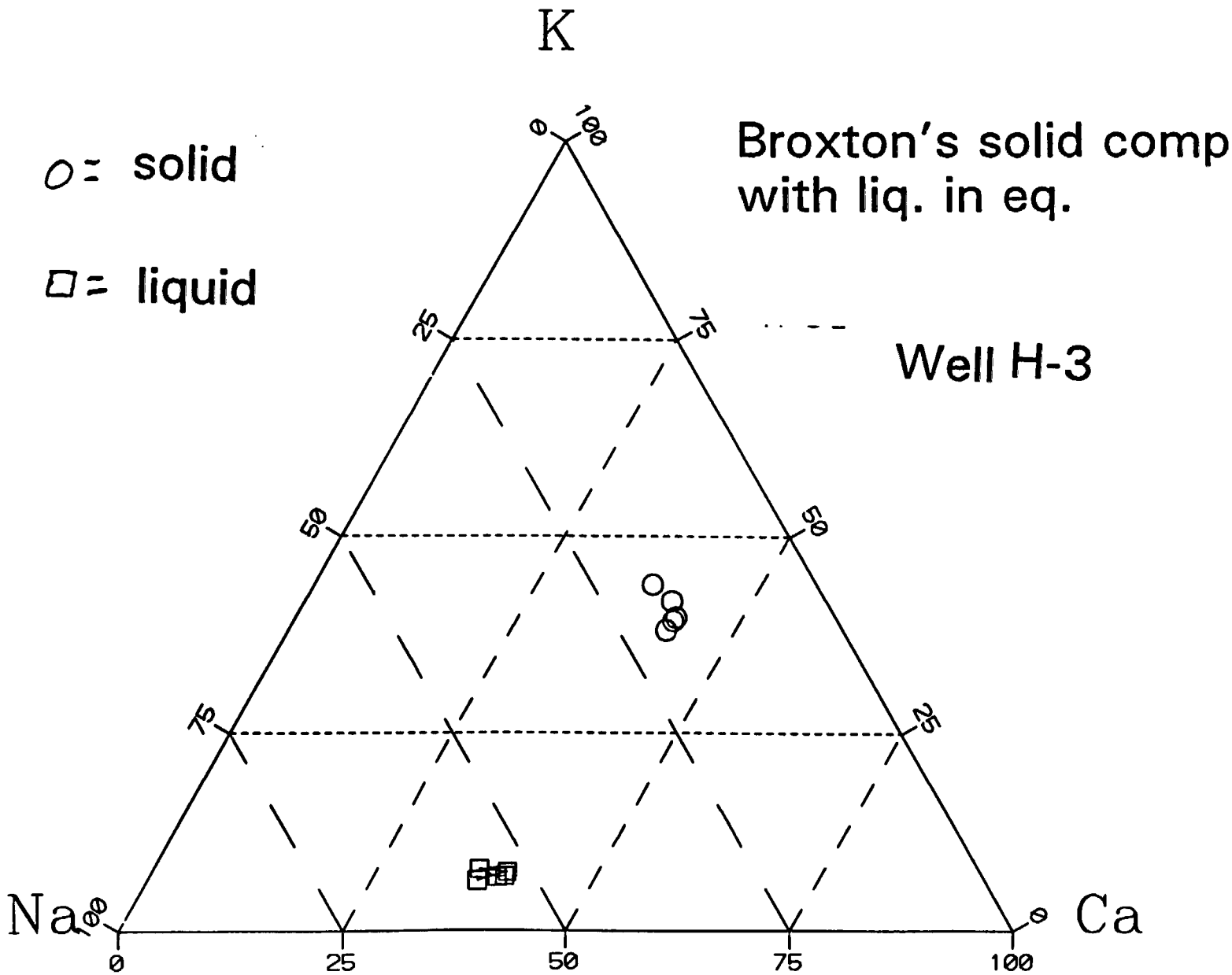
K
Na
Ca
0
25
50
75
100
○ = solid
□ = liquid
Broxton's solid comp
with liq. in eq.
Well H-3

Figure L-8. Zeolite to liquid compositions for Well H-4.

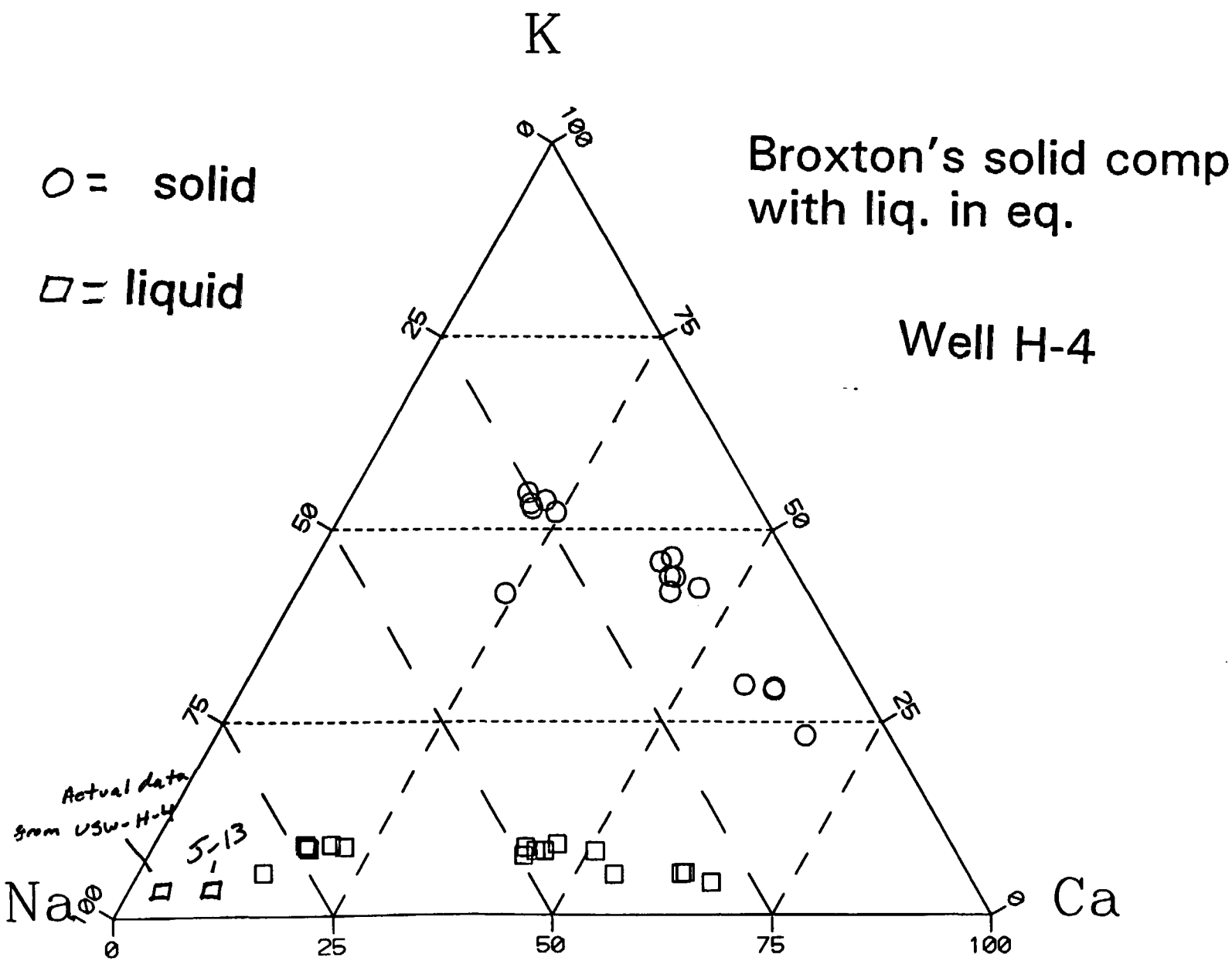

○ = solid

□ = liquid

Broxton's solid comp with liq. in eq.

Well H-4

L-7 REFERENCES

Appelo, C.A.T. and A. Willemsen, "Geochemical Calculations and Observations on Salt Water Intrusions, I., A Combined Geochemical/Mixing Cell Model," *Journal of Hydrology*, 94:313-330 [1987].

Broxton, D.E., R.G. Warren, R.C. Hagan, and G. Luedemann, "Chemistry of Diagenetically Altered Tuffs at a Potential Nuclear Waste Repository, Yucca Mountain, Nye County, Nevada," Los Alamos National Laboratory, LA-10802-MS, October 1986.

Montazer, P., and W.E Wilson, "Conceptual Hydrologic Model Flow in the Unsaturated Zone, Yucca Mountain, Nevada, Water Resources Investigations," U.S. Geological Survey, Water Resources Investigations Report, WRI-84-4345, 1984.

Montazer, P., E.P. Weeks, F. Thamir, S.N. Yard, and P.B. Hofricher, "Monitoring the Vadose Zone in Fractured Tuff, Yucca Mountain, Nevada," *Proceedings of the National Water Well Association Conference on Characterization and Monitoring of the Vadose (Unsaturated) Zone*, Worthington, Ohio, pp. 439-469, 1985.

Pabalan, R.T., "Nonideality Effects on the Ion Exchange Behavior of the Zeolite Mineral Clinoptilolite," in T.A. Abrajano and L.H. Johnson (eds.), "Scientific Basis for Nuclear Waste Management XIV," *Materials Research Society Symposium Proceedings*, 212:559-567 [1991].

Parkhurst, D.L., D.C. Thorstenson, and L.N. Plummer, "PHREEQE -- A Computer Program for Geochemical Calculations," U.S. Geological Survey, Water Resources Investigations Report, WRI-80-96, August 1980.

Peters, C.A., I.C. Yang, J.D. Higgins, and P.A. Burger, "A Preliminary Study of the Chemistry of Pore Water Extracted from Tuff by One-Dimensional Compression," in Kharaka and Maest (eds.), *Water-Rock Interaction*, Balkema, Rotterdam, 1992.

Thomas, K., "Summary of Sorption Measurements Performed with Yucca Mountain, Nevada, Tuff Samples and Water from Well J-13," Los Alamos National Laboratory, LA-10960-MS, December 1987.

WoldeGabriel, G., D.E. Broxton, D.L. Bish, and S.J. Chipera, "Preliminary Assessment of Clinoptilolite K/Ar Results from Yucca Mountain, Nevada, USA: A Potential High-Level Radioactive Waste Repository Site," in Kharaka and Maest (eds.), *Water-Rock Interaction*, Balkema, Rotterdam, 1992.

APPENDIX M

CONTENTS

		Page
M-1.	Introduction	M-1
M-2.	Solubility Limited Case	M-2
M-3.	Congruently Release Rate	M-3
M-4.	Conclusions	M-4

APPENDIX M
ENSEMBLE AVERAGING FOR SOURCE TERM PARAMETERS
R.B. Codell/NMSS

M-1. INTRODUCTION

For the sake of computational speed, the IPA Phase 2 analysis used a "lumped-parameter" approach, in which the entire geologic repository is represented by a relatively small number of representative waste packages. Since the entire repository source term, consisting of over 25,000 waste packages, is being represented by only seven zones or sub-areas, with only one waste package per repository sub-area, there must be careful consideration given to the way in which the repository sub-areas represent the ensemble of waste packages they are supposed to represent.

Presently, the arithmetic average of external environmental parameter values (e.g., temperature, infiltration) for all waste packages in the repository sub-area are chosen for a representative waste package. Additionally, there is only one set of source term parameter values (e.g., corrosion parameters, solubilities) representing the corrosion, liquid, and gaseous release submodels per repository sub-area. The present auxiliary analysis examines the relationships of several key independent variables, in the source term models, from the standpoint of their behavior under ensemble averaging.

The flow rate q and the volume V affect the dissolved release model in two ways:

- They determine the time that the waste package fills to the point of overflowing; and
- They determine the release rate for solubility limited radionuclides.

The demonstration of the effects of ensemble averaging on the cumulative release rate was performed for only two radionuclides, one solubility limited and the other limited by congruent dissolution of the UO_2 fuel. To further simplify the calculations, both radionuclides have infinite half lives, no other isotopes are present, and daughter products are not considered.

M-2. SOLUBILITY LIMITED CASE

For the stated conditions within a given vector, the concentration C_s within the waste package will be constant (i.e., the solubility). Therefore, the cumulative release for 10,000 years per waste package m_a for a solubility limited radionuclide by advection will be proportional to the flow rate through the waste package:

$$m_a = C_s q_l [10{,}000 - t_f] , \qquad \text{(M-1)}$$

where t_f = time to fill waste package, years = V_o/q.

The cumulative diffusive release m_d, is proportional to the concentration:

$$m_d = kC_s[10{,}000 - t_{fail}] , \tag{M-2}$$

where k is a proportionality constant related to the diffusion coefficient and retardation coefficient in the surrounding rock, which are constants within a given vector. The waste package failure time t_{fail}, is related to a number of parameters in the waste package failure model or disruptive failure models, and varies from place to place within a vector.

The cumulative release of the radionuclide for all waste packages is equal to the sum of the releases from each waste package after their filling, that is,

$$M = \sum_{i=1}^{N}\left[C_s q_i(10{,}000 - \frac{V_0}{q_i}) + kC_s(10{,}000 - t_{fail})\right] . \tag{M-3}$$

The average cumulative release per waste package is therefore the result of Equation (M-3), divided by N. After some rearrangement, Equation (M-3) can be shown to reduce to:

$$\langle m\rangle = C_s[10{,}000\langle q\rangle - \langle V_0\rangle + 10{,}000k - k\langle t_{fail}\rangle] , \tag{M-4}$$

where the angle brackets (< >) denote ensemble average over all N waste packages.

M-3. CONGRUENTLY RELEASE RATE

For the case where the release rate is controlled not by the solubility of the radionuclide, but by the rate of release from the fuel matrix, a different set of relationships controls the ensemble average. In this case, the concentration of the radionuclide in the waste package, C_o, is no longer a constant, but changes with time and is a function of the rate of release by advection and diffusion. Since C_o is no longer a constant, the integration for cumulative release over 10,000 years must be done formally:

$$M = \int_{t_{fail}}^{10{,}000} kC_o dt + \int_{t_f}^{10{,}000} q_i C_o dt . \tag{M-5}$$

For a long half life, C_o is related to the alteration rate of the matrix r, the inventory in the matrix M_o, and the flow rate, all of which are constant within a given vector. Therefore:

$$C_0 = \frac{rM_0}{q_i} , \tag{M-6}$$

$$m = \int_{t_{fail}}^{10,000} kC_0 dt + \int_{t_f}^{10,000} rM_0 dt \,. \tag{M-7}$$

Applying the same definitions for t_f and after evaluating the integrals, the cumulative release becomes:

$$m = rm_0\left[\frac{k}{q_i}(10,000 - t_{fail}) + 10,000 - \frac{v_0}{q_i}\right]. \tag{M-8}$$

The ensemble average for N waste packages can be found by summing, as in the case of the concentration limited release:

$$<m> = \frac{1}{N}\sum_{i=1}^{N} rm_0\left[10,000 + \frac{1}{q_i}\left[k(10,000 - t_{fail} - V_0\right]\right], \tag{M-9}$$

which reduces, after some rearrangement, to:

$$<m> = 10,000M_0kr <(\frac{1}{q})> - M_0kr <\left(\frac{t_{fail}}{q}\right)> + 10,000rM_0 + M_0r <\left(\frac{V_0}{q}\right)> . \tag{M-10}$$

M-4. CONCLUSIONS

For solubility limited releases of single, long-lived radionuclides, the ensemble average cumulative release per waste package is represented exactly by the arithmetic averages of the flow rate per waste package $<q>$, the waste package failure time $<t_{fail}>$, and the waste package failure volume $<V_0>$.

The ensemble mean parameters for the congruent release case, therefore, should be the $<1/q>$ (the harmonic mean), $<t_{fail}/q>$, and $<V_0/q>$.

Experiments with the release rate models, themselves, confirm that cumulative release of the long-lived solubility limited radionuclides is proportional to flow, which demonstrates that the arithmetic mean flow rate is the correct ensemble mean to use for these radionuclides. Release of congruently released radionuclides is not proportional to the flow rate, but for these radionuclides, the flow rate is relatively unimportant. A 35-fold increase in flow rate led to only about a 60 percent increase in releases. The effects of using the arithmetic mean of the V_0 and the parameters for the failure model have not been determined for IPA Phase 2.